



INDIAN AGRICULTURAL  
RESEARCH INSTITUTE, NEW DELHI

18873

L A R. I. S.

MGIPC—84—10 AR—21'6 49—1,000.

**Library,  
Indian Agricultural Research Institute,  
New Delhi (India).**



PROCEEDINGS  
OF THE  
ROYAL SOCIETY OF LONDON

SERIES A—MATHEMATICAL AND PHYSICAL SCIENCES

VOL. CLVIII



LONDON  
Printed and published for the Royal Society  
By Harrison & Sons, Ltd, 44-47, St. Martin's Lane  
Printers in Ordinary to His Majesty

3 February, 1937

18873

LONDON

HARRISON AND SONS, LTD., PRINTERS IN ORDINARY TO HIS MAJESTY  
ST MARTIN'S LANE

# CONTENTS

## SERIES A VOL CLVIII

No. A 893—1 January, 1937

	PAGE
On the Nature of Atmospheres IV By E. V. Appleton, F.R.S., and F. W. Chapman (Plates 1-3)	
The Effect of Space-Charge on the Secondary Current in a Triode By D. M. Myers, D. R. Hartree F.R.S., and A. Porter	23
On the Relations of the Tensor-calculus to the Spinor-calculus By E. T. Whittaker F.R.S.	38
The Auger Effect in Xenon and Krypton By L. H. Martin and F. H. Eggleston Communicated by T. H. Laby, F.R.S. (Plates 4-8)	46
The Modification of Apparent Thermionic Constants for Oxygenated Tungsten by the Temperature Variation of Adsorptive Equilibrium By M. C. Johnson and F. A. Vick Communicated by S. W. J. Smith F.R.S.	55
Dissociation Constants and Structures of Zwitterions By A. Neuberg Communicated by C. R. Harrington, F.R.S.	68
A Quantum Mechanical Discussion of the Cohesive Forces and Thermal Expansion Coefficients of the Alkali Metals By H. Fröhlich Communicated by N. F. Mott F.R.S.	97
Fine Structure in the Arc Spectrum of Platinum (A) The Nuclear Spin of Pt 195, (B) Even Isotope Displacement By S. Tolansky and E. Lee Communicated by W. I. Bragg, F.R.S.	110
Exact and Approximate Expressions for the Permeability of Potential Barriers to Light Particles By R. P. Bull Communicated by C. N. Hinshelwood, F.R.S.	128
A New Process of Negative Ion Formation—II By F. L. Arnot Communicated by H. Stanley Allen, F.R.S.	137
A New Process of Negative Ion Formation III—The Energy Distribution of the Negative Ions and Accommodation Coefficients of the Positive Ions By F. L. Arnot Communicated by H. Stanley Allen, F.R.S.	157
The Absorption Spectra of Triiodides By C. B. Allsopp Communicated by T. M. Lowry, F.R.S.	167
Dielectric Constants of Solids at High Frequencies and the Influence of Water of Crystallization on Dielectric Constant By E. F. Burton and L. G. Turnbull Communicated by O. W. Richardson, F.R.S.	182

	PAGE
A Quantitative Study of Pleochroic Haloes III—Thorium By G H Henderson, C M Mushkat, and D. P Crawford Communicated by Lord Rutherford, O M, F R S (Plates 9 and 10)	199
Pressure Broadening of Spectral Lines and van der Waals Forces I—Influence of Argon on the Mercury Resonance Line By H Kuhn Communicated by F A Lindemann, F R S	212
Pressure Broadening of Spectral Lines and van der Waals Forces II—Continuous Broadening and Discrete Bands in Pure Mercury Vapour. By H Kuhn Communicated by F A Lindemann, F R S (Plate 11)	230
Minutes of Meetings of 5, 12, 19, and 30 November, and 10 December, 1936	
No A 894—15 January, 1937	
The Interaction of Atoms and Molecules with Solid Surfaces VI—The Behaviour of Adsorbed Helium at Low Temperatures By J E Lennard-Jones, F R S, and A F Devonshire	242
The Interaction of Atoms and Molecules with Solid Surfaces VII—The Diffraction of Atoms by a Surface By J E Lennard-Jones, F R S, and A F Devonshire	253
The Interaction of Atoms and Molecules with Solid Surfaces VIII—The Exchange of Energy Between a Gas and a Solid By A F Devonshire Communicated by J E Lennard-Jones, F R S	269
The Electronic Structure of Some Polyenes and Aromatic Molecules I—The Nature of the Links by the Method of Molecular Orbitals By J E Lennard-Jones, F R S	280
The Electronic Structure of Some Polyenes and Aromatic Molecules II—The Nature of the Links of Some Aromatic Molecules By J E Lennard-Jones, F R S, and J Turkevich	297
The Electronic Structure of Some Polyenes and Aromatic Molecules III—Bonds of Fractional Order by the Pair Method By W G Penney Communicated by J. E Lennard-Jones, F R S . . . . .	306
Kinematics, Dynamics, and the Scale of Time By E A Milne, F R S	324
Explosion Waves and Shock Waves IV—Quasi-Detonation in Mixtures of Methane and Air By W Payman and W C F Shepherd Communicated by J F Thorpe, F R S (Plates 12–16)	348
The Lorentz Transformations in the New Quantum Electrodynamics By L Infeld Communicated by R H Fowler, F R S . . . . .	368
The Hyperfine Structure and Zeeman Effect of the Resonance Lines of Silver By D A Jackson and H Kuhn Communicated by F A Lindemann, F R S (Plates 17–19) .. . . .	372
The Contribution to the Electrical Resistance of Metals from Collisions Between Electrons. By W. G Baber Communicated by N F. Mott, F R S . . . . .	383

	PAGE
The Exchanges of Energy Between a Platinum Surface and Hydrogen and Deuterium Molecules By W B Mann and W C Newell Communicated by A O Rankine, F R S . . .	397
The Dielectric Polarization of <i>n</i> -Long Chain Ketones Near their Melting Points. By A. Müller. Communicated by Sir William Bragg, O.M., F.R.S. . . .	403
The Influence of Pressure on the Spontaneous Ignition and Limits of Inflammability of Ether-Air Mixtures By F T A Townend and E A C Chamberlain Communicated by W A Bone, F R S . . .	415
Spectrographic Studies of the Explosive Combustion of Methane By J Bell. Communicated by W A Bone, F R S (Plates 20-23) . . .	429
The Spectrum of Trebly-Ionized Lead, Pb IV By M F Crawford, A B McLay, and A M Crooker Communicated by O W Richardson, F R S . . .	435
Temperature Coefficients in the Anion Catalysed Decomposition of Nitramide. By E C Baughan and R P Bell Communicated by C N Hinshelwood, F R S . . .	464
Royal Society Expedition to Montserrat, B W I Preliminary Report on Seismic Observations By C F Powell Communicated by Sir Gerald Lenox-Conyngham, F R S (Plates 24 and 25) . . .	479

No A 895—3 February, 1937

On the Thermal Decomposition of Methyl Nitrite By A G Carter and Morris W Travers, F R S . . .	495
Mechanism of the Production of Small Eddies from Large Ones By G I Taylor, F R S, and A. E. Green . . .	499
Motion of an Infinite Elliptic Cylinder in Fluids with Constant Vorticity By Manohar Ray Communicated by M N. Saha, F R S . . .	522
The Polarization of Radio Echoes. By D F. Martyn and G H. Munro Communicated by Lord Rutherford, O M, F R S (Plate 26) . . .	536
The Theory of the Continuous Absorption Spectrum of Bromine By N S Bayliss Communicated by Sir David Masson, F R S . . .	551
The Spectrum of Ionized Tellurium—Extension of Te III By S G Krishnamurti and K R Rao Communicated by A Fowler, F.R.S. . .	562
On the Absolute Intensities of the Strong $\beta$ -Ray Lines of Ra (B + C), Th (B + C), and Ac (B + C). By K T. Li. Communicated by C. D Ellis, F R S. . .	571
Studies of Cosmic-Ray Showers by Quintuple Coincidences. By Hu Chien Shan Communicated by P. M. S. Blackett, F R S . . .	581

	PAGE
The Interaction of Atoms and Molecules with Solid Surfaces IX—The Emission and Absorption of Energy by a Solid By C. Strachan Communicated by J. E. Lennard-Jones, F.R.S. . . . .	591
The Effect of the Fitzgerald-Lorentz Contraction on the Frequency of Longitudinal Vibration of a Rod By A. B. Wood, C. A. Tomlinson, and L. Essen. Communicated by Sir Frank Smith, Sec. R.S. . . . .	606
The Ultra-Violet Absorption Spectra of Some Complex Aromatic Hydrocarbons—II By W. V. Mayneord and E. M. F. Roe Communicated by E. L. Kennaway, F.R.S. (Plate 27) . . . . .	634
Atmospheric Oscillations By C. L. Pekeris Communicated by G. I. Taylor, F.R.S. . . . .	650
The Micrography of Metals in Ultra-Violet Light By J. Smiles and H. Wrighton Communicated by J. E. Barnard, F.R.S. (Plates 28–34) . . . . .	671
The Emission Band Spectrum of Chlorine—I By A. Elliott and W. H. B. Cameron Communicated by S. R. Milner, F.R.S. (Plate 35) . . . . .	681
The <i>n</i> -Fatty Acids and Certain of their Derivatives By F. Francis, F. J. E. Collins, and S. H. Piper Communicated by M. W. Travers, F.R.S. . . . .	691
The Electrical Conductivity of Thin Metallic Films II—Caesium and Potassium on Pyrex Glass Surfaces By E. T. S. Appleyard and A. C. B. Lovell Communicated by A. M. Tyndall, F.R.S. . . . .	718
Ionization, Excitation, and Chemical Reaction in Uniform Electric Fields III—The Excitation of the Continuous Spectrum of Hydrogen By R. W. Lunt, C. A. Meek, and E. C. W. Smith Communicated by F. G. Donnan, F.R.S. . . . .	729
Index . . . . .	739

---

## On the Nature of Atmospherics—IV

By E. V. APPLETON, F.R.S., and F. W. CHAPMAN, M.Sc., Ph.D., King's College, London

(Received 26 June, 1936)

[PLATES 1-3]

### 1—INTRODUCTORY

The modern study of the rapid changes of the earth's electric field associated with lightning flashes was initiated by C. T. R. Wilson\* in 1916. Wilson made observations on the net changes of the earth's field due to the destruction of near-by thundercloud moments by lightning flashes and, since interest was centred solely in the magnitude of the initial and final values of the field, a relatively sluggish electrical indicator (capillary electrometer) was found most convenient. In observations of essentially the same character, Appleton, Watt, and Herd,† using a string electrometer as well as a capillary electrometer, made measurements at greater distances from the discharge channel. The work of Wilson, at distances usually within the region of audible thunder, had shown that the net changes of the earth's field associated with lightning flashes were more frequently positive than negative in sign. On the other hand, Appleton, Watt, and Herd found the opposite preponderance, and this led them to conclude that a thundercloud is frequently, if not always, bipolar and, further, that in order to account for the signs of the field changes it must be assumed that a very frequently occurring type of bipolar thundercloud is one with the positive charge uppermost. These conclusions were later confirmed by Schonland and Craib‡ in observations made in South African thunderstorms.

The measurements made by Appleton, Watt, and Herd on disturbances of the earth's electric field also included observations on the wave-form of those naturally occurring electric waves known to radio-engineers as atmospherics. In this series of observations the potential variations

\* 'Proc. Roy. Soc.' A, vol. 92, p. 555 (1916), and 'Phil. Trans.' A, vol. 221, p. 75 (1920).

† 'Proc. Roy. Soc.' A, vol. 111, p. 615 (1926).

‡ 'Proc. Roy. Soc.' A, vol. 114, p. 229 (1927).

developed across a condenser or resistance included in a damped wireless antenna were examined visually by means of a sensitive cathode-ray oscillograph. The results of a statistical analysis of a large number of individual drawings of wave-forms showed the type of atmospheric observed to be a relatively long aperiodic or quasi-periodic electrical disturbance of duration 2 to 3 milliseconds (msec) and intensity 0.1 volt per metre (v/m). High-frequency ripples on the main gross structure of quasi-frequencies up to 10 kilocycles per second (kc/s) were, however, noted and the interferent effects of atmospherics were attributed to such high-frequency components rather than to the effect of the relatively slow main disturbance.

Since there is no lack of evidence that we must look to thunderstorms, up to very considerable distances, as important sources of atmospherics, it appeared to us to be of interest to attempt to link up the observations of Wilson and others on the electrostatic field changes due to the destruction of thundercloud moments with the radiation field changes of atmospherics as studied by Appleton, Watt, and Herd, to study, in fact, the evolution of the atmospheric wave-form from the original disturbance. Our observations have thus been confined to those made within about 200–300 km from the discharge channel.

In repeating observations of the same type as those made by Appleton, Watt, and Herd, an attempt has been made to remove certain weaknesses in the technique which have been the subject of criticism. For example, the visual recording of the earlier series of observations has been replaced by photography of the transient disturbance as delineated on the cathode-ray screen. Moreover, by using the combination of a Wilson sphere as the exposed conductor connected to the input circuit of an electrometer triode† as the essential device by means of which the earth's electric field changes were recorded, it has been possible to vary the time constant of this circuit, and to satisfy ourselves that it exercised no deciding factor in the determination of the observed transient. Now it has been maintained by Lejay‡ that the earlier visual observations of atmospheric wave-forms were vitiated by the fact that the aerial system used had a time constant of the order of  $2 \times 10^{-3}$  seconds, and that it was this instrumental quantity which determined the observed durations and not the atmospheric which was the cause of the changes of potential in the aerial system. The arguments of Lejay we consider to be invalid for two reasons. In the first case he has confused the influence of a net change of field with

\* Appleton and Chapman, 'Nature,' vol. 134, p. 968 (1934).

† *Vide* Appleton, "Thermionic Vacuum Tubes," London, 1932, p. 71.

‡ Lejay, 'Bull. de l'Inst. de Physique du Globe,' p. 56 (1926).

the influence of a radiation field change. A net change of field would, it is true, cause a disturbance with a duration determined by the aerial time constant, but such disturbances were, as stated in the earlier paper, readily recognizable by their characteristic and relatively long duration, and were easily distinguished from the shorter atmospheric of distant origin which took place in an interval usually less than one-tenth of the time constant. Also, secondly, we have, in the present series, not been limited in our control of the aerial time constant and, by varying it, have satisfied ourselves that it exercises no recognizable influence on the delineation of wave-forms of the type and duration noted in the earlier observations.

At the same time, the present series of observations in which cathode-ray photography is employed, shows that the earlier observations by visual methods gave a limited and somewhat inadequate conception of the high-frequency components of atmospheric and that, in the visual series, the observer watching the oscillograph screen was liable to note the relatively large smooth radiation field and omit to record the short higher-frequency component which we now find always accompanies it. Our conception of atmospheric wave-forms, especially as regards their inter-ferent properties, is thus made much more satisfactory.

In the present series of observations the attempt has been made to supplement the observations on the temporal changes of  $E$ , the earth's electric field, by observations on the rate of change of field ( $i.e.$ , on  $dE/dt$ , where  $t$  is the time). In this way the study of the high-frequency components has been very much facilitated. Also, by confining our attention in a section of the work to atmospheric of known thunderstorm origin, it has been possible to follow the somewhat remarkable sequence of alterations of wave-form with distance. This alteration of wave-form is found to be partly such as might be expected from the simple laws of electrodynamics, the ratio of the radiation field to the electrostatic field increasing with distance. But there is also found marked evidence that the propagation of the atmospheric waves is subject to a dispersive influence which causes the high-frequency components to travel with a higher group velocity than the low-frequency components.

Quite apart from the question of the nature and origin of atmospheric, observations on the net change of field due to near-by lightning flashes, especially if the rapid changes can be followed, may be expected to give us information concerning the electrical nature of a lightning discharge since, at short distances, the variation of the electric field is proportional to the variation of the thundercloud moment during the flash.

## 2—BASIS OF METHOD USED

In order to study both the net change of the earth's electric field and the high-frequency detail in the field change, it was necessary to have a reasonably well-insulated exposed conductor as well as an electrometer system of rapid response. As the exposed conductor we used a Wilson sphere, while for the electrometer system we used an electrometer triode working by way of an amplifier and a cathode-ray oscillograph with photographic registration.

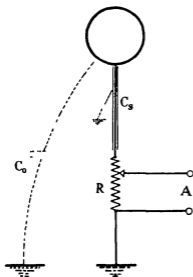


FIG 1—Illustrating diagrammatically the aerial system used for measurements of the rate of change of the earth's electric field (A, to oscillograph)

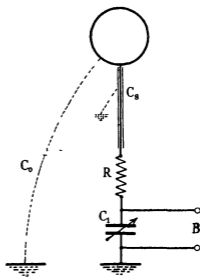


FIG 2—Illustrating diagrammatically the aerial system used for measurements of the earth's electric field (B, to electrometer triode)

Let us consider the effect of a rapid variation of the earth's electric field on such an exposed conductor of capacity  $C_0$  which is situated at a height  $h$  and earth-connected through a resistance  $R$  (see fig 1).  $C_s$  is the capacity between the down-lead and its cylindrical screen. If the system is non-oscillatory and the time constant  $(C_0 + C_s)R$  so small that the charge on the exposed conductor follows without appreciable lag the electric field variation, it has been shown that the potential  $v$  developed across the ends of the resistance  $R$  is proportional to the rate of change of the earth's electric field (i.e., to  $dE/dt$ , where  $E$  is the field and  $t$  the time). We have, in fact, the following relation

$$\frac{dE}{dt} = \frac{v}{h \cdot R \cdot C_0} \quad (1)$$

Measurements of  $dE/dt$  are especially suitable for emphasizing the high-frequency detail which is found in certain disturbances

To study the rapid change of  $E$ , the earth's electric field, the circuit shown diagrammatically in fig 2 was employed. Let us consider the effect on this system of a rapid change of  $E$ . Before the change occurs we consider the system as at earth potential so that the sphere retains a bound charge  $Q_0$  consistent with the normal potential  $V_0$  at the height  $h$ . We have then

$$V_0 + \frac{Q_0}{C_0} = 0 \quad (2)$$

Now let us suppose that the vertical electric field undergoes a change of magnitude  $f(t)$ , increasing the field at the height of the sphere by  $hf(t)$ . This will bring about a separation of charge  $Q$  in the insulated system and, if the time constant  $(C_1 + C_s)R$  is sufficiently small the separation of the charge will follow faithfully the changes of potential.

The expression of the fact that the potentials of  $C_0$  and  $C_1$  are still identical is that

$$V_0 + hf(t) + \frac{Q_0}{C_0} - \frac{Q}{C_0} = \frac{Q}{C_1 + C_s}, \quad (3)$$

or, subtracting (2), that

$$hf(t) = \frac{Q}{C_0} + \frac{Q}{C_1 + C_s} \quad (4)$$

Let us assume that the potential measured by the electrometer system across the capacity  $C_1$  is  $v$

Then

$$v = \frac{Q}{C_1 + C_s} \quad (5)$$

and

$$E = f(t) = \frac{v}{h} \left( \frac{C_0 + C_1 + C_s}{C_0} \right) \quad (6)$$

Formulae (1) and (6) are thus the relevant ones for our purpose. When the  $dE/dt$  method was used (formula (1)) the potential variations across the resistance  $R$  were amplified and then applied to the oscillographic plates. For measurements of  $E$  (formula (6)) the output circuit of the electrometer triode was connected via the same amplifier to the oscillograph. To a more detailed description of the circuit arrangements we now turn

### 3—THE EXPERIMENTAL ARRANGEMENT

As mentioned above, an insulated exposed sphere was used as the antenna. This was constructed so as to correspond in almost every

way with that previously described by Wilson, except that the insulation was throughout of pyrex glass and not of quartz. In order to assist in the maintenance of adequate insulation, a stream of warm air was circulated up the annular space between the vertical lead-in wire and the earthed cylindrical screen. This was effected by means of an electric lamp situated at the bottom of the vertical supporting system.

The exposed sphere had a capacity  $C_0$  of  $16.7 \mu\text{f}$  and the capacity  $C_s$  was experimentally found to be  $133.3 \mu\text{f}$ . As the antenna system was situated on the top of the east wing of King's College, London, and not on a flat site, it was necessary to determine its equivalent height by experiment. This was done, using the influence of the earth's electric field as follows. First the sphere was shielded with an earthed screen and the sudden potential developed across  $C_1$ , when the screen was removed, measured by a calibrated string electrometer. Let this quantity be  $v_1$ . The corresponding potential  $v_2$  obtained by suddenly increasing the height of the antenna system by a known small value  $h'$ , under the influence of the same field, was then measured and found to be, say,  $v_2$ . Then the effective height  $h$  of the sphere in its normal position is given by

$$h = \frac{v_1}{v_2} \cdot h' \quad (7)$$

The value of  $h$  was found in this way to be 3.5 metres.

As an insulating link between the antenna system and the amplifier, an electrometer triode was used. In this way it was possible to maintain a higher aerial insulating resistance than had been used in the previous experiments. The inherent insulation of the antenna and the grid of the electrometer triode was, in fact, so high that, for reasons given below, it was necessary to reduce its value by the deliberate insertion of a high-resistance leak  $\rho$  across the condenser  $C_1$ . In this way, since  $\rho$  was much smaller than the insulation resistance, the time constant  $(C_1 + C_s) \rho$  could be controlled and maintained at a value sufficiently high to permit correct delineation of the field changes and yet not high enough to cause the accumulation of charge on the grid of the electrometer triode due to slow variations of the earth's field.

In fig. 3 are shown the essential connexions of the sphere system, electrometer triode, amplifier, and oscillograph, details of the time-base oscillator being omitted.

A damping resistance  $R$ , anti-inductively and anti-capacitatively wound, was inserted in the aerial lead in order to prevent any possibility of free oscillations in the system.

The electrometer valve used was a Plotron FP-54 made by the General Electric Company of America. The whole of the sphere lead-in system and the electrometer valve was electrostatically shielded in a metal case with a dehydrating agent to prevent surface leakage. Under these conditions the input resistance of the electrometer triode itself could be maintained at  $10^{16}$  ohms approximately. The correct working control grid voltage of  $-4$  volts was applied either by periodically charging the sphere system to this potential or, as was more generally found necessary because of the slow variations of the potential gradient and the effects of the air-earth current, by permanently applying this bias voltage through the high resistance leak  $\rho$ , which was usually made of the order of 10 megohms.

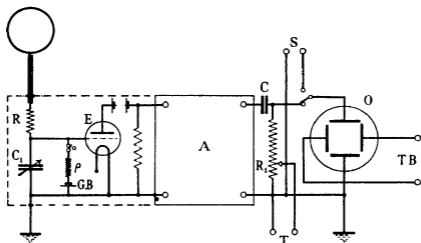


FIG 3—Showing diagrammatically the aerial system, amplifier, and recording cathode ray oscillograph. E, electrometer valve, A, resistance capacity coupled valve amplifier, O, cathode ray oscillograph, T, to thyatron camera shutter relay; S, to time calibrating oscillator, T B, to linear time-base.

A two-way switch, not shown in the diagram, provided facilities for joining the amplifier input terminals alternately to the plate circuit of the electrometer valve for E measurements, or across the resistance R, for measurements of  $dE/dt$ , in which case a further damping resistance was also inserted in the leads joining the resistance R to the amplifier.

Throughout the earlier observations of the present series a resistance coupled amplifier was used. The inherent difficulties in connexion with stability were, however, found to be troublesome and led us ultimately to change to an amplifier employing resistance-capacity coupling. A discussion of the characteristics and limitations of this amplifier is given below.

It was arranged that two or three stages of amplification could be selected as desired, but that in each case the same output valve should be in operation. This valve was adjusted to give a linear voltage swing of approximately 120 volts which corresponded to a maximum vertical deflexion of the cathode-ray trace of 2 cm. With the tube in its normal working conditions, deflexions greater than this value were considered as distorted, and the aerial adjustments and the amplifier were adjusted so that the output voltage excursions did not exceed this limit. The mean grid potentials of the first two valves of the amplifier were adjusted so that operating conditions were represented by linear portions of their characteristics.

The resistance-capacity amplifier was built on conventional lines and calls for little comment except that rather large coupling condensers (2 mfd. oil-filled type) were used in order that the uniform response should be maintained to as low a frequency range as possible. With two stages of amplification the magnification was 200, while with three stages this was increased to 4000.

The application of the amplifier output voltage to the deflecting plates of the cathode-ray oscillograph was effected by way of a 2 mfd. condenser (C, fig. 3). Across the same output terminals there was also inserted a 1 megohm resistance ( $R_1$ , fig. 3). A fraction of the transient voltage across this resistance was used to trip a thyatron relay which was used to operate the photographic recording camera.

### *Cathode-Ray Oscillograph Photography*

For recording, external photography of the fluorescent trace of a Cossor Cathode-ray Oscillograph was employed. In order to get high photographic sensitivity a camera lens of aperture  $f/0.99$  was used while the running voltage of the tube was increased to two or three thousand volts. The phenomenon of "origin distortion" in the cathode-ray oscillograph was eliminated by the usual method of deflecting the "electrostatic zero" to the side of the fluorescent screen and then restoring the electron beam to the centre by a suitable magnetic field.

Owing to the random incidence of the transients to be observed, certain difficulties arise in photography. It is, for example, impossible to leave a stationary film exposed for more than a very short time owing to the cumulative fogging produced by the background fluorescence on the cathode-ray screen. At first we tried the obvious method of making the field changes cause a horizontal deflexion of the spot, the film being rotated as a drum revolving about a horizontal axis. A resolution of

pulses with a quasi-period of about 0.01 msec was obtained by this method but, on the whole, we found it unsatisfactory, since only an exposure of about 30 seconds was possible owing to the fogging mentioned above. The alternative method of using a fast moving continuous film was out of the question on the grounds of expense. Except when discharges are very frequent indeed, it is obviously extremely wasteful in film. The second method of recording adopted proved much more satisfactory.\* It consisted in using the effect of afterglow, which is very marked in a certain type of Cossor cathode-ray oscillograph, and photographing the wave-form of the transient not *during* its occurrence but a fraction of a second *later*. In order to delineate the wave-form, the received impulse was made to cause a vertical deflexion of the cathode-ray beam while a suitable linear and unidirectional time base was provided by connecting the neon-tube relaxation oscillator to the horizontally-deflecting plates. The duration of the time stroke was varied from 100 to  $\frac{1}{10}$  of a millisecond, the former limit being used to provide conditions suitable for studying the grouping of atmospheric, and the latter limit to provide fine-structure delineation. Now the transient wave-form is portrayed on the screen long enough to permit photography by a camera subsequently opened automatically by the electrical effects of the transient itself. To provide for this, it was arranged that a small fraction of the transient amplifier output voltage should "trip" a thyratron which actuated a relay and so open the camera for  $\frac{1}{10}$  of a second. The photographic track on the special Cossor oscillograph used was of a reddish colour and, in photographing it, hypersensitive pan-chromatic film was found most suitable.

#### 4—LIMITATIONS OF THE APPARATUS

In observations such as we have attempted there are always limitations to the amplitudes and frequency detail of the wave-forms which can be recorded. In our case the inferior limit of amplitude was determined by the electrical noise level of the site, and we were unable to photograph during the day-time wave-forms the peak values of which were less than 0.1 v./m. During the night, when fewer local electrical machines were in operation, this figure could be slightly reduced.

The limitation of frequency detail was determined almost wholly by the limitations of the amplifier and of the photographic resolution. It will readily be seen that it is desirable for the amplifier to magnify, without

\* Chapman, 'Nature,' vol. 131, p. 620 (1933), and 'J. Phys.,' vol. 84, p. 25 P. (1935).

amplitude or phase distortion, frequencies from zero up to the highest possible value. In order to test the apparatus as to frequency response, tests were made, using a suddenly-applied direct and constant, potential across the input terminals. It will be seen that, roughly speaking, the high-frequency response of the system determines how quickly the output voltage responds to such a sudden application of input voltage, while the low frequency response of the amplifier determines how long such a maximum output voltage is maintained. In the test mentioned it was found that the cathode-ray spot reached its maximum deflexion in a time which was less than  $10^{-5}$  seconds so that we were certain that frequencies up to  $10^5$  c/s could be regarded as fairly accurately delineated.

For the amplification of low frequencies down to zero it will be seen that in the original resistance-coupled amplifier this is always faithfully accomplished, but that in a resistance-capacity amplifier this is not necessarily so. By the use of large coupling condensers and high grid leaks, however, it was arranged that the time constant of the grid circuit was 2 seconds, which was sufficient for our purpose, since we were interested in events the maximum duration of which rarely exceeded 0.1 second. This point was verified in the test mentioned above, since it was noted that the initial amplitude of the spot decayed with a time constant of the order of 2 seconds. This time constant was greater than that of the electrometer, which had to be reduced for reasons already given, and so exercised no deciding influence on the observations.

Using the original Western Electric oscillograph, Watt and Appleton reported that it was possible to follow the excursion of the cathode ray spot visually when its speed did not exceed  $10^4$  cm per second. With the Cossor Oscillograph and the photographic registration used in the present series of experiments, we estimate that the photographic trace can be recognized when the spot moves as fast as  $10^6$  cm per second. There is thus a gain of a hundredfold in this respect.

## 5—THE EXPERIMENTAL RESULTS AND THEIR DISCUSSION

In describing the experimental results it is convenient to trace the influence of increasing the distance from the discharge channel. We therefore begin with the field changes due to near flashes and continue with a description of the effects of more distant ones.

If observations are made sufficiently near the discharge channel the electric field is proportional to the electric moment of the cloud, so that a photographic record of what may be called the "fine-structure" of a net;

change of field may be expected to give us information concerning the nature of the discharge in the flash

*a—The Grouping of Discharge Components*

In the older measurements of the net change of field made with the capillary electrometer the effect of the change was shown by a discontinuity in the trace on the photographic record. In observations made at King's College since 1925 with the string electrometer it has been found that the majority of such net changes really take place in steps. This has been amply confirmed by the cathode-ray oscillograph records. In an analysis of some thousands of records of net changes obtained using a string electrometer, Dr J D Henderson and one of the authors have found that the most frequent type of discharge is one which takes place in a single "step" but that the next most frequent number of "steps" is either two or three, double and triple discharges being about equally frequent. Such "steps" obviously indicate that the thundercloud moment is frequently destroyed in a series of partial discharges. From the string electrometer records, which had a not very open time scale, the intervals between the successive partial discharges were found to range from 140 to 250 msec. Now if atmospherics originate in thundercloud discharges we might expect them to have the same tendency to occur in groups. In order to test this point we have therefore examined a record of the incidence of atmospherics with time, the time scale being comparable with that used in the string electrometer records of net changes. This record was taken using the cathode-ray direction finder of Watt and Herd, and, because the arrival azimuth of each component discharge is shown on it, is especially suitable for indicating clearly the components of a single group. Now it is very remarkable that this analysis of the radiation fields of atmospherics shows exactly the same features which are found in the analysis of net changes. The most frequent type of atmospheric is a single component but, after this, the numbers of components, 2 or 3, 4, 5, etc., occur with decreasing frequency. Moreover, the intervals between the components in the atmospheric are of exactly the same order of magnitude (varying from 60 to 300 msec) as that observed in the case of net changes.

With a still more open time scale such as we have used in the present series of experiments we have found further evidence of the tendency of discharges to occur in steps, and in this case, since a time base of 100 msec. was used, attention has been centred on a finer scale of grouping than that mentioned above, and intervals between successive components of the

order of 3 to 40 msec have been observed. In this case the high-speed records of the wave-forms show that the component discharges have very similar electrical characteristics.

Although it would appear that the range of grouping interval most frequently brought to the notice of the observer in any particular case depends on the nature of the responding electrical system and on the time scale employed there can be little doubt that these multiple electrical field changes are the result of intermittent lightning discharges such as were first shown to occur in Walter's experiments with a moving camera. Walter found intervals between component flashes of the order of 30 to 140 msec. Recent experiments of allied character carried out by Schonland, Malan, and Collens,\* using a Boys camera, show intervals between flashes ranging from 2 to 500 msec, with most frequent values of the order of 10 to 50 msec. A physical interpretation of the nature and origin of intermittent discharges has already been given by Simpson.

#### *b—The Evolution of an Atmospheric*

Observations on still quicker time-bases have been made to investigate the fine-structure of a single discharge. These show that the net change of field usually consists of either two or three parts. In the first part there is a smooth alteration of the field in the direction of the final net change. This change usually occupies from 1.0 to 10.0 msec. It is then followed by a very rapid change of field on which are superimposed ripples. This then may or may not be succeeded by a slower change (which may or may not be rippled) by which the final value of the field is reached. A typical net change of this type, observed at a distance of 3 km, is illustrated in fig. 4. As has been mentioned, the part (c) is very frequently either non-existent or not very marked. The magnitude of the change of field in (a) is generally about equal to that in (b). The transition from (a) to (b) is very abrupt.

Records obtained using much greater sensitivity (fig. 5) show that, although the (a) portion appears smooth on the gross structure, it really contains a fine-structure of a special type to which reference is made in § 6 and § 7.

It is from such a temporal variation of thunderstorm moment that the atmospheric is produced. Now as we proceed from the discharge channel we should expect the radiation field to become relatively more prominent than the electrostatic field, since the one varies inversely as

\* 'Proc. Roy. Soc.,' A, vol. 152, p. 595 (1935)

the first power of the distance and the other varies as the inverse cube. This is found to be so and, in order to demonstrate the variation of wave-form with the distance, Table I has been drawn up which is based on all the observations made. In the first column is given the distance from the discharge channel, which was found either by measurement of the interval

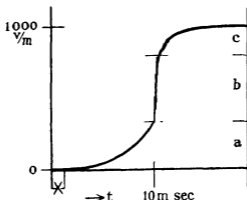


FIG 4—The typical variation of thunder cloud moment during a single lightning flash, as determined by the earth's electric field variation at a short distance from the discharge

between the lightning and the thunder or, in the case of the more distant storms, from the information given concerning storm centres in the daily weather reports of the Meteorological Office. In the second column is given  $E_s$ , the electrostatic field change, while in the third column is given the estimated value of the radiation field  $E_r$  from typical records. In

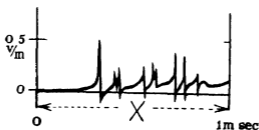



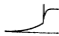
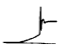
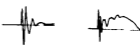
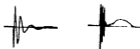
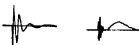


FIG 5—Illustrating fine structure of the initial part of "a" portion of the discharge (cf fig 4) obtained by using higher sensitivity

column four is drawn a picture of the typical wave-form at that distance. It is important to note that, for convenience of comparison, these pictures are drawn of about the same size, though, of course, the actual magnitudes of the field changes represented decrease with increasing distance from the source as indicated in the second and third columns.

TABLE I

Distance in km	$E_s$ in $v/m$ .	$E_r$ in $v/m$ .	Typical wave-form
3-5	1300	Not observed	
10	700	Not observed	
20-30	45	Not observed	
45-50	12	5	
60	3	3	
100	0.6	1.7	
150-200	0.1	Maximum peak value 0.8	
300-400	Not observed	Maximum peak value 0.3	

It will be seen that the high-frequency atmospheric wave-form has its origin in the rapid change of moment designated by (b) in fig. 4

*c—The Sequence of Wave-form Changes*

At a distance of about 200 km from the discharge channel the wave-form of an atmospheric disturbance is determined practically entirely by the radiation field of the discharge. During the distance range from 60 km to 200 km, however, certain marked changes of wave-form are noticed. These may be summarized as follows

- (a) The total duration of the atmospheric appears to increase
- (b) The wave-form becomes more regular and the higher frequency ripples less prominent (For example, at a distance of 40-70 km high-frequency ripples of quasi-period 0.01 msec occur on the steep front but these are not observable at greater distances)
- (c) The number of half-cycles observable in the atmospheric seems to increase

In the more distant records showing a smooth wave-form it is noted that the quasi-half-cycle increases throughout the atmospheric. At a distance of about 200 km a new phenomenon is often noticed. Many of the radiation wave-forms develop a slow tail of about two rounded half-cycles. Examples of how this develops are shown in fig. 6, Plates 1-3. It will be noticed that this type of wave-form is exactly of the type drawn by Appleton, Watt, and Herd in their visual series of observations.

*d—The Observations on Rate of Change of Field*

It should be mentioned at the outset that the records obtained by the  $dE/dt$  method would necessarily be expected to show up the high-frequency detail in the field changes. As an example of this we may quote the observations made near a flash when the E records show mainly the electrostatic field change, while the  $dE/dt$  records show up the quasi-oscillations which occur during the (b) and (c) portions of the discharge (see fig. 4). (The rate of change of field during the (a) portion is negligible compared with that developed during portions (b) and (c)). The  $dE/dt$  measurements show that during the parts (b) and (c) quasi-oscillations of period 0.01 to 0.25 msec. occur. The duration of a train of such quasi-oscillations may be as long as 1 msec.

As is to be expected with a net change of field, the  $dE/dt$  records at the point in question show asymmetrical excursions of the cathode ray

spot from the base line In records of this type it is noted that the quasi-period of the oscillations increases during the train, most probably indicating that the resistance of the discharge channel is increasing rapidly

At medium distances of about 60 km the  $dE/dt$  wave-forms become more symmetrical, and the ripples are less marked Quasi-periods of 0.1 to 0.2 msec become predominant, but values down to 0.05 msec. may be recognized

At distances of 200 km the  $dE/dt$  records show smooth wave-forms such as might be deduced from a graphical differentiation of the E records.

### 6—SOME SPECIMEN RECORDS

In fig. 6, Plates 1, 2, are shown a number of specimen records labelled 6 (i) to 6 (xxiii)

Record 6 (i) was taken on the 19 June, 1933, at a distance of approximately 10 km from the discharge, and shows a field change of a 1000 v./m, this taking place in two parts corresponding to the "a" and "b" portions in fig. 4 The time base was of duration 10 msec reading from left to right.

Record 6 (ii) is of similar character, but differs from record 6 (i) in showing a longer duration of the "a" portion of the discharge

Records 6 (iii) and 6 (iv) illustrate the fine structure of the initial part of the "a" change of moment and were obtained on the 25 June, 1935 It will be seen that superimposed on the alteration of field strength there are characteristic perturbations, each consisting of a first impulse in the direction of the change of moment immediately followed by an impulse of less intensity in the opposite direction Both records were obtained at about the same distance as those shown in figs. 6 (i) and 6 (ii), but the sensitivity of the apparatus was increased a thousand times

Record 6 (v) illustrates a typical result obtained by the  $dE/dt$  method on the 28 June, 1932 The distance of the discharge was not known It will be seen, however, that the excursions of the cathode ray spot are asymmetric about the zero line, indicating that there was a net positive change of field in this particular record. The record is of particular interest in illustrating the marked advantages of the  $dE/dt$  method for showing the fine structure of net change. Pulsations with quasi-periods as short as 10 micro-sec. are to be noted from the record

Records 6 (vi) to 6 (x) were all obtained on a time base of 10 msec. duration at a distance of from 40 to 60 km from the discharges of a storm on the 20 July, 1933 These records illustrate the evolution of the atmospheric wave-form from the discharge It will be seen that at

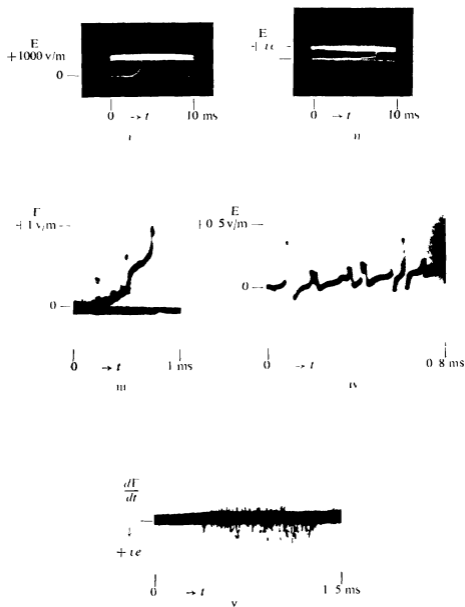
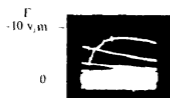
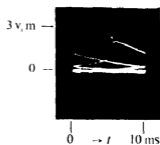


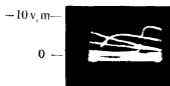
FIG. 6



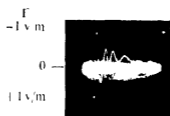
VI



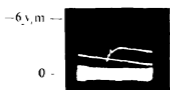
VII



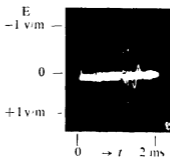
VIII



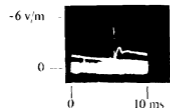
IX



X



XI



XII

XIII



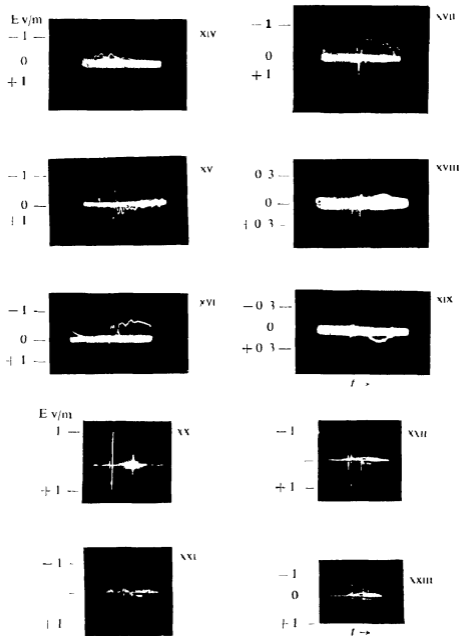


FIG 6—xiv to xix, time-base duration 5 millisecc, xx to xxiii, time-base duration 0.1 sec



this distance the initial radiation field is of the same order of magnitude as the net change

Records 6 (xi) and 6 (xii) taken on the 27 June, 1933, illustrate the high-frequency portion of the atmospheric as finally developed at a distance where the net change of field is too small to be recorded.

Records 6 (xiii) to 6 (xix) illustrate the atmospheric wave forms developed with increasing distance between 200 km and 400 km. In all cases the high frequency group and slower disturbance are to be noted. In the first three records of this group the high-frequency train and the low-frequency disturbance start almost simultaneously, but in the last records of the most distant disturbances recorded it will be noted that the short high-frequency train has run ahead so as to be distinct from the slow disturbance.

Owing to the electrical noise level at the site of the recording apparatus it has been impossible to record satisfactorily atmospherics of weaker intensity.

Records 6 (xx) to 6 (xxiii) show the tendency of atmospherics to occur in groups corresponding to a time sequence of partial discharges of varying intensity. The wave form of each component is unresolved, because the time stroke is relatively slow (duration 0.1 second). Quite often a small discharge is found to precede the most intense discharge, which usually occurs at the beginning of the group, by a brief time interval of the order of 1 msec. Such pre-discharges have already been noticed by Norinder\*.

#### 7—FURTHER DISCUSSION OF THE EXPERIMENTAL RESULTS

As has been mentioned above, the records of the fine-structure of the changes of field near a lightning flash give us information concerning the nature of the discharge so that from our observations it is possible to give an answer to the question so often debated: Is a lightning discharge oscillatory or non-oscillatory? The records of the electrostatic field changes show that the discharge as a whole is aperiodic, but that during both the periods of slow and rapid changes of moment there are superimposed minor pulsations, those occurring during the period of rapid change being the greater. A discharge of this type corresponds very closely with the electrical mechanism suggested by Simpson† who, in 1929, said:

“There can be little doubt that the resistance of a fully developed

\* ‘J. Franklin Inst.’ vol. 220, p. 69 (1935).

† ‘J. Inst. Elect. Eng.’ vol. 67, p. 1275 (1929).

lightning channel when most highly ionized may well be less than the critical value, and the channel therefore able to oscillate. The oscillations will be superimposed upon the main current but will not reverse its direction of flow. The effect is somewhat similar to that of a 'singing arc' in which the conducting path through the air between the electrodes is maintained by a unidirectional current, while the oscillations which give rise to the musical note are superimposed upon the current according to the frequency of the circuit."

The grouping of net-change and of atmospheric components obviously indicates the existence of partial discharges, and there can be little doubt that such components are to be associated with the intermittent lightning flashes as photographed by Walter and others which shows exactly the same order of temporal spacing. It may further be added that in a group of partial discharges there is a definite tendency for the wave-forms of the resulting atmospherics in a particular group to be very similar. This indicates that the component discharges are very similar in electrical nature, differing only in magnitude.

A further word is necessary in connexion with the comparison of the net-change records and the lightning discharge photographs taken with a rotating camera. Such photographs, especially those of Halliday, and Schonland, Malan, and Collens,\* show that the luminosity is intensely bright for a very short time but that, afterwards, the luminosity decays relatively slowly. The luminosity has generally ceased before the next component flash, but the fact that the next component follows the same track indicates persistence of ionization. Dr Halliday has very kindly measured up a few of his plates and estimates that the intense luminosity lasts for almost 0.02 to 0.04 msec but that the luminosity afterwards takes a millisecond or so to decay. It seems reasonable to suppose that the luminosity is intense when the current in the discharge channel is large. We therefore picture the intense luminosity as taking place during the part (b) of the typical net change in fig. 4. Support for this interpretation is to be found in the actual time intervals measured, for our net change records show that the rapid change (b) usually lasts from 0.05 to 0.1 msec.

Our observations show that the rapid change of thundercloud moment (b) portion in fig. 4) is preceded by a slower change in the same direction (a) portion in fig. 4). Now it has been shown by Walter† and others, from moving camera observations, that a single lightning flash to earth is

\* Schonland, Malan, and Collens, 'Proc. Roy. Soc. A', vol. 152, p. 595 (1935).

† Walter, 'Ann. Physik', vol. 10, p. 393 (1903), 'Jb. hamburg. wiss. Anst.', vol. 20, (1903), 'Ann. Physik', vol. 52, p. 421 (1935).

made up of a downward leader stroke followed by an upward and faster return stroke, the duration of these processes being of the order of 10 and 0.05 msec respectively. (The more recent experiments by Schonland, Malan, and Collens give, correspondingly, 10 and 0.04 msec) We are therefore able to identify the leader stroke causing the (a) portion of the field change and thus as causing quite a considerable change of thundercloud moment. This change takes place relatively slowly although, as described above, we have found the existence of characteristic small perturbations on the main structure spaced about 0.1 msec apart (figs 5 and 6). We believe that these perturbations on the field changes result from the branching and discontinuous nature of the first leader stroke as shown in the photographs taken by Schonland, Malan, and Collens.

The most rapid change of thundercloud moment occurs during the return stroke in which, according to our observations, about one-half of the total moment is destroyed in about 0.04 to 0.08 msec. Now Wilson's observations have shown that the order of magnitude of the charge dissipated in a typical lightning flash is of the order of 20 coulombs. We thus see that current of the order of 125,000 to 250,000 amperes must occur in a flash consisting of a single component, or half these values in a component of a two-component flash and so on.

It is of interest also to consider the correspondence between our results and those obtained by Norinder,\* who has made a very exhaustive series of measurements of  $dE/dt$  at distances within 16 km from discharge channels in Sweden. Norinder has observed values of the order of  $2 \times 10^7$  v./m./sec. at distances of up to 10 km from lightning flashes. From our observations it is clear that the most rapid change of field occurs during the return stroke ((b) portion) when, for similar distances, we find that a field of the order of 700 v./m. is destroyed in 0.05 msec, indicating a value of  $dE/dt$  equal to  $1.4 \times 10^7$  v./m./sec., which is of the same order of magnitude as that observed by Norinder.

In the observations under review it will be seen that the evolution of an atmospheric from a lightning flash has been traced to distances at which the wave-form is of the purely radiation type. In observations made on the more intense wave-forms of distant atmospherics (we have been precluded from examining the wave-forms of weaker atmospherics because of the electrical noise level at the site) it has been found that they are of exactly the same type as we have observed originating from British thunderstorms. The most frequent type of atmospheric is a brief train of about 8 half-cycles of quasi-period 0.1 to 0.15 msec. This wave-form is noted to be steep-fronted, and to show a sequence of quasi-half-

\* J. Franklin Inst., vol. 218, p. 738 (1934).

cycles increasing in duration. This disturbance is, in a minority of cases, followed by a relatively slow tail of wave-form similar to those described and analysed by Appleton, Watt, and Herd. It will thus now be seen that the earlier series of visual observations was incomplete in that attention was concentrated on the relatively longer and smoother disturbances the higher frequency forerunner of the longer disturbances having escaped attention. It is very probable that one of the reasons for this is that with the earlier form of oscillograph used these higher frequency components were not clearly visible to the naked eye.

As has been mentioned, the slow tail which accompanies some of the atmospherics begins to be appreciable at a distance of about 200 to 300 km, and that this is so suggests that it becomes of importance when ionospheric influences begin to be effective. The examples of wave-forms given in § 6 indicate how the high-frequency group and the slow tail begin almost simultaneously at near distances, but that, at greater distances, the high-frequency group arrives clearly ahead of the slow tail. This can only mean that the group velocity of the high-frequency train is greater than that of the slow tail.

Two problems, therefore, are involved in connexion with this phenomenon. What is the origin of the slow tail and why does the high-frequency group move forward relatively to it as the distance of propagation is increased? These problems are being the subject of further study so that the discussion of them here will be limited. The slow tail, as was suggested by Appleton, Watt, and Herd, appears necessarily to be the radiation field resulting from some aperiodic discharge. It might, at first, be thought that the high-frequency group and the slower disturbance are both the result of the dispersive transmission of a rapid pulse such as must originate from the (b) portion of the discharge. Now we have found that there is an empirical relation which expresses approximately the variation of the quasi-period with time for the components of the high-frequency group. It is, for example, found that the time of reception of any particular half-period in the group, measured with respect to the initial impulse, is approximately proportional to the square of the quasi-half-period. The slower disturbance subsequent to the high-frequency group is a unit not conforming to this relation, so that we can say that, unless there is some factor operative corresponding to anomalous dispersion for the missing frequencies, the high-frequency group and the slower disturbance do not originate from exactly the same portion of the discharge. Our records suggest that the slow disturbance is connected in some way with the slow (c) portion of the lightning discharge. Whether this is the result of the persistence of the discharge in the main channel after the intense stroke

(such as is indicated by the afterglow on the moving-camera photographs) or whether it is concerned with adjustments of current and space-charge between the top of the thundercloud and the ionosphere during the lightning flash is not yet clear to us

Concerning the difference between the group velocities of the high-frequency train and the slow tail it is possible to be more precise. We might suspect the influence of (a) the ground, (b) the atmosphere near ground level, and (c) the ionosphere. Calculation shows, assuming the known electrical constants of the ground, that there would be no appreciable differences in the group velocities of Zenneck waves, travelling along the ground, and of frequencies 10,000 c/sec and 500 c/sec. It may also be shown that the conductivity of the atmosphere near ground level is too small to affect the group velocity of the waves and that, moreover, the small effect present is such as to cause low frequencies to travel with a larger group velocity than higher frequencies, which is not found to be so in practice. We are therefore left with the conclusion that ionospheric influences are responsible for the gain in transit of the high-frequency group over the slow tail. It is well known that a medium containing free ions or electrons would produce an effect in this sense. Since the wavelengths concerned are long, only a relatively small ionic or electronic concentration is required, and since the time between two collisions with molecules is less for ions than for electrons at a given height, it is probable that ions are mainly effective in causing the group velocity to increase with increase of frequency. Although the two phenomena are not strictly comparable, it may be mentioned that Stoyko and Jouaust\* state that from their measurements of the apparent velocity of wireless time signals over long distances they conclude that short waves of 15 to 40 metres travel with a group velocity which is 10% higher than that of waves of from 15,000 to 20,000 metres. There seems little doubt that in their experiments any difference of group velocity must be ascribed to ionospheric influences.

The work was carried out as part of the programme of the Radio Research Board of the Department of Scientific and Industrial Research.

#### SUMMARY

A series of observations on rapid changes of the earth's electric field associated with lightning flashes has been made using a Wilson sphere as the exposed conductor and a cathode-ray oscillograph with photo-

\* 'C R Acad Sci Paris,' vol 196, p. 1291 (1933)

graphic registration The measurements have included observations on the temporal changes of both the electric field and the rate of change of the electric field

As a result of observations made on near discharges, it has been found that the discharge of the thundercloud moment is, in the main, an aperiodic one but that during the period of maximum current density subsidiary oscillations or pulsations are superposed on the main discharge.

The majority of net changes of field are found to take place in a series of steps The numbers of steps 1, 2, or 3, 4, 5, etc., occur with decreasing relative frequency Exactly the same relative frequencies of grouping are found in the incidence of atmospherics of distant origin Such partial discharges are obviously to be correlated with the intermittent flashes photographed by Walter and others

The decay of thundercloud moment during a lightning flash occurs in two parts, (a) a relatively slow reduction of about 30 to 50% of the whole in about 10 msec., followed by (b) a very rapid reduction in 0.04 to 0.08 msec. These correspond respectively to the leader-stroke and return-stroke in the lightning discharge discovered by Walter Evidence of a "fine structure" radiation field on the (a) portion has been observed

A new estimate is made of the maximum current flowing in a lightning discharge channel

From observations made at increasing distances from the discharge the evolution of the atmospheric wave-form has been studied At a distance of about 40-60 km the radiation field of the atmospheric is approximately equal to the electrostatic field change of the main discharge

The most frequently observed wave-form of the atmospheric ultimately developed is a brief steep-fronted train of about 6 to 10 half-cycles of quasi-period 0.1 to 0.15 msec. Many of such brief trains are followed by a slower disturbance of exactly the same type as those described by Appleton, Watt, and Herd in their visual observations of atmospheric wave-forms obtained, using a cathode-ray oscillograph of less satisfactory response Such a slow disturbance may possibly be due to an upward discharge from the top of the thundercloud to the ionosphere The quasi-oscillatory disturbance is found to move ahead of the slower disturbance during propagation, indicating a difference of group velocities brought about by ionospheric influences.

---

## The Effect of Space-Charge on the Secondary Current in a Triode

By D M MYERS, Engineering Laboratory, University of Oxford,  
D R HARTREE, F R S, and A. PORTER, University of Manchester

(Received 19 August, 1936)

### 1.—INTRODUCTION

When electrons strike a surface with sufficient velocity, secondary electrons may be emitted by it, some or all of which may be collected by a suitable electrode having a higher potential than the emitting surface ("Secondary electrons" are here taken to mean all electrons which leave the surface, whether reflected, rediffused, or actually emitted by the surface)

In the work to be described, a triode is considered, in which the anode receives electrons from the cathode, and emits secondary electrons which are collected by the grid, which is maintained at a higher positive potential than the anode. In the experimental work, a triode with an axially symmetrical configuration of electrodes was used, and such a triode will be considered in the theoretical work.

For a given energy of impact, the rate of emission of secondary electrons is proportional to the rate of arrival of primaries, the ratio is a function of the energy of impact of the primaries and, therefore, of the potential of the anode. We will, however, suppose that the secondary current which the anode could emit in the absence of space charge is unlimited, so that the actual magnitude of the secondary current is determined by the space-charge, and not by the emitting properties of the anode. If given potentials are applied to anode and grid, the secondary current and the space-charge of the secondary electrons will then rise until the field due to the total space-charge is sufficient to prevent a greater current of electrons from passing to the grid. This condition is described by the term "space-charge limitation" of secondary current.

If the grid is a complete cylindrical surface, then, in the limiting case of zero space-charge, all the secondary electrons emitted by the anode will reach the grid, except for the few which are emitted at very oblique angles. Any appreciable reduction in the number reaching the grid must then be due to space-charge limitation.

In the following sections, a theoretical determination is made of the radial variation of potential between grid and anode, and a relation is

found between the anode and grid potentials, and the primary and secondary anode currents, in the condition of space-charge limitation

## 2—GENERAL THEORY

Secondary electrons may be emitted with initial energies varying between zero and the energy of impact of the primary electrons, but only a small proportion has initial energies greater than a certain comparatively small value. The distribution of initial energies has been examined both by means of a "magnetic spectrum", and by the application of a retarding field near the emitting surface. Results obtained by several observers\* indicate that most of the secondary electrons have initial energies less than 4 or 5 electron volts.

If any continuous distribution of energies is assumed, the theoretical examination of the problem becomes very difficult. A reasonable approximation should be obtained, however, if all the secondary electrons are assumed to have the same initial energy.

In fig 1, the grid and anode are represented by G and A respectively, and have radii  $r_g$  and  $r_a$ . The cathode is taken as being at zero potential, and the grid and anode have applied potentials  $V_g$  and  $V_a$ . At a point P, whose distance from the cathode is  $r$ , and at which the potential is  $V$ , the volume densities of the primary and secondary electrons are  $\rho_p$  and  $\rho_s$ , and the respective velocities are  $v_p$  and  $v_s$ . The primary and secondary currents are  $i_p$  and  $i_s$  per unit length of anode.

Then if  $e$  and  $m$  represent the charge and mass of an electron, energy considerations show that

$$\frac{1}{2}mv_p^2 = eV \quad \text{and} \quad \frac{1}{2}mv_s^2 = e(V - V_a + V_s), \quad (1)$$

where  $eV$ , is the energy with which the secondaries are emitted. The equations of continuity are

$$i_p = 2\pi v_p r \rho_p \quad \text{and} \quad i_s = 2\pi v_s r \rho_s,$$

\* Barber, 'Phys. Rev.', vol 17, p 322 (1921), Sharman, 'Proc Camb phil Soc', vol. 23, pp 523, 922 (1927), Wells, 'Phil Mag', vol 5, p 367 (1928), Solter, 'Phys Rev', vol 36, p 1212 (1930), and others

and the potential  $V$  is related to the volume density of the primary and secondary electrons by Poisson's equation

$$\frac{1}{r} \frac{\partial}{\partial r} \left( r \frac{\partial V}{\partial r} \right) = 4\pi (\rho_p + \rho_s)$$

Eliminating the volume densities  $\rho$  and the velocities  $v$ , we obtain an equation for the potential  $V$  in the space between anode and grid, for given values of  $V_a$ ,  $i_p$ ,  $i_s$ , namely,

$$r \frac{d^2 V}{dr^2} + \frac{dV}{dr} = (2m/e)^{1/2} [i_p/V + i_s(V - V_a + V_s)^{1/2}] \quad (2)$$

The value,  $V_g$ , of  $V$  at  $r = r_g$  gives the grid voltage corresponding to given values of  $V_a$ ,  $i_p$ ,  $i_s$ .

Since equation (2) is second-order, two conditions are required to specify a definite solution. One condition is

$$V = V_a \text{ at } r = r_a, \quad (3)$$

the other can be obtained by the following considerations.

Under the conditions of space-charge limitation of secondary emission, the secondary current  $i_s$  for a given primary current and anode voltage is not "given", but depends on the potential distribution due to the space-charge. But for the solution of (2) it is most convenient to regard  $i_s$  as "given", and to impose on  $V$  a condition expressing that this  $i_s$  should be the secondary current determined by space-charge limitation, with the given  $i_p$  and  $V_a$ . We will see that this condition is

$$\frac{dV}{dr} = 0 \text{ at the radius where } V = V_a - V_s \quad (4)$$

If  $V$  nowhere falls as low as  $V_a - V_s$ , every electron leaving the anode can reach the grid, so that there is no space-charge limitation of the secondary current, hence  $V$  must fall at least to  $V_a - V_s$ . But if  $V$  falls below  $V_a - V_s$ , the secondary electrons are stopped at the nearest point to the anode at which  $V = V_a - V_s$  and return to the anode, so that they produce no secondary current (though they may contribute to the space charge). Hence the condition that there should be a secondary current limited by space-charge is that  $V$  should fall to  $V_a - V_s$  and no further, that is to say that  $V_a - V_s$  should be the minimum of  $V$ , and this is expressed by (4). We will write  $r_0$  for the radius at which this minimum of  $V$  occurs. Thus the general form of the solution of (2) is as shown in fig. 2

The process of solution of (2) subject to conditions (3) and (4) is considered in §§ 3, 4, 7. The relation between  $V$  and  $r$ , for given values of  $i_p$ ,  $i_s$ ,  $V_a$ ,  $V_s$ , and  $r_a$  is not, however, a convenient form of the result for direct comparison with experiment, since for a given triode only the value  $V = V_g$  at  $r = r_g$  is accessible to observation. But by evaluating a set of solutions with different values of  $i_p$ ,  $i_s$ ,  $V_a$ ,  $V_s$ , and rearranging the information expressed by these solutions, we can find the relation between  $i_s$  and  $V_g$  for given values of  $r_g$ ,  $V_a$ ,  $V_s$ , and  $i_p$ , and in this form the results are convenient for comparison with experiment.

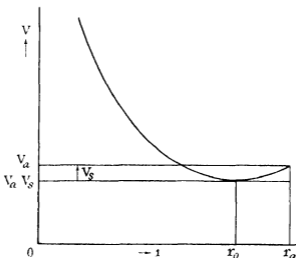


FIG. 2

### 3—REDUCTION AND TRANSFORMATION OF THE EQUATION

It is convenient to reduce the equation to a form involving only non-dimensional quantities, by writing it in terms of  $r/r_0$  and  $V/(V_a - V_s)$ . Let

$$r/r_0 = e^{-w} \quad (5)$$

(so that  $w$  increases from anode to grid),

$$\left. \begin{aligned} V/(V_a - V_s) &= \eta, \\ (2m/e)^{1/2} (V_a - V_s)^{-3/2} r_0 i_p &= \alpha, \end{aligned} \right\} \quad (6)$$

and

$$i_s/i_p = \beta. \quad (7)$$

Then equation (3) becomes

$$\frac{d^2 \eta}{dw^2} = \alpha e^{-w} [\eta^{-1} + \beta (\eta - 1)^{-1}] \quad (8)$$

with conditions

$$\eta = 1, \quad d\eta/dw = 0 \text{ at } w = 0 \quad (9)$$

No formal solution of this equation is known, but, except for the presence of the infinity in  $d^2\eta/dw^2$  at  $w = 0$ , it is suitable for solution numerically, or mechanically by means of the differential analyser. This will be considered in the next section.

In order to get away from the singularity at  $w = 0$ , before starting a numerical or mechanical integration of (8), it is necessary to use either an approximate analytical solution (for example, in the form of a series) in the neighbourhood of the singularity, or to transform the equation to a more manageable form.

The leading term in  $\eta$  for small  $w$  is found by substituting

$$\eta = 1 + cw^\gamma + o(w^\gamma)$$

and equating the leading terms on the two sides of the equation, this gives  $\gamma = \frac{1}{3}$ ,  $c = (9\alpha\beta/4)^{2/3}$ . The next term is found to be of order  $w^2$ , so that

$$\eta = 1 + (9\alpha\beta/4)^{2/3} w^{4/3} + O(w^2) \quad (10)$$

A series involving integer powers of  $w$  and of  $w^{2/3}$  can be found, but soon becomes elaborate, and it seems preferable to find, if possible, a transformation of equation (8) which will be suitable for numerical work near the origin. The behaviour of  $\eta$  near  $w = 0$ , expressed by (10), suggests trying  $z = (\eta - 1)^k$  as an auxiliary variable, with the expectation that  $k = \frac{3}{4}$  or  $k = \frac{3}{2}$  will give a manageable equation. Trial shows that the result of taking  $k = \frac{3}{2}$  is the most convenient, and gives

$$\frac{d^2z}{dw^2} = \frac{1}{3z} \left( \frac{dz}{dw} \right)^2 + \frac{3}{2} \alpha e^{-u} \left[ \frac{z^{1/3}}{(1 + z^{2/3})^{1/2}} + \beta \right], \quad (11)$$

where

$$z = (\eta - 1)^{3/2} \quad (12)$$

and, from (9),

$$z = 0, \quad dz/dw = 0, \quad d^2z/dw^2 = \frac{3}{2} \alpha \beta \text{ at } w = 0 \quad (13)$$

It is necessary to obtain the starting value of  $d^2z/dw^2$  from the series, since in equation (11) as it stands the first term on the right-hand side is indeterminate at  $w = 0$ .

Equation (11) is not convenient for mechanical solution from  $w = 0$  by the differential analyser, as for small  $w$  it involves the ratio  $(dz/dw)^2/z$  of two small quantities, which is not easy to handle on the machine, but it is quite convenient for numerical integration by a step-by-step method.

Care has to be taken about one point in the numerical integration; from (10), (12) it follows that

$$z = \frac{3}{4}\alpha\beta w^2 + O(w^{8/3})$$

and the term of order  $w^{8/3}$  makes the derivatives of  $d^2z/dw^2$  infinite at  $w = 0$ , and the usual finite-difference integration formula is not valid. It is necessary either to work out a special integration formula for the first interval, or to use so small an interval that, despite its infinite gradient at the origin, the term involving  $z^{1/3}$  in (11) has not increased from zero by more than can be allowed for at sight in obtaining the increment of  $dz/dw$  for the first interval of the integration. The second procedure seemed more satisfactory in practice, and was adopted.

Otherwise, the numerical integration is straightforward.

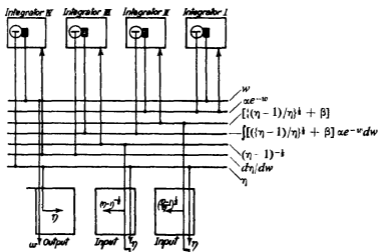


FIG. 3—Schematic set-up of differential analyser (Signs and scale factors omitted)

#### 4—SOLUTION OF EQUATION BY THE DIFFERENTIAL ANALYSER

For the solution of (8) by the differential analyser, it was written in the following form—

$$\frac{d^2\eta}{dw^2} = \alpha e^{-w} (\eta - 1)^{-\frac{1}{2}} \left[ \left( \frac{\eta - 1}{\eta} \right)^{\frac{1}{2}} + \beta \right]$$

The machine set-up is shown in schematic form in fig. 3, in which the notation follows that standardized by Bush.\*

The functions  $(\eta - 1)^{-\frac{1}{2}}$  and  $[(\eta - 1)/\eta]^{\frac{1}{2}}$  were supplied to the machine separately from two input tables. The reason for this is that the same

\* 'J. Franklin Inst.', vol. 212, p. 447 (1931)

input curves then apply for all values of  $\beta$ , the value of  $\beta$  being taken into account in the initial setting of the displacement of integrator II; if the equation were taken in the original form (8), only one input table would be necessary, but a separate curve of  $\eta^{-1} + \beta(\eta-1)^{-1}$  would be required for each value of  $\beta$ . The exponential  $e^{-w}$  was generated by integrator IV, and the value of  $\alpha$  was supplied in terms of the initial displacement of this integrator, or by gearing.

The numerical integration of (11) was normally taken to the first value of  $w$  reached in the step-by-step integration for which  $\eta > 1.05$ , the values of  $e^{-w}$ ,  $(\eta-1)^{-1}$ ,  $[(\eta-1)/\eta]^1 + \beta$ , and

$$(dz/dw) = -\frac{1}{2}z^{-1} dz/dw$$

for this value of  $w$  were calculated from the numerical solution, and the solution by the differential analyser was started from this point.

The solutions were recorded graphically, a set for a single value of  $\alpha$  and different values of  $\beta$ , namely 0.0, 0.1, 0.2, 0.4, 0.6, 0.8, 1.0, being recorded on the same sheet of paper, with the same zero, to facilitate interpolation as described in the next section. The values of  $\alpha$  taken were 0.1, 0.2, 0.4, 0.6, 0.8.

Solutions of (8) are likely to be useful in the investigation of other valve problems, and reproductions\* of the graphs of the machine solutions are consequently given in figs 4a-e.

Equation (3), being of the second order with the first derivative absent, is quite convenient for numerical work, and for one case ( $\alpha = 0.8$ ,  $\beta = 0.8$ ) a numerical solution was carried out to  $w = 2.5$ , and was compared with the machine solution at  $w = 2.0$ . The comparison was very satisfactory, the values of  $\eta$  for the machine solution and for the numerical solution being 4.29 and 4.28 respectively.

Solutions were only carried out for positive  $w$ , for the reason explained in § 6.

### 5—CASE I, $V_s = 0$ (SECONDARY ELECTRONS EMITTED WITH ZERO VELOCITY)

As already mentioned, the initial energy of the secondary electrons,  $V_s$ , is small, and as it seemed at first that it might be negligible, the theoretical results for  $V_s = 0$  were first taken for comparison with the results of

\* The original records are kept in the Library of the Engineering Laboratory, Oxford, and are available on loan to investigators requiring values of the solutions of equation (8) to an accuracy greater than that to which they can be read off from figs 4a-e.

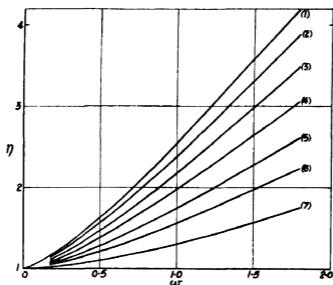
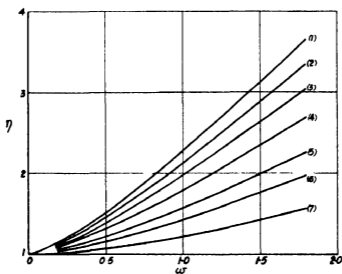


FIG 4a



Figs 4a-e—Graphs of solutions of equation (8). Each figure gives the solutions for a fixed value of  $\alpha$ , and various values of  $\beta$ , as follows —

Curve . . . . .	1	2	3	4	5	6	7
$\beta$ .. . . .	1.0	0.8	0.6	0.4	0.2	0.1	0.0

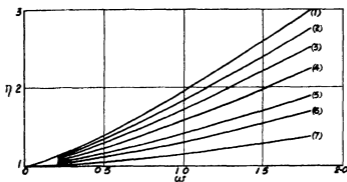


FIG 4c

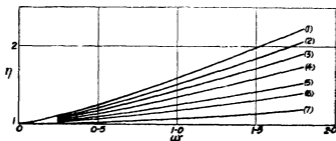


FIG 4d

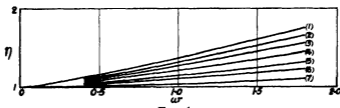


FIG 4e

FIGS 4a-e—(continued)

experiment We will consider this case first, as the comparison with experiment leads to very definite conclusions, also the theoretical results for  $V_s = 0$  form a basis for the later discussion of the effect of an appreciable initial energy of the secondary electrons

When  $V_s = 0$ , the conditions (3), (4) on the solution of (2) become

$$V = V_a, \quad dV/dr = 0, \quad \text{at } r = r_a;$$

also the singularity is at the anode itself, so that the integration of the equation starts from the anode and is carried into the grid The transformations (5), (6) then become—

$$r/r_a = e^{-w}, \quad V/V_a = \eta,$$

so that the set of solutions obtained, as described in § 4, give, on a reduced scale, the potential distribution in the triode, the origin  $w = 0$  corresponding to the anode, for each curve. In particular, the ordinate at  $w = \log(r_a/r_g)$  is  $(V_g/V_a)$ .

For a given triode,  $(r_a/r_g)$  is fixed, and we are interested in the relation between  $V_g$  and the other parameters such as  $V_a$ ,  $t_p$ .

By taking the set of curves for a constant value of  $\alpha$  and different  $\beta$  and reading off  $\eta = V_g/V_a$  at  $w = \log(r_a/r_g)$ , we obtain a relation between  $\beta = t_s/t_p$  and  $V_g/V_a$  for the given triode, which can then be plotted and expressed by a graph, and similar curves can be drawn for other values of  $\alpha$ . For a given value of  $V_a$  and any particular value of  $\alpha$ , each of these curves will relate to a definite value of  $t_p$ , since, for  $V_s = 0$ ,

$$\alpha = (2m/e)^{1/2} V_a^{-3/2} t_p r_a$$

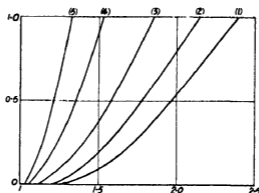


FIG. 5— $V_s = 0$ . Curves of  $\beta = t_s/t_p$  against  $\eta = V_g/V_a$  for  $r_a/r_g = 2.5$ , for different values of  $\alpha$ , namely, curve 1,  $\alpha = 0.8$ , curve 2,  $\alpha = 0.6$ , curve 3,  $\alpha = 0.4$ , curve 4,  $\alpha = 0.2$ , curve 5,  $\alpha = 0.1$ .

Intermediate values of  $t_p$  may be dealt with by interpolation between two curves.

Such a set of curves is shown in fig. 5, for the value of  $(r_a/r_g)$  for the triode used in the experimental work, they apply to any triode of the same dimensions.

An important feature of these results is that for any given anode potential and primary anode current, a certain minimum potential difference between grid and anode is necessary before any secondary current can flow from the anode.

6—CASE I,  $V_s = 0$ . COMPARISON WITH EXPERIMENT

Experiments were made with a triode specially designed for the measurement of primary anode current \*. In each set of observations the anode potential and primary current to the anode were kept constant, and the currents in the anode and grid circuits were measured when the grid was given various potentials greater than that of the anode. The secondary current was derived by subtracting the measured anode current from the primary current

The results of a typical set of observations are shown in fig 6, together with the theoretical curve with which they should coincide if  $V_s = 0$ , and the curves from which the latter was interpolated. It is clear that a wide discrepancy occurs between the two curves, the flow of secondary current commences when the grid is at only a slightly greater potential than the anode, which is contrary to the result indicated at the end of the previous section, and, over the range where the secondary current is not limited by the rate of emission of electrons by the anode, this current is much greater than anticipated theoretically

Now, in the theoretical treatment, the grid was assumed to be a complete circular cylindrical surface, whereas it was actually of helical form. It may be shown theoretically that the potential of points between the turns of the grid is not that of the grid itself but varies in such a way that it is always less than that of the grid, if the grid is at a higher potential than the anode. Moreover, it is possible for some electrons which leave the anode to pass through the grid wires and return to the anode after describing a path round one or more turns of the grid winding. It may therefore be expected that the secondary current of electrons from the anode to the grid will be slightly less than that determined theoretically. But the curves in fig 6 show the opposite effect, so the discrepancy cannot be accounted for in this way

Thus the experimental results are quite at variance with the results of the solution of equation (2) with  $V_s = 0$ , and the only apparent explanation is that the initial energy of the secondaries is not negligible, and this leads us to consider how it may be taken into account

7—CASE II,  $V_s \neq 0$ 

When  $V_s \neq 0$  we have

$$w = \log(r_0/r), \quad \eta = V/(V_a - V_s), \quad \alpha = (2m/e)^{1/2} (V_a - V_s)^{-3/2} r_0 j_p,$$

\* The primary current was measured by observing the temperature rise of the anode. An account of this triode and the method of using it will be published separately (Myers, 'Proc. phys. Soc., Lond.,' *in press*)

where  $r_0$  is the radius at which  $V$  takes its minimum value  $V_a - V_s$ ; the equation relating  $\eta$  and  $w$  is the same as when  $V_s = 0$ , though the variables now have slightly different meanings, and, to reach the anode, the solution is now required for negative values of  $w$

It is convenient to introduce the quantities—

$$\left. \begin{aligned} w' &= \log(r_a/r) = w + \log(r_a/r_0) \\ \eta' &= V/V_a = [1 - (V_s/V_a)] \eta \\ \alpha' &= (2m/e)^{1/2} V_a^{-3/2} I_p r_a = \left( \frac{V_a - V_s}{V_a} \right)^{3/2} \frac{r_a}{r_0} \alpha, \end{aligned} \right\} \quad (14)$$

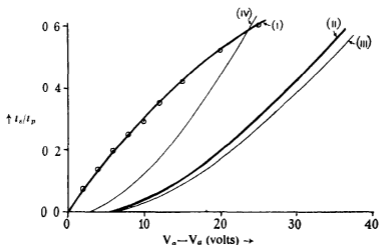


FIG. 6—Curves of  $i_s/i_p$  against  $V_p - V_a$  for  $V_a = 100$  volts. Curve (i) experimental curve for  $i_p = 34.9$  mA, observed points marked. Curve (ii), theoretical curve for  $V_s = 0$ ,  $i_p = 34.9$  mA, interpolated from curves (iii) and (iv). Curve (iii), theoretical curve for  $V_s = 0$ ,  $\alpha = 0.1$  ( $i_p = 37.1$  mA). Curve (iv), theoretical curve for  $V_s = 0$ ,  $\alpha = 0.2$  ( $i_p = 18.6$  mA).

as these are the quantities which can actually be measured in any actual experiment

To see the general effect of an initial velocity of the secondary electrons, consider the set of curves (fig. 7a) of  $\eta$  against  $w$ , for a given value of  $\alpha$  and different values of  $\beta$ . The value of  $w$  at the anode,  $w_a = -\log(r_a/r_0)$ , is now different for the different curves, and is given by the negative intersection of a line at height  $\eta_a = 1 = V_s/(V_a - V_s)$  above the common minimum of the curves.

If the curves are now shifted horizontally so that these intersections fall together at P (see fig. 7b), the abscissa from P of any point is

$$w + \log(r_a/r_0),$$

that is  $w'$ , from (14), and the ordinate from P is

$$(V - V_a)/(V_a - V_s) - [V_a/(V_a - V_s)](\eta' - 1),$$

the construction of curves of  $V_0/V_a$  against  $\beta = i_s/i_p$ , for a given triode (*i.e.*, given  $r_0/r_a$ ) and fixed  $\alpha$  can now be carried out as in § 5. For fixed  $V_a$ , these curves do not now refer to the same primary current  $i_p$ , since  $\alpha$ , not  $\alpha'$ , is the same for them all, and  $r_0$  is different for the different curves, hence to obtain a set of curves of  $i_s$  as a function of  $V_0$ , for fixed  $i_p$  and  $V_a$ , a further interpolation is now necessary, and this must be carried out for each value of  $\beta$ .

To find quantitatively the effect of any given initial velocity of the secondary electrons, it would be necessary to have the solution of (7) for

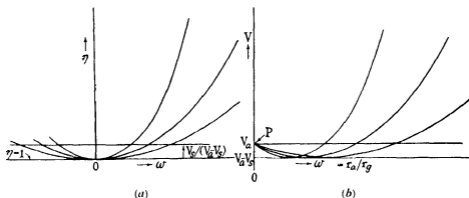


FIG. 7

negative values of  $w$ . This could be obtained without difficulty, but it does not seem likely that the solution would correspond closely to the actual situation inside a triode, as the secondary electrons in an actual triode probably have a velocity distribution, not a single velocity of emission. Thus to get an idea of the magnitude of the effect of an initial velocity of the secondary electrons, we can be content with an approximate solution of (7) for negative  $w$ .

Now the only difference between the solution of (7) for positive and negative  $w$  is the effect of the factor  $e^{-w}$ , which does not differ much from unity when  $w$  is small. Hence an approximation to the solution of (7) for negative  $w$  can be obtained by taking  $\eta(-w) = \eta(w)$ . This approximation is not good unless the minimum of  $V$  occurs close to the anode, but even when this is not the case, it may be as good an approximation as that involved in taking only a single velocity of emission.

With this approximation, curves of  $i_s$  against  $V_p$  were constructed, using the procedure outlined earlier in this section, for  $V_s = 0, 3$ , and 5 volts and for the same values of  $r_a/r_p$ ,  $V_a$ , and  $i_p$  as used in the experiments and in the calculated results for  $V_s = 0$ . The results are shown and compared with the observed results in fig 8. The change in shape of the calculated curve for small values of  $i_s/i_p$ , as  $V_s$  increases from 0 to 5 volts, should be noted. It will be seen that the observed results would agree very well with a theoretical curve with about  $V_s = 3.8$  volts, over the early part of the curve, this may be compared with the value 3 volts for polished copper, found by Sharman (*loc cit*) from measurements with a retarding field.

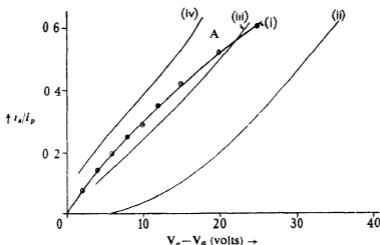


FIG 8—Curves of  $i_s/i_p$  against  $V_p - V_a$  for  $V_a = 100$  volts,  $i_p = 34.9$  mA. Curve (i), experimental curve, observed points shown. Curve (ii), theoretical curve for  $V_s = 0$  (cf fig 6). Curve (iii), approximate theoretical curve for  $V_s = 3$  volts. Curve (iv), approximate theoretical curve for  $V_s = 5$  volts.

While good agreement would thus be obtained with the early parts, OA, of the experimental curve, it is seen that beyond the point A, the experimental curve falls below the theoretical. This may be due to the helical form of the grid, whose effect has already been considered, or to the effect of a velocity distribution of the secondaries.

The authors wish to express their indebtedness to Miss B. M. Dent, of the Research Department of Metropolitan-Vickers Electrical Company, Limited, who carried out most of the initial numerical integrations of equation (11), as described in § 3 of this paper.

The experimental measurements were taken in the Engineering Laboratory, Oxford, and the authors wish to thank Mr. E. B. Moullin for the

provision to one of them (D M M) of facilities for carrying out this part of the work, and for his interest and advice in the preparation of the paper

One of us (D R H) wishes to thank the Department of Scientific and Industrial Research for a grant for assistance in carrying out a programme of development and application of the differential analyser at Manchester University, of which the work described in § 4 of this paper forms a part

#### SUMMARY AND CONCLUSIONS

The potential distribution in the space between the anode and grid of a triode with cylindrical electrodes has been determined theoretically in the condition where the grid collects current due to secondary emission from the anode, and this current is limited by electronic space-charge. Certain reasonable approximations were made in order to obtain an equation in a manageable form, particular solutions of the equation were derived by means of the mechanical Differential Analyser.

Corresponding results obtained experimentally on a triode having a nickel anode, were found to agree with the theoretical predictions, if the initial energy of secondary electrons was given a certain value, of the order of 4 volts, and this is taken as an approximate indication of the average initial energy of secondary electrons emitted by a nickel electrode.

---

## On the Relations of the Tensor-calculus to the Spinor-calculus

By E. T. WHITTAKER, F. R. S.

(Received 28 August, 1936)

### 1—INTRODUCTION

In this paper it is first shown (§ 2) that a six-vector which has the property of being identical with its own dual six-vector, and which, moreover has its invariant null, has properties equivalent to those of a spinor. It is then shown (§ 3) that the correspondence thus set up between tensor-analysis and spinor-analysis enables us to replace some complicated tensor-operations by simple spinor-operations. In § 4 the correspondence is applied to the tensorization of Dirac's relativistic equation of the electron, in connexion with its generalization to the space-time of general relativity. It is shown that Dirac's equations are equivalent to the vanishing of an ordinary vector.

### 2—A SPECIAL TYPE OF SIX-VECTOR, AND ITS EQUIVALENCE TO A SPINOR

We shall first suppose that space-time is Galilean, so that the metric is given by  $ds^2 = (dx^0)^2 - (dx^1)^2 - (dx^2)^2 - (dx^3)^2$ , where  $x^0 = ct$ ,  $x^1 = x$ ,  $x^2 = y$ ,  $x^3 = z$ . It is well known that in Galilean space-time, to every six-vector  $X^{pq}$  there corresponds a dual six-vector  $Y^{pq}$  such that

$$Y_{pq} = iX^{rs}, \quad X_{pq} = iY^{rs},$$

where  $pqrs$  is an even permutation of 0123 and  $i = \sqrt{-1}$ .

Consider now a complex six-vector  $R^{pq}$  which has the property of being identical with its own dual, this property is invariant under transformations of coordinates. We have then

$$R_{01} = iR_{23}, \quad R_{02} = iR_{31}, \quad R_{03} = iR_{12}. \quad (1)$$

The two invariants of this six-vector, namely

$$(R_{01}^2 + R_{02}^2 + R_{03}^2 - R_{23}^2 - R_{31}^2 - R_{12}^2)$$

and

$$(R_{01}R_{23} + R_{02}R_{31} + R_{03}R_{12}),$$

are therefore not distinct, each of them being a multiple of

$$(R_{01}{}^2 + R_{02}{}^2 + R_{03}{}^2);$$

we shall now suppose further that

$$R_{01}{}^2 + R_{02}{}^2 + R_{03}{}^2 = 0, \quad (2)$$

so that the invariants of  $R^{\mu\nu}$  are zero. Self-dual six-vectors whose invariant is null, such as  $R^{\mu\nu}$ , play a prominent part in what follows.

Now let the general Lorentz transformation,  $\iota e$ , the linear transformation which satisfies the equation

$$\dot{x}_0^2 + \dot{x}_1^2 - \dot{x}_2^2 - \dot{x}_3^2 = x_0^2 - x_1^2 - x_2^2 - x_3^2,$$

be

$$\dot{x}_i = \sum_{k=0}^3 a_{ik} x_k \quad (3)$$

Then the usual equations of transformation of a six-vector, combined with equations (1), give for the quantities  $R_{01}$ ,  $R_{02}$ ,  $R_{03}$ , the equations of transformation

$$\left. \begin{aligned} \tilde{R}_{01} &= (a_{00}a_{11} - a_{01}a_{10} - ia_{02}a_{13} + ia_{03}a_{12}) R_{01} \\ &\quad + (a_{00}a_{12} - a_{02}a_{10} - ia_{03}a_{11} + ia_{01}a_{13}) R_{02} \\ &\quad + (a_{00}a_{13} - a_{03}a_{10} - ia_{01}a_{12} + ia_{02}a_{11}) R_{03} \\ \tilde{R}_{02} &= (a_{00}a_{21} - a_{01}a_{20} - ia_{02}a_{23} + ia_{03}a_{22}) R_{01} \\ &\quad + (a_{00}a_{22} - a_{02}a_{20} - ia_{03}a_{21} + ia_{01}a_{23}) R_{02} \\ &\quad + (a_{00}a_{23} - a_{03}a_{20} - ia_{01}a_{22} + ia_{02}a_{21}) R_{03} \\ \tilde{R}_{03} &= (a_{00}a_{31} - a_{01}a_{30} - ia_{02}a_{33} + ia_{03}a_{32}) R_{01} \\ &\quad + (a_{00}a_{32} - a_{02}a_{30} - ia_{03}a_{31} + ia_{01}a_{33}) R_{02} \\ &\quad + (a_{00}a_{33} - a_{03}a_{30} - ia_{01}a_{32} + ia_{02}a_{31}) R_{03} \end{aligned} \right\} \quad (4)$$

Now if  $\alpha$ ,  $\beta$ ,  $\gamma$ ,  $\delta$  are any complex numbers satisfying the equation  $\alpha\delta - \beta\gamma = 1$ , then the transformation of two complex variables  $(\phi_1, \phi_2)$  represented by

$$\left. \begin{aligned} \phi_1 &= \alpha\phi_1 + \beta\phi_2 \\ \phi_2 &= \gamma\phi_1 + \delta\phi_2 \end{aligned} \right\} \quad (5)$$

is called a binary unimodular transformation, and it is well known that to every binary unimodular transformation there corresponds a definite Lorentz transformation, the coefficients  $a_{\mu\nu}$  of the Lorentz transformation

being given in terms of the coefficients of the binary unimodular transformation by the matrix-equation

$$\begin{pmatrix} a_{00} & a_{01} & a_{02} & a_{03} \\ a_{10} & a_{11} & a_{12} & a_{13} \\ a_{20} & a_{21} & a_{22} & a_{23} \\ a_{30} & a_{31} & a_{32} & a_{33} \end{pmatrix} = \frac{1}{2} \begin{pmatrix} \alpha & \beta & \gamma & \delta \\ \gamma & \delta & \alpha & \beta \\ -i\gamma & -i\delta & i\alpha & i\beta \\ \alpha & \beta & -\gamma & -\delta \end{pmatrix} \begin{pmatrix} \alpha^* \beta^* - i\beta^* \alpha^* \\ \beta^* \alpha^* - i\alpha^* \beta^* \\ \gamma^* \delta^* - i\delta^* \gamma^* \\ \delta^* \gamma^* - i\gamma^* \delta^* \end{pmatrix}, \quad (6)$$

where  $\alpha^*$ ,  $\beta^*$ ,  $\gamma^*$ ,  $\delta^*$  are the conjugate-complex quantities to  $\alpha$ ,  $\beta$ ,  $\gamma$ ,  $\delta$ . The group of Lorentz transformations† is isomorphic to the group of binary unimodular transformations, so that if two binary unimodular transformations  $B_1$ ,  $B_2$  correspond respectively in accordance with equation (6) to two Lorentz transformations  $L_1$ ,  $L_2$ , then the binary unimodular transformation  $B_1 B_2$  corresponds to the Lorentz transformation  $L_1 L_2$ . A pair of quantities ( $\phi_1$ ,  $\phi_2$ ) which undergo the binary unimodular transformation (5) when the coordinates are subjected to the Lorentz transformation defined by (3) and (6), is called a spinor ‡

Now substitute in equations (4) the values of the  $a_{pq}$  given by (6) we obtain

$$\left. \begin{aligned} \tilde{R}_{01} &= \frac{1}{2}(\sigma^2 - \beta^2 - \gamma^2 + \delta^2) R_{01} + \frac{i}{2}(\alpha^2 + \beta^2 - \gamma^2 - \delta^2) R_{02} \\ &\quad + (-\alpha\beta + \gamma\delta) R_{03} \\ \tilde{R}_{02} &= \frac{i}{2}(-\alpha^2 + \beta^2 - \gamma^2 + \delta^2) R_{01} + \frac{1}{2}(\alpha^2 + \beta^2 + \gamma^2 + \delta^2) R_{02} \\ &\quad + i(\alpha\beta + \gamma\delta) R_{03} \\ \tilde{R}_{03} &= (-\alpha\gamma + \beta\delta) R_{01} + i(-\alpha\gamma - \beta\delta) R_{02} + (\alpha\delta + \beta\gamma) R_{03} \end{aligned} \right\} \quad (7)$$

These equations give at once

$$\begin{aligned} \tilde{R}_{01} + i\tilde{R}_{02} &= \alpha^2 (R_{01} + iR_{02}) + \beta^2 (-R_{01} + iR_{02}) - 2\alpha\beta R_{03} \\ -\tilde{R}_{01} + i\tilde{R}_{02} &= \gamma^2 (R_{01} + iR_{02}) + \delta^2 (-R_{01} + iR_{02}) - 2\gamma\delta R_{03}, \end{aligned}$$

which by (2) are the squares of the equations

$$\left. \begin{aligned} (\tilde{R}_{01} + i\tilde{R}_{02})^{\frac{1}{2}} &= \alpha (R_{01} + iR_{02})^{\frac{1}{2}} + \beta (-R_{01} + iR_{02})^{\frac{1}{2}} \\ (-\tilde{R}_{01} + i\tilde{R}_{02})^{\frac{1}{2}} &= \gamma (R_{01} + iR_{02})^{\frac{1}{2}} + \delta (-R_{01} + iR_{02})^{\frac{1}{2}} \end{aligned} \right\}. \quad (8)$$

† More strictly speaking, not the *complete* Lorentz group, but the *restricted* Lorentz group, i.e., the group of four-dimensional rotations of determinant +1

‡ B. L. van der Waerden, 'Nachr. Ges. Wiss. Göttingen', p. 100 (1929). The name *spinor* is given more generally to quantities which bear the same kind of relation to ( $\phi_1$ ,  $\phi_2$ ) that tensors of rank greater than unity bear to vectors in ordinary tensor-analysis.

## On Relations of the Tensor-calculus to the Spinor-calculus 41

These equations show that the pair of quantities  $(R_{01} + iR_{02})^{\dagger}$ ,  $(-R_{01} + iR_{02})^{\dagger}$  constitute a spinor. Denoting this spinor by  $(\sqrt{2}\phi_1, \sqrt{2}\phi_2)$ , we have then

$$\sqrt{2}\phi_1 = (R_{01} + iR_{02})^{\dagger}, \quad \sqrt{2}\phi_2 = (-R_{01} + iR_{02})^{\dagger} \quad (9)$$

and

$$\left. \begin{aligned} R_{01} &= \phi_1^2 - \phi_2^2, & R_{02} &= -i(\phi_1^2 + \phi_2^2) & R_{03} &= -2\phi_1\phi_2 \\ R_{23} &= -i(\phi_1^2 - \phi_2^2), & R_{31} &= -(\phi_1^2 + \phi_2^2) & R_{12} &= 2i\phi_1\phi_2 \end{aligned} \right\} \quad (10)$$

Equations (9) and (10) set up a correspondence between self-dual six-vectors of vanishing invariant,  $R_{pq}$ , on the one hand, and spinors  $(\phi_1, \phi_2)$  on the other hand. Thus the calculus of spinors is included in the calculus of tensors†, in the sense that to every spinor there corresponds a tensor, and to every relation between spinors there corresponds a relation between tensors. When, however, we study this correspondence more closely, we find some remarkable features which will now be examined.

### 3—THE TENSOR-OPERATIONS CORRESPONDING TO CERTAIN SPINOR-OPERATIONS

In the spinor-calculus it is shown that ordinary vectors can be constructed by combining spinors with their complex conjugates. Thus if  $(\phi_1, \phi_2)$  and  $(\psi_1, \psi_2)$  are spinors, and if

$$\begin{aligned} D^0 &= \phi_1\psi_1^* + \phi_2\psi_2^*, & D^1 &= \phi_1\psi_2^* + \psi_1^*\phi_2, \\ D^2 &= i\phi_1\psi_2^* - i\psi_1^*\phi_2, & D^3 &= \phi_1\psi_1^* - \phi_2\psi_2^*, \end{aligned} \quad (11)$$

then  $D^p$  is a vector. Let  $R_{pq}$  and  $S_{pq}$  be the self-dual six-vectors corresponding to the spinors  $(\phi_1, \phi_2)$  and  $(\psi_1, \psi_2)$  respectively; the question now arises what tensor-operations, performed on the tensors  $R_{pq}$  and  $S_{pq}$ , will yield this vector  $D^p$ ? The answer is remarkable. Let us form the tensor

$$V^{pq} = \sum_k R^p_k S^{*qk}, \quad (12)$$

where  $S^*$  denotes the complex-conjugate of  $S$ . Then we find that  $V^{pq}$  is a particular kind of tensor of rank two, namely, it is the outer product of a vector with itself, and, in fact,

$$V^{pq} = -2D^p D^q, \quad (13)$$

† It will be remembered that at present we are considering only behaviour with respect to Lorentz transformations.

where  $D^p$  is the vector defined in (11). Thus when  $\sum_k R^p_k S^{*k}$  has been formed, the vector  $D^p$  can be determined. But we observe that *this involves passing from the tensor  $D^p D^q$  to the vector  $D^p$* , an operation which resembles extracting a square root in algebra. Thus while in the spinor-calculus the vector  $D^p$  is formed from the spinors  $(\phi_1, \phi_2)$  and  $(\psi_1, \psi_2)$  by simple direct operations, in the tensor-calculus  $D^p$  can be formed from the six-vectors  $R^{pq}$  and  $S^{pq}$  only by performing operations one of which is an inverse operation. This is characteristic of the relation between the tensor-calculus and the spinor-calculus: *the spinor-calculus enables us to construct by direct operations (addition, multiplication, contraction) new tensors which in the tensor-calculus can be constructed only by solving tensor equations*. We are reminded of the way in which the square roots that occur in trigonometry ( $\cos \theta = \sqrt{1 - \sin^2 \theta}$ ) can be evaded by making use of the substitution  $\cos \theta = \frac{1 - t^2}{1 + t^2}$ ,  $\sin \theta = \frac{2t}{1 + t^2}$ .

A still more striking example is the following. In the spinor-calculus it is shown that if  $(\phi_1, \phi_2)$  is a spinor defined over a domain in space-time, then

$$H_p = \phi_2 \frac{\partial \phi_1}{\partial x^p} - \phi_1 \frac{\partial \phi_2}{\partial x^p} \quad (14)$$

is an ordinary vector.  $H_p$  depends only on  $(\phi_1, \phi_2)$ , that is, wholly on the tensor  $R_{pq}$ , so we now inquire what operations performed on the tensor  $R_{pq}$  will yield this vector  $H_p$ . The answer is that if we form the tensor  $\sum_k R_{ks} (D^k)_p$ , where  $D^k$  is the vector already found, and the notation  $( )_p$  is used to denote covariant differentiation, which in our Galilean space-time is merely ordinary differentiation, then this tensor is the outer product of two vectors, and, in fact,

$$\sum_k R_{ks} (D^k)_p = 2D_s H_p \quad (15)$$

The vector  $H_p$  is thus obtained by tensor-analysis, but only by making use of the vector  $D^p$ , which itself was obtained by combining the tensor  $R_{pq}$  with the complex-conjugate of another arbitrary tensor  $S_{pq}$ †. The vector  $H_p$ , however, depends solely on  $R_{pq}$  and not at all on  $S_{pq}$ ; the part played by  $S_{pq}$  in the matter resembles that played by a catalytic agent in chemistry, we cannot perform the calculation without using  $S_{pq}$ , although  $S_{pq}$  disappears altogether from the final result. Here, then, *the spinor-calculus enables us to obtain by direct calculation a vector which*

† It is true that the tensor  $S_{pq}$  might be taken to be the same as  $R_{pq}$ , but even in this case  $D_p$  depends not solely on  $R_{pq}$  but on  $R_{pq}$  together with its complex-conjugate  $R^k_{pq}$ , which is a distinct tensor, so that the argument in the text still stands.

cannot be obtained by tensor-analysis except by the "catalytic" use of a tensor not related to the problem

The general problem of the construction of new tensors from known tensors has hitherto been studied chiefly in connexion with direct methods of tensor-formation, such as addition, multiplication, and contraction. There is a large field of possible research regarding tensors which can be defined only by the solution of tensor-equations or by the use of "catalytic" tensors. It would seem that in this field the spinor-calculus may be of great assistance.

#### 4—DIRAC'S RELATIVISTIC EQUATION OF THE ELECTRON

From what precedes it will be evident that the connexion between tensor-calculus and spinor-calculus may be used in order to solve difficult problems in tensor-calculus by re-stating them as problems in spinor-calculus. Conversely, the connexion may be used in order to solve difficult problems regarding spinors by re-stating them in terms of tensors, this is notably the case when the investigation of a problem in the space-time of special relativity has led to an equation expressed in terms of spinors, and it is desired to find the equation which is the extension of this to the space-time of general relativity, for tensors can be carried over at once from special relativity to general relativity, whereas spinors (at any rate, as defined originally) belong properly to special relativity, and spinor-equations can be transferred to general relativity only with difficulty. These remarks may be illustrated by reference to Dirac's relativistic equation of the electron.

We shall take Dirac's equations (omitting the terms depending on the external electromagnetic field, which complicate the equations without affecting the principles here involved) in the form†

$$\left. \begin{aligned} \frac{\partial \psi_1}{\partial x^0} + \frac{\partial \psi_2}{\partial x^1} - i \frac{\partial \psi_3}{\partial x^2} + \frac{\partial \psi_4}{\partial x^3} + \frac{mci}{\hbar} \psi_2 &= 0 \\ \frac{\partial \psi_2}{\partial x^0} + \frac{\partial \psi_1}{\partial x^1} + i \frac{\partial \psi_3}{\partial x^2} - \frac{\partial \psi_4}{\partial x^3} + \frac{mci}{\hbar} \psi_4 &= 0 \\ \frac{\partial \psi_3}{\partial x^0} - \frac{\partial \psi_4}{\partial x^1} + i \frac{\partial \psi_1}{\partial x^2} - \frac{\partial \psi_2}{\partial x^3} + \frac{mci}{\hbar} \psi_1 &= 0 \\ \frac{\partial \psi_4}{\partial x^0} - \frac{\partial \psi_3}{\partial x^1} - i \frac{\partial \psi_1}{\partial x^2} + \frac{\partial \psi_2}{\partial x^3} + \frac{mci}{\hbar} \psi_3 &= 0 \end{aligned} \right\} \quad (16)$$

† This is the form adopted by H. Weyl, "Gruppentheorie und Quantenmechanik" (1928), and by B. C. van der Waerden, "Nachr. Ges. Wiss. Gött.", p. 100 (1929), the  $\psi$ 's are connected with Dirac's original  $\psi$ 's by the relations

$$(\psi_1)_{\text{Dir}} = \frac{\psi_1 + \psi_2}{\sqrt{2}}, \quad (\psi_2)_{\text{Dir}} = \frac{\psi_3 + \psi_4}{\sqrt{2}}, \quad (\psi_3)_{\text{Dir}} = \frac{\psi_1 - \psi_2}{\sqrt{2}}, \quad (\psi_4)_{\text{Dir}} = \frac{\psi_3 - \psi_4}{\sqrt{2}}$$

With this form of the equations,  $(\psi_1^*, \psi_2^*)$  and  $(\psi_4, -\psi_3)$  are spinors, that is, are transformed according to equation (5) when the coordinates are subjected to the Lorentz transformation specified by (3) and (6). By § 2, to each of these spinors there corresponds a self-dual six-vector, calling these six-vectors  $M_{pq}^*$  and  $R_{pq}$  respectively, we have by (10)

$$M_{01}^* = \psi_1^{*2} - \psi_2^{*2}, \quad R_{01} = \psi_4^2 - \psi_3^2, \quad \text{etc} \quad (17)$$

Having obtained these two six-vectors, we can abandon spinor-analysis and proceed by tensor-analysis exclusively. First we determine four ordinary vectors  $A^p, B^p, C^p, C^{*p}$ , by the tensor-equations (like equations (12) and (13))

$$\left. \begin{aligned} \sum_k M_{pk} M^{*ek} &= -2A_p A^e, & \sum_k R_{pk} R^{*ek} &= -2B_p B^e, \\ \sum_k M_{pk} R^{ek} &= -2C_p C^e, & \sum_k M_{pk}^* R^{*ek} &= -2C_p^* C^{*e} \end{aligned} \right\} \quad (18)$$

These four vectors satisfy the relations

$$\left. \begin{aligned} \sum_p A_p A^p &= 0, & \sum_p B_p B^p &= 0, & \sum_p C_p C^p &= 0, & \sum_p C_p^* C^{*p} &= 0, \\ \sum_p A_p C^p &= 0, & \sum_p A_p C^{*p} &= 0, & \sum_p B_p C^p &= 0, & \sum_p B_p C^{*p} &= 0 \end{aligned} \right\} \quad (19)$$

i.e., each of these is perpendicular to itself and to two of the other three. The vector  $-e(A^p + B^p)$  is the "four-vector of electric charge and current" discovered by Darwin,<sup>†</sup> which determines the probability of finding the electron in unit volume at any place, and the probability that the electron in unit time passes through unit area perpendicular to a given direction.

Next, we obtain two vectors  $P_p$  and  $Q_p$  by the process which was used in (15), namely, we write

$$\sum_k M_{ks} (A^k)_p = 2A_s P_p, \quad \sum_k R_{ks}^* (B^k)_p = 2B_s Q_p \quad (20)$$

The divergences of the six-vectors  $M_{pq}$  and  $R_{pq}^*$  are, of course, also vectors, let us denote them by  $S_p$  and  $T_p$ , so

$$S_p = \sum_q (M_p^{\quad q})_q, \quad T_p = \sum_q (R_p^{\quad q})_q \quad (21)$$

From these vectors let us form the vector

$$\Omega_p = \frac{1}{2}S_p + \frac{1}{2}T_p + P_p + Q_p + \frac{mci}{\hbar}(C_p + C_p^*). \quad (22)$$

<sup>†</sup> 'Proc. Roy. Soc., A, vol. 118, p. 654 (1928).

The actual calculation can be carried out easily by working with spinors, we find at once

$$\begin{aligned}\frac{1}{2}S_0 &= \psi_1 \left( -\frac{\partial \psi_1}{\partial x^1} - i \frac{\partial \psi_1}{\partial x^2} + \frac{\partial \psi_2}{\partial x^3} \right) + \psi_2 \left( \frac{\partial \psi_2}{\partial x^1} - i \frac{\partial \psi_2}{\partial x^2} + \frac{\partial \psi_1}{\partial x^3} \right) \\ \frac{1}{2}T_0 &= \psi_3^* \left( \frac{\partial \psi_3^*}{\partial x^1} - i \frac{\partial \psi_3^*}{\partial x^2} - \frac{\partial \psi_4^*}{\partial x^3} \right) + \psi_4^* \left( -\frac{\partial \psi_4^*}{\partial x^1} - i \frac{\partial \psi_4^*}{\partial x^2} - \frac{\partial \psi_3^*}{\partial x^3} \right) \\ P_0 &= \psi_2 \frac{\partial \psi_1}{\partial x^0} - \psi_1 \frac{\partial \psi_2}{\partial x^0}, \quad Q_0 = \psi_4^* \frac{\partial \psi_3^*}{\partial x^0} - \psi_3^* \frac{\partial \psi_4^*}{\partial x^0} \\ C_0 &= -\psi_1 \psi_4 + \psi_2 \psi_3, \quad C_0^* = -\psi_1^* \psi_4^* + \psi_2^* \psi_3^*,\end{aligned}$$

and hence

$$\begin{aligned}\Omega_0 &= -\psi_1 \left( \frac{\partial \psi_1}{\partial x^1} + i \frac{\partial \psi_1}{\partial x^2} - \frac{\partial \psi_2}{\partial x^3} + \frac{\partial \psi_3}{\partial x^0} + \frac{mci}{\hbar} \psi_4 \right) \\ &\quad + \psi_2 \left( \frac{\partial \psi_2}{\partial x^1} - i \frac{\partial \psi_2}{\partial x^2} + \frac{\partial \psi_1}{\partial x^3} + \frac{\partial \psi_4}{\partial x^0} + \frac{mci}{\hbar} \psi_3 \right) \\ &\quad - \psi_3^* \left( -\frac{\partial \psi_3^*}{\partial x^1} + i \frac{\partial \psi_3^*}{\partial x^2} + \frac{\partial \psi_4^*}{\partial x^3} + \frac{\partial \psi_1^*}{\partial x^0} - \frac{m}{\hbar} \psi_2^* \right) \\ &\quad + \psi_4^* \left( -\frac{\partial \psi_4^*}{\partial x^1} - i \frac{\partial \psi_4^*}{\partial x^2} - \frac{\partial \psi_3^*}{\partial x^3} + \frac{\partial \psi_2^*}{\partial x^0} - \frac{mci}{\hbar} \psi_1^* \right)\end{aligned}$$

But the right-hand side vanishes in consequence of Dirac's equations (namely the first two of those given in (16) and the complex-conjugates of the other two), and similarly the components  $\Omega_1, \Omega_2, \Omega_3$  all vanish in consequence of Dirac's equations. Thus the vector  $\Omega_p$  vanishes in consequence of Dirac's equations. Conversely, the vanishing of the four components  $\Omega_0, \Omega_1, \Omega_2, \Omega_3$ , necessitates Dirac's equations, provided the determinant of the coefficients of the Dirac-expressions in the four equations  $\Omega_p = 0$  does not vanish, but this determinant is

$$\begin{vmatrix} -\psi_1 & \psi_2 & \psi_3^* & \psi_4^* \\ \psi_1 & -\psi_2 & \psi_3^* & -\psi_4^* \\ i\psi_1 & i\psi_2 & -i\psi_3^* & -i\psi_4^* \\ -\psi_2 & -\psi_1 & -\psi_4^* & -\psi_3^* \end{vmatrix},$$

which has the value  $-i(\psi_1\psi_3^* + \psi_2\psi_4^*)^2$ , and therefore cannot vanish unless  $\psi_1\psi_3^* + \psi_2\psi_4^*$  vanishes, which physically is exceptional, if not

impossible. Thus finally *Dirac's equations are equivalent to the statement that the vector  $\Omega_p$  is zero*

$$\Omega_p = 0 \quad (p = 0, 1, 2, 3) \quad (23)$$

Needless to say, the extension of the theory to the space-time of general relativity is much more straightforward when the equations are expressed in this tensorial form than when they are expressed in terms of spinors

## The Auger Effect in Xenon and Krypton

By L H MARTIN, Ph D, and F H EGGLESTON, B Sc, Natural Philosophy Laboratory, University of Melbourne

(Communicated by T H Laby, F R S — Received 15 June, 1936)

[PLATES 4-8]

### INTRODUCTION

In an earlier paper\* an account was given of a determination of the efficiency of emission of K series radiations from argon atoms ionized in the K shell. This efficiency, usually termed the K yield, was calculated from a statistical count of ordinary K photoelectron tracks and Auger pair tracks observed in a Wilson expansion chamber. These experiments have been extended to xenon and krypton, and the present paper describes the measurement of the K yields of these two gases.

Determinations of the K yields for elements of high atomic number with the cloud expansion chamber should be of especial value, as other methods† which depend on the measurement of X-ray energy by ionization currents encounter considerable difficulties owing to the increasing importance of scattering with short wave-length X-rays. The need for new measurements for the heavier elements has been emphasized recently by the striking divergence between the results of two extensive series of measurements, one due to Berkey‡ and the other to Arends,§ both of

\* Martin, Bower, and Laby, 'Proc Roy Soc,' A, vol 148, p. 40 (1935)

† Compton and Allison, "X-Rays in Theory and Experiment," p. 477

‡ 'Phys Rev,' vol 45, p. 437 (1934)

§ 'Ann Physik,' B, vol 22, p. 281 (1935)

whom used an ionization method Berkey found a well-defined maximum in the K yield-atomic number curve in the neighbourhood of atomic number 44 after which the K yield suddenly decreased with increasing atomic number, an effect which is in direct contradiction with the experiments of Arends and existing theory. In connexion with the latter, too, measurements of the K yields for elements of high atomic number are of importance as calculations made recently by Massey and Burhop\* show that a relativistic treatment of the Auger effect yields rather lower values of the K yield for the higher atomic numbers than was expected by Burhop† from his non-relativistic treatment

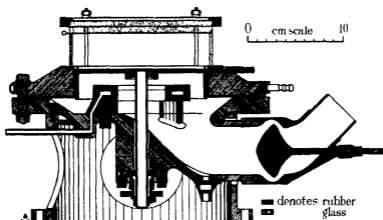


FIG 1

## EXPANSION CHAMBER

A line drawing of the expansion chamber is shown in fig 1. While this chamber retains most of the essential features of the model described in the previous paper, experience with it demanded some alterations in detail which have effected a marked improvement in its operation.

It has been found possible to keep the skirt of the piston short and yet prevent blowing between the cylinder and piston by the use of two piston rings which are well lubricated with oil-dag. Both stainless steel and aluminium alloy have been tried for the piston, and while the latter has the advantage of smaller mass, it is less resistant chemically and is liable to develop minute cracks which allow a slow loss of gas from the chamber. As it was found that for the present type of work the piston mass does

\* 'Proc Roy Soc,' A, vol 148, p 272 (1935)

† 'Proc Roy Soc,' A, vol 153, p 661 (1936).

not determine the effectiveness of the chamber, a stainless steel piston cut from 6-inch rod was employed. The best working speed of this piston was observed in terms of the initial pressure of the evacuated reservoir, the pressure being always just low enough to eliminate any effects due to slight variations in the frictional forces on the piston. Consistent expansions were obtained with pressures between 20 cm and 30 cm less than that in the chamber. At piston speeds corresponding to these pressures we probably obtained benefit from an effect recently recorded by Bearden,\* who found that a slow expansion increased the period of sensitivity of the chamber, provided the expansion ratio was great enough and ample vapour was available.

Apart from improved streamlining of gas conduits, the principal change in design lies in the method of applying oil damping to the piston. Oil is led from a reservoir to an annular flat surface which serves as a stop for the piston. The oil oozes through fine holes arranged in two rows alternately staggered, and forms a film on the stop approximately 1 mm thick. Time-displacement curves of the piston were recorded by an optical oscillograph† with oils of different viscosity (see Plate 4). Tests showed that castor oil at approximately 18° C gave a curve with the best characteristics. After a few expansions the oil feeds automatically under the action of the momentarily reduced pressure of each expansion. We have to thank Professor Laby for designing the piston rings and oil damping used in this chamber.

With the help of Dr N. B. Lewis of Kodak Australasia, we were able to make comparative tests on the relative merits of different photographic emulsions for track photography. On the assumption of sufficient illumination, it appeared that an emulsion with a steep H and D curve, giving a maximum contrast was to be preferred to one with a large H and D speed. This proved to be the case, the following being the order of merit of the three plates tested, all of which had a similar emulsion: (1) emulsion free from dyes, (2) hyper-speed orthochromatic, H and D 1200, (3) panchromatic, H and D 2000. Under identical conditions of illumination, tracks which were well recorded with dye free plates were barely visible with panchromatic plates manufactured with the same emulsion. The plates were developed in Eastman Kodak No. 72 contrast developer.

\* 'Rev. Sci. Instr.', vol. 6, p. 256 (1935).

† A simple but effective oscillograph was obtained by attaching to the piston a pea-lamp lit by A.C. A point image of this was formed by a camera lens on bromide paper attached to a vertical drum which was driven from a synchronous type gramophone motor. Time intervals of 0.01 sec. were registered clearly as variations in darkening of the trace.

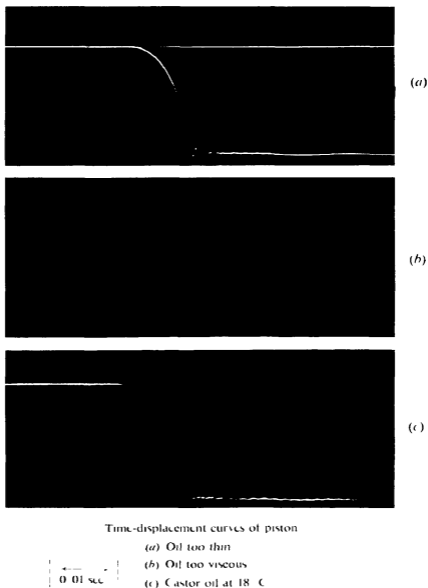
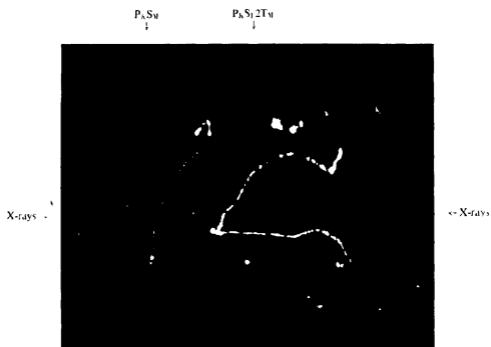
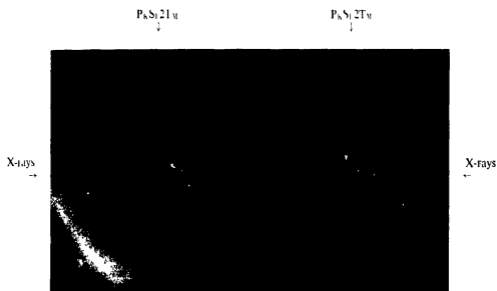


FIG. 3

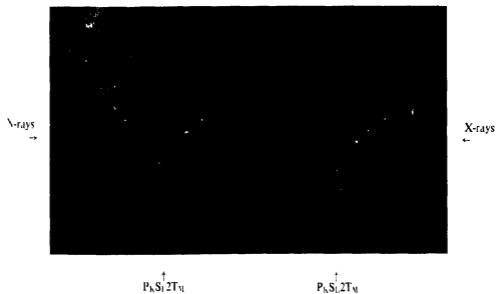


Auger effect in xenon





Anger effect in xenon





Pairs of plates were made with two cameras mounted each at  $45^\circ$  with the vertical and fitted with Zeiss Tessar  $f/4.5$  lenses, focal length 12.5 cm. Pyrex mercury vapour lamps were used, connected in series and excited by a discharge from a 0.25 m.f.d. condenser working between 30 and 35 kv.

### RESULTS

*Xenon*  $Z = 54$ —In view of the fact that X-rays of rather short wave-length are required to excite the K series of xenon ( $\lambda_k = 0.358 \text{ \AA.}$ ) with the consequent appearance of Compton recoil electrons of appreciable range, it was realized that there was a danger of confusing short primary K photoelectrons with high energy recoil electrons unless a beam of sufficient homogeneity was employed.

A beam of nominal wave-length 0.2  $\text{\AA.}$  was obtained by reflexion from a calcite crystal. The angular width of the beam was  $28'$ , so that actually a range of wave-lengths between 0.17  $\text{\AA.}$  and 0.22  $\text{\AA.}$  was reflected, but as the peak voltage on the tube never exceeded 80 kv. the shortest wave-lengths had a very small intensity. Actually tracks due to the shortest waves were never found in the chamber. Table I indicates the extreme lengths of the tracks produced by the above beam, calculated by assuming the range to be proportional to the square of the initial energy of the photoelectron.

TABLE I—RELATIVE LENGTHS OF TRACKS IN XENON

Primary K $h$ ( $v - v_K$ )	0.8 $\rightarrow$ 2.8 (max. observed 1.5)
Auger component $h$ ( $v_K - 2v_L$ )	1
Primary L $h$ ( $v - v_L$ )	4.6 $\rightarrow$ 8.4
Maximum Compton recoil	0.26

A xenon atmosphere of appropriate density was produced in the chamber by employing a 7% xenon hydrogen mixture. Typical tracks obtained with this gas are shown in Plates 5-7 together with the details relevant to each.

The plates were examined in pairs by two observers and unless agreement over the whole plate was possible the plates were discarded. It was necessary on occasions to neglect tracks at each end as confusion sometimes appeared due to tracks produced in the walls of the chamber where the X-rays entered and left. In all, 189 pairs of plates were selected for counting, the average number of tracks on each being between three and four. With the comparatively long tracks met with in this experiment, only a small percentage of the plates taken gave pictures free from

ambiguity, the successful plates mentioned above representing less than 25% of the total number

TABLE II—DETAILS OF COUNT FOR XENON

Identification	Type*	Number
$P_K \ h (\nu - \nu_K)$	$P_K$	143
$S_M \ h (\nu_I - 2\nu_M)$	$P_K S_M$	339
$S_L \ h (\nu_K - 2\nu_L)$	$P_K S_L$	24
$T_M \ h (\nu_L - 2\nu_M)$	$P_K S_L 1 T_M$	39
	$P_K S_L 2 T_M$	72

$$K \text{ yield} = \frac{482}{617} = 0.78$$

\* This column gives the composition of the various groupings of tracks observed, the energies of the individual primary, secondary, and tertiary components being given in column 1. Thus  $P_K S_L 1 T_M$  refers to a group consisting of the primary photoelectron, a secondary photoelectron from the L shell, and one tertiary photoelectron from the M shell.

The probable error of the count is  $0.648 \sqrt{\frac{\pi(1-\pi)}{n}}$ , where  $\pi$  is the ratio of the number of Auger groups counted to the total number  $n$  of K ionized atoms observed. This is slightly less than 5%.

*Krypton*  $Z = 36$ —A 10% krypton hydrogen mixture was used. Technically the krypton experiment does not present the same difficulties as those met in using xenon owing to the fact that longer wave-length X-rays can be employed to ionize this gas ( $\lambda_K = 0.864 \text{ \AA}$ ). Exciting X-rays with an average wave-length of  $0.4 \text{ \AA}$  were used, giving a primary K electron and an Auger component of about the same range. With this exciting radiation, the Compton recoil electrons are seen occasionally as tiny "sphere" tracks which cannot possibly confuse the count, the details of which are shown in Table III. The total number of plates counted was 127 pairs, the average number of tracks per plate lying between four and five. A typical example of the krypton tracks is shown in Plate 8.

TABLE III—DETAILS OF COUNT FOR KRYPTON

$$K \text{ yield} = \frac{\text{number } P_K}{\text{number } P_K + P_{KSL}} = \frac{285}{536} = 0.53$$

with a probable error 3%

The only previous measurements of these gases are those of Auger, made in his original discovery of the multiple ionization effect. The

value given by him for xenon is 0.71 with a probable error of 7% and for krypton 0.51 with a probable error of 3.5%. The agreement in the case of krypton is satisfactory, but our value for xenon is definitely greater than that of Auger. Our results for xenon are also out of agreement with those of Auger in a further important particular. This will be clear from the details of the counts shown in Table IV.

TABLE IV—DETAILS OF COUNTS IN XENON

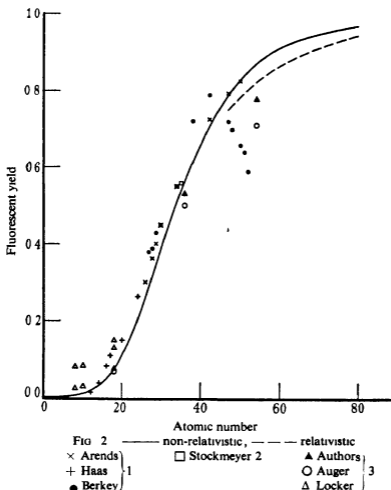
	Authors	Auger
$P_K$	143	36
$P_K S_M$	339	111
$P_K S_L$	24	25
$P_K S_L 1 T_M$	39	21
$P_K S_L 2 T_M$	72	13

While the ratio of the number of  $P_K S_M$  groups to  $P_K$  electrons is of the same order for both experiments, it will be seen that we have observed a relatively much greater number of  $P_K S_L 2 T_M$  groups than Auger. It is difficult to decide how far this might be due on our part to bias in the selection of plates for counting. In the preliminary selection of plates quadruple groups present no difficulties in identification, whereas a pair  $P_K S_L$ , often does owing to its origin not being well defined. In such a case of doubt the whole plate was discarded, and in view of the relatively small number of Auger groups counted, it might be possible for the  $P_K S_L$  group to appear to disadvantage. Such an argument does not account, however, for the lack of agreement shown in the relative numbers of  $P_K S_L 1 T_M$  and  $P_K S_L 2 T_M$  groups, since there is no difficulty in identifying either.

It might be expected *a priori* that the simultaneous emission of four electrons as the result of internal conversion would be a very rare event. On the other hand, the cloud chamber pictures cannot distinguish between such an event and one in which the atom is doubly ionized as the result of a  $P_K S_L$  process and then subsequently reorganizes with a further internal conversion process, yielding groups of the type  $P_K S_L 1 T_M$  or  $P_K S_L 2 T_M$ . Since the probability of internal conversion becomes increasingly greater with lower energy shells it might be expected therefore that the  $P_K S_L 2 T_M$  group would occur relatively often.

This discrepancy in the details of the counts made by Auger and ourselves does not, of course, affect in any way the values found for the K yield.

Fig 2 shows the more recent measurements of the K yield plotted against atomic number. These fall into three groups. (1) the measurements of Haas, Berkey, and Arends, in which the K yield is calculated from ionization measurements of the exciting and excited fluorescent rays, (2) the single measurement of Stockmeyer, who computed the K



yield from an ionization measurement of the energy of the Auger electrons when the K series of bromine is excited, and (3) the expansion chamber counts of Auger, Locher, and the authors

The measurements of Arends and the authors are in fair agreement and show no sign of a drop in the K yield after atomic number 44. Berkey's results have been criticized by Stephenson,\* who corrected them by

\* 'Phys. Rev.', vol 46, p 73 (1934)

allowing for the scattering of the exciting beam in the ionization chamber. While this correction definitely flattens out the maximum, the corrected K yields still decrease slowly after atomic number 44, and, in view of the general agreement between the values of Arends and those obtained from expansion chamber counts, it must be concluded that there exists some source of error in the measurements of Berkey for high atomic numbers as yet not accounted for

Attempts\* have been made to calculate theoretically the probability of internal conversion with atoms ionized in the K shell. Recent quantum mechanical calculations indicate that the probability of internal conversion in K ionized atoms is equal to  $(1 - bZ^4)^{-1}$  where the constant  $b$  evaluated by a direct computation of the probability for silver has the value†  $7.7 \times 10^{-7}$ . The curve for  $1 - (1 - 7.7 \times 10^{-7} Z^4)^{-1}$  is shown as a full line in fig. 2, and exhibits striking agreement with experiment for atoms of atomic number less than 40.

The question has sometimes been raised as to whether the process under discussion should be considered as an actual absorption of an X-ray quantum in the atom in which it is produced or a "radiationless" one arising from the direct interaction between the electrons concerned. The presence in the magnetic spectra‡ of X-ray photoelectrons of lines of energy  $h(\nu_K - 2\nu_{L_I})$ , although  $L_1 - K$  is a forbidden transition, might suggest that the process of multiple ionization is a "radiationless" one. From the point of view of quantum mechanics, both processes are equivalent and yield the same value for the probability of internal conversion §

Theoretical calculations have been extended recently to heavy atoms by Massey and Burhop,|| using Dirac's relativistic theory of the electron. They calculated the absolute probability of internal conversion for gold and silver, interpolated values of the K yield being shown in fig. 2 as a dotted curve. It is of interest to notice that the experimental values for xenon found by Auger and the authors appear to prefer the relativistic curve.

\* Wentzel, 'Z Physik,' vol 43, p 524 (1927)

† This is obtained from calculations of Massey and Burhop (*loc cit*). Owing to a slip in Burhop's paper (*loc cit*), the value obtained for  $b$  originally is somewhat smaller than this. The corrected value gives greatly improved agreement with experiment.

‡ Robinson and Young, 'Proc Roy Soc,' A, vol 128, p 92 (1930), Robinson, 'Nature,' 18 May, 1935

§ Mott and Massey, "The Theory of Atomic Collisions," p 266

|| *Loc cit*

We are indebted to Professor Laby for encouragement in this investigation, and to the Broken Hill Associated Smelters for generous assistance which made the construction and operation of the expansion chamber possible. The installation and preliminary experiments were carried out with the assistance of Mr J C Bower, prior to his departure to England. We have to thank Mr E H S Burhop for helpful discussion on the theory of the Auger Effect.

#### SUMMARY

An account is given of a statistical determination of the K yields of xenon and krypton carried out by means of a Wilson expansion chamber. The K yield for xenon is 0.78 and krypton 0.53.

Details of the xenon count show that in the majority of cases the ejection of K and L electrons from the same atom is accompanied by the ejection of two M electrons. Implications are discussed.

The experimental values of the K yield lie close to the theoretical curve expressing the variation of the K yield with atomic number.

---

# The Modification of Apparent Thermionic Constants for Oxygenated Tungsten by the Temperature Variation of Adsorptive Equilibrium

By M C JOHNSON and F A VICK, Physics Department, University of Birmingham

(Communicated by S W J Smith, FRS—Received 29 June, 1936)

## 1—INTRODUCTION

When the temperature variation of a saturated thermionic current  $i$  per unit area is represented by plotting  $\log (i/T^2)$  against  $1/T$ , it has been customary to identify the slope and the vertical intercept of the graph with the electronic work function  $\phi$  and the logarithm of the emission constant  $A$ , respectively, in Richardson's equation

$$i = AT^2 e^{-\phi/kT}$$

This identification has been reasonably successful for materials of a high degree of homogeneity, since they exhibit straight "Richardson plots" whose measurement offers values of  $A$  and  $\phi$  not inconsistent with electronic data from other sources. On the other hand, certain materials exhibit curved plots, indicating at once that no fixed  $A$  and  $\phi$  can be recorded. Others, with which we are here concerned, give plots which appear straight over an observed range but suggest values of  $A$  and  $\phi$ , disagreeing so radically with established theory or with indirect experiments that they have been regarded as anomalous. We prove in one instance that an extension of the range reveals such a plot as part of a curve, and that the curve contains implicit quantities not solely electronic and therefore not expressed by even a sequence of simple Richardson equations. Hence the slopes and intercepts of tangents to this curve are not identifiable with values of  $\phi$  and  $\log A$ .

## 2—THE INTERPRETATION OF RICHARDSON PLOTS FOR COMPOSITE SURFACES

Features having something in common with this instance are presented by the multiple plots of the alkalis,\* and the sequence of progressively

\* Reimann, "Thermionic Emission," Chapman and Hall (1934).

decreasing numerical values reported by various workers with "pure" platinum and associated metals\* together with certain more obviously composite surfaces. But the term "composite" is, we suggest, applicable more widely than has been recognized, not only to surfaces deliberately treated by vapour deposition or by internal diffusion of an added constituent, but also to certain metals of considerable chemical purity which are only rarely freed from intergranular traces capable of migrating at high temperatures.

Consider "clean" and "oxygenated" tungsten, which we shall refer to as W and OW respectively without prejudice as to the precise nature of the electronegative surface layer. The check on identification of the work function  $\phi$  is the comparison with photoelectric or contact potential data. The close agreement between the photoelectric threshold and the Richardson plots determines  $\phi$  for pure tungsten as  $4.54 \pm 0.02$  electron volts, but the plot for OW is usually quoted as giving 9.2 electron volts,† which is 50% in excess of the value deduced from the very reliable contact potential difference between W and OW measured by Reimann,‡ while photoelectric currents are here undetectable. The check on identification of the emission constant A is theoretical but of high reliability, the modern equation

$$A = (1 - r) \left( \frac{4\pi mk^2 e}{h^3} \right) \\ = (1 - r) \times 120 \text{ amps cm}^{-2} \text{ deg}^{-2},$$

where  $r$  is the reflexion coefficient, differs only by a factor of two from those which it superseded. Most pure metals, including W, exhibit values between 50 and 100  $\text{amps cm}^{-2} \text{ deg}^{-2}$ , agreeing in order of magnitude with the theory, since  $(1 - r) < 1$ . For OW, however, the Richardson plot usually quoted gives the extraordinary value for A of  $5 \times 10^{11}$  in the same units.

Explanations of anomalous constants have previously been attempted within the scope of still accepting the slope and intercept of the plot as representing these intrinsic thermionic properties. For instance, temperature coefficients to  $\phi$  itself have been explored, and large values of A have been attributed to the excessive "specific area" of microcrystalline surfaces, but quantitatively the latitude thereby introduced is not sufficient. R. H. Fowler§ has shown the inadequacy of a number of

\* Reimann, "Thermionic Emission," chap. 2 (1934).

† Kingdon, 'Phys. Rev.', vol. 24, p. 510 (1924).

‡ 'Phil. Mag.', vol. 20, p. 594 (1935).

§ 'Proc. Roy. Soc. A', vol. 122, p. 36 (1929).

such suggestions, and for OW has remarked that lack of equilibrium in the experimental conditions may place the numerical results on a different footing from genuine constants.

But the detailed consequences of abandoning the usual identification of the empirical data have not been developed. Therefore, in the present paper we begin by showing in what direction certain inevitable temperature variations of surface equilibrium must modify the graphs which supply such data. We suggest that a large class of experiments involves not only (a) the temperature variation of electron emission from each elementary surface area, but also (b) the temperature variation of surface covering. We then investigate experimentally the case of OW, and prove that an intrusion of temperature coefficients of adsorption and chemical reaction succeeds in masking its electronic properties. We find that these extraneous terms account fully for the most extreme numerical values which inevitably appeared anomalous when taken to represent work function and emission constant of OW. Our experiments exhibit these values as isolated members of a sequence of such "apparent" as distinct from real thermionic functions, this brings the data for OW into the class of curved or multiple plots, making it possible to discard similarly in their case the assumption that slope and intercept of a plot give genuine, even though changing, thermionic constants.

### 3—PRINCIPLE FOR ELECTRONEGATIVE SURFACE LAYERS

In fig 1 the lines *bc*, *bd*, represent idealized Richardson plots, the slope deciding the work function while the vertical intercept at zero abscissa is measured to obtain  $\log A$ . To a first approximation we neglect temperature variation of actual work functions, and assume that true Richardson plots are straight. Since an electronegative layer such as oxygen depresses the emission, let *bd* be the idealized plot for a surface completely covered with oxygen and *bc* for a completely uncovered surface of pure metal. The phenomenon with which we are concerned is most simply exhibited by thus assuming that  $A$  is the same for both, but if, as might well occur, the reflexion coefficient is greater for the covered surface, *bd* may be displaced downwards with the same slope and no generality lost from the argument. It cannot be displaced upwards, giving intersection of the two plots, as that would imply that some abscissa could be chosen for which the oxygenated surface would give a greater emission than the pure metal, contrary to all experience of electronegative layers.



covered metal. The amount of this excess is a function of the various temperature coefficients of adsorption and reaction which maintain the sequence of fractional gas coverings.

Once the possibility of this alteration in interpretation of plots has been established, it is necessary to decide whether the reported "constants" for oxygenated tungsten are not real thermionic functions but tangents to such a transition plot. Accordingly, we devise experiments covering a larger portion of the range between *bc* and *bd* than has hitherto been available, to demonstrate the curvature, to show to what accuracy certain regions may simulate linearity, and to ascertain whether the steepest portions are dependent on gas pressure and therefore not representative of a fully covered surface.

#### 4—REPLENISHMENT OF EVAPORATION LOSSES

The following experimental conditions will correspond to the distinction we have drawn between a true Richardson plot for a given state of composite surface and a transition plot representing passage from state to state. For the former to be obtained, yielding  $A$  and  $\phi$ , the constituents of the surface layers must remain in the same proportion and in the same state of aggregation throughout the temperature range, while the latter type of plot, to which we have suggested many accepted data belong, will only be repeatable and reversible if loss or change in aggregation in heating is balanced by complete recovery in cooling through the same range. The first condition is readily satisfied by the well-known contaminants which increase instead of decrease the emission, *e.g.*, caesiated tungsten can be made to yield a true Richardson plot because currents can be obtained at low enough temperatures for evaporation to be negligible.

The investigation of oxygen meets particular experimental difficulty, since any oxygen layer reduces the emission of tungsten to about  $10^{-5}$  of its normal, making high temperatures essential for currents to be detectable. At these temperatures evaporation cannot be neglected, and in a previous paper\* we have given oscillographic evidence contrasting the duration of surface lifetime of oxygen itself and of oxide, an order of magnitude of a second being reached at about  $2400^{\circ}$  K. for the former and below  $2000^{\circ}$  for the latter. Unless the surface is surrounded by oxygen, these properties entirely prevent true Richardson plots or even reversible transition plots from being obtainable. But, owing to the pressure dependence of the above oxidation, the supply of gas cannot be increased

\* Johnson and Vick, 'Proc. Roy. Soc. A', vol. 151, p. 296 (1935).

indefinitely in the hope of obtaining a full oxygen layer approaching static equilibrium, and the surface structure must be regarded as in dynamic equilibrium, the rapidity of replenishment itself accelerating the evaporation. In addition, the pressures used must not become high enough for ionization by collision to complicate the observed currents.

### 5—EXPERIMENTS

*a—Accuracy of Pressure Maintenance*—In the only recorded experiments of this type, from which the  $A$  and  $\phi$  are quoted, Kingdon\* admitted oxygen throughout at a rate designed to balance the "clean up" due to the oxide volatilizing from the filament and depositing on the walls. He then found that his results did not vary with alteration of this rate of admission, and concluded that the surface was kept fully covered and that the slope and intercept of his plot gave the  $\phi$  and  $A$  of OW itself. But at pressures below  $10^{-3}$  mm, multiples of any small admission do not necessarily yield multiples of gas pressure, the adsorbing capacity of the vitreous walls varying so greatly with time since their last baking that the loss of gas ranges from a few per cent to nearly 100%. Hence we adopt the opposite course of ceasing admissions long enough before the experiment (*e.g.*, 12 hours) to enable equilibrium with the walls to be complete, and making the enclosed volume large enough for subsequent loss by filament oxidation to be negligible. Low pressures can then be maintained and controlled by the nature and level of refrigerant at the several traps.

*b—The Thermionic Tube*—The emitting surface is a readily exchangeable filament 5 cm. long, 0.0101 cm. diameter, of thorium-free tungsten kindly given by the G. E. C. Research Laboratories, Wembley, emission from the isothermal central portion is collected by a nickel cylinder 1 cm. long and 1 cm. diameter with guard rings 2 cm. long†. These cylinders and the molybdenum spring mounting, etc., are heated in hydrogen and then *in vacuo* at 900° C. before assembly. During evacuation of the assembled tube, high frequency heating of the metal and oven baking of the pyrex walls is employed until trial Richardson plots guarantee that the steady state of pure tungsten emission has been reached, this is generally after many hours of ageing at over 2000° K., and intermittent flashing at 2600°, for each fresh filament in turn. Temperatures are obtained from filament currents, using the Jones-Langmuir tables.‡ The smallest anode

\* 'Phys. Rev.', vol. 24, p. 510 (1924)

† Johnson and Vick, 'Proc. Roy. Soc.', A, vol. 151, p. 296 (1935)

‡ Jones and Langmuir, 'Gen. elect. Rev.', vol. 30, p. 310 (1927).

voltage consistent with saturation is employed, to avoid the necessity for a Schottky correction, which in any case would be unreliable for a composite surface

*c—Measurement of Small Thermionic Currents*—Between  $10^{-8}$  and  $10^{-7}$  amp. a galvanometer is used with a universal shunt. A sequence of transient values is measured during attainment of equilibrium at each new temperature, but these are not discussed here, each recorded current representing the final steady value for each temperature. To extend sufficiently the temperature range, currents down to  $10^{-14}$  amp have to be measured. The usual electrometer methods for this region have the disadvantage, apart from their sensitivity to disturbance, that the time required for reading would prevent the detection of drifts, which are in our case important. We therefore pass the thermionic current through a known high resistance, apply the resulting potential difference between the grid and filament of a triode valve, and, by means of a potential divider, reset the grid bias until the anode current indicated by an ordinary galvanometer returns to its original value. The standard types of triode have an impedance between grid and filament of not greater than  $10^6$  ohms, so that resistances much in excess of  $10^6$  ohms cannot be placed in parallel with them for accurate measurement. We employ the Osram Type T "electrometer triode",\* which is designed to have the highest possible grid-filament impedance; its grid circuit has a resistance of  $10^{17}$  ohms, while the residual grid current is  $10^{-16}$ ,  $5 \times 10^{-16}$ ,  $10^{-14}$  amps. approximately for anode potentials of 3, 4, and 6 volts respectively. The actual circuit used is a modification of that devised by Morton† for the determination of glass electrode potentials. The grid potential can be changed by any amount up to 1.50 volt with an accuracy of 0.0005 volt. All the necessary potentials are derived from a single accumulator, which, together with all the circuits associated with the electrometer, is enclosed in earthed metal casing.

*d—Construction and Measurement of High Resistances*—Resistances between  $10^6$  and  $10^{13}$  ohms were constructed to the general design given by Curtiss ‡. A narrow longitudinal grinding on pyrex rod is filled with graphite and rubbed down. Contact is made by cast solder ends and the whole coated with "Synobel Insulating Varnish NX 5516" and baked at  $110^\circ \text{C}$  for three hours. Tests between 0.1 and 10 volts showed that Ohm's law is obeyed to within 0.1%.

\* Warren, 'G E C JI,' vol 6, p 118 (1935)

† 'J. Sci. Instr,' vol 9, p 289 (1932).

‡ 'Rev Sci Instr,' vol 4, p 679 (1933)

Up to  $10^9$  ohms the high resistances can be measured by the leakage of a standard condenser. Beyond this value we employ a method of comparison, using the electrometer. Current from a low resistance source is passed through a known high resistance  $R_1$  and unknown  $R_2$  in series. With  $R_2$  short-circuited by a soldered wire the potential difference  $E$  across  $R_1$  is measured by the electrometer. Then  $R_2$  is brought into circuit and the new potential  $e$  across  $R_1$  is measured. Then

$$R_2 = R_1 \left( \frac{E - e}{e} \right)$$

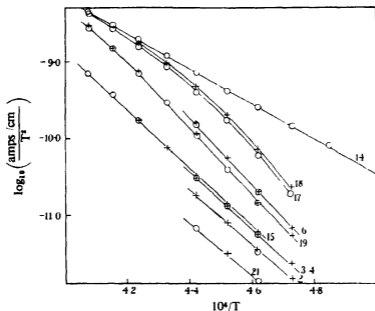


FIG 2—High temperature experimental plots. Curves 2, 3, 4, 6, filament 7, curves 14, 15, 17, 18, 19, filament 8, curve 21, filament 10

if we assume that  $E$  is unaltered by the addition of  $R_2$  in series with  $R_1$ . This is justified since  $R_1$  is never less than  $5 \times 10^8$  ohms. The resistance values were checked at intervals and, except for a more rapid change during the first week after baking, there was found only a slow rise of 1–2% in three months.

## 6—RESULTS AND CONCLUSIONS

In fig 2 are given some of the results between  $2000^\circ \text{K}$  and  $2500^\circ$ , obtained with the galvanometer. Each line includes points for ascending ( $\times$ ) and descending ( $O$ ) temperatures, showing constancy of pressure and

reversibility The lines corresponding to the largest pressures are to the bottom of the graph; the straight line at the top is one of the Richardson plots taken with every precaution for a clean W surface, and gives  $\phi = 4.55 \pm 0.03$  electron volts and  $A = 90$  amps  $\text{cm}^{-2} \text{deg}^{-2}$ . As we should expect, at the highest temperatures the lines approach asymptotically the line for clean W, but at the lower temperatures even of this range the slopes are approaching Kingdon's, the values for curves 6 and 19 (*e.g.*) being about 8.7 electron volts. That the surface layer is not

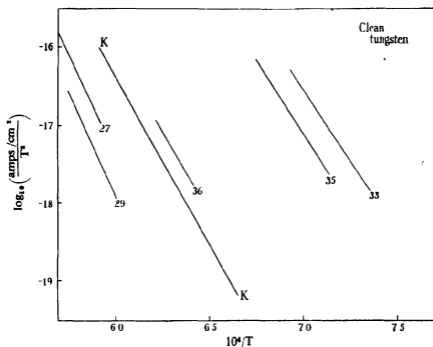


FIG. 3—Low temperature experimental plots

saturated is shown by the variation of current with pressure, although the change in slope with pressure is comparatively small.

With the electrometer, the main series of measurements, over a wide temperature range, was made with the pressure maintained constant, using the methods of § 5a. Other measurements over parts of the range were made at different pressures. At the lowest temperatures, a set of readings was taken with the same high resistance in the electrometer input, the temperature step for each pressure being adjusted to give the same range of thermionic currents. The results, together with Kingdon's line KK, are plotted in fig. 3 and show that even here the surface layer is not saturated, since we have lines on each side of KK. The slopes

gradually decrease with pressure, each line is approximately straight in this region, and the slope of Kingdon's line is confirmed

Each set of measurements made at the main pressure was plotted separately and the resulting lines redrawn on a large scale, together with that for the same pressure from fig 2. A curve drawn through all these lines then represents the change in emission from OW in a fixed pressure of oxygen over this wide temperature range. It is found possible to do this with considerable accuracy since, as we have seen, a slight change in pressure between lines produces little change in slope. The final graph

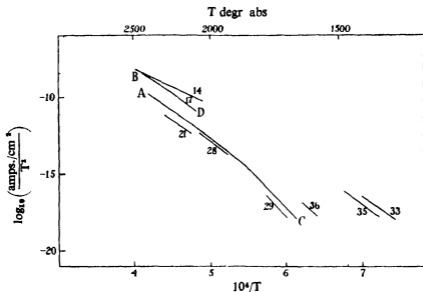


FIG. 4—Experimental transition curves.

is reproduced on a much smaller scale in fig. 4, together with the line for clean W, some of the results for other pressures, and the estimated line for fully oxygenated tungsten. This latter is drawn for the same value of A as for clean W, but with a slope deduced from Reimann's contact potential for OW to W, i.e., a work function of 6.35 electron volts for OW. Since A for OW may be less than that for W, the position shown for this line is an upper limit.

Comparison of these curves between 1300° and 2500° K. with the theoretical fig. 1 supports our view that all except the two limiting straight lines are not true Richardson plots but "transition plots" of the type described in § 3. Confirmatory details may be classified as follows:

- (1) The lines all lie between the boundaries set by clean and fully oxygenated tungsten.

- (ii) Not only do they include higher values of apparent  $A$  and  $\phi$  than those of Kingdon, but they are joined by continuous transition to those characterizing pure W, our extensions above and below the values previously recorded indicate that the latter are isolated members of a sequence constituting a curved plot
- (iii) It is significant that large apparent values of  $\phi$  occur not only at the high pressures and low temperatures, where emission is so small as to have been possibly attributable to a complete OW surface, but also with much larger emissions where no suggestion of more than partial covering of the surface could reasonably have been made.

These pressure effects, giving change of emission at constant temperature, prove that even the highest values of apparent  $A$  and  $\phi$  do not belong to a fully covered ( $\theta = 1$ ) surface, but to a fractionally covered ( $\theta < 1$ ) surface, *i.e.*, to one still capable of further covering if more of the available contaminant could be stabilized on the surface. The value of this fraction  $\theta$  is dependent on temperature because of the several energies of adsorption, activation, evaporation, etc. Hence its own net temperature coefficient, exponential with an index which includes all these energies, inevitably contributes to the slope of the plot and hence to the inferred exponent or apparent  $\phi$ . The amount of the contribution depends on the electrochemical status of the contaminant, for a gas so electronegative that "covered" emission is very small compared with "clean", and which is also subject to such energetic reactions as to have large chemical temperature coefficients, the transition plot even for a nearly full layer can be much steeper than any true Richardson plot. Hence no thermionic plots from such a surface could yield even approximately a true work function unless the condition  $\theta = \text{a constant}$  were completely satisfied.

In deciding whether such a limit could be attained in any thermionic experiment, *i.e.*, at any but very low temperatures, it is the secondary process of rapid oxidation, with volatilization of the products, which distinguishes this gas from other contaminants and impedes the final approach to unity of  $\theta$  for a hot surface. This suggests that knowledge of the work function of OW must be entirely dependent on the indirect evidence of contact potentials since no photoelectric currents are detectable.

We conclude that so far as thermionic data are concerned, these experiments enforce a distinction between any apparent constants  $A'$  and  $\phi'$

measured from a Richardson plot and the true emission constant  $A$  and work function  $\phi$ , such that

$$\begin{aligned} i &= A'T^2 e^{-\phi/kT} \\ &= AT^2 e^{-\phi/kT} [f(\theta)], \end{aligned}$$

where  $A$  and  $\phi$  are the particular values for some definite fractional covering,  $0 < 1$ . Since  $\theta$  in the simplest adsorption isotherm is of the form

$$\theta = F(p) e^{-u/lT} / 1 + F(p) e^{-u/kT},$$

the existence of a variable multiplier to the emission constant and a variable addition to the thermionic exponent is inherent in any experiment when the equilibrium of a trace of contaminant varies over the temperature range of the plot, causing excess in the measured intercept and slope

#### 7—THE RELATION BETWEEN APPARENT $A$ AND $\phi$

Reference to the tangents  $p, q, r$ , of the transition plot in fig. 1 indicates that the intercept or apparent  $\log A$  and the slope or apparent  $\phi$  must increase and decrease together, and trial by measuring ideal graphs shows that a rough approximation to proportionality between the two "constants" is obtainable for any form of plot not too steeply curved. It is of interest to show, fig. 5, how remarkably close the data of our experiments record such a proportionality, since this relation between thermionic constants has been the subject of a large number of investigations by Wilson, Richardson, Fowler, DuBridge,\* etc. Future interpretation of this relationship must be in accord with the fact shown in fig. 5, that it is obeyed by a set of apparent constants which we have proved are not purely thermionic quantities but contain chemical terms. The two straight lines which we reproduce are each obtained from one of the transition plots,  $i e$ , are each characteristic of a given gas pressure, the scattered points being from our curves at other pressures and from data collected by Reimann†. This suggests that if the scattered points published by various writers for other substances could also be grouped according to conditions of "constant reservoir of contaminant", whether internal or external to the emitter, a set of exact lines instead of a single diffuse line would likewise result. We have found this to be so in treating the recorded data for platinum

\* "Proc. Nat. Acad. Sci. Wash.," vol. 14, p. 788 (1928)

† "Thermionic Emission," p. 180 (1934)

It is a pleasure to thank Professor S. W. J. Smith, F.R.S., for his kindness, enabling us to carry out this investigation, and Mr. G. O. Harrison for much help in instrument construction.

### 8—SUMMARY AND APPLICATIONS

We have shown that the temperature coefficients of chemical reaction, at any composite surface whose state cannot be maintained steady, will cause definite changes in the plot of thermionic emission; these lead to intercepts and slopes being measured which neither coincide with nor are

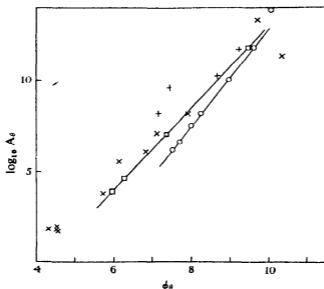


FIG. 5—Apparent work functions and emission constants (O) from curve AC, (□) from curve BD, (+) from other curves, (x) Reimann

even intermediate between the genuine thermionic constants for bare or covered surface. By means of a series of experiments on the pressure and temperature dependence of emission from a tungsten oxygen interface, we have shown that the "anomalous" constants of oxygenated tungsten are examples of the above principles.

The investigation is capable of further application as follows

(a) If lateral and normal migration of one component through the surface layers of another component is substituted for gas adsorption, similar considerations may be applied, *e.g.*, to platinum and the alkalis, with reasonable prospect that the ordered sequence of their apparent

constants reported under different conditions may similarly be simplified by recognizing that they contain temperature coefficients of diffusion, etc.

(b) For tungsten, where volume diffusion of impurity is slight, these data which contain  $\theta$  implicitly can, in principle, be made to yield information concerning the progressive change of  $\theta$  with temperature and pressure.  $\theta$ , however, defined through the work functions as in the dotted straight lines of fig. 1, is not simply proportional to the number of adsorbed particles. Accordingly, we deal elsewhere with the application of our method to the investigation of adsorption processes themselves, as involving theories not required in the present investigation

---

## Dissociation Constants and Structures of Zwitterions

By A. NEUBERGER

(From the Department of Pathological Chemistry, University College Hospital Medical School)

(Communicated by C. R. Harrington, F.R.S.—Received 30 June, 1936)

### I—THEORETICAL

Dissociation constants of amino-acids in relation to their structures have been discussed in recent years in several publications (Schmidt, *et al.*, 1929, Cohn, 1931, Greenstein, 1931, Melville and Richardson, 1935). A more quantitative treatment seems desirable, however, and such a treatment is attempted in this paper.

If in the aliphatic acid  $R-CH_2-COOH$  one of the hydrogen atoms attached to the  $\alpha$ -carbon atom is replaced by the positively charged  $NH_3^+$  group the ionization of the carboxyl group is increased about 280-fold. If substitution occurs in the  $\beta$ - or  $\gamma$ -positions the dissociation constant increases only about 12- or 5-fold respectively.

This effect can be divided into two parts

- (1) The influence of the charge in so far as it is conducted through the dielectricum of the solvent, this may be termed the charge effect.
- (2) The influence of the substituent which is transmitted through the chain of the molecule; this may be called the chain effect.

The chain effect comprises that part of the total charge effect, which is

transmitted through the molecule and not through the solvent, together with all changes induced by the distortion of the electronic configuration of the molecule.

#### CALCULATION OF MOLECULAR DIMENSIONS OF AMINO ACIDS

(a)—*Calculation from Dissociation Constants in One Solvent*—A quantitative treatment may be developed by investigating the energy changes involved in ionization

The dissociation constant  $K$  of an acid at the absolute temperature  $T$  is related to the free energy of ionization  $F$  by the equation

$$e^{-\Delta F/RT} = K \quad (1)$$

If a substituent be introduced into an acid the dissociation constant and, hence,  $F$  will in general be altered. In the simplest case the substituent carries a charge; examples of this kind where the charge is negative are afforded by dicarboxylic acids and dithiophenols, and have been treated by many authors. If the substituent carries a positive charge the electrical work can be calculated in exactly the same way, save that the sign is reversed. The acid  $^+H_3NCH_2COOH$ , for example, will give up hydrogen ions more readily than the acid  $CH_3COOH$ , since the positive charge of the substituent repels all similarly charged particles. In other words, the work necessary to remove proton from the carboxyl group will be smaller in the substituted acid.

If  $e$  is the charge of an electron and  $\psi$  the potential produced by the positive charge of the substituent at the distance  $r$ , which is the distance between the positive charge of the substituent and the carboxylic hydrogen atom, then the electrical work gained by removing the proton to infinity is given by the equation

$$W = e \psi \quad (2)$$

The difficulty arises in the evaluation of the potential  $\psi$ . Bjerrum (1923) has calculated  $\psi$  with the aid of certain simplifying assumptions which may be stated as follows.

(1) The potential of any one ion is not influenced by fields of other ions in the solution (Debye-Hückel effect); this condition is fulfilled at infinite dilution.

(2) Propagation of a non-electrostatic effect through the chain of the molecule does not exist, this assumption is certainly incorrect if the substituent is not very far removed from the dissociating group.

(3) The dielectric constant ( $D$ ) of the solvent is valid for the calculation of Coulomb forces in the immediate neighbourhood of ions; this assumption again cannot be correct for two reasons: firstly, the effect of the charge is conducted not only through the solvent but also through the molecule, and secondly, the structure of a highly polar solvent will be changed in the immediate neighbourhood of ions owing to electrical saturation and electrostriction. The structure of liquid water is still imperfectly understood, and it seems at present impossible to treat quantitatively the much more complicated conditions prevailing in the immediate neighbourhood of ions. Ingold (1931) has introduced corrections for the calculation of potentials in the surroundings of ions which must be regarded as qualitative in character and equivalent with the assumption that  $D$  in the immediate neighbourhood of ions is lower than in the bulk of the solvent, reference to his calculations will be made in a later part of this paper.

Accepting the above assumptions as approximations the potential  $\psi$  at a distance  $r$  is given by the equation

$$\psi = \frac{e}{Dr}. \quad (3)$$

By combining (2) and (3) we get

$$w = \frac{e^2}{Dr}, \quad (4)$$

for a single ion, or for a gm-molecule

$$W = \frac{Ne^2}{Dr}, \quad (4A)$$

where  $N$  is Avogadro's number. If the charge effect only is taken into account the distance of the charge from the dissociating group can be estimated as follows

Let us compare glycine and acetic acid having the dissociation constants  $K_1$  and  $K_2$  respectively. The difference between the free energies of ionization must be equal to the gain in electrical energy due to the positive charge of the substituent.

$$\Delta F_{\text{acetic acid}} - \Delta F_{\text{glycine}} = W = RT \ln \frac{K_1}{K_2}. \quad (5)$$

Combining this with equation (4A), we have

$$\frac{Ne^2}{RT \cdot D \cdot r} = \ln \frac{K_1}{K_2}. \quad (5A)$$

If we substitute the values  $\epsilon = 4.774 \times 10^{-10}$ ,  $N = 6.06 \times 10^{23}$ ,  $R = 83.5 \times 10^6$ ,  $T = 298^\circ$ , and  $D = 78.5$ , express  $r$  in Å., and convert to Briggsian logarithms we have

$$r = \frac{3.07}{p_{K_1} - p_{K_2}} \quad (6)$$

A similar calculation of  $r$  may be made by comparing the dissociation constant of glycine ester with the second dissociation constant of glycine.

(b)—*Calculation from Comparison of Dissociation Constants in Two Solvents*—It seems possible to take into account the chain effect by comparing dissociation constants of the unsubstituted and of the substituted acids in solvents of different dielectric constants (Ebert, 1925). Allowing for the chain effect, equation (5) can be written in the form

$$\Delta F_{\text{acetic acid}} - \Delta F_{\text{glycine}} = W + \phi = RT \ln \frac{K_1}{K_2} \quad (7)$$

where  $W$  is defined by (4A) and  $\phi$  is the change in free energy due to the chain effect which might assume positive or negative values. If it is assumed that the chain effect depends on the structure of the molecule only and not on the properties of the solvent,  $r$  can be calculated as follows

If glycine has the dissociation constant  $K_{1I}$  in the solvent I with the dielectric constant  $D_1$  and the dissociation constant  $K_{1II}$  in the solvent with the dielectric constant  $D_2$ , and acetic acid the dissociation constants  $K_{2I}$  and  $K_{2II}$  in the two solvents, we get the equations

$$\frac{N\epsilon^2}{D_1 r} + \phi = RT \ln \frac{K_{1I}}{K_{2I}}, \quad (8)$$

$$\frac{N\epsilon^2}{D_2 r} + \phi = RT \ln \frac{K_{1II}}{K_{2II}}, \quad (8A)$$

subtracting (8A) from (8) we obtain the equation

$$\frac{N\epsilon^2}{RT r} \left( \frac{1}{D_1} - \frac{1}{D_2} \right) = \ln \frac{K_{1I}}{K_{2I}} - \ln \frac{K_{1II}}{K_{2II}} \quad (9)$$

Expressing  $r$  in Å. and converting to Briggsian logarithms we get the expression

$$r = \frac{241}{p_{K_{1II}} - p_{K_{2II}} - (p_{K_{1I}} - p_{K_{2I}})} \left( \frac{1}{D_2} - \frac{1}{D_1} \right) \quad (10)$$

The chain effect is taken fully into account, but the difficulty of correct evaluation of the potential in the immediate neighbourhood of ions still remains

### INFLUENCE OF AN UNCHARGED SUBSTITUENT ON DISSOCIATION CONSTANTS

The influence of an uncharged substituent on the free energy of ionization is related, at least in the case of aliphatic acids, to the dipole moment of the new group (Nathan and Watson, 1933). Here again distinction has to be made between charge and chain effects, but the charge effect of a substituent with zero net charge will decrease much more quickly with the distance than in the case of a substituent with a free charge. If the centre of the positive charge of the dipole is at the distance  $r_1$  from the centre of the dissociating group, and the centre of the negative charge at the distance  $r_2$ , the net potential produced by the dipole will be  $\frac{e(r_2 - r_1)}{Dr_1 r_2}$ ;

if  $r_1 - r_2$  is small compared with  $r_1$  or  $r_2$ , the potential will be approximately proportional to  $r^2$  ( $r$  being the mean distance of the charges of the dipole from the dissociating group) and not to  $r$  as in the case of a charged substituent (*vide* Schwartzenbach and Egli, 1934).

Chain effects will also decrease very quickly with the distance of the substituent from the dissociating group, whether the substituent is charged or uncharged. This is shown, for instance, by the fact that the ultra-violet absorption spectrum of a carbonyl group is very much altered by a substituent in the  $\alpha$ -position, very much less if the same substituent occupies the  $\beta$ -position, and not at all if the substituent is further removed (*vide* Wolf, Briegleb, and Stuart, 1929). It is to be expected, therefore, that the chain effect, in so far as it consists of distortion of the electronic configuration of the dissociating group, is of small quantitative significance, provided that the substituent is separated by several carbon atoms from the dissociating group.

### GENERAL CHARACTERISTICS OF DISSOCIATION CONSTANTS OF $\omega$ -AMINO-ACIDS

Table I gives the dissociation constants of  $\omega$ -amino-acids of varying chain length, those of their esters, and those of the corresponding  $n$ -fatty acids. The  $p_K$  of  $n$ -dodecanoic acid cannot be determined owing to insolubility, but it can be assumed that a value of 4.845 is correct within  $\pm 0.01$ . Such an assumption is justified by the values for the higher fatty acids given by Larsson and Adell (1931) which show that an increase in length of the paraffin chain beyond that of  $n$ -butyric acid has only a very small influence on the ionization of the carboxyl group.

Inspection of Table I reveals several interesting points:

(1) The  $\text{NH}_3^+$  group has a strong influence on the dissociation constant of the carboxyl group which decreases with distance, but which is still quite marked when 11 saturated carbon atoms separate the amino from the carboxyl group; this behaviour is markedly different from that of an uncharged substituent. Table II demonstrates this point very clearly; in the  $\alpha$ -position the effect of bromine is nearly as large as that of  $\text{NH}_3^+$ , but with increasing distance from the carboxyl the effect of bromine falls off much more rapidly, until in the  $\delta$ -position the influence of the  $\text{NH}_3^+$  group is more than four times as great as that of Br. Other uncharged substituents such as OH or Cl behave quite similarly to Br. This marked difference between charged and uncharged substituents is in accordance with the theory developed above.

(2) The  $p_K$  values of primary aliphatic amines vary between 10.4 and 10.65. If only charge effects were taken into account, one would expect that the introduction of a negatively charged carboxyl group into an amine would increase the  $p_K$  so that the  $p_K$  of an amino-acid should be considerably higher than that of the corresponding amine, actually the reverse is the case. This can only be explained by assuming that the "chain effect" of the carboxyl group is opposite to and larger than the charge effect. This marked influence of the carboxyl group on amines is of the same order of magnitude and acts in the same direction as in the case of dicarboxylic acids, where the strengthening of the first carboxyl group is caused, apart from a constant statistical factor, by the chain effect of the  $\text{COOH}$  group. The chain effect of the  $\text{COO}^-$  group decreases more quickly with the distance than the charge effect. In  $\beta$ -alanine the chain effect predominates, the opposing effects are about equal in  $\gamma$ -amino-*n*-butyric acid, and it is not until we reach  $\delta$ -amino-*n*-valeric acid that  $p_K$  assumes a value which is higher than that of the corresponding amine owing to the preponderance of the charge effect.

(3) The  $p_K$  values of the ester decrease with increasing distance of the ester group from the amino group in the manner characteristic of an uncharged substituent.

(4) If the  $p_K$  values of amino-acids are compared with the  $p_K$  values of the corresponding esters, the influence of the negative charge becomes manifest. The introduction of a negative charge into the molecule causes an increase in the  $p_K$  of the amino group which is numerically nearly equal to the decrease in the  $p_K$  of the carboxyl group caused by the introduction of the positively charged  $\text{NH}_3^+$  group. This numerical equality becomes most marked in  $\delta$ -amino-*n*-valeric and  $\epsilon$ -amino-*n*-hexanoic acids where the distances between substituent and dissociating group are sufficiently large to cause chain effects to be small.

TABLE I

Substance	$\rho_{\Sigma_1}$	$\rho_{\Sigma_2}$	$r_1$	$r_2$	$r_{\text{theoret}}$	$\overbrace{r_1 \quad r_2}^{\text{Ingold}}$
Glycine	2 308*	9 772*				
Acetic acid	4 756†					
Glycine ester		7 75‡				
	2 448	2 022	1 25	1 52	3 6 ± 0 5	3 35 3 55
Alanine	2 340§	9 87§				
Propionic acid	4 874					
Alanine ester		7 80‡				
	2 534	2 07	1 21	1 48	3 6 ± 0 5	3 30 3 50
$\beta$ -Alanine	3 600¶	10 190¶				
Propionic acid	4 874					
$\beta$ -Alanine ester		9 130**				
	1 274	1 060	2 41	2 90	4 86 ± 0 5	4 20 4 45
$\gamma$ -Amino- <i>n</i> -butyric acid	4 230††	10 430††				
<i>n</i> -Butyric acid	4 820‡‡					
$\gamma$ -Amino- <i>n</i> -butyric acid ester		9 710§§				
	0 590	0 72	5 20	4 26	6 12 ± 0 5	6 10 5 40

$\gamma$ -Amino- <i>n</i> -valeric acid	4 02 <sup>¶</sup>	10 40 <sup>¶</sup>							
<i>n</i> -Valeric acid	4 821 <sup>   </sup>								
	0 809		3 8		6 12 $\pm$ 0 5	5 15			
$\beta$ -Amino- <i>n</i> -valeric acid	4 270 <sup>§§</sup>	10 766 <sup>§§</sup>							
<i>n</i> -Valeric acid	4 821 <sup>   </sup>								
$\beta$ -Amino- <i>n</i> -valeric acid ester		10 150 <sup>§§</sup>							
	0 551	0 616	5 57	5 0	7 38 $\pm$ 0 5	6 40	5 90		
$\epsilon$ -Amino- <i>n</i> -hexanoic acid	4 430 <sup>**</sup>	10 75 <sup>**</sup>							
<i>n</i> -Hexanoic acid	4 846 <sup>   </sup>								
$\epsilon$ -Amino- <i>n</i> -hexanoic acid ester		10 37 <sup>**</sup>							
	0 416	0 38	7 38	8 11	8 64 $\pm$ 0 5	7 85	8 45		
$\omega$ -Amino- <i>n</i> -dodecanoic acid	4 648 <sup>§§</sup>								
<i>n</i> -Dodecanoic acid	4 845 <sup>¶¶</sup>								
	0 197		15 5		16 2				
Glycylglycine	3 083 <sup>§§</sup>	8 265 <sup>§§</sup>							
<i>N</i> -Acetylglycine	3 685 <sup>§§</sup>								
Glycylglycine ester		7 710 <sup>¶¶</sup>							
	0 602	0 555	5 1	5 53	7 1 $\pm$ 0 5	6 01	6 35		

\* Harned and Owen (1930) † Harned and Ehlers (1933, *a*) ‡ Cohn (1931) § Nims and Smith (1933) | Harned and Ehlers (1933, *b*) ¶ Schmidt, *et al* (1929) \*\* Edsall and Blanchard (1933) †† Ley (1909) ‡‡ Harned and Sutherland (1934), §§ Part II of this paper ||| Larsson and Adell (1931) ¶¶ See text

TABLE II—COMPARISON OF THE DISSOCIATION CONSTANTS OF *n*-ALIPHATIC ACIDS SUBSTITUTED WITH BROMINE AND WITH  $\text{NH}_3^+$ 

Bromo-acids	$p_K$	Diff from $p_K$ of corresponding fatty acid	Amino-acids	$p_K$	Diff from $p_K$ of corresponding fatty acid
Bromoacetic acid	2.845	1.902	Glycine	2.308	2.448
$\alpha$ -Bromopropionic acid	2.967	1.907	Alanine	2.340	2.534
$\beta$ -Bromopropionic acid	4.009	0.865	$\beta$ -Alanine	3.600	1.274
$\gamma$ -Bromobutyric acid	4.585	0.235	$\gamma$ -Aminobutyric acid	4.230	0.590
$\delta$ -Bromovaleric acid	4.711	0.110	$\delta$ -Aminovaleric acid	4.270	0.551

## DIPOLE DISTANCES IN ZWITTERIONS

The present knowledge of the structures of molecules dissolved in polar solvents is very limited.

Data on amino-acid crystals obtained by means of X-ray analysis have been given by Hengstenberg and v. Lenel (1931) and Bernal (1931). Cohn (1935) using these results and accepted values for the distances C—C, C—N, and C—O, has estimated the dipole distance of glycine to be 3.2 Å, the position is much more complicated, however, when we come to structures of zwitterions in solution.

Wyman (1934) has attempted to interpret measurements of dielectric constants of aqueous solutions of amino-acids as showing that aliphatic amino-acids exist in solution as straight-chain molecules having a zigzag arrangement. But Kuhn (1935) pointed out that no measurements of dielectric constants of highly polar solvents such as water allow any quantitative interpretation. The fact that the increase of the dielectric constant of the solution brought about by equivalent amounts of different  $\omega$ -amino-acids rises with the chain length certainly indicates, however, that the dipole distance also rises with the chain length, i.e., no tendency to form ring-like structures exists.

The insolubility of all amino-acids so far known in non-polar solvents renders direct estimation of the dipole moments impossible,\* and it becomes therefore important to obtain information about the structures of zwitterions by other means.

Scatchard and Kirkwood (1932) and Kirkwood (1934) have extended

\* The dielectric measurements of Edsall and Wyman (1935) on *N*-dimethylanthranilic acid in benzene are difficult to interpret. It is uncertain firstly whether the zwitterionic form predominates in benzene and secondly to what extent association takes place.

the Debye-Hückel theory to zwitterions and have been able to correlate the activity coefficients of zwitterions with their dipole distances. Kirkwood (1934), using experiments of Cohn on the solubility of glycine in alcohol-water mixtures in the presence of salts, calculated the dipole distance of glycine to be 3.7 Å. Nearly identical results were obtained by Scatchard and Prentiss (1934) from freezing-point measurements. Approximate values of activity coefficients of long-chain zwitterions, recorded in the second part of this paper, also suggest values of the dipole distances which are in accordance with the theory that these zwitterions are more or less straight-chain molecules.

The difference between  $p_K$  of an amino-acid and the  $p_K$  of the corresponding fatty acid should, if all the assumptions discussed above were correct, give an estimate of  $r_1$  the distance between the centre of the positive charge of the  $\text{NH}_3^+$  group and the centre of the hydrogen atom of the carboxyl group. Values obtained by employing equation (6) are given in Table I, column 3. If similar calculations are applied to the difference between  $p_K$  of the amino-acid and the  $p_K$  of the corresponding ester, values for  $r_2$ , the distance between the centre of the negative charge of the carboxyl group and the dissociating hydrogen atom of the  $\text{NH}_3^+$  group, are obtained,  $r_1$  and  $r_2$  should be almost equal, which is shown to be the case.

The distances  $r_1$  and  $r_2$  are not very different from  $R_1$  the dipole distance, they may be slightly larger, since the distance O—H or N—H in the direction of the chain has to be added. A mean value for  $r_{\text{gly,lin}} = 3.6 \text{ Å} \pm 0.5$  is based on the assumption that no appreciable bending of the molecule occurs. All other values of  $r_{\text{theor.}}$  are based on the assumption that the molecules exist in solution in the straight-chain form having a zigzag arrangement, thus the increase of chain length brought about by the introduction of an additional methylene group is estimated to be 1.26 Å. The increase of  $r$  effected by introduction of a glycine residue as in glycyglycine is assumed to be 3.5 Å in accordance with the X-ray measurements of Meyer and Mark (1928) and Astbury (1933).

Table I shows that the values of  $r$  obtained with the aid of equation (6) are all of the correct order of magnitude. There is very good agreement where the charged substituent is separated from the dissociating group by more than 5 carbon atoms, as in  $\epsilon$ -amino-*n*-hexanoic acid or in  $\omega$ -amino-*n*-dodecanoic acid. Where the distance between substituent and dissociating groups is small, the values of  $r_1$  and  $r_2$  are much below  $r_{\text{theor.}}$ . The fact that a similar behaviour was noted in the case of dicarboxylic acids, suggests that the disagreement in the case of the lower  $\omega$ -aminoacids is not due to any specific interaction between the positive and

negative charges leading to a bending of the chain of the molecule, but rather to the inapplicability of the assumptions involved in deriving equation (6). The two disturbing effects, the change of the dielectric constant of the solvent in the immediate neighbourhood of ions and the propagation of the effect of the substituent through the molecule, are operative only at a short distance from the charge. The actual value of  $D$  in the immediate neighbourhood of a charged particle is probably smaller than that used in obtaining equation (6) and therefore low values of  $r$  are to be expected.

In Table I, columns 6 and 7, values of  $r_1$  and  $r_2$  are recorded using Ingold's evaluations of  $\psi$ . It can be seen that by this method, where correction is made for disturbances in the immediate neighbourhood of ions, values of  $r$  are obtained which agree very well with those calculated on the basis of straight chain structure.

The fact that, by applying a theory based on assumptions which are only approximately correct, we obtain results in agreement with another theory is certainly not absolute evidence that any of the hypotheses is correct. But the fact that the agreement is very close in the case of long chain zwitterions where we would expect equation (6) to hold is certainly significant. The evidence which can be obtained from dissociation constants certainly favours the view that no appreciable bending from the straight-chain structure occurs.

Kuhn (1935) has calculated much smaller dipole distances of zwitterions on the basis of statistical considerations, he assumes, however, that there is absolutely free rotation of the carbon atoms. There is not much experimental evidence for such a view. Dielectric measurements in water are devoid of any quantitative significance, and his and Wyman's formulae have to be regarded as purely qualitative statements.

#### MEASUREMENTS OF DISSOCIATION CONSTANTS IN MIXED SOLVENTS

Amino-acids are insoluble in most pure organic solvents. Data are available, however, for  $p_K$  values of amino-acids in aqueous-alcoholic solutions (Michaelis and Mizutani, 1925, Neuberger, 1934, Jukes and Schmidt, 1934, Ogston and Brown, 1935). All these measurements were made on cells of the type

$H_2$	Amino-acid in aqueous alcohol	Sat KCl	Sat. KCl HgCl	Hg
-------	----------------------------------	------------	------------------	----

Such cells are somewhat unsatisfactory, since they involve a liquid junction between two solvents, but if, e.g., glycine and acetic acid in 90%

alcohol are compared, it can be assumed that the liquid junction potentials are nearly the same in each case and that the difference between the apparent  $p_K$  values thus obtained does not differ very much from that between the true  $p_K$  values. All these measurements were made without extrapolation to  $\mu = 0$  and the results therefore can only be regarded as approximate.

In Table III the values of  $p_{K_1}$  of glycine and of  $p_{K \text{ acetic acid}}$  in various concentrations of alcohol are recorded together with the values of  $r$ .

TABLE III

% alcohol	Dielectric constant	$p_{K \text{ acetic acid}}$	$p_{K_1 \text{ glycine}}$	$r$
0	78.5	4.71	2.44	1.30 (equation (6))
25	67.0	5.09	2.70	4.25
50	52.5	5.74	3.08	3.85
75	38.0	6.49	3.55	4.85
90	29.5	7.18	3.93	5.20

The measurements were made according to a method described in an earlier paper (Neuberger, 1934),  $\mu = 0.005$ . The values of Wyman (1931) for the dielectric constants of the alcohol-water mixtures were used.

derived therefrom according to equation (10). It is evident that the values are of about the correct order of magnitude.

In Table IV are recorded data for isomeric amino-*n*-valeric acids. These figures are quoted from Jukes and Schmidt (1934), the measurements were made in 72% alcohol. In column 3 are given the values of  $r$  which are obtained from equation (6), whilst the values recorded in

TABLE IV

Substance	$p_K$ in water	$p_K$ in 72% alcohol	$r$ from aqueous data	$r$ from alcoholic data	$r_{\text{theor.}}$
<i>n</i> -Valeric acid	4.81	6.83	—	—	—
$\alpha$ -Amino- <i>n</i> -valeric acid	2.36	3.60	1.25	2.3	$3.6 \pm 0.5$
$\gamma$ -Amino- <i>n</i> -valeric acid	4.02	5.35	3.85	4.6	$6.1 \pm 0.5$
$\delta$ -Amino- <i>n</i> -valeric acid	4.21	5.74	5.10	6.1	$7.35 \pm 0.5$

column 4 are obtained with the aid of equation (10) from the figures obtained in 72% alcohol. The dissociation constant of *n*-valeric acid in 72% alcohol has been derived by extrapolation from the data of Mizutani (1925) and Jukes and Schmidt (1935).

It would be desirable to have more accurate data for the dissociation constants of zwitterions in aqueous alcohol from cells not involving liquid

junctions; in any case, however, there is an inherent difficulty in the interpretation of data obtained in mixed solvents, since it is quite probable that redistribution of solvent molecules around ions will occur owing to differences in polarizability of the two types of solvent molecules

A critical review of all the data which are available at present thus provides strong cumulative evidence for the straight-chain structure of zwitterions, even if the straight-chain structure cannot be regarded as conclusively established, all observations can be explained by assuming that such bending of the chain as may occur is not very appreciable

## II—MEASUREMENTS OF DISSOCIATION CONSTANTS OF ZWITTERIONS AND RELATED COMPOUNDS

The object of the measurements recorded in this part was primarily to provide additional data concerning the dissociation constants of  $\omega$ -amino-acids, such data were necessary to permit the development of the theoretical treatment which has been given in Part I

Further use has been made of the data in two directions. It follows from the zwitterionic theory that the change of the apparent dissociation constants of zwitterions with varying ionic strength of the solution should be different from the corresponding change of the dissociation constants of ordinary acids and bases. The respective behaviours to be anticipated are formally developed below and the new data have been utilized to investigate the degree to which the behaviour of zwitterions does, in fact, accord with expectation

Secondly, the new measurements permit the approximate calculation of the activity coefficients of more complicated zwitterions

The measurements have been made on cells of the type



where S is an aqueous solution containing a mixture of an organic acid or base and its corresponding salt in very small concentrations. Ionic strengths have been varied by addition of KCl to the solutions

The potential E measured can be written in the form

$$E = E_0 + E_D + \frac{RT}{f \log e} \cdot \log C_{\text{H}^+} \cdot f_{\text{H}^+}, \quad (1)$$

where  $E_0$  denotes the "ideal" electrode potential at unit mean activity of the hydrogen ion and  $E_D$  the net liquid junction potential. It can be seen that the value of  $E_0$  depends on the values assigned to  $E_D$  and  $f_{\text{H}^+}$ . If Henderson's formula is assumed to be correct, the value of  $E_D$  depends

mainly on the transport number of  $K^+$  Guggenheim and Schindler (1934), using values given by Longworth (1930), and MacInnes and Dole (1931), for the transport number of  $K^+$  and employing values for the activity coefficients of HCl resulting from measurements not involving liquid junctions, obtained for  $E_0$  a value of 333.7 mv at 25°. Measurements on different systems showed that values for dissociation constants and activity coefficients could be obtained which agreed very well with measurements from "cells without transference" or with conductivity experiments

In this way the value of  $f_{H^+}$  as defined in (1) becomes numerically identical with the thermodynamically well-defined magnitude, the mean activity coefficient of the hydrogen ion  $C_{H^+} f_{H^+}$  is now equal to the mean activity of the hydrogen ion and the negative logarithm of this magnitude is termed  $p_H$ . Such a statement about the identity of  $p_H$  and the mean activity of hydrogen ions is approximately correct for solutions containing simple electrolytes, but its validity is very doubtful for complicated systems containing electrolytes of high valency. It has to be emphasized that activity coefficients of single ions as opposed to mean activity coefficients are devoid of thermodynamical significance (Taylor, 1927) and are used in the present paper only as a convenient means of expression.

If the acid HB dissociates into the ions  $H^+$  and  $B^-$  the equilibrium constant  $K_0$  of the reaction is defined by the equation

$$K_0 = \frac{a_{H^+} a_{B^-}}{a_{HB}} = \frac{C_{H^+} C_{B^-}}{C_{HB}} \frac{f_{H^+} f_{B^-}}{f_{HB}}, \quad (2)$$

where  $a$  denotes activity,  $C$  concentration, and  $f$  activity coefficient.  $K_0$  is independent of the ionic strength of the solution.

Using negative logarithms and employing the equation

$$-\log C_{H^+} f_{H^+} = p_H,$$

we can write

$$p_K = p_H + \log \frac{C_{HB}}{C_{B^-}} + \log f_{HB} - \log f_{B^-} \quad (2A)$$

The apparent dissociation constant  $K$  may be defined by the equation

$$p_K = p_H + \log \frac{C_n}{C_{B^-}}, \quad (3)$$

where  $p_K$  depends on the ionic strength of the solution.

It can be assumed that the activity coefficient of the electrically neutral molecule HB is approximately unity up to moderately strong concen-

trations of salt. Then we get for an ordinary acid the relationship which is only approximately correct

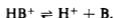
$$p_K = p_{K_0} + \log f_B \quad (4)$$

The activity coefficient of any one ion depends not only on the ionic strength of the solution but also on specific properties of all ions present. But for not too concentrated solutions the following equation approximately holds,

$$-\log f_B = \frac{0.5 \sqrt{\mu}}{1 + \sqrt{\mu}}, \quad (5)$$

where  $\mu$  is the ionic strength (Guggenheim, 1935). Actually this equation corresponds to the original term of the Debye-Huckel theory if the "ionic diameter"  $a$  is assumed to be 3.08 Å.

For the dissociation of a base or—using Brönsted's terminology—of a cationic acid which dissociates according to the scheme



where  $B$  is a neutral molecule we get the following equations:

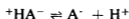
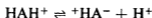
$$p_{K_0} = p_H + \log \frac{C_{HB^+}}{C_B} + \log f_{HB^+} - \log f_B \quad (6)$$

$$p_K = p_H + \log \frac{C_{HB^+}}{C_B} \quad (6A)$$

$$p_K = p_{K_0} - \log f_{HB^+} \quad (6B)$$

From (6B) which again is only approximately correct, it follows that the apparent constant of  $p_K$  of a cationic acid varies with the ionic strength of the solution in the opposite direction from that of an ordinary acid. Thus it should be possible to decide whether a part of any titration curve is due to an acidic or basic group by varying the ionic strength of the solution.

For a zwitterion the dissociation is represented by the steps



We get

$$p_{K_1} = p_H + \log \frac{C_{HAH^+}}{C_{{}^+HA^-}} + \log f_{HAH^+} - \log f_{{}^+HA^-} \quad (7)$$

$$p_{K_1} = p_H + \log \frac{C_{HAH^+}}{C_{{}^+HA^-}} \quad (7A)$$

$$p_{K_1} = p_{K_0} - \log f_{HAH^+} + \log f_{{}^+HA^-}. \quad (7B)$$

If the zwitterion  $^+HA^-$  could be assumed to have unit activity at all concentrations,  $p_{K_1}$  would vary with the ionic strength in the same way as the apparent constant of a cationic acid. But this assumption is not correct. The decrease in activity of an ion in solutions of electrolytes of finite concentration is due to the electrostatic interaction of the ions; an "ionic atmosphere" is formed round an ion due to Coulomb forces. In the case of a zwitterion similar interaction will occur between the charged poles of the zwitterion and ions in the solution. This electrostatic effect will be larger, the larger is the distance between the charges in the zwitterion compared with the "thickness of the ionic atmosphere", the characteristic length  $1/\kappa$  of the Debye-Hückel theory. In other words, the deviation from unit activity will be most pronounced for zwitterions having the positive and negative charges very far apart, it will be small in solutions of small ionic strength but will increase more quickly with increase in ionic strength than the corresponding magnitude of an ordinary ion. These more qualitative assumptions are supported by exact calculations of Scatchard and Kirkwood (1932), who found that  $\log f$  for a molecule of a zero net charge should be approximately proportional to the ionic strength of the solution and not to its square root. Equation (7b) can now be written in the form

$$p_{K_1} = p_{K_1}^0 + \frac{0.5 \sqrt{\mu}}{1 + \sqrt{\mu}} - \beta\mu, \quad (7c)$$

where  $\beta$  is a function mainly of the distance between the charges in the zwitterion but depends probably to some extent on the properties of the salt present. For the second dissociation constant we arrive at a similar equation

$$p_{K_2} = p_{K_2}^0 - \frac{0.5 \sqrt{\mu}}{1 + \sqrt{\mu}} + \beta\mu \quad (8)$$

This different behaviour of zwitterions in the matter of the change of the apparent dissociation constant with the ionic strength of the solution was first pointed out by Guntelberg and Schrödt (1928) in studies upon indicators. If equations (7c) and (8) are regarded as being correct, an approximate estimate of  $-\beta\mu = \log f_{HA^-}$  should be possible.

In order to verify these assumptions, the apparent dissociation constants of several zwitterionic ampholytes and related compounds having varying distances between the charged groups have been measured at different ionic strengths. In preparing some of these ampholytes, several new compounds were obtained which are described in the experimental part.

## EXPERIMENTAL

*Preparation of Compounds**(a)— $\omega$ -Aminododecanoic Acid*

*Ethyl  $\omega$ -Bromoundecanoate*— $\omega$ -Bromoundecanoic acid (10 gm) was esterified according to Walker and Lumsden (1901) After drying over concentrated  $\text{H}_2\text{SO}_4$  in a vacuum the ester crystallized in beautiful needles at about  $5^\circ$  to melt again at room temperature Yield, 93%

*Ethyl  $\omega$ -Cyanoundecanoate*—Ethyl  $\omega$ -bromoundecanoate (10.15 gm) and potassium cyanide (2.75 gm) were dissolved in warm alcohol (74 ml.) and boiled on a water bath for 4 hours The alcohol was then evaporated under reduced pressure and the residue poured into water The oil which separated was extracted with ether and the extract washed once with water An oil solidifying at  $0^\circ$  was obtained by evaporation from the dried ethereal solution and was recrystallized from 60% alcohol, the crystals being drained on a chilled porous plate in the refrigerator The recrystallized product was free from halogen (Found N (Kjeldahl) 5.65%  $\text{C}_{14}\text{H}_{25}\text{O}_2\text{N}$  requires 5.85%) M P about  $10^\circ$  Yield 73%

The combined aqueous liquors from the above experiment gave, on acidification, an oil which was extracted with ether and hydrolysed with concentrated HCl on a water bath for a short time, the resulting solution being evaporated under reduced pressure The crystalline residue was recrystallized from aqueous alcohol, and then had M P  $127^\circ$  which is the M P of decanedicarboxylic acid; 13.1 mg of the crystalline material required 5.55 ml  $N/50$  NaOH, using phenolphthalein as indicator  $\text{C}_{10}\text{H}_{18}\text{O}_4$  as dibasic acid requires 5.70 ml Thus, it can be assumed that the product of hydrolysis is decanedicarboxylic acid, which has originated from a small amount of cyanoundecanoic formed during the reaction, owing to the alkalinity of the potassium cyanide

*$\omega$ -Aminododecanoic Acid Ethyl Ester Hydrochloride*—Ethyl  $\omega$ -cyanoundecanoate (6.8 gm) was dissolved in a small quantity of absolute alcohol containing HCl (2 equiv) and hydrogenated in presence of platonic oxide (Adams) The product crystallized out in the reduction vessel but was dissolving on warming The mixture was filtered, clarified with charcoal, again filtered and evaporated to low bulk under diminished pressure After keeping in the cold for a short time the crystals which had separated were collected and washed with acetone The mother liquor gave on addition of dry ether a further crystalline precipitate Yield 76%

$\omega$ -Aminododecanoic acid ethyl ester hydrochloride is soluble in water and hot alcohol, but practically insoluble in most organic solvents M P  $138^{\circ}$  (Found N (Kjeldahl) 4.85%, Cl (Carius) 12.91%;  $C_{14}H_{30}O_2NCl$  requires N, 5.02%, Cl, 12.70%)

*$\omega$ -Aminododecanoic Acid Hydrochloride*— $\omega$ -Aminododecanoic acid ethyl ester hydrochloride (2.9 gm) was added to concentrated HCl (30 ml) and the solution boiled for one hour, diluted with water, clarified with charcoal, filtered hot and evaporated to a small volume. In the cold a crystalline precipitate appeared which was collected, dried, and recrystallized from water. Yield 76% M P  $163^{\circ}$ , a sample mixed with the original preparation of Le Sueur and Withers (1914) having the same M P (Found N (Kjeldahl) 5.47%,  $C_{12}H_{20}O_2NCl$  requires N, 5.56%)

(b) — *$\delta$ -Aminovaleric Acid*

*$\delta$ -Aminovaleric acid ethyl ester hydrochloride* which has not been described before, was prepared by esterification of  $\delta$ -aminovaleric acid hydrochloride (Schotten, 1884, 1888) with absolute alcohol and hydrogen chloride in the usual manner. The residue obtained on evaporation was taken up in absolute alcohol, addition of ether produced a crystalline precipitate which was collected and recrystallized from alcohol-ether. Yield 90% M P not very sharp  $100$ – $102^{\circ}$ . The substance is slightly hygroscopic (N (Kjeldahl) found, 7.90%,  $C_7H_{16}O_2NCl$  requires 7.71%)

(c)— *$\gamma$ -Aminobutyric Ethyl Ester Hydrochloride*

$\beta$ -Cyanopropionic acid (4 gm) (Dakin, 1917) was dissolved in a small quantity of absolute alcohol containing HCl (2 equiv) and hydrogenated in presence of 0.4 gm of platonic oxide. After 10 hours the hydrogen uptake stopped at 75% of the theoretical amount. After filtering off the catalyst the solution was saturated with hydrogen chloride in order to complete the esterification. The alcoholic solution was concentrated under reduced pressure and the esterification repeated once more. Removal of the alcohol left an oil which crystallized after addition of alcohol and ether. Yield, 64% M P  $70$ – $72^{\circ}$  (Tafel (1900) gives  $65$ – $70^{\circ}$ ) (Found N (Kjeldahl) 8.54%;  $C_6H_{14}O_2NCl$  requires N, 8.38%)

Glycylglycine and glycylglycine ester were prepared from glycine ester by standard methods and were recrystallized twice.

*N*-Acetylglycine was recrystallized from a laboratory sample, the preparation has M P  $202^{\circ}$ .

*Potentiometric Methods*

0.1 *N* calomel electrodes prepared according to Gjaldbaek (1924) were used throughout. The KCl was a very pure "Kahlbaum" preparation recrystallized twice and dried for a week in a high vacuum over  $P_2O_5$ .

The water was redistilled immediately before use from a distillation apparatus fitted with a silica condenser tube and care was taken to exclude  $CO_2$ .

The HCl was prepared by dilution from HCl of constant boiling point. NaOH was prepared from a stock solution according to Clark (1923). The diluted solution of NaOH which was standardized against HCl was free from any appreciable amounts of  $CO_2$  as shown by titration with bromophenol blue and phenolphthalein.

All measurements were made at  $25^\circ \pm 0.03$ .

All alkaline solutions were made up with exclusion of  $CO_2$  and transferred to the hydrogen electrode vessel under hydrogen, which had been freed from  $CO_2$ .

The potentiometer was a Cambridge Company instrument which allowed accurate reading to 0.1 mv. The galvanometer was a Cambridge A.M. standard type with an internal resistance of 450 ohms.

The Weston cell was newly standardized by the National Physical Laboratory.

Great care was taken to obtain absolutely reproducible liquid junctions and cylindrical symmetry at the junctions, a point which has been emphasized by Guggenheim (1930).

The value chosen for  $E_0$  was 334.4 mv, a value slightly higher than that used by Guggenheim (1935), since calomel electrodes prepared at different times which agreed very well amongst themselves, gave values with 0.1 *N* HCl and with the acetic acid-sodium acetate system which were higher by about 0.7 mv than those of Guggenheim.

In most cases it was necessary to correct for hydrolysis. The concentration of  $H^+$  was calculated from the  $p_H$  by formula (9)

$$pC_{H^+} = p_H - \frac{0.5 \sqrt{\mu}}{1 + \sqrt{\mu}}, \quad (9)$$

where  $pC_H$  is the negative logarithm of the  $H^+$  concentration. The concentration of  $OH^-$  is given by the exact formula

$$pC_{OH} = p_{K_w} - p_H + \log f_{OH} - \log f_{H^+} \quad (10)$$

\* I am indebted to Professor J. C. Drummond for the loan of this instrument.

In this paper the activity coefficient of water has been neglected and it has been assumed that  $-\log f_{\text{OH}}$  equals  $\frac{0.5\sqrt{\mu}}{1+\sqrt{\mu}}$ . For  $p_{K^*w}$ , the thermodynamic dissociation constant of water the value of 13.997 given by Harned and Hamer (1933) has been used. Thus we get the less accurate formula (11)

$$pC_{\text{OH}} = 13.997 - p_H - \frac{0.5\sqrt{\mu}}{1+\sqrt{\mu}} \quad (11)$$

The application of formulae (9) and (11) to solutions of ionic strength  $> 0.1$  may lead to small errors in  $K_c$  since equation (5) does not apply to very concentrated solutions.

For the calculation of liquid junctions Henderson's formula has been used. The equivalent conductivities of most organic electrolytes studied in the present investigation are not known. Where no values were available the arbitrary value of  $\Lambda_\infty = 40$  was assumed. The organic electrolytes were present in such small concentrations in all experiments that the error arising from this source could not be  $> 0.15$  mv, even if the mobilities of the ions concerned were five times higher or five times smaller than the assumed value.

## RESULTS

In Table V the results of the potentiometric measurements are recorded, the measured potentials corrected to a hydrogen pressure of 760 mm are given in column 1, whilst in column 2 the potentials are recorded after correction for liquid junction. In column 4,  $\alpha$  denotes the degree of neutralization, i.e., the relative amount of the acidic form in per cent of the total;  $c$  in column 5 gives the total molar concentration of the acid or base present either dissociated or undissociated,  $\mu$  denotes the ionic strength of the solution which was varied by addition of KCl.

The potentials became steady after about 15–20 min and remained constant within 0.1–0.2 mv. for many hours except in the case of glycine ester, where a slow drift was observed, when the  $p_H$  was higher than about 7.2, e.g., at  $p_H$  7.7 a drift of about 0.5–0.8 mv. per hour was noted in 0.008 *N* solution. In very dilute solutions ( $\mu < 0.005$ ) potentials were constant but could often be reproduced in different experiments only within about 1 mv., a fact which has been noted also by other investigators. In the case of  $\omega$ -aminododecanoic acid it was necessary to use solutions containing an excess of the cationic form since the free acid, the zwitterion, is only slightly soluble in water.

TABLE V

	E	E <sub>corr</sub>	p <sub>H</sub>	a	c	μ	p <sub>K</sub>
<i>N</i> -Acetyl glycine	555 5	553 5	3 647	50 6	0 008	0 004	3 647
	533 8	531 8	3 337	25 5	0 008	0 002	3 673
	583 5	581 9	4 184	75 9	0 0075	0 0056	3 664
	556 5	554 6	3 659	50 35	0 006	0 003	3 659
	554 4	553 6	3 632	50 35	0 006	0 023	3 632
	551 5	551 5	3 583	50 35	0 006	0 103	3 583
	550 8	551 2	3 561	50 35	0 006	0 203	3 561
	548 1	548 9	3 502	50 35	0 006	0 503	3 502
Glycylglycine first p <sub>K</sub>	526 9	525 3	3 227	50 0	0 008	0 004	3 088
	506 8	505 2	2 887	79 0	0 008	0 0062	3 088
	552 7	551 1	3 664	25 0	0 008	0 002	3 116
	529 3	527 5	3 264	50 0	0 006	0 003	3 094
	531 3	530 5	3 317	50 0	0 006	0 023	3 152
	532 1	531 3	3 337	50 0	0 006	0 063	3 166
	532 2	532 2	3 344	50 0	0 006	0 103	3 169
	532 35	532 65	3 351	50 0	0 006	0 203	3 164
	532 7	533 5	3 366	50 0	0 006	0 503	3 149
β-Amino valeric acid first p <sub>K</sub>	591 45	590 5	4 322	50 5	0 008	0 008	4 303
	564 4	563 0	3 865	25 3	0 008	0 008	4 294
	619 9	618 5	4 803	75 8	0 008	0 008	4 301
	581 8	591 0	4 338	50 6	0 006	0 016	4 314
	596 1	597 0	4 437	50 6	0 006	0 506	4 409
	593 1	593 1	4 374	50 6	0 006	0 106	4 342
	595 65	596 0	4 424	50 6	0 005	0 205	4 397
	593 7	593 4	4 378	50 6	0 005	0 055	4 351
	593 1	592 5	4 363	50 6	0 005	0 025	4 337
	596 8	597 55	4 449	50 6	0 005	0 405	4 419
	593 5	593 1	4 373	50 6	0 005	0 045	4 346
ω-Aminododecanoic acid first p <sub>K</sub>	585 1	583 7	4 215	25 3	0 006	0 006	4 663
	585 1	584 3	4 225	25 3	0 006	0 026	4 672
	586 9	585 3	4 241	25 7	0 005	0 005	4 669
	587 7	587 0	4 270	25 7	0 005	0 025	4 701
	587 8	587 5	4 280	25 7	0 005	0 055	4 721
	588 2	588 2	4 2909	25 7	0 005	0 105	4 736
	563 1	561 6	3 841	10 11	0 006	0 006	4 671
	564 65	564 95	3 897	10 11	0 006	0 206	4 710
	564 9	564 9	3 897	10 11	0 006	0 106	4 726
Glycylglycine second p <sub>K</sub>	798 0	796 6	7 814	27 58	0 008	0 002	8 233
	853 4	851 9	8 749	75 8	0 008	0 006	8 251
	824 4	822 9	8 259	50 3	0 008	0 004	8 248
	794 5	793 1	7 759	25 0	0 008	0 002	8 236
	822 65	821 55	8 236	50 3	0 008	0 014	8 225

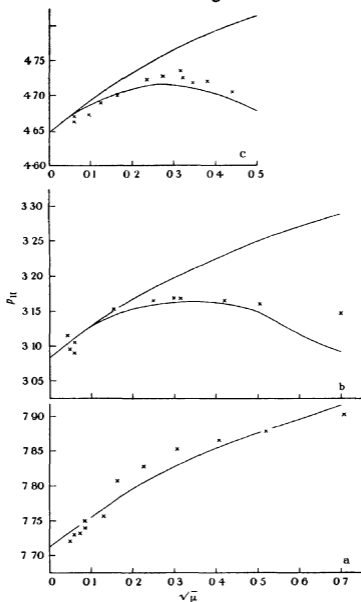
TABLE V—contd.

	E	E <sub>corr</sub>	p <sub>H</sub>	a	c	μ	p <sub>K</sub>
Glyoylglycine second p <sub>K</sub> —(continued)	821.9	821.1	8.228	50.3	0.006	0.024	8.217
	821.1	820.7	8.221	50.3	0.006	0.044	8.210
	820.0	819.8	8.206	50.3	0.006	0.084	8.197
	819.65	819.85	8.207	50.3	0.006	0.164	8.196
	820.6	821.3	8.231	50.3	0.006	0.404	8.220
Glycylglycine ester	755.2	753.8	7.090	19.25	0.008	0.008	7.718
	765.6	764.4	7.265	25.3	0.008	0.008	7.735
	*790.6	789.2	7.689	50.5	0.008	0.008	7.681
	773.2	774.0	7.433	25.3	0.006	0.506	7.903
	771.6	771.9	7.396	25.3	0.006	0.166	7.866
	771.4	771.4	7.388	25.3	0.006	0.106	7.858
	768.6	767.9	7.328	25.3	0.006	0.026	7.808
δ-Aminovaleric acid second p <sub>K</sub>	966.15	964.95	10.660	51.72	0.008	0.012	10.740
	941.2	940.0	10.238	26.43	0.008	0.010	10.737
	963.6	962.4	10.619	51.72	0.006	0.009	10.721
	960.6	961.4	10.600	51.72	0.006	0.509	10.758
	963.15	962.4	10.615	50.19	0.006	0.019	10.746
	957.7	957.3	10.531	50.19	0.006	0.049	10.647
	958.6	959.1	10.561	50.19	0.006	0.409	10.725
	960.9	961.1	10.591	51.72	0.006	0.209	10.726
	959.7	959.7	10.571	51.72	0.006	0.109	10.679
	960.2	959.9	10.574	51.72	0.006	0.059	10.661
	962.4	962.2	10.613	51.72	0.006	0.029	10.696

\* A slight amount of hydrolysis had taken place

The thermodynamic constants were obtained by graphical extrapolation, as shown in Figs. 1 and 2, or by applying equations (4), (5), (6B), (7C), and (8), those values for  $\beta$  in equations (7C) and (8) were chosen which fitted the experimental results most satisfactorily. Both methods—calculation and graphical extrapolation—gave results which agreed within 0.005 or less. It can be assumed that the  $p_K$  values thus obtained are accurate within 0.01; a greater accuracy can probably not be obtained from cells involving liquid junctions. In the case of glycine ester the error might possibly be larger on account of slight hydrolysis.

The dissociation constants of  $\gamma$ -aminobutyric acid ester and of  $\delta$ -aminovaleric acid ester could not be determined by the technique described above, owing to the rapidity with which hydrolysis and/or lactam formation occurs on partial neutralization of solutions of the ester hydrochlorides. The usual technique of electrometric titration was therefore used in these cases, the junctions being made with a saturated KCl-agar bridge.



Figs 1a, 1b, and 1c— $\times$  Experimental *a*, glycylglycine ester, *b*, glycylglycine  $pK$ , *c*,  $\omega$ -aminododecanoic acid. The curve in fig 1a and the upper curves in figs 1b and 1c have been plotted according to equation

$$pK = pK_s + \frac{0.5 \sqrt{\mu}}{1 + \sqrt{\mu}}$$

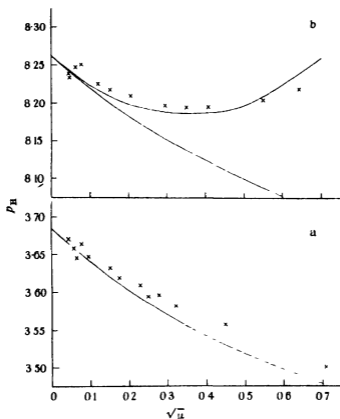
The lower curve in fig. 1b is plotted according to equation

$$pK = pK_s + \frac{0.5 \sqrt{\mu}}{1 + \sqrt{\mu}} - 0.4 \mu,$$

and in fig 1c according to equation

$$pK = pK_s + \frac{0.5 \sqrt{\mu}}{1 + \sqrt{\mu}} - 0.55 \mu$$

Usually, about 20 ml of 0.01*N* solution of the ester hydrochloride were placed in the titration vessel and a continuous stream of hydrogen passed through, while the solution was being brought to the temperature of the thermostat. After about half an hour an amount of 0.1 *N* NaOH



Figs 2c and 2b— $\times$  Experimental *a*, *N*-acetyl glycine, *b*, glycylglycine  $p_K$ . The curve in fig 2a and the lower curve in fig 2b are plotted according to equation

$$p_K = p_{K_s} - \frac{0.5 \sqrt{\mu}}{1 + \sqrt{\mu}}$$

The upper curve in fig 2b is plotted according to equation

$$p_K = p_{K_s} - \frac{0.5 \sqrt{\mu}}{1 + \sqrt{\mu}} + 0.4 \mu$$

corresponding to 5–25% of the ester was run into the solution, readings of the potentials were taken after 1, 2 min, etc.; the times were noted by means of a stop-clock. The  $p_H$  was calculated from the potentials without corrections for barometric pressure or liquid junction potentials; the

higher ionic strengths. This effect is most pronounced in the case of  $\omega$ -aminododecanoic acid, but is marked also in glycylglycine and  $\delta$ -aminovaleric acid (Figs 1*b* and 1*c*). The second values decrease first with increasing ionic strength, as in ordinary acids, then remain constant and finally decrease at higher ionic strengths (fig 2*b*). It can be seen that within the limits of experimental error the experimental results can be well expressed by the equation

$$p_K = p_{K_s} \pm \frac{0.5 \sqrt{\mu}}{1 + \sqrt{\mu}} \mp \beta \mu$$

as postulated

$\beta \mu$  is approximately equal to the logarithm of the activity coefficient of the zwitterion. The values for  $\beta$  obtained from the experimental results are about 0.55 for  $\omega$ -aminododecanoic acid, 0.40 for glycylglycine, and 0.35 for  $\delta$ -amino-*n*-valeric acid, these values are many times higher than those used to accommodate salting-out effects in the extended Debye-Hückel theory.

The values for the activity coefficients of zwitterions thus obtained, are only rough approximations, but it is interesting to note that if these values are used to evaluate  $r$ , the dipole distances of these amino-acids, by means of the theory of Scatchard and Kirkwood (1932), one arrives at quite reasonable values, viz., about 7 Å for  $\delta$ -amino-*n*-valeric acid, 8 Å for glycylglycine, and 11 Å for  $\omega$ -aminododecanoic acid.

I wish to express my gratitude to Professor C. R. Harington, F.R.S., for his continued interest and his help in the preparative work, to Professor A. C. Chibnall for a gift of  $\omega$ -bromo-*n*-undecanoic acid, and to the Academic Assistance Council for a personal grant.

## SUMMARY

### PART I

1—The influence of a charged substituent on the free energy of ionization of a dissociating group has been analysed into an electrostatic part, which is propagated through the solvent and another part, called chain effect, which is transmitted through the molecule. Following Bjerrum's treatment of dicarboxylic acids, the change in the dissociation constant due to substitution has been correlated with the molecular structure of zwitterions. The assumptions involved in these calculations have been discussed.

2—Approximate values for the dipole distances of zwitterions have been obtained from the comparison of their dissociation constants with those of

related compounds. The values thus obtained provide strong evidence for the assumption that  $\omega$ -amino-acids exist in solution as nearly straight-chain molecules

3—Comparison of dissociation constants of zwitterions and corresponding fatty acids in water and in aqueous alcohol supplies a further method for calculating dipole distances. Values thus obtained are of the correct order of magnitude

## PART II

1— $\omega$ -Amino-*n*-dodecanoic acid has been prepared from  $\omega$ -cyano-*n*-undecanoic acid and  $\gamma$ -amino-*n*-butyric acid from  $\beta$ -cyanopropionic acid by catalytic reduction

2—Dissociation constants of the above and other  $\omega$ -amino-acids, their esters, of glycylglycine and *N*-acetylglycine have been measured. The measurements have been made on cells involving liquid junction potentials which were small, reproducible, and could be easily calculated, and the thermodynamic constants were obtained by extrapolation to zero ionic strength

3—It has been shown that the apparent dissociation constants of zwitterions change with the ionic strength of the solution in a manner different from either acids or bases. The measurements allow an approximate evaluation of the activity coefficients of zwitterions

## REFERENCES

- Astbury, W. T. (1933) 'Trans. Faraday Soc.', vol. 29, p. 193  
 Bernal, J. D. (1931) 'Z. Kristallogr.', vol. 78, p. 363  
 Bjerrum, N. (1923) 'Z. phys. Chem.', vol. 106, p. 219  
 Clark, W. M. (1923) 'The Determination of Hydrogen Ions,' 2nd ed. Baltimore.  
 Cohn, E. J. (1931). 'Ergebn. Physiol.', vol. 38, p. 781  
 — (1935) 'Ann. Rev. Biochem.', vol. 4, p. 93  
 Dakin, H. D. (1917) 'Biochem. J.', vol. 11, p. 79  
 Ebert, L. (1925) 'Ber. dtsch. chem. Ges.', vol. 58, p. 175  
 Edsall, J. T., and Blanchard, M. H. (1933) 'J. Amer. chem. Soc.', vol. 55, p. 2337  
 — and Wyman, J., jr. (1935) 'J. Amer. chem. Soc.', vol. 57, p. 1964  
 Fischer, E., and Zemlén, G. (1909) 'Ber. dtsch. chem. Ges.', vol. 42, p. 4878  
 Gjaldback, J. K. (1924) 'K. danske vidensk. Selsk. Math.-fys. Med.', vol. 5 (9)  
 Greenstein, J. P. (1931) 'J. Biol. Chem.', vol. 98, p. 473  
 — (1933) 'J. Biol. Chem.', vol. 101, p. 603  
 Güntelberg, E., and Schrodt, E. (1928) 'Z. phys. Chem.', vol. 135, p. 393.  
 Guggenheim, E. A. (1930) 'J. Amer. chem. Soc.', vol. 52, p. 1315  
 — (1935) 'Phil. Mag.', vol. 19, p. 588  
 — and Schindler, T. D. (1934) 'J. phys. Chem.', vol. 38, p. 533

- Harned, H S, and Ehlers, R W (1933, *a*). 'J. Amer chem Soc.,' vol 55, p 652.  
—— (1933, *b*) 'J Amer chem Soc,' vol 55, p 2379  
Harned, H S, and Hamer, W J (1933) 'J Amer. chem Soc,' vol. 55, p 2194.  
—— and Owen, B B (1930) 'J Amer chem Soc,' vol 52, p 5091  
—— and Sutherland, R O (1934) 'J Amer chem Soc,' vol 56, p 2039  
Hengstenberg, J, and v Lenel, F (1931) 'Z Krystallogr,' vol 77, p 424.  
Ingold, C K (1931) 'J chem Soc,' p 2179  
Jukes, T H, and Schmidt, C L A (1934) 'J biol Chem,' vol 108, p 359  
—— (1935) 'J biol Chem,' vol 110, p 9  
Kirkwood, J G (1934) 'J chem Phys,' vol 2, p 351  
Kuhn, W (1935) 'Z phys Chem,' A, vol. 175, p 1  
Larsson, E, and Adell, B (1931) 'Z phys Chem,' A, vol 156, p 381  
Ley, H (1909) 'Ber dtsh chem Ges,' vol 42, p 354  
Le Sueur, H R, and Withers, J C (1914) 'J chem Soc,' vol 105, p 2800  
Longworth, L G (1930) 'J Amer chem Soc,' vol 52, p 1897  
MacInnes, D A, and Dole, M (1931) 'J Amer chem Soc,' vol 53, p 1357  
Melville, J, and Richardson, G M (1935) 'Biochem J,' vol 29, p 187  
Meyer, K H, and Mark, H (1928). 'Ber dtsh chem Ges,' vol 61, p 1932  
Michaelis, L, and Mizutani, M (1925) 'Z phys Chem,' vol 118, p 135  
Mizutani, M (1925) 'Z phys Chem,' vol 118, p 350  
Nathan, W S, and Watson, W B (1933) 'J chem Soc,' p. 890.  
Neuberger, A (1934) 'Proc Roy Soc,' B, vol 115, p 179  
Nims, L F, and Smith, D K (1933) 'J biol Chem,' vol 101, p 401  
Ogston, A G, and Brown, J F (1935) 'Trans Faraday Soc,' vol. 31, p 574  
Ostwald, W (1889) 'Z phys Chem,' vol 3, p 170  
Scatchard, G, and Kirkwood, J G (1932) 'Phys Z,' vol 38, p 297  
—— and Prentiss, S S (1934) 'J Amer chem Soc,' vol 56, p. 1586  
Schmidt, C L A, Appleman, W R, and Kirk, P (1929) 'J biol Chem,' vol. 81,  
p 723  
Schotten, C (1884) 'Ber dtsh chem Ges,' vol 17, p 2544  
—— (1888) 'Ber dtsh chem Ges,' vol 21, p 2235  
Schwartzbach, G, and Egli, H. (1934). 'Helv. chim. Acta.,' vol 17, p 1183  
Tafel, J (1900) 'Ber dtsh chem Ges,' vol 33, p 2231  
Taylor, P B (1927) 'J phys Chem,' vol 31, p 1478  
Walker, J, and Lumsden, J S (1901) 'J Chem Soc,' vol 79, p 1191  
Wolf, K L, Briegleb, E G, and Stuart, H A (1929). 'Z phys Chem,' B, vol. 6,  
p 163  
Wyman, J, jr (1931) 'J Amer chem Soc,' vol 53, p 3292  
—— (1934) 'J Amer chem Soc,' vol 56, p 536
-

# A Quantum Mechanical Discussion of the Cohesive Forces and Thermal Expansion Coefficients of the Alkali Metals

By H. FRÖHLICH

(Communicated by N. F. Mott, F.R.S.—Received 7 July, 1936)

1—The first successful calculation of the cohesive forces in metals was made by Wigner\* and his collaborators, who have obtained wave functions for electrons in metallic Li and Na by numerical integration. The purpose of this paper is twofold: firstly, we shall show that good approximate wave functions for the alkali metals can be obtained by simple analytical methods, the results agreeing well with those of the more exact calculations and with experiment, and secondly, we shall use these wave functions to calculate for the alkali metals the thermal expansion coefficient, a quantity which has not previously been derived from the theory.

2—Following Wigner and Seitz, we surround each atom by a polyhedron, which we replace by a sphere (the atomic sphere) of radius  $r_1$  defined by

$$\frac{4\pi}{3} r_1^3 = \text{atomic volume.}$$

Within this sphere we take for the potential energy  $V(r)$  that of an electron in the field of the ion. Let  $E(r_1)$  be the energy of an electron in the lowest state in the lattice; then  $E(r_1)$  is given by the Schrödinger equation†

$$\frac{d^2\psi}{dr^2} + \frac{2}{r} \frac{d\psi}{dr} + (E(r_1) - V(r))\psi = 0, \quad (1)$$

together with the boundary condition

$$\frac{d\psi}{dr} = 0, \quad r = r_1 \quad (2)$$

\* Wigner and Seitz, 'Phys. Rev.', vol. 43, p. 1804 (1933), vol. 46, p. 509 (1934), Wigner, 'Phys. Rev.', vol. 46, p. 1002 (1934), Seitz, 'Phys. Rev.', vol. 47, p. 400 (1935), Wigner and Bardeen, 'Phys. Rev.', vol. 48, p. 84 (1935).

† In the following, we shall always use atomic units unless otherwise stated.

For given  $E$ , (2) is in general satisfied by two values of  $r_1$ , which approach each other as  $E$  decreases. Let  $r_0$  be the value of  $r_1$  for which these two values coincide. For smaller values of  $E$  than that corresponding to  $r_0$ , no solution of (1) and (2) exist, so that  $E(r_0)$  is the minimum value of  $E(r_1)$ . We then have, in addition to (2)

$$\frac{d^2\psi}{dr^2} = 0, \quad r = r_0, \quad (3)$$

and hence from (1)

$$E(r_0) = V(r_0)$$

For the alkali metals,  $r_0$  lies outside the radius of the ion, in the region where

$$V(r) = -2/r$$

Therefore

$$E(r_0) = -\frac{2}{r_0} \quad (4)$$

The calculation of  $E(r_0)$  therefore is reduced to a calculation of  $r_0$ .

The wave function  $\psi_0$  which belongs to the energy  $E(r_0)$  is by (2) and (3) nearly constant near  $r = r_0$ , we therefore set, near  $r = r_0$ ,

$$\psi_0(r) = 1 + \phi(r), \quad \phi(r) \ll 1 \quad (5)$$

$$\phi(r_0) = 0 \quad (6)$$

Substituting the wave function (5) in (1) and neglecting  $(E(r_0) - V(r))\phi$ , which is a small quantity of the second order, we find for  $\phi$

$$\frac{d^2\phi}{dr^2} + \frac{2}{r} \frac{d\phi}{dr} + \left(\frac{2}{r} - \frac{2}{r_0}\right)\phi = 0,$$

the equation being valid only near  $r = r_0$ . The solution of this equation satisfying (2), (3), and (6) is given by

$$\psi_0 = 1 + \frac{(r - r_0)^2}{3rr_0} \quad (7)$$

This solution holds for values of  $r$  which are greater than the radius of the ion and for which

$$\frac{(r - r_0)^2}{3rr_0} \ll 1 \quad (8)$$

This condition is satisfied for all values of  $r$  for which we shall require  $\psi_0$ .

3—We shall now give a method of solving the Schrödinger equation (1) for an arbitrary energy  $E$ , if a solution  $\psi_n$  has already been obtained for a certain energy  $E_n$ . We write the energy  $E$  in the form

$$E = E_n + \epsilon, \quad (9)$$

and the wave function

$$\psi = \psi_n(r)f(r), \quad (10)$$

where  $f$  is to be determined. Then we find for  $f(r)$  the equation

$$\frac{d^2 f}{dr^2} + 2 \frac{\Phi'}{\Phi} \frac{df}{dr} + \epsilon f = 0, \quad (11)$$

where

$$\Phi = r\psi_n, \quad \Phi' = \frac{d\Phi}{dr}$$

In this equation no terms have been neglected. It is possible to give for any  $\psi_n$  an approximate solution of (11) for small values of  $\epsilon$ . This solution satisfies in general different boundary conditions from  $\psi_n$ . In our special case, we shall take for  $\psi_n$  the function  $\psi_0$ . As  $\psi_0$  is nearly constant in the greatest part of the atomic sphere,  $\psi'_0$  is zero and (11) reduces to

$$\frac{d^2 f}{dr^2} + \frac{2}{r} \frac{df}{dr} + \epsilon f = 0 \quad (11A)$$

The bounded solution is\*

$$f = \frac{\sin \beta r}{\beta r},$$

with

$$\beta^2 = \epsilon \quad (12)$$

According to (10) and (7), we have†

$$\psi = \left(1 + \frac{(r - r_0)^3}{3rr_0}\right) \frac{\sin \beta r}{\beta r}. \quad (13)$$

As long as  $\psi_0$  is approximately a constant for  $r < r_0$ , (13) is a solution for any energy for those values of  $r$  for which (8) holds. If, furthermore,  $\epsilon$  is small, so that

$$\beta r = \sqrt{\epsilon} r < 1, \quad (12A)$$

we may expand the sine and, using (12), obtain

$$\psi = 1 + \frac{(r - r_0)^3}{3rr_0} - \frac{\epsilon r^2}{6} \quad (13A)$$

\* The general solution is

$$f = \frac{\sin \beta r}{\beta r} + c \frac{\cos \beta r}{r}$$

It can be proved that the constant  $c$  must be very small, so that we may put  $c = 0$ . For Na, for example, the error in the energy is less than 3%.

† In equation (11A) we have neglected the term  $\frac{(r - r_0)^3}{3rr_0}$ , whereas we did not do so in (13). It may easily be shown that this is correct in the sense of our approximation.

Substituting this expression into (21), we find

$$m = \frac{1}{\omega}, \quad a_{n+1} = -a_n \frac{(m-n)(m-n-1)}{2\omega(n+1)}$$

The coefficients  $a_n$  of this series initially decrease, but as  $n \rightarrow \infty$ , however, the series diverges. For values of  $\omega$  and  $r$  for which we shall use this function the third coefficient is only of the order of 1% of the first. Therefore, taking into account the first two terms only, we shall obtain a good approximation. We thus find for the wave function  $\psi$  given by (18)

$$\psi = r^{m-1} e^{-\omega r} \left( 1 - \frac{m(m-1)}{2\omega r} \right) \quad (22)$$

This wave function is a solution of the Schrödinger equation (1) with the eigen-value (15). As pointed out above, at the radius  $r = r_0$  we have to equate the values of  $\psi$  and  $d\psi/dr$  given by (22) to the corresponding values obtained from equation (13), substituting for  $\beta$  the value (12), (15). We thus obtain a relation between the radius  $r_0$  and the ionization energy  $\omega^2$

$$r_0^2 - \frac{1+\omega}{2\omega^3} r_0 + \frac{(1-\omega)^2}{2\omega^5} + \left( \frac{r_0}{\omega} - \frac{1-\omega}{2\omega^4} \right) x \cot x = 0,$$

where

$$x = \sqrt{(2r_0 - \omega^2 r_0^2)}$$

This equation can easily be solved for given values of  $\omega$ . Thus  $r_0$  is obtained as a function of the ionization energy  $I = \omega^2$ . The result may be seen from fig. 2 and Table I.

TABLE I

	Li	Na	K	Rb	Cs
Ionization potential (obs.)	0.397	0.378	0.319	0.308	0.287
$r_0$ (calc.)	2.97	3.24	4.15	4.36	4.80

5—In order to find the total energy, we have to add to (14A) the Fermi energy  $F$ . Since the wave function of the lowest state is nearly flat, as for free electrons, the Fermi energy  $F$  may be set equal to the value for free electrons

$$F = \frac{2}{r_1^2}.$$

Neglecting the small corrections for the correlations between electrons,\* the total energy is, using (14A),

$$U(r_1) = -\frac{2}{r_1} - \frac{r_1^2 - r_0^2}{r_1^3} + \frac{2}{r_1^2}$$

\* Wigner, *loc. cit.*

From this equation the radius  $\rho$ , at which the minimum of the total energy occurs, may be calculated

$$\frac{\partial U}{\partial r_1} = \frac{3(r_1^2 - r_0^2)}{r_1^4} - \frac{4}{r_1^3} = 0, \quad r_1 = \rho, \quad (23)$$

or

$$\rho = 0.73 + (r_0^2 + 0.53)^{1/2} \quad (24)$$

Furthermore, we obtain the heat of sublimation  $S$

$$S = -U(\rho) - I = \frac{2}{\rho} - \frac{0.73}{\rho^2} - I, \quad (25)$$

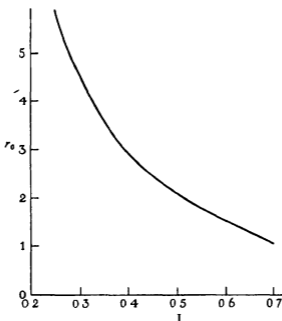


FIG. 2.

and the compressibility  $\kappa$

$$\frac{1}{\kappa} = \frac{1}{12\pi\rho} \left( \frac{\partial^2 U}{\partial r_1^2} \right)_{r_1=\rho} = \frac{0.159}{\rho^4} - \frac{0.116}{\rho^5} \quad (26)$$

#### THERMAL EXPANSION COEFFICIENT

6—Let us denote by  $\nu_i$  the frequency of any one of the normal modes of a crystal, and by  $\gamma$  the quantity

$$\gamma = - \frac{d(\log \nu_i)}{d(\log v)},$$

where  $v$  is the volume of the crystal. If, following Grüneisen,\* one makes the assumption that  $\gamma$  is the same for all the normal modes of the crystal, then it may easily be shown that the thermal expansion coefficient  $\alpha$  is given by

$$\alpha = \gamma \kappa c_v / v,$$

where  $c_v$  is the heat capacity of a volume  $v$  and  $\kappa$  the compressibility. It follows that  $\alpha$  is proportional, for varying temperatures, to  $c_v$ . Since this prediction is in agreement with experiment\* it is probably true that  $\gamma$  is the same for most normal modes.

To obtain  $\gamma$ , we shall thus imagine that a single atom is withdrawn from its mean position a small distance  $a$ , the other atoms being kept at rest. The potential energy of this atom is increased by an amount  $\epsilon(a)$ . Therefore the frequency  $\nu_0$  of its oscillation, according to the well-known formula for the harmonic oscillator, is given by

$$2\pi\nu_0 = \left( \frac{2\epsilon(a)}{a^2 M} \right)^{\frac{1}{2}},$$

where  $M$  is the mass of the atom. The frequency  $\nu_0$  will not be the frequency of any actual normal mode, but since  $\gamma$  is assumed to be the same for all normal modes, we shall not be far wrong if we take

$$\gamma = - \frac{d(\log \nu_0)}{d(\log v)} = - \frac{1}{2} \frac{d(\log \epsilon(a))}{d(\log v)} \quad (27)$$

7—Now we have to calculate the change  $\epsilon(a)$  in the energy of the displaced atom. It is not possible to calculate the energy of a single atom, but only the energy of the whole crystal. Since only one atom is displaced, the energy change of each electronic state depends on the size of the crystal. One should expect, however, to find the energy change of the displaced atom, by solving the Schrödinger equation in its atomic sphere with the same boundary condition (2) as in the ordinary case. In order to show that this boundary condition describes a possible electronic state, we must look for such a deformation of the crystal, in which the lowest electronic state ( $i$  e., the energy of each atom) has changed by  $\epsilon(a)$ . Such a deformation may easily be found. We displace all atoms of a whole plane, for example, the (100) plane, by a distance  $a$  perpendicular to the plane, all atoms of the next parallel plane by  $-a$ , etc. We shall imagine the atomic spheres not to be displaced. The wave

\* Grüneisen, 'Handb. der Physik,' vol 10, p 1 (1926). I wish to thank Professor Mott for calling my attention to the work of Grüneisen and for valuable discussions.

† This has been suggested to me by Mr. K. Fuchs.

function in each atomic sphere is now no longer spherically symmetrical but contains further terms which may be expanded in a series of spherical harmonics. Now it is easy to see that the  $s$  term satisfies our boundary condition just as for undisplaced atoms. The  $p$  term satisfies it in all parts of the atomic sphere which are bounded either by atoms of the same plane as the atom in question, or by atoms of a neighbouring plane.\* For a face-centred cubic lattice, the boundary condition is thus satisfied for the whole atomic sphere. In a body-centred cubic lattice, on the other hand, the atomic sphere is bounded not only by the eight nearest neighbours but also by the six next nearest neighbours. Four of these are in the same plane as the atom in question. For the  $p$  term, therefore, the boundary condition is satisfied in twelve of the fourteen planes which form the polyhedron round the atom. There is no possibility of calculating the energy difference between a face-centred and a body-centred lattice, if we replace the polyhedron by a sphere. Therefore, the error due to the fact that the boundary condition for a body-centred lattice is not satisfied at two planes should be negligible. As we shall find below, higher terms than  $p$  terms have no influence on the calculation of the energy  $\epsilon(a)$ . Thus we shall obtain  $\epsilon(a)$  by solving the Schrödinger equation with the same boundary condition (2) as for the undisplaced atom †. We have not, of course, proved that this leads to the frequency  $\nu_0$  which we would obtain on the assumption of independent oscillations of all atoms. For the calculation of  $\gamma$ , this is irrelevant, since we assume that  $\gamma$  has the same value for all frequencies.

We shall now give the solution of the Schrödinger equation for the displaced atom. Let  $x$  be the distance from the nucleus,  $r$  the distance from the centre of the atomic sphere, and  $\theta$  the angle between  $r$  and the displacement  $a$ . Then we have

$$x^2 = r^2 + a^2 - 2ra \cos \theta \quad (28)$$

We shall denote by  $\Psi$  the wave function and by  $E$  the energy of the electron. If  $E_1$  is the energy for the undisplaced atom, we have

$$E = E_1 + \epsilon(a) \quad (29)$$

Let  $\psi_s$  be the wave function of the  $s$  term of the undisplaced atom (energy  $E$ ),  $\phi_P P_1(\cos \theta)$  and  $\chi_E P_2(\cos \theta)$  respectively the  $p$  and  $d$  wave functions

\* The boundary condition is not exactly satisfied on the whole plane, but in the same approximation as for the undisplaced atom.

† Each atomic sphere forms now an electrical dipole. It may easily be proved that the energy due to the interaction of one dipole with its nearest and next nearest neighbours vanishes exactly for a body-centred cubic lattice.

(The  $P_n(\cos \theta)$  are the spherical harmonics) Then we may write  $\Psi$  in the form

$$\Psi = \psi_E(x) + \lambda \phi_E(x) P_1(\cos \theta) + \mu \chi_E(x) P_2(\cos \theta) + \dots,$$

where  $\lambda$  and  $\mu$  are constants. In order to satisfy our boundary condition, we have first to expand  $\Psi$  as a power series of spherical harmonics with respect to the (undisplaced) atomic sphere. For this purpose, we expand  $\Psi$  as a power series in  $a$ , taking into account only terms up to  $a^2$ . The coefficients contain  $\cos \theta$ . Thus the series can be written alternatively as a series of spherical harmonics, making use of (28) and of

$$\cos^2 \theta = \frac{1}{3} + \frac{2}{3} P_2.$$

Thus we find

$$\begin{aligned} \Psi = & \left[ \psi_E(r) + \frac{a^2}{6} \left( \frac{2}{r} \psi_E''(r) + \psi_E'''(r) \right) - \frac{\lambda}{3} a \phi_E'(r) \right] P_0 \\ & + [-a \psi_E'(r) + \lambda \phi_E(r)] P_1(\cos \theta) + \dots \end{aligned} \quad (30)$$

The dashes denote differentiation with respect to  $r$ . At  $r = r_1$  the boundary condition (2) must be satisfied for the terms with  $P_0$  and  $P_1$  of the expression (30). This leads to the two equations

$$\begin{aligned} \psi_E' + \frac{a^2}{6} \left( \frac{2}{r} \psi_E'' + \psi_E''' - \frac{2}{r^3} \psi_E' \right) - \frac{\lambda}{3} a \phi_E'' &= 0, \quad r = r_1 \\ -a \psi_E'' + \lambda \phi_E' &= 0, \quad r = r_1 \end{aligned}$$

Eliminating  $\lambda$  we obtain

$$\psi_E' = -\frac{a^2}{6} \left( \frac{2}{r} \psi_E'' + \psi_E''' - \frac{2}{r^3} \psi_E' \right) + \frac{a^3}{3} \psi_E'' \frac{\phi_E''}{\phi_E'}, \quad r = r_1$$

As  $\epsilon(a)$  is a small quantity ( $\sim a^2$ ), we expand this expression at  $E = E_1$  with respect to  $E$ . Using the Schrödinger equation, equation (29), and the condition  $\psi_E(r_1) = 0$ , we find

$$\frac{1}{\psi_E} \left( \frac{\partial \psi_E}{\partial E} \right)_{E=E_1} \epsilon(a) = -\frac{a^2}{6} \left( V' + 2(E_1 - V) \frac{\phi_E''}{\phi_E'} \right) + a^4, \quad r = r_1. \quad (31)$$

In this expression  $\phi_E$  is the radial part of the  $p$  function for the energy  $E_1$ .  $\phi$  satisfies the equation

$$\phi'' + \frac{2}{r} \phi' + \left( E_1 - V - \frac{2}{r^2} \right) \phi = 0.$$

We write  $\phi$  in the form

$$\phi(r) = \psi_{E_1}(r) g(r),$$

and find

$$g'' + \left( \frac{2}{r} + \frac{2\psi'_{E_1}}{\psi_{E_1}} \right) g' - \frac{2}{r^2} g = 0$$

As in equation (11), we have  $\psi'_{E_1} \cong 0$  near  $r = r_1$  and therefore

$$g = r + \frac{c}{r^2}$$

It can be proved that the constant  $c$  must be very small so that we find\*

$$\phi_{E_1}(r) = r \psi_{E_1}(r), \quad r \sim r_1 \quad (32)$$

In § 3 we have found that for small  $\varepsilon$

$$\psi_E = \psi_{E_1} \left( 1 - \varepsilon \frac{r^2}{6} \right),$$

or with  $\psi'_{E_1}(r_1) = 0$

$$\left( \frac{\partial \psi'_E}{\partial E} \right)_{E=E_1, r=r_1} = - \left( \frac{r^2}{6} \psi_{E_1} \right)'_{r_1} = - \frac{r_1}{3} \psi_{E_1}(r_1) \quad (33)$$

Thus we obtain† from (31) with (32) and (33), using the Schrödinger equation and  $\psi'_{E_1}(r_1) = 0$ ,

$$\frac{\varepsilon(a)}{a^2} = \frac{V'(r_1)}{2r_1} - (E_1 - V(r_1))^2$$

If we introduce for  $E(r_1)$  the expression given by equation (14A), we find with  $V = -2/r$

$$\frac{\varepsilon}{a^2} = \frac{1}{r_1^3} - \frac{(r_1^2 - r_0^2)^2}{r_1^6}. \quad (34)$$

In this expression, the first term  $\frac{1}{r_1^3} (= \frac{e^2}{2r_1^3})$  is equal to the value of  $\varepsilon/a^2$ , calculated on the assumption of constant electronic charge distribution.

Since

$$v = \frac{4\pi}{3} r_1^3,$$

\* For Na,  $\phi_{E_1}$  has also been calculated by numerical integration using the same potential  $V(r)$  as Wigner and Seitz (*loc cit*) used for the  $s$  function  $\psi_{E_1}$ . This has shown that near  $r = r_1$  (32) is correct within 2%.

† In c.g.s. units this expression is

$$\frac{\varepsilon(a)}{a^2} = \frac{V'(r_1)}{2r_1} - \frac{2m}{\hbar^2} (E_1 - V(r_1))^2$$

we may calculate  $\gamma$  from (27) and (34) and we obtain

$$\gamma = \frac{1}{3} \frac{3r_1^3 + 4r_1^2(r_1^2 - r_0^2) - 6(r_1^2 - r_0^2)^2}{r_1^3 - (r_1^2 - r_0^2)^2}, \quad r_1 = \rho \quad (35)$$

According to (23), the equilibrium value  $\rho$  of  $r_1$  is determined by

$$\rho^3 - r_0^3 = \frac{4}{3} \rho$$

Introducing this expression into (35) we find finally

$$\gamma = 1 - \frac{48}{\rho} \frac{\rho - 1}{2} \frac{46}{16} \quad (36)$$

#### DISCUSSION OF THE RESULTS

8—In § 5 we have obtained the simple formulae (24), (25), and (26) for the radius of the atomic sphere  $\rho$ , the heat of sublimation  $S$ , and the compressibility  $\kappa$

These formulae contain the assumption that the approximation of free electrons is a good one. This assumption has been used on two points: (1) in the calculation of the lowest energy state (§ 3), (2) in the expression for the Fermi energy, which has been taken to be equal to the zero point energy of free electrons. Our assumption is the better fulfilled, the greater the difference between the radius  $r_0$  and the ionic radius. According to fig. 2, this means, qualitatively speaking, that the ionization potential must be small.

In Table II we compare the theoretical results for  $\rho$ ,  $S$ , and  $\kappa$  with experiments, using for  $r_0$  the values of Table I. The experimental value of  $\rho$  is given by

$$\frac{4\pi}{3} \rho^3 = \frac{\text{atomic weight}}{\text{density}}$$

The experimental values of  $S$  are those of Rabinowitsch and Thilo.\* All values must, of course, be taken at the absolute zero of temperature. For the compressibilities this is not possible, since no experimental values for low temperatures exist†. We therefore give (a) the values at room temperatures and (b) values obtained by linear extrapolation to  $T = 0$  whenever this is possible. The values of  $\kappa$  at the zero of temperature, obtained in this way, are certainly too low‡, the right values must lie

\* 'Z phys. Chem.,' B, vol. 6, p. 298 (1930). These values are about 20% higher than those of Sherman, used by Wigner and Seitz.

† Landolt-Börnstein Tables.

‡ Grüneisen, 'Handb. der Physik,' vol. 10, p. 37 (1926).

between (a) and (b). In equations (24)–(26) the units are Rydberg's and Bohr's radii; to obtain in c.g.s. units multiply  $\rho$  by  $0.528 \times 10^{-8}$ ,  $S$  by  $2.15 \times 10^{-11}$ , and  $1/\kappa$  by  $143 \times 10^{12}$ .

TABLE II

	Li	Na	K	Rb	Cs
$\rho$ (Å)—					
Theoretical (equation (24))	1.99	2.13	2.60	2.72	2.94
Experimental	1.69	2.10	2.61	2.82	3.01
$S$ (k-cal/mol)—					
Theoretical (equation (25))	24.5	22	17	16	15
Experimental	46	30	26.5	25	24
$10^4 \kappa$ (cm <sup>2</sup> /kg)—					
Theoretical (equation (26))	11	14	30	35	53
Experimental (a)	9	16	40	52	70
„ (b)	7	10	20	—	—

Except for Li, the values of  $\rho$  are correct to within 4%. With regard to  $S$ , it must be kept in mind that  $S$  is the difference between two much bigger quantities, the total energy and the ionization energy. The difference between the theoretical and experimental values of the total energy is less than 10%. An exact comparison for  $\kappa$  is not possible, but it seems that the theoretical values fit very well (except for Li).

As Seitz (*loc cit*) has shown, the Fermi energy for Li is only about 0.7 of the Fermi energy of free electrons. This accounts for the greater discrepancies for Li. From the point of view of our theory, Li is most likely to show deviations from the model of free electrons, since it has the highest ionization potential.

9—The calculation of the thermal expansion coefficient  $\alpha$  has been reduced by Grüneisen's formula to the calculation of the coefficient  $\gamma$  (27). In § 7 (36) we have calculated  $\gamma$ . In Table III we compare the theoretical values for  $\gamma$  with the experimental values, given by Grüneisen (*loc cit*).

TABLE III

	Li	Na	K	Rb	Cs
Theoretical (equation (36))	2.1	2.0	1.8	1.8	1.8
Experimental	1.2	1.3	1.3	1.5	1.3

The results are not so good as above (Table II), but still satisfactory, if one considers that the thermal expansion coefficient is a quantity which is very sensitive against small changes in the wave function.

I should like to express my thanks to the Academic Assistance Council for a grant, and to Professors Tyndall and Mott for their kind hospitality in their Laboratory

#### SUMMARY

A method is developed which allows the quantitative analytical calculation of the binding of alkali metals, using as only empirical parameter the ionization potential. With this method the lattice constant, heat of sublimation, compressibility, and thermal expansion coefficient have been calculated. Satisfactory agreement with the experimental values is obtained

---

### Fine Structure in the Arc Spectrum of Platinum

#### (A) The Nuclear Spin of Pt 195

#### (B) Even Isotope Displacement

By S. TOLANSKY, Ph D, and E. LEE, B.Sc., Manchester University

(Communicated by W. L. Bragg, F.R.S.—Received 6 July, 1936)

#### 1—INTRODUCTION

The platinum isotope 195 has an odd atomic weight and an even atomic number, that is the nucleus contains an odd neutron. It has been shown elsewhere by one of us\* that the distribution of nuclear spins in the nuclei with an odd neutron is totally different to that in the nuclei containing an odd proton. The number of mechanical moments known for those nuclei with odd neutrons is considerably less than that known for the other type, and for this reason we undertook the examination of the arc spectrum of platinum with a view to ascertaining the nuclear spin from the fine structures.

Dempster† has investigated the isotopic constitution of platinum with the mass spectrograph and reports the following isotopes, 192, 194, 195, 196, 198, the relative abundances being such that 192 is extremely weak, 194, 195, 196 all about similar, and 198 somewhat weaker than these. It

\* Tolansky, 'Nature,' vol. 135, p. 620 (1935)

† 'Nature,' vol. 135, p. 5 (1935)

is to be expected from this that some of the arc lines of platinum will exhibit a fine structure pattern due to the magnetic splitting of the 195 isotope and at the centre of gravity of this pattern will be a strong central component due to the grouping together of the even isotope components. If there is even isotope displacement, the centre component will be split up into three, the intensities of which will be such that two are strong and one weak. (The 192 isotope is so weak that it is being entirely neglected in the whole of this discussion.)

The terms we have examined are of the type  $5d^8 ns mp$ ,  $5d^9 ns$ , etc., that is complex terms, and previous work indicates that this type of term usually exhibits even isotope displacement. It is therefore to be expected that the central component will often be split up. This, indeed, is the case.

A partial gross structure analysis of the Pt I spectrum has been made by Hausmann\* and extended by Livingood †. The allocations of the classified lines examined by us are shown in fig. 1 (using the notation of Livingood). Some of the most prominent lines, and, in fact, some of the lines very helpful for a fine structure analysis lie in the ultra-violet region. We only have at our disposal a two prism glass spectrograph and a silvered Fabry-Perot interferometer, and with this means have studied the fine structures of thirty-six lines in the region  $\lambda\lambda$  6800–4320. After completing the experimental work and whilst engaged upon the analysis, two papers on the fine structures in the Pt I spectrum were published by Jaekel and Kopfermann‡ and by Jaekel§. These authors examined the region  $\lambda\lambda$  5900–2350 and amongst their reported lines are eight of the lines studied by us. The eight structures reported by Jaekel and observed by us are in very good general agreement.

Amongst the twenty-seven terms involved in the lines we have studied, none has the  $J$  value of 0, whilst amongst the ultra-violet lines observed by Jaekel four involve terms with  $J = 0$ . As will be shown later, the nuclear spin of the isotope 195 is  $\frac{1}{2}$ , and owing to the predominance of higher  $J$  values only two fine structure components can usually be detected in a line. The interval between these is the algebraic sum of the fine structure intervals of the two terms involved. The true values in all the terms can only be easily obtained if the transitions can be linked through to a term with  $J = 0$  as Jaekel has succeeded in doing. Amongst the well-determined structures found by Jaekel is the interval for the  $5d^8 6s7s {}^5F_4$

\* 'Astrophys J.', vol. 66, p. 333 (1927).

† 'Phys. Rev.', vol. 34, p. 185 (1929).

‡ 'Z. Phys.', vol. 99, p. 492 (1936).

§ 'Z. Phys.', vol. 100, p. 513 (1936).



results and those of Jaeckel, although entirely different line combinations have been used as the basis for analysis in the two cases. The differences are largely to be attributed to incomplete resolution in the patterns.

#### EXPERIMENTAL

The arc spectrum of platinum was excited in a water-cooled hollow cathode discharge. The cathode, consisting of a cylinder of platinum foil, was about 8 cm long, the diameter being about half an inch. Helium was continuously circulated through the tube until it was quite clean. After this, circulation was not found to be essential. When using the helium at the usual 1–2 mm pressure employed in a hollow cathode tube, the spectrum was only moderately strong, and was not obviously strengthened by the use of argon instead of helium. However, a very great increase in brilliance was obtained by raising the helium pressure to 15 mm. Under these conditions the lines excited appear to be modified somewhat in intensities when compared with the normal pressure. This perhaps accounts for a number of the lines measured by us and not reported by Jaeckel.

The fine structures were studied by means of a variable gap large-aperture silvered Fabry-Perot interferometer (silvered by sputtering in argon) placed in the parallel beam of a two prism glass spectrograph with camera focal length about 125 cm. Exposures varied from a few seconds to two hours. The observed fine structures are shown in Table I. The structures are given in  $\text{cm}^{-1} \times 10^{-3}$ , and to avoid cumbersome repetition later this unit will be conveniently called a millicentimetre<sup>-1</sup> being denoted by  $\text{mcm}^{-1}$ . Below each component a visual estimate of the relative intensity is given in brackets. The line allocations are those given by Livingood. Those components which the analysis proves to belong to the even isotopes are shown in heavy type, and it is to be noted that often a component due to  $^{195}$  is superposed upon one of these. This will be discussed later. In the last column the structures reported by Jaeckel are given for the purpose of comparison, and it is seen that the agreement is good. We appear to have achieved a higher resolution than Jaeckel in some of the lines. This may be due to the fact that our source was water cooled, that of Jaeckel being hot.

In Table I the  $5d$  electrons have been omitted for the sake of avoiding cumbersome repetition. Where one electron is indicated, such as in  $6p\ ^3P_2$  or  $6s\ ^3D_3$ , etc., it is to be understood that a  $5d^9$  group precedes the electron mentioned. When two electrons are given in the table, e.g.,  $6s\ ^3F_4$  or  $6s6p\ ^3G_6$ , then a  $5d^9$  group precedes the two electrons. Un-

TABLE I—FINE STRUCTURES IN THE VISIBLE ARC LINES OF PLATINUM

Wave-length	Allocation	Structure, $\text{cm}^{-1} \times 10^{-3}$		Structure (Jaekel)
		Red	Violet	
6760 0	$6p\ ^3F_4-7s\ ^3D_3$	Single		
6710 4	$6s6p\ D_3\ (Z_2)-7s\ ^3D_3$	0 45 109 (2) (12) (1)		
6523 4	$6s6p\ D_1\ (Y_2)-7s\ ^3D_3$	0 40 74 (6) (4) (1½)		
6398 9	$6s\ ^1G_4-6p\ ^3F_4$	0 ~70 (8) (1)		
6326 8	$6s\ ^1G_4-6s6p\ D_3\ (Z_2)$	0 88 158 (7) (8) (9)		
6318 7	$6s6p\ D_1\ (X_1)-7s\ ^3D_3$	0 75 145 176 (4) (5) (6) (3)		
6283 8	$6s6p\ F_3-7s\ ^3D_1$	0 75 175 (4) (15) (5)		
6026 0	$6s6p\ ^3F_4-6s7s\ ^3F_4$	336 0 273 (3) (25) (4)		
5840 3	$6s\ ^3F_4-6p\ ^3P_1$	0 175 260 815 (1) (4) (4½) (7)		
5514 3	$6s6p\ D_3\ (17_3)-M_3$	163 0 223 (4) (20) (3)		
5478 5	$6s6p\ ^3F_5-6s7s\ ^3F_4$	103 0 76 (2) (15) (3)	105 0 69	
5475 8	$6p\ ^3F_4-7s\ ^3D_3$	0 84 89 140 (4) (5) (6) (2)	0 40 81 135	
5390 8	$6p\ ^3F_4-7s\ ^3D_1$	0 46 91 138 259 (4) (2) (8) (10) (3)	0 49 91 132 258	
5369 0	$6s\ ^3F_4-6p\ ^3F_4$	0 110 145 285 316 (1) (2) (4) (5) (4)	0 135 293	
5301 0	$6s6p\ ^1G_4-6s7s\ ^3F_4$	66 0 40 (1) (7) (2)		
5227 6	$6s\ ^3D_3-6p\ ^3P_1$	0 81 168 308 (9) (10) (12) (2)	0 84 171 308	
5165 0	$6s6p\ ^3D_3\ (12_3)-H_3$	Single (broad)		

TABLE I—(continued)

Wave-length	Allocation	Structure, $\text{cm}^{-1} \times 10^{-4}$				Structure (Jaechel)
		Red		Violet		
5059 5	$6p\ ^3P_2-7s\ ^3D_3$	0	~40			0 ~70
		(7)	(1)			
4998 1	$6s6p\ D_3-M_3$	129	0	79		
		(2)	(13)	(3)		
4980 5	$6s6p\ F_4-O_4$	100	0	131		
		(3)	(15)	(2)		
4853 9	$6s6p\ ^3F_4-M_3$	175	0	227		
		(4)	(20)	(3)		
4658 0	$6s6p\ ^3D_3-6s7s\ ^3F_4$	0	374	438	706	0 405 706
		(4)	(12)	(10)	(5)	
4640 8	$6p\ ^3D_3-7s\ ^3D_1$	Single				
4552 4	$6s6p\ ^3G_3-6s7s\ ^3F_3$	100	0	71		102 0 85
		(2)	(15)	(3)		
4547 9	$6s6p\ D_3\ (Z_3)-E_3$	Single				
4511 2	$6p\ ^3F_4-E_3$	Single				
4498 7	$6s6p\ ^3D_4-7s\ ^3D_3$	0	53			
		(1)	(1)			
4442 6	$6s^3\ ^3F_3-6p\ ^3P_3$	0	171	261	335	
		(1)	(5)	(6)	(7)	
4411 4	$6p\ ^3F_3-6s7s\ ^3F_4$	0	183	238	388	
		(2)	(8)	(7)	(3)	
4327.2	$6s6p\ ^3G_3-6s7s\ ^3F_4$	0	40			
		(7)	(1)			
6263 9	Unclassified	112	0	98		
		(2)	(12)	(3)		
6237 9	Unclassified	120	0	104		
		(2)	(15)	(3)		
5845 0	Unclassified	159	0	125		
		(3)	(21)	(4)		
4879.5	Unclassified	388	0	309		
		(3)	(20)	(4)		
4560 1	Unclassified	335	0	406		
		(5)	(25)	(4)		

fortunately, five lines with very excellent structures have not yet been classified and cannot be made use of in analysis

#### ANALYSIS OF THE PT 195 STRUCTURES

From the fact that in each fine structure pattern only two components are found for the 195 isotope it is at once obvious that the nuclear spin is  $\frac{1}{2}$ . In a transition such as  $\Delta J = 2 \rightarrow 2$  the four resulting components have intensities 13 9 1 1 whilst in a  $\Delta J = 4 \rightarrow 4$  transition the intensities are 50 40 1 1. In view of the predominance of higher J value tran-

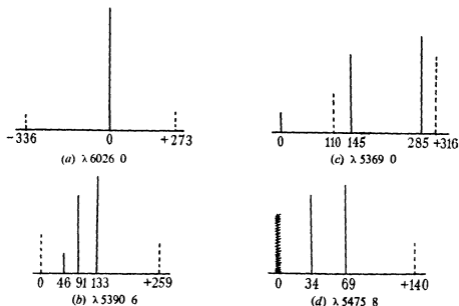


FIG 2

sitions and also because of the difficulties introduced by the even isotopes, it can be seen that in general only two fine structure components will be observable for the 195 isotope. The lines group themselves into obvious types. The first type is that exhibited by  $\lambda$  6026 0 (fig 2a). In this case there is no even isotope displacement so that the strong central component is the sum of the even isotopes. The two outer weaker components (dotted) are attributed to 195. The even isotope line lies at the approximate centre of gravity of the 195 pattern, a point which will be discussed later. The second type of line, of which  $\lambda$  5390 6 is an example, (fig 2b) exhibits even isotope displacement and outer wing components due to 195 (dotted). Variations occur, the 195 pattern in some cases falling within the even isotope pattern, as illustrated in fig 2c. The third type

occurs most frequently, and in this, one of the 195 components falls upon an even isotope line, usually the 198 line. This is shown in fig 2*d*, a hatched line indicating the blend.

As previously pointed out, the absence of a line with  $J = 0$  introduces a difficulty into our analysis. If the measurements are very accurate, or if the very weak components could be measured, an exact analysis could be obtained by considerations of the centre of gravity as shown by an undisplaced even isotope compound line. If the upper and lower  $J$  values differ, then the separations of the 195 isotope lines from the central even isotope line enables an analysis to be carried out. This process implies complete absence of perturbation and is also very sensitive to small errors in measurement. Jaeckel, who has measured structure in four ultra-violet lines involving  $J = 0$ , is able to calculate absolute displacements. We have therefore decided to adopt Jaeckel's value  $783 \text{ mcm}^{-1}$  for the structure in the term  $5d^8 6s 7s^2 F_4$ . On this basis all our lines have been analysed.

The analysis of some of the lines is shown in fig 3. In all the cases illustrated the even isotope lines have been omitted, the discussion on these being left over to Part B. Fig 3*a* shows the analysis of  $\lambda 4411.2$ . The weak dotted transition has not been observed, and this is not surprising since the intensity ratios calculated for the components are 36:27:1. The interval derived for the lower term is  $395 \text{ mcm}^{-1}$ , which compares well with  $383 \text{ mcm}^{-1}$  given by Jaeckel from the study of ultra-violet lines. The lower term  $5d^9 6p^3 F_3$  links through to many others. For example, this gives the analysis of  $\lambda 5475.8$  (shown in fig 3*b*). As seen in fig 3*b*, the interval found for the upper term  $5d^9 7s^2 D_3$  is  $255 \text{ mcm}^{-1}$ . Jaeckel gives  $248 \text{ mcm}^{-1}$ . The line  $\lambda 5390.8$  is shown in fig 3*c* and as the term  $5d^9 6p^3 F_3$  has already been evaluated the analysis shows that the interval for the  $5d^9 7s^2 D_3$  term is  $136 \text{ mcm}^{-1}$ . This value can now be used to analyse the extreme red line  $\lambda 6710.4$ , which involves this term and  $5d^8 6s 6p D_3 (Z_3)$ . The analysis is shown in fig 3*d*. The interval found for the lower term is  $245 \text{ mcm}^{-1}$ . This is in good agreement with Jaeckel's value,  $252 \text{ mcm}^{-1}$  deduced from ultra-violet lines.

The extended details of the remainder of the analysis need not be given. Independent values have often been obtained for one term from many lines. Thus  $\lambda\lambda 6760.0, 4511.2$  both involve  $5d^9 6p^3 F_4$  and give 255 and  $250 \text{ mcm}^{-1}$  respectively for this term (Jaeckel gives 253, obtained from quite different lines). Small errors arise in cases like that shown in fig. 2*d* where there is overlapping of components, or where the 195 structure is too small to be resolved, due to the fact that the intervals in

upper and lower terms are approximately equal. However, in most cases the terms involved occur in other transitions also, so that this difficulty is largely overcome. The full list of term structures observed by us is

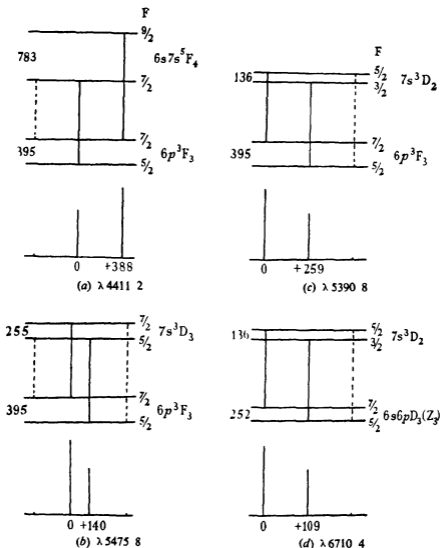


FIG 3

given in Table II. In column 3 the values reported by Jaeckel are given. The structures are given in  $\text{mcm}^{-1}$  and as before, in the term notations, the groups of  $5d$  electrons have been omitted. A negative sign implies an inverted term, that is the larger  $F$  value lies deeper.

TABLE II—FINE STRUCTURE INTERVALS AND INTERVAL FACTORS IN THE ARC TERMS

Term	Interval $\text{cm}^{-1} \times 10^{-3}$		Interval factor
	Authors	Jaeckel	
$M_1$	-228	—	-65
$E_2$	~250	—	~71
$6s7s\ ^1F_4$	788	788	174
$6s7s\ ^3F_3$	900	902	164
$7s\ ^3D_3$	136	126	54
$7s\ ^3D_3$	255	248	73
$6s6p\ D_2\ (17_a)$	158	—	45
$6s6p\ D_1\ (13_a)$	436	—	174
$6s6p\ ^3D_2$	—	308	123
$6s6p\ ^3F_4$	174	—	39
$6s6p\ ^3F_3$	604	609	110
$6s6p\ ^3D_3\ (Z_2)$	252	252	72
$6p\ ^3F_4$	253	253	56
$6s6p\ D_2\ (Y_2)$	200	208	80
$6s6p\ D_1\ (X_1)$	-40	-78	~-39
$6s6p\ ^1G_4$	1006	—	155
$6s6p\ ^3D_2$	77	72	21
$6p\ ^3F_3$	395	383	111
$6s6p\ ^1G_3$	730	719	132
$6p\ ^3P_2$	170	168	67
$6s^2\ ^1G_4$	403	—	90
$6s^2\ ^3F_3$	189	210	80
$6s\ ^1D_2$	480	482	192
$6s^2\ ^3F_3$	170	193	~52
$6s6p\ V_1$	—	284	189
$6p\ ^3P_1$	—	-102	-68
$6s6p\ U_0$	—	0	0
$6s\ ^3D_1$	—	-252	-168
$6s^2\ ^3P_1$	—	197	79
$5d^{10}\ ^1S_0$	—	0	0
$6s^2\ ^3F_4$	—	140	31
$6s\ ^3D_3$	—	-203	-81
$6s\ ^3D_3$	—	696	199
$6s6p\ ^3D_4$	300	626	—

In the last column (4) the interval factors are given. The fine structure interval factor is defined by  $A$  where  $A(F+1)$  is the separation between two fine structure levels  $F+1$  and  $F$ .  $A$  is negative when  $F+1$  lies deeper than  $F$ . Amongst the term values common to the observations of Jaekel and ourselves, the only serious discrepancy in both interval factor of 195 and also in even isotope displacement occurs in  $5d^8 6s6p {}^5D_4$ . As different lines have been employed, we are led to suspect the classification of one of these,  $\lambda 4498.1$  being most suspect.

TABLE III—FINE STRUCTURE INTERVAL FACTORS AND EVEN ISOTOPE DISPLACEMENTS ( $\text{CM.}^{-1} \times 10^{-3}$ )

$5d^8 6s$	${}^3D_1$	-168	(90)	$5d^8 6p$	${}^3P_1$	-68	(75)
	${}^3D_2$	-81	(117)		${}^3P_2$	67	(86)
	${}^3D_3$	199	(82)		${}^3F_3$	111	(56)
	${}^1D_2$	192	(120)		${}^3F_4$	56	(27)
$5d^8 7s$	${}^3D_2$	54	(12)	$5d^8 6s7s$	${}^5F_4$	174	(103)
	${}^3D_3$	73	(20)		${}^5F_5$	164	(103)
$5d^8 6s^2$	${}^3F_2$	80	(200)	$5d^8 6s6p$	${}^5F_6$	39	(107)
	${}^3F_3$	52	(203)		${}^5F_7$	110	(112)
	${}^3F_4$	31	(203)		${}^5G_5$	132	(108)
	${}^1G_4$	90	(83)		${}^5G_6$	155	(107)
	${}^3P_2$	79	(160)		${}^5D_2$	123	~(50)
$5d^{10} {}^1S_0$	0	(0)	${}^5D_3$		21	~(85)	
$M_2$	-65	(107)	$D_2 (13_2)$		174	(107)	
$E_2$	~71	~(0)	$V_1$		189	(75)	
			$U_0$		0	(70)	
			$D_3 (Z_3)$		72	(70)	
			$D_1 (X_1)$	-39	(84)		
			$D_2 (Y_2)$	80	(40)		
			$D_2 (17_2)$	45	(107)		

In Table III the interval factors, which are taken from the mean values in Table II, are rearranged into groups depending upon the electron configurations. In addition to the interval factors, the even isotope displacements (which are derived later) are shown in brackets. In certain cases it is possible to observe the coupling effect due to a single electron forming a multiplet group. Considering first the deeply lying  $5d^8 6s D$  multiplet formed by the addition of the  $6s$  electron to the  $5d^8 {}^3D$  multiplet

of Pt II. As is shown in fig. 4, this approximately fits the coupling scheme suggested by White \*

In this figure the  $5d^9 {}^4D$  terms of Pt II are shown at A. The long black arrow represents the resultant L value of the  $5d^9$  electrons (it equals 2).

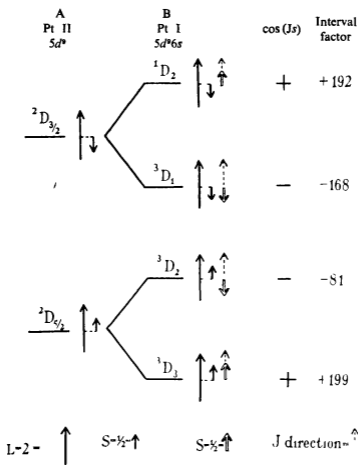


FIG 4

The small black arrow represents the resultant S value of this group (this is equal to  $\frac{1}{2}$ ). From the multiplet analysis it is fairly certain that the coupling approximates to pure  $jj$  coupling. B shows how the  $5d^9 6s^2 D$  multiplet arises by the addition of the  $6s$  electron in  $jj$  coupling. The white arrow represents the spin vector of the  $6s$  electron (this is equal to  $\frac{1}{2}$ ). Now, White has pointed out that to a first approximation when an  $s$

\* 'Phys Rev,' vol. 35, p. 1146 (1930)

electron couples with a complex group like  $5d^9$  the interval factor is proportional to  $(s/J) \cos(Js)$ , that is to say it is determined by the angle made by the direction of the  $s$  electron with the resultant  $J$  direction (the  $J$  direction is shown by the dotted arrow). In pure  $jj$  coupling the ratios of the interval factors of the  $^1D_2$ ,  $^3D_1$ ,  $^3D_2$ ,  $^3D_3$  terms should be as  $+3 \cdot -3 \cdot -2 \cdot +2$ . From the fig. it is seen that the observed intervals are correct as regards signs only. The numerical values do not fit these ratios, but the discrepancies in all but  $^3D_2$  may be due to the incomplete  $jj$  coupling which exists. The smallness of the interval factor of  $^3D_2$  strongly suggests that a perturbation is taking place.

Attention may be drawn to the fact that, apart from perturbation, the smallness of the  $5d^9 6s^3D_2$  term interval factor implies that a considerable part of the total coupling is contributed by the  $5d^9$  electrons. This is at first surprising for in  $jj$  coupling there are  $5d_{3/2}$  and  $5d_{5/2}$  electrons, and at most it might be expected that the  $5d_{3/2}$  electron will not be more penetrating than a  $p_{3/2}$  electron whose degree of penetration is quite small. There is an indication that this term may be perturbed. This is shown by two things, namely the calculated Zeeman effect  $g$  factor for this term is 1.17 according to theory, whilst the value found is 1.01, and secondly, the isotope displacement in this term is about 33% greater than the mean value in the other two terms of the triplet. A perturbation in the interval factor will probably be accompanied by a perturbation in the isotope displacement too. There is always, too, the possibility that a faulty classification has been made. In any event the difference of 31 between the  $^3D_1$  and  $^3D_3$  terms will be due to the  $5d^9$  electron group.

The smaller values given by the  $5d^9 7s^3D$  terms show that the major portion of the interval factor in the previous group is due to the more penetrating  $6s$  electron. Of particular interest is the  $5d^8 6s^3F_2$ ,  $^3F_3$ ,  $^3F_4$  group of terms. These lie fairly close together and are all deep terms. The even isotope displacement is practically identical in the three, a fact which seems to indicate the absence of perturbation. The terms of the group show a regular decrease in interval factor with increasing  $J$  value. If it is assumed, as is usually done, that the two  $6s$  electrons exactly compensate each other and thus make no contribution to the coupling, then it must be concluded that these fairly large interval factors arise entirely from the coupling of the  $5d^8$  electrons, and the differences of the values is due to the rearrangement of these electrons in the respective term configurations. If, therefore, there is no residual interaction due to  $6s^2$  we must conclude, from the evidence in both the multiplets considered, that  $5d_{3/2}$  electrons are capable of appreciable nuclear coupling. If it can be shown, on the other hand, that the  $6s^2$  group has a residual interaction,

then the  $d_{3/2}$  coupling need not be sufficiently great to give an interval factor as large as that of  $5d^8 6s^2 {}^3F_4$ , for instance

Table III shows that amongst the other term groups, the fine structure interval factor increases with  $J$  in the multiplets  $5d^9 6p {}^3P$ ,  $5d^8 6s6p {}^5F$ ,  $5d^8 6s6p {}^5G$  and decreases in  $5d^9 6p {}^3F$ . It is not surprising that large and small interval factors are found in terms with  $6s6p$  electrons, since the  $jj$  coupling allows the presence of a  $p_{1/2}$  electron which is deeply penetrating in a heavy atom like platinum and will at times act in opposition to the  $6s$  electron.

Finally it may be suggested that the penetrating property of the  $5d_{3/2}$  electrons (presumably it is only the  $5d_{3/2}$  electrons which have any marked effect) is linked up with the very high atomic weight. The  $d_{5/2}$  effect may, of course, also contribute to the interval factor.

## 2—EVEN ISOTOPE DISPLACEMENT

On referring back to Table I it will be seen that a large number of the lines exhibit even isotope displacement. In this displacement effect it is to be expected that the three main even isotopes will be equidistant in every term, and therefore in every line which shows displacement. From the intensities of the lines it can be seen that the abundance ratios of the isotopes are 198·196 195 194 1 4 4 5. The 195 abundance is difficult to determine since there are two components to a line, but the value is almost certainly 4 or  $4\frac{1}{2}$ . The abundance ratio can be seen from the intensities in fig. 2.

Previous experience leads one to expect that complex configurations such as  $5d^8 6s^2$ ,  $5d^9 6s$ ,  $5d^8 6s6p$ , etc., will all exhibit even isotope displacement and this at once introduces a difficulty, for if all the observed terms exhibit even isotope displacement the lines will only show differences in term displacements. Thus, even if a complete analysis is carried out successfully, all that will be known is the relative displacement in one term compared with another and not the absolute value, and it is very likely that a constant will have to be added to or subtracted from all the displacements found, in order to arrive at the true term displacements. Amongst the deeply lying terms involving the ultra-violet lines studied by Jaeckel and Kopfermann is the term  $5d^{10} {}^1S_0$ . This is the only term in the spectrum with the  $5d^{10}$  shell completely filled, and Jaeckel and Kopfermann assume that the isotope displacement in this term is very small or zero. This assumption seems to be very reasonable (although there is no theoretical justification as yet), but it must be recognized that it may not be true. Since, however, these authors have referred all their even isotope

displacements relative to this value, we shall do the same in order to compare the term displacements derived by us from entirely different lines. It is to be remembered that a constant must be added to all displacements if later work proves that there is displacement in  $5d^{10}1S_0$ .

Since none of our lines involves the  $5d^{10}1S_0$  term, we must adopt the value given by Jaekel and Kopfermann for some other term involved in our lines, and, for convenience, we adopt the displacement of  $12 \text{ mcm.}^{-1}$  that they give for the  $5d^9 7s^3D_2$  term. On the basis of this value, the displacement of  $45 \text{ mcm.}^{-1}$  in the line  $\lambda 5390.8$  is accounted for in the

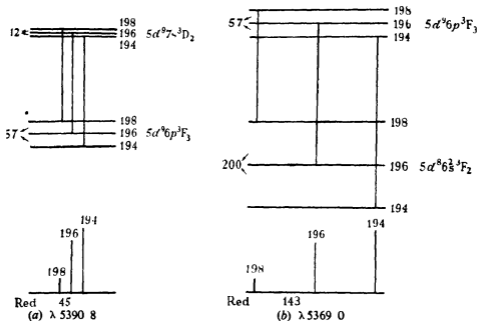


FIG 5

manner shown in fig 5a. This analysis gives  $57 \text{ mcm.}^{-1}$  as the isotope displacement for the lower term  $5d^9 6p^3F_3$ , the value found by Jaekel and Kopfermann being  $55 \text{ mcm.}^{-1}$ . The terms link through to each other as, for instance,  $\lambda 5369.0$  gives 200 as the displacement in  $5d^9 6s^3F_2$ , which is exactly the value found by Jaekel and Kopfermann (see fig 5b). The agreement obtained by widely different lines is exhibited in the term  $5d^9 6s6p D_2$  ( $Y_3$ ), for which we deduce a value of  $49 \text{ mcm.}^{-1}$  from the red line  $\lambda 6523.4$ , whilst the ultra-violet lines of Jaekel and Kopfermann give the displacement as  $47 \text{ mcm.}^{-1}$ . The self-consistency of our measurements can be inferred from the fact that two independent ways of deriving the displacement in  $5d^9 6p^3F_3$  gave 57 and  $59 \text{ mcm.}^{-1}$  respectively, the former being the more reliable value.

In every term (other than  $5d^{10}1S_0$ , of course) the displacements are such that the lightest isotope 194 lies deepest. Presumably 192 if it could be observed would lie still deeper than 194. In Table IV we give

TABLE IV—EVEN ISOTOPE DISPLACEMENTS IN  $\text{cm}^{-1} \times 10^{-3}$ 

Term	Authors	Jaekel and Kopfermann
$M_2$	$\sim 107$	—
$E_2$	$\sim 0$	—
$6s7s\ ^3F_4$	107	$\sim 100$
$6s7s\ ^3F_3$	107	$\sim 100$
$7s\ ^3D_3$	12	12
$7s\ ^3D_1$	$\sim 23$	15
$6s6p\ D_3\ (17_3)$	107	—
$6s6p\ D_3\ (13_3)$	107	—
$6s6p\ ^3D_2$	—	$\sim 50$
$6s6p\ ^3F_4$	107	—
$6s6p\ ^3F_3$	109	116
$6s6p\ ^3D_2\ (Z_3)$	$\sim 13$	45
$6p\ ^3F_4$	$\sim 15$	$\sim 40$
$6s6p\ D_2\ (Y_2)$	50	47
$6s6p\ D_1\ (X_1)$	83	85
$6s6p\ ^3G_6$	107	—
$6s6p\ ^3D_3$	$\sim 45$	85
$6p\ ^3F_3$	57	55
$6s6p\ ^3G_5$	107	109
$6p\ ^3P_2$	35	37
$6s\ ^3G_4$	93	—
$6s\ ^3F_4$	200	200
$6s\ ^3D_3$	116	123
$6s\ ^3F_3$	199	205
$6s6p\ V_1$	—	75
$6p\ ^3P_1$	—	$\sim 75$
$6s6p\ U_0$	—	$\sim 70$
$6s\ ^3D_1$	—	$\sim 90$
$6s\ ^3P_2$	—	160
$5d^{10}\ ^1S_0$	—	0
$6s\ ^3F_4$	—	203
$6s\ ^3D_2$	—	117
$6s\ ^3D_1$	—	82
$6s6p\ ^3D_4$	$\sim 76$	110

all the isotope displacements we have observed together with those found by Jaekel and Kopfermann.

In the cases where the 195 lines are completely separated from the even isotope lines it is possible to calculate the position of the centre of gravity

of the 195 pattern if the unobserved weak component is taken into account. The position of this component can be placed exactly when the term intervals are known (there are two weak components if the upper and lower  $J$  values are identical). This calculation can be made for the lines  $\lambda$  5390.8 and 5369.0, and the result is shown in fig. 6. In both cases it is seen that the centre of gravity of the 195 pattern does not fall exactly half-way between the components 194, 196 but is displaced towards the lighter. This has also been noticed by Jaekel and Kopfermann. This interesting fact is identical with what has been observed in the case of mercury. This fact is only revealed in lines having isotope displacement and completely separated 195 components.

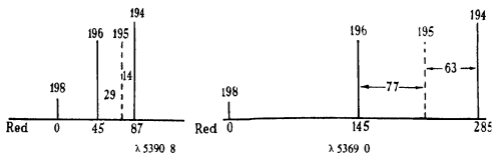


FIG. 6

On going back to Table III, which shows the isotope displacements in the arranged term groups (in the brackets) a number of interesting points can be deduced. In spite of the fact that the isotope displacement is linked to a complex term, it is apparent that the value of the displacement is largely determined by the presence of one or more penetrating electrons, the degree of penetration deciding the value of the displacement. The largest displacements are found in the  $5d^9 6s^2$  terms which means that in isotope displacement the two  $6s$  electrons do not compensate each other, but are additive in effect. The displacements in the  $5d^9 6s$  group vary between 82–120 and in the  $5d^9 7s$  group they are 12 and 20. This shows in a marked way the large reduction in displacement produced by changing from a  $6s$  to the much less penetrating  $7s$  electron. The displacements in the  $5d^9 6p$  group are decidedly less than those in the  $5d^9 6s$  group, but are by no means negligible, illustrating the relatively deep penetration shown by a  $6p_{1/2}$  electron in heavy atoms. In view of this, the wide variation (35–112) found in the  $5d^9 6s6p$  terms is only to be expected, for the influences of the  $6s$  and  $6p$  electrons may add or subtract. The displacement in  $6s^2$  terms is approximately twice that in  $6s$  terms.

In a general way it can be seen that the isotope displacements within a multiplet are not directly dependent upon the  $J$  value, as is the case in fine structure interval factors due to a nuclear spin. Too many multiplets exhibit the same isotope displacement in different  $J$  values for there to be any direct relationship. In the  $6s^2$  group the individual electron  $j$  values oppose, giving small magnetic coupling, but as the effects are additive in isotope displacement, it is apparent that the coupling mechanism is quite different in both cases. The independence of isotope displacement on  $J$  value shows why the  $J$  compensation in  $6s^2$  which nullifies the magnetic coupling, fails entirely to operate in isotope displacement.

#### SUMMARY

Lines of the Pt I spectrum in the region  $\lambda\lambda$  6800–4320 are excited in a water-cooled hollow cathode and examined for fine structure with a silvered Fabry-Perot interferometer. Thirty-six lines are studied. The isotopes observed in platinum are 198, 196, 195, 194, the abundance ratios being approximately 1 4 4 5. The 195 isotope has a nuclear spin of  $\frac{1}{2}$  which is the value shown by a very large number of nuclei with an odd nuclear neutron. A fine structure analysis is carried out for 195, interval factors being calculated in a large number of terms. It is shown that the  $5d^8$  and  $5d^9$  electron groups have an appreciable coupling with the nucleus, from which it is concluded that in a heavy atom  $5d_{3/2}$  electrons exhibit a certain degree of penetration.

All the terms observed exhibit even isotope displacement, some of which attain the large value of  $200 \text{ cm}^{-1} \times 10^{-3}$  per isotope. In all the isotope displacements the lighter isotope, 194, lies deepest, and it is shown that the centre of gravity of the 195 pattern is not half-way between the isotope lines 194, 196, but lies nearer to 194. The value of the even isotope displacement in a term appears to be determined by the degree of penetration exhibited by any penetrating electrons in the term electron configuration. In a  $6s^2$  electron group the two  $6s$  electrons do not compensate but are additive in producing isotope displacement. The displacements are not a function of  $J$ , differing thus from the magnetic splitting in the odd isotope, which depends upon  $J$ .

---

# Exact and Approximate Expressions for the Permeability of Potential Barriers to Light Particles

By R. P. BELL

(Communicated by C. N. Hinshelwood, F.R.S.—Received 7 July, 1936)

In order to calculate the permeability of an energy barrier to a particle of mass  $m$  and energy  $W$  it is necessary to solve the Schrödinger equation for the potential energy function  $V(x)$  representing the barrier. An exact solution has only been obtained for one type of barrier represented by a continuous curve (which we shall call the Eckart barrier\*), and in this case the resulting expression for the permeability is an inconvenient one for application to problems of reaction velocity†. Most treatments of this subject have therefore been based on the following approximate method. If the wave function is written in the form

$$\psi(x) = e^{s(x)},$$

the one-dimensional Schrödinger equation becomes

$$\frac{d^2\psi}{dx^2} + \left(\frac{ds}{dx}\right)^2 + \frac{8\pi^2m}{h^2} \{W - V(x)\} = 0 \quad (1)$$

This equation can be solved approximately provided that the first term is small compared with the second, i.e., if

$$\left| \frac{\frac{d^2\psi}{dx^2}}{\left(\frac{ds}{dx}\right)^2} \right| \ll 1 \quad (2)$$

The first approximation is

$$\psi \sim e^{\pm \int \frac{2\pi\sqrt{2m}}{h} (V-W)^{\frac{1}{2}} dx}, \quad (3)$$

and the condition (2) becomes

$$\left| \frac{h}{2\pi\sqrt{2m}} \frac{d}{dx} \left\{ \frac{1}{(V-W)^{\frac{1}{2}}} \right\} \right| \ll 1 \quad (4)$$

Condition (4) is obviously not satisfied in the neighbourhood of the points  $x = x_1$  and  $x = x_2$  at which  $W = V$ . However, if  $W$  is consider-

\* 'Phys. Rev.', vol 35, p 1303 (1930).

† See Bell, 'Proc. Roy. Soc.', A, vol 139 (1933)

ably less than  $E$ , the maximum value of  $V$ , the regions in which  $(V - W)^{-\frac{1}{2}}$  varies too rapidly will be small compared with the distance between them. Under these conditions equation (3) can be used to connect the solutions on the right- and left-hand sides of the barrier using the conditions of continuity at  $x = x_1$  and  $x = x_2$ . This gives for the permeability

$$G \sim e^{-\frac{4\pi\sqrt{2m}}{h} \int_{x_1}^{x_2} (V-W)^{\frac{1}{2}} dx} \quad \text{when } W < E \quad (5)$$

This expression tends to unity as  $W$  approaches  $E$ , and it is generally used in conjunction with the further assumption

$$G = 1 \quad \text{when } W > E \quad (6)$$

This approximate method of treatment must, however, fail for small values of  $|E - W|$  for small positive values, (5) fails on account of condition (4), and for small negative values, assumption (6) neglects the partial "reflexion" of particles which must take place in this region. This range of energy values is of particular interest for chemical problems, and it is impossible in general to determine the error inherent in the approximate treatment unless the exact solution is available for comparison. Such a comparison has been made for the Eckart barrier\* in which case the approximate treatment introduces at most a twofold error. We do, however, know that actual potential barriers are very much flatter at the top than the Eckart curve, and this might imply a much larger error: thus in the extreme case of a rectangular barrier of similar dimensions† the discrepancy between the two methods of treatment amounts to several powers of ten for  $W \sim E$ .

It has been previously shown‡ that equation (5) assumes a particularly convenient form for a parabolic barrier. This type of barrier has a larger radius of curvature at the maximum than the Eckart barrier, and hence approximates more closely to the barriers met with in chemical problems. It is therefore of interest to investigate the exact solution for this case.

If the dimensions of the parabolic barrier are those shown in fig. 1, the potential energy between  $x = -a$  and  $x = +a$  is given by

$$V(x) = E \left( 1 - \frac{x^2}{a^2} \right),$$

\* Bell, 'Proc Roy Soc,' A, vol 148, p 241 (1935)

† For the exact solution in this case see, e.g., Condon, 'Rev mod Phys,' vol 3, p 43 (1931)

‡ Bell, 'Proc Roy Soc,' A, vol 148, p 241 (1935), 'Proc Roy Soc,' A, vol 154, p 414 (1936)

and the Schrödinger equation for this region is

$$\frac{d^2\psi_{II}}{dx^2} + \frac{8\pi^2m}{h^2} \left( W - E + \frac{Ex^2}{a^2} \right) \psi_{II} = 0 \quad (7)$$

Making the substitutions

$$\xi = \left\{ \frac{2\pi\sqrt{2mE}}{ha} \right\}^{1/2} x, \quad \lambda = \frac{2\pi a \sqrt{2mE} (W - E)}{hE}, \quad (8)$$

equation (7) becomes

$$\frac{d^2\psi_{II}}{d\xi^2} + (\lambda + \xi^2) \psi_{II} = 0 \quad (9)$$

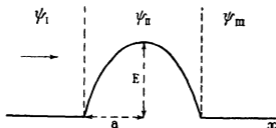


FIG. 1

This differs from the wave equation for the harmonic oscillator only in the sign of  $\xi^2$ , and it may be solved by a formally similar procedure. For large values of  $\xi$  (9) has the asymptotic solutions

$$\psi_{II} = e^{\pm i\xi^2} \quad (10)$$

Neither of these solutions becomes infinite at any point, and we may therefore write for the general solution

$$\psi_{II} = AF_+(\xi) e^{+i\xi^2} + BF_-(\xi) e^{-i\xi^2}, \quad (11)$$

where  $F_+(\xi)$  and  $F_-(\xi)$  must satisfy the equation

$$\frac{d^2F_{\pm}}{d\xi^2} \pm 2i\xi \frac{dF_{\pm}}{d\xi} + (\lambda \pm i) F_{\pm} = 0. \quad (12)$$

If  $F_{\pm}(\xi)$  are expressed as infinite power series in  $\xi$ , a two-term recursion formula can be obtained for the coefficients. However, on account of the complex nature of the coefficients and slow convergence of the series for relevant values of  $\xi$ , it is not practicable to apply this formal solution in the present problem.

Fortunately, it is possible to obtain useful information by considering the special case  $W = E$  ( $\lambda = 0$ ). Since the approximate treatment of (5) and (6) only fails for small values of  $|W - E|$ , the exact value of the permeability for  $W = E$  will give an indication of the maximum error involved in the approximations. It is convenient to consider the more general potential function

$$V(x) = E \left\{ 1 - \left| \left( \frac{x}{a} \right)^{2q-2} \right| \right\}, \quad (13)$$

which represents a continuous symmetrical barrier for all values of  $q > 3/2$  and reduces to the parabolic barrier when  $q = 2$ . Making the substitution,

$$\xi = \left\{ \frac{2\pi a \sqrt{2mE}}{h} \right\}^{1/q} \frac{x}{a} = \beta^{1/q} \frac{x}{a}, \quad (14)$$

the wave equation becomes

$$\frac{d^2 \psi_{II}}{d\xi^2} + \xi^{2q-2} \psi_{II} = 0. \quad (15)$$

This equation can be solved exactly in terms of Bessel functions,\* the general solution being

$$\psi_{II} = \xi^{\frac{1}{2}} \left\{ A J_{\frac{1}{2q}} \left( \frac{\xi^q}{q} \right) + B J_{-\frac{1}{2q}} \left( \frac{\xi^q}{q} \right) \right\} \quad (16)$$

If the particles of energy  $E$  are approaching the barrier from the left-hand side, then  $\psi_I$  and  $\psi_{III}$  (see fig. 1) can be written

$$\left. \begin{aligned} \psi_I &= e^{\frac{2\pi i}{h} \sqrt{2mE} x} + C e^{-\frac{2\pi i}{h} \sqrt{2mE} x} \\ &= \exp(i\beta^{1-\frac{1}{q}} \xi) + C \exp(-i\beta^{1-\frac{1}{q}} \xi) \\ \psi_{III} &= D \exp(i\beta^{1-\frac{1}{q}} \xi), \end{aligned} \right\} \quad (17)$$

the permeability being given by the ratio of the amplitudes of the forward waves in regions III and I, i.e., by  $|D|^2$ . This may be evaluated by using the conditions of continuity of  $\psi$  and  $d\psi/d\xi$  at  $\xi = \pm \beta^{1/q}$  (i.e.,  $x = \pm a$ ). Differentiating (16) and using the relations

$$\frac{dJ_n(z)}{dz} = (n/z)J_n(z) - J_{n+1}(z) = -(n/z)J_n(z) + J_{n-1}(z), \quad (18)$$

\* This result, and all theorems used in this paper involving Bessel functions and gamma functions, may be found in any standard work on analysis.

we have

$$\frac{d\psi_{II}}{d\xi} = \xi^{q-1} \left\{ A J_{\frac{1}{2q}-1} \left( \frac{\xi^q}{q} \right) - B J_{1-\frac{1}{2q}} \left( \frac{\xi^q}{q} \right) \right\}. \quad (19)$$

The conditions of continuity then become

$$\left. \begin{aligned} e^{-t\beta} + C e^{t\beta} &= \beta^{\frac{1}{2q}} \left\{ -A J_{\frac{1}{2q}} \left( \frac{\beta}{q} \right) + B J_{1-\frac{1}{2q}} \left( \frac{\beta}{q} \right) \right\}, \\ t \beta^{1-\frac{1}{q}} e^{t\beta} - C t \beta^{1-\frac{1}{q}} e^{-t\beta} &= \beta^{1-\frac{1}{2q}} \left\{ A J_{\frac{1}{2q}-1} \left( \frac{\beta}{q} \right) + B J_{1-\frac{1}{2q}} \left( \frac{\beta}{q} \right) \right\}, \\ D e^{t\beta} &= \beta^{\frac{1}{2q}} \left\{ A J_{\frac{1}{2q}} \left( \frac{\beta}{q} \right) + B J_{1-\frac{1}{2q}} \left( \frac{\beta}{q} \right) \right\}, \\ D t \beta^{1-\frac{1}{q}} e^{t\beta} &= \beta^{1-\frac{1}{2q}} \left\{ A J_{\frac{1}{2q}-1} \left( \frac{\beta}{q} \right) - B J_{1-\frac{1}{2q}} \left( \frac{\beta}{q} \right) \right\}. \end{aligned} \right\} \quad (20)$$

Elimination of the coefficients A, B, and C gives

$$D = \frac{t e^{t\beta} \left\{ J_{\frac{1}{2q}} \left( \frac{\beta}{q} \right) J_{1-\frac{1}{2q}} \left( \frac{\beta}{q} \right) + J_{1-\frac{1}{2q}} \left( \frac{\beta}{q} \right) J_{\frac{1}{2q}-1} \left( \frac{\beta}{q} \right) \right\}}{\left\{ J_{1-\frac{1}{2q}} \left( \frac{\beta}{q} \right) + t J_{-\frac{1}{2q}} \left( \frac{\beta}{q} \right) \right\} \left\{ J_{\frac{1}{2q}-1} \left( \frac{\beta}{q} \right) + t J_{\frac{1}{2q}} \left( \frac{\beta}{q} \right) \right\}} \quad (21)$$

Using the relation

$$J_n(z) J_{-n+1}(z) + J_{-n}(z) J_{n-1}(z) = \frac{2 \sin n\pi}{\pi z}, \quad (22)$$

we have finally for the permeability  $G_0$

$$G_0 = |D|^2 = \frac{4q^2 \sin^2(\pi/2q)}{\pi^2 \beta^2 \left\{ J_{\frac{1}{2q}} \left( \frac{\beta}{q} \right) + J_{\frac{1}{2q}-1} \left( \frac{\beta}{q} \right) \right\} \left\{ J_{1-\frac{1}{2q}} \left( \frac{\beta}{q} \right) + J_{1-\frac{1}{2q}} \left( \frac{\beta}{q} \right) \right\}}. \quad (32)$$

We shall first consider various limiting values for this expression  
Using the ordinary Bessel function series

$$J_n(z) = \frac{z^n}{2^n \Gamma(n)} \left\{ 1 - \frac{z^2}{2(2n+2)} + \dots \right\}, \quad (24)$$

we have

$$\left. \begin{aligned} \lim_{\beta \rightarrow 0} G_0 &= \lim_{\beta \rightarrow 0} \frac{4q^2 \sin^2(\pi/2q)}{\pi^2 \beta^2 J_{\frac{1}{2q}}^2 \left( \frac{\beta}{q} \right) J_{\frac{1}{2q}-1}^2 \left( \frac{\beta}{q} \right)} \\ &= \left\{ \frac{1}{\pi} \sin \frac{\pi}{2q} \Gamma \left( -\frac{1}{2q} \right) \Gamma \left( \frac{1}{2q} - 1 \right) \right\}^2 = 1, \end{aligned} \right\} \quad (25)$$

which is, of course, the correct value for an infinitely thin barrier or an infinitely light particle. Further, the theorem

$$\lim_{z \rightarrow \infty} \frac{z^{\frac{1}{2}} J_n(z)}{\cos \{z - (2n + 1) \pi/4\}} = \left(\frac{2}{\pi}\right)^{\frac{1}{2}} \quad (26)$$

gives

$$\lim_{\beta \rightarrow \infty} G_0 = \sin^2 \frac{\pi}{2q} \quad (27)$$

provided that  $q$  is finite. (It is interesting to note that this limiting value depends only on the shape of the barrier, and is valid when the particle and the barrier assume macroscopic dimensions. Classical mechanics would normally be applied to such a system, but makes no prediction as to the permeability, when  $W$  is exactly equal to  $E$ .) If  $q \rightarrow \infty$ , the curve becomes a rectangular barrier, and it can be shown that

$$\lim_{q \rightarrow \infty} G_0 = \frac{1}{1 + \beta^2} \quad (28)$$

which agrees with the usual expression for a rectangular barrier of width  $2a$ .

For values of  $\beta/q > 1$ , (23) is most conveniently evaluated by using the asymptotic expansions for the Bessel functions. Neglecting terms in  $1/\beta^2$  and higher powers we have

$$\left. \begin{aligned} J_{\pm \frac{1}{2q}} \left( \frac{\beta}{q} \right) &\sim \cos \left\{ \frac{\beta}{q} - \frac{\pi}{4} \left( 1 \pm \frac{1}{q} \right) \right\} - \frac{1-q^2}{8q\beta} \sin \left\{ \frac{\beta}{q} - \frac{\pi}{4} \left( 1 \pm \frac{1}{q} \right) \right\}, \\ J_{\pm \left( \frac{1}{2q} - 1 \right)} \left( \frac{\beta}{q} \right) &\sim \mp \sin \left\{ \frac{\beta}{q} - \frac{\pi}{4} \left( 1 \pm \frac{1}{q} \right) \right\} \\ &\quad \pm \frac{3q^2 - 4q + 1}{8q\beta} \cos \left\{ \frac{\beta}{q} - \frac{\pi}{4} \left( 1 \pm \frac{1}{q} \right) \right\} \end{aligned} \right\} \quad (29)$$

Substituting these values in (23) and again neglecting terms in  $1/\beta^2$ , we obtain

$$G_0 \sim \frac{\sin^2 \frac{\pi}{2q}}{1 - \frac{q-1}{2\beta} \cos \frac{\pi}{2q} \cos \frac{2\beta}{q}} \quad (30)$$

In the case of the parabolic barrier ( $q = 2$ ), equation (30) is accurate to within a few per cent for all values of  $\beta > 2$ . It hence gives ample

accuracy for problems of chemical kinetics, *e.g.*, for the barriers previously considered as appropriate to reactions involving hydrogen and deuterium\*  $\beta$  varies from 8.75 to 26.4. For many purposes the limiting value (27) is sufficiently accurate, as may be seen from fig. 2, which shows the value of  $G_0$  from  $\beta = 0$  to  $\beta = 30$ .

It is clear that for parabolic barriers no great error is introduced by the approximation involved in equations (5) and (6). The maximum error is committed by the assumption that  $G = 1$  when  $W = E$ , the true value being nearly  $\sin^2 \pi/4 = 0.5$ . Actual reaction velocity calculations usually involve integration over a range of particle energies, in which case the net error will be less than this. Further, since the error committed depends chiefly on the shape of the barrier and is almost independent of

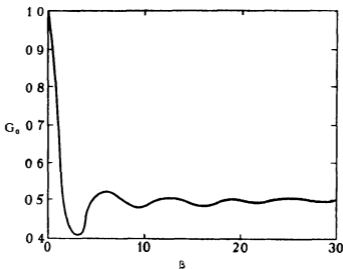


FIG. 2

$E$ ,  $a$ , and  $m$ , the approximate treatment can be safely used for quantitative comparisons between similar reactions. If  $q > 2$ , *i.e.*, if the barrier is flatter than a parabola, the absolute error will be somewhat larger. The appropriate value for  $q$  in any actual case depends on the curvature of the barrier near the top, and hence cannot be predicted accurately in our present state of knowledge.

If the true value of  $G_0$  is not very different from the value unity predicted by (5), we should anticipate that the variation of  $G$  with  $W$  will be given approximately by (5), even for small negative values of  $(W - E)$ . In the case of the parabolic barrier this may be verified by the use of an

\* Bell, 'Proc. Roy. Soc., A', vol. 148, p. 241 (1935).

approximate solution valid in this region. If in equation (12) the first term can be neglected compared with the second, *i.e.*, if

$$\left| \frac{\frac{d^2 F}{d\xi^2}}{\xi \frac{dF}{d\xi}} \right| \ll 1, \quad (31)$$

then the equation can be solved approximately, giving

$$F_{\pm} \sim \frac{1}{\xi^{\frac{1}{2}}} e^{\pm \frac{1}{2} \lambda \log \xi} \quad (32)$$

Condition (31) then becomes

$$\left| \frac{1}{2\xi^2} (-3 \pm i\lambda) \right| \ll 1, \quad i.e. \quad \frac{1}{\xi^2} \ll 1, \quad \left| \frac{\lambda}{\xi^2} \right| \ll 1. \quad (33)$$

With this proviso, the approximate wave equation inside the barrier can be written (*cf* equation (11))

$$\psi_{II} \sim \frac{1}{\xi^{\frac{1}{2}}} [A \exp \{ \frac{1}{2} i (\xi^2 + \lambda \log \xi) \} + B \exp \{ -\frac{1}{2} i (\xi^2 + \lambda \log \xi) \}] \quad (34)$$

Equation (34) must fail near the centre of the barrier, but becomes more accurate with increasing  $\xi$ . It will be a fairly good approximation at the edges of barriers appropriate to chemical reactions (where in general  $\xi^2 > 8$ ) and hence may be used for joining the solutions in regions I and III (equation (27)). Writing

$$\left. \begin{aligned} \gamma &= \left\{ \frac{2\pi a \sqrt{2mE}}{k} \right\}^{\frac{1}{2}}, \\ U_{\pm} &= \frac{1}{\gamma^{\frac{1}{2}}} \exp \{ \pm \frac{1}{2} i (\gamma^2 + \lambda \log \gamma) \} \\ W_{\pm} &= \frac{1}{\gamma^{\frac{3}{2}}} (1 \mp 2i\gamma^2 \mp i\lambda) \exp \{ \pm \frac{1}{2} i (\gamma^2 + \lambda \log \gamma) \} \end{aligned} \right\} \quad (35)$$

the equations of continuity at  $\xi = \pm \gamma$  become

$$\left. \begin{aligned} e^{-i\gamma^2} + C e^{i\gamma^2} &= -A i e^{-i\pi\lambda} U_+ - B i e^{i\pi\lambda} U_- \\ i\gamma e^{-i\gamma^2} - C i\gamma e^{i\gamma^2} &= A i e^{-i\pi\lambda} W_+ + B i e^{i\pi\lambda} W_- \\ D e^{i\gamma^2} &= A U_+ + B U_- \\ D i\gamma e^{i\gamma^2} &= -A W_+ - B W_- \end{aligned} \right\}, \quad (36)$$

giving on solving for D

$$D = \frac{i\gamma e^{-i\gamma^2} (U_+ W_- - U_- W_+)}{\gamma (U_+ W_- - U_- W_+) \cosh \frac{\pi\lambda}{2} - i (W_+ W_- + \gamma^2 U_+ U_-) \sinh \frac{\pi\lambda}{2}}. \quad (37)$$

If the conditions (33) are used to simplify this expression, we obtain finally for the permeability

$$G = |D|^2 \sim e^{\pi\lambda}, \quad (38)$$

which is identical with equation (5) for a parabolic barrier

The chief results of the foregoing discussion may be summed up as follows

1—The usual approximation for the permeability of a potential barrier (equation (5)) must fail when the energy of the particle  $W$  is near the maximum value of the potential energy  $E$ . The error involved can only be ascertained by comparison with an exact solution

2—An exact solution has been derived for the particular case  $W = E$  for potential barriers having the general equation

$$V(x) = E \{ 1 - (x/a)^{2q-2} \}$$

It is hence shown that for barriers appropriate to chemical kinetics the maximum error in the approximate treatment involves a factor of nearly  $\sin^2 \pi/2q$  and is almost independent of the mass of the particle and the dimensions of the barrier

3—Equation (5) may therefore be used for a semi-quantitative treatment of absolute reaction rates and will give accurate results for the relative rates of similar reactions. In the case of a parabolic barrier these conclusions have been confirmed by an approximate treatment valid for small negative values of  $W - E$

#### SUMMARY

A discussion is given of the range of validity of approximate expressions for the permeability of potential barriers, and it is pointed out that the errors involved in such approximations can only be evaluated by comparison with exact solutions. A formal exact solution of the wave equation is obtained for a parabolic potential barrier, but does not lend itself to calculations of the permeability. It is, however, shown that when the energy of the particle is equal to the maximum potential energy a convenient exact solution can be obtained for a more general type of barrier, and that this solution can be used to estimate the maximum error involved in the approximate treatment. It is concluded that for barriers appropriate to chemical reactions the approximate expressions can be used for semi-quantitative calculations of absolute rates and will give accurate results for the relative rates of similar reactions. In the case of a parabolic barrier these conclusions are confirmed by an independent type of asymptotic solution.

---

## A New Process of Negative Ion Formation—II

By F L ARNOT, Ph.D., Lecturer in Natural Philosophy, The University,  
St Andrews

(Communicated by H Stanley Allen, F R S—Received 7 July, 1936)

### INTRODUCTION

It has been known for many years that negative ions are formed in various gases through which a stream of electrons is passed. It has generally been believed that these negative ions are all formed by one of two processes, which may be termed the "radiative process" and the "dissociation process". The latter process can occur only in a molecular gas, whereas the radiative process can occur in monatomic as well as molecular gases.

In the dissociation process the impinging electron dissociates the molecule and attaches itself to one of the products of dissociation, the energy of the electron in excess of that necessary for dissociation together with the electron affinity of the resulting negative ion being carried away in kinetic form by the products of dissociation. The radiative process is a direct attachment of the electron to the atom or molecule without dissociation, the kinetic energy of the electron together with the electron affinity of the atom or molecule being radiated.

During an investigation of negative ion formation in mercury vapour, carried out with the assistance of Mr J C Milligan, I obtained results which were inconsistent with either of these two processes. This led me to suggest a new process of formation in which the negative ions are formed from positive ions which extract two electrons from any negatively-charged electrode, including the filament, to which they are driven. Subsequent investigation then showed conclusively that the negative ions produced in mercury vapour were formed by this process.\*

This paper contains the results of an extension of this work† to hydrogen, nitrogen, oxygen, and carbon dioxide. It will be shown that in each of these gases the large majority, if not all, of the negative ions detected are formed by the new process, and not by either of the two processes that have in the past been presumed to account for their formation.

\* 'Proc Roy Soc,' A, vol 156, p 538 (1936)

† The reading of this paper will be facilitated by first reading Paper I

## APPARATUS

The apparatus used in this work, which is shown in fig 1, has been fully described in two previous papers \* It will be sufficient to repeat here that it consists essentially of an ionization chamber and a magnetic analyser. The analyser, which is evacuated through a liquid air trap of large

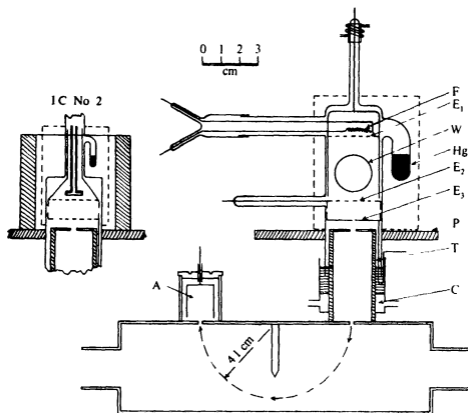


FIG 1—The apparatus

diameter by the right-hand outlet, was set in a gap of 1 cm. between the poles of a large electromagnet. The left-hand outlet was connected through another liquid air trap to a McLeod gauge.

All the results given in this paper were obtained with ionization chamber No 2 shown as an inset in fig 1. This contained in addition to the filament two nickel gauze electrodes. The upper electrode will be denoted by  $E_1$  and the lower one by  $E_2$ . The tungsten filament was 0.15 mm in

\* Arnot and Milligan, 'Proc Roy Soc,' A, vol 153, p. 359 (1936), vol. 156, p 538 (1936)

diameter and 8 mm in length on all occasions, the potential drop across this length being less than 1.5 volts.

The potential used to accelerate the electrons to  $E_1$  will be denoted throughout this paper by  $V_0$ . The potential between  $E_1$  and  $E_2$  will be denoted by  $V_1$ , and the potential between  $E_2$  and the iron cylinder T by  $V_2$ . The potential  $V_0$  will always be given as positive, and consequently when  $V_1$  or  $V_2$  is given as negative this potential drop will be in a direction to *retard* electrons and negative ions.

The gas to be investigated was stored over phosphorus pentoxide in a large glass bulb of 1½-litre capacity at a pressure of a few centimetres of mercury. The gas from the bulb passed through a fine glass capillary, then through a liquid air trap, and entered the ionization chamber through a side-tube sealed on in place of that containing mercury in fig. 1. After passing through the apparatus, the gas was pumped off into the atmosphere. All the gases used were obtained from commercial cylinders, and no impurities were detected in the positive ion analysis curves, except a very slight trace of  $\text{CO}^+$ , which was probably due to gas emitted from the filament and electrodes, and was too small to have any appreciable effect on the results. For all runs the pressure of residual gas was below  $10^{-6}$  mm of Hg. The electrometer was worked at a voltage sensitivity of about 1000 mm. per volt, the capacity of the insulated system being 122 cm.

No difficulty was experienced in running a tungsten filament in oxygen below a pressure of about  $5 \times 10^{-4}$  mm of Hg. Above a pressure of  $10^{-3}$  mm of oxygen the emission increased rather rapidly due to oxidization of the filament, but at a pressure of  $2 \times 10^{-4}$  mm and a filament emission of 1 milliamp it was only necessary to reduce slightly the filament current about every five minutes to keep the emission constant within 10%. The filament was no doubt protected by an outside layer of oxide, so that further oxidization was possible only by diffusion of oxygen through this layer. The oxide layer increases the work function of the filament, and it was consequently necessary to run the filament at a considerably higher temperature in oxygen to obtain the same filament emission as was given at a lower temperature in an inert gas.

## RESULTS

### 1—Analysis of the Ions

Positive ion analysis curves were taken for each gas, and the results obtained were in good agreement with previous work on positive ions.\*

\* See Smyth, 'Rev. Mod. Phys.', vol. 3, p. 347 (1931).

Nitrogen gave  $N_2^+$  and  $N^+$ , the ratio of the two peaks varying greatly with the pressure, as shown by fig 4. Oxygen gave  $O_2^+$  and  $O^+$ , the ratio of  $O_2^+$  to  $O^+$  varying between about 7 at the lowest and highest pressures used to about 10 at intermediate pressures, as shown in fig 5. Hydrogen gave  $H^+$ ,  $H_2^+$ , and a little  $H_3^+$ . Carbon dioxide gave  $CO_2^+$ ,  $CO^+$ ,  $O^+$ , and  $C^+$ .

Analysis of the negative ions showed that only atomic negative ions were produced in hydrogen and nitrogen. Oxygen gave  $O^-$  and  $O_2^-$ ,

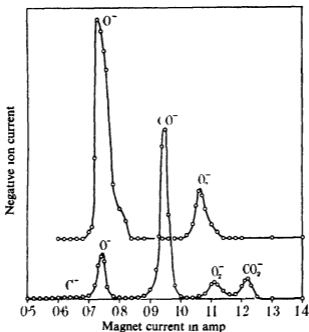


FIG. 2.—Analysis of the negative ions formed in oxygen (upper curve) and in carbon dioxide (lower curve)

while carbon dioxide gave  $CO_2^-$ ,  $CO^-$ ,  $O_2^-$ ,  $O^-$  and a very small amount of  $C^-$ . By suitably arranging the potentials, the conversion of the positive ions into negative ions could be caused to take place on the filament, on  $E_1$  or on  $E_2$ .

Negative ion analysis curves for oxygen and for carbon dioxide are shown in fig 2, the upper curve being for oxygen and the lower one for carbon dioxide†. These curves were taken with the following arrangement of potentials.  $V_0 = 60$  volts,  $V_1 = -180$  volts,  $V_2 = 200$  volts. All electrons and negative ions from the filament are stopped between  $E_1$

† The presence of a slight bulge on the high-energy side of the  $O^-$  peak is significant, and will be referred to in the following paper, p. 164.

and  $E_4$ . Positive ions produced between  $E_1$  and  $E_2$  are accelerated through  $E_2$ , retarded and reversed in the 200-volt field between  $E_2$  and the iron cylinder T. They will consequently pass back and forth through the gauze  $E_2$ , some of them being absorbed by the gauze in each passage of the ions through it.  $E_2$  is consequently bombarded by positive ions equally on both sides. Some of the positive ions hitting the gauze  $E_2$  on the under side are converted into negative ions which then enter the analyser with an energy of 200 volts.

The intensity of the C<sup>-</sup> peak is too small to show up in fig. 2. In a curve of negative ions produced on  $E_1$  a C<sup>-</sup> peak quite definitely appears having an intensity equal to 0.03 that of the O<sup>-</sup> peak.

### 2—Energy Distribution of the Negative Ions

The energy distribution of the negative ions, which is intimately connected with the subject of accommodation coefficients, will be given and discussed in the following paper. It may, however, be stated here that the negative ions come off the surface on which they are formed with a wide range of energy, extending from zero to beyond 60 volts for O<sup>-</sup>, and to beyond 109 volts for H<sup>-</sup>. This energy is derived from the parent positive ions of 200 volts' energy from which the negative ions are formed, and for which the accommodation coefficient of the surface is less than unity.

It is also necessary at this stage to say something about the energy distribution of the H<sup>-</sup> ions formed in hydrogen. In gases other than hydrogen the negative ion peaks obtained by magnetic analysis are all quite sharp, as is shown in fig. 2, for, although the energy distribution curves extend over a wide energy range, yet the large majority of the negative ions are confined within an energy range of only a few volts\*. In hydrogen, however, a peculiar and very interesting effect occurs. Instead of the large majority of the ions being confined to a *single* narrow band of energy, the H<sup>-</sup> ions are resolved into *two* energy bands, so producing a double peak in magnetic analysis, as shown in fig. 3.

The curves in fig. 3 were all taken with  $V_0 = 60$  volts, and  $V_2 = 200$  volts. Thus the ions were accelerated off the gauze  $E_2$  into the analyser by a field of 200 volts. The negative potential  $V_1$  which controls the energy of the positive ions striking  $E_2$  was varied. The positive ions hitting  $E_2$  have an energy of  $V_1$  volts (see p. 147).

The H<sup>-</sup> ions form a double peak because the accommodation coefficient has two principal values. If these two values of the accommodation

\* See figs. 5, 7, and 8 in the following paper.

coefficient were independent of the energy with which the positive ions hit the surface, then the peaks would move together as  $V_1$  is decreased. However, the movement of the high energy peak to lower energies as  $V_1$  is decreased is more rapid than would be expected. This means that the lower value of the accommodation coefficient increases as  $V_1$  decreases. This will be more fully discussed in the second paper (*see p 163*)

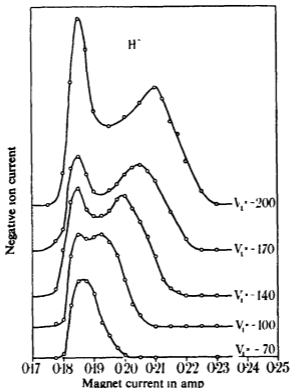


FIG 3—Analysis of the  $H^-$  ions formed from positive ions of energy  $V_1$

### 3—Variation of Peaks with Pressure

In fig 4 the two lower curves represent the variation with pressure of the two positive ion peaks in nitrogen,  $N^+$  and  $N_2^+$ . The upper curve, which is the sum of the two lower curves, represents the variation with pressure of the total positive ionization. The points represented by circles, which deviate from the upper curve only by the experimental error, represent the variation of the negative ion peak with pressure. The circles have been fitted at one point to the upper curve.

These results show quite definitely that the  $N^-$  ions originate from both  $N^+$  and  $N_2^+$ ; and that the probability of  $N^-$  arising from  $N_2^+$  is equal to

the probability of its arising from  $N^+$ , since the negative ionization is proportional only to the total positive ionization, and not to the distribution of this positive ionization amongst the monatomic and diatomic forms.

The reason for this is probably that the  $N_2^+$  ions all dissociate immediately on striking the surface, so that we have the two processes—

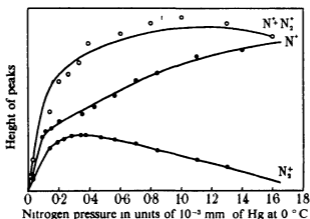
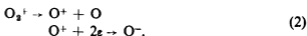


FIG 4—Pressure variation curves for nitrogen. Circles represent points of negative ion curve fitted to total positive ionization curve

both occurring at the surface. The dissociation of all the  $N_2^+$  ions on striking the surface would also account for the absence of  $N_2^-$  ions, for it is not likely that  $N_2$  has no electron affinity in view of the fact that CO, which has a similar outer electronic structure to  $N_2$ , does have an electron affinity, as shown by the  $CO^-$  peak in fig. 2. The  $N^+$  and  $N_2^+$  curves were taken with  $V_0 = 140$  volts,  $V_1 = -180$  volts,  $V_2 = -40$  volts, and the  $N^-$  results with  $V_0 = 140$  volts,  $V_1 = -180$  volts,  $V_2 = 200$  volts. The  $N^-$  ions thus originated on the gauze  $E_2$ .

The results for oxygen are shown in fig. 5. Here the  $O^+$  ionization is so small compared to the  $O_2^+$  ionization over the whole pressure range that the curve for  $O_2^+ + O^+$  has not been drawn, since this will differ from the  $O_2^+$  curve only very slightly and would tend to confuse the figure. The two broken curves, which have been fitted separately to the  $O_2^+$  curve at the maximum represent the variation of pressure of the  $O^-$  and  $O_2^-$  ions.

The shape of the  $O^-$  curve follows that of the  $O_2^+$  (and hence that of the  $O_2^+ + O^+$ ) curve quite closely. In view of the results for nitrogen, shown in fig. 4, it may be concluded that the  $O^-$  ions probably arise from both  $O_2^+$  and  $O^+$  ions by the two processes



Since  $O_2^-$  ions are formed in oxygen, we must conclude that some of the  $O_2^+$  ions do not dissociate on striking the surface of the gauze  $E_2$ . We then get the process

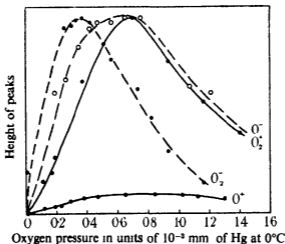


FIG. 5—Pressure variation curves for oxygen

Since the number of  $O_2^-$  ions produced is much smaller than the number of  $O^-$  ions (see fig. 2), the probability of process (3) occurring is less than that of process (2), which involves dissociation of the  $O_2^+$  ion.

The reason why the maximum of the  $O_2^-$  curve occurs at a lower pressure than the maximum of the  $O^-$  curve is probably due to greater scattering and neutralization of the  $O_2^-$  ions. The curves of fig. 5 were taken with the same arrangement of potentials as were used for the curves of fig. 4, except that  $V_0$  was 60 volts in place of 140 volts.

In fig. 6 the two lower curves represent the variation with pressure of the two  $H^-$  peaks shown in fig. 3. Since the fast ion, denoted by  $H_f^-$ , reaches a maximum at a lower pressure than the normal ion  $H_n^-$  we conclude that the fast ion is more readily "ionized", i.e., neutralized, than the

normal or slower ion This is to be expected, since the probability of a negative ion losing its electron on collision will increase with the velocity of the ion The upper curve in fig 6 represents the sum of the two lower curves

Fig. 7 represents the variation with pressure of the three positive hydrogen ions  $H^+$ ,  $H_2^+$ , and  $H_3^+$  The  $H^+$  and  $H_3^+$  ionization is negligible compared with the  $H_2^+$  ionization over this pressure range, and consequently the negative ions must arise almost entirely from the  $H_2^+$  ions. That this is so is shown by the fact that the broken curve, which is the

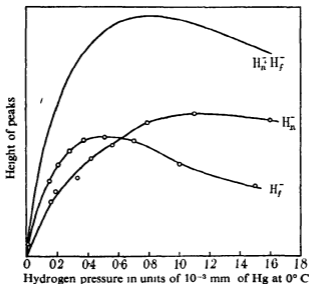
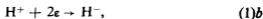


FIG. 6—Pressure variation curves for atomic negative ions of hydrogen  $H_n^-$  is curve for normal ions,  $H_f^-$  for fast ions

upper curve of fig 6 representing the total  $H^-$  ionization, closely follows the  $H_2^+$  curve The two curves have been fitted at one point Thus the negative ions in hydrogen arise almost entirely from the process



the  $H_2^+$  being dissociated on striking the gauze  $E_2$

Negative ions undoubtedly also arise directly from the atomic positive ions as in oxygen and nitrogen, and it is quite probable also that the  $H_2^+$  ions dissociate on striking the surface, so giving a  $H^+$  ion which extracts two electrons from the surface and comes off as a negative ion, as in

(1)*b* The results shown in figs 6 and 7 were obtained with the same arrangement of potentials as were used for the results in nitrogen, shown in fig 4

Satisfactory pressure variation curves were not obtained in carbon dioxide, for the pressure could not be reduced to zero. Even after evacuating for several hours with the  $\text{CO}_2$  turned off, strong positive and negative ion currents were still obtained. It appeared that something in the ionization chamber strongly absorbed  $\text{CO}_2$ , which was then given off under electron bombardment or by the heat from the filament. That this was so

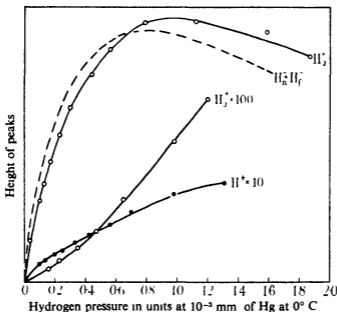


FIG 7—Pressure variation curves for positive ions and for total negative ionization in hydrogen

was shown by the following test. After running the filament for a few hours with the  $\text{CO}_2$  turned off and with liquid air on the McLeod and pump traps, the pumps were shut off. The pressure in the apparatus rose to a steady value of  $3 \times 10^{-4}$  mm, due to the gas from the back of the diffusion pump. The liquid air was then removed from the pump trap. No change of pressure was observed. Finally, the liquid air was removed from the McLeod trap. The pressure in the apparatus then rose to  $1.5 \times 10^{-2}$  mm of Hg. This pressure was definitely due to  $\text{CO}_2$ , and not to water vapour, for the pressure remained at  $1.5 \times 10^{-2}$  when a mixture of solid  $\text{CO}_2$  and alcohol was placed on the McLeod trap. Positive ion analysis confirmed the conclusion that the gas was  $\text{CO}_2$ . It appears likely

that the  $\text{CO}_2$  was absorbed by a film of carbon deposited on the electrodes, and produced from dissociation of the carbon dioxide, for after running the filament for an hour or so in oxygen the  $\text{CO}_2$  peaks disappeared, which would be accounted for by the oxidation of the carbon film

The positive ions detected in  $\text{CO}_2$  were  $\text{CO}_2^+$ ,  $\text{CO}^+$ ,  $\text{O}^+$ , and  $\text{C}^+$ . Negative ions corresponding to each of these atoms and molecules, and in addition the ion  $\text{O}_2^-$ , were found, as shown in fig. 2. The  $\text{CO}_2^-$  ions must be produced directly from  $\text{CO}_2^+$  without dissociation at the surface, and the  $\text{O}_2^-$  ions from  $\text{CO}_2^+$  by dissociation. The other negative ions no doubt come from the corresponding positive ions, and also probably from  $\text{CO}_2^+$  dissociating at the surface. Thus the ions  $\text{CO}^-$ ,  $\text{O}^-$ , and  $\text{C}^-$  arise respectively from  $\text{CO}^+$ ,  $\text{O}^+$ , and  $\text{C}^+$  extracting two electrons from the surface, and it is probable that each of them can be formed as well from  $\text{CO}_2^+$ . Some of the  $\text{O}^-$  and  $\text{C}^-$  ions also probably come from  $\text{CO}^+$  dissociating at the surface.

#### 4—The Probability of Conversion of Positive Ions into Negative Ions

To obtain the probability of conversion of the positive ions into negative ions on the gauze  $E_2$  as a function of the energy of the positive ions  $V_0$  was set at 60 volts,  $V_2$  at 200 volts, and  $V_1$  was varied from — 200 volts to — 60 volts. When working in nitrogen, oxygen, and carbon dioxide the stray field of the magnet was sufficient to prevent the electrons from penetrating far into the space between  $E_1$  and  $E_2$  when  $V_0$  was 60 volts. The positive ions should therefore all be produced close to  $E_1$  and should all receive the full energy  $V_1$  in falling to  $E_2$ . The analysis of the positive ions gave quite sharp peaks showing that they were fairly homogeneous in energy, and the position of the peaks showed that the positive ions had practically the full energy  $V_1$ .

Positive ions of energy  $V_1$  produced between  $E_1$  and  $E_2$  will then be reversed by the field  $V_2$  between  $E_2$  and the iron cylinder  $T$ , and again reversed by the field  $V_1$  between  $E_2$  and  $E_1$ . They will consequently pass back and forth through the gauze  $E_2$ , some of them being absorbed by the gauze in each passage of the ions through it. Thus  $E_2$  will be bombarded by positive ions of energy  $V_1$  equally on both sides.

The positive ions converted into negative ions on the under side of the gauze, and accelerated into the analyser by  $V_2$ , will thus be due to a positive ion current equal to half that received by  $E_2$ . The negative ions formed on the upper side of  $E_2$  will be accelerated by  $V_1$  away from the analyser. The positive ion current to  $E_2$  was kept constant while the energy of the positive ions was decreased by reducing  $V_1$ , and the height

of the negative ion peak measured at each value of  $V_1$ . The results obtained in nitrogen, oxygen, hydrogen, and carbon dioxide are shown respectively in figs 8, 9, 10, and 11

Owing to the presence of two  $H^-$  peaks in hydrogen which moved closer together as  $V_1$  was decreased, as shown in fig 3, it was not justifiable to

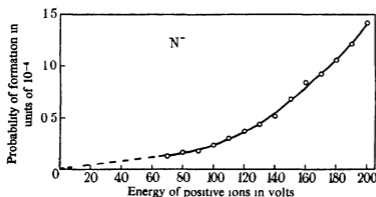


FIG. 8—Probability of conversion of positive ions into negative ions in nitrogen

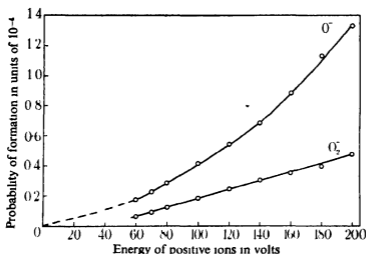


FIG. 9—Probability of conversion of positive ions into negative ions in oxygen

measure simply the height of the peaks. The results given in fig. 10 were thus obtained by measuring the area under each of the peaks in fig 3 and plotting this against the corresponding value of  $V_1$ . Also, owing to the much smaller stray magnetic field present when measuring the  $H^-$  peaks, the positive ion current to  $E_2$  will not be so homogeneous in energy.

The absolute value of the probability of formation was found as follows. A complete negative ion peak was obtained by magnetic analysis for

$V_1 = -180$  volts, and its area measured by an Amsler planimeter. Then, keeping  $V_0$  at 60 volts and  $V_1$  at  $-180$  volts,  $V_2$  was changed from 200 volts to  $-50$  volts, so that the positive ions now entered the analyser

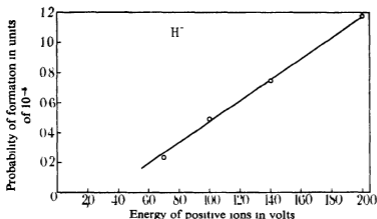


FIG. 10—Probability of conversion of positive ions into negative ions in hydrogen

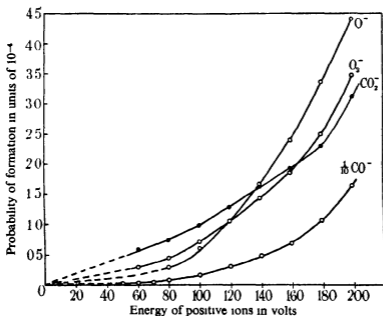


FIG. 11—Probability of conversion of positive ions into negative ions in carbon dioxide.

The positive ion current to the iron cylinder T was set to have the same value as that which formerly gave rise to the negative ions, namely half the total positive ion current that formerly passed to  $E_2$ . The intense

positive ion current then entering the Faraday cylinder was measured by connecting a 0.1 microfarad condenser across the quadrants of the electrometer, and the area of each of the positive ion peaks so obtained was measured with a planimeter.

First consider a monatomic gas in which the negative ions are all produced from the atomic positive ions. Let  $A$  be the area of the atomic positive ion peak, and  $a$  the area of the negative ion peak formed from the positive ions of  $V_1$  volts' energy, and  $C$  and  $c$  the capacities of the electrometer system for the measurement of the positive and negative ions respectively. Then the probability of a positive ion of  $V_1$  volts' energy being converted into a negative ion on the nickel gauze  $E_2$  is

$$a/A \times c/C$$

The value found\* for 180-volt  $\text{Hg}^+$  ions was  $6.4 \times 10^{-4}$ .

In dealing with a diatomic gas the problem is more involved, for we have seen that the negative ions are formed, not only from the atomic positive ions, but also from the diatomic positive ions. It appears fairly certain from the evidence given on p. 143 that in nitrogen all the  $\text{N}_2^+$  ions dissociate immediately on striking the surface. If this is so the  $\text{N}^-$  ions are all ultimately formed from  $\text{N}^+$ , and therefore, if we put  $A$  equal to the sum of the areas of the  $\text{N}^+$  and  $\text{N}_2^+$  peaks, we shall obtain the probability of conversion of  $\text{N}^+$  ions into  $\text{N}^-$  ions. This has been done in fig. 8.

In oxygen there are two negative ion peaks. The  $\text{O}_2^-$  ions are formed only from the  $\text{O}_2^+$  ions. Putting  $a$  equal to the area of the  $\text{O}_2^-$  peak and  $A$  equal to the area of the  $\text{O}_2^+$  peak, we obtain the probability of conversion of  $\text{O}_2^+$  ions into  $\text{O}_2^-$  ions. The  $\text{O}^-$  ions are formed from the  $\text{O}_2^+$  ions and probably also from the  $\text{O}^+$  ions, but the area of the  $\text{O}^+$  peak is only 7% of the area of the  $\text{O}_2^+$  peak, and this ratio will not be affected by changing  $V_1$ , which controls the energy of the positive ions. Since the experimental error is probably of this order, the number of  $\text{O}^-$  ions formed directly from the  $\text{O}^+$  ions can be neglected. This would not be justifiable if the probability of formation of  $\text{O}^-$  from  $\text{O}^+$  was much greater than from  $\text{O}_2^+$ , but fig. 5 shows that the  $\text{O}^-$  ions are practically all formed from  $\text{O}_2^+$  ions. Therefore, putting  $a$  equal to the area of the  $\text{O}^-$  peak, and  $A$  equal to the area of the  $\text{O}_2^+$  peak, we obtain the probability of conversion of  $\text{O}_2^+$  ions into  $\text{O}^-$  ions. The probabilities shown in fig. 9 have been determined in this way.

If the  $\text{O}_2^+$  ions, with the exception of the negligible number that form  $\text{O}_2^-$ , all dissociate immediately on striking the surface as in nitrogen, so

\* Arnot and Milligan, 'Proc. Roy. Soc.', A, vol. 156, p. 538 (1936).

that the  $O^-$  ions are formed directly from  $O^+$  ions, the probability of conversion of  $O^+$  ions into  $O^-$  ions will be the same as that for conversion of  $O_2^+$  ions into  $O^-$  ions. In dealing with nitrogen the probability could not be expressed as that of the conversion of  $N_2^+$  into  $N^-$ , as has been done for oxygen, since the area of the  $N^+$  peak is by no means negligible, being 40% of the  $N_2^+$  peak.

In hydrogen the same procedure can be adopted as for oxygen. The area of the  $H^+$  and  $H_2^+$  peaks, taken together, is only 1.8% of the area of the  $H_2^+$  peak, and consequently all the  $H^-$  ions can be considered to arise from  $H_2^+$  ions, which is confirmed by fig. 7. The probabilities shown in fig. 10 were therefore obtained by putting  $a$  equal to the area of the  $H^-$  peak, and  $A$  equal to the area of the  $H_2^+$  peak, and so represent the probability of conversion of  $H_2^+$  ions into  $H^-$  ions. If we consider the  $H_2^+$  ions to dissociate on hitting the surface, so that it is the  $H^+$  ion which extracts the two electrons from the surface to form the  $H^-$  ion, then this probability is also that of the conversion of  $H^+$  ions into  $H^-$  ions.

The  $CO_2^-$  and  $O_2^-$  peaks in carbon dioxide can only arise from the  $CO_2^+$  ions, and consequently we put  $A$  equal to the area of the  $CO_2^+$  peak to find the probability of conversion of  $CO_2^+$  into  $CO_2^-$  and  $CO_2^+$  into  $O_2^-$ . The  $CO^-$  ions can be formed from  $CO^+$  and also from  $CO_2^+$  ions. The area of the  $CO^+$  peak is 29% of the area of the  $CO_2^+$  peak and hence cannot be neglected, and so we cannot adopt the procedure used for oxygen and hydrogen. Also, since  $CO_2^+$  can dissociate into a variety of different products, we cannot adopt the procedure used for nitrogen. The best we can do is to put  $A$  equal to the sum of the areas of the  $CO_2^+$  and  $CO^+$  peaks. The probability so obtained is the probability that one positive ion of a mixture of 77.4% of  $CO_2^+$  and 22.6% of  $CO^+$  will be converted into a  $CO^-$  ion.

The  $O^-$  ions can arise from the  $CO_2^+$ ,  $CO^+$ , and  $O^+$  ions. The area of the  $O^+$  peak is only 6.5% of the combined area of the  $CO_2^+$  and  $CO^+$  peaks, and so can be neglected since this will introduce an error probably less than the experimental error. Putting  $A$  equal to the sum of the areas of the  $CO_2^+$  and  $CO^+$  peaks, we obtain the probability that one positive ion of a mixture of 77.4% of  $CO_2^+$  and 22.6% of  $CO^+$  will be converted into an  $O^-$  ion. This is less than the probability of formation of a  $CO^-$  ion from the same mixture, as shown by fig. 11, which implies that the ionized product of the dissociation of  $CO_2^+$  by impact with the gauze is more likely to be  $CO^+$  than  $O^+$ , which would be expected from the structure of the molecule.

No probability curve was obtained for the  $C^-$  ion. Since its intensity was about 3% of the intensity of the  $O^-$  ion, its probability of formation

from a mixture of 77.4% of  $\text{CO}_2^+$  and 22.6% of  $\text{CO}^+$  will be of the order of 3% of the probability of formation of  $\text{O}^-$

The probabilities of formation in units of  $10^{-4}$  of the various negative ions on a nickel surface from positive ions of 180 volts' energy are given in the third column of Table I. In the second column is given the positive ion from which the negative ion is formed. It should be remarked again that if the probability of dissociation of the  $\text{H}_2^+$  and  $\text{O}_2^+$  ions on striking the gauze is unity for the  $\text{H}_2^+$  and almost\* unity for the  $\text{O}_2^+$  ions, then the probabilities given for the formation of  $\text{H}^-$  and  $\text{O}^-$  from the respective diatomic positive ions will also be their probabilities of formation from monatomic ions.

TABLE I.—PROBABILITY OF CONVERSION OF 180-VOLT POSITIVE IONS INTO NEGATIVE IONS ON A NICKEL SURFACE

Negative ion	Positive ion from which formed	Probability of formation Units of $10^{-4}$
$\text{Hg}^-$	$\text{Hg}^+$	6.4
$\text{H}^-$	$\text{H}_2^+$	0.104
$\text{N}^-$	$\text{N}^+$	1.07
$\text{O}^-$	$\text{O}_2^+$	1.10
$\text{O}_2^-$	$\text{O}_2^+$	0.42
$\text{CO}_2^-$	$\text{CO}_2^+$	2.31
$\text{O}_4^-$	$\text{CO}_2^+$	2.51
$\text{CO}^-$	77.4% $\text{CO}_2^+$ + 22.6% $\text{CO}^+$	10.8
$\text{O}^-$		3.37
$\text{C}^-$		(0.1)

#### 5—Search for Negative Ions Formed by Electron Attachment

The two processes which have in the past been presumed to account for the formation of negative ions are the "dissociation process" and the "radiative process". Both processes consist in the attachment of a free electron to a neutral atom or molecule, and differ only in the manner of disposal of the excess energy.

In the dissociation process, which can occur only in a molecular gas, the impinging electron dissociates the molecule and attaches itself to one of the products of dissociation, the energy of the electron in excess of that necessary for dissociation, together with the electron affinity of the resulting negative ion, being carried away by the products of dissociation.

The radiative process, which can occur in monatomic as well as molecular gases, is a direct attachment of a free electron to a neutral atom or

\* Not quite unity since about  $10^{-4}$  of the  $\text{O}_2^+$  ions form  $\text{O}_4^-$  ions.

molecule without dissociation, the kinetic energy of the electron, together with the electron affinity of the atom or molecule, being radiated

In the work described above the negative ions were all formed between  $E_2$  and the iron cylinder T, where, owing to the arrangements of potentials, there are no free electrons. Actually, it has been shown that the negative ions are formed on  $E_2$  from positive ions. It is quite definite, therefore, that the negative ions observed here are not formed by either the dissociation or the radiative process.

In order to see if negative ions formed by either of these two processes could be detected, the following arrangement of potentials was used.  $V_1$  was set at 2 volts and  $V_2$  at 10 volts, while  $V_0$  was varied from 188 volts down to 2 volts. The positive ions striking  $E_2$  will all have energies between 0 and 10 volts, and those striking  $E_1$  between 0 and 12 volts. The probability of conversion of positive ions of these energies into negative ions is shown by figs. 8, 9, 10, and 11 to be very small—too small to be detected.

All the negative ions formed between  $E_1$  and  $E_2$  by electron attachment, either by the dissociation or radiative process, will be accelerated into the analyser with an energy between 10 and 12 volts. When  $V_0$  was varied from 188 to 2 volts and a search made for negative ions of these energies, none could be detected. At the higher values of  $V_0$ , negative ions having an energy of ( $V_0 + 12$ ) volts, and therefore due to conversion of positive ions on the filament, were detected.

It thus appears that the large majority, if not all, of the negative ions formed in these gases when bombarded with electrons of energy greater than 2 volts are formed by the new process of positive ion conversion, and not by either of the two processes that have in the past been presumed to account for their formation.

#### DISCUSSION

The results presented above, together with those given in paper I, show conclusively that negative ions are formed in mercury vapour, hydrogen, nitrogen, oxygen, and carbon dioxide from positive ions which extract two electrons from any negatively-charged electrode, including the filament, to which they are driven. Neglecting the kinetic energy of the positive ion when it meets the surface, this process is energetically possible provided

$$V_i + V_f > 2\phi,$$

where  $V_i$  is the ionization potential of the positive ion,  $V_f$  the electron affinity of the negative ion that is formed, and  $\phi$  the work function of the

surface For a nickel surface  $\phi$  is 5.03 volts \* The values of  $V_i$ ,  $V_f$  and the excess energy  $V_i + V_f - 2\phi$  for various processes of formation are given† in Table II Processes resulting in a diatomic negative ion are not given since no data exist for electron affinities of diatomic ions

TABLE II

Negative ion	Positive ion from which formed	$V_i$ volts	$V_f$ volts	Excess energy $V_i + V_f - 2\phi$ volts
Hg <sup>-</sup>	Hg <sup>+</sup>	10.39	1.79	2.12
H <sup>-</sup>	H <sup>+</sup>	13.5	0.76	4.20
H <sup>-</sup>	H <sub>2</sub> <sup>+</sup>	15.5	0.76	6.20
N <sup>-</sup>	N <sup>+</sup>	14.5	0.04	4.48
N <sup>-</sup>	N <sub>2</sub> <sup>+</sup>	16.5	0.04	6.48
O <sup>-</sup>	O <sup>+</sup>	13.5	3.80	7.24
O <sup>-</sup>	O <sub>2</sub> <sup>+</sup>	13.0	3.80	6.74
O <sup>-</sup>	CO <sup>+</sup>	14.1	3.80	7.84
O <sup>-</sup>	CO <sub>2</sub> <sup>+</sup>	14.4	3.80	8.14
C <sup>-</sup>	CO <sup>+</sup>	14.1	1.37	5.41
C <sup>-</sup>	CO <sub>2</sub> <sup>+</sup>	14.4	1.37	5.71

When the negative ion is formed from the positive ion without the latter dissociating during the process, such as in the formation of a monatomic negative ion from a monatomic positive ion or a diatomic negative ion from a diatomic positive ion, the excess energy must be taken up by an electron or atom of the surface. It is not at all likely that it will be radiated. When the excess energy exceeds the work function of the surface it may be entirely employed in setting free another electron with kinetic energy equal to the difference between the excess energy and the work function.

When the positive ion dissociates, such as in the formation of O<sup>-</sup> from O<sub>2</sub><sup>+</sup>, the excess energy may be taken up by the products of dissociation. The disposal of the energy in this way will depend upon the stage in the process at which dissociation occurs. For example, if the O<sub>2</sub><sup>+</sup> ion is dissociated by its impact with the surface into O and O<sup>+</sup>, and the O<sup>+</sup> ion is then converted into O<sup>-</sup> by the extraction of two electrons, the process is essentially the same as the formation of O<sup>-</sup> from the atomic positive ion, and the excess energy must be taken up by an electron or atom of the surface. But if the O<sub>2</sub><sup>+</sup> ion acquires two electrons from the surface, so

\* Fox and Bowie, 'Phys. Rev.', vol. 44, p. 345 (1933).

† Ionization potentials are taken from Smyth, 'Rev. Mod. Phys.', vol. 3, p. 347 (1931), and electron affinities from Glockler, 'Phys. Rev.', vol. 46, p. 111 (1934).

becoming a doubly-excited molecule which then dissociates into  $O^-$  and  $O$ , the excess energy can be taken up in kinetic form by the products of dissociation

Further experiments must be made to decide definitely between these two alternatives, but since  $N^-$  is formed with the same probability from  $N_2^+$  as from  $N^+$  (see fig. 4 and accompanying text), it appears more probable that the  $N_2^+$  ions are dissociated by the impact, and the  $N^-$  ion is then formed from the resulting  $N^+$  ion. If preliminary dissociation occurs in nitrogen it probably also occurs in oxygen and hydrogen, since the work of dissociation of both  $O_2^+$  and  $H_2^+$  is less\* than that of  $N_2^+$ .

Assuming that preliminary dissociation on impact with the surface occurs in hydrogen and oxygen as well as in nitrogen, so that the negative ions are formed from the atomic positive ions, it is found that the probability of formation of negative ions from positive ions of the same energy increases approximately linearly with the atomic number of the ion, as is shown by Table III

TABLE III

Ion	Atomic number	Probability of formation, Units of $10^{-6}$
$H^-$	1	1.04
$N^-$	7	10.7
$O^-$	8	11.0
$Hg^-$	80	64.0

For any one ion the probability of the excess energy being absorbed by an electron or atom of the surface will increase with the degree of penetration of the positive ion into the surface, *i.e.*, with the kinetic energy of the positive ion. This would account for the increased probability of conversion as the energy of the positive ions is increased, as shown by figs. 8, 9, 10, and 11. The positive ions which are not converted into negative ions will come off the surface as reflected positive ions and neutral atoms.

I am indebted to Mr. J. C. Milligan for his assistance when doing the work on nitrogen.

\* The work of dissociation of the ionized molecule  $D_i$  is given by

$$D_i = I_a - I_m + D$$

where  $I_a$  is the ionization potential of the atom,  $I_m$  that of the molecule, and  $D$  the work of dissociation of the normal molecule. Using the values for  $I_a$ ,  $I_m$ , and  $D$  given by Smyth ('Rev. Mod. Phys.', vol. 3, p. 347 (1931)), the values of  $D_i$  are respectively 7.1 volts, 5.6 volts, and 2.4 volts for  $N_2^+$ ,  $O_2^+$ ,  $H_2^+$ .

## SUMMARY

In paper I of this series it was shown that negative ions were produced in mercury vapour by a new process of formation. The present paper is an extension of this work to hydrogen, nitrogen, oxygen, and carbon dioxide. Only monatomic negative ions were found in hydrogen and nitrogen. Oxygen gave diatomic as well as monatomic negative ions. Carbon dioxide gave  $\text{CO}_2^-$ ,  $\text{CO}^-$ ,  $\text{O}_2^-$ ,  $\text{O}^-$ , and  $\text{C}^-$ .

It is shown that all of these ions, like those of mercury, are produced by the new process of formation in which positive ions acquire two electrons from any negatively charged surface, including the filament, to which they are driven. Any negative ions produced by the processes which have been presumed in the past to form negative ions were too few to be detected.

The probability of conversion of positive ions into negative ions increases with the kinetic energy, and with the atomic number of the positive ion. For positive ions of 180 volts' energy the probability of conversion in all of the above gases has values between  $10^{-5}$  and  $10^{-3}$ , depending upon the negative ion formed.

---

## A New Process of Negative Ion Formation

### III—The Energy Distribution of the Negative Ions and Accommodation Coefficients of the Positive Ions

By F L ARNOT, Ph.D., Lecturer in Natural Philosophy, The University,  
St Andrews

(*Communicated by H Stanley Allen, F R S—Received 7 July, 1936*)

#### INTRODUCTION

In the previous paper it has been shown that the negative ions found in hydrogen, nitrogen, oxygen, and carbon dioxide are formed from positive ions which acquire two electrons from a negatively-charged surface, and are then accelerated away from the surface as negative ions

It will be shown in this paper that the negative ions come off the surface on which they are formed with a wide range of energy, extending from zero up to beyond 60 volts for  $O^-$  and beyond 109 volts for  $H^-$ . This energy is derived from the parent positive ions which have 200 volts' kinetic energy on striking the surface.

This provides a new and far more informative method than has been previously used of obtaining accommodation coefficients for positive ions \* The results show that the accommodation coefficient for a positive ion of a particular energy has not a single value, but extends over a wide and continuous range within which one, and sometimes two, values are more probable than others

#### EXPERIMENTAL METHOD

The apparatus used in this work was that described in the previous paper. It has been shown in Part I,† dealing with the formation of negative ions in mercury vapour, that the height of peaks obtained at approximately the same magnet current is accurately proportional to the area under them, and that retarding potential curves obtained by plotting the height of the peak coincide with those obtained by plotting the area of the peak against the retarding potential.

\* The term "accommodation coefficient" is defined on p. 162.

† 'Proc. Roy Soc., A, vol 156, p 538 (1936).

The retarding potential was placed between the Faraday cylinder A and the analyser. For each value of the retarding potential the height of the peak was measured by taking several readings over the top of the peak at

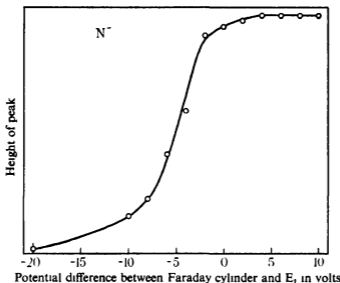


FIG. 1—Retarding potential curve for atomic negative ions of nitrogen

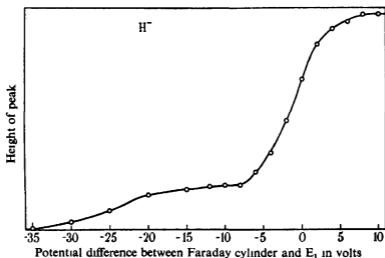


FIG. 2—Retarding potential curve for atomic negative ions of hydrogen

slightly different magnet currents. This procedure was necessary because, as the retarding potential is increased, the top of the peak moves to higher values of the magnet current, since ions of higher energy have greater

momentum, and hence require a stronger field to bring them into the Faraday cylinder

### RESULTS

Retarding potential curves for  $N^-$  and  $H^-$  are given in figs. 1 and 2 respectively. Both the  $N^-$  and the  $H^-$  ions were produced by conversion

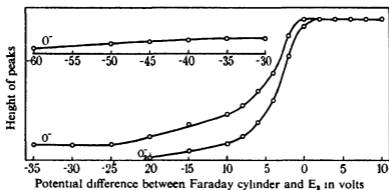


FIG 3—Retarding potential curves for atomic and diatomic negative ions of oxygen.

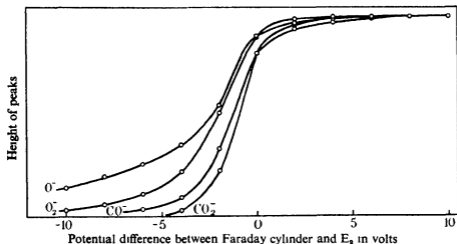


FIG 4—Retarding potential curves for the negative ions formed in carbon dioxide

of 140-volt positive ions\* on  $E_1$ , the potentials being  $V_0 = 60$  volts,  $V_1 = 140$  volts,  $V_2 = 0$ . Both curves represent the height of the negative ion peak plotted against the potential difference between the Faraday cylinder and the gauze  $E_1$  on which the negative ions originate.

\* Results to be described later (see p 164) indicate that practically all the positive ions hitting  $E_1$  have 140 volts energy. The reason for this is probably due to the formation of a thin positive ion sheath over  $E_1$ .

Retarding potential curves for the  $O^-$  and  $O_2^-$  ions obtained in oxygen are shown in fig 3, and those for the ions  $CO_2^-$ ,  $CO^-$ ,  $O_2^-$ , and  $O^-$  obtained in carbon dioxide are given in fig 4. All of these negative ions were produced by conversion of 200-volt positive ions† on  $E_2$ , the potentials being  $V_0 = 100$ ,  $V_1 = -200$ ,  $V_2 = 200$  for fig. 3, and  $V_0 = 60$ ,  $V_1 = -200$ ,  $V_2 = 200$  for fig. 4. Retarding potential curves of positive ions described in the work on mercury vapour showed that no contact potential existed between the nickel gauzes and the Faraday cylinder, which was nickel-plated.

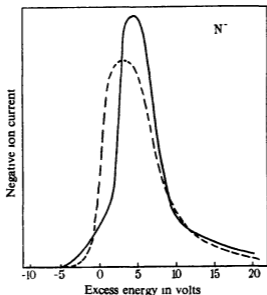


FIG. 5.—Energy distribution curves for atomic negative ions of nitrogen. Continuous curve is for ions formed on  $E_1$ . Broken curve is for ions formed on the filament.

By differentiation of the retarding potential curves we obtain the corresponding energy distribution curves shown in figs 5, 6, 7, and 8. The energy scales in these figures represent the energy of the negative ions in excess of that which they would have if they left the gauze on which they originate with zero energy. Thus the ions appearing at +10 volts all left the gauze after formation with 10 volts' energy. This excess energy must be derived from the energy of the positive ions from which they originate, and for which the accommodation coefficient of the gauze is less than unity. It will now be clear that the *negative* potentials in the retarding potential curves become *positive* energies in the energy distribution.

† Positive ion analysis curves show by the sharpness and position of the peaks that most of the positive ions have 200 volts' energy.

curves, since negative ions overcoming a negative retarding potential have a positive excess energy

The continuous curve in fig. 5 is the differential of fig. 1, and represents the energy distribution of the  $N^-$  ions formed from 140-volt positive ions

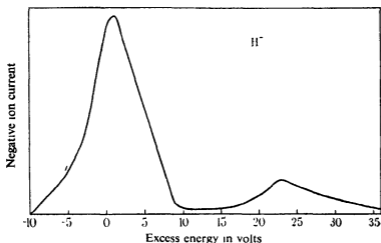


FIG. 6—Energy distribution curve for atomic negative ions of hydrogen

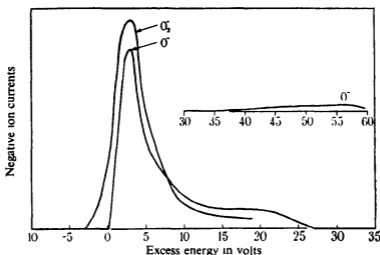


FIG. 7—Energy distribution curves for atomic and diatomic negative ions of oxygen.

on the gauze  $E_1$ . The broken curve in fig. 5 is the differential of a retarding potential curve for  $N^-$  ions formed from 200-volt positive ions on the filament.

The negative ions having a *negative* excess energy can be accounted for as was done in paper I on  $\text{Hg}^-$  ions, partly by assuming that they lose energy by collision with neutral atoms in the ionization chamber and analyser, and partly by the finite resolving power of the apparatus.

We thus see that the negative ions in each gas come off the surface on which they are formed with a wide range of energy extending from zero up to 10, 20, or even beyond 36 volts for  $\text{H}^-$ , and beyond 60 volts for  $\text{O}^-$ .

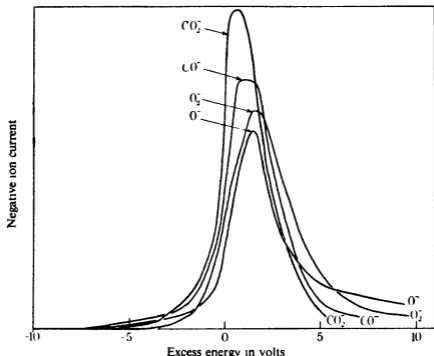


FIG. 8.—Energy distribution curves for the negative ions formed in carbon dioxide

This energy must be derived from the kinetic energy of the positive ions for which the accommodation coefficient is less than unity.

The accommodation coefficient  $\alpha$  is defined by the equation

$$\alpha = \frac{E_i - E_r}{E_i - E_s}$$

where  $E_i$ ,  $E_r$ , and  $E_s$  are respectively the kinetic energy of incidence of the positive ions, that of reflexion in the form of negative ions, and that characteristic of the temperature of the reflecting surface. For no loss of energy on reflexion  $\alpha$  is zero, while for complete adjustment on impact, as when the ion is absorbed and re-evaporated,  $\alpha$  is unity. In this work

$E_+$  is about 0.04 volt, and is therefore negligible. Thus  $\alpha$  represents the fraction of the total kinetic energy of the positive ion lost on impact with the surface.

It is evident from the results given above that the accommodation coefficient does not have a single value, but can take a wide range of values for any one ion incident with a particular energy. It is also clear that the energy distribution curves represent the *probability distribution of the accommodation coefficient*. We see that in each gas the most probable value of the accommodation coefficient is such that the positive ion after reflexion as a negative ion from the surface retains an energy of the order of a volt or two, and that in general the probability of this coefficient having a smaller value decreases as the value of the coefficient decreases.

A very interesting effect is found to occur in hydrogen. It will be seen from figs 2 and 6 that the  $H^-$  ion has a greater probability of being emitted from the surface with an energy of 1 volt or of 23 volts than with any other value. This means that the accommodation coefficient has *two* quite different and widely separated values that are more probable than intermediate values. This effect in hydrogen is shown up very strikingly in the magnetic analysis of the  $H^-$  peak which is given in fig. 3 of the previous paper. These curves in fig. 3 of the previous paper were all taken with  $V_0 = 60$  volts and  $V_2 = 200$  volts. Thus the ions were accelerated off the gauze  $E_2$  into the analyser by a field of 200 volts. The kinetic energy of the positive ions striking the gauze  $E_2$  is given by  $V_1$ .

The lower energy peak in each curve is composed of the  $H^-$  ions, which are shown by fig. 6 in this paper to leave the gauze with a mean energy of 1 volt when the positive ions striking the gauze have an energy of 140 volts. The accommodation coefficient for this peak is therefore 0.993. If this were independent of the initial energy of the positive ions we should expect the position of the peak to move down from 0.1850 amps. to 0.1846 amp. when  $V_1$  is changed from 200 volts to 70 volts. This movement would be quite imperceptible, and is thus in accordance with the evidence of fig. 3 of the previous paper, showing that the position of the peak remains constant at 0.185 amp.

From the position of the higher energy peak relative to that of the lower energy peak in fig. 3 of the previous paper, we can calculate the mean energy with which the  $H^-$  ions composing the higher energy peak leave the gauze, and from this energy the accommodation coefficient for this peak can be found. The results obtained are shown in Table I.

We see that when the positive ions have an energy of 140 volts the negative ions come off the gauze  $E_2$  with an energy of 23 volts, which is in exact agreement with the value found by the retarding potential method

for ions reflected from the gauze  $E_1$ , shown in fig. 6. This shows that most of the ions striking  $E_1$  really do have an energy of 140 volts, as stated in the footnote on p. 159, and explained there by the presence of a thin positive ion sheath over  $E_1$ . We also see from Table I that the accommodation coefficient for this peak increases as the energy of the positive ions is decreased.

TABLE I—ACCOMMODATION COEFFICIENTS CALCULATED FROM FIG. 3 OF THE PREVIOUS PAPER

Energy of positive ions	Position of peak	Energy retained by ion, $E_r$	Accommodation coefficient
Volts	Amps	Volts	$\alpha$
200	0.210	59	0.706
170	0.204	38	0.777
140	0.199	23	0.838
100	0.192	9.5	0.905

This effect in hydrogen, that of the accommodation coefficient having two distinct values that are more probable than intermediate values, also occurs in oxygen, as shown by figs. 3 and 7. We see that the energy distribution curve for  $O^-$  has two peaks, one occurring at 3 volts, and the other between 55 and 60 volts. Now the positive ions in fig. 7 have an energy of 200 volts, and we see from Table I that when the positive ions of hydrogen have an energy of 200 volts the higher energy peak occurs at 59 volts. Since we get a high energy peak in both hydrogen and oxygen occurring at about 60 volts, and corresponding to an accommodation coefficient of 0.7, it seems very likely that this effect is due to some property of the nickel surface at which the ion is reflected, and is independent of the ion itself.

The presence of this high energy  $O^-$  peak is apparent in fig. 2 of the previous paper. Calculation shows that if 200-volt  $O^-$  ions appear at a magnet current of 0.73 amp.,  $O^-$  ions of 260 volts' energy should appear at 0.83 amp. A distinct bulge on the side of the  $O^-$  peak in fig. 2 of the previous paper does occur at about 0.83 amp. The two peaks are not resolved as they are in hydrogen, since the resolving power of the analyser is much less at these higher fields.

An important difference between the energy distribution curves given in this paper and those for negative ions of mercury\* is that, whereas the maximum of the mercury curves occurred precisely at zero excess energy, the maximum of each of the curves shown here occurs at a positive value

\* 'Proc. Roy. Soc.' vol. 156, p. 538 (1936)

of the excess energy This means that the majority of the  $\text{Hg}^-$  ions leave the electrode on which they are formed with zero energy, whereas the majority of each of the lighter negative ions investigated in this paper come off the electrode on which they are formed with a finite energy of the order of a few volts

The reason for this is probably due to the fact that the mercury ions are heavier than the tungsten atoms forming the surface off which they were reflected, whereas the ions investigated here are all lighter than the atoms of the nickel surface on which the negative ions are formed Compton\* recently put forward the theory, based on the classical principle of momentum transfer between a moving and a stationary particle, that the accommodation coefficient for positive-ions striking a metal surface should be less than unity only if the mass of the metal atom exceeds that of the positive ion Although this theory requires modification since, in its

TABLE II—PRINCIPAL AND MINIMUM VALUES OF THE ACCOMMODATION COEFFICIENT

Ion	Energy of incidence Volts	Principal values of $\alpha$		Minimum value of $\alpha$
		—	—	
$\text{Hg}^+$	200	1 000	—	< 0 90
	200	0 993	0 706	< 0 455
	170	0 993	0 777	< 0 530
	140	0 993	0 838	< 0 580
$\text{H}^+$	100	0 993	0 905	< 0 700
	70	0 993	—	< 0 800
	140	0 968	—	< 0 84
$\text{N}^+$	140	0 968	—	< 0 84
$\text{O}^+$	200	0 985	0 715	< 0 70
$\text{O}_2^+$	200	0 985	—	< 0 89
$\text{CO}_2^+$	200	0 997	—	< 0 97

present form, it is unable to explain why many of the  $\text{Hg}^-$  ions come off the surface with high energy, yet it does account for the fact that the *most probable value* of the accommodation coefficient is unity for mercury ions and less than unity for the ions formed in hydrogen, nitrogen, oxygen, and carbon dioxide

Table II contains the principal values and an upper limit to the minimum values of the accommodation coefficient determined from figs 5, 6, 7, and 8. The principal values of  $\alpha$  are calculated from the position of the maxima occurring in the energy distribution curves. An extrapolation of these

\* 'Proc Nat Acad Sci Wash,' vol 18, p 705 (1932) See also Compton and Lamar, 'Phys Rev,' vol 44, p 338 (1933)

curves to obtain the minimum values of  $\alpha$  is too uncertain owing to the possibility of a second maximum appearing as in hydrogen and oxygen. An upper limit to the minimum value has therefore been calculated from the end points of the curves. The actual minimum value is probably considerably smaller than this upper limit. In hydrogen the upper limit has been determined from the curves of fig. 3 of the previous paper. We see that for 200-volt  $H^+$  ions the minimum value of  $\alpha$  is less than 0.455, which means that some  $H^-$  ions come off the surface with an energy greater than 109 volts. The values for mercury, which are taken from paper I, are for a tungsten surface, the other values are for a nickel surface.

It will be seen from fig. 8 that the probability of an ion coming off the surface with a small energy depends upon the type of ion, and increases in the order  $O^-$ ,  $O_2^-$ ,  $CO^-$ ,  $CO_2^-$ . The probability of the ion coming off with a high energy increases in the reverse order,  $CO_2^-$ ,  $CO^-$ ,  $O_2^-$ ,  $O^-$ . In other words, the probability of the accommodation coefficient having a *high value* is least for the  $O^-$  ions and greatest for the  $CO_2^-$  ions, and increases with the type of ion in the order  $O^-$ ,  $O_2^-$ ,  $CO^-$ ,  $CO_2^-$ . Conversely the probability of the accommodation coefficient having a *small value* is least for the  $CO_2^-$  ions and greatest for the  $O^-$  ions, and increases in the order  $CO_2^-$ ,  $CO^-$ ,  $O_2^-$ ,  $O^-$ . Fig. 7 confirms the conclusion that the probability of the accommodation coefficient having a high value is greater for diatomic than for monatomic oxygen ions, whereas a low value is more probable for the monatomic ions than for the diatomic ions.

#### SUMMARY

The energy distribution of positive ions rebounding as negative ions from a nickel surface has been measured for the ions formed in hydrogen, nitrogen, oxygen, and carbon dioxide. The negative ions come off the surface on which they are formed with a wide range of energy, extending from zero to beyond 60 volts for  $O^-$  and beyond 109 volts for  $H^-$  when the parent positive ions strike the surface with an energy of 200 volts.

This provides a new and far more informative method than has been previously used of obtaining accommodation coefficients for positive ions. The results show that, for the positive ions formed in each gas, the accommodation coefficient for ions of a particular energy has a wide range of values amongst which there is always one, and sometimes two, most probable values.

---

## The Absorption Spectra of Triiodides

By C B ALLSOPP, M A , Ph D

(Communicated by T M Lowry, F R S—Received 8 July, 1936)

The absorption spectra of the triiodides are of particular interest in view of the striking fact, to which attention was directed ten years ago by Professor Lowry,\* that the same twin maxima of intensity occur at about 3500 Å and 2900 Å respectively in the absorption spectra both of iodoform  $\text{CHI}_3$  and of potassium triiodide  $\text{KI}_3$ . This similarity could not be accounted for by the conventional theories of valency, which would assign three covalent C—I bonds to the former compound, whereas the most plausible formula for the other contains an  $\text{I}_3^-$ -ion, with the probable configuration  $\text{K}^+ \text{I}_3^{--}$  [III]

Subsequent investigations revealed similar maxima in the spectra of  $\alpha$ -dimethyltelluronium diiodide  $\text{TeMe}_2\text{I}_2$  and of the so-called "  $\beta$ -diiodide "  $[\text{TeMe}_3] \text{TeMeI}_4$ ,† in those of the corresponding diethyl compounds  $\text{TeEt}_2\text{I}_2$  and  $[\text{TeEt}_3] \text{TeEtI}_4$ ,‡ and in that of the diiodide of cyclo-telluropentane  $\text{C}_5\text{H}_{10}\text{TeI}_2$ .§ The formulae of these compounds have been written as containing either an I<sup>-</sup>-ion (in the diiodides) or covalently bound iodine (in the tetraiodides) || Two bands, with a much wider separation than in  $\text{CHI}_3$  or  $\text{KI}_3$ , have also been recorded in the spectrum of thallium triiodide  $\text{TlI}_3$ ,¶ they were used as evidence that the triiodide is neither a completely ionized thallic iodide nor a thalious periodide, but must contain at least a part of the iodine linked covalently to the metal. Finally, the original bands were again recorded in the spectra of  $\text{CsI}_3$  and  $\text{CsI}_2\text{Br}$  and of the quaternary ammonium halides  $\text{QmI}_3$  and  $\text{QmI}_2\text{Br}$ , in which Qm represents the *p*-bromophenyltrimethylammonium radical \*\*. There is strong chemical evidence that the halogen atoms in these compounds form complex ions in which one atom has a positive charge and the two others negative ones, the electropositive atom

\* ' J Chem Soc. ' p 622 (1926)

† Lowry, Goldstein, and Gilbert, ' J Chem Soc. ' p 307 (1928)

‡ Gilbert and Lowry, ' J Chem Soc. ' p 3179 (1928)

§ Gilbert and Lowry, ' J Chem Soc. ' p 2658 (1928)

|| See Lowry and Huther, ' Rec Trav chim ' Pays-Bas, vol. 55, p 688 (1936), Lowry and Miss ter Horst, *ibid*, p 697

¶ Berry and Lowry, ' J Chem Soc. ' p 1748 (1928)

\*\* Gilbert, Goldstein, and Lowry, ' J Chem Soc. ' p 1092 (1931)

always being the heaviest halogen in the complex \* This evidence is supported by the X-ray analysis of  $\text{CsICl}_2$ , which indicates for the complex anion a linear structure with the iodine centrally placed between two chlorines†, corresponding electronic configurations for the ions have been formulated on the basis of measurements of their magnetic susceptibilities ‡ On these grounds, the formulae for the  $\text{I}_3^-$  and  $[\text{I}_2\text{Br}]^-$  ions could be written  $[\ddot{\text{I}}\ddot{\text{I}}\ddot{\text{I}}]$  and  $[\ddot{\text{I}}\ddot{\text{I}}\ddot{\text{Br}}]$  respectively Comparison with the absorption spectra of the ions  $\text{IBr}_2$ ,  $\text{IBrCl}$ , and  $\text{ICl}_2$ , in which the iodine is always electropositive, then showed that the twin bands only appear when negative iodine is linked to positive iodine, and not at all when positive iodine alone is present

The same bands have recently been discovered by de Boer§ in quite different circumstances, namely in the spectrum of iodine adsorbed as a unimolecular layer on the surface of a  $\text{CaF}_2$  crystal, when the maxima have wave-lengths 3450 Å and 2840 Å respectively, and are nearly ten times more intense than those in the spectra of  $\text{KI}_3$  or  $\text{CsI}_3$  Chilton and Rabinowitsch|| also found two similar maxima, but at longer wave-lengths (c 4975 Å and 4375 Å) in the spectrum of iodine adsorbed on chabasite De Boer's interpretation of these spectra is as follows. The energy difference between the two maxima is about 0.8 volt, which is almost the difference between the energies of the iodine atom in its normal and its excited, metastable states ( $2P_1$  and  $2P_1'$ ) The absorption spectrum of the iodine molecule  $\text{I}_2$ , in the vapour or in its violet solutions, also contains two bands, the first at about 5000 Å corresponding with dissociation into one excited and one unexcited atom,¶ and the second at 7320 Å, corresponding with dissociation into two normal atoms\*\* The separation between these two bands is also equal to about 0.8 volt The twin bands of the spectrum of adsorbed iodine may therefore be identified with those of the free molecule with a displacement of 1.9 volts towards shorter wave-lengths on account of the change in binding energy on adsorption A similar explanation would be valid for the spectrum observed by Chilton and Rabinowitsch Alternatively, it might be that through the strong polarization of the adsorbed  $\text{I}_2$  molecules a complex

\* McCombie and Reade, 'J Chem Soc,' vol 123, p 142 (1923), vol 125, p 148 (1924), p 2528 (1926)

† Wyckoff, 'J Amer Chem Soc,' vol 42, p 1100 (1920)

‡ Gray and Dakers, 'Phil Mag,' vol 11, p 81 (1931)

§ 'Z phys Chem,' B, vol 14, p 163 (1931), vol 21, p 208 (1933)

|| 'Z phys Chem,' B, vol 19, p 107 (1932)

¶ Franck, 'Z phys Chem,' vol 144, p 120 (1926).

\*\* Brown, 'Phys Rev,' vol 38, p 1187 (1931)

ion containing fluorine is formed, with a structure  $[FII]^{-\frac{1}{2}+\frac{1}{2}}$  identical with that of the polyiodide ions described above. In either case, the primary act on absorption of light must produce both neutral and excited iodine atoms, the band of longer wave-length corresponding with the former process and that of shorter wave-length with the latter. The same effect has since been found in the spectrum of bromine adsorbed on a  $CaF_2$  surface, when the same explanation is again valid.\*

Twin bands, at much shorter wave-lengths but with a similar difference of energy, also occur in the absorption spectra of the vapours and of the aqueous solutions of the alkali iodides,† and Lederle‡ has shown that in aqueous solutions of  $LiI$ ,  $NaI$ ,  $KI$ ,  $SrI_2$ ,  $MgI_2$ ,  $ZnI_2$ , and  $CdI_2$  their appearance is independent both of the cation and of concentration, so that they are characteristic of hydrated  $I^-$ . The difference of energy between the maxima again led to the association of these bands with the production of a neutral or of an excited  $I$  atom, and the first step in the absorption is then 'the loss by the iodine ion of its electron, either to the cation or to a water molecule attached to the anion, producing either two separated neutral atoms or a free iodine atom in the two cases respectively. The wave-lengths of these maxima are 2262 Å and 1935 Å, and they have the same intensity,  $\log \epsilon = 4.13$ . Lederle also found them in alcoholic solutions of  $HgI_2$  and  $CdI_2$ , but they are then displaced towards longer wave-lengths and their relative intensities are changed.

The occurrence of two bands of equal intensity and the same difference of frequency (about  $6000\text{ cm}^{-1}$ ) in all these spectra suggests at once that they have a common origin, *i.e.*, in the simultaneous production of a normal and an excited (metastable) iodine atom during the absorption process. Experiments which are described in the present paper reveal that the same twin bands are also characteristic of the triiodides of the trivalent elements As, Sb, and Bi, the intense colour of which (brick red, orange red, and black) indicates the presence of covalently bound iodine, since the iodine ion is colourless, and that they also occur in the spectra of iodine compounds of quadrivalent tin, and some properties of the bands which have now been observed give no reason for supposing that any alternative postulate as to their origin is necessary.

\* Custers and de Boer, 'Physica,' vol. 1, p. 265 (1934).

† Franck, Kuhn, and Rollefson, 'Z. Physik,' vol. 43, p. 155 (1927), Hilsch and Pohl, 'Z. Physik,' vol. 57, p. 145 (1930), Franck and Scheibe, 'Z. phys. Chem., A,' vol. 139, p. 22 (1928), Franck and Haber, 'S.B. preuss. Akad. Wiss. Berl.,' p. 250 (1931).

‡ 'Z. phys. Chem., B,' vol. 10, p. 121 (1930).

1—ABSORPTION SPECTRA OF  $\text{AsI}_3$ ,  $\text{SbI}_3$ , AND  $\text{BiI}_3$ 

The maxima in the absorption curves for alcoholic solutions of  $\text{AsI}_3$ ,  $\text{SbI}_3$ , and  $\text{BiI}_3$ , which are reproduced in fig 1, were as follows:—

$\text{AsI}_3$   $\log \epsilon = 4.21$  at  $3560 \text{ \AA}$ ,  $\log \epsilon = 4.34$  at  $2940 \text{ \AA}$ ,

$\text{SbI}_3$   $\log \epsilon = 4.07$  at  $3570 \text{ \AA}$ ,  $\log \epsilon = 4.20$  at  $2920 \text{ \AA}$ ,

$\text{BiI}_3$   $\log \epsilon = 4.02$  at  $3560 \text{ \AA}$ ,  $\log \epsilon = 4.19$  at  $2940 \text{ \AA}$

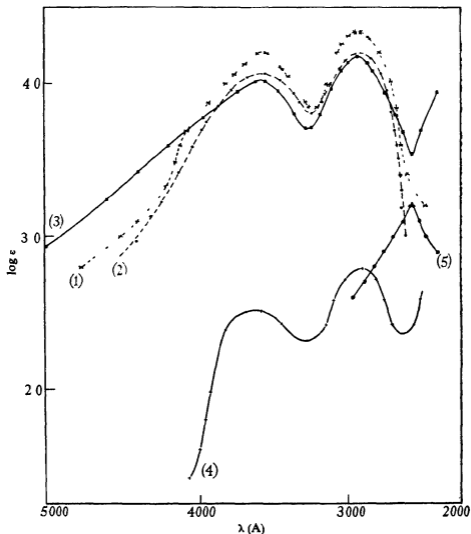


FIG 1—Molecular extinction coefficients of (1)  $\text{AsI}_3$ , (2)  $\text{SbI}_3$ , (3)  $\text{BiI}_3$ ; (4)  $\text{SnCH}_3\text{I}_3$ ; in alcohol; (5) product of reaction of  $\text{AsI}_3$  with ether

The frequency differences were 5920, 6240, and 5920  $\text{cm}^{-1}$  respectively. The similarity of the curves, and the value of the difference of frequency, suggests that the bands have the same origin as those already described, but a number of phenomena observed during the measurements seemed to indicate that the spectra of the solutions might not be characteristic of the triiodide molecules themselves. Thus (i) the crystals dissolve very slowly in alcohol and the yellow colour of the solutions is not developed immediately, (ii) the original material could not be recovered from the solutions, which, even on slow evaporation in the cold *in vacuo*, yielded only tarry residues; (iii) the twin bands for the three compounds are extremely similar to one another, so that they might easily have been due to some common product of interaction of the trivalent iodides with the solvent. They could not, however, be attributed to iodoform, the bands of which are from four to seven times less intense, and are also separated slightly more widely both in wave-length and in intensity, moreover, the smell of iodoform was never detected in the solutions. The bands are also more intense than those of  $\text{KI}_3$  in water, but the solutions of  $\text{CsI}_3$  and  $\text{QmI}_3$  in alcohol give maxima of still greater intensity. These observations would therefore be compatible with the formulation of the three triiodides as univalent periodides, but this hypothesis is excluded by the well-established valencies of the elements in question. The suggestion that  $\text{HI}_3$  might be formed by some process analogous to its reversible formation in alcoholic solutions of elementary iodine\* leads to even more serious difficulties, since the absence of a visible band at 4470 Å showed that there was no free iodine in the solutions. It can therefore only be supposed that if alcoholysis does occur, it is incomplete and leaves some at least of the halogen atoms bound directly to the metal, although the gradual development of the colour of the solutions might also be due to the disintegration of polymeric complexes.

*Decomposition by Ether*—More definite conclusions were reached when attempts were made to observe the absorption spectrum of  $\text{AsI}_3$  in ether. For this purpose 0.0057 gram of  $\text{AsI}_3$  was dissolved in 25 cc. of ether, which had been dried over sodium and distilled from phosphoric oxide. The solution had a yellow colour which faded after a few hours. It then showed a single maximum,  $\log \epsilon = 3.21$  at 2570 Å (fig. 1, curve 5). This is at the same wave-length as that of methyl iodide, namely  $\log \epsilon = 2.7$  at 2600 Å.,† but is three times more intense. It was therefore

\* Batley, 'Trans. Faraday Soc.', vol. 24, p. 438 (1928).

† Lowry and Sass, 'J. Chem. Soc.', p. 622 (1926).

attributed to the formation of ethyl iodide in accordance with the equation  $2\text{AsI}_3 + 3\text{Et}_2\text{O} = \text{As}_2\text{O}_3 + 6\text{EtI}$

*Experiments in Carbon Tetrachloride*—An attempt to obtain a spectrum of  $\text{SbI}_3$  under conditions in which no interaction with the solvent can occur was finally made by allowing metallic antimony and iodine to interact in presence of carbon bisulphide, and diluting with a large bulk of carbon tetrachloride, in which solvent alone the crystalline iodide is insoluble. For this purpose, a solution of iodine (0.5 gm) in  $\text{CS}_2$  (25 cc) was shaken intermittently for some hours with an excess of metallic antimony until the colour of the iodine was discharged. The greenish-grey solution was then diluted with 100 volumes of  $\text{CCl}_4$ , whereby the concentration of  $\text{CS}_2$  was reduced to a point at which it no longer prevented a comparison of the absorptive power of the solution with that of the solvent. The almost colourless solution thus obtained gave the molecular extinction coefficients recorded in fig. 2. The curve (1) now shows a single maximum  $\log \epsilon = 4.63$  at 3150 Å, which is twice as strong as the twin maxima of the alcoholic solutions, and is intermediate in wave-length, with a step-out at 3850 Å. Fig. 2 also shows by means of the broken curves the progressive development of the twin maxima when solutions of  $\text{SbI}_3$  in  $\text{CS}_2$  were diluted with alcohol instead of with carbon tetrachloride. Immediately after dilution, the solution (2) showed the same maximum at 3150 Å as in  $\text{CCl}_4$ , although it was ten times less intense. After 36 hours it had disappeared completely and had been replaced by twin maxima at 3450 Å and 2900 Å separated by a shallow minimum as shown in curve (3). The final appearance of the spectrum, when the solution had developed a characteristic yellow colour after standing for a week, is shown in the thin continuous curve (4).

In view of the fact that  $\text{SbI}_3$  can be recrystallized without change from  $\text{CS}_2$ , this striking result might be held to indicate conclusively the secondary nature of the spectra containing the twin bands which were obtained from the alcoholic solutions, but closer inspection of curve (1) shows that such a conclusion is unnecessary, since the maximum at 3150 Å may be identified with the band at 2900 Å in curve (4), and the step-out at 3850 Å with the band at 3600 Å, the whole spectrum being displaced by about 250 Å on passing from  $\text{CCl}_4$  to  $\text{C}_2\text{H}_5\text{OH}$  as solvent. This phenomenon can be explained satisfactorily if it is assumed that (i) both spectra are due to  $\text{SbI}_3$ , and (ii) the twin bands have the same significance as those in the spectra which were described above.  $\text{SbI}_3$  is insoluble in  $\text{CCl}_4$  alone but remains in solution in  $\text{CS}_2$  when this is flooded with  $\text{CCl}_4$ . This may be attributed to the formation of a molecular complex

$x\text{SbI}_3 \cdot y\text{CS}_2$ , which is not necessarily stable, and which still gives rise to the spectrum of  $\text{SbI}_3$ . Evidence for such a complex may be found in the readiness of the triiodides to form molecular compounds (*see below*) and in the high polarity of the  $\text{CS}_2$  molecules. On the addition of alcohol, in which the  $\text{SbI}_3$  is soluble, the triiodide would distribute itself between the  $\text{CS}_2$  and the alcohol, the decrease of intensity of the maximum in curve (2) indicating that about 90% goes to the alcohol (which is in large

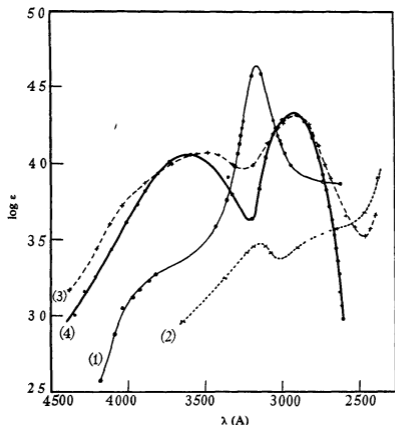


FIG. 2—Influence of solvent on the absorption spectrum of  $\text{SbI}_3$ . (1)  $\text{CS}_2$ ; (2), (3), and (4), alcohol.

excess) immediately, and the subsequent attainment of equilibrium then corresponds with the transition from curve (2) to curve (4). Association of  $\text{SbI}_3$  with an excited  $\text{CS}_2$  molecule ( $\text{CS}_2$  itself absorbs at almost identical wave-lengths) would be expected to favour the release during irradiation of an iodine atom in an excited rather than in an unexcited state, so that the band of shorter wave-length would be enhanced and the intensity of the other diminished, just as is actually observed; whilst the displacement

of the whole spectrum could be attributed to the slightly lower energy required to remove iodine from the activated complex

There is thus no conclusive evidence to show that the twin bands in the spectra obtained with the alcoholic solutions of the triiodides are not characteristic of the molecules of these compounds, and this conclusion has now received complete confirmation from the measurements of the absorption spectra of the *vapours* of  $\text{SbI}_3$  and  $\text{BiI}_3$  made by Butkow, who records the following values for the wave-lengths of the maxima of the bands\* —

$\text{BiI}_3$	4150, 3386, and 2810 Å ,
$\text{SbI}_3$	3430, and 2770 Å

No discrete band of longer wave-lengths was found in the spectrum of the solutions of  $\text{BiI}_3$ , although the absorption curve does not fall off so rapidly towards longer wave-lengths as do those of the other two compounds, but the other two pairs of maxima clearly correspond with those found for the alcoholic solutions, the displacement of each spectrum being about 100 Å on passing from the vapour to the dissolved state

## 2—INFLUENCE OF SOLVENT ON THE ABSORPTION SPECTRUM OF IODOFORM

In view of the marked influence of  $\text{CS}_2$  on the absorption spectrum of antimony triiodide, the absorption spectrum of iodoform was re-examined under similar conditions. The bands now observed for solutions in various solvents are shown in fig. 3, the positions and intensities of the maxima being as follows:—

Solvent	Curve No	Band I		Band II	
		$\lambda_{\text{max}}$	$\log \epsilon_{\text{max}}$	$\lambda_{\text{max}}$	$\log \epsilon_{\text{max}}$
$\text{C}_2\text{H}_5\text{OH}$	1	3490	3.23	2960	3.26
$\text{CCl}_4$	2	3510	3.31	3065	3.20
$\text{CCl}_4 + \text{CS}_2$	3	3490	3.27	2985	3.04
$\text{C}_2\text{H}_5\text{OH}^\dagger$ (irradiated)	4	3600	3.52	2920	3.95

† In the course of these measurements, a marked effect of irradiation on the absorption spectrum of an alcoholic solution of  $\text{CHI}_3$  was observed. Curve (4) was obtained after a solution had been exposed for several hours to the intense ultra-violet radiation from a mercury arc. The twin bands have moved apart, the intensities of both have increased (that at shorter wave-lengths about fivefold), whilst the band of longer wave-length is much wider. These irradiated solutions do not obey Beer's law. The effects may all be attributed to the presence of free iodine, which could be identified in the solutions, and serve to indicate the care necessary in recording absorption spectra of this type.

\* 'Z. Physik,' vol. 90, p. 810 (1934). The experiments described in the present paper were carried out in 1932.

These wave-lengths must be compared with those of the same pair of maxima, at 3450 Å and 2940 Å respectively, observed for the *vapour* of iodoform by Iredale \* The agreement is so close as to leave no doubt that the spectra obtained with the solutions are those characteristic of the iodoform molecule

On passing from alcoholic solutions to those obtained by making a saturated solution of iodoform in  $\text{CS}_2$  and then diluting 100 times in

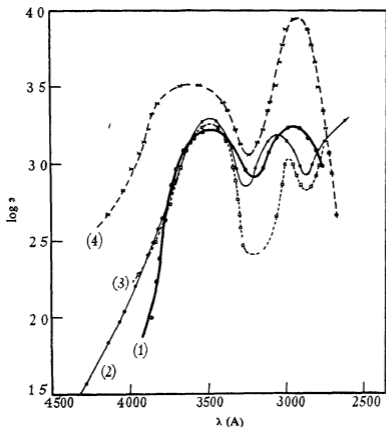


FIG 3—(1) Absorption spectrum of iodoform in alcohol, (2)  $\text{CCl}_4$ , (3)  $\text{CCl}_4 + \text{CS}_2$ ; (4) alcohol after irradiation

$\text{CCl}_4$ , there is again a striking change in the appearance of the absorption curve, but in a manner quite different from that for  $\text{SbI}_3$  under similar conditions, since it is now the maximum of *shorter* wave-length which is changed, both its intensity and its width being diminished (curve 3), whilst the other band remains unaffected and the spectrum as a whole is hardly displaced. A much larger change in position was, in fact, observed

\* 'Z. phys. Chem.,' B, vol 20, p 340 (1933)

with a solution in  $\text{CCl}_4$  alone (curve 2) This difference in behaviour in the presence of  $\text{CS}_2$  might be due to a difference in the origin of the two spectra, but the similarity of the curves and of the wave-lengths makes this unlikely; and there is also a slight difference in the conditions of measurement in the two cases, since iodoform is freely soluble in  $\text{CCl}_4$  and it is therefore not necessary to postulate the formation of a complex molecule with  $\text{CS}_2$  in order to account for the stability of the solutions in the mixed solvent The change might then be attributed to a kind of Stark effect in the presence of activated  $\text{CS}_2$  molecules It is interesting to relate the diminution in the area of the band, and thus presumably the diminution in probability of production of an excited I atom, in the presence of  $\text{CS}_2$ , with the observed retardation of the photochemical oxidation of iodoform in the presence of this compound \*

### 3—MOLECULAR COMPOUNDS OF THE TRIIODIDES AND OF IODOFORM

In addition to the similarity of their absorption spectra, the triiodides have in common with iodoform the property of forming molecular compounds† Martin‡ has isolated the complexes  $\text{KI}_3 \cdot 2\text{C}_6\text{H}_5\text{CN}$  and  $\text{HI}_3 \cdot 4\text{C}_6\text{H}_5\text{CN}$ , and Kleinboldt and Schneider§ have established the existence of  $\text{AsI}_3 \cdot 3\text{S}_8$ ,  $\text{SbI}_3 \cdot 3\text{S}_8$ ,  $\text{SnI}_4 \cdot 2\text{S}_8$ ,  $\text{CHI}_3 \cdot 3\text{S}_8$ , and  $\text{C}_2\text{I}_4 \cdot 4\text{S}_8$ , in which one  $\text{S}_8$  molecule is attached to each iodine atom This structure was confirmed by observations of Hertel|| on the X-ray spectra of the crystals of  $\text{CHI}_3 \cdot 3\text{S}_8$  and  $\text{AsI}_3 \cdot 3\text{S}_8$ , which have similar symmetry (space group most probably =  $\text{C}_{3v}^1$ ), and readily form mixed crystals, although  $\text{AsI}_3$  and  $\text{CHI}_3$  themselves are quite unlike

This readiness to form molecular compounds has been cited above as evidence for the existence of complexes of the type  $x\text{SbI}_3 \cdot y\text{CS}_2$ , and it therefore seemed desirable to examine the absorption spectrum of  $\text{SbI}_3 \cdot 3\text{S}_8$  and to compare it with that of the isomorphous  $\text{CHI}_3 \cdot 3\text{S}_8$ ¶ Measurements were made with the following solutions  $\text{SbI}_3 \cdot 3\text{S}_8$  and  $\text{CHI}_3 \cdot 3\text{S}_8$  in  $\text{CCl}_4$ ,  $\text{SbI}_3$  or  $\text{CHI}_3$  in  $3\text{S}_8 + \text{CS}_2 + \text{CCl}_4$ ,  $\text{SbI}_3$  in  $12\text{S}_8 + \text{CS}_2 + \text{CCl}_4$  These were prepared by mixing the elements in the correct stoichiometrical proportions in carbon bisulphide, when the

\* Cf Dubrissay and Emschwiller, 'C R Acad Sci, Paris,' vol 195, p 660 (1932).

† See, for instance, Auger, 'C R Acad Sci, Paris,' vol 146, p 477 (1908)

‡ 'J Chem Soc,' p 2640 (1932)

§ 'J prakt Chem,' vol 120, p 238 (1929)

|| 'Z phys Chem,' B, vol 15, p 51 (1931)

¶ Martin's benzonitrile compounds are unsuitable for this purpose in view of the disturbing influence of the phenyl group, he was not able to isolate complexes containing aliphatic nitriles

compound could either be crystallized out and redissolved in  $\text{CCl}_4$  or the solution diluted directly to 100 times its volume with this solvent in the same way as for the corresponding solutions of  $\text{SbI}_3$  and  $\text{CHI}_3$ . The antimony solutions required an excess of sulphur for stability, and the comparison solvent used in the measurements always contained the equivalent amount of sulphur in order to compensate for the increase in absorption due to this. The range of wave-lengths over which observations could be made was thus limited, but the following results could be established.  $\text{CHI}_3$  in  $3\text{S}_8 + \text{CS}_2 + \text{CCl}_4$  gives a band with  $\lambda_{\text{max}} = 3490 \text{ \AA}$ ,  $\log \epsilon_{\text{max}} = 3.32$ ,  $\text{CHI}_3 \cdot 3\text{S}_8$  in  $\text{CCl}_4$  alone gives a step-out at the same wave-length,  $\log \epsilon = 3.45$ , on the side of longer wave-lengths of the intense absorption due to sulphur,  $\text{SbI}_3$  in  $12\text{S}_8 + \text{CS}_2 + \text{CCl}_4$  gives a very flat maximum at  $3560 \text{ \AA}$ ,  $\log \epsilon = 3.28$ , and  $\text{SbI}_3 \cdot 3\text{S}_8$  in  $\text{CCl}_4$  alone also has a step-out at  $3580 \text{ \AA}$ ,  $\log \epsilon = 3.15$ . From this it is clear that, in contrast to the behaviour of  $\text{SbI}_3$  alone in  $\text{CS}_2 + \text{CCl}_4$ , the presence of the sulphur, attached to the iodine atoms, retains the band at longer wave-lengths with an intensity still comparable with that of the same band for  $\text{CHI}_3$  under similar conditions, which would be expected if the saturation of the iodine valencies by the sulphur had prevented the formation of a complex of  $\text{SbI}_3$  with the  $\text{CS}_2$  and had so prevented the change in the intensities of the bands which could be attributed to the excitation of the  $\text{CS}_2$  molecules when that occurred.

#### 4—IODINE COMPOUNDS OF TIN

The absorption spectrum of a specimen of  $\text{CH}_3\text{SnI}_3$  has also been measured. A solution of this compound in  $\text{CCl}_4$  had a faint yellow colour which rapidly changed to that of free iodine on exposure to visible light, but the almost colourless alcoholic solutions remained stable long enough for the curve (4) of fig 1 to be recorded. The two maxima are again observed, at  $3600 \text{ \AA}$ ,  $\log \epsilon = 2.52$ , and at  $2910 \text{ \AA}$ ,  $\log \epsilon = 2.80$ . Their separation ( $6580 \text{ cm}^{-1}$ ) is a little greater than for the trivalent triiodides, and their intensity lower, but their relative intensities are similar.

These results may be compared with those which have been recorded elsewhere\* for a solution of  $\text{SnI}_4$  in hexane, when maxima were found at  $3560 \text{ \AA}$  and  $2850 \text{ \AA}$  (separation =  $7690 \text{ cm}^{-1}$ ) with an intensity about  $\log \epsilon = 4.0$ . In both cases, the spectra are again consistent with the simultaneous production of unexcited and excited iodine atoms

\* Grant, 'Trans Faraday Soc.', vol 31, p 433 (1935)

## DISCUSSION

The results of the experiments which have been described, together with those of other observers, are collected in Table I. Allowing for the fact that the frequency differences are based on the wave-lengths of

TABLE I—ABSORPTION SPECTRA OF COMPOUNDS CONTAINING

Substance	Solvent	Band I		Band II		Frequency difference cm <sup>-1</sup>
		$\lambda_{\max}$	$\log \epsilon_{\max}$	$\lambda_{\max}$	$\log \epsilon_{\max}$	
		A		A		
I <sup>-</sup>	Water	2262	4.13	1935	4.13	7650
KI <sub>3</sub>	EtOH	3550	3.9	2900	3.9	5020
CsI <sub>3</sub>	EtOH	3600	4.46	2900	4.60	6700
	Water	3520	3.3	2900	3.44	6070
QmI <sub>3</sub>	EtOH	3580	4.38	2900	4.55	6550
CsI <sub>3</sub> Br	EtOH	3580	4.02	2900	4.22	6550
QmI <sub>3</sub> Br	EtOH	3600	4.16	2900	4.38	6700
I <sub>2</sub> on CaF <sub>2</sub>	—	3500	c 5.0	2850	c 5.0	6520
TeMe <sub>3</sub> I <sub>3</sub>	EtOH	3570	3.7	2840	4.05	7200
TeEt <sub>3</sub> I <sub>3</sub>	C <sub>6</sub> H <sub>14</sub>	3350	4.36	2700	4.65	7190
[TeMe <sub>3</sub> ] TeMeI <sub>4</sub>	C <sub>6</sub> H <sub>14</sub>	3360	4.49	2640	4.70	8120
[TeEt <sub>3</sub> ] TeEtI <sub>4</sub>	C <sub>6</sub> H <sub>14</sub>	3350	4.51	2670	4.80	7600
C <sub>6</sub> H <sub>10</sub> TeI <sub>3</sub>	EtOH	3560	4.28	2880	4.45	6630
TlI <sub>3</sub>	MeOH	4000	3.9	2600	4.35	13460
CHI <sub>3</sub>	EtOH	3490	3.23	2960	3.26	5230
	CCl <sub>4</sub>	3510	3.31	3065	3.20	4240
AsI <sub>3</sub>	Vapour	3450	—	2940	—	5020
	EtOH	3560	4.21	2940	4.34	5920
SbI <sub>3</sub>	EtOH	3570	4.07	2920	4.20	6240
	Vapour	3430	—	2770	—	6950
BiI <sub>3</sub>	EtOH	3560	4.02	2940	4.19	5920
	Vapour	3386	—	2810	—	5950
SnCH <sub>3</sub> I <sub>3</sub>	EtOH	3600	2.52	2910	2.80	6580
SnI <sub>4</sub>	CCl <sub>4</sub>	3650	c 4.0	2850	c 4.1	7690

maxima of absorption, and not on the limits of the continuous bands, the constancy of the separation is good,\* and, in view of the similarity of the absorption curves, in all these cases (except TlI<sub>3</sub>) leads to the conclusion that the spectra have a common origin, as has been suggested above, in the simultaneous production of excited (metastable) and normal iodine

\* The relationship of the separation of the maxima to the separation of the limits is discussed by Iredale, 'Z. phys. Chem.', B, vol. 20, p. 340 (1933)

atoms, in  $^2P_1$  and  $^3P_1$  states, during the absorption process. None of the effects now observed is out of accordance with this point of view. It remains, therefore, to investigate whether there are probable mechanisms by which this could occur in each of the following systems: (i) a hydrated  $I^-$ -ion; (ii) a triatomic  $I_3^-$  or  $(I_2Br)^-$ -ion, (iii) an adsorbed  $I_2$  molecule, and (iv) iodides of trivalent and quadrivalent elements in which the iodine is linked covalently to the metal. In case (i), the mechanism has already been established quantitatively (*see above*): the ion loses its charge, leaving an iodine atom which may be released in an excited state. A similar process might be postulated to account for the appearance of the bands in the spectra of the tellurium diiodides, if the formulae of these compounds are to be written as containing  $I^-$ . In case (ii), as de Boer has suggested, the adsorbed  $I_2$  may first be released as a neutral molecule which then dissociates either into two normal atoms or into one normal and one excited atom. This mechanism could also apply to the polyhalide ions, when  $[III]$  or  $[BrII]$  could each release  $I_2$  (from  $I^+ + I^-$ ), and this is in accordance with the observation that the two iodine bands do not occur in the spectrum when only  $I^+$  is present, as in  $[BrIBr]$ , when the corresponding product would be  $IBr$ .

There remain only the compounds in which the iodine is covalently bound. The photochemical decomposition of iodoform has been studied by Iredale,\* who also concludes that the primary process results in the liberation of an iodine atom, either in its normal or in its excited state, according as the energy is absorbed in the band of longer or shorter wave-length. It must be noted that the twin bands do not appear in the spectrum either of methyl iodide or of methylene diiodide, each of which contains only a single band, with maxima at 2600 Å and 2960 Å respectively.† With methyl iodide, however, the primary process is the liberation of an excited  $I$  atom,‡ and the same is probably true for  $CH_2I_2$ , so that of the two bands of the iodoform spectrum only that of higher energy would be expected to appear in the other two spectra. In  $CH_3I$  this band should have rather shorter wave-length in view of the greater energy required to disrupt the C—I bond when only a single halogen atom is present.

\* Iredale, 'Z. phys. Chem.', B, vol. 20, p. 340 (1933), Gibson and Iredale, 'Trans. Faraday Soc.', vol. 32, p. 571 (1936).

† Lowry and Sass, 'J. Chem. Soc.', p. 622 (1926), *see also* Gregory and Style, 'Trans. Faraday Soc.', vol. 32, p. 724 (1936).

‡ Herzberg and Scheibe, 'Trans. Faraday Soc.', vol. 25, p. 716 (1929), 'Z. phys. Chem.', B, vol. 7, p. 390 (1930), Iredale, 'J. phys. Chem.', vol. 33, p. 290 (1929).

In the four iodine derivatives of methane, the tendency to decompose freely on irradiation increases rapidly from  $\text{CH}_3\text{I}$  to  $\text{CI}_4$ , as the probability that a normal iodine atom will be produced increases. The spectrum of  $\text{CI}_4$ , therefore, should contain the twin bands, and this has been found to be the case\*. It may therefore be expected that the primary act in the irradiation of the tervalent iodides or of stannic or tellurium compounds containing three or four iodine atoms all bound covalently would also involve the liberation of a neutral iodine atom. Thus, the first stage in the decomposition of  $\text{AsI}_3$  could be  $\text{AsI}_3 \rightarrow \text{AsI}_2 + \text{I}$  (normal) accompanied by  $\text{AsI}_3 \rightarrow \text{AsI}_2 + \text{I}$  (excited) with about the same probability of either process occurring. In this way, the similarity of the spectra which have been described can be completely accounted for, and it may reasonably be concluded that the origin to which they have been attributed is correct.

#### EXPERIMENTAL

*Materials*—I am indebted to Baron Uzumasa for the following preparations. *Arsenic triiodide* was prepared by the method of Oddo and Giachery;† the red crystals were recrystallized from carbon bisulphide and washed with ether. *Antimony triiodide* was prepared by the method of Vournasos,‡ the orange-red product was sublimed, and washed with ether and then with carbon bisulphide until the red colour of free iodine could no longer be seen in the extract. The crystals obtained by direct combination in presence of carbon bisulphide (*see above*) were shown by Mrs Wooster to give the same X-ray spectrum as those prepared by the method of Vournasos. *Bismuth triiodide* was prepared by the method of Vournasos,‡ the grey crystalline precipitate was freed from mother liquor and sublimed in a current of carbon dioxide at about  $200^\circ$ , the black sublimate was then washed with ether and with carbon bisulphide until free from iodine.

*Method*—The absorption spectra were recorded by the methods previously described\*. The points plotted in figs 1–3, with the exception of

\* These measurements were not included above as the data are not considered to be sufficiently accurate. A solution of  $\text{CI}_4$  in  $\text{CCl}_4$  gave bands with maxima at 3860 Å. and 3040 Å. (frequency difference =  $6980 \text{ cm}^{-1}$ ), but as the iodine band at 5200 Å. was also developed strongly, no reliance can be placed on intensity measurements.

† 'Gazz. chim. ital.', vol. 53, p. 63 (1923).

‡ 'C. R. Acad. Sci., Paris,' vol. 166, p. 526 (1918).

§ Allsopp, 'Proc. Roy. Soc., A', vol. 143, p. 618 (1934).

those in the "transitional" curves of fig 2, represent the means of several readings

The author wishes to express his gratitude to Professor T M Lowry, F R S, for suggesting this problem, and for his continual interest and advice while the work was being carried out, he also thanks Professor J E Lennard-Jones, F R S, and Dr G B B M Sutherland for helpful suggestions, and Professor K Fajans for valuable discussion of the data

#### SUMMARY

Twin bands, which are now observed in the absorption spectra of alcoholic solutions of  $\text{AsI}_3$ ,  $\text{SbI}_3$ ,  $\text{BiI}_3$ , and  $\text{SnCH}_3\text{I}_3$ , are very similar to those found in the spectra of solutions of iodoform. The influence of solvents on the absorption spectra of the triiodides and of iodoform is investigated and discussed, and it is shown that the twin bands in these cases can have the same origin as those found in the spectra of the iodide ion, of adsorbed iodine molecules, of the polyhalides of the alkalis, and of a number of iodine derivatives of quadrivalent and hexavalent tellurium, namely in the simultaneous production during irradiation of iodine atoms in the normal and in the excited, metastable state

---

# Dielectric Constants of Solids at High Frequencies and the Influence of Water of Crystallization on Dielectric Constant

By E F BURTON and L G. TURNBULL

(Communicated by O W Richardson, F R S—Received 10 July, 1936)

## 1—INTRODUCTION

The determination of the dielectric constant of one constituent of a mixture, when the dielectric constants of the other component and the mixture itself are known, has been a problem which has been given much attention for many years. The familiar Clausius-Mossotti relationship for the dielectric constant of any substance is

$$\frac{\epsilon - 1}{(\epsilon + 2)d} = A$$
, where  $\epsilon$  is the dielectric constant of the substance,  $d$  the density, and  $A$  a constant depending upon the polarizability of the molecule. This relation was developed independently by Clausius,\* Mossotti,† Lorenz,‡ Lorentz,§ Rayleigh,|| and Debye¶, but even in the case of pure liquids deviations well outside the experimental error have been found.

The case of mixtures was first treated by Lorentz.\*\* He states "If one does not consider all the molecules to be alike, but assumes several kinds, one obtains the formula for the refractive index of a mixture. In the first place it may be assumed that the ratio  $\frac{n^2 - 1}{(n^2 + 2)d}$  is equal to a constant, where  $n$  and  $d$  refer to the mixture, and secondly that between this quantity and the analogous constants  $\frac{n_1^2 - 1}{(n_1^2 + 2)d_1}$ ,  $\frac{n_2^2 - 1}{(n_2^2 + 2)d_2}$ , etc., which refer separately to the constituents of the mixture, the relation

$$\frac{n^2 - 1}{(n^2 + 2)d} = \frac{a_1(n_1^2 - 1)}{d_1(n_1^2 + 2)} + \frac{a_2(n_2^2 - 1)}{d_2(n_2^2 + 2)} + \text{etc}$$
 must hold. Here  $a_1$ ,

\* "Mechanische Wärme Theorie," vol 2, p 94 (1874)

† Lebedew, 'Ann Physik,' vol 44, p 288 (1891)

‡ 'Ann. Physik,' vol 11, p 70 (1880)

§ 'Ann Physik,' vol 9, p 641 (1880)

|| 'Phil Mag,' vol 34, p 481 (1892)

¶ 'Verh phys-med. Ges,' vol 15, p. 777 (1913).

\*\* 'Ann Physik,' vol 9, p 654 (1880).

$a_2$ , etc., are the amounts of the constituents present in unit mass" Replacing  $n^2$  by  $\epsilon_m$ , etc. and  $\left(\frac{a_1}{d_1} \times d\right)$  by  $v_1$  etc., one obtains

$$\frac{\epsilon_m - 1}{(\epsilon_m + 2)} = v_1 \cdot \frac{\epsilon_1 - 1}{\epsilon_1 + 2} + v_2 \frac{\epsilon_2 - 1}{\epsilon_2 + 2} + \text{etc}$$

where  $\epsilon_m, \epsilon_1, \epsilon_2$  refer to the dielectric constants of the mixture and two components respectively, while  $v_1, v_2$  are the volume ratios of the components to that of the whole mixture ( $v_1 + v_2 + \dots = 1$ ) However, the formula will hold only for spheres isotropically arranged in a uniform field.

Wiener\* realized that for a mixture of particles in a liquid medium the geometrical shape of the particles might influence the distribution of the electric field and consequently the dielectric constant of the mixture He derived the following formula for two components

$$\frac{\epsilon_m - 1}{\epsilon_m + u} = v_1 \frac{\epsilon_1 - 1}{\epsilon_1 + u} + v_2 \frac{\epsilon_2 - 1}{\epsilon_2 + u},$$

where the symbols have the same meaning as above, and  $u$  is a constant depending on the geometrical shape of the particles involved Of course, when  $u = 2$  Wiener's formula becomes that obtained by Lorentz

Fricke† worked out the cases of spheroids immersed in a liquid medium and obtained

$$\frac{\epsilon_m - \epsilon_2}{\epsilon_m + u\epsilon_2} = v_1 \frac{\epsilon_1 - \epsilon_2}{\epsilon_1 + u\epsilon_2},$$

where  $u$  is a factor depending upon  $\epsilon_1, \epsilon_2$  and on the geometry of the particles. It is to be noted that since  $v_2$  may be replaced by  $1 - v_1$ , Fricke's equation is practically that of Wiener

## 2—DETERMINATION OF THE VALUE OF THE CONSTANT $u$ IN FRICKE'S EQUATION

In the present investigation, the authors have tested the validity of Fricke's formula, and have found it to hold for mixtures of powdered salts in oil The first salt chosen was sodium chloride, the dielectric constant of which was known from reliable observations ( $\epsilon_1 = 5.81$ ) The mean dielectric constant of the mixture of the powdered salt and a light water-free oil was measured for different volume-concentrations ( $v_1$ ) Using

\* 'Ber sächs Ges (Akad), Wiss,' vol 62, p 256 (1910)

† 'Phys. Rev,' vol 24, p 575 (1924)

the known value of the dielectric constant of the salt itself, a graph of the dielectric constant of the mixture ( $\epsilon_m$ ) against the volume-concentration gave the rectangular hyperbola, in accord with Fricke's equation, as shown in fig 1. The experimental points were found by using two types of measuring cells, one to check the other. The lower limit at  $v_1 = 0$  corresponds to the dielectric constant of the oil medium itself, the upper limit at  $v_1 = 1$  is the known value for the dielectric constant of the sodium

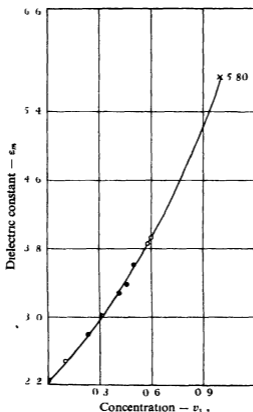


FIG. 1—○ Cell A, ◊ cell B. NaCl in Oil  $\mu = 164$

chloride, at a frequency used in these experiments and at room temperature. However, for the unknown salt, it would seem that considerable error might result in the extrapolation of the curve beyond the experimental points, the limit of these being at a volume concentration of approximately 0.6.

Putting

$$\frac{\epsilon_1 - \epsilon_2}{\epsilon_1 + u\epsilon_2},$$

in Fricke's equation, equal to a constant  $C$ , we have

$$\frac{\epsilon_m - \epsilon_1}{\epsilon_m + u\epsilon_1} = C v_1,$$

from which we obtain :

$$\log \frac{\epsilon_m - \epsilon_1}{\epsilon_m + u\epsilon_1} = \log v_1 + \log C$$

Plotting  $\log \frac{\epsilon_m - \epsilon_1}{\epsilon_m + u\epsilon_1}$  against  $\log v_1$ , there results a straight line, inclined at an angle of  $45^\circ$  with the axis of  $v_1$  (see fig 2). This will be true, however, for one value of  $u$  only, any other value giving a line inclined at some other angle than  $45^\circ$ . By inserting various values of  $u$ , it was possible to find the proper value in the following manner. Arbitrary values of  $u$  were chosen, and for each value of  $u$ , a straight line was plotted as described above (fig 2a and 2b), the values of  $u$  will not be likely to differ very much from 2. The tangent of each line was measured, plotting  $u$  against the tangent obtained resulted in a smooth curve as shown by the full line in fig 3. The value of  $u$  corresponding to a line giving the value of the tangent unity, could be read from the graph. This was the value, used in the ultimate extrapolation of the straight line to the volume-concentration  $v_1 = 1$ . For sodium chloride the proper value of  $u$  was found to be 1.64. This is the value of  $u$  which should be inserted in Fricke's formula for the purpose of calculating  $\epsilon_1$ ; or it is the value of  $u$  which determines the straight line (at  $45^\circ$  to the axis) used for extrapolation to  $v_1 = 1$ . This extrapolation gave  $\epsilon_1 = 5.80$ .

Before measuring the dielectric constants of unknown salts, those of several salts, the values of which were known, were investigated, and good agreement with other observers was found. The procedure in these cases was as follows. From the experimental values of  $\epsilon_m$  up to  $v_1 = 0.6$ , the proper value of  $u$  was determined as indicated above. Using this value of  $u$ , the straight line which gives the relation between  $\log \frac{\epsilon_m - \epsilon_1}{\epsilon_m + u\epsilon_1}$  and  $\log v_1$ , is drawn and extrapolated to  $v_1 = 1$ , at which point  $\epsilon_m$  becomes  $\epsilon_1$ , the dielectric constant of the pure salt. The following is a table comparing these values of  $\epsilon_1$  with those of the International Critical Tables at room temperature and at the frequency used in this investigation.

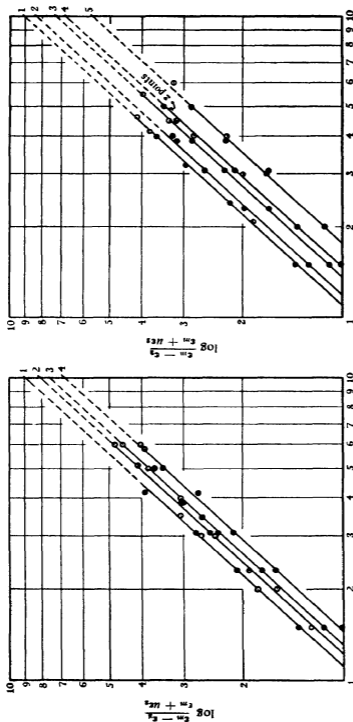


Fig 2a—1,  $\text{MgSO}_4 \cdot 10\text{H}_2\text{O}$ , 2,  $\text{MgSO}_4 \cdot 7\text{H}_2\text{O}$ , 3,  $\text{K}_2\text{Al}_2(\text{SO}_4)_4 \cdot 24\text{H}_2\text{O}$ , 4,  $\text{NaCl}$ , 5,  $\text{Na}_2\text{B}_4\text{O}_7 \cdot 10\text{H}_2\text{O}$ ; 1,  $\text{CuSO}_4 \cdot 5\text{H}_2\text{O}$ , 2,  $\text{Na}_2\text{B}_4\text{O}_7 \cdot 10\text{H}_2\text{O}$ , 3,  $\text{K}_2\text{Al}_2(\text{SO}_4)_4 \cdot 24\text{H}_2\text{O}$ , 4,  $\text{NaCl}$ , 5,  $\text{Na}_2\text{B}_4\text{O}_7 \cdot 10\text{H}_2\text{O}$

TABLE I

Salt	Author's value	International Critical Tables
Potassium Iodide	5.17	5.2
Sodium Chloride	5.80	5.81
Potassium Alum	6.36	6.32 (19° C and $3 \times 10^4$ cycles sec.)

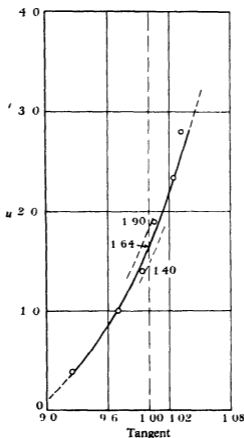


FIG. 3—NaCl.

## 3—EXPERIMENTAL METHOD

A resonance method was used in the determination of the dielectric constants of the samples investigated. The apparatus has been described by McKay.\* Briefly, it consisted of a quartz-crystal oscillator which

\* 'Canad J Res,' vol 12, p 377 (1935)

supplied power, at a frequency of  $2 \times 10^6$  cycles per second, to a resonance circuit in which the measuring cell could be placed. The resulting current was fed through two capacitatively-coupled amplifiers to the detector. A galvanometer in the detector circuit gave deflexions which were a measure of the amplified high frequency current, see fig. 4. The two most interesting features of this apparatus were (1) a symmetrical resonance curve, (2) a resonance capacity independent of the shunt resistance. The former was used in the determination of the resonance capacity in the following way. A condenser (A, in fig. 4) of approximately  $350 \mu\text{fd}$  capacity, placed in parallel with the measuring cell (D), could be switched

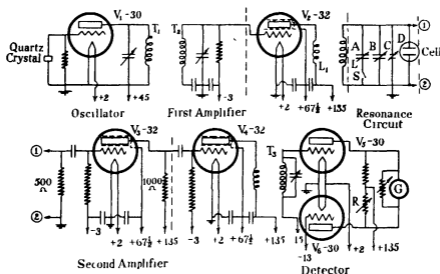


FIG. 4

in and out of the resonance circuit by means of a capacityless switch (S), in such a manner as to determine two points on opposite sides of the resonance peak. Thus when the condenser (A) was switched in and out of the circuit, the galvanometer showed a change in deflexion. In order to locate these two points symmetrically with respect to the peak, a third condenser (B) was necessary. This had a maximum capacity of approximately  $350 \mu\text{fd}$  and was in parallel with the other two condensers (A and D). By means of this, adjustments could be made until the galvanometer showed no change on switching condenser A in and out of the resonance circuit. This indicated that the two points in question were equidistant from the resonance peak and on opposite sides. The average of these two points gave the resonance capacity. Any necessary final adjustments could be made with a small calibrated variable cylindrical condenser (C)

of maximum capacity  $7.5 \mu\text{fd}$  and reading to  $0.003 \mu\text{fd}$ , in parallel with the resonance circuit.

All parts of the apparatus were made quite rigid, and the galvanometer was placed on a massive iron block, damped in oil and suspended by four steel springs. Storage cells were used to heat the valve filaments, and in the final set up, the actual "galvanometer drift" was less than 3 mm. per minute, enabling capacity settings to be made with considerable accuracy.

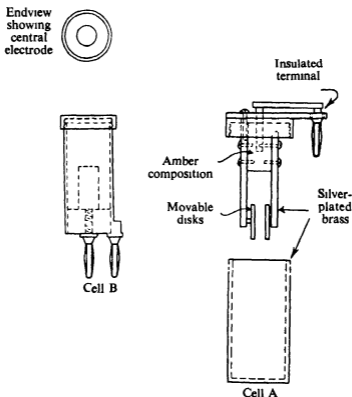


FIG 5

#### 4—MEASURING CELLS

The cells were of two types, as shown in fig. 5. The first of these (A) consisted of two parallel brass disks, rigidly fixed to an amberoid spacer, the whole of which could be securely screwed to a cylindrical brass receptacle. The second (B) was of the cylindrical type. Each condenser was silver plated and had an air capacity of approximately  $2 \mu\text{fd}$ .

## 5—MEASUREMENTS

The salt in question was first finely ground in a mortar, and sifted through a copper screen (6400 mesh). The powder was then mixed in certain determined proportions with a light water-free oil of known dielectric constant.

The effective capacity ( $C$ ) of the empty cell was first determined. It is seen that this is the sum of two capacities, the air capacity of the cell ( $CO$ ) and the capacity of the leads ( $CL$ ), so that

$$C = CO + CL \quad (1)$$

A certain volume of benzene, the dielectric constant ( $\epsilon_B$ ) of which was accurately known at room temperature and at the resonance frequency of the apparatus, was next introduced into the cell. The resultant capacity ( $C'$ ) was then measured. Then

$$C' = \epsilon_B CO + CL \quad (2)$$

From equations (1) and (2),  $CO$  and  $CL$  were determined. The next step was the addition of the salt-oil mixture to the empty cell. Care was taken to introduce the same volume of the aggregate as was occupied by the benzene. The capacity  $C''$  was noted, following the same reasoning as above.

$$C'' = \epsilon_M CO + CL \quad (3)$$

Using the values found for  $CO$  and  $CL$  from (1) and (2) above,  $\epsilon_m$ , the dielectric constant of the salt-oil mixture could be calculated. The dielectric constant of the water-free oil was found in the same way, a mean of several determinations giving it as 2.23.

TABLE II

Salt	Dielectric constant
Na Cl	5.80
$K_2 Al_2(SO_4)_4 \cdot 24 H_2O$	6.36
K I	5.17
$Mg SO_4 \cdot 7 H_2O$	6.20
$Mg SO_4 \cdot 1 H_2O$	7.36
$Cu SO_4 \cdot 5 H_2O$	6.55
$Cu SO_4 \cdot 1 H_2O$	10.1
$Na_2 B_4 O_7 \cdot 10 H_2O$	6.00
$Na_2 B_4 O_7 \cdot 2 H_2O$	7.44

## 6—RESULTS

Table II gives the dielectric constants of the salts investigated. These values have been found from the extrapolated straight lines as shown in

fig 2 Tables III to XI give the dielectric constants of the salt-oil mixtures at different volume concentrations Figs 1, 6, 7, 8, 9, and 10 show the hyperbolic curves which fit the observed points.

TABLE III  
SODIUM CHLORIDE—NaCl IN OIL

Concentration ( $v_1$ )	Dielectric constant of mixture ( $\epsilon_m$ )
(B) 0 100	2 49
(A) 0 231	2 80
(A) 0 308	3 02
(A) 0 417	3 28
(A) 0 461	3 38
(A) 0 500	3 62
(B) 0 580	3 87
(B) 0 600	3 93

Calculated dielectric constant for NaCl = 5 80

TABLE IV  
POTASSIUM ALUM,  $K_2 Al_2(SO_4)_4 \cdot 24 H_2O$  IN OIL

Concentration ( $v_1$ )	Dielectric constant of mixture ( $\epsilon_m$ )
(B) 0 200	2 81
(A) 0 231	2 88
(B) 0 300	3 16
(A) 0 308	3 14
(A) 0 346	3 26
(A) 0 385	3 43
(A) 0 400	3 45
(A) 0 500	3 75
(B) 0 500	3 83
(B) 0 600	4 23

Calculated dielectric constant for potassium alum = 6 36

TABLE V  
POTASSIUM IODIDE, KI IN OIL

Concentration ( $v_1$ )	Dielectric constant of mixture ( $\epsilon_m$ )
(B) 0 100	2 45
(B) 0 300	2 92
(A) 0 308	2 91
(A) 0 385	3 18
(B) 0 400	3 17
(A) 0 500	3 48

Calculated dielectric constant for KI = 5 17

TABLE VI

MAGNESIUM SULPHATE,  $\text{MgSO}_4 \cdot 7\text{H}_2\text{O}$  IN OIL

Concentration ( $v_1$ )	Dielectric constant of mixture ( $\epsilon_m$ )
(B) 0 150	2 61
(A) 0 211	2 83
(A) 0 308	3 04
(A) 0 385	3 25
(B) 0 513	3 71
(B) 0 600	4 04

Calculated dielectric constant for  $\text{MgSO}_4 \cdot 7\text{H}_2\text{O} = 6.20$

TABLE VII

MAGNESIUM SULPHATE (DEHYDRATED),  $\text{MgSO}_4 \cdot \text{H}_2\text{O}$  IN OIL

Concentration ( $v_1$ )	Dielectric constant of mixture ( $\epsilon_m$ )
(B) 0 100	2 54
(B) 0 200	2 86
(A) 0 231	2 97
(B) 0 300	3 20
(A) 0 308	3 25
(B) 0 350	3 38
(B) 0 418	3 78

Calculated dielectric constant for  $\text{MgSO}_4 \cdot \text{H}_2\text{O} = 7.36$

TABLE VIII

COPPER SULPHATE,  $\text{CuSO}_4 \cdot 5\text{H}_2\text{O}$  IN OIL

Concentration ( $v_1$ )	Dielectric constant of mixture ( $\epsilon_m$ )
(A) 0 200	2 80
(B) 0 300	3 09
(A) 0 306	3 15
(A) 0 385	3 38
(B) 0 400	3 51
(B) 0 450	3.71
(B) 0 500	3.88
(A) 0 500	3.89

Calculated dielectric constant for  $\text{CuSO}_4 \cdot 5\text{H}_2\text{O} = 6.55$

TABLE IX

COPPER SULPHATE (DEHYDRATED),  $\text{CuSO}_4 \cdot 1 \text{H}_2\text{O}$  IN OIL

Concentration ( $v_1$ )	Dielectric constant of mixture ( $\epsilon_m$ )
(B) 0 105	2 58
(B) 0 209	2 97
(A) 0 241	3 12
(A) 0 320	3 52
(A) 0 398	3 80
(B) 0 414	4 00
(B) 0 464	4 21

Calculated dielectric constant for  $\text{CuSO}_4 \cdot 1 \text{H}_2\text{O} = 10 \cdot 1$ 

TABLE X

SODIUM BORATE,  $\text{Na}_2\text{B}_4\text{O}_7 \cdot 10 \text{H}_2\text{O}$  IN OIL

Concentration ( $v_1$ )	Dielectric constant of mixture ( $\epsilon_m$ )
(B) 0 100	2 48
(A) 0 231	2 78
(A) 0 308	3 01
(A) 0 385	3 24
(B) 0 450	3 46
(B) 0 550	3 77

Calculated dielectric constant for  $\text{Na}_2\text{B}_4\text{O}_7 \cdot 10 \text{H}_2\text{O} = 6 \cdot 00$ 

TABLE XI

SODIUM BORATE (DEHYDRATED),  $\text{Na}_2\text{B}_4\text{O}_7 \cdot 2 \text{H}_2\text{O}$  IN OIL

Concentration ( $v_1$ )	Dielectric constant of mixture ( $\epsilon_m$ )
(B) 0 100	2 56
(A) 0 231	3 01
(A) 0 308	3 29
(A) 0 385	3 56
(B) 0 400	3 61

Calculated dielectric constant for  $\text{Na}_2\text{B}_4\text{O}_7 \cdot 2 \text{H}_2\text{O} = 7 \cdot 44$ 

## 7—SOURCES OF ERROR

In measuring the dielectric constants of the salt oil mixtures, precautions must be taken to get rid of any air trapped in the mixture, as this tends to decrease the measured effective capacity and hence the dielectric constant of the mixture. Constant tapping of the cell containing the aggregate frees the entrapped air.

With very low concentrations, no air seemed to be mixed with the salt and oil, but the salt appeared to settle out rapidly, especially in the case of sodium chloride, tending to increase the dielectric constant of the mixture. The dielectric constants for small concentrations of powder in oil were obtained by stirring the salt quickly in the oil, pouring the aggregate into the cylindrical cell B, fig 5, while connected in the resonance

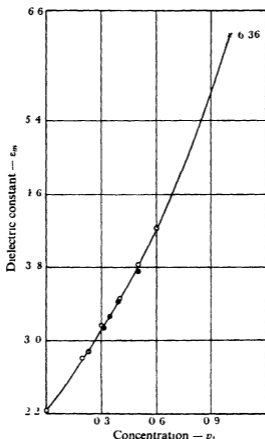


FIG 6— $K_2Al_2(SO_4)_4 \cdot 24 H_2O$  in oil,  $\mu = 2.04$   $\otimes$  cell A,  $\circ$  cell B

circuit, and immediately measuring the capacity. From time to time the air capacity (CO) of the cell and the capacity of the leads (CL) were re-measured, the change in capacity in each case was negligible.

#### 8—THE EFFECT OF WATER OF CRYSTALLIZATION ON DIELECTRIC CONSTANT

Whenever examined the dielectric constant of the dehydrated salt was found to be considerably greater than that of the hydrated salt. In the case of copper sulphate this is especially marked.

If the constant  $\frac{\epsilon - 1}{(\epsilon + 2)} \frac{1}{d}$  of the Clausius-Mossotti relationship be multiplied by the molecular weight  $M$ , an expression known as the molecular refractivity,  $\frac{\epsilon - 1}{\epsilon + 2} \frac{M}{d}$  results. This value has been worked out for the hydrated and dehydrated salt in all the cases examined. It was

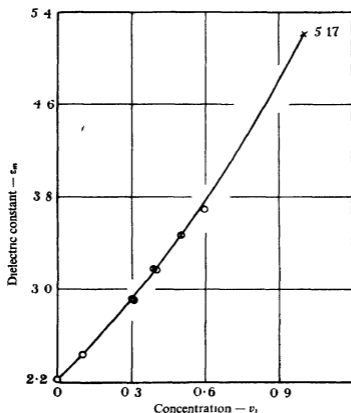


FIG. 7—KI in oil,  $u = 2.36$  ⊗ cell A, ○ cell B

found that the change in molecular refractivity per molecule of water of crystallization was approximately constant.

Table XII shows the change in molecular refractivity per molecule of water of crystallization as calculated by the authors, along with the values found by Heydweiller\* for barium chloride and sodium carbonate.

It is interesting to note that taking the dielectric constant of ice† at 0°C.

\* 'Z. Physik,' vol. 3, p. 308 (1920).

† Abegg, 'Ann. Physik,' vol. 65, p. 229 (1898).

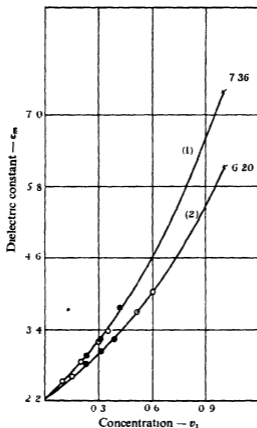


FIG. 8—Curve 1,  $\text{MgSO}_4 \cdot 1 \text{H}_2\text{O}$ ,  $\mu = 1.86$ , curve 2,  $\text{MgSO}_4 \cdot 7 \text{H}_2\text{O}$  in oil;  $\mu = 1.40$   $\odot$  cell A,  $\circ$  cell B

TABLE XII

Molecular refractivity of hydrated salt		Molecular refractivity of dehydrated salt		Difference in molecular refractivity	Difference per molecule of water of crystallization
$\text{Na}_2\text{B}_4\text{O}_7 \cdot 10 \text{H}_2\text{O}$	138	$\text{Na}_2\text{B}_4\text{O}_7 \cdot 2 \text{H}_2\text{O}$	73	65	8.1
$\text{MgSO}_4 \cdot 7 \text{H}_2\text{O}$	93	$\text{MgSO}_4 \cdot 1 \text{H}_2\text{O}$	37	56	9.3
$\text{CuSO}_4 \cdot 5 \text{H}_2\text{O}$	71	$\text{CuSO}_4 \cdot 1 \text{H}_2\text{O}$	42	29	7.3
* $\text{Na}_2\text{CO}_3 \cdot 10 \text{H}_2\text{O}$	115	* $\text{Na}_2\text{CO}_3$	17	98	9.8
* $\text{BaCl}_2 \cdot 2 \text{H}_2\text{O}$	58	* $\text{BaCl}_2$	42	16	8.0

\* From Heydweiller

and frequency of  $5 \times 10^6$  cycles per second,  $\epsilon$ , 3.2, the molecular refractivity of ice is 8.3

If further investigations should substantiate the result that each molecule of water of crystallization carries with it a fixed contribution to the molecular refractivity, the simplicity of the result should be of interest

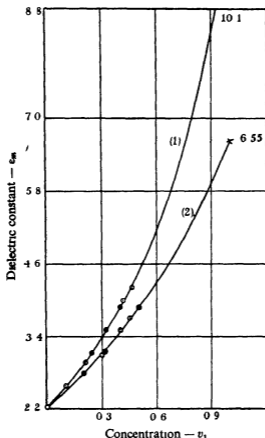


FIG. 9—Curve 1,  $\text{CuSO}_4 \cdot 1\text{H}_2\text{O}$ ,  $u = 1.34$ , curve 2,  $\text{CuSO}_4 \cdot 5\text{H}_2\text{O}$  in oil;  $u = 1.90$  ⊗ cell A, ○ cell B

in any theory concerning the dielectric constants of the salts, and in the role played by the water molecule in such hydrated salts.

### 9—SUMMARY

The dielectric constants of sodium chloride, alum, magnesium sulphate (crystalline and dehydrated), copper sulphate (crystalline and dehydrated), potassium iodide, borax (crystalline and dehydrated), have been measured

at room temperature. The method, using a resonance circuit at a frequency of  $2 \times 10^6$  cycles per second, involved the determination of the dielectric constant of mixtures of the salt and water-free oil in different proportions. The dielectric constant of the salt is then calculated from the formula of Frické, the dielectric constant of the oil being known

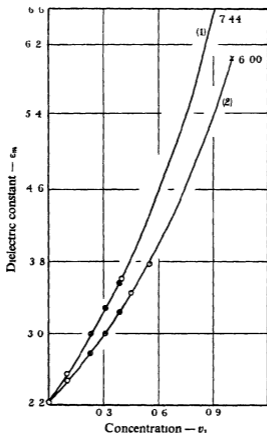


FIG 10—Curve 1, borax (dehydrated),  $\mu = 2.00$   $\text{Na}_2\text{B}_4\text{O}_7 \cdot 2\text{H}_2\text{O}$ , curve 2,  $\text{Na}_2\text{B}_4\text{O}_7 \cdot 10\text{H}_2\text{O}$  in oil,  $\mu = 1.30$   $\otimes$  cell A,  $\circ$  cell B

In the few cases where concordant results have been obtained by other investigators, such results are in good agreement with those reported here.

It has been pointed out that when a salt possessing water of crystallization is dehydrated, its dielectric constant increases. It is seen that the change in molecular refractivity per molecule of water of crystallization is approximately constant

## A Quantitative Study of Pleochroic Haloes III—Thorium

By G H HENDERSON, Ph D, C M MUSHKAT, M Sc, and D P  
CRAWFORD, M Sc, Dalhousie University, Halifax, N S

(*Communicated by Lord Rutherford, O M, F R S—Received 14 July,  
1936*)

[PLATES 9, 10]

This paper gives an account of measurements of thorium haloes in biotite, made with the halo photometer. This apparatus, which has been earlier applied to uranium haloes,\*† gives a permanent record of the structure of a halo, yielding ring diameters and intensity of blackening throughout the halo.

Thorium haloes are very rare compared with those due to uranium. Out of more than a hundred biotites examined up to the present, only one gave a reasonable number of clearly defined haloes due to thorium. This material came from the Star Lake district in Manitoba, near the Ontario boundary. It was a brown biotite occurring as easily cleavable crystals a few mm in diameter. Haloes were not very plentiful in the small amount of material available, but they were in rich variety including thorium, uranium, and compound uranium-thorium, as well as several other types of halo, which will be dealt with in another paper. A few good thorium haloes were also found in a brown biotite from Pierrepont, St. Lawrence Co., N. Y., and one or two more have been recognized in other biotites.

Thorium haloes were first described and measured by Joly,‡ further measurements have been given by Imori and Yoshimura§ and by van der Linde.||

They are here classified, by their appearance under the microscope, into three stages of development: embryonic, normal, and over-exposed. The embryonic halo consists of a disk of small diameter surrounded by a single

\* Henderson and Bateson, 'Proc. Roy. Soc., A', vol. 145, p. 563 (1934).

† Henderson and Turnbull, 'Proc. Roy. Soc., A', vol. 145, p. 582 (1934). These papers will be referred to subsequently as I and II respectively.

‡ 'Phil. Trans.', vol. 217, p. 51 (1917).

§ 'Sci. Pap. Inst. phys. chem. Res. Tokyo', vol. 5, p. 11 (1926).

|| 'Zbl. Min. Geol. Paläont.', Abt. A, vol. 177 (1926).

ring The disk has a sharply defined edge, which has often the appearance of a ring In faint embryonic haloes the disk shows greatest blackening near the central nucleus but in later stages it appears darkened fairly uniformly In the very faintest haloes the disk alone is visible The radius of this disk will be associated with the alpha particles from thorium itself and that of the ring with the combined effects of the alpha particles from RdTh and ThX The ring appears to be somewhat more sharply defined on the inside than on the outside The annular region between disk and ring often appears lighter in colour than even the mica outside the halo It will be seen from the records that this is only apparent, being probably due to contrast Nevertheless, the appearance of disk and ring separated by a light, sharply defined annular region is very characteristic of embryonic thorium haloes, enabling them to be distinguished at a glance A photomicrograph of a typical embryonic halo, in a rather advanced stage, is shown in fig 1, Plate 9

The term normal has been applied to those haloes showing the most pronounced ring structure As this stage is approached the disk takes on a uniformly blackened appearance and the ring becomes darker Outside this ring there appear three weaker rings The innermost of these three is due to Tn together with ThC, while the next is due to ThA The third, of considerably greater radius, is due to ThC' In addition, there sometimes appears a faint ring in the annular space between disk and inner ring Occasionally there can also be seen signs of a ring inside the disk A typical normal halo is shown in fig 2, Plate 9 On the original print there can be seen clearly, starting from the outside, the large ThC' ring, then the two rings followed by the heavier RdTh-ThX ring, then in the annular space a faint ring (due to the radium family), and finally the disk, on the original negative there can be seen traces of a ring within the disk

The normal stage is rather evanescent. When the development proceeds so far that the outermost ring is prominent, all inner detail quickly becomes lost In the over-exposed stage there is left only the outer ring surrounding a blackened disk corresponding to ThA

Reversal has not been observed in the thorium haloes examined.

## RESULTS

Some 80 haloes from the Star Lake biotite and 8 from the Pierrepont biotite gave good photometer records. Typical examples of these records are shown in figs. 3, 4, and 5, Plate 10, representing embryonic, normal, and compound haloes respectively.



well-defined groups which differ from those for uranium both in position and in relative numbers of rings in the different groups. Five of them can be ascribed to the thorium family, two to members of the uranium family present in compound haloes, and one is of unknown origin.

Numerical values for the various groups of those rings classed as "certain" are given in Table I. The first column gives the radius (in microns) of the various groups, the same values are also shown at the top of fig. 6. The second column gives the air equivalent of these mean radius in cm. at 15° C. and 760 mm., using the conversion factor 4.89,

TABLE I

Radius in microns	Air equivalent cm. at 15° C.	Associated $\alpha$ -particles	Number of rings	Probable error of mean %
41.80	8.55	ThC' 8.62	23	0.2
33.5	6.85	RaC' 6.97	6	0.4
27.77	5.68	ThA 5.68	60	0.2
23.86	4.88	Tn 5.06 ThC 4.78	17	0.3
20.00	4.09	ThX 4.35 RdTh 4.02	41	0.2
15.2	3.10	Ra 3.39 U II 3.28 Io 3.19	11	0.5
12.38	2.53	Th (H & N) 2.59 Th (K & K) 2.87	77	0.3
5.9	1.21	?	7	3.1

which will be referred to in a later section. The third column gives the accepted ranges in air of the associated  $\alpha$ -particles; the same information, converted into microns, is given at the bottom of fig. 6. The fourth column gives the numbers of rings included in the groups and the fifth the probable error of the mean.

While the division into groups is apparent from fig. 6, some definite criterion must be adopted for assigning the individual ring radius into groups in order to obtain the numerical data given in Table I. For this purpose a group was deemed to be constituted of all those rings whose radius did not differ from the mean of the group by more than  $1.0\ \mu$ . This value, while somewhat arbitrarily chosen, is not unreasonable. Out

of the 40 microns of abscissae under the curve of fig. 6, only 16 microns are occupied by the eight groups, yet 91% of all the rings are found in the groups. The remaining 9% (25 out of 267) is largely confined to the outskirts of these groups. The concentration of rings near the centre of a group is so great that had the limits of the group been chosen considerably wider than  $\pm 1.0 \mu$ , there would have been no appreciable change in the mean radius given in Table I and only a slight increase in the probable errors.

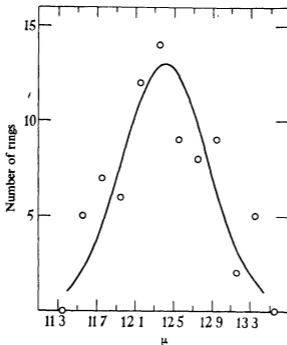


FIG. 7

As was stated earlier, the rings in fig. 6 have been plotted at intervals of  $1 \mu$ , and consequently the figure cannot show satisfactorily the distribution within a single group. In fig. 7 the numbers of ring radii for the  $\alpha$ -particles from Th have been plotted at intervals of  $0.2 \mu$ . The number of rings is rather small for such narrow intervals but is sufficient to show the distribution with the group.

The probable error of an individual ring radius for Th is  $0.30 \mu$ . The Gaussian curve for this value is shown in fig. 7. Thirty-five of the rings lie within the limits  $\pm 0.30 \mu$  measured from the mean, while forty-two lie outside these limits. This is as near the theoretical equality as could be expected with the numbers of rings and intervals used.

The errors given in the last column of Table I refer, of course, to the accidental errors of measurement only and are inserted to give some idea of their magnitude. The systematic errors will be referred to in a later section.

#### COMPARISON WITH $\alpha$ -PARTICLE RANGES

This comparison is most easily demonstrated by the integrated ionization curve for the thorium family, fig 8. The range of Th has been taken to be 2.59 cm and the ranges of the other members of the family are as in the third column of Table I. The basic ionization (Bragg) curve is a

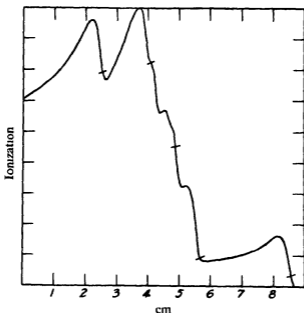


FIG. 8.

mean of the curves of Henderson\* and of Curie and Behounek†. The radii from thorium haloes are indicated on the curve.

Beginning at the outside of the halo the first group of rings has a mean radius of  $41.80 \mu$  equivalent to 8.55 cm of air. This is undoubtedly due to the  $\alpha$ -particles from  $\text{ThC}'$ , whose accepted range is 8.62 cm at  $15^\circ \text{C}$ . This group is much smaller intensity than the analogous  $\text{RaC}'$  group (II, fig 9). One reason for this is the fact that only 65% of the atoms of the thorium family branch to give this  $\alpha$ -particle. Another reason is that the range for  $\text{ThC}'$  is greater, and consequently the inverse square law leads to a smaller relative intensity.

\* 'Phil Mag.', vol 42, p. 536 (1921)

† 'J Phys Radium,' vol 7, p 125 (1926)

A weak group next appears at  $33.5 \mu$ ,  $6.85 \text{ cm}$  air equivalent, due to  $\text{RaC}'$   $\alpha$ -particles of  $6.97 \text{ cm}$  range occurring in compound uranium-thorium haloes. In pure uranium haloes the  $\text{RaC}'$  group is the most prominent. Consequently, we will not expect that rings due to the other members of the uranium family, which are necessarily present, will perturb greatly the thorium groups. Moreover, the other groups due to the uranium family (with the exception of that due to the combined effects of Ra, U II, and Io) occur too close to thorium groups to be resolved. This may readily be seen by comparing Table I with Table II below.

A strong group next occurs at  $27.77 \mu$ ,  $5.68 \text{ cm}$  air equivalent, due to ThA,  $5.68 \text{ cm}$  accepted range. The curve for this group appears to be rather wide in fig. 6, due simply to the fact that it happens to have "straddled" the intervals.

The  $\alpha$ -particles due to Tn,  $5.06 \text{ cm}$  and to ThC,  $4.78 \text{ cm}$  (35% branch) fall too close together to permit resolution of ring radii, and to them jointly must be ascribed the group at  $23.86 \mu$ ,  $4.88 \text{ cm}$  air equivalent. This group appears weaker than might be expected, but a study of figs. 3, 4, and 5 will show that this ring appears on a rapidly rising part of the photometer curve and is difficult to distinguish.

The strong group at  $20.00 \mu$ ,  $4.09 \text{ cm}$  air equivalent, is due to the joint effects of ThX,  $4.35 \text{ cm}$  and of  $\text{RdTh}$   $4.02 \text{ cm}$ .

The weak group at  $15.2 \mu$  seems to be due to the joint effects of Ra, U II, and Io. In pure uranium haloes this group comes at  $15.3 \mu$ . It is the only one (apart from  $\text{RaC}'$ ) which could be expected to be resolved from the thorium groups. These rings appeared to be more prominent in the Pierrepont biotite than in that from Star Lake.

It will thus be seen that there is good agreement of all the above-mentioned mean group radii with the accepted  $\alpha$ -particle ranges. Furthermore, all members of the thorium family are accounted for satisfactorily.

The strongest group of all, due to Th, at  $12.38 \mu$ ,  $2.53 \text{ cm}$  air equivalent, is of special interest because of the large discrepancy between the most recently published values of the range in air of the Th  $\alpha$ -particle. Henderson and Nickerson\* found a range of  $2.59 \pm 0.05 \text{ cm}$ , while Kurie and Knopf† obtained  $2.87 \pm 0.03 \text{ cm}$ . Both values were obtained by measuring tracks in a Wilson cloud chamber. It will be seen that the range found from haloes is much closer to the former value.

In the course of our work with the halo photometer it has been shown that there is good agreement of the measured ring radii with accepted

\* 'Phys. Rev.', vol. 36, p. 1344 (1930)

† 'Phys. Rev.', vol. 43, p. 311 (1933)

$\alpha$ -particle ranges In particular for RaC', ThC', RaA, and ThA, the agreement is well within 1%, and these include all the longer range  $\alpha$ -particles which are sufficiently separated from other groups to be resolved by the photometer In these cases the accuracy in range determination attainable by direct laboratory methods is considerably greater than that attainable with the halo photometer The two shortest range  $\alpha$ -particle groups, from U I and Th, are, however, in a different category Although the Th group and, to a lesser extent, the U I group are far enough from others to be resolved, direct measurement is difficult on account of the weak activity of these substances No difficulty of this kind is found with haloes, where the radioactive effects are cumulative over geological time It would then appear that the accuracy of the halo method is comparable with that of direct laboratory measurements under the difficult experimental conditions obtainable with Th

It is very fortunate that the Th ring is very clearly defined, being the most noticeable feature of the whole halo in both embryonic and normal stages This is due largely to the fact that there are no nearby rings to mask it, as may be seen from fig 8 The case is much less favourable with the smallest ring in the uranium halo, due to U I This is so ill-defined, due to a neighbouring group, that it remained unobserved for many years until discovered by Kerr-Lawson \* The radius of the U I ring in uranium haloes was found by the halo photometer to be equivalent to 2.58 cm † This is 5.5% lower than the accepted range in air of 2.73 cm For Th, under much more favourable conditions, the ring radius, equivalent to 2.53 cm, is 2.3% lower than the 2.59 cm range from Henderson and Nickerson and 12% lower than the range of 2.87 found by Kurie and Knopf Further discussion of this question will be given elsewhere.

Finally, one other group of rings is found with a radius of 5.9  $\mu$  equivalent to an  $\alpha$ -particle of 1.21 cm range These rings appear inside the dark disk due to Th and are not well defined An example of such a ring is shown on the photometer record of fig 3 There are only 7 "certain" rings included in this group, but if "doubtful" rings be included the number rises to 31, giving a mean of 5.91  $\mu$  and a probable error of the mean of 1.2% In uranium haloes (II) two short groups of mean radii 8.6  $\mu$  and 5.2  $\mu$  were found and named K and L respectively While it is possible that the group found in the thorium haloes is yet a third group, it should be remembered that systematic errors become large with such small

\* Univ. Toronto Stud. Geol., Nos. 24 and 27 (1927).

† Mean of values in I and II

rings It is more probable, therefore, that these rings belong to the L group If this is so the mean radius of 40 rings in both uranium and thorium haloes is  $5.75 \mu$  This is equivalent to an  $\alpha$ -particle range of  $1.18 \text{ cm}$ , with a probable error in the mean of  $1\%$ , due to accidental errors

#### DISCUSSION OF MEASUREMENTS

For the purpose of this discussion it is well first to recapitulate the various steps which must be taken in attaining the results given in the last section The first step is to calibrate the halo photometer by means of a microscope test plate By photometering this in exactly the same way as the halo, we find the enlargement factor  $E$ , which is the distance in centimetres along the record corresponding to  $1 \text{ micron}$  on the travelling microscope stage If  $D$  is the distance in  $\text{cm}$  corresponding to a ring diameter, *i.e.*, between "kinks" on the curve symmetrically situated on opposite sides of the halo record, then the ring radius in microns is  $D/2E$  Next, this value is decreased by a correction  $\delta$ , for the finite size of the nucleus Finally, the corrected radii are converted into equivalent centimetres of air  $R$ , by dividing by the conversion factor  $C$  This factor  $C$  is the distance in microns of mica equivalent to  $1 \text{ cm}$  of air at  $15^\circ \text{C}$  and  $760 \text{ mm}$  and is the reciprocal of the stopping power of a sheet of biotite  $1 \mu$  thick

Thus

$$R = (D/2E - \delta)/C$$

*Enlargement Factor*—The microscope test plate was subdivided into divisions of  $0.01 \text{ mm}$  nominal length Calibration records of the test plate were taken frequently in the course of the work, generally using the same divisions The photometer screw ( $1 \text{ mm}$  pitch) had been carefully surveyed over several turns of the screw by means of the test plate A very uniform portion of the screw amounting to about a tenth of a turn was always used in obtaining calibration and halo records The mean distance in  $\text{cm}$  on the record corresponding to a nominal  $0.01 \text{ mm}$  division on the test plate was  $2.036 \text{ cm}$  and the probable error of the mean  $0.2\%$  When this work was nearly completed the test plate was sent to the National Research Laboratory, Ottawa, and measured in terms of the International Metre It was found that the divisions were quite uniform but that the length of the 8 divisions usually used in calibration was actually  $0.0794 \text{ mm}$  in terms of the International Metre Accordingly, the test plate divisions were in error by about  $0.75\%$  and the corrected

value of the enlargement factor  $E$  was 0.2051 cm. equivalent to 1 micron.\*

The distance  $D$  on the record was measured between the feet of that portion of the curve which was due to the particular group of  $\alpha$ -particles in question. The definiteness with which these points could be determined depended on the quality of the halo from which the record was obtained.

*Nuclear Correction*—The nuclei of all haloes giving rings classed as "certain" were measured under the microscope with a screw micrometer eyepiece. The amount of correction to be applied on account of this is rather uncertain. Since the measurement of ring radius is made to the foot of the ionization curve due to the  $\alpha$ -particle group, this point should have been reached by those particles starting from the nearest point of the surface of the nucleus. Accordingly, the correction should be equal to the nuclear radius. Since in judging the position of the foot of the curve we are more likely to estimate it too low than too high, the correction should be somewhat less than the nuclear radius.

We have also attempted to estimate this correction empirically from measurements on uranium haloes in a biotite from Renfrew, Ont., which had been previously studied (II). The mean radius of the  $RaC'$  ring was 34.6 nominal microns for a number of haloes with demonstrably small nuclei. For a number of other haloes with larger nuclei the excess of the  $RaC'$  ring over 34.6  $\mu$  was taken and divided by the measured radius of the nucleus. The errors involved are naturally large. The ratio of excess range in mica to nuclear radius was found to be 1.13 with a probable error in the mean of 7%.

\* In Papers I and II all results given in microns should, therefore, be decreased by 0.75%, while all results given in equivalent centimetres of air remain unaltered. This may be shown as follows. It will be recalled from I that the radius of the  $RaC'$  ring was found to be 34.4 nominal microns. Since the range of these  $\alpha$ -particles is 6.97 cm, the conversion factor was taken to be  $34.4/6.97 = 4.94$  nominal microns equivalent to 1 cm of air. We now know that the enlargement factor was too small by 0.75%. Hence all ring radii given in microns in I and II must be decreased by 0.75%. Since all results in centimetres of air are obtained by putting the measured  $RaC'$  ring radius equal to 6.97 cm, the other air values are not to be changed.

The  $RaC'$  ring radius becomes 34.1 standard microns and the corrected conversion factor should be  $34.1/6.97 = 4.89 \mu$  equivalent to 1 cm of air at 15° C. and 760 mm. Since in I we gave a reason for supposing that the conversion factor was, if anything, too high and since the new value agrees equally as well as the old with recalculated values from the chemical constitution of the biotite, we have no hesitation in making this revision.

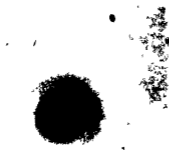


FIG 1



FIG 2

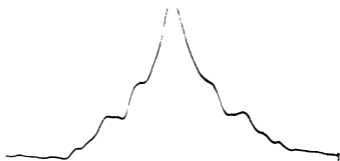


FIG. 3

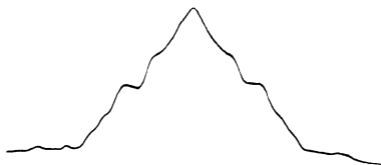


FIG. 4

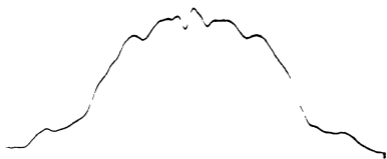


FIG. 5

The correction finally adopted was equal to the nuclear radius. The average nuclear radius of all the haloes used in this work was  $1.1 \mu$  and the largest  $2.0 \mu$ . It is believed that the error in determining the nuclear radius is not greater than  $0.1 \mu$ .

*Conversion Factor*—We have adopted the same (corrected) conversion factor,  $C = 4.89$ , for the thorium biotites, as was used for those containing uranium haloes. One reason for doing this is that uranium haloes for a number of biotites previously studied have proved to be remarkably uniform and have given consistent results when using the same conversion factor. Further and more direct justification was also available. It was fortunate that the Star Lake material contained several other types of haloes besides thorium. Some 12 good uranium haloes were photometrized and measured. The ring radii were found to be distributed in the same characteristic groups as with earlier work (II). The mean radii are shown in Table II, in comparison with previous results.

TABLE II

	RaC'	An and AcC	RaA	Rn and RaF	Ra, U II, Io	U I
Star Lake biotite	6.97	5.57	4.72	3.91	3.14	2.60
Paper II	7.00	5.55	4.70	3.93	3.12	2.59
Paper I	6.97	5.50	4.69	4.00	3.16	2.52

Of these results it should be remembered that only one has been adjusted. That is, the RaC' ring in Paper I has been set equal to the accepted range for RaC', thus giving the conversion factor. All others have been obtained using this same factor. The agreement is good and the errors for the Star Lake biotite are of about the same magnitude as in the other results. Other checks are obtainable from the uranium rings shown in Table I and from another type of halo which will be discussed in a forthcoming paper. Thus there seems to be ample justification for adopting the conversion factor 4.89 in this work.

*Accuracy of Measurements*—Since the photometer is used as a transfer instrument, all errors due to it are included in the probable errors given in Table I, which appear to follow an approximate Gaussian distribution law. Systematic errors may arise from three sources, the test plate, the nuclear correction, and the conversion factor. The value of 79.4 microns given by the National Research Laboratory for the 8 divisions of the test plate used for calibration was stated to be accurate to  $0.2 \mu$ , i.e., to

0.25% This error applies, of course, only to results expressed in microns

The nuclear radius,  $r$ , is relatively small, being on the average about 8% of the ring radius of Th and proportionally less for the larger rings. There might be some question as to whether a correction  $\delta = r$ , which we have applied, is not too large. Joly estimated  $\delta = r/2$ , which is almost certainly a lower limit of possibility. Applying corrections of  $r$  and  $r/2$  we obtain ranges from Th haloes of 2.53 and 2.64 cm respectively, differing by about 4%. The uncertainty, if any, in the amount of correction is likely to be considerably less than the difference between these extreme cases. We estimate that the error in the range of Th, due to this possible cause, is not greater than 1.5%. For the larger rings and for haloes with smaller nuclei it would be correspondingly less. The error in ring radius due to errors in the measurement of the nuclear radius under the microscope is comparatively negligible.

The conversion factor has been deduced from the measurements of the RaC' ring. Using this factor we have checks on four other  $\alpha$ -particle groups in the uranium and thorium families whose ranges are accurately known and which are separated enough from other groups to be resolved by the halo photometer. For RaA, ThC', and ThA, the halo ranges are less than the standard air ranges by 0.4%, 0.8%, and 0.0% respectively. For UI, under difficult conditions, the halo range is smaller by 5.5%. If the latter be given a weight of half the others the average difference is about 1%.

The question might be raised as to whether it is justifiable to use the same conversion factor for  $\alpha$ -particles of different ranges. The careful experiments of Briggs\* on mica (probably muscovite) have a bearing on this point. He found the conversion factor to decrease very slightly as the range decreases. For UI or Th the factor would appear to be about 1% less than for RaC', but the effect is not much greater than the experimental errors. If this should be true for biotite, the halo ranges for these short  $\alpha$ -particle groups should be increased by this amount, but in view of the uncertainties involved it has seemed inadvisable to do more than point out this possibility.

Summarizing this discussion on accuracy, we consider a very conservative estimate of error in the range of Th to be 3% and somewhat less for longer ranges. It will be observed that this is much less than the difference between the two recent direct determinations of the range for Th obtained by Henderson and Nickerson and by Kurie and Knopf and that it agrees with the former well within the estimated limits of error.

\* 'Proc. Roy. Soc.,' A, vol. 114, p. 341 (1927).

## CONCLUSIONS

The results of this study of thorium haloes by the method of the halo photometer are in complete accord with the comparable results on uranium haloes (I and II). All members of the thorium family are accounted for satisfactorily, and the process of blackening within the thorium halo seems to be quite analogous to that for uranium. The method lends itself to the measurement of  $\alpha$ -particle ranges with moderate precision. While such measurements normally cannot compete in accuracy with direct laboratory determinations, they may be of comparable value when direct measurements are difficult, as is the case with Th.

Both the Star Lake and Pierrepont biotites are of Pre-Cambrian age\*. The good agreement of the  $\alpha$ -particle ranges deduced from these ancient haloes with the results of present day laboratory experiments furnishes striking proof of the invariability of physical laws throughout the vast extent of geological time.

This work has been carried out with the help of a grant from the Carnegie Corporation of New York, to whom acknowledgment is gratefully made. We also wish to thank Mr F. W. Sparks, M. A., who has given us much valuable assistance. For samples of biotite generously sent us we wish to thank Professor J. S. DeLury of Winnipeg, Mr H. S. Spence, of the Mines Branch, Ottawa, and Dr W. F. Foshag, of the U. S. National Museum, Washington.

## SUMMARY

Pleochroic haloes due to the thorium family have been studied by means of the halo photometer. Five rings are found in the halo, which satisfactorily account for all the  $\alpha$ -particles of this family. The ranges are in good agreement with accepted values and the range found for Th, 2.53 cm, at 15° C and 760 mm, furnishes valuable evidence as to the magnitude of this constant. A ring corresponding to  $\alpha$ -particles of very short range, 1.18 cm, and of undetermined origin, has been found in these haloes. A full discussion is given of the accuracy of measurement.

\* For this information I am indebted to Professor J. S. DeLury, of Winnipeg, and Professor A. F. Buddington, of Princeton, respectively.

# Pressure Broadening of Spectral Lines and van der Waals Forces

## I—Influence of Argon on the Mercury Resonance Line

By H KUHN, Clarendon Laboratory, Oxford

(Communicated by F A Lindemann, F R S—Received 15 July, 1936)

[PLATE 11]

It is the purpose of this and the following paper to consider the type of broadening of a spectral line, produced by approaches of other atoms to the radiating atom, which we shall call throughout "transits". The aspect with which we are particularly concerned is the transits of single atoms producing the wing of the broadened line. The intensity distribution in spectra of this type, which are intermediate between ordinary pressure broadening and continuous molecular spectra, can be interpreted in a simple way, yielding results on the van der Waals forces†. The first paper gives an account of intensity measurements in the single transit region of the mercury line 2537 Å broadened by the admixture of argon.

### THEORETICAL FOUNDATIONS

*Transits of Atoms and Pressure Broadening*—The forces between two atoms can conveniently be described by plotting the potential  $V$  of the force, multiplied by  $1/h$ , as a function of the distance  $r$  (fig 1). At large distances, two normal atoms always attract each other. The potential of this force, generally called van der Waals force, is predicted by wave mechanics‡ to be approximately an inverse sixth power function of the distance:

$$\frac{1}{h} V_a = - \frac{C_6}{r^6}. \quad (1)$$

At smaller distances, the potential law changes. It either passes into a very strong exponential attraction due to chemical forces, forming a potential trough of the depth of about 10 — 100 kT at room temperature (dotted curve); or it passes directly into a repulsion, forming a potential

† Kuhn, 'Phil. Mag.', vol 18, p 987 (1934)

‡ F. London, 'Z. Physik', vol. 63, p. 245 (1930), 'Z. phys. chem.', B., vol 11, p 222 (1930).

minimum of the depth  $D$  of the order of  $kT$  or less (solid curve  $a$ , *e.g.*, Hg—A interaction).

In the region of the chemical attraction force ( $r_1$ , dotted curve), the second atom will nearly always be caught, forming a stable oscillating and rotating molecule, the spectrum of which is in general a discrete band spectrum. The opposite, however, is true at greater distances  $r_2$  ( $|V_2| \ll kT$ ), *i.e.*, in the region of the van der Waals forces. The Boltzmann factor  $e^{-V_2/kT}$  approaches unity, and the ratio  $N_a/N_m$  of the

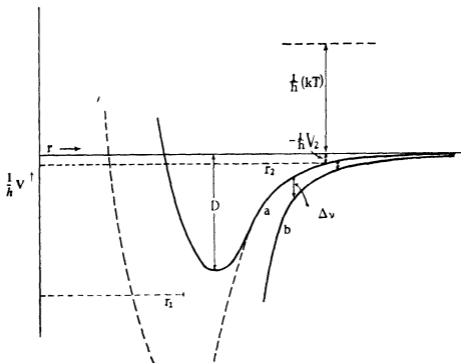


FIG. 1—Qualitative diagram of the van der Waals potential of ground state ( $a$ ), and excited state ( $b$ ). See footnote†, page 216

number of free atoms at the distance  $r_2$  to those caught as molecules of the same internuclear distance is approximately given by the ratio of the corresponding impulse phase volumes. As the kinetic energy of the molecule can never greatly exceed its negative potential energy,† the ratio  $N_m/N_a$  will be of the order  $(|V_2|/kT)^{3/2}$ .

The system of two atoms in a state of transit emits or absorbs a continuous spectrum. Its intensity‡ at large distances where  $-V \ll kT$

† See Oldenberg, 'Z. Physik,' vol. 56, p. 563 (1929)

‡ The word intensity is used here in a wider sense, including intensity of absorption.

will be large compared with that of the discrete band spectrum produced by molecules of the same internuclear distance. At smaller distances, e.g., near the potential minimum, if chemical forces are absent, both will have comparable intensities †. On account of the greater statistical probability of larger distances, i.e., smaller perturbations, the intensity of the continuous spectrum due to the transits will increase as the atomic line is approached. It therefore shows the typical features of a pressure broadening effect, which was first pointed out by Jablonski ‡. Nevertheless, the phenomenon of pressure broadening cannot be completely described as the statistical distribution (occurrence distribution, Häufigkeitsverteilung) of the perturbed eigen frequencies produced by the forces of neighbouring atoms. A general theory would involve a complicated Fourier analysis of the eigen frequencies varying in time. Lenz§ has succeeded in finding approximate solutions, but they give little hope of further progress and experimental applications.

The Michelson-Lorentz theory of collision broadening, in its refined form given by Weisskopf||, can be considered as describing the limiting case of swiftly-moving atoms with fields of force varying rapidly with the distance. If the law of force is known, it yields upper limits of the force constants.

The statistical occurrence distribution describes the opposite limiting case of infinitely slow motion. It cannot be applied, even as a rough approximation, to small frequency distances  $\Delta\nu$  from the line, of the order of the half-value width¶, at greater values of  $\Delta\nu$ , however, i.e., in the wing of the line, the occurrence distribution is generally a good approximation. Here, the deviation of the true intensity distribution from the occurrence distribution, due to the motion of the atoms, can be estimated as a diffuseness, imposed on the occurrence distribution ††. The half-value

† See also Finkelburg, 'Z. Physik,' vol 96, p 699 (1935).

‡ 'Z. Physik,' vol 70, p 723 (1931).

§ 'Z. Physik,' vol 80, p 423 (1933).

|| 'Z. Physik,' vol 75, p 287 (1932), 'Phys. Z.', vol 34, p 1 (1933).

¶ An attempt by Margenau ('Phys. Rev.', vol 40, p 387 (1932), vol 43, p 129 (1933)) to calculate the intensity distribution of pressure broadening as an occurrence distribution failed because of the neglect of the kinetic effect (see Lenz, 'Z. Physik,' vol 83, p 139 (1933)), its apparent agreement with experiment being due to an error in the statistical method (see Kuhn, *loc. cit.*).

†† Kuhn and London, 'Phil. Mag.', vol 18, p 983 (1934), later, Margenau ('Phys. Rev.', vol 48, p. 755 (1935)), apparently without knowledge of this publication, has tried to solve the same problem with a mathematical method which seems more general, but his result explicitly evaluated does not differ from our (2), except by an unessential numerical factor. This formula can, however, not be applied to small

width  $\delta\nu$  of the diffusion function can be derived from the function  $\nu(t)$  which describes the variation of the eigenfrequency with the time. If higher derivatives are neglected, it can be written as

$$\delta\nu = \frac{1}{\pi} \sqrt{\left| \frac{d\nu(t)}{dt} \right|} = \frac{\sqrt{\nu}}{\pi} \sqrt{\left| \frac{d\nu}{dx} \right|}. \quad (2)$$

If  $\nu$  is a function of the distance  $r$  of one neighbour only, the maximum blurring  $\delta'\nu$  of a certain frequency  $\nu(r)$  is produced by central impacts ( $x \equiv r$ ). When the frequency law is  $\nu_0 - \nu \sim -\frac{1}{r^3}$  (see below), we get

$$\delta'\nu \sim \sqrt{\nu} \sqrt{\frac{1}{r^2}}.$$

In this particular case, the ratio  $\frac{\delta\nu}{\nu_0 - \nu}$  is a crude measure for the relative influence of the motion. Using the maximum value  $\delta'\nu$  instead of  $\delta\nu$ , we get

$$\frac{\delta'\nu}{(\nu_0 - \nu)} \sim \sqrt{\nu} \times r^2,$$

showing that the influence of the kinetic effect is smallest at small inter-atomic distances, i.e., at large  $(\nu_0 - \nu)$  values.

The absolute value of  $\delta\nu$  derived from (2) is a rough estimate only. The evaluation shows that, at large values of  $\Delta\nu$ , the influence of the motion is small enough to be either neglected or treated as a correction.

### REGION OF SINGLE TRANSITS

For the wings of the line which are due to comparatively near approaches ( $\approx 3 - 6 \times 10^{-8}$  cm), another important simplification can be made. The interaction of the radiating atom with one neighbour, the single transit, becomes predominant, multiple transits can be neglected. Based on these two facts, a simple calculation of the intensity distribution in the wings of the broadened line is possible†. If a single atom at a distance  $r$  produces the perturbation  $(\nu_0 - \nu)$  of the atomic frequency  $\nu_0$ , the intensity  $I(\nu)$  of the frequency  $\nu$  is proportional to the number of occurrences of the nuclear distance  $r$ .

$$I(\nu) d\nu = A \times 4\pi r^2 dr. \quad (3)$$

values of  $\Delta\nu$ , where the correction is as big as the statistical effect itself. Unfortunately, Margenau restricts its application to this frequency range, his results are thus hardly useful for comparison with experimental facts.

† Kuhn, 'Phil. Mag.', vol 18, p 987 (1934).

From equation (3), the intensity distribution  $I(v)$  can be calculated if the function  $v(r)$  is known, *e.g.*, any theoretical function  $v(r)$  can be checked by experiment

The function  $v(r)$  can be replaced by the potential  $V_a(r)$  and  $V_b(r)$  of the forces between the neighbouring atom and the radiating atom in the normal and excited states respectively†

$$v(r) - v_0 = \frac{1}{h} (V_b(r) - V_a(r)) \quad (4)$$

In (4),  $r$  appears as a parameter which does not vary during the process of emission or absorption. This application of the Franck-Condon principle to atomic transits has been proved correct by Weisskopf‡. It must be taken as a statistical statement only, as  $V(r)$  changes considerably during the lifetime of an excited atom. If very high excitations are excluded,  $V_b$  is a function of the same type as the potential energy  $V_a$  for normal atoms which was discussed above, so that

$$\frac{1}{h} V_b = -\frac{C_b}{r^6}. \quad (1')$$

The constant  $C_b$  is generally greater than  $C_a$ . From (1), (1'), and (4) it follows that

$$\Delta v(r) = v(r) - v_0 = -\frac{C}{r^6}, \quad (4')$$

where  $C$ , which is equal to  $C_b - C_a$ , is in most cases a positive constant. In fig. 1,  $\Delta v(r)$  is given by the vertical distances (double arrows) between the curves *a* and *b*.

In the range of validity of (3) and (1) the occurrence distribution of the intensity can at once be calculated by introducing (4') into (3), which yields

$$I(v) = \frac{2\pi A}{3} \times \frac{C^{1/2}}{(v_0 - v)^{3/2}} \quad (3')$$

In absorption,  $I(v)$  must be replaced by the absorption coefficient  $k_v = \log_e \frac{i_0}{i}$  where  $i_0$  and  $i$  are the intensities of the incident and transmitted light.

† In this and the following equations and also in the figures,  $V_b$  is normalized so as to be zero for the system of the excited atom at infinite distance from the normal one. The  $V_b$  scale is therefore shifted by  $h\nu_0$  from the  $V_a$  scale.

‡ 'Z. Physik,' vol. 75, p. 287 (1932), 'Phys. Z.,' vol. 34, p. 1 (1933).

The value of  $A$  can be found from the integral of the absorption coefficient  $k_\nu$  over the whole frequency range, which is known to be

$$S = \int k_\nu^* d\nu = Nlf \times \frac{\pi e^2}{cm}, \dagger$$

where  $f$  is the oscillator strength of the line,  $N$  the number of absorbing atoms per ccm,  $l$  the length of the absorption cell,  $c$  the velocity of light, and  $m$  and  $e$  mass and charge of the electron (in E S U). If  $\bar{V} = 1/n$  is the volume per atom of the broadening gas,  $\nu_e$ ,  $n$  the number of atoms per  $\text{cm}^3$ , we find

$$A = \frac{S}{\bar{V}} = nNlf \times \frac{\pi e^2}{cm},$$

and finally

$$k_\nu = nNlf \times \frac{2\pi^2 e^2}{3cm} \times \frac{C^{1/2}}{(\nu_0 - \nu)^{3/2}} \quad (3'')$$

This equation can be compared with experiment in two ways (1) The  $3/2$  power law of the decrease of  $k_\nu$  with  $(\nu_0 - \nu)$  can be tested, (2) the constant  $C$ , derived from the measured intensities by means of (3'') can be compared with  $C$  values found by applying the Lorentz-Weisskopf theory to intensity measurements at small  $(\nu_0 - \nu)$  values. As the latter method is less accurate, a rough agreement only can be expected.

Minkowski<sup>‡</sup> found a very good confirmation of the  $3/2$  power law in case of the sodium resonance lines broadened by argon and sufficiently good agreement with the  $C$  value from Lorentz broadening. As the method is so far the only experimental test of the potential law of the van der Waals forces, it seemed desirable to investigate as another example the mercury resonance line 2537 Å broadened by argon. Minkowski's measurements have shown that even for the NaA-broadening the effect of the atomic motion is negligible in the wing of the line. This should be more so for the broadening of Hg lines, due to the smaller relative speeds of the atoms.

#### EXPERIMENTAL PROCEDURE

A few drops of mercury were distilled into the absorption vessel which was a silica tube, 20 cm in length and 2.5 cm in diameter, with plane end plates. The tube was then filled with argon of the pressure  $p_0$  (660 mm., 512 mm., and 219 mm. respectively) at 0° C, and sealed off. In order

† The asterisk is to indicate that  $k_\nu$  is to be integrated over a region far beyond the validity of (3').

‡ 'Z. Physik,' vol. 93, p. 731 (1935)

to keep the tube at a uniform temperature, a thick copper tube 35 cm in length was fitted into the iron tube of an electric furnace and the absorption tube was placed inside. The ends of the copper tube were closed by asbestos plates with 2 cm wide circular holes, the ends of the furnace were closed by asbestos-coated metal disks with silica windows. The temperature was measured by means of a mercury thermometer with completely immersed stem. After the temperature had been kept constant for about 15 minutes, the pressure of the mercury vapour could be assumed to be equal to the saturation pressure. By thus varying the pressure  $P$  of the mercury over a very wide range, the region of conveniently strong absorption could be shifted from the near neighbourhood of the line to a distance of about 15 Å. Provided the broadening by the mercury itself is small, the absorption coefficient should be expected to be proportional to the density of mercury. The coincidence of the coefficients for the same wave-length, derived from photographs at different pressures of mercury verified this expectation. The temperature change during the exposure was always less than  $0.5^{\circ}\text{C}$ . On the whole, the uncertainty of the temperature average in the tube can be supposed to be less than  $1^{\circ}\text{C}$ , the uncertainty of  $P$  therefore about 5%.

A quartz autocollimation spectrograph with a focal length of 2.5 m. for  $\lambda$  2537 Å was used. The side of the  $30^{\circ}$  prism was coated with aluminium by evaporation *in vacuo*. In order to exclude scattered light, a small circular screen had to be placed near the centre of the objective lens. The dispersion, measured by means of iron normals, was 2.16 Å/mm at 2537 Å.

As a light source for the continuous background of the absorption experiment an "end-on" hydrogen discharge tube was used. The capillary, of 8 mm internal diameter and 25 cm length, was cooled by running water, the aluminium electrodes were very big and air cooled. The tube could be run continually with 0.6 amps A.C. The main advantage of this light source for intensity measurements is its constancy; the current, and therefore the intensity of the light, could easily be kept constant within 1%.

Due to this fact and to the high dispersion of this spectrograph, the simple and reliable photometric procedure of Koch could be adopted †. After an absorption photograph had been taken with narrow slit (0.012 mm), a series of exposures was made on the same plate with the same light source at reduced current, varying the slit width from 0.5 to 0.08 mm in 9 stages. In order to mark the frequency  $\nu_0$  of the unper-

† See Ornstein, 'Phys. Z.', vol 28, p. 688 (1927).

turbed mercury line, the spectrum of a silica mercury lamp was superposed on each photograph. Ilford Process plates were found suitable, and a uniform development was ensured by strong automatic rocking. The thermoelectric photometer of the Oxford Observatory was used, partly with 7-fold, partly with 49-fold magnification. The blackening of the plate at a certain wave-length which would correspond to the intensity  $I_0$  without absorption could, with sufficient accuracy, be derived from the blackenings outside the absorption region by interpolation on the photometer records. The photometer curves of the absorption photographs were evaluated by means of calibration curves, yielding

$$k_\nu/2.3 = k'_\nu - \log_{10} I_0/I,$$

as a function of  $N$  and  $n$ , where  $N = \frac{P \times 273 \times 2.7 \times 10^{19}}{760 \times T}$  and  $n = \frac{p_0 \times 2.7 \times 10^{19}}{760}$  are the numbers per ccm of mercury and argon atoms respectively,  $P$  being the pressure of Hg in mm,  $T$  the absolute temperature during the measurement,  $p_0$  the pressure of argon at  $0^\circ \text{C}$ , which was measured before sealing off. Fig. 2, Plate 11, shows a photometer trace taken with 7-fold magnification, of an absorption spectrogram at  $P = 1.58 \text{ mm}$ ,  $p_0 = 512 \text{ mm}$ ,  $T = 409^\circ \text{ abs}$ .

## RESULTS

### 1—Long Wave-Length Broadening

In order to compare the results with equation (3''), in fig. 3

$$\log_{10} \frac{k'_\nu T}{p_0 P} = \log_{10} \left( \frac{k_\nu}{nN} \times 1.5 \times 10^{25} \right)$$

is plotted against  $\log_{10} (\nu_0 - \nu)$  for values of  $\nu_0 - \nu > 0$ . The intensity produced by broadening of the Hg line by the pressure of mercury itself was known from measurements reported in the following paper. It was noticeable only in measurements with small  $p_0$  and large  $P$  and was subtracted from the measured  $k'_\nu$  values.

The expected proportionality of  $k'_\nu$  to  $N$  and  $n$  is confirmed experimentally by the fact that the points on the  $\log \frac{k_\nu}{nN}$  curve show no systematic deviation for different values of either  $n$  or  $N$ . The measurements at  $p_0 = 219 \text{ mm}$ . are marked by crosses. The proportionality to  $n$  shows that multiple collisions play no part in this frequency region.

In the range of validity of (3''), the dots should lie on a straight line with the gradient  $-3/2$ . In fact, at large values, the measurements fit a line of this gradient very well (solid curve, fig. 3). (The scale of the abscissae is twice that of the ordinates.) Comparing this result with Minkowski's measurements of the Na—A broadening, it is surprising that the region of the  $\Delta\nu^{-3/2}$  law begins only at rather large  $\Delta\nu$  values, the region of a steeper gradient (about 2.3, broken line) stretching comparatively far.

More surprising, however, is the result of the evaluation of the C-value from the intensity measurements by means of (3''')

$$\begin{aligned}\sqrt{C} &= \frac{k_r}{nN} (\nu_0^* - \nu^*)^{3/2} \times \frac{1}{\hbar} \times \frac{3mc^{5/2}}{2\pi^2 e^2} \quad (\nu^* = \text{wave number}) \\ &= \frac{k_r T}{p_0 P} (\nu_0^* - \nu^*)^{3/2} \times 1.22 \times 10^{-18} = 3.2 \times 10^{-17} \quad (3''') \\ C &= (1.0 \pm 0.2) \times 10^{-33}\end{aligned}$$

The C-value derived from measurements† of the half-value width by means of Weisskopf's‡ formula for the Lorentz cross-section gives  $C = 6.5 \times 10^{-33}$ . From this and also from mere theoretical estimates, C is expected to be of the order of  $5 \times 10^{-33}$ . This discrepancy is far too great to be explained by the inaccuracy of either the half-value width method or the theoretical estimate. An explanation, however, which simultaneously accounts for the unexpectedly large region of the steeper gradient in fig. 3 presents itself on closer inspection of the theoretical basis of the argument.

If a mercury atom in the excited state  $^3P_1$  approaches an argon atom in its fundamental state  $^1S_0$ , the orientation of the angular momentum  $J = 1$  of the Hg atom in the axial field of force of the atom pair produces two quantum states  $\Omega = \pm 1$  and  $\Omega = 0$ . We have, therefore, two potential curves with the statistical weights 2 and 1 instead of the one curve *b* in fig. 1. The question if the two curves are appreciably separated in the region of the polarization forces has been discussed by Margenau (*loc. cit.*) by means of London's formulae for a  $^1P_1$  state, which is practically identical with the present one. No use could, however, then

† Fuchtbauer, Joos, and Dinkelacker, 'Ann. Physik,' vol. 71, p. 204 (1923).

‡ Here, as in most cases, the corrected formula (Kuhn, 'Phil. Mag.,' *loc. cit.*) has to be used. But the correction for the mean free path must be applied twice, at the beginning as well as at the end of the free path (Mr. F. London drew my attention to this fact), so that the correct formula has to be written  $\lambda = \frac{1}{N\pi p^2} - \lambda_p$ .

be made of this extension of the theory, because in considering multiple interactions an average value for the two orientations had to be used. If  $C_b^0$  and  $C_b^1$  are the force constants for the two orientations, the theory predicts that  $C_b^1$  is about  $\frac{1}{2}C_b^0$ †. As the average value  $C_b$  is greater, but

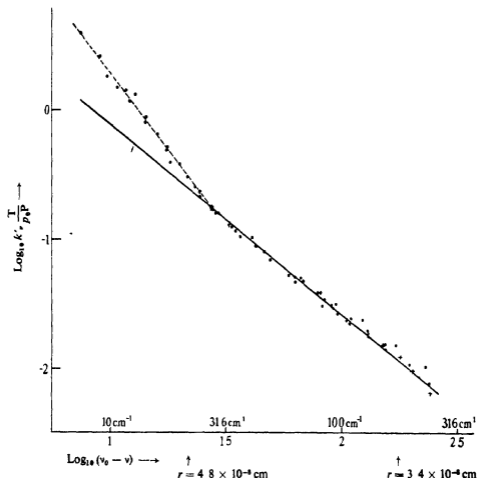


Fig. 3—Absorption in the long wave-length wing, + measurements at  $p_0 = 219$  mm ; ● measurements at  $p_0 = 512$  and  $660$  mm , — theoretical curve  $k' \sim \Delta v^{-4/3}$ .

of the same order of magnitude as  $C_a$ , it is quite possible that  $C_b^1 < C_a$  (see fig. 4).

If this is true, only the  $a \rightarrow b^0$  transitions are responsible for the long

† This is strictly true only for normal and metastable states, but because of the weakness of the transition  $^1S - ^3P_1$ , the term  $^3P_1$  can be considered as a metastable one.

wave-length wing of the broadening. As  $\Omega = 0$  has the statistical weight 1 compared with 3 for  $\Omega = 0$  and  $\Omega = 1$  together, every third transit only is able to give the transition  $a \rightarrow b^0$ , therefore  $n/3$  instead of  $n$  has to be written in equation (3'''), yielding a nine times larger value for  $C$ :

$$C^0 = C_b^0 - C_a = (9.0 \pm 2) \times 10^{-33},$$

*i.e.*, the "effective" pressure of Argon is only 1/3 of its full pressure

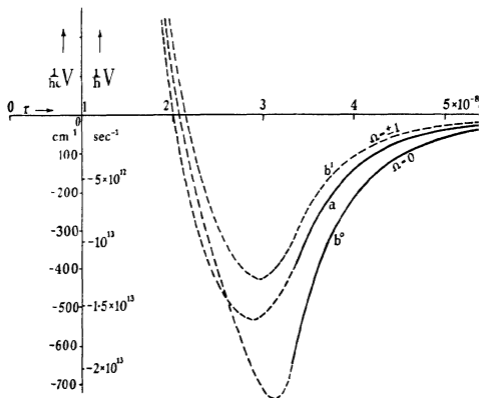


FIG 4—Potential of the van der Waals force, with splitting of the excited state, — quantitative, derived from measurements, - - - qualitative

In the Lorentz effect, however, the action of both the  $b^1$  and the  $b^0$  curves is superposed, as only the phase change, disregarding its sign, matters here, so that the argon acts with its full pressure. In this effect,  $C$  is some sort of average between  $|C_b^1 - C_a|$  and  $|C_b^0 - C_a|$ , and consequently rather smaller than  $C_b^0 - C_a$ , so that there is no longer a discrepancy between the  $C$  value derived from the red wing broadening and the Lorentz effect value.

The new assumption also explains the above-mentioned fact of the unusually wide frequency range in which the intensity law is of the Lorentz type (gradient  $\approx 2$ , broken curve, in fig 3) compared with the statistical wing effect, the Lorentz effect is favoured by the joint efficiency of both states  $\Omega = 0$  and  $\Omega = \pm 1$

In fig 4,  $V_a$  and  $V_b^0$  are plotted quantitatively, assuming the theoretical, fairly accurate value  $C_a = 1.7 \times 10^{-32}$  yielding  $C_b^0 = 2.6 \times 10^{-32}$ .  $V_b^1$  is only qualitatively drawn. A comparison of figs 3 and 4 shows that

the  $\Delta\nu^{-3/2}$  law is valid even in the region in which  $|V_a| = \frac{1}{0.9} h \times \Delta\nu$  is of

the order of  $kT$  ( $\approx 300 \text{ cm}^{-1}$ ). This seems surprising at first sight, as the number of atoms should increase by the factor  $e^{-|V_a|/kT} \approx e$ . But we have to assume that the continuous spectrum is produced by free atoms, *i.e.*, atoms in the state of transit, not by those caught as molecules. In a region with the potential energy  $V_a$ , all atoms, the kinetic energy  $\tau$  of which is smaller than  $|V_a|$ , are caught as quantized molecules. The number of free atoms is nearly equivalent to the number of atoms with  $\tau > |V_a|$ .<sup>†</sup> The number of these free atoms, however, is almost independent of  $V_a$ ,

only their average velocity is increased by the factor  $\frac{kT + |V_a|}{kT}$ .<sup>‡</sup> The

increase of the density of atoms due to the Boltzmann factor is mainly an increase of bound atoms. The fact that the absorption in the region under discussion is continuous and obeys the  $\Delta\nu^{-3/2}$  law shows that HgA molecules of the same internuclear distance have their main absorption in a different region of wave-lengths. The fact of quantization makes the classical statistical evaluation of the frequency distribution less correct for molecules (*see also* below).

The question arises whether it is possible to observe the statistical effect of the  $\Omega = \pm 1$  state as a wing on the side of shorter wave-lengths. In the following paragraph, the impossibility of observing this wing because of overlapping by other effects will be shown.

<sup>†</sup> In fact, an atom can even be caught as a molecule if its kinetic energy is somewhat larger than its potential energy, *see* Oldenberg, 'Z. Physik,' vol 56, p. 563 (1929).

<sup>‡</sup> This would strictly be true for a two-dimensional gas, where

$$\int_{\tau=-\infty}^{\tau=\infty} f(\tau) e^{-|V_a|/kT} d\tau = \int_{\tau=0}^{\tau=\infty} f(\tau) d\tau,$$

if  $f(\tau)$  is the distribution function in absence of forces. In three dimensions, the integral cannot be evaluated, but an approximation shows that the left side of the equation exceeds the right one by a factor of about  $\sqrt{1 + |V_a|/kT}$ , which is only a small correction in the present case.

## 2—Short Wave-Length Broadening

For not too large values of  $\nu - \nu_0$  (fig 5), the absorption decreases with nearly the second power of  $\nu - \nu_0$ . To show this,  $\log_{10} \frac{k'T}{p_0 P}$  is plotted against  $\log_{10} (\nu - \nu_0)$ , the broken line indicating the Lorentz law. The actual gradient is slightly steeper, as for sodium,<sup>†</sup> and in qualitative agreement with Lenz's formulae

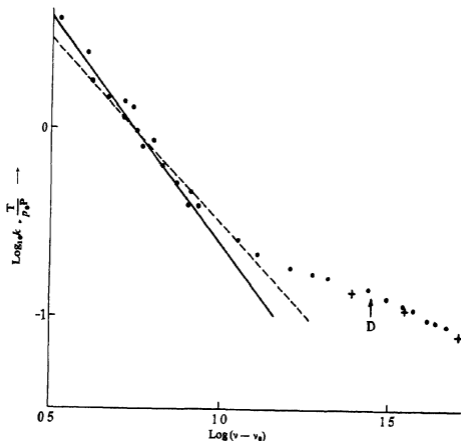


FIG 5—Absorption at short wave-lengths

For larger values of  $\Delta\nu$  (fig 6), the intensity curve is more complicated. The small gradient near the arrow D in figs. 2 and 5 is probably due to the discrete band D ( $\lambda = 2534.5 \text{ \AA}$ ), which will be discussed later. The most remarkable feature is the two maxima A and B at  $2531.9 \text{ \AA}$  and

<sup>†</sup> Minkowski, *loc cit*

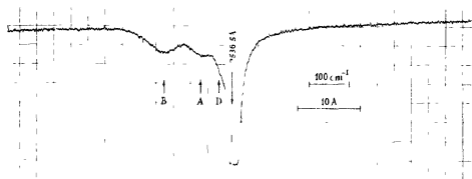


FIG. 2—Part I

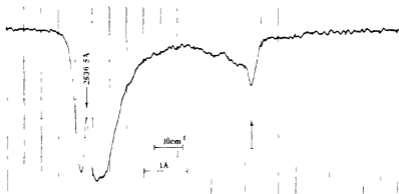


FIG. 1—Part II

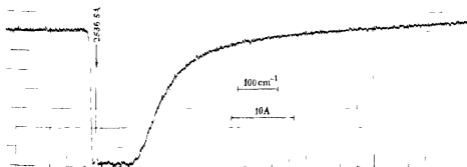


FIG. 2—Part II



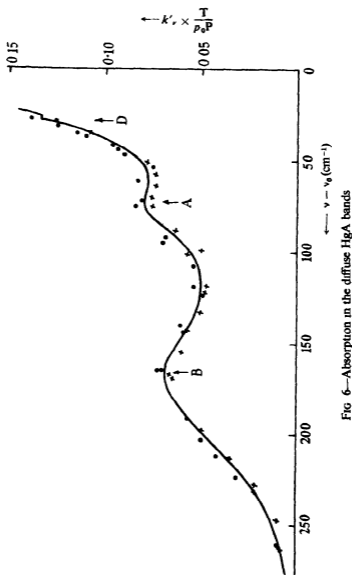


FIG 6—Absorption in the diffuse HgA bands

2525.7 Å., which have already been observed by Oldenberg† in absorption and in fluorescence. In fig 6,  $k'_{\nu} \times \frac{T}{p_0 P}$  is plotted as a function of  $(\nu - \nu_0)$ . Very similar diffuse bands have also been found on the short

† Oldenberg, 'Z. Physik,' vol. 47, p. 184 (1928) , vol 55, p 1 (1929)

wave-length side of lines of other metals in the presence of rare gases † An interpretation has been given,‡ in which the presence of two maxima was attributed to the existence of two potential curves corresponding to the two orientations of the angular momentum. The difference between the energy curves  $b^1$  and  $b^0$  at large internuclear distances, found above, favours the general idea of this interpretation of the Oldenberg bands. Its details, however, require modification. The statistical investigation, by means of (3), of the region of positive  $V_a$  shows that no intensity maximum exists which corresponds to the average or to the most probable kinetic energy. Also the total intensity of the two bands is too great to be due to this region only. If the Boltzmann factor is neglected, the integral  $\int k_\nu d\nu$ , taken over the two diffuse bands in fig 6, gives the phase volume  $4\pi r^2 \Delta r$  responsible for their absorption

$$4\pi r^2 \Delta r = \int k_\nu d\nu \times \frac{cm}{nNl\pi f e^2} \approx 15 \times 10^{-23} \text{ cm}^3$$

With an average value of  $r = 3 \times 10^{-8}$  cm, we obtain  $\Delta r = 1.4 \times 10^{-8}$  cm, which is too large for the region of positive  $V$  values only. Both these objections would be removed by assuming a considerable increase of the transition probability with decreasing distance. This can only be expected for lines which are forbidden by the J-selection rules but not here.

It must therefore be assumed that the transitions to the two curves  $b^0$  and  $b^1$  from the whole region of repulsion of the curve  $a$  are responsible for the two diffuse bands. A gain in intensity as  $\nu$  increases can arise if the gradients of the curves  $a$  and  $b$  approach each other with decreasing  $r$ , as can be seen from (3) if written in the form

$$I(\nu) = 4\pi A \frac{r^2}{\left| \frac{d\nu}{dr} \right|} = A' \frac{r^2}{\left| \frac{d(V_b - V_a)}{dr} \right|}$$

As the value of  $r$  decreases further the intensity may decrease again because of the Boltzmann factor for positive  $V$ , thus forming a maximum of intensity || Probably, also the quantized initial states contribute to

† Krefft and Rompe, 'Z. Physik,' vol 73, p 681 (1931)

‡ Kuhn and Oldenberg, 'Phys. Rev.,' vol 41, p 72 (1932)

§ An interesting example of this kind was recently investigated by Preston ('Phys. Rev.,' *in the press*)

|| A similar alternative explanation of the bands was given by Preston (appearing shortly in 'Phys. Rev.,' kindly communicated to me by Professor Oldenberg)

the continuous maxima by means of transitions to the positive potential parts of  $b^1$  and  $b^0$

The fact that the two diffuse bands appear in absorption and in emission at nearly the same frequencies is a strong argument in favour of this interpretation, in which the statistical occurrence of the different values

$\nu = \frac{1}{h} (V_b - V_a)$  plays the main part in the production of the maxima

A remeasurement of Oldenberg's fluorescence photographs gave as the wave-lengths of the maxima . 2532 0 Å. and 2526 4 Å. Whether the deviation of the second value from that one found in absorption is real or due to the inaccuracy of the fluorescence measurement is not certain

### 3—Discrete Bands

The absorption photographs at higher pressures showed, superposed on the long wave-length wing, several faint but very sharp bands, degraded towards short wave-lengths. The wave-lengths of the two strongest ones could be measured with an accuracy of 0.1 Å. and were found to be 2542.0 and 2544.0 Å. They are obviously identical with the first members of the series of bands observed by Oldenberg (*loc cit*) in the fluorescence of a mercury argon mixture ( $2541.7 \pm 0.2$  Å.,  $2543.7 \pm 0.2$  Å.), and must be explained correspondingly as due to HgA molecules. Their intensity is so small that they did not seriously interfere with the intensity measurements of the continuous absorption. The degradation of these bands towards short wave-lengths seems to indicate a decrease of the equilibrium distance of the HgA molecules with excitation, in contradiction to fig. 4. But it is doubtful whether the bands are single bands or groups, so that the degradation is possibly not merely due to rotation structure. Therefore, the dotted parts of the potential curves in fig. 4, though largely hypothetical, are still the most plausible interpretation of the experimental facts. The sharp band on the short wave-length side of the line, at  $2534.5 \pm 0.2$  Å. (D in figs. 2, 3 and 5), is very much stronger, and probably contains the bulk of the absorption of the molecules.

The experimental fact that the envelope of the intensity distribution in the discrete spectrum does not coincide with that in the continuous spectrum indicates that the Franck-Condon principle in its simplest form is not a very good approximation for this type of molecules. The experiments described in the following paper lead to the same conclusion.

## TRANSITION PROBABILITIES

The preceding discussions are based on the assumption that the transition probability is not changed by the perturbation of the energies involved in optical impacts. If the transition is not forbidden by the J-selection rule, no such change can be expected theoretically, and it must be stressed that no experimental evidence of it exists. The decrease of the absorption integral over the broadened mercury line 2537 Å. at very high pressures of A, CO<sub>2</sub>, or N<sub>2</sub>† cannot—as it is often done—be interpreted as a decrease of the transition probability. A rough estimate shows that the effect can be completely accounted for by the absorption in the wings of the line escaping the observation which was limited to a small frequency region. The volume  $v = \frac{4\pi}{3}(r_1^3 - r_2^3)$  inside which the absorption frequency is changed sufficiently is a considerable fraction of the total average volume  $v_0$  per atom, under the conditions of these experiments ‡.

In general, investigations of line intensities will hardly be able to reveal changes of transition probabilities due to impacts, because any such changes will be connected with considerable changes of frequency. The results of Hamos,§ who found no changes of the lifetime of the sodium fluorescence in the presence of rare gases, is therefore not unexpected.

An apparently striking example of a decrease in intensity of a continuous absorption in Cs vapour due to an addition of a few cm of neon has recently been described by Braddick and Ditchburn ||. If it were due to a decrease in the transition probability, it would involve a strong influence of a Ne atom on the absorbing particle (atom or molecule) at a distance of about  $10^{-8}$  cm. But there can be little doubt that the observed decrease in absorption is due to a decrease in the amount of Cs vapour present in the tube after the addition of neon, for it is well known that Cs vapour at high temperature is very rapidly absorbed by glass, so that the actual pressure of the Cs vapour in the absorption tube does not correspond to the vapour pressure of the Cs metal in the side tube, but depends also on the rate at which it diffuses from the side tube. This, of course, becomes slower if the neon pressure is increased.

† Fuchtbauer, Joos, and Dinkelacker, 'Ann. Physik,' vol. 71, p. 204 (1923).

‡ Using  $r_1 = 5$ ,  $r_2 = 2 \times 10^{-8}$  cm, the ratio  $v/v_0$  is 0.36 at 45 atm. argon pressure (considering single impacts only), which agrees with the rate of decrease (0.3) found by Fuchtbauer, Joos, and Dinkelacker.

§ 'Z. Physik,' vol. 74, p. 379 (1932).

|| 'Proc. Roy. Soc. A,' vol. 150, p. 478 (1935).

## SUMMARY

The continuous spectrum which forms the wing of a pressure broadened spectral line is produced by transits of atoms at distances within the range of the van der Waals forces (optical impacts). Within certain limiting conditions, the intensity distribution is very nearly identical with the occurrence distribution of the perturbed eigenfrequencies of single transits. It is therefore able to yield quantitative results on the van der Waals forces.

The absorption coefficient in the wings of the Hg line 2537 Å broadened by argon is measured at different pressures of argon and mercury by means of photographic photometry. Its proportionality to the densities of Hg and Ar proves that it is produced by single transits.

The discussion of the results leads to the conclusion of a considerable splitting of the excited state into two components, due to orientation of the J-vector against the axis of the collision pair. Between  $\Delta\nu = 25$  and  $\Delta\nu = 250 \text{ cm}^{-1}$ , the measured absorption coefficients are proportional to  $\Delta\nu^{-3/2}$  as predicted by theory. This proves the validity of the  $C/r^6$  potential law of the polarization forces for internuclear distances between  $3.4$  and  $4.8 \times 10^{-8} \text{ cm}$ . The constant  $C$  for the component  $\Omega = 0$  of the excited state is found to be  $C_0 = 2.6 \times 10^{-32}$ .

---

# Pressure Broadening of Spectral Lines and van der Waals Forces

## II—Continuous Broadening and Discrete Bands in Pure Mercury Vapour

By H KUHN, Clarendon Laboratory, Oxford

(Communicated by F A Lindemann, F.R.S.—Received 15 July, 1936)

### INTRODUCTION

The spectrum of single transits, forming part of the pressure broadening, has been quantitatively investigated for Na—A and for Hg—A transits \* It was found to be very nearly identical with the occurrence distribution of the perturbed eigenfrequencies, the intensity† distribution being in agreement with the theoretical prediction‡  $I(\nu) \sim \Delta\nu^{-3/2}$  within the limits of its validity. As this agreement is a direct experimental test on the sixth power potential law of the van der Waals forces, given by London's wave mechanical theory, it seemed to be of interest to investigate a case in which the velocity of the atoms is considerably less, so that any possible influence of the motion is smaller still. The interaction between two mercury atoms, *i.e.*, the broadening of the mercury resonance line by the mercury pressure itself, was therefore chosen for quantitative investigation.

An excited atom interacts with a normal atom of the same kind at very large distances with a potential of force proportional to  $1/r^3$ , if *r* is the internuclear distance. The influence of this "resonance force" on pressure broadening has been treated theoretically by Weisskopf §. Though it is considerable at very low pressures, resulting in large "optical impact diameters" for the Lorentz effect, it is very small at higher densities. This is connected with the dipole property of the forces: the interactions of several neighbouring atoms mainly cancel each other, leaving a very small residue only, the so-called coupling broadening. It was thus expected‡ that in the wing effect the resonance forces can be completely neglected.

\* Minkowski, 'Z. Physik,' vol 93, p 731 (1935), Kuhn, preceding paper.

† The word intensity is used here in a broader sense, including intensity of absorption.

‡ Kuhn, 'Phil. Mag.,' vol 18, p. 987 (1934).

§ Weisskopf, 'Z. Physik,' vol 75, p 287 (1932).

The wing effect must be considered as a single interaction with respect to the polarization forces ( $V \sim 1/r^6$ ), but simultaneously as a highly multiple interaction with respect to the resonance forces ( $V \sim 1/r^3$ ). This is due to their slow decrease with the distance which is at a first approximation counterbalanced by the increase of the number of atoms within a certain distance ( $N \sim r^3$ ).

The absorption of mercury vapour is known\* to extend with increasing density mainly towards long wave-lengths. The far end of this wing of the absorption has been quantitatively investigated by Kuhn and Freudenberg,† the nearer part of it recently by de Groot ‡. In this latter investigation, agreement was found with the  $\Delta\nu^{-3/2}$  law of intensity by measuring the limits of absorption at different pressures. This agreement is a rough one only, on account of the experimental inaccuracies, and also because the frequency range is rather bigger than that in which the  $1/r^6$  potential law can be expected to hold. Photometric measurements extending to smaller frequency distances from the line seemed desirable.

Experimental arrangement and procedure were essentially the same as those described in the preceding paper. The side tube of the absorption cell was slightly longer, so that its end was the coolest part, and contained the liquid mercury. Its temperature was measured by means of a mercury thermometer. The correction of the emergent stem was determined experimentally. The possible error was about  $0.5^\circ$ .

## RESULTS

The asymmetry of the broadening is much more pronounced than in the broadening by argon. Fig. 1 (Part II), Plate 11, shows a photometer curve of the absorption at 7.68 mm pressure with 49-fold magnification of the photometer. The continuous long wave-length wing is interrupted by the well-known discrete bands with their strongest peak at 2540.34 Å, marked by an arrow. Fig. 2 (Part II), Plate 11, shows the further extension of the wing towards long wave-lengths at higher pressure (94.36 mm) with sevenfold magnification.

In fig. 3, the measured values of  $\log_{10} \frac{k' T^2}{P^2} = \log_{10} \left( \frac{k'}{N^2} \times 1.5 \times 10^{35} \right)$  of the continuous long wave-lengths wing are plotted against  $\log_{10} (\nu_0 - \nu)$ .  $P$  is the mercury vapour pressure,  $N$  the number of atoms per ccm,  $T$

\* Wood and Guthrie, 'Astrophys. J.', vol. 29, p. 24 (1909). See also Wood, 'Physical Optics,' New York, 1934, p. 636.

† Kuhn and Freudenberg, 'Z. Physik,' vol. 76, p. 38 (1932).

‡ De Groot, P. Zeeman, "Verhandelingen," p. 312, Haag, 1935.

the absolute temperature, and  $k_v = \log_e \frac{i_0}{i} = 2.3 \log_{10} \frac{i_0}{i} = 2.3 k'$ , the absorption coefficient. The points derived from plates at different values of  $P$  lie very well on the same curve. This shows that the absorption coefficient is proportional to  $N^2$ , in agreement with the assumption that the absorption is due to single transits. The presence of the discrete bands causes the interruption of the curve.

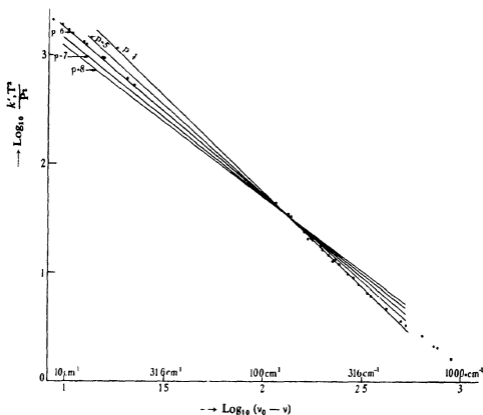


FIG. 3—Continuous absorption in the long wave-length wing

In the short wave-length wing, the absorption drops very rapidly, so that no great accuracy of measurement was obtained, particularly as only the sevenfold magnification of the photometer was used. Again,  $\log_{10} \frac{k' T^2}{P_2}$  is plotted as a function of  $\log_{10} (\nu - \nu_0)$ , but the measurements are hardly accurate enough to prove the proportionality of  $k'$  to  $N^2$ . The only certain result is a decrease much quicker than with the inverse square of  $\Delta\nu$  (fig. 4).

For the discrete bands near 2540 Å, the absorption coefficient

$$k'_v = 1/2 \cdot 3 \times k_v = \log_{10} \frac{I_0}{I},$$

at 7.68 mm pressure ( $T = 449^\circ$ ) is plotted as a function of  $\Delta\nu$  (in  $\text{cm}^{-1}$ ) in fig 5 (broken curve). The subtraction of the continuous absorption

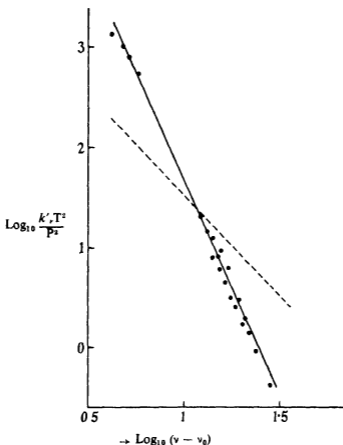


FIG 4—Short wave-length broadening. Experimental curve, - - - theoretical curve of Lorentz-broadening

(dotted curve) which is derived by interpolation from fig 3 gives the absorption coefficients of the discrete absorption (full curve). On the plates, the absorption minima (arrows I and II) appear as black lines, the steep drops (arrows III and IV) as strong edges.

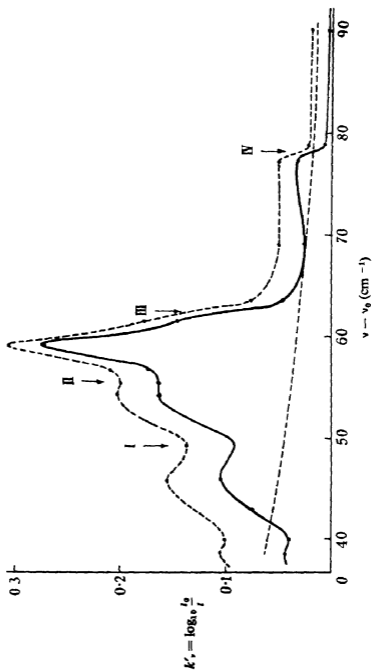


FIG 5—Absorption in the discrete  $\text{Hg}_3$  bands  $P = 7.68 \text{ mm}$

## DISCUSSION OF THE RESULTS

1—*The Continuous Broadening*

The pressure broadening, measured in half-value widths, due to atoms of the same kind, has been found to be much stronger (about 100 times) than that due to foreign atoms or molecules,\* but the experiments that show this are rather indirect. Theoretically, Weisskopf† showed that the resonance forces can give rise to very great optical impact radii. That this difference, if it is real, disappears in the wings of the broadened lines, was expected and was found in the experiments reported here. At distances of about  $10 \text{ cm}^{-1}$  from the centre of the line, the absorption coefficient in pure mercury vapour of 7.68 mm is about the same as the absorption coefficient of a mixture of 0.156 mm mercury and 660 mm argon. This corresponds to a broadening efficiency of the mercury of less than twice that of argon.

Since the effect of the resonance forces is negligible, and the relative speed of the atoms even smaller than with mixtures of A and Hg or A and Na, the intensity distribution in the wing of the line must be expected to be practically identical with the occurrence distribution of the frequencies perturbed by polarization forces. As only single transits are effective, at the low pressures involved, we expect again the absorption coefficient as a function of  $\Delta\nu$  to be

$$k_\nu = \frac{\alpha}{(\nu_0 - \nu)^{3/2}}. \quad (1)$$

In order to show how far the experimental results support the sixth power distance law of the polarization potential, as given by London, a more general potential law

$$V = -\frac{C}{r^p},$$

may be tested for all integer values of  $p$ . It results in an intensity distribution,†

$$k_\nu = \frac{\beta}{(\nu_0 - \nu)^{\frac{p+3}{p}}} \quad (1')$$

giving straight lines of different gradients for the different  $p$ -values, if  $\log k$  is plotted against  $\log (\nu_0 - \nu)$ .

\* Minkowski, 'Z. Physik,' vol 36, p 839 (1926), Orthmann and Pringsheim, *ibid*, vol 46, p 160 (1928).

† *Ibid*, vol 75, p 287 (1932).

‡ Kuhn, 'Phil Mag,' vol 18, p 987 (1934).

In fig. 3 (the scale of the abscissae is twice that of the ordinates) the straight lines represent the potential laws  $p = 4, 5, 6, 7, 8$ . They show that only  $p = 5$  and  $p = 6$  need be considered for comparison with the measurements. For several reasons (Boltzmann-factor and limits of validity of the theoretical potential law), the absorption at large  $\Delta\nu$  values cannot be explained quantitatively. The region of smaller frequency differences is therefore of main interest. The measurements between  $\Delta\nu = 9 \text{ cm}^{-1}$  and  $\Delta\nu = 160 \text{ cm}^{-1}$  can be very closely approximated by the curve  $p = 6$ , definitely better than by any other integer exponent. Using the whole region observed, up to  $1000 \text{ cm}^{-1}$ , the line fitting the values most closely would yield a value between 5 and 6 (about 5.2). But apart from the theoretical reasons against using the whole range of frequencies, the deviations from linearity are greater than the possible experimental errors.

Assuming  $p = 6$ , the constant  $\alpha$  yields the constant  $C$  of the potential law

$$\alpha = N^2 h^2 \frac{2\pi^2 e^2}{3mc} \times C^{\frac{1}{2}} \quad (2)$$

The numerical result derived from the dotted curve is

$$C = C_b - C_a = 5.4 \times 10^{-32} \quad (3)$$

Using London's theoretical, fairly accurate value  $C_a = 3.8 \times 10^{-32}$  for the ground state, the constant for the excited state is found as  $C_b = 9.2 \times 10^{-32}$ . This value of  $C_b$  would have a direct physical significance only if the excited state were single or had a very small splitting. But the reverse must be expected from theoretical reasons and from comparison with the Hg—A interaction (see preceding paper). In the present case, the absence of a short wave-length wing of any considerable extent shows that not only  $C_b^0$  but also  $C_b^1$  is greater than  $C_a$  (see the qualitative fig. 6). The transitions  $\alpha^0$  and  $\alpha^1$  to both curves  $b_0$  and  $b^1$  contribute to the long wave-length wing, the constant  $C$  in equation (2) being given by

$$\sqrt{C} = \frac{1}{2} (\sqrt{C_b^0 - C_a} + 2\sqrt{C_b^1 - C_a}),$$

where the value of the second root is probably much smaller than that of the first one. The absorption of a certain frequency is produced by transitions  $\alpha^0$  and  $\alpha^1$  (fig. 6) at different internuclear distances. The transitions  $\alpha^1$  must be expected to show considerable deviations from the  $\Delta\nu^{-3/2}$  distribution even for values of  $\Delta\nu$  considerably less than the heat of dissociation. The deviation from the line  $p = 6$  beyond  $160 \text{ cm}^{-1}$  in fig. 3 is probably due to their contribution to the absorption. The rough

validity of the  $\Delta\nu^{-3/2}$  distribution which extends as far as  $1000\text{ cm}^{-1}$  is apparently caused by the  $\alpha^0$  transitions, which, for the same frequency, involve greater internuclear distances than  $\alpha^1$  transitions

The general agreement for large values of  $\Delta\nu$  between the experimental curve and that required by the above theory shows that the Boltzmann factor  $e^{-V/kT}$  must be disregarded in computing the occurrence distribu-

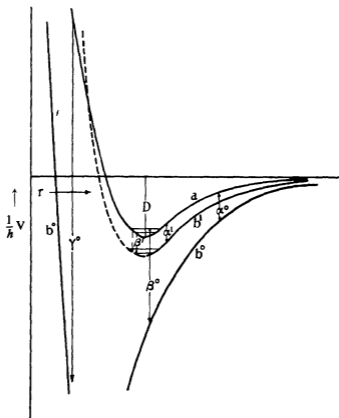


FIG. 6—Qualitative diagram of van der Waals potential curves, with splitting of excited level  $b$

tion. An explanation of this was given in the corresponding case of the HgA interaction. In the present case, it has a strong experimental support. In a former investigation\* on the influence of temperatures up to  $1150^\circ\text{C}$  on the mercury absorption spectrum, it was found that a large region of continuous absorption extending from the resonance line as far as  $6000\text{ cm}^{-1}$  showed no influence of the temperature comparable with the

\* Kuhn and Freudenberg, 'Z. Physik,' vol 76, p 38 (1932)

influence on the discrete  $\text{Hg}_2$  bands. This result, very unexpected at that time, is exactly what the explanation given here would predict

For positive energies, *i.e.*, very small internuclear distances, the distribution function has to be multiplied by  $e^{-v/kT}$ ; the conclusion that the negative temperature coefficient beyond  $6000\text{ cm}^{-1}$  indicates initial states of positive potential energy (transitions  $\gamma^0$  in fig. 6), is unaltered. The interpretation of the exponential decrease of the absorption coefficient at very large  $\Delta v$  values by means of the Boltzmann-factor is also upheld, for in the limiting case of sufficiently large potential energies, the volume factor is small compared with the Boltzmann-factor and can be neglected for rough estimates. This is identical with the assumption of central impacts made by Kuhn and Freudenberg

## 2—The Discrete Bands

The band system at about  $2540\text{ Å}$ . (fig. 5) is the only discrete absorption observed near the resonance line. In the qualitative picture of the potential curves in fig. 6 it must be ascribed to the transitions  $\beta^1$  from the quantized states of curve *a* to the quantized states of curve *b*<sup>1</sup>. As the statistical weights of *b*<sup>1</sup> and *b*<sup>0</sup> are 2 and 1 respectively, the observed bands represent the total absorption connected with the transition  $^1\text{S}_0 \rightarrow ^3\text{P}_1$  of  $2/3$  of all molecules. The transitions  $\beta^0$  of the remaining  $1/3$  of the molecules would be expected, according to the Franck-Condon principle, to give bands of much longer wave-lengths, probably at least  $1000\text{ cm}^{-1}$  from the atomic line. It is true that this principle does not hold strictly for quantized molecules. The mere fact that the intensity distribution in the discrete bands is quite different from that of the continuous spectrum for  $\text{Hg}_2$  and  $\text{HgA}$  shows that the deviations from this principle are very marked in the case of these loose molecules. For rough statements, however, on the wave-length region of a band system, it can certainly be relied on. The region of very large frequency distances was not investigated with the present arrangement. Lord Rayleigh\* found a diffuse structure at frequency distances beyond  $2000\text{ cm}^{-1}$ . The presence of a true quantization structure cannot be regarded as excluded. On account of their probable extension over a large spectral range and their faintness due to the small statistical weight, the bands may be difficult to observe.

The absorption integral over the whole band system  $2540\text{ Å}$ . is connected with the number  $N_m$  of molecules per ccm. by the equation of the electron theory

$$\int k_\nu d\nu = 2 \cdot 3 \int k'_\nu d\nu = \frac{2}{3} \times 2N_m f \frac{\pi e^2 l}{cm},$$

\* 'Proc Roy Soc,' A, vol 116, p 702 (1927)

$f$  is the oscillator strength characteristic for the electron transition,  $l$  the length of the absorption cell. The factor  $2/3$  is the statistical factor mentioned above, the factor 2 expresses the fact that the molecule contains two atoms. It is almost certain that the  $f$  value (which is a measure of the transition probability) of the transition  $^1S - ^3P_1$  of the Hg atom is not appreciably changed by the formation of a van der Waals molecule (see preceding paper). Using the value  $f = 0.026$  of the free atom\* will therefore be a very good approximation. Under the conditions of the experiment represented in fig. 5 ( $P = 7.68$  mm,  $T = 448^\circ$  abs.,  $l = 20$  cm), the integral is found to be

$$\int k_\nu d\nu = 8.7,$$

giving a number of molecules per ccm of

$$N_m = 1.5 \times 10^{13} = 8.7 \times 10^{-6} N_a,$$

if  $N_a$  is the number of free atoms per ccm.

This measurement of the concentration of molecules which is correct within probably 10 or 20% can be used for calculating the heat of dissociation. The formula of Gibson and Heitler† gives in the present case of a  $^1S$  term of the atom

$$\frac{D}{kT} = \ln \frac{p_a^2}{p_m} - \frac{3}{2} \ln \frac{\pi m_a kT}{h^2} + \ln \frac{8\pi^2 I}{h^2} - \ln \left( 1 - e^{-\frac{h\nu_0}{kT}} \right) - \ln 2$$

The pressures  $p_a$  and  $p_m$  of the atoms and molecules respectively have to be written in dyne/sq. cm if absolute c.g.s. units are used.  $I$  is the moment of inertia,  $m_a$  the mass of a Hg atom,  $\nu_0$  the vibration frequency of the molecule. Using  $I = 1.69 \times 10^{-87}$  ( $r = 3.2 \times 10^{-8}$  cm) and  $\nu_0 = 36$  cm $^{-1}$  as the values previously assumed to be the most likely ones,‡ the result is

$$D = 2.1 \text{ cal } (= 0.092 \text{ volt} = 740 \text{ cm}^{-1}).$$

The Gibson-Heitler formula, however, assumes the potential law of a harmonic oscillator. This is a perfectly good approximation for ordinary molecules, where higher oscillation states are infrequent. In the present case, however, the higher oscillation states are abundant. Their phase volume is greater than that of a harmonic oscillator, and the above value of  $D$  is therefore an upper limit only.

\* Ladenburg and Wolfsohn, 'Z. Physik,' vol. 63, p. 616 (1930).

† Gibson and Heitler, 'Z. Physik,' vol. 49, p. 465 (1928).

‡ 'Z. Physik,' vol. 76, p. 38 (1932).

The heat of dissociation has been measured earlier by determining the decrease of the total absorption in the bands 2540 Å with increasing temperature, a method first used by Franck and Grotian\*. Koernicke† found  $D = 1.4$  cal., Kuhn and Freudenberg (*loc cit*)  $D = 1.6$  cal. This method also involves the assumption of the harmonic force law. It is contained in the value of the specific heat of the molecule. In this case, however, the inaccuracy of the assumption makes the value of  $D$  too low, the values 1.4 and 1.6 cal. are lower limits. All these results can thus be summarized.

$$1.5 \text{ cal} < D < 2.1 \text{ cal.}$$

London's theoretical estimate,‡  $D = 2.0$  cal., based on the calculation of the polarization force, is rather an upper limit, as the repulsion forces are neglected.

As no complete vibration analysis of the  $\text{Hg}_2$  bands has yet been possible, the value  $\nu_0 = 36 \text{ cm}^{-1}$  is not quite certain. The values 18 and  $54 \text{ cm}^{-1}$ , though less likely, could not be excluded with certainty. The first one would make  $D$  smaller by 0.6 cal., the latter would increase it by 0.4 cal.

The internuclear distance  $r$ , and therefore  $I$ , is not accurately known. The value  $r = 3.2 \times 10^{-8} \text{ cm}$  is derived from the densities of liquid mercury and of solid alloys. A deviation of 10% which is just possible would alter the value of  $D$  by about 10% only. This inaccuracy is therefore comparatively unimportant.

In a former paper (*loc cit*), one of the two potential curves of the excited state—the  $b^1$  curve—was assumed to form a shallow potential minimum, much like that of the ground state. The transitions to the repulsion branch of  $b^1$  were supposed to give the small extension of the broadening to short wave-lengths. Though the argument of the positive temperature coefficient observed is not unambiguous here, as it could also result from a Lorentz effect, the very steep gradient of the absorption curve (fig. 4) is in favour of this explanation rather than of a Lorentz effect.

In computing the integral  $\int k_\nu d\nu$  from the photometric measurements of the discrete bands, it was assumed that there was no finer structure, unresolved on account of insufficient resolving power of the spectrograph. At the pressures involved this assumption is justified, as the width of the individual rotation lines is probably greater than their distance. How-

\* *Ibid*, vol 4, p 89 (1921).

† *Ibid*, vol 33, p 219 (1925).

‡ 'Z. phys. Chem.', B, vol 11, p. 222 (1930).

ever, in order to test this point experimentally, a rough comparison was made with the photographs at the same pressure of mercury and 219 mm. pressure of argon. The absence of any noticeable enhancing effect of the argon on the  $\text{Hg}_2$  band absorption showed that the additional broadening of the lines due to the argon did not change the total absorption. In case of any unresolved fine structure, it would certainly have increased.

The author expresses his gratitude to the Imperial Chemical Industries, through whose assistance this work has been made possible, and to Professor F. A. Lindemann for his kind interest in the research. He is also greatly indebted to Dr. D. A. Jackson for the continued use of his spectrograph and to Professor H. H. Plaskett for permission to use his photometer.

#### SUMMARY

The broadening of the absorption line 2536.5 Å of mercury vapour under the influence of its own pressure is measured. The distribution of the absorption coefficient in the long wave-length wing of the line agrees with the theoretically predicted  $\Delta\nu^{-3/2}$  law, thus confirming the exponent  $p = 6$  in the potential law  $V \sim r^{-p}$  of the van der Waals forces.  $p = 5$  or  $p = 7$  would give less good agreement, any other integral value of  $p$  striking disagreement with the measurements.

Former measurements of the temperature coefficients of the continuous absorption are discussed.

The total absorption in the discrete band system 2540 Å. is measured. It yields an absolute value of the concentration of  $\text{Hg}_2$  molecules. It can be used for calculating the heat of dissociation of the  $\text{Hg}_2$  molecule by means of the Gibson and Heitler formula. The resulting value of 2.1 cal. is shown to be an upper limit, whereas the former thermal measurements ( $\approx 1.5$  cal.) are lower limits.



ever, in order to test this point experimentally, a rough comparison was made with the photographs at the same pressure of mercury and 219 mm. pressure of argon. The absence of any noticeable enhancing effect of the argon on the  $\text{Hg}_2$  band absorption showed that the additional broadening of the lines due to the argon did not change the total absorption. In case of any unresolved fine structure, it would certainly have increased

The author expresses his gratitude to the Imperial Chemical Industries, through whose assistance this work has been made possible, and to Professor F. A. Lindemann for his kind interest in the research. He is also greatly indebted to Dr. D. A. Jackson for the continued use of his spectrograph and to Professor H. H. Plaskett for permission to use his photometer.

#### SUMMARY

The broadening of the absorption line 2536.5 Å of mercury vapour under the influence of its own pressure is measured. The distribution of the absorption coefficient in the long wave-length wing of the line agrees with the theoretically predicted  $\Delta\nu^{-3/2}$  law, thus confirming the exponent  $p = 6$  in the potential law  $V \sim r^{-p}$  of the van der Waals forces.  $p = 5$  or  $p = 7$  would give less good agreement, any other integral value of  $p$  striking disagreement with the measurements.

Former measurements of the temperature coefficients of the continuous absorption are discussed.

The total absorption in the discrete band system 2540 Å. is measured. It yields an absolute value of the concentration of  $\text{Hg}_2$  molecules. It can be used for calculating the heat of dissociation of the  $\text{Hg}_2$  molecule by means of the Gibson and Heitler formula. The resulting value of 2.1 cal. is shown to be an upper limit, whereas the former thermal measurements ( $\approx 1.5$  cal.) are lower limits.

# The Interaction of Atoms and Molecules with Solid Surfaces

## VI—The Behaviour of Adsorbed Helium at Low Temperatures

By J. E. LENNARD-JONES, F.R.S., and A. F. DEVONSHIRE, The University Chemical Laboratory, Cambridge

(Received 8 August, 1936)

### 1—INTRODUCTION

The heat of adsorption of helium atoms on solid surfaces is so small that no one has succeeded in measuring it directly. Its value could probably be inferred from a series of accurate measurements of adsorption isotherms by using the formulae given in Paper III of this series,<sup>†</sup> or it could be calculated from known interatomic force fields as has sometimes been done.<sup>‡</sup> Such calculations indicate that the heat of adsorption on crystals of the rock salt type would probably be of the order of 100 to 200 cal./gm. atom. Another method of determining it has, however, been found in Paper V<sup>§</sup> from the diffraction experiments of Frisch and Stern<sup>||</sup> for these indicate that helium atoms on a lithium fluoride crystal have two quantized vibration levels perpendicular to the surface, whose energies are  $-57.5$  cal. and  $-129$  cal. (reckoned from a zero in which the atoms are in the gas phase at rest). The lower one gives the heat of adsorption.

From these energy levels it is possible to deduce some information as to the nature of the potential field between helium atoms and lithium fluoride crystals by choosing a function of the right properties (such that it vanishes at infinity, gives attraction at large distances and repulsion at short distances, and has a minimum at a finite distance from the surface), for which the vibrational wave equation can be solved. Such a function is the Morse potential function,<sup>¶</sup> which contains two parameters  $D$  and  $\kappa$ , the former giving the depth of the potential minimum and the latter

<sup>†</sup> Lennard-Jones and Devonshire, 'Proc. Roy. Soc.,' A, vol. 156, p. 6 (1936), using, for example, equation (29).

<sup>‡</sup> Lennard-Jones, 'Trans. Faraday Soc.,' vol. 38, p. 333 (1932).

<sup>§</sup> Devonshire, 'Proc. Roy. Soc.,' A, vol. 156, p. 37 (1936), Lennard-Jones and Devonshire, 'Nature,' vol. 137, p. 1039 (1936).

<sup>||</sup> Frisch and Stern, 'Z. Phys.,' vol. 84, p. 430 (1933).

<sup>¶</sup> Cf. Lennard-Jones and Strachan, 'Proc. Roy. Soc.,' A, vol. 150, p. 442 (1935).

the rate at which the field falls off (exponentially) at large distances. The two energy levels given above are thus sufficient to determine  $D$  and  $\kappa$  and they are found to be  $-175$  cal and  $(1 \cdot 10) 10^8 \text{ cm}^{-1}$ .

Our object in this paper is to use this information to construct a map of the potential field between the (100) surface of a LiF crystal and a helium atom outside it. The field must be periodic along the surface, owing to the periodic nature of the surface layer. The experiments of Stern and his collaborators† have shown that the surface of a LiF crystal has the same effect as a square grating of the size of the lattice of ions of one sign. This is probably due to the greater van der Waals field exercised by the  $F^-$  ions, those of the  $Li^+$  ions being negligibly small, or it may be due to the presence of an adsorbed film of atoms (possibly of oxygen atoms) held to alternate lattice points. When we refer to the field of the crystal, we shall mean the field of the crystal as used by Stern, whether containing an adsorbed film or not.

Calculations have been made elsewhere‡ of the potential energy of inert gases in the field of alkali halide crystals, and maps have been drawn showing the three-dimensional character of the field. An examination of these results shows that the field above any point of the surface can be represented satisfactorily by a Morse function (at any rate in the interesting region near the minimum) and that the depth of minimum changes from point to point of the surface in accordance with its doubly periodic character. The depth of this minimum fluctuates by an amount which is approximately one-third of its average value. Proceeding in this way, we have constructed the map shown in fig. 1, which gives two cross-sections of the field. The absolute minimum is above the centre of a lattice cell. In order to pass from one cell to one of the next nearest cells, an adsorbed atom must surmount a potential col, in order to pass over a lattice point, it must surmount a higher potential col.

Having obtained this rough contour plan of the field, we have attempted to draw inferences as to the probable behaviour of adsorbed helium atoms in it, particularly at low temperatures, where the behaviour of helium is of special interest.

## 2—THE ENERGY LEVELS AND WAVE FUNCTIONS OF AN ADSORBED HELIUM ATOM

The mathematical function which is plotted in fig. 1 is

$$V(x, y, z) = V_0(x, y, z) + V_1(x, y, z), \quad (1)$$

† Stern and Estermann, 'Z. Phys.' vol. 61, p. 95 (1930).

‡ Lennard-Jones, 'Trans. Faraday Soc.', vol. 38, p. 333 (1932).

where

$$V_0 = D (e^{-2\kappa(x-b)} - 2e^{-\kappa(x-b)}), \quad (2)$$

$$V_1 = -2\beta D e^{-2\kappa(x-b)} (\cos ax + \cos ay), \quad (3)$$

$\beta$  is a small constant, and  $2\pi/a$  is equal to the length of the lattice spacing. For each value of  $x$  and  $y$ ,  $V$  is a Morse function, the depth of the potential

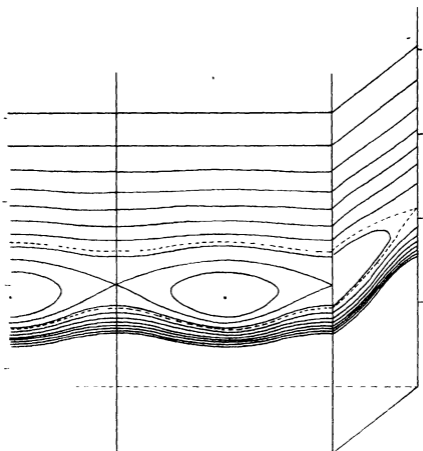


FIG. 1—Sections of the equipotential surfaces of a helium atom above a LiF surface.

minimum varying from  $D/(1 - 4\beta)$  over the centre of a lattice cell ( $x = 0, y = 0$ ) to  $D/(1 + 4\beta)$  over a lattice point. Fig. 1 shows a section of the equipotential surfaces by the planes  $x = a\pi$  and  $y = 0$ .

We shall find it convenient to write

$$(\hbar^2/2m) U_0(z) = V_0(z), \quad (4)$$

and

$$(\hbar^2/2m) U_1(z) = (V_1(z)/2) (\cos ax + \cos ay) \quad (5)$$

The wave equation for a particle in this field, viz.,

$$\{\nabla^2 + (2m/\hbar^2) E - U_0(z) - 2U_1(z)(\cos ax + \cos ay)\} \psi = 0, \quad (6)$$

is not separable, but we compare it with one which is, viz.,

$$\{\nabla^2 + (2m/\hbar^2) E - U_0(z) - 2U_1^{(n)}(\cos ax + \cos ay)\} \psi = 0, \quad (7)$$

where  $U_1^{(n)}$  is a constant. Now the solution of (7) is given by

$$E = E_l^{(n)}(\xi) + E_m^{(n)}(\eta) + E_n, \quad (8)$$

$$\psi(x, y, z) = g_l^{(n)}(\xi, x) g_m^{(n)}(\eta, y) f_n(z), \quad (9)$$

where  $E_n$  is a characteristic value and  $f_n(z)$  the corresponding wave function of the equation

$$\left\{ \frac{\partial^2}{\partial z^2} + \frac{2m}{\hbar^2} E - U_0(z) \right\} f(z) = 0, \quad (10)$$

while  $E_l^{(n)}(\xi)$  is a characteristic value and  $g_l^{(n)}(\xi, x)$  the corresponding wave function of the equation

$$\left\{ \frac{\partial^2}{\partial x^2} + \frac{2m}{\hbar^2} E^{(n)} - 2U_1^{(n)} \cos ax \right\} g(x) = 0, \quad (11)$$

with similar definitions of  $E_m^{(n)}(\eta)$  and  $g_m^{(n)}(\eta, y)$ . As we shall see presently,  $l$  and  $m$  take integral values 0, 1, 2, ..., and  $\xi, \eta$  are fractions between  $\pm \frac{1}{2}$ .

The solutions of (6) can be expressed in terms of those of (7) if we regard  $2(U_1(z) - U_1^{(n)})(\cos ax + \cos ay)$  as a perturbation, then the first order correction to the energy level given in (8) contains a factor

$$\int_{-\infty}^{\infty} f_n^*(z) \{U_1(z) - U_1^{(n)}\} f_n(z) dz, \quad (12)$$

and this vanishes if

$$U_1^{(n)} = \int_{-\infty}^{\infty} f_n^*(z) U_1(z) f_n(z) dz, \quad (13)$$

the  $f_n$  functions being normalized. Hence to a first approximation the energy levels of (6) and (7) are the same, provided  $U_1^{(n)}$  is defined as in (13).

The solutions of the equation (10) in  $z$  have been given in earlier papers of this series† and need not be repeated here, except to the extent that

$$E_n = -\kappa^2 \hbar^2 (d - n - \frac{1}{2})^2 / 2m, \quad (14)$$

† Cf. Lennard-Jones and Strachan, 'Proc. Roy. Soc., A, vol. 150, p. 442 (1935).

where  $n$  is an integer and  $d$  is a number defined by

$$d = (2mD)^{1/2} / \kappa \hbar \quad (15)$$

We note, however, that with the particular form of  $U_1(z)$  given by (3) and (5)† it is easy to obtain an explicit formula for  $U_1^{(n)}$ , viz.,

$$\begin{aligned} U_1^{(n)} &= - (2m/\hbar^2) \beta D \int_{-\infty}^{\infty} f_n^*(z) e^{-2\kappa u} f_n(z) dz \\ &= - (2m/\hbar^2) \beta D (d - n - \frac{1}{2})/d. \end{aligned} \quad (16)$$

We now consider the part of the solution in  $x$  and  $y$ . If in equation (11) we put

$$\begin{aligned} ax = \theta, \quad \frac{2U_1^{(n)}}{a^2} &= - \left( \frac{4m}{a^2 \hbar^2} \right) \beta D (d - n - \frac{1}{2})/d = - 4q^{(n)}, \\ 2mE^{(n)}/a^2 \hbar^2 &= \alpha^{(n)}, \quad \theta = \pi - \phi, \end{aligned} \quad (17)$$

we obtain the well-known Mathieu equation

$$\left\{ \frac{\partial^2}{\partial \phi^2} + \alpha^{(n)} - 4q^{(n)} \cos \phi \right\} g^{(n)}(\phi) = 0 \quad (18)$$

The most general solution of this equation which is everywhere finite is given by‡

$$g_l^{(n)}(\xi, \phi) = \exp(i\xi\phi) G_l^{(n)}(\xi, \phi), \quad (19)$$

where  $G_l^{(n)}(\xi, \phi)$  has period  $2\pi$  in  $\phi$ , and  $\xi$  takes values between  $\frac{1}{2}$  and  $-\frac{1}{2}$ , while  $l$  is a quantum number which takes the values 0, 1, 2, ... The characteristic values of  $\alpha^{(n)}$  lie in a set of bands, each band having a definite value of  $l$  and each level in a band a definite value of  $\xi$ . We shall label the levels in such a way that  $\xi = 0$  at the bottom of each band. For each finite value of  $\xi$ , the wave functions  $g(\xi, \phi)$  and  $g(-\xi, \phi)$  are degenerate, but the end points  $\xi = \pm \frac{1}{2}$  are equivalent, and there is only one wave function and it is real. The energy bands can be represented on a cylinder, as Jones and Zener have shown,§ energies being measured parallel to the axis, while  $\xi$  is a cyclic coordinate whose variation through the range  $-\frac{1}{2}$  to  $\frac{1}{2}$  for a given  $l$  provides a closed curve on the cylindrical surface. The real wave functions at the ends of the bands have periods of either  $2\pi$  or  $4\pi$ , the top of one band having the same periodicity as the bottom of the next.

† Lennard-Jones and Strachan, *loc. cit.*, the actual matrix there worked out is that of  $(e^{-2\kappa u} - e^{-\kappa u})$  but the work can easily be used to give the required result.

‡ Floquet, cf. Whittaker and Watson, "Modern Analysis," p. 412 (1920).

§ Jones and Zener, 'Proc. Roy. Soc., A', vol. 144, p. 106 (1934).

For small values of  $q$  a method of determining  $\alpha_i(\xi)$  as a power series in  $q$  for the cases  $\xi = 0$  and  $\xi = \pm \frac{1}{2}$  has been used by Lennard-Jones and Pike,<sup>†</sup> following a suggestion made by Whittaker and Watson.<sup>‡</sup> This can be extended to other values of  $\xi$  and results in the equations

$$\alpha_i(\xi) = (\frac{1}{2}l + |\xi|)^2 + \frac{8q^2}{4(\frac{1}{2}l + |\xi|)^2 - 1} + O(q^4), \quad (20)$$

which is valid provided  $\frac{1}{2}l + |\xi|$  is not approximately  $\frac{1}{2}$  or 1. For values of  $\frac{1}{2}l + |\xi|$  equal to  $\frac{1}{2}$  or 1, corresponding to the top or bottom of a band, the same method gives the formulae

$$\left\{ \begin{aligned} \alpha_0(0) &= -8q^2 + O(q^4), \\ \alpha_0(\frac{1}{2}) &= \frac{1}{4} - 2q - 2q^2 + 2q^3 + O(q^4), \end{aligned} \right\} \quad (21)$$

$$\left\{ \begin{aligned} \alpha_1(0) &= \frac{1}{4} + 2q - 2q^2 - 2q^3 + O(q^4), \\ \alpha_1(\frac{1}{2}) &= 1 - \frac{1}{4}q^2 + O(q^4), \\ \alpha_2(0) &= 1 + \frac{1}{4}q^2 + O(q^4), \end{aligned} \right\} \quad (22)$$

the bracketed pairs belonging to the same band. A formula for the energy gap between bands has been given by Lennard-Jones and Pike,<sup>||</sup> giving  $4q, 8q^2, \dots$  in agreement with the above values.

The wave functions corresponding to the energy level given in (20) are,<sup>¶</sup> putting  $m = \frac{1}{2}l + |\xi|$ ,

$$\begin{aligned} g_i(\xi) &= \exp(\pm im\phi) \\ &+ \exp(\pm i\overline{m-1}\phi) \left\{ \frac{2q}{2m-1} + \frac{q^2}{(m-1)(2m-1)^2} + O(q^3) \right\} \\ &+ \exp(\pm i\overline{m+1}\phi) \left\{ -\frac{2q}{2m+1} - \frac{q^2}{(m+1)(2m+1)^2} + O(q^3) \right\} \\ &+ \exp(\pm i\overline{m-2}\phi) \left\{ \frac{q^2}{(m-1)(2m-1)} + O(q^3) \right\} \\ &+ \exp(\pm i\overline{m+2}\phi) \left\{ \frac{q^2}{(m+1)(2m+1)} + O(q^3) \right\} + \dots \end{aligned} \quad (23)$$

<sup>†</sup> 'Trans. Faraday Soc.', vol. 30, p. 830 (1934).

<sup>‡</sup> "Modern Analysis," p. 420 (1920).

<sup>§</sup> Cf. Lennard-Jones and Pike, 'Trans. Faraday Soc.', vol. 30, p. 830, equation (14) (1934).

<sup>||</sup> *Loc. cit.*, equation (16).

<sup>¶</sup> *Ibid.*, equation (15).

while the wave equations corresponding to the ends of the bands given in (22) are

$$\left. \begin{aligned} g_0(0) &= A \{1 - 4q(1 - 8q^2) \cos \phi + 2q^2 \cos 2\phi + \dots\} \\ g_0(\tfrac{1}{2}) &= \sin \phi/2 - \{q(1 - q - 2q^2/3)\} \sin 3\phi/2 \\ &\quad + \{q^2(1 - q)/3\} \sin 5\phi/2 - \dots \\ g_1(0) &= \cos \phi/2 - q(1 + q - 2q^2/3) \cos 3\phi/2 \\ &\quad + \{q^2(1 + q)/3\} \cos 5\phi/2 - \dots \\ g_1(\tfrac{1}{2}) &= \sin \phi - (2q/3 - 43q^2/27) \sin 2\phi + (q^2/6) \sin 3\phi - \dots \\ g_2(0) &= \cos \phi + 2q(1 - 20q^2/3) - (2q/3 + 43q^2/27) \cos 2\phi \\ &\quad + (q^2/6) \cos 3\phi - \dots \end{aligned} \right\} \quad (24)$$

The wave functions and energy values near the extremities of the bands, that is for very small values of  $\xi$ , can be found by writing

$$g_i(\xi) = \exp(i\xi\phi) G_i(\xi), \quad (25)$$

and supposing that  $G_i(\xi)$  can be expressed as a linear function of the real functions which belong to the extremity of the band and the one nearest to it. Thus writing

$$G_i(\xi) = aG_i(0) + bG_{i-1}(\tfrac{1}{2}), \quad (26)$$

substituting in equation (18) and treating the terms in  $\xi$  and  $\xi^2$  as perturbations, we deduce the secular equation for  $\alpha$

$$\begin{vmatrix} \alpha - \alpha_i(0) - \xi^2 & i\xi \\ -i\xi & \alpha - \alpha_{i-1}(\tfrac{1}{2}) - \xi^2 \end{vmatrix} = 0, \quad (27)$$

giving for sufficiently small values of  $\xi$

$$\alpha = \alpha_i(0) + \frac{i^2 \xi^2}{\alpha_i(0) - \alpha_{i-1}(\tfrac{1}{2})}, \quad \alpha = \alpha_{i-1}(\tfrac{1}{2}) - \frac{i^2 \xi^2}{\alpha_i(0) - \alpha_{i-1}(\tfrac{1}{2})} \quad (28)$$

These formulae combined with (21) and (22) suffice to give  $\alpha$  as a function of  $\xi$  near the end of a band.

For these two levels we find

$$\frac{b}{a} = \frac{i\xi}{\alpha_i(0) - \alpha_{i-1}(\tfrac{1}{2})}, \quad \frac{b}{a} = \frac{\alpha_i(0) - \alpha_{i-1}(\tfrac{1}{2})}{i\xi}, \quad (29)$$

respectively, thus determining the wave functions.

## 3—THE LATERAL MIGRATION OF ADSORBED HELIUM ATOMS

The velocity corresponding to any solution of the part of the wave equation in  $x$  or of  $y$  is given by†

$$v_1(\xi) = \frac{1}{a\hbar} \frac{\partial}{\partial \xi} E_1(\xi) = \frac{a\hbar}{2m} \frac{\partial}{\partial \xi} \alpha_1(\xi), \quad (30)$$

so that the velocity can readily be inferred for any adsorbed state from the formulae given in the preceding paragraph. The average velocity for all the states in a band is given by

$$\begin{aligned} \bar{v}_1 &= 2 \int_0^l v_1(\xi) d\xi = \frac{a\hbar}{2m} 2 \int_0^l \frac{\partial}{\partial \xi} \alpha_1(\xi) d\xi \\ &= \frac{a\hbar}{m} \{ \alpha_1(\frac{1}{2}) - \alpha_1(0) \}, \end{aligned} \quad (31)$$

and is thus proportional to the width of the band. Values of  $\alpha_1(0)$  and  $\alpha_1(\frac{1}{2})$  have been tabulated over a fairly wide range of values for  $q$  for small values of  $l$ ‡

For the field between helium atoms and the (100) surface of LiF we find, as explained in § 1, a value for  $D$  of 175 cal. per gram atom and a value for  $\kappa$  of  $(1/10) 10^8 \text{ cm}^{-1}$ , whence  $d = 3.5$ . The value of  $\beta$  which we have chosen to give fig. 1, drawn after the pattern of the fields of neon near NaF and argon near KCl,§ is 0.038, and from equation (17) we then find that  $q$  is equal to 0.05. This is sufficiently small to render the formulae of the preceding section applicable.

The velocity parallel to the  $x$  axis corresponding to states near the bottom of the lowest band can be inferred from equation (30), using equation (20) and putting  $l = 0$ , and proves to be  $(0.92)(a\hbar\xi/m)$ . If  $q$  were zero the velocity would be  $a\hbar\xi/m$  and so the effect of the periodic field is to increase the apparent mass of the atom by 8%—otherwise the atom moves freely as though there were no field in  $x$  or  $y$ . Migration therefore occurs even for the lowest energies. According to classical mechanics, on the other hand, the same particle in the same field could not migrate until its energy were sufficient to surmount the potential col at  $x = a\pi$ , that is  $E > 2\beta D(d - n - \frac{1}{2})/d$ , which for the numerical values used here means that  $E$  must correspond to a temperature  $(\frac{1}{2}kT)$  of

† Jones and Zener, *loc. cit.*

‡ Ince, 'Proc. Roy. Soc. Edinburgh,' vol. 46, pp. 20, 316 (1925), Goldstein, 'Proc. Camb. Phil. Soc.,' vol. 23, p. 303 (1927).

§ Lennard-Jones, 'Trans. Faraday Soc.,' vol. 38, p. 333 (1932).

11 5° K The *average* velocity parallel to the  $x$  axis in the first band is 0.66 times its value for  $q = 0$

In fig 2 the positions of the bands for  $q = 0.05$  for motion in the  $x$  direction are plotted against a background showing the form of the potential field. The lowest band is below the height of the potential barrier so that atoms with these energies moving "classically" would continue to vibrate about a fixed point.

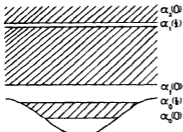


FIG 2—The energy bands for motion parallel to the  $x$ -axis

The energy and velocity is plotted as a function of  $\frac{1}{2}l + \xi$  in fig 3, the dotted lines being the corresponding values for  $q = 0$ .

When the results expressed in fig. 3 are combined with the similar ones for a perpendicular direction, it is found that a particle tends to travel in certain favoured directions according to its total energy. This is shown in figs 4 (a), 4 (b), 4 (c), and 4 (d), where for one quadrant the velocity

is plotted as a vector, the end points of those vectors which correspond to states of equal energy being joined in a series of contours. These contours for small energies near the bottom of a band are nearly circular, but for higher energies they become more like a square with rounded

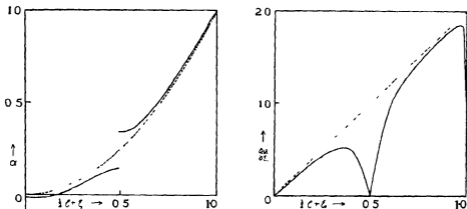


FIG 3—The energy and velocity corresponding to various states within the energy bands

corners (as in (a)), then this pattern becomes indented at the mid-points and finally assumes the shape of four loops meeting at the origin (as in (b)); the pattern then changes to a quasi-square with loops at the corners, and eventually to a square-like configuration and finally to circles again.

The conclusion which we draw from these results is that the periodic field of a surface does not prevent the migration of helium atoms even at the lowest temperatures. When the concentration of adsorbed atoms is large† their mutual interaction must be taken into account, and atoms

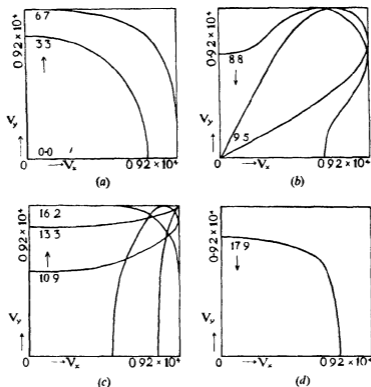


FIG. 4—Velocity curves for states of equal energy, for the lowest band in the plane ( $v_x, v_y$ ). Energies are in cal/mole, and are measured from the bottom of the band, velocities are measured in cm/sec.

must be allotted to the various energy states according to the Bose-Einstein Statistics. But seeing that three-dimensional arrays of helium atoms are liquid at very low temperatures, it seems reasonable to infer

† Using the formula (24) of Paper III, Lennard-Jones and Devonshire, *loc cit*, and the energy levels of  $-57.5$  cal and  $-129$  cal, we calculate the following pressures ( $P$  in atmospheres) at which the surface is half covered at various temperatures —

T	6	8	10	12	14	16	18	20
P	(5.6) $10^{-4}$	(1.2) $10^{-3}$	9 $10^{-3}$	0.34	0.90	1.90	3.46	5.61

The fraction of surface covered at other pressures can easily be deduced from the equation  $\theta = ap/(1 + ap) = p/(p + P)$

that two-dimensional films would have similar properties. In that case an adsorbed film of helium atoms should remain mobile even at very low temperatures. It would be interesting if this property could be demonstrated experimentally. If the rate of diffusion of adsorbed helium along a surface could be measured accurately, it could be used to determine the apparent mass of helium atoms and from this result information could be derived as to the energy bands in the surface field.

#### SUMMARY

The energy levels of adsorbed helium atoms for motion perpendicular to a surface of a lithium fluoride crystal, deduced in a previous paper from the diffraction experiments of Frisch and Stern, are used to construct a map of the potential field between gas atom and solid. Calculations are then made of the lateral velocity of migration of helium atoms in this field. Whereas according to classical mechanics helium atoms would remain vibrating about a mean position at very low temperatures, according to quantum mechanics the atoms can migrate along the surface, however low the temperature. There is an apparent increase of mass of about 8% but otherwise the atoms move as though the lateral potential barriers did not exist.

---

# The Interaction of Atoms and Molecules with Solid Surfaces

## VII—The Diffraction of Atoms by a Surface

By J. E. LENNARD-JONES, F.R.S., and A. F. DEVONSHIRE, The University  
Chemical Laboratory, Cambridge

(Received 8 August, 1936)

### 1—INTRODUCTION

In the hands of Stern and his collaborators, an accurate technique has been evolved for the measurement of the intensities of reflected and diffracted beams of atoms from the surfaces of crystals, but surprisingly little use has been made of these results to deduce information of theoretical interest except to verify the validity of the de Broglie relation for atomic beams †. In this paper we attempt a theory of the diffraction of atoms at surfaces with a view to finding explicit formulae for the intensities of diffracted beams in terms of the constants of the surface field in order that a comparison of the theory and experiment might yield information as to the magnitudes of these constants. A precise knowledge of surface fields would be of value in that it would make possible a calculation of other properties of atoms on surfaces, such as the adsorption and migration of adsorbed atoms, as has already been done in the preceding paper (Part VI) for helium on lithium fluoride. ‡

### 2—THE INTENSITY OF DIFFRACTED BEAMS

Formulae have already been given in general terms in Paper V † for the intensities of diffracted beams. In this paper we evaluate these formulae for a definite type of surface field. We find that surface fields over a square lattice can be represented satisfactorily by the function

$$V(x, y, z) = D \{ e^{-2\kappa(x-b)} - 2e^{-\kappa(x-b)} \} + 2\beta D e^{-2\kappa(x-b)} \{ \cos ax + \cos ay \} \quad (1)$$

where the meaning of the symbols has been explained in preceding papers. Perpendicular to the surface, the potential has then the form of a Morse function, but the depth and position of the minimum varies from point

† Cf., however, Paper V, Devonshire, 'Proc. Roy. Soc.,' A, vol. 156, p. 37 (1936).

‡ P. 242

to point of the surface in a periodic manner. A contour map of a field of this type has been plotted in Paper VI, and has the right kind of properties, having a close similarity to contour maps calculated directly from interatomic fields.† In fields due to van der Waals forces the second term of equation (1) is smaller than the first term (of the order of a fifth), and we accordingly treat it as a perturbation of solutions of the wave equation which involve the first term alone. This method has been justified by its success with helium on lithium fluoride, as shown in Paper V.

The solutions of the equation

$$\left\{ \frac{\hbar^2}{2m} \frac{\partial^2}{\partial z^2} + E - D(e^{-2\kappa(z-b)} - 2e^{-\kappa(z-b)}) \right\} \psi = 0 \quad (2)$$

are known and, using the notation of Paper V and putting

$$u = z - b, \quad d = (2mD)^{1/2}/\kappa\hbar, \quad (3)$$

we have for the solutions corresponding to discrete energy values‡

$$E_n = -\kappa^2 \hbar^2 (d - n - \frac{1}{2})^2 / 2m, \quad (4)$$

$$f_n(z) = N_n^{-1} \exp(-de^{-\kappa u}) (2de^{-\kappa u})^{d-n-1/2} L_{2d-2n-1}^{2d-2n-1}(2de^{-\kappa u}), \quad (5A)$$

where

$$N_n^2 = \frac{\{\Gamma(2d-n)\}^2}{\kappa(2d-2n-1)n!}, \quad (5B)$$

and  $L_{2d-2n-1}^{2d-2n-1}(x)$  is the generalized Laguerre polynomial. The solutions corresponding to continuous energy values are given by§

$$f(k_3, z) = N(k_3) (2de^{-\kappa u})^{-1/2} W_{d, \mu}(2de^{-\kappa u}), \quad (6A)$$

where

$$\mu = (2mE)^{1/2}/\kappa\hbar = k_3/\kappa \quad (6B)$$

$$N^*(k_3) N(k_3) = \frac{\Gamma(\frac{1}{2} - i\mu - d) \Gamma(\frac{1}{2} + i\mu - d)}{\Gamma(2i\mu) \Gamma(-2i\mu)}, \quad (6C)$$

and  $W_{d, \mu}(x)$  is the confluent hypergeometric function.||

With this normalization  $f(k_3, z)$  has the asymptotic form of

$$2 \cos(\mu\kappa u + \alpha),$$

or of  $2 \cos(k_3\mu + \alpha)$ , implying incident and reflected waves of unit amplitude

† Lennard-Jones, 'Trans. Faraday Soc.', vol. 38, p. 333 (1932)

‡ Lennard-Jones and Strachan, 'Proc. Roy. Soc., A', vol. 150, p. 442 (1935).

§ Strachan, 'Proc. Roy. Soc., A', vol. 150, p. 456 (1935)

|| Whittaker and Watson, "Modern Analysis" (1920), chap. 16.

When a beam incident on a crystal surface has unit amplitude and is represented by a wave function

$$\psi_0 = \exp \{i(k_1 x + k_2 y)\} f(k_3, z), \quad (7)$$

the formulae given in Paper V show that to the first order of approximation one of the diffracted beams is given by

$$\psi_1 = \alpha(k'_3, k_3) \exp \{i(k_1 + a)x + ik_2 y + ik'_3 z\}, \quad (8)$$

where

$$\alpha(k'_3, k_3) = \frac{1}{2k'_3} \int_{-\infty}^{\infty} f(k'_3, z) U_1(z) f(k_3, z) dz \quad (9A)$$

$$= \frac{1}{2k'_3} (k'_3 | U_1 | k_3), \quad (9B)$$

and

$$(k'_3)^2 = k_3^2 - 2ak_1 - a^2 \quad (10)$$

For the field given by (1) we have

$$\frac{\hbar^2}{2m} U_1(z) = \beta D e^{-\beta z} \quad (11)$$

The ratio of the intensity of the diffracted beam to the incident one is then

$$\begin{aligned} R &= \frac{k'_3}{k_3} |\alpha(k'_3, k_3)|^2 = \frac{1}{4k_3 k'_3} |(k'_3 | U_1 | k_3)|^2 \\ &= \frac{\beta^2 D^2 (2m)^2}{4k_3 k'_3 \hbar^4} \frac{|\Gamma(\frac{1}{2} + i\mu - d)|^2}{|\Gamma(2i\mu)|^2} \frac{|\Gamma(\frac{1}{2} + i\mu' - d)|^2}{|\Gamma(2i\mu')|^2} I^2 \\ &= \frac{\beta^2 \kappa^2 d^4}{4\mu\mu'} \frac{|\Gamma(\frac{1}{2} + i\mu - d)|^2}{|\Gamma(2i\mu)|^2} \frac{|\Gamma(\frac{1}{2} + i\mu' - d)|^2}{|\Gamma(2i\mu')|^2} I^2, \end{aligned} \quad (12)$$

where  $I$  is defined by the integral

$$I = \frac{1}{4d^2 \kappa} \int_0^\infty W_{d, i\mu}(\eta) W_{d, -i\mu}(\eta) d\eta, \quad (13)$$

and  $\eta = 2d \exp(-\kappa u)$

The integral  $I$  is evaluated in the next section and is found to be (equation (28))

$$\begin{aligned} I &= \frac{\pi^2}{2d^2 \kappa (\cosh 2\mu\pi - \cosh 2\mu'\pi)} \\ &\quad \times \left\{ \frac{\mu^2 - \mu'^2 + 2d}{|\Gamma(\frac{1}{2} + i\mu - d)|^2} + \frac{\mu^2 - \mu'^2 - 2d}{|\Gamma(\frac{1}{2} + i\mu' - d)|^2} \right\}, \end{aligned} \quad (14)$$

and we then find, using the relation

$$|\Gamma(2i\mu)|^2 = \pi/2 \mu \sinh 2\mu\pi,$$

that

$$R = \frac{\beta^2 \pi^2}{4} \frac{\sinh 2\mu\pi \sinh 2\mu'\pi}{(\cosh 2\mu\pi - \cosh 2\mu'\pi)^2} \\ \times \frac{\{(\mu^2 - \mu'^2 + 2d) |\Gamma(-d + i\mu' + \frac{1}{2})|^2 + (\mu^2 - \mu'^2 - 2d) |\Gamma(-d + i\mu + \frac{1}{2})|^2\}}{|\Gamma(-d + i\mu' + \frac{1}{2})|^2 |\Gamma(-d + i\mu + \frac{1}{2})|^2}.$$

This formula gives  $R$  in terms of the constants of the field, viz.,  $d$ ,  $\kappa$ , and  $\beta$  ( $d$  being defined in equation (3)) and the component of velocity of the incident beam perpendicular to the surface (by equation (6b)), that of the diffracted beam being then determined by the relation (10); we have, in fact, from (10) and (6b),

$$(\mu')^2 = \mu^2 - (2a\mu_x/\kappa) - a^2/\kappa^2, \quad (16)$$

where  $\mu_x = k_1/\kappa$ . Using the abbreviations

$$A_\mu = |\Gamma(-d + i\mu + \frac{1}{2})|^2, \quad A_{\mu'} = |\Gamma(-d + i\mu' + \frac{1}{2})|^2, \quad a_0 = a/\kappa,$$

and using (16), we can write for  $R$

$$R = \frac{\beta^2 \pi^2}{4} \frac{\sinh 2\mu\pi \sinh 2\mu'\pi}{(\cosh 2\mu\pi - \cosh 2\mu'\pi)^2} \frac{A_{\mu'}}{A_\mu} \\ \times \left\{ (2a_0\mu_x + a_0^2) \left( 1 + \frac{A_\mu}{A_{\mu'}} \right) + 2d \left( 1 - \frac{A_\mu}{A_{\mu'}} \right) \right\}^2 \quad (17)$$

The numerical values of  $A_\mu$  and  $A_{\mu'}$  can be obtained from the formulae given by Jahnke and Emde† on writing  $A_\mu$  in the equivalent form

$$A_\mu = 2\pi^2 / \{ (\cosh 2\mu\pi - \cos 2\mu_0\pi) |\Gamma(d + \frac{1}{2} + i\mu)|^2 \},$$

where  $\mu_0 = d - \frac{1}{2}$ . For large values of  $d$  the asymptotic formula

$$|\Gamma(d + \frac{1}{2} + i\mu)|^2 = 2\pi e^{-(2d+1)} \{ \mu^2 + (d + \frac{1}{2})^2 \}^d e^{-2\mu \tan^{-1} \{ \mu/(d + \frac{1}{2}) \}} \\ \left[ 1 + \frac{2d+1}{12 \{ (d + \frac{1}{2})^2 + \mu^2 \}} + O\left(\frac{1}{d^3}\right) \right],$$

can be used; in fact, this is surprisingly accurate even for values of  $d$  as

† 'Tables of Functions,' Teubner (1933).

small as 2 or 3. The following values of  $A_\mu$ , worked out for  $d = 3.5$ , give some indication of its variation with  $\mu$  —

$\mu$	0.5	1.0	1.5	2.0
$A_\mu$	$6.20 \times 10^{-2}$	$2.73 \times 10^{-2}$	$1.65 \times 10^{-2}$	$1.13 \times 10^{-2}$
$\mu$	2.5	3.0	4.0	
$A_\mu$	$8.59 \times 10^{-7}$	$7.18 \times 10^{-8}$	$6.43 \times 10^{-10}$	

### 3—EVALUATION OF THE INTEGRAL I

To evaluate the integral I defined in (13), we express  $W_{d,\mu}(\eta)$  as a Barnes integral, viz †

$$W_{d,\mu}(\eta) = \frac{e^{-\eta/2} \eta^d}{2\pi i} \int_{-\infty}^{\infty} \frac{\Gamma(s) |\Gamma(-s-d+i\mu+\frac{1}{2})|^2}{|\Gamma(\frac{1}{2}+i\mu-d)|^2} \eta^s ds$$

The contour of integration has to be chosen in such a way that the poles of  $\Gamma(s)$  lie to the left and those of

$$\Gamma(-s-d+i\mu+\frac{1}{2}) \Gamma(-s-d-i\mu+\frac{1}{2})$$

lie to the right

Now ‡

$$\int_0^\infty e^{-\eta} \eta^{l-1} W_{d,\mu}(\eta) d\eta = \frac{\Gamma(l+i\mu+\frac{1}{2}) \Gamma(l-i\mu+\frac{1}{2})}{\Gamma(l-d+1)}, \quad (18)$$

provided that

$$R(l \pm i\mu + \frac{1}{2}) > 0$$

Changing the order of integration in I after substituting for  $W_{d,\mu}(\eta)$  as a contour integral and using formula (17), which is permissible since the path of integration over  $s$  can be chosen so that the condition (18) is satisfied, we have

$$\begin{aligned} I &= \frac{1}{4d^2\kappa} \frac{1}{2\pi i} \int_{-\infty-i}^{\infty-i} \frac{\Gamma(s+d+i\mu'+\frac{1}{2}) \Gamma(s+d-i\mu'+\frac{1}{2}) \Gamma(-s-d+i\mu+\frac{1}{2}) \Gamma(-s-d-i\mu+\frac{1}{2})}{s(s+1) \Gamma(-d+i\mu+\frac{1}{2}) \Gamma(-d-i\mu+\frac{1}{2})} ds \\ &= \frac{1}{4d^2\kappa} \frac{1}{2\pi i} \int_{-\infty-i}^{\infty-i} \left\{ \frac{\Gamma(s+d+i\mu'+\frac{1}{2}) \Gamma(s+d-i\mu'+\frac{1}{2}) \Gamma(-s-d+i\mu+\frac{1}{2}) \Gamma(-s-d-i\mu+\frac{1}{2})}{\Gamma(-d+i\mu+\frac{1}{2}) \Gamma(-d-i\mu+\frac{1}{2})} \right\} \\ &\quad \times \left\{ 1 + \frac{\mu'^2 + (d+\frac{1}{2})^2}{s} - \frac{\mu'^2 + (d-\frac{1}{2})^2}{s+1} \right\} ds. \quad (19) \end{aligned}$$

† Whittaker and Watson, "Modern Analysis," p. 343 (1920).

‡ Lennard-Jones and Devonshire, Paper III, § 4

Now†

$$\begin{aligned} \frac{1}{2\pi i} \int_{-\infty i}^{\infty i} \Gamma(s+d+i\mu'+\tfrac{1}{2}) \Gamma(s+d-i\mu'+\tfrac{1}{2}) \Gamma(-s-d+i\mu+\tfrac{1}{2}) \\ \times \Gamma(-s-d-i\mu+\tfrac{1}{2}) ds \\ = \Gamma(1+i\mu+i\mu') \Gamma(1+i\mu-i\mu') \Gamma(1-i\mu+i\mu') \\ \times \Gamma(1-i\mu-i\mu'), \quad (20) \end{aligned}$$

and

$$\begin{aligned} J &= \frac{1}{2\pi i} \int_{-\infty i}^{\infty i} s^{-1} \Gamma(s+d+i\mu'+\tfrac{1}{2}) \Gamma(s+d-i\mu'+\tfrac{1}{2}) \\ &\quad \times \Gamma(-s-d+i\mu+\tfrac{1}{2}) \Gamma(-s-d-i\mu+\tfrac{1}{2}) ds \\ &= \Gamma(1+i\mu+i\mu') \Gamma(1-i\mu-i\mu') \\ &\quad \times \frac{1}{2\pi i} \int_{-\infty i}^{\infty i} s^{-1} \mathbf{B}(s+d+i\mu'+\tfrac{1}{2}, -s-d+i\mu+\tfrac{1}{2}) \\ &\quad \times \mathbf{B}(s+d-i\mu'+\tfrac{1}{2}, -s-d-i\mu+\tfrac{1}{2}) ds \\ &= \Gamma(1+i\mu+i\mu') \Gamma(1-i\mu-i\mu') \\ &\quad \times \frac{1}{2\pi i} \int_{-\infty i}^{\infty i} s^{-1} \int_0^1 \int_0^1 u^{s+d+i\mu'-\frac{1}{2}} (1-u)^{-s-d+i\mu-\frac{1}{2}} \\ &\quad \times v^{s+d-i\mu'-\frac{1}{2}} (1-v)^{-s-d-i\mu-\frac{1}{2}} du dv \quad (21) \end{aligned}$$

The factor in the integrand involving  $s$  is

$$s^{-1} (uv)^s \{(1-u)(1-v)\}^{-s},$$

which has a pole at  $s=0$ , to the left of the path of  $s$ . The integral with respect to  $s$  of this factor, taken round a semicircle of radius  $R$  to the left of the imaginary axis,  $\rightarrow 0$  as  $R \rightarrow \infty$  if  $uv/(1-u)(1-v) > 1$ , and the corresponding integral to the right of the imaginary axis  $\rightarrow 0$  as  $R \rightarrow \infty$  if  $uv/(1-u)(1-v) < 1$ . Hence

$$\frac{1}{2\pi i} \int_{-\infty i}^{\infty i} \frac{1}{s} \left\{ \frac{uv}{(1-u)(1-v)} \right\}^s ds = \begin{cases} 0, & \text{if } u+v < 1 \\ 1, & \text{if } u+v > 1 \end{cases}$$

If we change the order of integration in equation (21) and integrate with respect to  $s$ , we deduce that

$$\begin{aligned} J &= \Gamma(1+i\mu+i\mu') \Gamma(1-i\mu-i\mu') \iint u^{d+i\mu'-\frac{1}{2}} (1-u)^{-d+i\mu-\frac{1}{2}} \\ &\quad \times v^{d-i\mu'-\frac{1}{2}} (1-v)^{-d-i\mu-\frac{1}{2}} du dv, \quad (22) \end{aligned}$$

† "Modern Analysis" (1920), par. 14.52.

where the double integral is over the range

$$0 < u < 1, \quad 0 < v < 1, \quad u + v > 1,$$

and hence, putting  $u = 1 - z$ , we have

$$J = \Gamma(1 + i\mu + i\mu') \Gamma(1 - i\mu - i\mu') \int_0^1 v^{d-i\mu'-i} (1-v)^{-d-i\mu-i} \\ \times \int_0^v (1-z)^{d+i\mu'-i} z^{-d+i\mu-i} dv dz. \quad (23)$$

Now

$$(1-z)^{d+i\mu-i} = \sum_{n=0}^{\infty} \frac{z^n}{n!} \frac{\Gamma(-d-i\mu'+\frac{1}{2}+n)}{\Gamma(-d-i\mu'+\frac{1}{2})},$$

and therefore

$$J = \Gamma(1+i\mu+i\mu') \Gamma(1-i\mu-i\mu') \\ \times \left[ \sum_{n=0}^{\infty} \frac{\Gamma(-d-i\mu'+\frac{1}{2}+n)}{n! \Gamma(-d-i\mu'+\frac{1}{2})} \frac{1}{(n-d+i\mu+\frac{1}{2})} \int_0^1 v^{n+i\mu-i\mu'} (1-v)^{-d-i\mu-i} dv \right] \\ = \Gamma(1+i\mu+i\mu') \Gamma(1-i\mu-i\mu') \frac{\Gamma(-d-i\mu+\frac{1}{2})}{\Gamma(-d-i\mu'+\frac{1}{2})} \\ \times \left[ \sum_{n=0}^{\infty} \frac{\Gamma(-d-i\mu'+\frac{1}{2}+n)}{\Gamma(-d-i\mu'+\frac{1}{2}+n) n! (n-d+i\mu+\frac{1}{2})} \right] \\ = \Gamma(1+i\mu+i\mu') \Gamma(1-i\mu-i\mu') \frac{\Gamma(-d-i\mu+\frac{1}{2})}{\Gamma(-d-i\mu'+\frac{1}{2})} \frac{1}{i(\mu+\mu')} \\ \times \left[ \sum_{n=0}^{\infty} \frac{\Gamma(n+1+i\mu-i\mu')}{n!} \left( \frac{1}{n-d-i\mu'+\frac{1}{2}} - \frac{1}{n-d+i\mu+\frac{1}{2}} \right) \right] \\ = \Gamma(1+i\mu+i\mu') \Gamma(1-i\mu-i\mu') \frac{\Gamma(-d-i\mu+\frac{1}{2})}{\Gamma(-d-i\mu'+\frac{1}{2})} \frac{1}{i(\mu+\mu')} \\ \times \left[ \Gamma(1+i\mu-i\mu') \Gamma(i\mu'-i\mu) \left\{ \frac{\Gamma(-d-i\mu'+\frac{1}{2})}{\Gamma(-d-i\mu+\frac{1}{2})} - \frac{\Gamma(-d+i\mu+\frac{1}{2})}{\Gamma(-d+i\mu'+\frac{1}{2})} \right\} \right], \quad (24)$$

using the formula†.

$$\sum_{n=0}^{\infty} \frac{\Gamma(a+n) \Gamma(b+n)}{n! \Gamma(c+n)} = \frac{\Gamma(a) \Gamma(b) \Gamma(c-a-b)}{\Gamma(c-a) \Gamma(c-b)}, \quad (25)$$

for the case  $c = b + 1$ . It can easily be shown that this formula can be

† "Modern Analysis" (1920), p. 282.

used, as in equation (24), to give the difference of two divergent hypergeometric series, provided that difference is convergent. Hence

$$J = \Gamma(1 + i\mu + i\mu') \Gamma(1 - i\mu - i\mu') \Gamma(1 + i\mu' - i\mu) \Gamma(1 + i\mu - i\mu') \\ \times \left\{ 1 - \frac{\Gamma(-d + i\mu + \frac{1}{2}) \Gamma(-d - i\mu + \frac{1}{2})}{\Gamma(-d - i\mu' + \frac{1}{2}) \Gamma(-d + i\mu' + \frac{1}{2})} \right\} \frac{1}{\mu^2 - \mu'^2} \quad (26)$$

Similarly the last term in equation (19) can be integrated by putting  $s = s' - 1$ , the effect is similar to changing  $d$  to  $d - 1$  in  $J$ , so that we have

$$\frac{1}{2\pi i} \int_{-\infty}^{\infty} (s+1)^{-1} \Gamma(s + d + i\mu' + \frac{1}{2}) \Gamma(s + d - i\mu' + \frac{1}{2}) \\ \times \Gamma(-s - d + i\mu + \frac{1}{2}) \Gamma(-s - d - i\mu + \frac{1}{2}) ds \\ = \Gamma(1 + i\mu + i\mu') \Gamma(1 - i\mu - i\mu') \Gamma(1 + i\mu' - i\mu) \Gamma(1 + i\mu - i\mu') \\ \times \left\{ 1 - \frac{\Gamma(-d + i\mu + \frac{3}{2}) \Gamma(-d - i\mu + \frac{3}{2})}{\Gamma(-d - i\mu' + \frac{3}{2}) \Gamma(-d + i\mu' + \frac{3}{2})} \right\} \frac{1}{\mu^2 - \mu'^2} \quad (27)$$

From equations (19), (20), (26), and (27) we then deduce that

$$I = \Gamma(1 + i\mu + i\mu') \Gamma(1 - i\mu - i\mu') \Gamma(1 + i\mu' - i\mu) \Gamma(1 + i\mu - i\mu') \\ \times \frac{1}{\mu^2 - \mu'^2} \left\{ \frac{\mu^2 - \mu'^2 + 2d}{\Gamma(-d + i\mu + \frac{1}{2}) \Gamma(-d - i\mu + \frac{1}{2})} \right. \\ \left. - \frac{\mu'^2 - \mu^2 + 2d}{\Gamma(-d + i\mu' + \frac{1}{2}) \Gamma(-d - i\mu' + \frac{1}{2})} \right\} \frac{1}{4d^2\kappa} \\ = \frac{\pi^2}{2d^2\kappa (\cosh 2\mu\pi - \cosh 2\mu'\pi)} \left\{ \frac{\mu^2 - \mu'^2 + 2d}{\Gamma(-d + i\mu + \frac{1}{2}) \Gamma(-d - i\mu + \frac{1}{2})} \right. \\ \left. + \frac{\mu^2 - \mu'^2 - 2d}{\Gamma(-d + i\mu' + \frac{1}{2}) \Gamma(-d - i\mu' + \frac{1}{2})} \right\} \quad (28)$$

In the proof of equation (20) we have tacitly assumed that  $R(d) < \frac{1}{2}$ , since the convergence of some of the integrals involved, e.g., in (23) depends on this, but by the theory of analytic continuation the equation will hold throughout the domain in which both sides of the equation are analytic functions of  $d$ .

#### 4—THE PROBABILITY OF SELECTIVE ADSORPTION AND SELECTIVE EVAPORATION

Diffracted beams of the first order will in general only occur, provided that the component of velocity perpendicular to the surface is sufficiently large for  $k'_z$ , defined in equation (10), to be real and positive, but even

when  $k'_3$  is imaginary there are certain critical directions of approach for which diffraction occurs, the atoms subsequently sliding along the surface with an oscillatory motion perpendicular to the surface. This process has been referred to as *selective adsorption*<sup>†</sup> and has already been discussed in Paper V. It was there shown that the number of atoms which are captured into an oscillatory state of quantum number  $n$  per unit area per unit time for given values of  $k_1$  and  $k_2$  is

$$\frac{h}{4mk_3} |(n|U_1|k_3)|^2 g(k_3), \quad (29)$$

where

$$(n|U_1|k_3) = \int_{-\infty}^{\infty} f_n^*(z) U_1(z) f(k_3, z) dz, \quad (30)$$

and  $k_3$  corresponds to one of the critical directions of approach, defined by

$$k_3^2 = a^2 + 2ak_1 + 2mE_n/\hbar^2, \quad (31)$$

the energy levels  $E_n$  are, of course, negative when measured from the same zero as  $k_1$ ,  $k_2$ , and  $k_3$ .  $g(k)$  is defined in such a way that  $g(k_3) dk_3$  is the number of molecules in the range  $(k_3, k_3 + dk_3)$  per unit volume.

We now propose to examine the probability of this process in more detail by using the analytical expression for a surface field given by (1). We then have

$$(n|U_1|k_3) = \beta\kappa^2 d^2 \int_{-\infty}^{\infty} f_n^*(z) \exp\{-2\kappa(z-b)\} f(k_3, z) dz \quad (32)$$

This is an integral of the type already evaluated in Paper III (§4). In the notation there used

$$\frac{(n|U_1|k_3)}{\beta\kappa^2 d^2} = \frac{N(k_3)}{N_n} \frac{\Gamma(2d-n)}{n!} \frac{1}{4d^2\kappa} (J_{d+1} - n(2d-n-1)J_d),$$

where  $J_d$  is defined in equation (42) of that paper,  $N(k_3)$  and  $N_n$  are the appropriate normalization factors defined in equations (5b) and (6c) above, and hence it may be shown that

$$\begin{aligned} |(n|U_1|k_3)|^2 &= \frac{\pi\beta^2\kappa^3}{4} \frac{(2d-2n-1)}{n! \Gamma(2d-n)} \frac{\mu \sinh 2\mu\pi}{(\cosh 2\mu\pi - \cos 2\mu_0\pi)} \\ &\times \left\{ \mu^2 + (d-n-\frac{1}{2})^2 + 2d \right\}^2 \left| \Gamma\left(\frac{1}{2} + d + i\mu\right) \right|^2, \end{aligned} \quad (33)$$

where  $\mu_0 = d - \frac{1}{2}$

<sup>†</sup> Lennard-Jones and Devonshire, 'Nature,' vol. 137, p. 1069 (1936).

Using this formula, we can now evaluate the probability of selective adsorption per collision between a gas atom and the surface. From equation (29) we deduce that the number of atoms which are selectively adsorbed per unit area per unit time is given by

$$\Sigma_n (p/kT) (\hbar^3/2\pi mkT)^{\frac{1}{2}} \int_{-\infty}^{\infty} \int_{-\infty}^{\infty} (h/4mk_3) |(n|U_1|k_3)|^2 \times \exp [-(\hbar^2/2m)(k_1^2 + k_2^2 + k_3^2)/kT] dk_1 dk_2, \quad (34)$$

the integral over  $k_3$  having already been carried out in deriving (29). Not all collisions can be effective in the process. Only those in which  $k_1$  and  $k_2$  satisfy the relation (*cf* equation (10))

$$k_3^2 = a^2 + 2ak_1 + E_n(2m/\hbar^2), \quad (35A)$$

or

$$k_3^2 = a^2 + 2ak_2 + E_n(2m/\hbar^2), \quad (35B)$$

can result in selective adsorption. The first gives a tangentially diffracted beam with a change in  $k_1$  but none in  $k_2$ , the second a similar beam with a change in  $k_2$  but none in  $k_1$ . They might be referred to as the first order selectively adsorbed beams. Others of higher orders may occur due to other periodic terms in the potential  $V$  (equation (1)), but these will be less frequent, being proportional to the square of the amplitude of these periodic terms, and may be neglected, at any rate for the present. Since  $k_3$  must be positive, equation (35) defines a lower limit for  $k_1$  or for  $k_2$  for each vibrational level. For smaller values we must place  $(n|U_1|k_3)$  equal to zero. Taking the two processes (35A) and (35B) together, the expression (34) becomes

$$2\Sigma_n (p/kT) (\hbar^3/2\pi mkT)^{\frac{1}{2}} \int_{-\infty}^{\infty} (h/4mk_3) |(n|U_1|k_3)|^2 \times \exp [-(\hbar^2/2m)(k_1^2 + k_2^2)/kT] dk_1. \quad (36)$$

The total number of collisions with the surface per unit area per unit time is  $(p/kT)(kT/2\pi m)^{\frac{1}{2}}$ , and hence the probability of the process per collision is

$$c' = \frac{2\hbar^2}{kT(2\pi mkT)^{\frac{1}{2}}} L, \quad (37)$$

where

$$L = \Sigma_n \int_{-\infty}^{\infty} (h/4mk_3) |(n|U_1|k_3)|^2 \exp [-(\hbar^2/2m)(k_1^2 + k_2^2)/kT] dk_1. \quad (38)$$

We denote this quantity by  $c'$  because we have used  $c$  in Papers III and IV to denote the average probability of condensation on to a surface and it connotes another method of condensation. This expression is a sum

of curvilinear integrals, the path of integration for a particular value of  $n$  being along the parabola given by (35A). It is convenient to change the variable to  $\mu$  since it is proportional to  $k_3$  (equation 6B), and as  $(n|U_1|k_3)$  is finite for all positive values of  $\mu$ , the range of integration is from zero to infinity. We then have

$$dk_1/k_3 = \kappa d\mu/a,$$

so that substituting for  $(n|U_1|k_3)^2$  from equation (33), we get

$$c' = \frac{\hbar^3 \beta^2 \kappa^4}{16a (2\pi m k T)^{\frac{1}{2}}} \sum_n \frac{2d-2n-1}{n! \Gamma(2d-n)} \int_0^\infty \frac{\mu \sinh 2\mu\pi}{(\cosh 2\mu\pi - \cos 2\mu_0\pi)} \\ \times \{ \mu^2 + (d-n-\frac{1}{2})^2 + 2d^2 \} \Gamma(\frac{1}{2} + d + i\mu)^2 \\ \times \exp [(-\hbar^2/2m)(k_1^2 + k_3^2)/kT] d\mu \quad (39)$$

The exponential can easily be expressed in terms of  $\mu$  by means of the notation (35A), but the integral can only be evaluated by quadrature. Some numerical values are given in the last section.

It has also been shown in Paper V, equation (14), that the inverse process takes place and that the amplitude of the evaporated beam is

$$\alpha_n(k_3) = \frac{1}{2k_3} (n|U_1|k_3),$$

provided there is one adsorbed atom per unit area in the state defined by  $(k'_1, k'_3, n)$  such that its quantum numbers after evaporation are  $(k_1, k_3, k_3)$ . This means that the number leaving the surface by the diffraction mechanism for this concentration of adsorbed atoms is equal to

$$(\hbar/4mk_3) |(n|U_1|k_3)|^2, \quad (40)$$

where the matrix element is the same as that given by (33). This process might conveniently be called *selective evaporation*, seeing that adsorbed atoms must be in certain selected states before the phenomenon may occur.

The average rate of evaporation per adsorbed molecule is obtained from (34) by multiplying by the probability of the occurrence of a given state and integrating over all states, we must also take account of diffraction by both the main axes of the surface lattice.

The average rate of evaporation is thus found to be

$$\frac{2(\hbar^3/2\pi m k T)^{\frac{1}{2}} \int_{-\infty}^{\infty} \sum_n (\hbar/4mk_3) |(n|U_1|k_3)|^2 \exp [(-\hbar^2/2m)k'_1{}^2 - E_n]/kT] dk'_1}{\sum_n \exp(-E_n/kT)} \\ = \frac{2\hbar (L/2\pi)}{(2\pi m k T)^{\frac{1}{2}} \sum_n \exp(-E_n/kT)}, \quad (41)$$

using  $L$  for the integral defined in (38), and the identity

$$k_1^2 + k_2^2 = (k'_1)^2 + E_n (2m/\hbar^2),$$

and  $k'_1 = k_1 + a$

The average time which elapses before evaporation takes place by the diffraction mechanism, being defined as the reciprocal of this, is

$$\tau' = \frac{(2\pi mkT)^{\frac{1}{2}} \sum_n \exp(-E_n/kT)}{2\hbar (L/2\pi)} \quad (42)$$

From these formulae for  $c'$  and  $\tau'$  we see that

$$c' \tau' = (h/kT) \sum_n \exp(-E_n/kT) \quad (43)$$

This is the same relation as we found between  $c$  and  $\tau$  in Paper III for ordinary evaporation. It follows that equilibrium between the gas phase and the adsorbed phase will be set up by this mechanism and will be expressed by a Langmuir adsorption isotherm of the same form as that found previously. Thus the number of atoms condensing per unit area per second equated to the number evaporating, when a fraction  $\theta$  of the surface is covered, is expressed by

$$(1 - \theta) (p/kT) (kT/2\pi m)^{\frac{1}{2}} c' = (\theta n_s / \tau'),$$

$n_s$  being the number of adsorbed atoms per unit area when the surface may be regarded as completely covered. Using (43), this becomes

$$p = \frac{\theta}{1 - \theta} \frac{kT}{h} \frac{n_s (2\pi mkT)^{\frac{1}{2}}}{\sum_n \exp(-E_n/kT)}, \quad (44)$$

which is a detailed formula for the adsorption isotherm. It is identical with that given in Paper III, equation (24), for the case that adsorbed atoms migrate freely along a surface like a two-dimensional gas. Under these conditions equation (44) expresses statistical equilibrium whatever the form of the surface field, for the special field considered in this paper the values of the discrete energy levels are given by equation (4).

From the formula for  $\tau'$  we can derive an expression for the mean free path of a selectively adsorbed atom. By free path we mean the distance travelled before the probability of its evaporation due to diffraction by the surface lattice becomes equal to unity. Thus we write

$$l = \bar{v} \tau',$$

where  $\bar{v}$  is the mean velocity of those adsorbed atoms which are in such a state that they can evaporate without change of energy. Their lateral

velocity must be such that either  $k'_1$  or  $k'_2$  exceeds a lower limit  $k_n$ , defined by

$$-a^2 + 2ak_n + 2mE_n/\hbar^2 = 0$$

Hence

$$\frac{m\bar{v}}{\hbar} = \frac{\sum_n \exp(-E_n/kT) \int_{k_n}^{\infty} \int_{k_n}^{\infty} (k'_1{}^2 + k'_2{}^2)^{\frac{1}{2}} \exp\{-(k'_1{}^2 + k'_2{}^2) \hbar^2/2mkT\} dk'_1 dk'_2}{\sum_n \exp(-E_n/kT) \int_{k_n}^{\infty} \int_{k_n}^{\infty} \exp\{-(k'_1{}^2 + k'_2{}^2) \hbar^2/2mkT\} dk'_1 dk'_2}.$$

It is sufficiently accurate to equate  $\bar{v}$  and  $(\bar{v}^2)^{\frac{1}{2}}$ , and this is easier to calculate, thus

$$\frac{m^{\frac{3}{2}}\bar{v}^{\frac{3}{2}}}{\hbar^3} = \frac{\sum_n \exp(-E_n/kT) \int_{k_n}^{\infty} \int_{k_n}^{\infty} (k'_1{}^2 + k'_2{}^2) \exp\{-(k'_1{}^2 + k'_2{}^2) \hbar^2/2mkT\} dk'_1 dk'_2}{\sum_n \exp(-E_n/kT) \int_{k_n}^{\infty} \int_{k_n}^{\infty} \exp\{-(k'_1{}^2 + k'_2{}^2) \hbar^2/2mkT\} dk'_1 dk'_2},$$

and this can easily be expressed in terms of the Gaussian error function

#### 5—THE DETERMINATION OF SURFACE FIELDS FROM DIFFRACTION EXPERIMENTS

From the explicit formula which we have given above in equation (17) for the ratio of the intensity of a first order diffracted beam to the incident beam, it should be possible in principle to determine the constants of a surface field. The ratio  $R$  is a function of the three constants of the field, viz.,  $\kappa$ ,  $\beta$ , and  $d$  (or its equivalent  $D$ ), and so a series of measurements of  $R$  for incident beams of various velocities ( $\mu$ ) should be sufficient to determine them. In practice, however, it will be necessary to eliminate irregular scattering before this ideal can be achieved. Neither the reflected nor the diffracted beams, as now observed, are sharp, and this may be due to incoherent scattering by irregularities in the surfaces of the crystals or to the presence of adsorbed films, and further refinements may be necessary. It would also simplify comparison of theory and experiment if monochromatic atomic beams could be used.

On the theoretical side it is to be noted that the formula evaluated in this paper is based on the first order perturbation theory, and so is more likely to be accurate the smaller the fraction of atoms diffracted by the surface. In spite of these limitations, the theoretical formula may yet be valuable in conjunction with other methods as a means of deducing quantitative information of surface fields. At present there is no known method of deducing the fluctuation of a surface field parallel to the surface, though experiments on the migration of atoms and the activation

energy necessary to produce migration may provide information of this character. It may therefore be necessary or desirable to use surfaces and atoms for which two of the constants,  $d$  and  $\kappa$ , can be determined by other means. One such method is by the observation of the phenomenon of selective adsorption, as has been described in Paper V, or by the measurement of adsorption isotherms and comparison with a formula such as that of (44) above, or by the variation of accommodation coefficients with temperature as described in Paper VIII to follow. When  $d$  and  $\kappa$  are known by these or other methods, the formula for  $R$  involves only one unknown ( $\beta$ ).

Under these conditions one method of determining  $\beta$  is as follows. The crystal is rotated until the incident beam is perpendicular to one of the main axes of the surface lattice (assumed square). Then in formula (17) we can place  $\mu_x = 0$ , and

$$(\mu')^2 = \mu^2 - a^2/\kappa^2 \quad (45)$$

The diffracted beam lies in a plane which is inclined at an angle  $\psi$  to the reflected beam as shown in fig. 1, where

$$\cos \psi = k'_3/k_3 = \mu'/\mu = (1 - a^2/\kappa^2 \mu^2)^{1/2}, \quad (46)$$

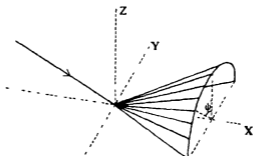


FIG. 1

and so  $\psi$  depends only on  $\mu$  when  $a$  and  $\kappa$  are known. Measurements of  $R$  as a function of  $\mu$  are therefore equivalent to measurements of  $R$  as a function of  $\psi$ . We can, in fact, write equation (17) in the form

$$R = \beta^2 F(\mu) = \beta^2 G(\psi). \quad (47)$$

In Table I we give a few calculated values of  $G(\psi)$  when  $d = 3.5$  (or  $D = 175$  cal.) and  $\kappa = (1.10) 10^8$  cm.<sup>-1</sup>, such as we have found for helium atoms on LiF by the method of selective adsorption, and  $a = (2.20) 10^8$  cm.<sup>-1</sup> for the surface lattice of LiF.

One interesting feature of  $G(\psi)$  for this special case emerges from the table and that is its relative constancy over a wide range of  $\psi$ . This is in agreement with the observations, for diffraction curves, calculated on the assumption that the probability of diffraction is independent of the  $z$  component of incident velocity, agree fairly well with the experimental curve.<sup>†</sup>

TABLE I—THE FUNCTION  $G(\psi)$  FOR  $d = 3.5$ ,  $a_0 = a/\kappa = 2$

$\psi$	$G(\psi)$	$\psi$	$G(\psi)$
9.5	341	45.0	113
14.0	231	51.3	109
18.4	175	57.0	107
24.0	147	63.4	106
29.1	132	68.2	105
33.7	124	78.7	91
39.8	117		

If now an experimental curve for  $R$  can be found for this case as a function of  $\psi$ , a comparison with the table should be sufficient to determine  $\beta$ . In one or two cases where estimates have been made of the potential energy of a rare gas in the field of an alkali halide crystal,<sup>‡</sup> the depth of the potential minimum fluctuated by above one-third of its average value. In the type of field used in this paper the depth of the potential minimum varies from  $D/(1 - 4\beta)$  to  $D/(1 + 4\beta)$ , so that  $8\beta/(1 - 16\beta^2)$  should be about one-third or  $\beta$  about 0.04. A value of  $\beta$  of this amount seems to give values of  $R$  approximately equal to those observed, so far as they can be estimated from the experimental curves,<sup>§</sup> assuming the same fraction of reflected and diffracted beams affected by irregular scattering.

Estimates of the order of magnitude of the probability of selective adsorption can be made from the numerical constants of the surface field between helium and lithium fluoride. Taking the values for  $D$  and  $\kappa$  already given and a value of 0.038 for  $\beta$ ,<sup>||</sup> the values of  $c'$  shown in Table II for various temperatures were obtained. In Table II are also included the corresponding values of  $\tau'$  in seconds and also the mean free path of a selectively adsorbed atom in centimetres, calculated by the formulae of the preceding section. Both  $c'$  and  $\tau'$  decrease as the temperature increases,  $c'$  being almost inversely proportional to temperature for this

<sup>†</sup> Frisch and Stern, 'Z. Phys.', vol. 84, p. 430 (1933).

<sup>‡</sup> Lennard-Jones, 'Trans. Faraday Soc.', vol. 38, p. 333 (1932).

<sup>§</sup> Frisch and Stern, *loc. cit.*

<sup>||</sup> Cf. Paper VI, §3.

particular case, but  $\tau'$  changes only by a factor of three in the range of temperature 30 to 300° abs. It follows that the free path is also nearly constant over the same range. Actually it has a minimum at about 100° abs., for, while  $\tau'$  decreases, the mean velocity of translation in the adsorbed state increases as the temperature increases.

TABLE II—THE PROBABILITY AND DURATION OF ADSORPTION AND THE MEAN FREE PATH

T (° abs.)	30	50	100	300
$c'$	0.032	0.018	0.009	0.0025
$\tau'$ (secs.)	$6.27 \times 10^{-10}$	$3.47 \times 10^{-10}$	$2.22 \times 10^{-10}$	$2.12 \times 10^{-10}$
$l$ (cm.)	$3.32 \times 10^{-5}$	$2.08 \times 10^{-5}$	$1.69 \times 10^{-5}$	$2.58 \times 10^{-5}$

The calculations of the free path refer to the case of an atom being diffracted by a perfect crystal surface, free from adsorbed gas. At the end of the path the atom would again be diffracted and would leave the crystal in the direction corresponding to perfect reflexion of the incident beam. Under these conditions, the phenomenon would not be observed. But if the atom, speeding along the surface, encountered an imperfection in the crystal or another adsorbed atom or for any other reason were incoherently scattered, or if it lost energy to the solid, it would be permanently lost to the reflected beam. Since Frisch and Stern observed the phenomenon of the diminution of reflexion at the critical directions we may infer that the atoms selectively adsorbed were so lost in a time of the order of  $10^{-10}$  sec. or in travelling  $10^{-5}$  cm.

#### SUMMARY

A theory of the diffraction of atoms at surfaces is worked out and explicit formulae are given for the intensities of diffracted beams. It is shown how a comparison of theory and experiment may be made in order that the constants of surface fields may be determined.

A formula is given for the probability that an atom approaching a surface along a critical direction will be diffracted so as to be captured by the surface field. The inverse process, whereby atoms running along a surface are diffracted so as to be evaporated, is examined and a specific formula evaluated for the average time which elapses before the phenomenon occurs. The free path of an atom evaporated by this mechanism appears in a particular case to be of the order of  $10^{-5}$  cm. It is shown that equilibrium between a gas and an adsorbed film can be established by the diffraction mechanism and that the condition for equilibrium is expressed by a Langmuir adsorption isotherm.

## The Interaction of Atoms and Molecules with Solid Surfaces

### VIII—The Exchange of Energy Between a Gas and a Solid

By A F DEVONSHIRE, University Chemical Laboratory and Trinity Hall, Cambridge

(*Communicated by J E Lennard-Jones, F R S —Received 8 August, 1936*)

#### 1—INTRODUCTION

In previous papers of this series† the problem of energy interchange between a gas atom and a solid has been discussed for the case when the gas atom makes a transition between two adsorbed states or between an adsorbed state and a free state. In this paper we shall discuss the case of a transition between two free states and apply the results to the determination of the thermal accommodation coefficient.

In recent years a number of theoretical papers‡ on this subject have appeared, following the new and accurate experimental work of Roberts,§ who worked with helium and neon on tungsten. The authors, however, neglect, or only roughly take into account, the attractive field which is known to exist between the solid and the gas, the fact that atoms become adsorbed on the surface is clear evidence of the existence of such a field. In this paper we shall suppose that the interaction potentials between solid and gas atom can be represented by a Morse potential function, for it has the right characteristics, in that it is attractive at large distances and repulsive at small ones, and has a minimum in between. The formulae of this paper are accordingly more general than previous ones and contain them as special cases. They are applicable to experimental results such as those of neon on tungsten for which earlier theories would not be adequate.

† Lennard-Jones and Strachan, 'Proc Roy Soc,' A, vol 150, p 442 (1935), Strachan, 'Proc Roy Soc,' A, vol 150, p 456 (1935), Lennard-Jones and Devonshire, 'Proc Roy Soc,' A, vol 156, p 6 (1936).

‡ Jackson, 'Proc Camb Phil Soc,' vol 28, p 136 (1932), Jackson and Mott, 'Proc Roy Soc,' A, vol 137, p 703 (1932), Jackson and Howarth, 'Proc Roy Soc,' A, vol 142, p 447 (1933), vol 152, p 515 (1935), Landau, 'Phys Z Sowjet,' vol 8, p. 489 (1935).

§ 'Proc Roy Soc,' A, vol 129, p 146 (1930), vol 135, p 192 (1932), vol 142, p 518 (1933), 'Proc Camb Phil Soc,' vol 30, p 74 (1933).

## 2—THE ACCOMMODATION COEFFICIENTS IN TERMS OF THE TRANSITION PROBABILITY

When a gas at one temperature is allowed to come in contact with a solid at another temperature there is a flow of energy from the one to the other and the rate of interchange is defined in terms of the *thermal accommodation* coefficient, a term first introduced by Knudsen. This coefficient ( $\alpha$ ) may be defined as follows

Let  $T_1$  be the temperature of the solid,  $T_2$  of the gas,  $E_1$  and  $E_2$  the mean energies of the atoms striking the surface at these temperatures, and  $E'_2$  the mean energy per atom on leaving the surface after a collision. Then

$$\alpha = (E'_2 - E_2)/(E_1 - E_2)$$

$\alpha$  is thus a function of  $T_1$  and  $T_2$ , and for theoretical purposes it is more convenient to define it by the equation

$$\alpha = \lim_{T_1 \rightarrow T_2} \frac{E'_2 - E_2}{E_1 - E_2}$$

In determining  $\alpha$  we shall assume that all the gas atoms move perpendicularly to the surface, and that the solid can be regarded as composed of harmonic oscillators which only take up or give up one quantum of energy at a time. This latter assumption has been justified by Strachan,<sup>†</sup> who has shown that the probability of the solid changing a given amount of energy by a one-quantum jump is always much larger than the probability of change by a two-quantum jump.

The number of atoms striking unit area per unit time in the energy range ( $E, E + dE$ ) is

$$(F/kT) \exp(-E/kT) dE,$$

where  $F$  is the total number of atoms striking unit area in unit time. Hence, if we denote by  $G(E, E + h\nu) d(h\nu)$  the probability per collision that the atom will take up a quantum of energy from the solid in the frequency range ( $\nu, \nu + d\nu$ ), the total energy taken up from the solid per unit time is equal to

$$(F/kT_2) \int_0^{\nu_m} h^2 \nu d\nu \int_0^\infty G(E, E + h\nu) \exp(-E/kT_2) dE,$$

where  $\nu_m$  is the maximum frequency of the solid. Similarly the energy given up to the solid per unit time is

$$(F/kT_2) \int_0^{\nu_m} h^2 \nu d\nu \int_0^\infty \Gamma(E + h\nu, E) \exp\{-(E + h\nu)/kT_2\} dE,$$

<sup>†</sup> Strachan, Paper IX of this series.

where  $\Gamma(E + h\nu, E) d(h\nu)$  is the probability per collision that an atom with energy  $E + h\nu$  will give up a quantum of energy to the solid in the frequency range  $(\nu, \nu + d\nu)$ . Hence the average energy taken up per atom striking the surface is given by

$$E'_2 - E_2 = (1/kT_2) \int_0^{\nu_m} h^2 \nu d\nu \int_0^\infty [G(E, E + h\nu) \exp(-E/kT_2) - \Gamma(E + h\nu, E) \exp\{-(E + h\nu)/kT_2\}] dE \quad (1)$$

But by the law of detailed balancing

$$\Gamma(E + h\nu, E) = G(E, E + h\nu) \exp(h\nu/kT_1),$$

and therefore

$$\begin{aligned} E'_2 - E_2 &= (1/kT_2) \int_0^{\nu_m} h^2 \nu d\nu \int_0^\infty G(E, E + h\nu) \exp(-E/kT_2) \\ &\quad \times [1 - \exp\{h\nu/kT_1 - h\nu/kT_2\}] dE \\ &= \frac{T_1 - T_2}{k^2 T_2^3} \int_0^{\nu_m} h (h\nu)^2 d\nu \int_0^\infty G(E, E + h\nu) \exp(-E/kT_2) dE, \end{aligned} \quad (2)$$

if  $T_1 - T_2$  is small. Now

$$E_1 - E_2 = k(T_1 - T_2), \quad (3)$$

and hence

$$\alpha = \frac{E'_2 - E_2}{E_1 - E_2} = \frac{h}{k^2 T_2^3} \int_0^{\nu_m} (h\nu)^2 d\nu \int_0^\infty G(E, E + h\nu) \exp(-E/kT_2) dE. \quad (4)$$

### 3—THE TRANSITION PROBABILITY

If we denote by  $\phi(E) dE$  the wave function corresponding to the continuous energy range normalized so that

$$\int_0^\infty \phi^*(E') \phi(E) dz = \delta(E' - E),$$

then  $\phi(E) dE$  corresponds to a flux  $dE/h$  of atoms on the surface and hence  $(dE/h) \Gamma(E, E')$  is the rate of transition between the state  $\phi(E) dE$  and the state  $\phi(E') dE$ , where  $E' > E$ .

We shall assume, as in preceding papers of this series, that the field between the gas atom and the crystal is given by a Morse function, namely

$$\begin{aligned} V(z, Z) &= D e^{-2\kappa(z-b-Z)} - 2D e^{-\kappa(z-b-Z)} \\ &= D(e^{-2\kappa(z-b)} - 2e^{-\kappa(z-b)}) + 2\kappa D Z (e^{-2\kappa(z-b)} - e^{-\kappa(z-b)}), \end{aligned} \quad (5)$$

approximately, where  $z$  is the coordinate of the gas atom,  $Z$  of the crystal atom, and  $z = 0$  is the surface of the crystal. The unperturbed equation for the gas atom is then

$$\left\{ \frac{\hbar^2}{2m} \frac{\partial^2}{\partial u^2} + E - De^{-2\kappa u} + 2De^{-\kappa u} \right\} \phi = 0, \quad (6)$$

where  $u = z - b$ , and it has been shown† that the rate of transition from the state  $l$  to the state  $s$  is given by

$$\frac{4\kappa^2 D^2}{M} |(E_l | e^{-2\kappa u} - e^{-\kappa u} | E_s)|^2 \frac{3}{2\nu_m^3} \frac{\nu}{\hbar} \frac{1}{(\exp \hbar\nu/kT - 1)}, \quad (7)$$

where

$$E_l - E_s = \hbar\nu$$

Hence

$$\hbar^{-1} G(E, E + \hbar\nu) = \frac{4\kappa^2 D^2}{M} g(E, E + \hbar\nu) \frac{3}{2\nu_m^3} \frac{\nu}{\hbar} \frac{1}{(\exp \hbar\nu/kT - 1)}, \quad (8)$$

where

$$g(E, E + \hbar\nu) = \left| \int_{-\infty}^{\infty} \phi^*(E, u) (e^{-2\kappa u} - e^{-\kappa u}) \phi(E + \hbar\nu, u) du \right|^2 \quad (9)$$

Now‡

$$\phi(E, u) = N(E) (2de^{-\kappa u})^{-1} W_{d, \mu}(2de^{-\kappa u}),$$

where

$$d = (2mD)^{1/2}/\kappa\hbar, \quad \mu = (2mE)^{1/2}/\kappa\hbar,$$

$$N^*(E) N(E) = \frac{1}{4\pi\mu} \frac{2m}{\kappa\hbar^2} \frac{\Gamma(\frac{1}{2} - i\mu - d) \Gamma(\frac{1}{2} + i\mu - d)}{\Gamma(2i\mu) \Gamma(-2i\mu)},$$

and  $W_{d, \mu}(x)$  is the confluent hypergeometric function.

Now the integral in equation (9) depends on

$$I_1 = \int_{-\infty}^{\infty} (2de^{-\kappa u})^{-1} W_{d, \mu}(2de^{-\kappa u}) e^{-2\kappa u} W_{d, -i\mu}(2de^{-\kappa u}) du,$$

and on

$$I_2 = \int_{-\infty}^{\infty} (2de^{-\kappa u})^{-1} W_{d, \mu}(2de^{-\kappa u}) e^{-\kappa u} W_{d, -i\mu}(2de^{-\kappa u}) d\eta.$$

† Lennard-Jones and Strachan, 'Proc Roy Soc,' A, vol 150, p 442 (1935), cf equations (18) and (20)

‡ Strachan, 'Proc Roy Soc,' A, vol 150, p. 456 (1935)

The first of these has already been evaluated in the preceding paper† and the second can be evaluated by similar methods. We find

$$I_2 = \frac{\pi^2 2d}{2d^2 \kappa (\cosh 2\mu\pi - \cosh 2\mu'\pi)} \left\{ \frac{1}{\Gamma(-d + i\mu + \frac{1}{2}) \Gamma(-d - i\mu + \frac{1}{2})} - \frac{1}{\Gamma(-d + i\mu' + \frac{1}{2}) \Gamma(-d - i\mu' + \frac{1}{2})} \right\},$$

and therefore that

$$\int_{-\infty}^{\infty} (2de^{-\kappa u})^{-1} W_{d, i\mu} (2de^{-\kappa u}) (e^{-2\kappa u} - e^{-\kappa u}) W_{d, -i\mu} (2de^{-\kappa u}) d\eta \\ = \frac{\pi^2 (\mu^2 - \mu'^2)}{2d^2 \kappa (\cosh 2\mu\pi - \cosh 2\mu'\pi)} \left\{ \frac{1}{A_\mu} + \frac{1}{A_\mu} \right\},$$

with the abbreviation‡

$$A_\mu = |\Gamma(-d + i\mu + \frac{1}{2})|^2$$

Hence

$$g(E, E') = \frac{1}{16\pi^2 \mu \mu'} \left( \frac{2m}{\kappa \hbar^2} \right)^2 \{ A_\mu A_{\mu'} / |\Gamma(2i\mu)|^2 \cdot |\Gamma(2i\mu')|^2 \} \\ \times \left| \int_{-\infty}^{\infty} (2de^{-\kappa u})^{-1} W_{d, i\mu} (2de^{-\kappa u}) (e^{-2\kappa u} - e^{-\kappa u}) W_{d, i\mu'} (2de^{-\kappa u}) du \right|^2 \\ = \frac{\hbar^2 v^3}{16D^2} \left( \frac{2m}{\kappa^2 \hbar^2} \right)^2 \frac{\sinh 2\mu\pi \sinh 2\mu'\pi}{(\cosh 2\mu\pi - \cosh 2\mu'\pi)^2} \frac{(A_\mu + A_{\mu'})^2}{A_\mu A_{\mu'}}, \quad (10)$$

where

$$\hbar v = E' - E$$

Therefore

$$G(E, E + \hbar v) = \frac{v^3}{v_m^3} \frac{24\pi^4}{\kappa^3 \hbar^2} \frac{1}{\{\exp(\hbar v/kT) - 1\}} \\ \times \frac{\sinh 2\mu\pi \sinh 2\mu'\pi}{(\cosh 2\mu\pi - \cosh 2\mu'\pi)^2} \frac{(A_\mu + A_{\mu'})^2}{A_\mu A_{\mu'}}, \quad (11)$$

and hence

$$\alpha = \frac{3}{v_m^3} \int_0^{v_m} \frac{v^3 (\hbar v/kT)^3}{\{\exp(\hbar v/kT) - 1\}} dv \int_0^M \frac{8\pi^4 m}{\kappa^2 \hbar^2} \\ \times \frac{\sinh 2\mu\pi \sinh 2\mu'\pi}{(\cosh 2\mu\pi - \cosh 2\mu'\pi)^2} \frac{(A_\mu + A_{\mu'})^2}{A_\mu A_{\mu'}} \exp(-E/kT) dE, \quad (12)$$

† Paper VII, p. 255 above, cf. equation (13)

‡ Cf. Paper VII, after equation (16)

where  $v_m$  is given by the equation

$$h v_m = k \Theta,$$

$\Theta$  being the characteristic temperature of the solid

#### 4—EFFECT OF USING A ONE-DIMENSIONAL MODEL

If we consider the gas molecules as moving in three dimensions but assume that the component of momentum parallel to the surface is unchanged on impact, the only change in our derivation of  $\alpha$  will be to replace equation (3) by

$$E_1 - E_2 = 2k(T_1 - T_2),$$

and hence to halve the value of  $\alpha$ . If, on the other hand, the average proportional change of energy corresponding to motion parallel to the  $x$  or  $y$  directions was the same as the average proportional change for motion in the  $z$ -direction  $\alpha$  would be unaltered. It seems most likely, *a priori*, that the true state of affairs lies in between these two possibilities and that, therefore, the effect of using a one-dimensional model is to increase  $\alpha$  by a small factor

#### 5—COMPARISON WITH CLASSICAL THEORY

In a recent paper Landau† has criticized the work of Mott, Jackson, and Howarth on the grounds that their formulae have only a limited range of validity and has suggested that, for the heavier gases, where the energy loss or gain of a gas atom on collision with the surface is small compared with its total energy over a fairly wide temperature range, the classical theory could be used. He has shown that for the case of an exponential repulsive field  $\alpha$  should then be proportional to  $T^{\frac{1}{2}}$ . So long as one-quantum transitions give the greater part of the contribution to the accommodation coefficient, the classical theory cannot be valid, but it is of interest to see that in the case Landau considered the formula (12) for  $\alpha$  can be evaluated, and gives exactly half the result he obtained, after correcting a mistake in his formula. Throughout the greater part of his paper he assumes that the crystal can be regarded as a fluid in reckoning up the normal modes, but in equation (32) he quotes a formula for the characteristic temperature derived for the case of a solid, and this inconsistency makes his results too small by a factor one-third.

† Landau, 'Phys. Z. Sowjet.', vol 8, p. 489 (1935)

If in equation (12) we put  $d = 0$  it becomes

$$\alpha = \frac{3}{v_m^3} \int_0^{v_m} \frac{v^3 (h\nu/kT)^3}{\{\exp(h\nu/kT) - 1\}} dv \int_0^\infty \frac{m}{M} \frac{8\pi^4 m}{\kappa^2 \hbar^2} \times \frac{\sinh \mu\pi \sinh \mu'\pi}{(\cosh \mu\pi - \cosh \mu'\pi)^2} \exp(-E/kT) dE, \quad (13)$$

and under certain conditions the integrals can be evaluated explicitly. For we have

$$\frac{\sinh \mu\pi \sinh \mu'\pi}{(\cosh \mu'\pi - \cosh \mu\pi)^2} = \frac{\sinh \mu\pi \sinh \mu'\pi}{4 \sinh^2 \frac{1}{2}(\mu - \mu')\pi \sinh^2 \frac{1}{2}(\mu + \mu')\pi} \\ = \frac{1}{4 \sinh^2 \frac{1}{2}(\mu - \mu')\pi},$$

approximately if

$$\mu\pi \gg 1, \quad (14)$$

and

$$(\mu' - \mu)\pi = \left(\frac{2m}{\kappa^2 \hbar^2}\right)^{\frac{1}{2}} \{(E + h\nu)^{\frac{1}{2}} - E^{\frac{1}{2}}\} \\ = \left(\frac{2m}{\kappa^2 \hbar^2}\right)^{\frac{1}{2}} \frac{h\nu}{2E^{\frac{1}{2}}},$$

approximately if

$$E \gg h\nu \quad (15)$$

Again if

$$kT \gg h\nu, \quad (16)$$

we have

$$\exp(h\nu/kT) - 1 = h\nu/kT,$$

approximately, and finally if the integrand is small for  $\nu > v_m$  we can replace the upper limit in the integration over  $\nu$  by  $\infty$ , and we then have

$$\alpha = \frac{3}{v_m^3} \frac{m}{M} \frac{8\pi^4 m}{\kappa^2} \frac{1}{(kT)^3} \int_0^\infty \int_0^\infty \frac{v^4 \exp(-E/kT)}{4 \sinh^2 \{\pi^2 m^{\frac{1}{2}} \nu / \kappa E^{\frac{1}{2}}\}} dv dE.$$

If we now use the formula

$$\int_0^\infty \frac{x^4 dx}{\sinh^2 x} = \frac{\pi^4}{30},$$

to integrate over  $\nu$  we deduce that

$$\alpha = \frac{3}{v_m^3} \frac{m}{M} \frac{2\pi^4 m}{\kappa^2} \frac{\pi^4}{(kT)^3} \frac{(2\kappa^2)^{\frac{1}{2}}}{(\pi^4 m)^{\frac{1}{2}}} \int_0^\infty E^{\frac{1}{2}} \exp(-E/kT) dE \\ = \frac{1}{2} \frac{1}{m^{\frac{1}{2}} M} \left(\frac{2\kappa^2 kT}{\pi v_m^3}\right)^{\frac{1}{2}} \\ = \frac{1}{2} \frac{1}{m^{\frac{1}{2}} M} \left(\frac{8\pi^{\frac{1}{2}} \kappa^2 T}{k\Theta^3}\right)^{\frac{1}{2}}. \quad (17)$$

This formula is derived on the assumption of a one-dimensional model. If we use a three-dimensional model but assume, as Landau did, that the field is dependent only on the  $z$ -coordinates of the gas atom and the crystal atom, so that the motion parallel to the surface is unchanged, we then have (cf § 4)

$$\alpha = \frac{1}{8} \frac{1}{m^{\frac{1}{2}} M} \left( \frac{8\pi\hbar^2 \kappa^2 T}{k \Theta^2} \right)^{\frac{1}{2}} \quad (18)$$

This value for  $\alpha$  is exactly half that obtained by Landau (after correction) on the assumption of a classical theory. The conditions (14), (15), and (16) always break down over some part of the range of integration, but equations (17) and (18) will still be approximately true if they hold over the greater part of the region in which the integrand of (13) makes an effective contribution to the integral. This will be the case if

$$2\pi^4 mkT / \kappa^2 \hbar^2 \gg 1$$

The fourth condition is that the integrand should be small for  $v > v_m$ . Now the essential factor in the integrand may be written approximately

$$\begin{aligned} & v^4 \exp \{ - (2\pi^4 m v^2 / \kappa^2 E)^{\frac{1}{2}} - (E/kT) \} \\ & \leq v^4 \exp \{ - (2\pi^4 m v^2 / \kappa^2 kT)^{\frac{1}{2}} (2^{-\frac{1}{2}} + 2^{\frac{1}{2}}) \} \\ & < v^4 \exp \{ - (12\pi^4 m v^2 / \kappa^2 kT)^{\frac{1}{2}} \}, \end{aligned}$$

which is small for  $v > v_m$  if

$$(12\pi^4 m v_m^2 / \kappa^2 kT)^{\frac{1}{2}} \gg 10,$$

that is if

$$T \ll \frac{12\pi^4 m v_m^2}{10^2 \kappa^2 k},$$

or

$$T \ll \frac{12\pi^4 mk \Theta^2}{10^2 \kappa^2 \hbar^2}.$$

Hence the necessary conditions for (17) to be valid are

$$\frac{2\kappa^2 \hbar^2}{\pi^2 mk} \ll T \ll (0.006 \Theta^2) \frac{\pi^2 mk}{2\kappa^2 \hbar^2}.$$

The upper limit corresponds to that given by Landau and the lower limit is always small. For example, for helium on tungsten with  $\kappa = 2 \times 10^8 \text{ cm}^{-1}$  and  $\Theta = 200^\circ \text{ K}$ , the conditions become

$$10^\circ \ll T \ll 24^\circ,$$

so that the formula (18) is not valid for any value of  $T$ . For the heavier

gases the conditions hold over a fairly wide range of temperature, but in this case the formula is hardly applicable as the attractive field is much larger and cannot be neglected. It does not seem possible to make any approximation which would make the general formula (12) integrable in finite terms.

## 6—DISCUSSION OF RESULTS

The case of a simple exponential repulsive field can be obtained by putting  $d = 0$  in equation (12), and then our value for  $\alpha$  is equal to that given by Jackson and Howarth† multiplied by a factor  $3/2$ . This discrepancy seems to be due to an error in the original paper by Jackson‡. If we denote by  $N$  the number of gas atoms per unit volume, and by  $T_2$  the temperature, the average properties of the gas atoms leaving the surface may be specified by numbers  $N'$  and  $T'_2$ , which must be related to  $N$  and  $T_2$  in such a way that the number of atoms striking unit area in unit time is the same in both cases. This will be so if

$$N' (T'_2)^{1/2} = N T_2^{1/2},$$

whereas Jackson assumed that

$$N' = N$$

In order to obtain agreement with experiment, they multiplied their results by a "roughness factor", between 1.5 and 2, to allow for the possibility of a gas atom making a double collision with the surface, and so the effect of the correction is only to reduce this rather arbitrary factor.

We have applied our formula for  $\alpha$  to the case of helium and neon on tungsten, taking the characteristic temperature of tungsten to be  $205^\circ$ . In fig. 1 we have drawn curves for neon on tungsten showing the variation of  $\alpha$  with temperature for different values of  $D$  and  $\kappa$ . The experimental values of Roberts are marked with a cross, and the curve which best fits these results corresponds to  $\kappa = 0.75 \times 10^8$ ,  $D = 493$  cal. The value of  $\alpha$  increases rapidly as  $\kappa$  increases, so that if  $D$  were known the value of  $\kappa$  could be deduced from the value of  $\alpha$  within quite narrow limits. The experimental results are not, however, sufficient to enable us to determine both  $D$  and  $\kappa$  accurately, but they do suggest that they are both rather small. The greater part of the contribution to the integral over  $v$  comes from the region where  $v$  is fairly small, so that the value of the upper

† 'Proc. Roy. Soc.', A, vol. 142, p. 447 (1933).

‡ *Loc. cit.*

limit has little effect on the result. Hence  $\alpha$  is approximately inversely proportional to  $v_m^2$ , that is to  $\Theta^3$ .

In fig. 2 we have drawn two curves for helium on tungsten, the first

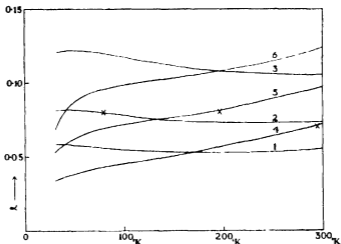


FIG 1—Accommodation coefficient for neon on tungsten. Curve 1 corresponds to  $\kappa = 0.707 \times 10^8$ ,  $D = 448$  cal/mol, 2 to  $\kappa = 0.742 \times 10^8$ ,  $D = 493$  cal/mol, 3 to  $\kappa = 0.786 \times 10^8$ ,  $D = 553$  cal/mol, 4 to  $\kappa = 10^8$ ,  $D = 212$  cal/mol, 5 to  $\kappa = 1.09 \times 10^8$ ,  $D = 252$  cal/mol, 6 to  $\kappa = 1.154 \times 10^8$ ,  $D = 283$  cal/mol

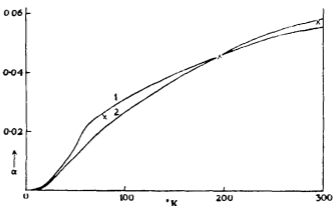


FIG 2—Accommodation coefficient for helium on tungsten. Curve 1 corresponds to  $\kappa = 1.154 \times 10^8$ ,  $D = 60$  cal/mol, with a roughness factor of 1.1; 2 to  $\kappa = 2 \times 10^8$ ,  $D = 0$ , with a roughness factor of 1.06

being taken from Jackson and Howarth's paper (with the correcting factor  $3/2$  inserted), and both being multiplied by a small "roughness factor" so as to fit on to the experimental point at  $195^\circ$  K. It will be

seen that even if we assume only quite a small heat of adsorption it is necessary to reduce the value of  $\kappa$  considerably in order to obtain agreement with experiment

It is to be noted that the theory is only valid as long as the surface is reasonably free from adsorbed gas. For this reason the theory may not be applicable to very low temperatures when there may be several layers of adsorbed atoms.

In conclusion, I should like to thank Professor Lennard-Jones for suggesting this problem and for many helpful discussions with him while it was being worked out

#### SUMMARY

A formula for the thermal accommodation coefficient of a monatomic gas on a solid is obtained for the case when there is an attractive field between the gas and the solid. The theory is applied to the case of helium and neon on tungsten. Satisfactory agreement with experiment is obtained, and an estimate is made of the values of the constants of the potential field

---

## The Electronic Structure of Some Polyenes and Aromatic Molecules

### I—The Nature of the Links by the Method of Molecular Orbitals

By J E LENNARD-JONES, F R S, The University Chemical Laboratory,  
Cambridge

(Received 9 September, 1936)

#### I—INTRODUCTION

The characteristic property which some molecules have of transmitting influences from one part to another is an indication that the electrons constituting the bonds cannot be segregated into closed localized pairs. This feature is represented in the Pauling method by the superposition of a number of canonical structures, each of which corresponds to a chemical picture of localized bonds. The state of the molecule has properties which are different from those of the individual canonical structures, but can be defined or interpreted in terms of a set of them. The energy of the lowest or normal state is usually lower than that of any one canonical structure, even than that which would appear from the orthodox method of drawing bonds to be the most stable. The amount by which the energy sinks as a result of the superposition has been called resonance energy by Pauling, and numerical estimates of its value have been made for a large number of organic molecules<sup>†</sup>. In calculating this energy change, however, no account seems to have been taken of the change in the lengths of the links which may be caused by the interaction of the electrons. Links are regarded as single or double, and the appropriate energy content calculated as though they were isolated single or double links, whereas the interaction between adjoining links may result in a length and an energy of link, to which the description single or double is no longer appropriate.

Pauling<sup>‡</sup> has recently discussed the relationship between the nature and the lengths of links in typical organic molecules. Taking the known

<sup>†</sup> Pauling and Wheland, 'J Chem Phys,' vol 1, p 362 (1933), Pauling and Sherman, 'J Chem Phys,' vol 1, pp 606, 679 (1933)

<sup>‡</sup> Pauling, Brockway, and Beach, 'J Amer Chem Soc,' vol. 57, p 2705 (1935).

lengths of links in ethylene, benzene, graphite, and ethane, and the fractional order of their links (as two, three-halves, four-thirds, and unity) derived from the coefficients which occur in the linear sum of canonical structures, Pauling has derived an empirical relation between them. From it he deduces in other cases the extent to which the double-bonded character enters into other links. Pauling's method will be made more precise in a paper which follows this.

In this paper we shall use a different method, based on the properties of molecular orbitals. We suppose, as Hückel,<sup>†</sup> Pauling,<sup>‡</sup> and others have done, that the aromatic character of unsaturated hydrocarbons is due to the existence of a  $\pi$ -electron at each carbon nucleus. Apart from these electrons, the molecule consists of single bonds due to the interaction of directed  $\sigma$ -electrons. This interaction may be calculated by either the method of localized pairs or by the orbital method as Penney<sup>§</sup> has done, and we shall suppose that part of the problem solved. We therefore begin with a molecular framework in which there are three single bonds associated with each carbon atom, probably in a plane inclined at angles of  $120^\circ$  to each other. At each carbon atom there is also a  $\pi$ -electron, which is antisymmetrical with regard to the plane containing the single links. We shall refer to these electrons as the *mobile* electrons as they are closely analogous to the conduction electrons of metals, and may be regarded as having a certain degree of mobility. They cannot be regarded as localized in the same sense as electrons participating in a single bond, nor can they be paired according to their spins in a unique way to correspond to any one conventional structural formula. In dealing with them according to the method of molecular orbitals, each electron is assumed to move throughout the whole molecule in the field of the nuclear framework and all the other electrons and is allotted to an orbital in conformity with the Pauli Principle. The net effect of all the mobile electrons cannot be described in terms of conventional single and double bonds. They cause the lengths of the carbon-to-carbon links to be intermediate between those of isolated single and double links, the links are, in fact, of an order between one and two and may be described as of fractional order. The method leads to an expression for the total energy of a molecule of this type from which the amount of resonance in it can be inferred.

<sup>†</sup> Hückel; E, 'Z. Phys.', vol. 70, p. 204 (1931), vol. 72, p. 310 (1931), vol. 76, p. 628 (1932), 'Physical Soc., Int. Conf. Phys.', London, p. 1 (1935).

<sup>‡</sup> *Loc. cit.*

<sup>§</sup> 'Proc. Roy. Soc., A', vol. 146, p. 223 (1934).

## 2—DESCRIPTION OF THE METHOD

If each  $\pi$ -electron were paired with an electron of an H or other atom, the distance separating neighbouring carbon atoms would be that of a single link. Each such link would represent an equilibrium between the forces causing the C—C link to shrink (the attractive exchange forces,  $J_{ii}$ ) and the forces causing repulsion between the paired electrons on each carbon core (the repulsive exchange forces,  $-\frac{1}{2}J_{ij}$ ). Included in the latter would be the effect of the  $\pi$ -electrons, each assumed paired with an electron from some other system. In this state of equilibrium we suppose the "pairing atoms" removed, and seek to find what changes are introduced by the interaction of the  $\pi$ -electrons, each now free on its carbon atom. This interaction will tend to cause neighbouring carbon atoms to move towards each other, but we have to remember that this will be opposed by those forces which produced equilibrium in the single links. We assume these forces unaltered by the removal of the "pairing atoms", though this is not strictly accurate, because of the removal of one electron on each of these atoms which was contributing to the forces of repulsion and because of the change from a tetrahedral arrangement of links at each carbon to a trigonal one. These are refinements which it may be possible to introduce as our knowledge of the electronic structure becomes more detailed.

At first we suppose the framework to consist of a succession of C—C links, all equally spaced, but the mobile electrons will introduce forces tending to upset this regularity. Hence it is necessary to calculate the energy of these electrons moving in a nuclear framework in which the initial symmetry is destroyed. One such final configuration might be that in which links were alternately long and short. The configuration of the nuclear framework would then be specified by two coordinates  $x_1$  and  $x_2$ . For any given values of  $x_1$  and  $x_2$ , it is necessary to determine the possible energy values and wave functions of an electron moving in this field of alternating rhythmic symmetry. Let these be  $E_1(x_1, x_2)$ ,  $E_2(x_1, x_2)$ , ...,  $E_n(x_1, x_2)$ , and let the degeneracy of the wave functions excluding spin be  $\alpha_1, \alpha_2, \dots, \alpha_n$ .

We now allot electrons one at a time to those orbitals, beginning with those of lowest energy to conform with the Pauli principle. This means that  $2\alpha_1$  electrons (allowing for spin) can be allotted to the level  $E_1$  and so on until all the electrons are allocated. Hence the orbital energy of the mobile electrons is given by

$$\mathcal{E}(x_1, x_2) = 2\alpha_1 E_1(x_1, x_2) + 2\alpha_2 E_2(x_1, x_2) + \dots \quad (1)$$

Work is, however, required to produce the  $x_1, x_2$  configuration from that of single links. If  $V(x)$  is the energy required to change the length of a single link from its equilibrium value until it becomes equal to  $x$ , and there are  $v_1$  links of length  $x_1$  and  $v_2$  of lengths  $x_2$ , the energy of compression is given by

$$\psi(x_1, x_2) = v_1 V(x_1) + v_2 V(x_2) \quad (2)$$

For example, in a conjugated hydrocarbon chain the number of  $\pi$ -electrons is even and may be denoted by  $2v$ . If we take the length of the first and alternate links to be  $x_1$ , and the rest to be  $x_2$ , then  $v_1 = v$  and  $v_2 = v - 1$ .

The total energy of the configuration is then

$$\mathcal{F}(x_1, x_2) = \mathcal{E}(x_1, x_2) + \psi(x_1, x_2), \quad (3)$$

and the configuration of lowest energy will be such that

$$\frac{\partial \mathcal{F}}{\partial x_1} = \frac{\partial \mathcal{F}}{\partial x_2} = 0 \quad (4)$$

In general, if a configuration be specified by  $p$  coordinates,  $x_1, x_2, \dots, x_p$ , then the condition for equilibrium will be

$$\frac{\partial \mathcal{F}}{\partial x_1} = \frac{\partial \mathcal{F}}{\partial x_2} = \dots = \frac{\partial \mathcal{F}}{\partial x_p} = 0, \quad (5)$$

but usually the difficulty of extending the calculation in this way is to calculate the energy of the molecular orbitals  $E_1, E_2$  in a configuration of such complexity and lack of symmetry.

In practice, the potential energy of the single link is most easily expressed in terms of a parabolic function, as for a simple harmonic oscillator, or in terms of a Morse function. In the applications we shall make of this method the difference between  $x_1, x_2$ , and  $s$ , the normal length of a pure single link, is so small that the potential  $V$  can be approximated to by a parabola and then  $V(x_1) = \kappa(x_1 - s)^2$ , where  $\kappa$  is a suitable force constant.

To calculate the energy of the orbitals, we suppose the potential energy expressed in the form of a sum

$$v(r) = \sum_f v_f(r_f), \quad (6)$$

where  $v_f$  is the potential energy of a  $\pi$ -electron at a distance  $r_f$  from the  $f$ th attracting centre due to the nuclear framework and the average effect

of all the other electrons. Let  $\psi_f$  be the wave functions of the  $\pi$ -electron in the field of  $v_f$  alone and let  $E_0$  be its energy, so that

$$\left[ -\frac{\hbar^2}{8\pi^2m} \nabla^2 + v_f \right] \psi_f = E_0 \psi_f \quad (7)$$

To find the wave function  $\Psi$  in the field  $v(r)$ , we express it as a linear sum of the  $\psi_f$ 's, now assumed known, thus

$$\Psi = \sum a_f \psi_f, \quad (8)$$

and we have to find the coefficients  $a_f$  and  $E$  to satisfy the equation

$$\left[ -\frac{\hbar^2}{8\pi^2m} \nabla^2 + v \right] \Psi = E \Psi \quad (9)$$

as well as possible. This leads to the familiar secular equation for the energy

$$\text{Det} (H_{fg} - E d_{fg}) = 0, \quad (10)$$

where

$$\begin{aligned} H_{fg} &= \int \psi_f^* \left[ -\frac{\hbar^2}{8\pi^2m} \nabla^2 + v \right] \psi_g d\tau = \int \psi_f^* [E_0 + v'_g] \psi_g d\tau \\ &= E_0 d_{fg} + \int \psi_f^* v'_g \psi_g d\tau, \end{aligned} \quad (11)$$

on using equation (7) and putting  $v'_g = v - v_g$ ,  $d_{fg}$  is the "overlap" integral. Then the determinant in (10) becomes

$$\text{Det} \{ (E_0 - E) d_{fg} + (v'_g)_{fg} \} = 0, \quad (12)$$

where

$$\begin{aligned} (v'_g)_{fg} &= \int \psi_f^* v'_g \psi_g d\tau \\ &= \sum' \int \psi_f^* v_g \psi_g d\tau \\ &= \sum' (v_g)_{fg}, \end{aligned} \quad (13)$$

and the summation includes the matrix elements of all the  $v_g$ 's except  $v_g$ . Usually these matrix elements will be very small except when  $e = f = g - 1$ , or  $e = f = g + 1$ , or when  $f = g$  and at the same time  $e = g - 1$  or  $g + 1$ , the former are "resonance" integrals, the latter Coulomb integrals. Similarly the "overlap" integrals  $d_{fg}$  will be small except when they refer to neighbouring atoms, that is  $f = g \pm 1$ . The secular determinant often simplifies considerably when all matrix elements except these are neglected

## 3—THE UNSATURATED HYDROCARBON CHAINS

In the unsaturated hydrocarbon chains with  $2\nu$  carbon atoms along the main chain, which we may label  $C_1, C_2, \dots, C_\nu, \dots, C_{2\nu}$ , the secular equation (12) has  $2\nu$  rows and columns and there are  $2\nu$  solutions for the orbital energy  $E$ . It seems reasonable to assume that there will be a centre of symmetry midway between  $C_\nu$  and  $C_{\nu+1}$  and then at most there will be  $\nu$  different distances between carbon atoms in equilibrium. If all the distances on each side of the centre of symmetry are assumed to be different, then the potential energy  $V_s$  at each carbon will be different and the matrix elements given in (13) will be different. The problem then becomes one of great complexity. It seems necessary, therefore, to attempt to solve the problem by successive approximations.

The first would be to assume all the lengths equal. This, in fact, is what Huckel† has done, though, being concerned only with the energies of the molecules, he has neglected  $\psi$  given in (2) and has not actually calculated the equilibrium distances. The neglect of  $\psi$  must, however, lead to errors in the evaluation of the energy.

The next approximation is to assume the links to alternate in length without specifying which are the long and which the short links. The method must determine that. This, then, requires two coordinates, and instead of using  $x_1$  and  $x_2$  we shall use the notations  $x_d$  and  $x_s$ , the former signifying the length of those links which are denoted by a double bond in the usual classical formula, and  $x_s$  signifying the lengths of the "single" links. The potential at each carbon except for the terminal atoms can then be taken to be the same, though it will not be symmetrical, and the important exchange integrals are of two types, viz.,  $(v_f)_{f,f+1}$  and  $(v_f)_{f,f-1}$ , one being a resonance integral across a long link and the other across a short link. When  $f$  is odd  $(v_f)_{f,f+1}$  is across a "double" link and  $(v_f)_{f,f-1}$  across a "single" link. The former we shall denote by  $\beta_d$ , the latter by  $\beta_s$ .

$$\begin{aligned}(v_f)_{f,f+1} &= \beta_d \text{ (} f \text{ odd)} \\ &= \beta_s \text{ (} f \text{ even)}\end{aligned}\tag{14}$$

The main Coulomb terms are also of two types, viz.,  $(v_{f+1})_{f,f}$  and  $(v_{f-1})_{f,f}$ . The first of these is the potential energy of the field  $v_{f+1}$  averaged over the electronic orbital  $\psi_f$  at nucleus  $f$ , and the second a similar average of the potential energy of the field  $v_{f-1}$ . When  $f$  is odd

† *Loc cit.*

the former is across a "double" link and the latter across a "single" link, and so we write

$$\begin{aligned}(v_{f+1})_{f,f} &= \alpha_d (f \text{ odd}) \\ &= \alpha_s (f \text{ even})\end{aligned}\quad (15)$$

It is usual in applications of the method of molecular orbitals to assume that the overlap integrals  $d_{ff}$  occurring in the secular equation can be neglected, but it is not necessary to do so entirely. Those between neighbouring atoms are of two types according as the link which separates them is long or short, and so we can write

$$\begin{aligned}d_{f,f+1} &= \delta_d (f \text{ odd}) \\ &= \delta_s (f \text{ even}),\end{aligned}\quad (15a)$$

where  $\delta_d$  and  $\delta_s$  will be fractions less than unity. Those between more widely separated atoms will be still smaller and may be neglected. If the wave functions are normalized, then  $d_{ff}$  is equal to unity.

We neglect Coulomb and exchange integrals except between neighbouring atoms and also those integrals which involve three different nuclei, as these will undoubtedly be small. We shall also assume the potential field due to the terminal atoms to be the same as the rest.

The secular equation is then

$$\begin{array}{ccccccc} E_0 + \alpha_d - E & , & (E_0 - E) \delta_d + \beta_d & , & 0 & , & 0 \\ (E_0 - E) \delta_d + \beta_d & , & E_0 + \alpha_s + \alpha_d - E & , & (E_0 - E) \delta_s + \beta_s & , & 0 \\ 0 & , & (E_0 - E) \delta_s + \beta_s & , & E_0 + \alpha_s + \alpha_d - E & , & 0 \\ . & & . & & . & & . \\ 0 & , & 0 & , & 0 & , & E_0 + \alpha_s + \alpha_d - E & , & (E_0 - E) \delta_d + \beta_d \\ 0 & , & 0 & , & 0 & , & (E_0 - E) \delta_d + \beta_d & , & E_0 + \alpha_d - E \end{array} = 0, \quad (16)$$

the exchange terms occurring only on each side of the diagonal and being alternately  $\beta_d$  and  $\beta_s$ . The diagonal terms are all the same except the first and last. The effect of this asymmetry will be smaller the longer the chain, and no great error will be introduced by taking all the diagonal elements to be the same, which we abbreviate to  $\epsilon$ , viz.,

$$\epsilon = E_0 + \alpha_s + \alpha_d - E. \quad (17)$$

To evaluate the roots of this equation, we could proceed as follows: first, neglect  $\delta_s$  and  $\delta_d$  and solve for  $E$  in terms of  $\beta$ 's, giving the first

approximation, viz., a series of roots  $E_1^{(1)}$ ,  $E_2^{(1)}$ , . . . ,  $E_n^{(1)}$ , replace the  $\beta$ 's occurring in these roots by  $(E_0 - E^{(1)})\delta_s + \beta_s$  and  $(E_0 - E^{(1)})\delta_d + \beta_d$ , having given to  $E$  the appropriate value obtained in the first approximation. This process could be continued to any required accuracy, giving  $E$  as a power series in the  $\delta$ 's. In this paper, however, we shall assume the  $\delta$ 's small enough to be negligible.

The equation to be solved is then

$$\Delta_{2\nu}(\epsilon) = \begin{vmatrix} \epsilon, & \beta_d, & 0, & 0, & 0 \\ \beta_d, & \epsilon, & \beta_s, & 0, & 0 \\ 0, & \beta_s, & \epsilon, & 0, & 0 \\ / & & & & \\ 0, & 0, & 0, & \epsilon, & \beta_d \\ 0, & 0, & 0, & \beta_d, & \epsilon \end{vmatrix} = 0 \quad (18)$$

This equation is of even degree in  $\epsilon$ . It follows that the roots of  $\epsilon$  occur in pairs of the type  $\pm \epsilon$ . It also follows that the above determinant is unaltered by writing  $-\epsilon$  wherever  $\epsilon$  appears, so that

$$\Delta_{2\nu}(-\epsilon) = \Delta_{2\nu}(\epsilon)$$

Multiplying these determinants together, we have

$$\Delta_{2\nu}(\epsilon) \Delta_{2\nu}(-\epsilon) = \begin{vmatrix} z, & 0, & \alpha, & 0, & 0, & 0, & 0, & 0 \\ 0, & y, & 0, & \alpha, & 0, & 0, & 0, & 0 \\ \alpha, & 0, & y, & 0, & 0, & 0, & 0, & 0 \\ 0, & \alpha, & 0, & y, & 0, & 0, & 0, & 0 \\ / & & & & & & & \\ 0, & 0, & 0, & 0, & y, & 0, & \alpha, & 0 \\ 0, & 0, & 0, & 0, & 0, & y, & 0, & \alpha \\ 0, & 0, & 0, & 0, & \alpha, & 0, & y, & 0 \\ 0, & 0, & 0, & 0, & 0, & \alpha, & 0, & z \end{vmatrix}, \quad (19)$$

where

$$y = -\epsilon^2 + \beta_s^2 + \beta_d^2, \quad z = -\epsilon^2 + \beta_d^2, \quad \alpha = \beta_s\beta_d. \quad (20)$$

By transposition of rows and columns, this determinant can be transformed to one of the type

$$\begin{vmatrix} D_r & 0 \\ 0 & D_r \end{vmatrix}$$

where

$$D_r = \begin{vmatrix} z, & \alpha, & 0, & 0, & 0, & 0 \\ \alpha, & y, & \alpha, & 0, & 0, & 0 \\ 0, & \alpha, & y, & \alpha, & 0, & 0 \\ 0, & 0, & \alpha, & y, & 0, & 0 \\ 0, & 0, & 0, & 0, & y, & \alpha \\ 0, & 0, & 0, & 0, & \alpha, & y \end{vmatrix}. \quad (21)$$

and is a determinant of  $v$  rows and columns. It follows that

$$\Delta_{2v}(\epsilon) = \pm D_r(\epsilon) \quad (22)$$

Now  $D_r$  can be expanded as a bordered determinant and gives

$$D_r = z\mathscr{D}_{v-1} - \alpha^2\mathscr{D}_{v-2}, \quad (23)$$

where  $\mathscr{D}_r$  is the determinant obtained from  $D_r$  by changing  $z$  to  $y$ .

We can write for  $\mathscr{D}_r$

$$\mathscr{D}_r = (-\alpha)^r \begin{vmatrix} 2 \cos \theta, & -1, & 0, & 0 \\ -1, & 2 \cos \theta, & 0, & 0 \\ & & \ddots & \\ 0, & 0, & 2 \cos \theta, & -1 \\ 0, & 0, & -1, & 2 \cos \theta \end{vmatrix}, \quad (24)$$

where

$$2 \cos \theta = -y/\alpha, \quad (25)$$

and, expanding it, we find

$$\frac{(-1)^r \mathscr{D}_r}{\alpha^r} = \frac{2 \cos \theta (-1)^{r-1} \mathscr{D}_{r-1}}{\alpha^{r-1}} - \frac{(-1)^{r-2} \mathscr{D}_{r-2}}{\alpha^{r-2}}, \quad (26)$$

whence it can be shown by induction that

$$\frac{(-1)^r \mathcal{D}_r}{\alpha^r} = \frac{\sin(\nu+1)\theta}{\sin\theta}. \quad (27)$$

Since the recurrence relation between  $\mathcal{D}_r$  in (26) is equivalent to

$$\mathcal{D}_r = y\mathcal{D}_{r-1} - \alpha^2 \mathcal{D}_{r-2}, \quad (28)$$

we have for  $D_r$  from (23)

$$\begin{aligned} D_r &= \mathcal{D}_r + (z-y)\mathcal{D}_{r-1} \\ &= \mathcal{D}_r - \beta_s^2 \mathcal{D}_{r-1} \\ &= (-1)^r \alpha^r \frac{\sin(\nu+1)\theta}{\sin\theta} - \beta_s^2 (-1)^{r-1} \alpha^{r-1} \frac{\sin\nu\theta}{\sin\theta} \\ &= (-1)^r \alpha^r \{ \sin(\nu+1)\theta + (\beta_s/\beta_d) \sin\nu\theta \} / \sin\theta \end{aligned} \quad (29)$$

The roots are therefore given by

$$\frac{\sin(\nu+1)\theta}{\sin\nu\theta} = -\frac{\beta_s}{\beta_d}, \quad (30)$$

and then the values of  $\epsilon$  are given by (25) and (20). We note in passing that if  $\beta_s = \beta_d = \beta$  the roots of equation (29) are given by

$$\frac{\sin(\nu+\frac{1}{2})\theta}{\sin\frac{1}{2}\theta} = 0, \quad (31)$$

or

$$\theta = (2r\pi)/(2\nu+1) \quad (r = 1, \dots, \nu), \quad (32)$$

and from (25) we then get

$$\epsilon = 2\beta \cos \frac{r\pi}{2\nu+1} \quad (r = 1, \dots, 2\nu). \quad (33)$$

The roots of equation (30) cannot be obtained so easily, but when  $\beta_s$  is not very different from  $\beta_d$ , equation (29) can be solved by using the results just obtained for  $\beta_s = \beta_d$ . Thus we can write equation (30) in the form

$$\frac{\sin(\nu+\frac{1}{2})\theta}{\sin\frac{1}{2}\theta} = \left(1 - \frac{\beta_s}{\beta_d}\right) \frac{\sin\nu\theta}{\sin\theta}, \quad (34)$$

and express the roots as

$$\theta_r = 2r\pi/(2\nu+1) + \zeta_r, \quad (35)$$

where  $\zeta_r$  is small. Then substituting in (34), we get

$$\begin{aligned}\zeta_r &= \frac{1}{2\nu+1} \left(1 - \frac{\beta_r}{\beta_d}\right) \frac{\sin \nu\theta_r}{\cos \frac{1}{2}\theta_r \cos (\nu + \frac{1}{2})\theta_r}, \\ &= -\frac{1}{2\nu+1} \left(1 - \frac{\beta_r}{\beta_d}\right) \tan \frac{r\pi}{2\nu+1},\end{aligned}\quad (36)$$

neglecting small quantities of the second order

The energy levels are then given by equation (25) as

$$\epsilon = \pm (\beta_s^2 + \beta_d^2 + 2\beta_s\beta_d \cos \theta_r)^{\frac{1}{2}} \quad (r = 1, 2, \dots, \nu) \quad (37)$$

Allotting two electrons each to the lowest  $\nu$  energy levels, we find for the orbital energy

$$\epsilon(x_s, x_d) = 2 \sum_{r=1}^{\nu} (\beta_s^2 + \beta_d^2 + 2\beta_s\beta_d \cos \theta_r)^{\frac{1}{2}} \quad (38)$$

To avoid any ambiguity in sign, it is better to write this as

$$\epsilon(x_s, x_d) = 2\beta_d \sum_{r=1}^{\nu} \{1 + 2(\beta_s/\beta_d) \cos \theta_r + (\beta_s/\beta_d)^2\}^{\frac{1}{2}},$$

and the sign is determined by  $\beta_d$ , the ratio  $\beta_s/\beta_d$ , being positive. Actually  $\beta_d$  is negative, as defined in this paper. The compressional energy is

$$\mathcal{V}(x_s, x_d) = \nu\kappa_s(x_d - s)^2 + (\nu - 1)\kappa_s(x_s - s)^2, \quad (39)$$

so that the equations for equilibrium are

$$\sum_{r=1}^{\nu} \frac{(\beta_s + \beta_d \cos \theta_r) \frac{\partial \beta_s}{\partial x_s} - \beta_s \beta_d \sin \theta_r \frac{\partial \theta_r}{\partial x_s}}{(\beta_s^2 + \beta_d^2 + 2\beta_s\beta_d \cos \theta_r)^{\frac{1}{2}}} + (\nu - 1)\kappa_s(x_s - s) = 0 \quad (40A)$$

and

$$\sum_{r=1}^{\nu} \frac{(\beta_d + \beta_s \cos \theta_r) \frac{\partial \beta_d}{\partial x_d} - \beta_s \beta_d \sin \theta_r \frac{\partial \theta_r}{\partial x_d}}{(\beta_s^2 + \beta_d^2 + 2\beta_s\beta_d \cos \theta_r)^{\frac{1}{2}}} + \nu\kappa_s(x_d - s) = 0 \quad (40B)$$

The further development of the theory requires a knowledge of  $\beta$  as a function of the interatomic distance, and this in turn requires a knowledge of the field in which these electrons move

It is not possible to find this without a complete solution of the electronic structure of the molecule by methods such as that of the self-consistent field, and this problem is intractable at present. It is necessary, therefore, to determine  $\beta$  by other means. One such method is to use the known properties of ethane and ethylene. The energy required to break these

links is known and also the force constants of the potential field, these having been determined from the known spacing of the vibration levels †. The potential field can be represented by a Morse function, but since the displacements from the equilibrium position with which we shall be concerned are only of the order of one-fifth of an Angstrom, it is sufficiently accurate to represent the potential near the equilibrium configuration by a parabolic function

Thus for a single link we can write

$$E_s = E_s^0 + \kappa_s (x - s)^2,$$

and for a double link

$$E_d = E_d^0 + \kappa_d (x - d)^2$$

Now the different values of the energy and length of the link in ethylene from those of ethane are due mainly to the  $\pi$ -electrons, both of which on the orbital theory are allotted to a level of energy  $\beta$ . Hence we may write

$$\begin{aligned} 2\beta &= E_d - E_s \\ &= E_d^0 - E_s^0 + \kappa_d (x - d)^2 - \kappa_s (x - s)^2 \end{aligned} \quad (41)$$

This equation gives  $\beta$  as a function of interatomic distance within the limits for which the parabolic potential term is valid. For greater interatomic distances we could use Morse functions and the method would still be applicable, though more cumbersome. Hence we have

$$2\beta_s = E_d^0 - E_s^0 + \kappa_d (x_s - d)^2 - \kappa_s (x_s - s)^2 \quad (42A)$$

$$2\beta_d = E_d^0 - E_s^0 + \kappa_d (x_d - d)^2 - \kappa_s (x_d - s)^2, \quad (42B)$$

and so

$$\frac{\partial \beta_s}{\partial x_s} = \kappa_d (x_s - d) - \kappa_s (x_s - s), \quad (43A)$$

$$\frac{\partial \beta_d}{\partial x_d} = \kappa_d (x_d - d) - \kappa_s (x_d - s) \quad (43B)$$

To solve equations (40A) and (40B) for  $x_s$  and  $x_d$ , we still require  $\partial \theta_s / \partial x_s$  and  $\partial \theta_d / \partial x_d$ . From equation (30) we have for the value of  $\theta$  appropriate to the equilibrium configuration

$$\frac{\partial \theta}{\partial x_s} = -\frac{1}{f(\theta)} \frac{\partial \beta_s}{\beta_d \partial x_s}, \quad \frac{\partial \theta}{\partial x_d} = \frac{\beta_s}{f(\theta) \beta_d^2} \frac{\partial \beta_d}{\partial x_d}, \quad (44)$$

where

$$f(\theta) = \frac{(\nu + 1) \cos(\nu + 1)\theta + \nu \cos \nu \theta}{\sin \nu \theta} - \frac{\nu \cos \nu \theta}{\sin \nu \theta} \left(1 - \frac{\beta_s}{\beta_d}\right). \quad (45)$$

† Cf Sutherland and Dennison, 'Proc. Roy. Soc.,' A, vol. 148, p. 270 (1935).

If  $\left(1 - \frac{\beta_s}{\beta_d}\right)$  is a small quantity, then the equilibrium values of  $\theta$  are given by (35), and to the first order we have

$$f_\theta(\theta_r) = (2\nu + 1) \cot \nu\theta = - (2\nu + 1) \cot \frac{r\pi}{2\nu + 1}, \quad (46)$$

since  $\cos(\nu + 1)\theta_r = \cos \nu\theta_r$ , for  $\theta_r = 2r\pi/(2\nu + 1)$ . The derivatives for this special case can also be obtained directly from (35) and (36). It follows that  $f(\theta)$  can then be expressed in the form

$$f(\theta_r) = - (2\nu + 1) \cot \frac{r\pi}{2\nu + 1} + \left(1 - \frac{\beta_s}{\beta_d}\right) \left\{ 2\nu \cot \frac{r\pi}{2\nu + 1} - \tan \frac{r\pi}{2\nu + 1} \right\} + O\left(1 - \frac{\beta_s}{\beta_d}\right)^2. \quad (47)$$

Substituting equations (43A), (43B), and (44) in equations (40A), (40B), and (41), we get

$$x_s = s - \frac{(s - d)}{1 + (\kappa_s/\kappa_d) \{(\nu - 1/S_1) - 1\}}, \quad (48)$$

and

$$x_d = s - \frac{(s - d)}{1 + (\kappa_s/\kappa_d) \{(\nu/S_2) - 1\}}, \quad (49)$$

where

$$S_1 = \sum_{r=1}^{\nu} \frac{\{\cos \theta_r + (\beta_s/\beta_d) (1 + (\sin \theta_r)/f(\theta_r))\}}{\{1 + 2(\beta_s/\beta_d) \cos \theta_r + (\beta_s/\beta_d)^2\}^{\frac{1}{2}}} \quad (50)$$

$$S_2 = \sum_{r=1}^{\nu} \frac{\{1 + (\beta_s/\beta_d) \cos \theta_r - (\beta_s/\beta_d)^2 (\sin \theta_r)/f(\theta_r)\}}{\{1 + 2(\beta_s/\beta_d) \cos \theta_r + (\beta_s/\beta_d)^2\}^{\frac{1}{2}}} \quad (51)$$

They are expressed as functions of  $(\beta_s/\beta_d)$ , since this is essentially positive.

The equations for  $x_s$  and  $x_d$  can be solved by successive approximations. Thus we first assume  $\beta_1$  and  $\beta_2$  equal in  $S_1$  and  $S_2$ , and then we get values for  $x_s$  and  $x_d$ . Equations (42A) and (42B) then determine  $\beta_s$  and  $\beta_d$ . These are substituted in  $S_1$  and  $S_2$ , using the expressions given in (35), (36), and (47) for  $\theta_r$  and  $f(\theta_r)$ . The approximations converge very rapidly, and the first step usually gives  $x_s$  and  $x_d$  to a fiftieth or hundredth of an Angstrom.

The expressions for  $S_1$  and  $S_2$  reduce considerably when  $\beta_s = \beta_d$ . Denoting them by  $S_1^{(0)}$  and  $S_2^{(0)}$ , we have

$$S_1^{(0)} = \frac{2\nu + 2}{2\nu + 1} \sum_{r=1}^{\nu} \cos \frac{r\pi}{2\nu + 1} - \frac{1}{2\nu + 1} \sum_{r=1}^{\nu} \sec \frac{r\pi}{2\nu + 1} \quad (52)$$

$$S_2^{(0)} = \frac{2\nu}{2\nu + 1} \sum_{r=1}^{\nu} \cos \frac{r\pi}{2\nu + 1} + \frac{1}{2\nu + 1} \sum_{r=1}^{\nu} \sec \frac{r\pi}{2\nu + 1}, \quad (53)$$

and the first summation in each is easily effected, giving

$$\sum_{r=1}^{\nu} \cos \frac{r\pi}{2\nu+1} = \sin^2 \frac{\nu\pi}{2(2\nu+1)} / \sin \frac{\pi}{2(2\nu+1)}. \quad (54)$$

To determine the lengths of the links for very long chains, we require the limiting values of  $S_1/\nu$  and  $S_2/\nu$  as  $\nu$  becomes large. Now

$$\text{Lt}_{\nu \rightarrow \infty} \frac{1}{2\nu+1} \sum_{r=1}^{\nu} \cos \frac{r\pi}{2\nu+1} = \int_0^{\pi/2} \cos \theta \, d\theta / \pi = 1/\pi,$$

and

$$\begin{aligned} \frac{1}{2\nu+1} \sum_{r=1}^{\nu} \sec \frac{r\pi}{2\nu+1} &\rightarrow \int_0^{\nu\pi/2\nu+1} \sec \theta \, d\theta / \pi \\ &= (1/\pi) \log \tan \left( \frac{\pi}{4} + \frac{\nu\pi}{2(2\nu+1)} \right) \\ &= (1/\pi) \log \cot \{ \pi/4 (2\nu+1) \} \\ &= (1/\pi) \log \{ 4(2\nu+1)/\pi \} \end{aligned}$$

Hence

$$\text{Lt}_{\nu \rightarrow \infty} (S_1/\nu) = 2/\pi = \text{Lt}_{\nu \rightarrow \infty} (S_2/\nu), \quad (55)$$

and so for very long chains

$$x_s = x_d = s - \frac{(s-d)}{1 + (\kappa_s/\kappa_d)(\pi/2 - 1)} \quad (56)$$

Thus the lengths of the links of conjugated hydrocarbon chains tend to become equal and approach an asymptotic value intermediate between that of a true single and a true double link

The values of  $S_1^{(0)}$  and  $S_2^{(0)}$  have been worked out for a number of special cases and are given in Table I.

TABLE I—THE VALUES OF  $S_1^{(0)}$  AND  $S_2^{(0)}$  FOR VARIOUS VALUES OF  $\nu$

$C_{2\nu}H_{2\nu+1}$	$\nu$	$S_1^{(0)}$	$S_2^{(0)}$	$(\nu-1)/S_1^0$	$\nu/S_2^0$
Butadiene ..	2	0.4472	1.7888	2.236	1.118
Hexatriene .. . . .	3	0.9667	2.5269	2.069	1.188
Octatetraene .	4	1.519	3.240	1.976	1.235
Decapentene ....	5	2.088	3.939	1.916	1.270
Duodecahexene	6	2.669	4.627	1.874	1.297
	$\infty$	$\infty$	$\infty$	1.571	1.571

#### NUMERICAL VALUES

In order to determine the lengths of the links in conjugated hydrocarbon chains from equations (48) and (49), it is necessary to know the

lengths  $s$  and  $d$  of single and double links. For  $s$  we take the value of 1.54 Å., generally accepted for the carbon to carbon distance in ethane and diamond †. The length of a double carbon-carbon link is not known with the same certainty. Sidgwick† estimates it to be 1.32 Å. while Badger‡ gives it as 1.37. In a re-examination of the data Penney§ estimates it to be 1.33 Å., and this is the value we shall assume.

The force constants of ethane and ethylene have been derived by Sutherland and Dennison|| from infra-red spectra. Denoting the part of the potential energy, which involves the carbon to carbon distance, by  $\frac{1}{2} c x_0^2$ , they find for ethane  $c = 4.96 \times 10^6$  dynes/cm. and for ethylene  $c = 9.79 \times 10^6$  dynes/cm. We accordingly take  $\kappa_s = 2.48 \times 10^6$  dynes/cm., and  $\kappa_d = 4.9 \times 10^6$  dynes/cm. and the constant we require is  $\kappa_s/\kappa_d = 0.507$ .

The values of the alternate short and long links in the chain molecules  $C_nH_{2n+2}$ , calculated from these numerical constants using Table I, are given in Table II. They are the first approximations to the solution of equations (48) and (49). The second approximations for butadiene and hexatriene are given below. The short links in butadiene and hexatriene are slightly longer than double links, but the long links are decidedly different from normal single links. The last column gives the average lengths of the links, a number which is remarkably constant.

TABLE II—THE LENGTHS OF LINKS IN CONJUGATED HYDROCARBON CHAINS

$C_nH_{2n+2}$	$v$	$x_s$	$x_d$	$\{vx_d + (v-1)x_s\}/(2v-1)$
Ethylene	1	—	(1.33)	1.33
Butadiene	2	1.41	1.34	1.36
Hexatriene	3	1.40	1.35	1.37
Octatetraene	4	1.40	1.35	1.37
Decapentene	5	1.40	1.36	1.37
Duodecahexene	6	1.39	1.36	1.37
Infinitely long chain	$\infty$	1.38	1.38	1.38

The total energy of the mobile electrons can also be calculated from the formulae given above. Thus for butadiene we have

$$\begin{aligned}
 2\beta_s &= E_d^0 - E_s^0 + \{\kappa_d(1.41 - 1.33)^2 - \kappa_s(1.41 - 1.54)^2\} 10^{-16} \text{ ergs} \\
 &= \{E_d^0 - E_s^0 - 1.45\} \text{ kcal} \\
 2\beta_d &= \{E_d^0 - E_s^0 - 14.2\} \text{ kcal}
 \end{aligned}$$

† Cf. Sidgwick, "Covalent Link in Chemistry," p. 82 (1933).

‡ Badger, 'Phys. Rev.', vol. 45, p. 648 (1934).

§ Penney, the following paper, p. 317.

|| Sutherland and Dennison, 'Proc. Roy. Soc. A', vol. 148, pp. 257, 264 (1935).

The values of  $E_s^0$  and  $E_d^0$  are not known with certainty Sidgwick† estimates  $E_s^0$  to be 71.14 kcal, and  $E_d^0$  to be 125.2. Pauling and Sherman‡ use different values, while 72.6 and 128.3 have also been adopted by Hückel§. It will facilitate comparison if we also take these latter figures. Then we get

$$\text{Butadiene} \begin{cases} \beta_s = -28.6 \text{ kcal} \\ \beta_d = -35.0 \text{ kcal} \end{cases}$$

We note that  $\beta_s$  and  $\beta_d$  are not very different, and expansions given in the above theory for  $1 - (\beta_s/\beta_d)$  small could be used in this case.

The energy levels of the mobile electrons in butadiene are easily shown to be

$$\frac{1}{2} \{ \beta_s \pm (\beta_s^2 + 4\beta_d^2)^{\frac{1}{2}} \} \quad \text{and} \quad \frac{1}{2} \{ -\beta_s \pm (\beta_s^2 + 4\beta_d^2)^{\frac{1}{2}} \},$$

so that the total energy of the four electrons in the lowest state is thus

$$\mathcal{E}(x_s, x_d) = -2 |(\beta_s^2 + 4\beta_d^2)^{\frac{1}{2}}| + 2\kappa_s(x_d - s)^2 + \kappa_s(x_s - s)^2$$

From this expression, using the above values of  $\beta_s$  and  $\beta_d$ , we can derive the second approximation to  $x_s$  and  $x_d$  and then the next approximation to  $\beta_s$  and  $\beta_d$ , thus —

*Butadiene (2nd approximation)*

$x_s$	$x_d$	$\beta_s$	$\beta_d$
1.43	1.34	26.5	35.0

The corresponding value of the total energy is -116.8 kcal.

The energy of the same electrons in two pure double bonds would be  $-4\beta_d + 2\kappa_s(s-d)^2$  or  $2(E_d^0 - E_s^0)$ , that is -111.4 kcal. The "resonance" energy of the  $\pi$ -electrons in butadiene is thus -5.4 kcal. Hückel|| obtains for the resonance energy  $0.48\beta$  where  $\beta$  is estimated to be between 15 and 20 kcal/mol, but the links are assumed equal and the energy of compression is neglected.

The resonance energy of hexatriene can be calculated in a similar way. The energies of the orbitals are  $\pm \epsilon_r$ , where

$$\epsilon_r = \left\{ 2(3\beta_s^2 + 4\beta_d^2)^{\frac{1}{2}} \cos\left(\frac{\phi + 2r\pi}{3}\right) - \beta_s \right\} / 3$$

† "The Covalent Link in Chemistry," pp. 111, 113 (1933)

‡ "J. Chem. Phys.," vol. 1, pp. 606, 679 (1933)

§ "Physical Soc.," Int. Conf. of Physics, p. 25 (1935)

|| *Loc. cit.*, Table I

and  $r = 0, 1$ , and  $2$ ;  $\phi$  is given by

$$\cos \phi = \frac{1}{2} (16\beta_s^2 - 9\beta_d\beta_s^2) (4\beta_d^2 + 3\beta_s^2)^{-3/2}.$$

The three lowest roots are  $\epsilon_0$ ,  $-\epsilon_1$ , and  $-\epsilon_2$ , and the energy due to the six  $\pi$ -electrons is

$$\mathcal{E} = 2(\epsilon_0 - \epsilon_1 - \epsilon_2) + 3\kappa_s(x_d - s)^2 + 2\kappa_s(x_s - s)^2.$$

The equilibrium values of  $x_s$  and  $x_d$  to the second approximation prove to be 1.42 and 1.34 respectively and the corresponding values of  $\beta_s = -27.6$  kcals. and  $\beta_d = -35.0$  kcals., we get a value for  $\mathcal{E}$  of  $-178.5$  kcals. The resonance energy, being the difference between this and the configuration of three double bonds and two single bonds, is 11.4 kcals.

#### SUMMARY

A general method is developed for calculating the lengths of links and the energies of conjugated organic molecules by means of molecular orbitals. General formulae are given for the lengths of the links in conjugated hydrocarbon chains, and it is shown that in short chains there are two kinds of links, one rather longer than a true double link and the other intermediate between a true single and a true double link. In long chains both links tend to become equal to 1.38 Angstroms.

---

# The Electronic Structure of Some Polyenes and Aromatic Molecules

## II—The Nature of the Links of Some Aromatic Molecules

By J. E. LENNARD-JONES, F.R.S., and J. TURKEVICH,† The University  
Chemical Laboratory, Cambridge

In this paper we apply methods similar to those of the preceding paper to the series of cyclic molecules  $C_{2n}H_{2n}$ , of which cyclobutadiene and benzene are the first members. The question we set out to answer is whether or not these molecules in the state of lowest energy exist as regular polygons. An alternative form is a series of alternating links, as represented by the Kekulé structural formula for benzene.

We shall assume as before that the configuration of each such molecule can be specified by two parameters  $x_s$  and  $x_d$ , the former referring to a single link and the latter a double link, in the conventional chemical formula. The secular equation is then

$$\Delta_{2n}(\epsilon) = \begin{vmatrix} \epsilon & \beta_s & 0 & 0 & 0 & \beta_d \\ \beta_s & \epsilon & \beta_d & 0 & 0 & 0 \\ & & & & & \\ & & & & & \\ 0 & 0 & 0 & \beta_d & \epsilon & \beta_s \\ \beta_d & 0 & 0 & 0 & \beta_s & \epsilon \end{vmatrix} = 0, \quad (1)$$

where

$$\epsilon = \alpha_s + \alpha_d - E \quad (2)$$

This differs from the secular determinant for an open chain in the appearance of  $\beta_d$  in the first and last rows.

† Travelling Fellow, Princeton University, U.S.A.

The determinant is an even power series in  $\epsilon$ , and we may use the same method as that given in the preceding section. We have

$$\Delta_{2\nu}(\epsilon) \Delta_{2\nu}(-\epsilon) = \begin{vmatrix} y, & 0, & \alpha, & 0, & 0, & 0, & \alpha, & 0 \\ 0, & y, & 0, & \alpha, & 0, & 0, & 0, & \alpha \\ \alpha, & 0, & y, & 0, & 0, & 0, & 0, & 0 \\ 0, & \alpha, & 0, & y, & 0, & 0, & 0, & 0 \\ \\ 0, & 0, & 0, & 0, & y, & 0, & \alpha, & 0 \\ 0, & 0, & 0, & 0, & 0, & y, & 0, & \alpha \\ \alpha, & 0, & 0, & 0, & \alpha, & 0, & y, & 0 \\ 0, & \alpha, & 0, & 0, & 0, & \alpha, & 0, & y \end{vmatrix}, \quad (3)$$

where

$$y = -\epsilon^2 \beta_s^2 + \beta_d^2, \quad \alpha = \beta_s \beta_d \quad (4)$$

By transposition of rows and columns, this determinant of  $2\nu$  rows and columns may be brought into the form

$$\begin{vmatrix} \nabla_\nu & 0 \\ 0 & \nabla_\nu \end{vmatrix} \quad (5)$$

where  $\nabla_\nu$  is a determinant of  $\nu$  rows and columns, viz.,

$$\nabla_\nu = \begin{vmatrix} y, & \alpha, & 0, & 0, & 0, & \alpha \\ \alpha, & y, & \alpha, & 0, & 0, & 0 \\ 0, & \alpha, & y, & 0, & 0, & 0 \\ \\ 0, & 0, & 0, & y, & \alpha, & 0 \\ 0, & 0, & 0, & \alpha, & y, & \alpha \\ \alpha, & 0, & 0, & 0, & \alpha, & y \end{vmatrix} \quad (6)$$

We infer at once that

$$\Delta_{2\nu}(\epsilon) = \pm \nabla_\nu(y) \quad (7)$$

Expanding  $\nabla_r$  as a bordered determinant of  $\mathcal{D}_{v-1}$  defined in Paper I (23), we have

$$\nabla_r = y \mathcal{D}_{v-1} - 2\alpha^2 \mathcal{D}_{v-2} - 2(-\alpha)^v. \quad (8)$$

Now we have from Paper I, equation (27),

$$\mathcal{D}_v = (-\alpha)^v \frac{\sin(v+1)\theta}{\sin\theta}, \quad (9)$$

where

$$\cos\theta = -y/2\alpha = (\epsilon^2 - \beta_s^2 - \beta_d^2)/2\beta_s\beta_d \quad (10)$$

Hence we find after some reduction

$$\nabla_r = (-1)^{v+1} 4\alpha^v \sin^2 v\theta/2, \quad (11)$$

and so the roots of

$$\nabla_r = 0,$$

are given by

$$v\theta = 2r\pi \quad (r = 0, 1, \dots, v-1) \quad (12)$$

The energy levels are therefore

$$\epsilon = \pm (\beta_s^2 + \beta_d^2 + 2\beta_s\beta_d \cos 2r\pi/v)^{1/2}, \quad (13)$$

where  $r$  takes the values  $0, 1, \dots, v-1$ . When the integrals  $\beta_s$  and  $\beta_d$  are negative, as defined in this paper, it is better to write

$$\epsilon_r = \beta_d \{ [1 + 2(\beta_s/\beta_d) \cos 2r\pi/v + (\beta_s/\beta_d)^2]^{1/2} \}, \quad (14)$$

and the bonding orbitals are given by  $r = 0, 1, \dots, v-1$ .

Some of these levels are doubly degenerate. Thus when  $v$  is odd the lowest and highest levels are single and the intermediate ones are doubly degenerate. When  $v$  is even there are four single levels, viz., the lowest and highest bonding levels and the lowest and highest antibonding levels, the rest being doubly degenerate. Because of this characteristic difference between the two cases it is necessary to deal with them separately.

*Case (i),  $v$  odd*

When  $v$  is odd the orbital energy plus compressional energy of the  $2v$  electrons is

$$\mathcal{J}(x_s, x_d) = \sum_{r=0}^{v-1} 2\epsilon_r + v\kappa_s(x_d - s)^2 + v\kappa_s(x_s - s)^2, \quad (15)$$

and the conditions for equilibrium are

$$\sum_{r=0}^{v-1} \frac{\{(\beta_s/\beta_d) + \cos 2r\pi/v\} (\partial\beta_s/\partial x_s)}{[1 + 2(\beta_s/\beta_d) \cos 2r\pi/v + (\beta_s/\beta_d)^2]^{1/2}} + v\kappa_s(x_s - s) = 0, \quad (16A)$$

and

$$\sum_{r=0}^{v-1} \frac{\{(\beta_s/\beta_d) \cos 2r\pi/v + 1\} (\partial\beta_d/\partial x_d)}{[1 + 2(\beta_s/\beta_d) \cos 2r\pi/v + (\beta_s/\beta_d)^2]^{1/2}} + v\kappa_s(x_d - s) = 0 \quad (16B)$$

Solving these equations for  $x_s$  and  $x_d$ , we find

$$x_s = s - \frac{s-d}{1 + (\kappa_s/\kappa_d) \{(\nu/\Sigma_1) - 1\}} \quad (17A)$$

$$x_d = s - \frac{s-d}{1 + (\kappa_s/\kappa_d) \{(\nu/\Sigma_2) - 1\}}, \quad (17B)$$

here

$$\Sigma_1 = \sum_{r=0}^{\nu-1} \frac{(\beta_s/\beta_d) + \cos 2r\pi/\nu}{|1 + 2(\beta_s/\beta_d) \cos 2r\pi/\nu + (\beta_s/\beta_d)^2|} \quad (18A)$$

$$\Sigma_2 = \sum_{r=0}^{\nu-1} \frac{1 + (\beta_s/\beta_d) \cos 2r\pi/\nu}{|1 + 2(\beta_s/\beta_d) \cos 2r\pi/\nu + (\beta_s/\beta_d)^2|}. \quad (18B)$$

When  $\beta_d = \beta_s$ , we see that  $\Sigma_1 = \Sigma_2$  and  $x_s = x_d$ , and so these are solutions of (17A) and (17B). To verify that this is a stable configuration, it is necessary to prove also that  $\frac{\partial^2 \chi}{\partial x_s^2}$  and  $\frac{\partial^2 \chi}{\partial x_d^2}$  are positive and that  $\frac{\partial^2 \chi}{\partial x_s^2} \frac{\partial^2 \chi}{\partial x_d^2} > \left(\frac{\partial^2 \chi}{\partial x_s \partial x_d}\right)^2$  in this configuration. It is not difficult to establish this in particular cases. When  $\nu$  is odd, the cyclic molecules  $C_{2\nu}H_{2\nu}$  form regular polygons.

We then have in the equilibrium configuration

$$\Sigma_1^0 = \Sigma_2^0 = \sum_{r=0}^{\nu-1} |\cos r\pi/\nu| = \text{cosec } \pi/2\nu, \quad (19)$$

and the orbital energy is (putting  $\beta_s = \beta_d = \beta$ )

$$2 \sum_{r=0}^{\nu-1} \epsilon_r = 4\beta \sum_{r=0}^{\nu-1} |\cos r\pi/\nu| = 4\beta \text{ cosec } \pi/2\nu$$

Thus for benzene ( $\nu = 3$ ) we have  $\Sigma_1^0 = 2$  and the orbital energy is  $8\beta$ .

*Case (ii),  $\nu$  even.*

When  $\nu$  is even, then the lowest energy level is  $\beta_s + \beta_d$ , or  $-|\beta_s| - |\beta_d|$  and the highest bonding orbital ( $r = \nu/2$ ) is  $\beta_s - \beta_d$  or  $-|\beta_s| + |\beta_d|$ , since  $|\beta_s| > |\beta_d|$ . In this case the orbital energy is

$$4\beta_d + 4 \sum_{r=1}^{\nu/2-1} \beta_s \{1 + 2(\beta_s/\beta_d) \cos 2r\pi/\nu + (\beta_s/\beta_d)^2\}^{\frac{1}{2}}, \quad (20)$$

and we find

$$x_s = s - \frac{s-d}{1 + (\kappa_s/\kappa_d) \{(\nu/\Sigma_1) - 1\}} \quad (21A)$$

$$x_d = s - \frac{s-d}{1 + (\kappa_s/\kappa_d) \{(\nu/\Sigma_2) - 1\}}, \quad (21B)$$

where

$$S_1 = 2 \sum_{r=1}^{v/2-1} \frac{(\beta_s/\beta_d) + \cos 2r\pi/v}{\{1 + 2(\beta_s/\beta_d) \cos 2r\pi/v + (\beta_s/\beta_d)^2\}^{1/2}} \quad (22A)$$

$$S_2 = 2 + 2 \sum_{r=1}^{v/2-1} \frac{1 + (\beta_s/\beta_d) \cos 2r\pi/v}{\{1 + 2(\beta_s/\beta_d) \cos 2r\pi/v + (\beta_s/\beta_d)^2\}^{1/2}}. \quad (22B)$$

In the special case of cyclobutadiene ( $v = 2$ ), we find  $S_1 = 0$  and  $S_2 = 2$ . It is then necessary to write, instead of equation (21A),

$$x_s = s - \frac{(s-d)S_1}{S_1 + (\kappa_s/\kappa_d)\{v - S_1\}} = s,$$

and  $x_d = d$ .

Thus this method indicates that an isolated cyclobutadiene should have two normal single links and two normal double links. The energy of the  $\pi$ -electrons, being  $4\beta_d$ , is the same as that of two isolated ethylene molecules. As energy will be required to alter the angle between the single bonds from the normal tetrahedral angle to a right angle, we may infer that cyclobutadiene will have a less energy content than two ethylene molecules and will tend to dissociate.

From the formulae for  $S_1$  and  $S_2$ , it is clear that  $S_2$  is always greater than  $S_1$  and so  $x_d$  is always less than  $x_s$  in these molecules. When  $v$  is even, the cyclic molecules  $C_{2v}H_{2v}$  consist of links of alternating lengths. Hence the theory predicts an essential difference in structure of the cyclic molecules  $C_{2v}H_{2v}$  according as  $v$  is odd or even†.

To solve equations (21A) and (21B) in any particular case, the simplest procedure is to evaluate  $S_1$  and  $S_2$  for  $\beta_s = \beta_d$ , then to find  $x_s$  and  $x_d$ . From them  $\beta_s$  and  $\beta_d$  can be determined and so the next approximate  $S_1$  and  $S_2$ . For  $\beta_s = \beta_d$ , the series in  $S_1$  and  $S_2$  may be summed for the general case, and denoting them by  $S_1^0$  and  $S_2^0$ , we have

$$S_1^0 = \cot(\pi/2v) - 1 \quad (23A)$$

$$S_2^0 = \cot(\pi/2v) + 1 \quad (23B)$$

In cyclo-octatetraene, for example, we have  $v = 4$  and  $S_1^0 = \sqrt{2}$ ,  $S_2^0 = \sqrt{2} + 2$ .

The results of the calculations for a few molecules, using the same constants as given in Paper I, § 3, are given in Table III. The resonance

† This result applies only to isolated atoms. In an assembly the rate of change from one form to another will depend on the temperature and on the height of the energy barrier separating the two equilibrium configurations. Calculations indicate that this height for cyclo-octatetraene is 8 kcal. and that the change from one form to the other will take place rapidly at room temperature.

energy given in the last column is the difference between the total energy due to the mobile electrons and two, three, and four double links respectively

TABLE III—THE LENGTHS OF LINKS AND ENERGIES OF SOME CYCLIC MOLECULES

$C_nH_n$	$v$ even		$v$ odd	Energy (mobile electrons) (kcal )	Resonance energy (kcal )
	$x_s$	$x_d$	$x_s = x_l$		
Cyclobutadiene	1.54	1.33	—	111.4	0.0
Benzene	—	—	1.37	197.3	30.2
Cyclo-octatetraene	1.43	1.35	—	241.6	18.8

The figures given in this table can be used to calculate the total energy content of the molecules. Thus for benzene we have six (C—C) links and six (C—H) links plus the energy of the mobile electrons. Using the value of (C—C) and (C—H) given by Huckel,<sup>†</sup> viz., 72.6 and 93.9 kcal, we find a total energy of 1197.3 kcal. Huckel gives the observed energy content as 1202 kcal, while Sidgwick<sup>‡</sup> gives it as 1193.2 kcal. Agreement is remarkably close.

The only observation of the sizes of links with which these calculations can be compared is that of benzene, which is given by Pauling and Brockway<sup>§</sup> as 1.39 Å, the difference between observation and calculation being only 0.02 Å. In this connexion it is to be noted that the calculations are based on the estimate of 1.33 for the length of link in ethylene, and any revision of this figure would modify the results for benzene by about the same amount.

#### DIPHENYL AND NAPHTHALENE

Similar methods can be applied to more complex molecules, and for purposes of illustration we have investigated the structure of diphenyl and naphthalene, the former because the connecting link between the phenyl groups is usually regarded as single and its properties are of some chemical interest, the latter because the benzene nucleus has been found above to be a regular polygon, and it seemed of interest to investigate the effect of the two rings on each other.

<sup>†</sup> 'Int. Conf. Phys.', p. 25 (1935).

<sup>‡</sup> "Covalent Link in Chemistry," p. 112 (1933).

<sup>§</sup> 'J. Chem. Phys.', vol. 2, p. 867 (1934).

(i) *Diphenyl*—It is likely that the connecting link between the two phenyl groups will slightly upset their symmetry and cause inequalities in the lengths of the links. We could take this into account by supposing there were four characteristic links in diphenyl, one joining the benzene nuclei, and three others in each ring, the whole molecule having two planes of symmetry through the mid-point of the central link. The method described in this paper could deal with this problem, though the calculations would be laborious. In order to simplify the calculations somewhat, we shall assume the rings to remain regular hexagons, and shall specify the molecular configuration by two parameters,  $x_1$  and  $x_2$ , the former referring to the connecting link and the latter to the rings.

The secular equation for this system is of the twelfth order, and if the field at each carbon atom is taken to be the same, there are two types of exchange integrals,  $\beta_1$  across the connecting link and  $\beta_2$  across all others. Every row of the determinant then contains three contiguous non-zero elements, viz.,  $\beta_2$ ,  $\epsilon$ , and  $\beta_2$ , except the first and seventh, which contain four, the first is ( $\epsilon$ ,  $\beta_2$ , 0, 0, 0,  $\beta_2$ ,  $\beta_1$ , 0, 0, 0, 0, 0) and the seventh is ( $\beta_1$ , 0, 0, 0, 0, 0,  $\epsilon$ ,  $\beta_2$ , 0, 0, 0,  $\beta_2$ ), where  $\epsilon$  is the same as in equation (17), the total Coulomb contributions to the energy being taken to be equal. The determinant factorizes as

$$(\epsilon^2 - \beta_2^2)^2 f(\epsilon) f(-\epsilon) = 0,$$

where

$$f(\epsilon) = \epsilon^4 - \beta_1 \epsilon^3 - 5\beta_2^2 \epsilon^2 + 3\beta_1 \beta_2^2 \epsilon + 4\beta_2^4,$$

and so the roots are found to be  $\pm \beta_2$  (doubly degenerate) and

$$\begin{aligned} &\pm \{k_1 + k_2 + k_3 - (\beta_1/4)\}, & \pm \{k_1 - k_2 - k_3 - (\beta_1/4)\}, \\ &\pm \{-k_1 + k_2 - k_3 - (\beta_1/4)\}, & \pm \{-k_1 - k_2 + k_3 - (\beta_1/4)\}, \end{aligned}$$

where  $k_1$ ,  $k_2$ ,  $k_3$  are the positive square roots of

$$k_r^2 = (3\beta_1^2 + 40\beta_2^2)/48 + (\beta_2/6)(9\beta_1^2 + 73\beta_2^2)^{1/2} \cos(\phi + 2r\pi)/3$$

$$(r = 0, 1, \text{ and } 2),$$

and

$$\cos \phi = \beta_2(108\beta_1^2 + 595\beta_2^2)(9\beta_1^2 + 73\beta_2^2)^{-1/2}$$

The six lowest roots are  $\beta_2$  (twice), and those of the roots given above in which the sign of  $k_1$  is positive. Hence the orbital energy of the twelve mobile electrons is

$$\mathcal{E}(x_1, x_2) = 8\sqrt{k_1} + 4\beta_2,$$

and the compressional energy

$$\mathcal{V}(x_1, x_2) = \kappa_s(x_1 - s)^2 + 12\kappa_r(x_2 - s)^2.$$

The equilibrium values of  $x_1$  and  $x_2$ , using the same constants as before, prove to be 1.44 and 1.40 Angstroms. The resonance of the mobile electrons, according to this theory, causes a shortening of the link connecting the phenyl groups and a lengthening of the links within the groups. The equilibrium values of  $\beta_1$  and  $\beta_2$  are -25.4 kcal. and -29.6 kcal. respectively. This gives a total energy of the mobile electrons in the equilibrium configuration of -399.6 kcal./mol. or a resonance energy of 65.4 kcal., being 5 kcal. greater than two benzene rings. The total energy content of diphenyl then proves to be 2268.9 kcal./mol., while Hückel† gives the observed value as 2305 kcal./mol.

(ii) *Naphthalene*—The conventional formula for naphthalene contains a double link in the bond common to the two rings, and from this the links alternate as single and double. Accepting this picture, we denote the single links by  $x_1$  and the double links by  $x_2$ , with corresponding exchange integrals  $\beta_1$  and  $\beta_2$ . The secular equation can be arranged in the form

$$\begin{vmatrix} \epsilon & \beta_2 & 0 & 0 & 0 & \beta_1 & 0 & 0 & 0 & 0 \\ \beta_2 & \epsilon & \beta_1 & 0 & 0 & 0 & 0 & 0 & 0 & 0 \\ 0 & \beta_1 & \epsilon & \beta_2 & 0 & 0 & 0 & 0 & 0 & 0 \\ 0 & 0 & \beta_2 & \epsilon & \beta_1 & 0 & 0 & 0 & 0 & 0 \\ 0 & 0 & 0 & \beta_1 & \epsilon & \beta_2 & 0 & 0 & 0 & \beta_1 \\ \beta_1 & 0 & 0 & 0 & \beta_2 & \epsilon & \beta_1 & 0 & 0 & 0 \\ 0 & 0 & 0 & 0 & 0 & \beta_1 & \epsilon & \beta_2 & 0 & 0 \\ 0 & 0 & 0 & 0 & 0 & 0 & \beta_2 & \epsilon & \beta_1 & 0 \\ 0 & 0 & 0 & 0 & 0 & 0 & 0 & \beta_1 & \epsilon & \beta_2 \\ 0 & 0 & 0 & 0 & \beta_1 & 0 & 0 & 0 & \beta_2 & \epsilon \end{vmatrix} = 0,$$

of which the roots are

$$\begin{aligned} & \pm \frac{1}{2} \{ \beta_1 \pm \sqrt{\beta_1^2 + 4\beta_2^2} \}, \\ & \pm \frac{1}{3} \{ 2(7\beta_1^2 - \beta_1\beta_2 + 4\beta_2^2)^{\frac{1}{2}} \cos(\phi + 2r\pi)/3 - (\beta_1 + \beta_2) \}, \end{aligned}$$

with  $r = 0, 1$ , and  $2$ , where

$$\cos \phi = \frac{1}{2} (34\beta_1^3 - 15\beta_1^2\beta_2 - 6\beta_1\beta_2^2 + 16\beta_2^3)(7\beta_1^2 - \beta_1\beta_2 + 4\beta_2^2)^{-\frac{1}{2}}$$

The equilibrium values of  $x_1$  and  $x_2$  prove to be 1.39 and 1.37 Angstroms respectively. It would clearly be better to take four parameters

† Hückel, 'Int. Conf. Phys.', p. 25 (1935)

for the molecule, one for the bond common to the two rings and three other lengths in each ring, assuming the molecule to have two planes of symmetry. Labelling the common link as A and the others in order from it as B, C, and D, Penney in the paper following this finds the lengths  $A = 1.42$ ,  $B = 1.40$ ,  $C = 1.38$ , and  $D = 1.40$ . It is interesting to note that the average value of the links denoted by  $x_1$  above, viz.,  $(4B + 2D)/6$ , is equal to 1.40, while the average value of  $x_2$ , viz.,  $(A + 4C)/5$ , is equal to 1.39, so that the averages are in excellent agreement with the method of this paper. The average length of the links in naphthalene has been measured by Robertson† by X-ray methods and estimated to be 1.41.

The exchange integrals  $\beta_1$  and  $\beta_2$  are equal to 30.6 kcal/mol and 32.4 kcal/mol respectively, and the equilibrium value of the energy is 331.1 kcal/mol, giving a total energy, when added to  $11(C - C) + 8(C - H)$ , of 1880.9 kcal/mol. The observed value given by Huckel is 1904 and by Sidgwick is 1881.5 kcal/mol. The resonance energy, reckoned as the difference between 331.1 and five double bonds, is 52.6 kcal.

We are indebted to Mr. A. F. Devonshire and Mr. C. A. Coulson for checking the formulae of this and the preceding paper and for considerable help with the numerical work.

#### SUMMARY

General formulae are given for the lengths of links of cyclic aromatic molecules. Benzene is shown to be a regular hexagon of length 1.37 Angstroms, whereas other cyclic molecules are found to be irregular and to consist of alternately long and short links. Calculations have been made of the energies of these molecules and the effect of "resonance" is estimated.

The method has also been applied to diphenyl and naphthalene.

† 'Proc. Roy. Soc.,' A, vol. 142, p. 674 (1933)

# The Electronic Structure of Some Polyenes and Aromatic Molecules

## III—Bonds of Fractional Order by the Pair Method

By W G PENNEY, Stokes Student of Pembroke College, Cambridge\*

(Received 9 September, 1936)

Lennard-Jones and Turkevich in the preceding paper have investigated by the orbital method the nature of the binding in various aromatic molecules due to the mobile electrons. The purpose of the present paper is to make somewhat similar calculations by the pair method. The author has had the benefit of several discussions with Professor Lennard-Jones, and he is glad to take this opportunity of acknowledging them.

### INTRODUCTION

Many molecules are such that their structure can be satisfactorily represented by simple bond diagrams. For this to be so it is necessary that any two atoms in the molecule are either not linked directly, or are linked by a single, double, or multiple bond. Excellent examples of molecules whose structure can be represented by simple bond diagrams are methane, ethane, ethylene, and acetylene. From an appeal to the experimental data it is found that for molecules of this class bond energies are closely conserved and that internuclear distances can be accurately predicted by associating with each atom an "ionic" radius which varies with the order of the linkage involved.

A large number of molecules, however, cannot be represented by simple bond diagrams. Notable examples are the aromatic carbon compounds containing condensed ring systems, and graphite. For these no unique bond system is possible, and in order to explain the observed chemical behaviour it is necessary to postulate the simultaneous existence of several bond structures, each with a certain probability. The usual way of describing this situation, following Pauling, is to say that there is "resonance" between the various bond structures. Huckel,<sup>†</sup> Rumer,<sup>‡</sup>

\* Now at Imperial College, London.

<sup>†</sup> 'Z. Phys.', vol 70, p 204 (1931); vol 72, p 310 (1931), vol 76, p 628 (1932).

<sup>‡</sup> 'Nachr. Ges. Wiss. Göttingen', M P Kl., p 337 (1932).

and Pauling and his collaborators\* have developed a mathematical theory of resonance. They have applied the general methods of the quantum mechanics of polyatomic molecules, due mainly to Slater, Pauling, Mulliken, Hund, and Lennard-Jones,† to these condensed ring systems. It appears that the effect of resonance is to increase the stability beyond that which would otherwise be expected, thus accounting for the observed facts.

When there is resonance between two or more bond structures it is no longer possible to say that all of the linkages are of integral order. Thus, for example, in the benzene ring where the main resonance is between the two Kekulé structures, the carbon-carbon linkages are something between single and double bonds. If it were only possible to devise a method of calculating the exact, fractional order of this linkage, we could then interpolate between single- and double-bond energies, and single- and double-bond ionic radii. Molecules in which resonance occurs could then be dealt with as easily as those in which it does not.

An interesting problem, therefore, is to find some way of calculating the order of a bond. Pauling, Brockway, and Beach‡ have already described a method, but, as we shall show, it is not entirely satisfactory. Nevertheless, if it is applied systematically it gives good results. We propose another method which has several advantages, and which may give even better results.

Our discussion develops on the following lines. First a brief account is given of Pauling and Wheland's treatment§ of the benzene ring in terms of canonical structures. This enables us to illustrate and criticize the general method used by Pauling, Brockway, and Beach for estimating the order of carbon-carbon bonds. An alternative method is suggested and is illustrated by simple examples. The method is then used to estimate the order of the bonds in different molecules where there is resonance, and to show that by simple interpolation between integral order bonds good estimates of the heats of formation of these molecules are possible. A similar application is made to obtain the dependence of the ionic radius of the carbon atom on the bond order, following fairly closely the treatment of Pauling, Brockway, and Beach. This section involves

\* Pauling and Wheland, 'J. Chem. Phys.', vol. 1, p. 362 (1933); Pauling and Sherman (J.), *ibid.*, vol. 1, pp. 606, 679 (1933); Wheland, *ibid.*, vol. 2, p. 474 (1934).

† An excellent summary of the present state of the quantum theory of polyatomic molecules has been given by Van Vleck and Sherman (A.), 'Rev. mod. Phys.', vol. 7, p. 167 (1935).

‡ 'J. Amer. Chem. Soc.', vol. 57, p. 2705 (1935).

§ 'J. Chem. Phys.', vol. 1, p. 362 (1933).

finding a fairly accurate solution of the graphite problem by the method of electron pairs. Finally the order of the bonds in butadiene, hexatriene, octatetraene, and naphthalene are calculated and predictions are made of the various C—C distances.

*The Benzene Ring*—Three of the bonds of each carbon atom in the benzene ring are unimportant for a discussion of resonance, and hence may be ignored. The essential feature is simply a ring of six monovalent atoms. For such a system two-bond diagrams are much more probable than any others since they have three pairs of neighbours linked by a bond. These two structures are usually referred to as the Kekulé structures because they yield the two Kekulé structures for the benzene ring when the three neglected bonds on each carbon atom are replaced. In order to calculate the most stable state of a ring of six monovalent atoms, one constructs wave functions corresponding to different bond structures, and uses these wave functions as a basis for setting up the secular equation. If the system contains  $2N$  atoms, the number of independent singlet states is  $(2N)!/N!(N+1)!$ , and hence this is the degree of the equation obtained by the Slater method for the lowest root. Rumer, Weyl, and Teller\* proved that if the orbits are formally arranged in a ring and various bond diagrams constructed by joining up  $N$  pairs by straight lines, then those bond diagrams which do not involve any crossing of bonds also number  $(2N)!/N!(N+1)!$ . Further, if each bond is taken to signify that the spins of the electrons occupying the two orbits linked by the bond have a resultant rigorously zero, then each bond diagram represents a singlet state of the system, and no one of the non-crossing set can be expressed in terms of the others. Hence the non-crossing set can be used to set up the secular equation. Pauling calls these structures "canonical", and has shown how to evaluate the matrix elements of unity and the Hamiltonian between states represented by these structures†. He and his collaborators were able to set up and solve the secular equations for systems corresponding to many different complicated organic molecules.

There are five canonical structures for the ring of six monovalent atoms. They are shown in fig 1.

Pauling and Wheland‡ showed that, subject to the usual approximations of neglecting overlapping of orbitals centred on different nuclei and interactions between non-neighbours, the normalized wave function of the

\* 'Nachr. Ges. Wiss. Gött., M P Kl.', p. 499 (1932).

† Pauling, 'J. Chem. Phys.', vol. 1, p. 280 (1933).

‡ 'J. Chem. Phys.', vol. 1, p. 362 (1933).

most stable configuration of the system is given in terms of those of the canonical structures by

$$\Psi = 0.410 (\psi_I + \psi_{II}) + 0.178 (\psi_{III} + \psi_{IV} + \psi_V) \quad (1)$$

and that the energy, apart from the additive Coulomb term, is

$$W = 2.61J, \quad (2)$$

$J$  being the exchange integral between neighbours. If one neglects the three excited structures the wave function and energy of the lowest state are

$$\Psi = 0.632 (\psi_I + \psi_{II}), \quad W = 2.40J \quad (3)$$

The two Kekulé structures occur with equal probability, and any two neighbours which are linked by a single bond in one Kekulé structure are

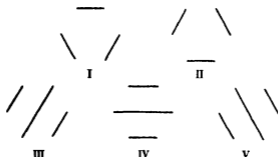


FIG. 1—The five canonical structures for the resonance problem of the benzene ring.

not linked at all in the other. Hence we may say that the linkage between any two neighbours is half the time single bond and half the time "no" bond. Returning to the benzene ring, the linkage between neighbouring carbon atoms is half double bond and half single bond. This is the convention adopted by Pauling, Brockway, and Beach for the order of the linkage in benzene. More generally for any system of monovalent atoms, if the ground state is given in terms of the canonical structures by the sum

$$\Psi = \sum_i a_i \psi_i,$$

$\psi_i$  being the wave function of the canonical structure  $i$ , then the order of the linkage connecting any two atoms is

$$x = (\sum_i g_i a_i^2) / (\sum_i a_i^2), \quad (4)$$

where  $g_i$  is unity if the structure  $i$  has a bond between the two atoms, and is zero otherwise.

From the relations (1)–(4) we see that if the excited canonical structures of the benzene ring are neglected, the order of the carbon-carbon linkage is 1.5, and if the excited structures are included the order *falls* to 1.46. According to the convention (4), the inclusion of the excited structures has *increased* the stability but *lowered* the order of the linkage.

Another serious objection to the convention (4) is that it leads one to expect results different from the true ones. Thus if one says that the order of the carbon-carbon linkage in benzene is 1.5, one would expect the heat of formation to be that of six carbon-hydrogen bonds, three double carbon-carbon bonds, and three single carbon-carbon bonds, *i.e.*, just the same as that of a single Kekulé structure\*. But one of the things which the theory of resonance sets out to explain is why the heat of formation of benzene is greater than that of a single Kekulé structure. A much better convention would therefore be one which gives the carbon-carbon linkage in benzene to be greater than 1.5. We can then say that the effect of resonance is to increase the importance of the double bonds at the expense of the single bonds, and thus to increase the stability.

A much less serious objection to the convention (4) is that in order to calculate the order of the linkage the secular equation must be set up, and the complete wave function expressed, in terms of the canonical structures. As far as setting up the secular equation is concerned, however, many different sets of structures, some involving "crossed" bonds, are equally good. The calculated energy levels are, of course, invariant, but a quantity such as  $x$  above, in which the running suffix  $i$  now covers the particular set of structures used to set up the secular equation, is not.

#### METHOD PROPOSED FOR CALCULATING THE ORDER OF THE LINKAGE

The method we propose for calculating the order of the linkage is based on the vector model introduced by Dirac,<sup>†</sup> and applied by Van Vleck,<sup>‡</sup> Serber,<sup>§</sup> and others to detailed problems involving permutation

\* On the other hand, the statement correctly predicts that none of the bonds is as vulnerable to attack as the localized double bonds of a Kekulé structure. However, any fractional order between one and two, and not too near either limit, would also do this.

† "The Principles of Quantum Mechanics," chap. xi, Oxford Univ. Press, 1930.

‡ 'Phys. Rev.', vol. 45, p. 405 (1934).

§ 'Phys. Rev.', vol. 45, p. 461 (1934), 'J. Chem. Phys.', vol. 2, p. 697 (1934).

degeneracy. The fundamental formula is that the Hamiltonian of a system of  $2N$  orbits is formally equivalent to a Hamiltonian

$$H = \text{const} - \frac{1}{2} \sum (1 + 4\mathbf{s}_i \cdot \mathbf{s}_j) J_{ij},$$

the summation being over all pairs. Here  $J_{ij}$  is the exchange integral between the orbits  $i$  and  $j$ , and  $\mathbf{s}_i$  is the spin vector matrix of an electron in the orbit  $i$ . The problem of permutation degeneracy has thus been replaced by one of formal cosine coupling between angular momentum vectors.

The energy of the most stable state of the system is therefore

$$W = \text{const} - \frac{1}{2} \sum (1 + 4\overline{s_i s_j}) J_{ij}, \quad (5)$$

where  $\overline{s_i s_j}$  is the diagonal element of  $\mathbf{s}_i \cdot \mathbf{s}_j$  for this state of least energy. One of our approximations is that the only  $J_{ij}$  terms that need be included in (5) are those between neighbours. If we now assume that the systems with which we are dealing are so highly symmetrical that all orbits are equivalent, then all  $J_{ij}$  between neighbours are equal, and are equal, let us say, to  $J$ . In this special case all  $\mathbf{s}_i \cdot \mathbf{s}_j$  between neighbours are equivalent, and  $W$  and  $\mathbf{s}_i \cdot \mathbf{s}_j$  are diagonalized simultaneously. Apart from the additive constant the energy is

$$W = -\frac{1}{2} kJ (1 + 4\overline{s_i s_j}), \quad (6)$$

where  $k$  is the number of pairs of neighbours, and  $i$  and  $j$  represent any pair of neighbouring orbits. If we can calculate  $W$  as a numerical multiple of  $J$  (this being exactly what one does when one solves the secular equation), the value of  $\overline{s_i s_j}$  can be found quite simply from (6).

Now when the two orbits  $i$  and  $j$  are linked by a bond the two electrons occupying these orbits by definition have resultant spin zero, and hence  $\mathbf{s}_i \cdot \mathbf{s}_j$  is a diagonal matrix with eigenvalues  $(-3/4)$ . On the other hand, when there is no bond between the orbits,  $\mathbf{s}_i \cdot \mathbf{s}_j$  is a matrix whose diagonal elements are all zero\*. Therefore, as the two orbits pass from conditions representing a single bond to conditions where there is no bond the diagonal elements of  $\mathbf{s}_i \cdot \mathbf{s}_j$  vary from  $(-3/4)$  to 0. The fractional order  $p$  of any intermediate type of bond can be defined by linear extrapolation between these two limits as  $(-4/3) \times (\text{mean value of } \mathbf{s}_i \cdot \mathbf{s}_j)$ , i.e.,

$$p_{ij} = -4\overline{s_i s_j} / 3 \quad (7)$$

A somewhat simpler, but less fundamental, explanation of the quantity  $p$  can be obtained directly from the formula of perfect pairing. It is

\* For a proof of these statements see, for example, Van Vleck, "The Theory of Electric and Magnetic Susceptibilities," Oxford Univ. Press, 1932, chapter xii.

assumed that all orbits are equivalent, and that the energy of the most stable state can be calculated. There are in all  $k$  equivalent pairs of neighbouring orbits, and therefore the average energy per pair is  $W/k$ . The contribution to the energy of the system of a pair of neighbouring orbits linked by a bond is  $J$ : when the orbits participate in different bonds, and hence are not linked together, the contribution of their interaction is  $-\frac{1}{2}J$ . The actual linkage when the whole system is in its most stable state can be expressed as  $p$  times a single bond plus  $(1 - p)$  times "no" bond in such a way that the energy comes out right

$$\begin{aligned} W/k &= p(J) + (1 - p)(-\frac{1}{2}J), \\ p &= (1 + 2W/kJ)/3 \end{aligned} \quad (8)$$

Substituting for  $W$  from (6), it is easily verified that (8) reduces to (7)

As an example, consider the ring of six atoms. The lowest energy state is  $W = 2.61J$ . There are six pairs of equivalent neighbours, and hence

$$2.61J = -\frac{1}{2} \times 6(1 + 4\overline{s_i s_j})J, \quad \overline{s_i s_j} = -0.4675,$$

and the order of the linkage from (7) is 0.623. Thus, according to our definition of the order of the linkage, the carbon-carbon linkage in benzene is of order 1.623. It is nearer to a double bond than to a single bond, in agreement with the experimental evidence.

Several other simple systems give excellent examples of fractional linkage. Three atoms arranged symmetrically in a straight line about the central atom\* have an energy  $J$ , and the order of the linkage is  $2/3$ . The energy of four similar monovalent atoms arranged in a square\* is  $2J$ , and the order of the linkage is  $2/3$ . When the atoms are arranged in a regular tetrahedron† the energy is 0 and the linkage falls to  $1/3$ . Eight similar atoms arranged in a regular octagon‡ have an energy  $3.29J$  and the order of the linkage is 0.607. Eight atoms arranged at the corners of a cube‡ have an energy  $3.65J$  and the order of the linkage is 0.536.

To sum up, the strength of the definition (7) for the order of a linkage is that it gives a very close connexion between the order of the linkage and the stability. When there is resonance in the system, the stability

\* The solutions of the three and four electron problems can be expressed in closed form (see, for example, Van Vleck and Sherman (A.), 'Rev. Mod. Phys.', vol. 7, p. 167 (1935)). The energy expressions which we quote are obtained directly by substituting the appropriate values for the various exchange integrals.

† Penney, 'Proc. Roy. Soc. A', vol. 146, p. 223 (1934).

‡ Serber, 'J. Chem. Phys.', vol. 2, p. 697 (1934).

is greater than that expected from a simple bond diagram and the average order of the linkages correspondingly increased

#### THE ORDER OF THE LINKAGE IN GRAPHITE

Later in the paper we shall need the order of the linkage in graphite, and this is a convenient place to consider it. As is well known, graphite consists of parallel sheets of carbon atoms arranged in hexagonal lattices. The primary bonds from any carbon atom all lie in the plane of the sheet, and the forces that hold the different sheets together are mainly of a van der Waals type. Thus it is sufficient in calculating the order of the linkage to consider only one sheet. As in the benzene ring, three of the four bonds on each carbon atom can be temporarily ignored and our problem resolves itself chiefly into calculating the exchange energy per atom of a sheet of similar monovalent atoms arranged in a hexagonal lattice\*. Once again we shall neglect non-orthogonality and interactions between non-neighbours. Even so, no simple rigorous solution seems possible, but an approximate method which should give fairly accurate results is the following.

Imagine the lattice built up from hexagons. Now the rigorous solution of the six-ring problem is known. Let us therefore diagonalize the interactions within each hexagon, and allow for the interaction between any two neighbouring orbits in different hexagons by the usual term ( $-\frac{1}{2}J$ ). There are three interactions between neighbouring orbits of other hexagons per hexagon, and the average exchange energy per atom, according to the approximation based on the six-ring problem, is therefore  $(2 \cdot 61J - 3 \times 0 \cdot 5J)/6$ , i.e.,  $0 \cdot 185J$ .

To get an idea of the error of the above calculation, consider a similar approximation for the energy of diphenyl  $C_6H_5-C_6H_5$ . Here there are two rings of six with one interaction between them. According to the above method of approximation, the energy should be

$$(2 \times 2 \cdot 6055J - 0 \cdot 50J) = 4 \cdot 711J.$$

The accurate solution is  $4 \cdot 867J$ . Hence, by properly allowing for the resonance in the link that joins the two rings, the energy is increased by  $0 \cdot 156J$ . In other words, instead of adding ( $-\frac{1}{2}J$ ) for each of the non-preferred interactions, a much better approximation is to add ( $-0 \cdot 344J$ ). By this method we calculate the energy of the ortho-, meta-, and para-diphenylbenzene problems as  $7 \cdot 13J$ , instead of  $7 \cdot 103J$ ,  $7 \cdot 094J$ , and

\* Lennard-Jones, 'Trans. Faraday Soc.', vol 30, p 58 (1934)

7.086J respectively, obtained by Pauling and Sherman\* from a very nearly rigorous solution of the secular equation. Returning to the graphite problem in terms of the six-ring, the energy per atom becomes 0.263J.

Let us now build up the lattice from the ten-atom problem of the naphthalene molecule. Here there are four neglected interactions per ten atoms. The energy of the ten-atom system is 4.04J, and the energy per atom of the lattice according to this approximation is

$$(4.04J - 1.38J)/10 = 0.266J$$

This agrees well with the estimate based on the six-ring.

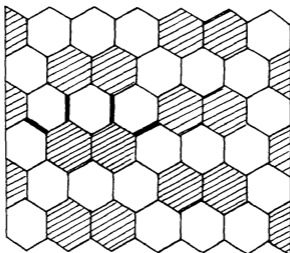


FIG. 2—The resonance problem of graphite in terms of that of naphthalene. Our approximation is to diagonalize the eleven "preferred" interactions within each naphthalene system and to allow for each of the four "non-preferred" interactions by a term  $-0.344J$ . A typical set of four "non-preferred" interactions is shown in heavy lines. Other approximations agreeing well with the above may be made in terms of benzene, anthracene, and phenanthracene.

The solution of the graphite problem may also be obtained in terms of units based on the anthracene and phenanthracene molecules. Unfortunately, the solution of neither of these molecules has been worked out. From thermo-chemical data, however, Pauling and Sherman† estimate the energy of the anthracene system as 5.55J and of the phen-

\* \* J. Chem. Phys., vol. 1, p. 606 (1933)

† \* J. Chem. Phys., vol. 1, p. 679 (1933)

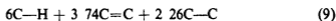
anthracene system as 5.68J. In both cases there are five non-preferred interactions per fourteen atoms of the unit. Correcting for these, the exchange energy per atom is 0.273J from the anthracene approximation and 0.283J from the phenanthracene approximation.

From what has been said above, it appears that the exchange energy per atom in the sheet is 0.27J, with a possible error of about  $\pm 0.01$ J. The number of neighbouring pairs of atoms per atom is  $3/2$ . Hence from (6)  $\overline{s_i s_j}$  is  $-0.342$ , and from (7) the order of the linkage is 0.45. The order of the linkage in graphite, according to our convention, is therefore 1.45.

According to Pauling, Brockway, and Beach,\* the order of the linkage in graphite is  $4/3$ . Their argument is that there are three non-excited canonical structures for the sheet of monovalent atoms, and any pair of neighbouring atoms are linked in one structure by a bond but are not linked in the other two. Hence the order of the linkage by their rule is  $1/3$ , and in graphite is  $4/3$ . This argument, it seems to us, depends a good deal on intuition. Thus for an infinite sheet of atoms, any excited structure of finite order is surely to a first approximation as important as the non-excited structures. But the number of excited structures of degree  $n$  is proportional to the  $n$ th power of the number of atoms in the sheet. Hence it is very difficult to tell what is the exact value of the fraction  $x$  of equation (4). The difficulty is similar to that encountered in ferromagnetism when allowance is made for non-orthogonality. Just as there, the ratio of the numerator to the denominator is roughly the same as if the first terms only are taken †. Our method of defining the order of the linkage is not open to this objection.

#### HEATS OF FORMATION OF AROMATIC COMPOUNDS WITH FRACTIONAL LINKAGES

From a knowledge of the C—H, C—C, and C=C, bond energies and the order of the linkages in various aromatic compounds involving resonance, the heats of formation may be calculated. We have shown that the order of the linkage in benzene is 1.623. An approximation for the heat of formation of benzene is therefore



Two sets of bond energies are available in the literature, those of

\* 'J. Amer. Chem. Soc.', vol. 57, p. 2705 (1935).

† See, for example, Van Vleck, 'Phys. Rev.', vol. 49, p. 232 (1936).

Sidgwick,\* and those of Pauling and Sherman† Superficially there is a considerable difference between them, due mainly to the uncertainty in the heat of sublimation of solid carbon. However, this heat of sublimation is involved both in the "observed" heats of formation and in the bond energies, and for this reason either set of bond energies gives excellent agreement between "calculated" and "observed" heats of formation. The C—H bond energy is determined from methane, the C—C from ethane, and the C=C from ethylene. Hence if an arbitrary increase  $\Delta$  is made in the assumed heat of sublimation of carbon, the C—H bond changes by  $-\frac{1}{4}\Delta$ , the C—C bond by  $-\frac{1}{2}\Delta$ , the C=C bond by  $-\Delta$ , and the result of the interpolation formula (9) by  $-5.63\Delta$ . The "observed" heat of formation of benzene changes by  $-6\Delta$ . The variation  $\Delta$  has therefore introduced a discrepancy  $0.37\Delta$  between the heat calculated from (9) and the "observed" heat. The difference between the value for the sublimation energy of carbon used by Sidgwick and Bowen and that used by Pauling and Sherman corresponds to a  $\Delta$  of about one electron volt.

TABLE I

Molecule	Heat of formation (S B)		Heat of formation (P S)	
	"Observed"	"Calculated"	"Observed"	"Calculated"
Benzene	51.7	51.9	58.2	58.7
Toluene	63.0	63.2	70.6	71.0
Ethylbenzene	74.3	74.5	82.9	83.3
Propylbenzene	85.6	85.9	95.3	95.6
Naphthalene	81.7	81.9	92.5	93.2

According to Sidgwick and Bowen, the C—H bond energy is 4.070 e-volts, the C—C bond energy is 3.170 e-volts, and the C=C bond energy is 5.443 e-volts‡. The corresponding figures according to Pauling and Sherman are 4.323, 3.65, and 6.56. Table I shows the heats of formation of a few molecules calculated from (9) and the corresponding "observed" heats. The letters S B stand for Sidgwick and Bowen, and P S for Pauling and Sherman. The agreement is seen to be very good, being within 0.2 e-volts with the S B scheme and within 0.5 e-volts with the P S scheme.

\* Sidgwick and Bowen, 'Ann. Rep. Chem. Soc.', p. 110 (1931); Sidgwick, "The Covalent Link in Chemistry," Cornell Univ. Press, 1933.

† Pauling, 'J. Amer. Chem. Soc.', vol. 54, p. 3570 (1932); Pauling and Sherman (J.), 'J. Chem. Phys.', vol. 1, p. 606 (1933).

‡ We prefer electron-volts to kilo-calories as units of energy because the numbers giving the heats of formation of organic molecules do not then run into thousands. 1 e-volt = 23.054 kcal.

Calculations similar to the above may be made for many other molecules. We do not make them because of the difficulty of understanding why they have anything like the accuracy which, in fact, they appear to have

#### THE IONIC DIAMETER OF CARBON AS A FUNCTION OF THE BOND ORDER

We can call the internuclear distance between two linked carbon atoms the ionic diameter of the carbon atom for this particular linkage. The ionic diameter of carbon for single bonds is known from the spacing in

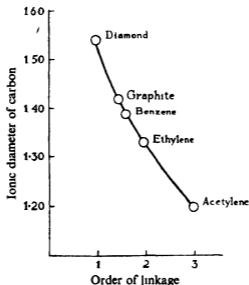


FIG 3—The ionic diameter of carbon as a function of bond order.

diamond to be 1.54 Angstroms. The ionic diameter for double bonds is the internuclear distance in ethylene. Badger\* gives this as 1.37 Angstroms, but we shall show that more recent knowledge of C—H distances requires that this estimate be revised to 1.33 Angstroms. The ionic diameter for triple bonds is the internuclear distance in acetylene, and this is known very accurately from the work of Herzberg, Patat, and Spinks† to be 1.20 Angstroms. We have therefore the ionic diameter of carbon for single, double, and triple bonds. Fig. 3 shows the ionic diameter plotted against the bond order, and a smooth curve is drawn

\* 'Phys Rev,' vol 45, p 648 (1934)

† 'Z Phys,' vol 92, p 87 (1934).

through the single-, double-, and triple-bond points. Two further points can be filled in and both lie beautifully on the curve. They are 1.39 Angstroms for the ionic diameter in benzene\* where the bond order is 1.623, and graphite where the ionic diameter is 1.42 Angstroms† and the bond order is 1.45.

We have now to justify our use of the value 1.33 Angstroms for the internuclear distance in ethylene. The quantities measured by Badger are moments of inertia, and he finds for them 5.7, 27.5, and 33.2 respectively in units  $10^{-40}$  gm cm<sup>2</sup>. Since ethylene is plane, only two of the three are independent, and the greatest, for example, is the sum of the other two. Three coordinates are needed to specify the shape of the molecule, and these are conveniently chosen as the H—C—H angle, the C—H distance, and the C—C distance. If one of these were known the other two could be calculated from the known moments of inertia. In methane the C—H distance is 1.093 Angstroms,‡ and in acetylene it is 1.058 Angstroms§. The C—H distance in ethylene is surely between these limits, and is almost certainly nearer to the methane value. Setting up the equations for the moments of inertia and solving them for the C—C distance and the H—C—H angle, we find that with the C—H distance the same as in acetylene the C—C distance is 1.352 Angstroms and the H—C—H angle 122°, and with the C—H distance the same as in methane the C—C distance is 1.320 Angstroms and the angle 116°. We consider that the most likely values are 1.08 Angstroms for the C—H distance, 1.33 Angstroms for the C—C distance, and 118° for the H—C—H angle.

#### PREDICTED INTERNUCLEAR DISTANCES IN MOLECULES INVOLVING RESONANCE

The molecules considered up to the present are specialized in the sense that each carbon atom entering into the resonance is equivalent. We shall now generalize our treatment to remove this restriction provided that the departures from equivalence are small. As examples we shall consider the following molecules—butadiene, hexatriene, octatetraene, and naphthalene.

*Conjugated Chains*—The *butadiene* molecule  $H_2C \cdot CH = CH \cdot CH_2$  has the four carbon atoms lying in a staggered chain, with a centre of sym-

\* Pauling and Brockway, 'J Chem Phys,' vol. 2, p. 867 (1934)

† Finch and Wilman, 'Proc Roy Soc,' A, vol. 155, p. 345 (1936)

‡ Ginsburg and Barker, 'J Chem Phys,' vol. 3, p. 668 (1935)

§ Herzberg, Patat, and Spinks, 'Z Phys,' vol. 92, p. 87 (1934)

metry at the middle of the central carbon-carbon link. For brevity we may refer to the central link as the "A" link, and to the outer two links as the "B" links. There are two canonical structures for the resonance problem, the more stable having bonds in the B links and none in the A, and the less stable having a bond in the A link and none in the B. Call the exchange integrals for the A link ( $J + a$ ), and those for the B links ( $J + b$ ). Then the secular equation is

$$\begin{vmatrix} -W + \frac{1}{2}J - \frac{1}{2}a + 2b & -\frac{1}{2}W + \frac{1}{2}J + \frac{1}{2}a + b \\ -\frac{1}{2}W + \frac{1}{2}J + \frac{1}{2}a + b & -W + a - b \end{vmatrix} = 0$$

The exact solution of this equation is easily found. However, it will be sufficient for our purpose to solve it under the assumption that  $a$  and  $b$  are small compared with  $J$ , and to retain only first powers of  $a$  and  $b$ . The lower energy level is then

$$W = (3)^{\frac{1}{2}}(J + b) \quad (10)$$

If we refer to the four orbits, beginning at one end, as 1, 2, 3, and 4, then from symmetry arguments 1 and 4 are equivalent, and 2 and 3 are equivalent. From (5) the energy of the most stable state is

$$W = \frac{1}{2}(1 + 4\overline{s_2}, \overline{s_3})(J + a) - (1 + 4\overline{s_1}, \overline{s_2})(J + b)$$

Comparing this with (10), we obtain

$$\overline{s_2}, \overline{s_3} = -1/4, \quad \overline{s_1}, \overline{s_2} = \overline{s_3}, \overline{s_4} = -0.683$$

Hence from (7) the order of the A linkage in the resonance problem is 0.333, and the order of the B linkage is 0.911. Adding 1.0 for the localized carbon-carbon single bonds, the A linkage in butadiene is of order 1.33, and the B linkage of order 1.91. The length of the A link from fig. 3 is thus 1.43 Angstroms, and the length of the B link 1.34 Angstroms. These agree exactly with the results given by Lennard-Jones in paper I.

Consider now the *hexatriene* molecule. Once again we shall label the links from the centre as A, B, and C. There are five canonical structures, one of which is unexcited, three are singly excited, and one is doubly excited. The approximations made by Pauling and Sherman\* are that all exchange integrals between neighbours are equal, that singly excited structures occur with equal weight, and that the doubly excited structure can be neglected. With these approximations the energy and normalized wave function for the ground state are

$$W_0 = 2.482J \quad \psi_0 = 0.674 \psi_1 + 0.197 (\psi_{II} + \psi_{III} + \psi_{IV}).$$

\* 'J. Chem. Phys.', vol. 1, p. 679 (1933).

Writing the exchange integrals for the A link as  $(J + a)$ , for the B links as  $(J + b)$ , and for the C links as  $(J + c)$ , in which  $a$ ,  $b$ , and  $c$  are small, the energy  $W$  by first order perturbation theory is  $\int \psi_e H \psi_e dv$ , where  $H$  is the Hamiltonian. We find

$$W = 2.482J + 0.709a + 0.123b + 1.650c$$

Proceeding from this equation as in the analogous case of butadiene, the order of the A linkage in hexatriene is 1.806, the B linkage is 1.374, and the C linkage is 1.883. These give the length of the A link as 1.36, of the B links as 1.42, and of the C links as 1.35, the units being Angstroms.

There are four types of linkage in the *octatetraene* molecule. In harmony with the notation used for butadiene and hexatriene, we label them from the centre as A, B, C, and D. Assuming that all exchange integrals between neighbours are equal, that the six singly excited structures occur with equal weight, and that higher excited structures can be neglected, the energy and wave function of the lowest state from the work of Pauling and Sherman can be shown to be

$$W = 3.22J, \quad \psi = 0.556\psi_I + 0.145(\psi_{II} + \psi_{III} + \psi_{VII})$$

Introducing the modified exchange integrals  $(J + a)$ ,  $(J + b)$ ,  $(J + c)$  and  $(J + d)$ , the energy works out at

$$W = 3.22J + 0.19a + 1.29b + 0.10c + 1.64d.$$

The order of the A linkage in octatetraene is 1.46, of the B linkage is 1.76, of the C linkage is 1.37, and of the D linkage is 1.88. The lengths in Angstroms are 1.41, 1.37, 1.42, and 1.35 respectively.

TABLE II

Molecule	A linkage		B linkage		C linkage		D linkage	
	Order	Length	Order	Length	Order	Length	Order	Length
Butadiene	1.33	1.43	1.91	1.34	—	—	—	—
Hexatriene	1.81	1.36	1.37	1.42	1.88	1.35	—	—
Octatetraene	1.46	1.41	1.76	1.37	1.37	1.42	1.88	1.35

Table II gives a summary of our results on the three conjugated double-bond systems considered above. It will be seen that the old picture of alternate single and double links is decidedly in error. The agreement between the links calculated by our method and those calculated by the method of Lennard-Jones, Paper I, is excellent, the discrepancy never exceeding 0.02 Angstrom. Considerable confidence may therefore

be placed in these estimates provided that no modification is necessary later for the internuclear distance in ethylene

As a last example of conjugated chain molecules, we consider the very long chain  $\text{H}_2\text{C}=\text{CH}-\text{CH}=\text{CH}-\text{CH}=\text{CH}_2$ . If end effects are neglected, all exchange integrals between neighbours in the resonance problem are equal. To calculate the exchange energy per atom of the chain, a method of approximation may be adopted similar to that used with graphite. Thus we divide up the chain first of all into fours and base our approximations on the four-electron resonance problem of butadiene. The energy of the four preferred interactions is 1.732J, adding to this -0.5J for the non-preferred interaction, we obtain as the energy per four atoms of the chain 1.232J. Hence the energy per atom according to this approximation is 0.31J. Proceeding to the approximation based on hexatriene, the energy of the six preferred interactions is 2.482J; adding -0.5J for the non-preferred interaction and dividing by six gives the energy per atom of the chain as 0.33J. Similarly, the approximation based on octatetraene gives the energy of the eight preferred interactions as 3.22J and the energy per atom of the chain as 0.34J. The three approximations which have just been made must be successively better, we see that the true energy of the chain per atom must lie very close to 0.35J.

The order of the linkage in the resonance problem from (8) is therefore 0.567. Adding unity for the single C—C bonds, the linkage in the long chain is of order 1.567. This is slightly less than that in benzene (1.623), but greater than that in graphite (1.45). The internuclear distance in the long chain from fig. 3 is 1.38 Å, a result agreeing exactly with that of Lennard-Jones in Paper I.

We can even predict end effects by our method, for it cannot matter to any measurable extent whether the end link is part of the long chain or part of the octatetraene molecule. Thus the outside link is more like a double bond, and the next link is more like a single bond, than are the others. Similar alternation persists further in, but dies out rapidly. From an inspection of the figures for octatetraene, the lengths of the links in the long chain in Ångströms, proceeding inwards from one end, are 1.35, 1.42, 1.37, 1.39, 1.38, ..., and end effects therefore have little influence on links four or more from the end.

*Naphthalene*—We conclude this section by evaluating the order of the linkages in the naphthalene molecule. The resonance problem is that of ten orbits arranged in two equal hexagons with a side in common. There are forty-two canonical structures, of which three are unexcited, sixteen are singly excited, twenty are doubly excited, and three are triply excited.

Pauling and Wheland,\* and Sherman,† have shown that the energy of the most stable state is 4.04J. There are in all 11 interactions between neighbours. Hence the average order of the linkage from (6) and (7) is 0.578. Adding 1 for the single bonds of naphthalene, the average order of the carbon-carbon linkage is 1.578, and the average carbon-carbon distance from fig. 3 is 1.40 Angstroms. Robertson‡ finds from X-ray measurements that the mean carbon-carbon distance in naphthalene is 1.41 Angstroms. The agreement is quite satisfactory.

The order of the individual linkages may be calculated as follows. According to Pauling and Wheland, it is a good approximation in the resonance problem to neglect doubly- and triply-excited structures. When this is done, the energy and normalized wave function of the ground state are

$$W = 3.979J, \quad \psi = 0.240 [\psi_I + 0.851 (\psi_{II} + \psi_{III}) + 0.303 (\psi_{IV} + \psi_{VIX})] \quad (11)$$

Let us call the various linkages of types A, B, C, and D as shown in fig. 4. Writing  $(J + a)$  for the exchange integral in the A link, and

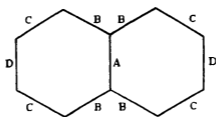


FIG. 4

similarly for the other links, we have for the energy by first order perturbation theory  $W = \int \psi^2 H d\tau$ , and this leads directly to

$$W = 3.979J + 0.150a + 1.097b + 2.143c + 0.590d$$

Proceeding exactly as with the similar equations for butadiene, we find that the A link in naphthalene is of order 1.433 and length 1.42, the B links are of order 1.516 and length 1.40, the C links are of order 1.690 and length 1.38, and the D links are of order 1.530 and length 1.40, the units of length being Angstroms. The lengths predicted by Pauling,

\* 'J. Chem. Phys.', vol. 1, p. 362 (1933).

† 'J. Chem. Phys.', vol. 2, p. 488 (1934).

‡ 'Proc. Roy. Soc. A', vol. 142, p. 674 (1933).

Brockway, and Beach\* are 1.40, 1.44, 1.39, and 1.42 Angstroms respectively.

The order of the linkages and their lengths may also be calculated on the assumption that all excited canonical structures may be neglected. With this approximation, the orders and lengths, given in brackets, are respectively for A, B, C, and D, 1.60 (1.39), 1.37 (1.42), 1.78 (1.36), and 1.37 (1.42). It is not obvious, however, why it should be a good approximation to neglect the excited structures. Thus, for example, in evaluating  $W$  by first order perturbation theory from the wave function (11), the diagonal element  $(0.240)^2 \int \psi_1^2 H dv$  arising from the most stable canonical structure is only 0.116J, whereas the term arising solely from the excited structures, namely  $(0.0728)^2 \int [\psi_{IV} + \psi_{XIV}]^2 H dv$  is as large as 1.349J. In view of the fact that first excited structures, because of their number, are vital in a proper evaluation of the energy, it is necessary to examine whether the second excited structures are also important. The error caused by neglecting them is apparently of the same order of magnitude as that due to the assumption that all first excited structures occur with equal coefficient, and is therefore properly neglected to our degree of approximation.

The author wishes to express his thanks to Pembroke College, Cambridge, for the award of the Stokes Studentship, during the tenure of which the work described in this paper was carried out.

#### SUMMARY

The most satisfactory way of interpreting the conclusions of the electron-pair theory of "resonance" is to say that linkages involving resonance are of fractional order. A convention is suggested by which the exact order of linkages may be calculated. The essential feature is that it gives a direct relation between the bond order and the bond energy. Thus, for example, the bond order in benzene is 1.623, and the excess of this figure over 1.5 measures the effect of the resonance. Once the bond order has been determined, the bond energy may be estimated by interpolating between single- and double-bond energies. The heats of formation of hydrocarbons with resonance may in this way be found as easily as those of ordinary molecules. Similar interpolation may be made for other properties, such as internuclear distance, which are closely connected with

\* 'J. Amer. Chem. Soc.', vol 57, p 2705 (1935).

bond energy From the known internuclear distances in compounds containing carbon, the dependence of the ionic diameter of carbon on the bond order may be found (*see* fig 3) Using the theory to evaluate the bond orders in the conjugated systems butadiene, hexatriene, octatetraene, naphthalene, and the infinite chain, the various internuclear distances can then be predicted The results are appreciably different from those expected on the classical idea of alternating single and double bonds

---

## Kinematics, Dynamics, and the Scale of Time

By E. A. MILNE, F.R.S.

(Received 28 August, 1936)

### OUTLINE OF THE ARGUMENT

1—In two previous papers\* the laws of dynamics and the Newtonian approximation to the law of gravitation have been derived on a purely kinematic basis That is, they have been deduced rationally, starting from the individual observer's awareness of a temporal sequence for events at himself, and from his assigning of measures of distance and epoch by means of light-signals and appropriately rated and synchronized clocks, explicit procedure for this rating and synchronization having been stated in terms of the observer's own experiences No appeal was made in the derivations to any empirical laws of dynamics or gravitation, or even to the principle of relativity or to the principle of the constancy of the velocity of light Recourse to these last two was avoided by careful statement of exactly what is meant by "uniform velocity", by introduction of the notion of *kinematic equivalence*† Laws of dynamics and gravitation emerged by embodying in analysis the programme outlined by Mach, according to which all the matter in the universe is relevant

\* "On the Foundations of Dynamics," 'Proc Roy Soc,' A, vol 154, p 22 (1936) (cited hereafter as I), "The Inverse Square Law of Gravitation," *ibid*, vol 156, p 62 (1936), (cited as II) These papers are sequels to the author's "Relativity, Gravitation, and World-Structure" (1935), cited as W.S. A purely kinematic proof of a certain fundamental relation  $G(\xi) \equiv -1$  has since been obtained

† See W.S., chap 2, II, § 5a

to the description of dynamical laws of nature and must necessarily be taken into account in describing the motion even of a free particle, this programme was carried out by introducing the notion of *statistical equivalence*,\* which amounts to a definition of the systems of moving particles proposed for consideration (as affording a representation of the universe) as those whose motion and distribution satisfy what has been called the *cosmological principle*† It is particularly to be noticed that the cosmological principle is not a concealed law of nature but is simply a definition defining the subject of study, just as in any gravitational problem we must define what we are discussing—one-body problem, three-body problem, etc

The reason that, in systems defined by means of the cosmological principle, not only no recourse to empirical laws of nature is needed but regularities playing the part of laws of nature can be derived, is that essentially the cosmological principle is a mode of specifying an extrapolation of certain kinds of *phenomena* If laws of nature are supposed to be derived as inductive generalizations from observed phenomena, then it is preferable to extrapolate phenomena and derive the corresponding laws rather than to extrapolate laws and predict phenomena We have no more warrant for extrapolating laws than for extrapolating the phenomena from which they have been learned We have no justification for believing in world-wide principles as a sort of super-authority. But

\* W S, chap 3, in particular § 64, and II, § 5b, less precise enunciations were given earlier in 'Nature,' vol 130, p 9 (1932), and 'Z Astrophys,' vol 6, p 1 (1933).

† Robertson has claimed ('Astrophys. J,' vol 83, p 270 (1936)) to have enunciated the same principle earlier That there is something in common between his statements and mine is obvious, but his enunciations always lack the essential element of precision and clarity In his "Relativistic Cosmology" ('Rev Mod Phys,' vol 5, p 65 (1933), he quotes Weyl ('Phys Z,' vol 24, p 230 (1923), and 'Phil Mag,' vol. 9, p 936 (1930)), but in neither his own nor in Weyl's papers was I able to find any clear statement equivalent to the cosmological principle Robertson now cites his paper, 'Proc nat Acad Sci Wash,' vol 11, p 822 (1929), here the enunciation takes the form that an observer must be "unable to detect any difference between his observations and those of any *contemporary* observer" (my italics), but he states no test by means of which an observer can ascertain the epoch of his experiences which is contemporary with a given epoch at another observer, Robertson failed, in fact, to attend to the rating and synchronization of clocks, which is carried out by prior analysis of kinematic equivalence Further, Robertson required that the observed distribution should "satisfy Einstein's field equations for some suitable choice of the matter-energy tensor" This alone is sufficient to show how far removed from the idea of the cosmological principle were Robertson's ideas of 1929, for in my application of the principle I dispense with any appeal to Einstein's field equations Lastly, Robertson has so far not noticed the difference between the notion of kinematical equivalence and that of statistical equivalence

when the extrapolated phenomena are fitted together so as to make a self-consistent universe, it is then found that no *laws* need be assumed at all, the actual laws "obeyed" can be inferred simply from the definitions of the systems contemplated. We begin with local phenomena, which are shown to be possible and self-consistent, and we can end with local laws, and whether the actual universe follows the details of the extrapolation is quite immaterial. We simply require that local phenomena and local laws be such that they are capable of being fitted together to form a complete universe.

The rôle of observation is then to *identify* in nature entities corresponding to those mentioned in the original definitions. Whether the laws are "exact", why they are "simple", and how they come "to hold good"—the three questions that can be asked about any "law of nature"—are questions to which the answers are then immediate. The laws of dynamics are exact and simple, and hold good, because they are logical inferences from axiomatic definitions, obtained by a fairly short deductive train of thought. It is thus no longer necessary to appeal, as a warrant for a belief in the "truth" of these laws of nature, to the so-called "principle of induction", which has never been satisfactorily stated, much less demonstrated.\* These laws of nature arise naturally and inevitably, as do theorems in a geometry, and, as in geometry, observation vindicates not the truth of the theorems (which depend for their validity only on the logical self-consistency of the original axioms and the absence of errors from the reasoning connecting the theorems with the axioms) but the applicability of the axiomatic definitions to the things occurring in nature.

2—Our previous papers now make possible the discussion of a "semi-isolated" dynamical system. By a "semi-isolated" system we mean one for which the individual "influences" (to use for convenience the language of the theory of causation) of separate external systems may be disregarded, but for which the general effect of the general distribution of matter in the universe, appropriately "smoothed out", must necessarily be taken into account. In other words, we take into account the general "gravitational field" of the parts of the cosmos external to the system under discussion. Successive examples of a "semi-isolated" system are offered by a single extra-galactic nebula, a single solar system or globular cluster, a single planet. These require handling in different ways, but it will be shown to be possible to derive for such systems the

\* The present point of view is thus somewhat removed from that of Jeffreys in his book "Scientific Inference."

classes of theorems conveniently called "energy theorems", "virial theorems", and "angular momentum theorems". Such theorems are derived by taking the equation of motion of a single particle, operating scalarly or vectorially with the position-vector or velocity-vector of the particle, and summing for a number of particles. The theorems we derive from our rational dynamics, taking into account the "pull" of the substratum or smoothed-out external universe, appear at first sight to differ from the corresponding theorems of Newtonian dynamics, more especially in the explicit occurrence of the time  $t$ , reckoned as measured from the natural origin of time. This same time  $t$  has also occurred in our formulation of the law of gravitation, in that  $\gamma$ , the coefficient playing the part of the Newtonian constant of gravitation, has appeared to be proportional to  $t$ .

3—The essential step of the present paper is then to show that these theorems, together with the original equation of motion, can all be thrown into strictly Newtonian form by transferring the time-variable from  $t$  to  $\tau$ , where

$$\tau = t_0 \log (t/t_0) + t_0, \quad (\text{A})$$

$t_0$  being the present value of the age of the universe at ourselves, reckoned on the  $t$ -scale,  $\gamma$  becomes a constant  $\gamma_0$ . This is simply equivalent to a renumbering of clock graduations from  $t$  to  $\tau$ , and as in the present formulation of kinematics and dynamics all physical quantities—lengths, velocities, forces, energies, moments, Doppler shifts, etc.—are determined fundamentally by time-measures, the measures of all these quantities must be converted from the  $t$ -scale to the  $\tau$ -scale. It is found that when  $t$  is transformed to  $\tau$  explicitly whenever it occurs in the equations of motion and derived theorems, the various other physical quantities all appear in the transformed equations in their  $\tau$ -measures calculated according to Newtonian dynamics. For example, if  $\mathbf{F}$  is the measure of a force on the  $t$ -scale, the force emerges in the transformed equations as  $(t/t_0)\mathbf{F}$ , but this quantity  $(t/t_0)\mathbf{F}$  is precisely the measure  $\Phi$  of the same force on the  $\tau$ -scale. The equation of motion of a particle then appears in the form  $m d^2\Pi/d\tau^2 = \Phi$ , where  $\Pi$  is the position-vector on the  $\tau$ -scale.

4—If, then, we adopt from empirical experience the Newtonian forms of the equations of motion and the derived theorems, that is, if we take these forms as *given*, it follows that the variable  $\tau$  introduced above is the time of dynamical experience, whilst the kinematic variable is  $t$ . We perform an act of identification, and identify the variable  $\tau$  as the time

kept by dynamical time-keepers, such as a swinging pendulum, a rotating earth, or a revolving planet, to the order of accuracy to which our approximations relate \* A detailed discussion of each of these species of time-keeper will be given

5—This result seems to be of some importance We have that at the present epoch  $\tau_0 = t_0$  and  $(d\tau/dt)_{t=t_0} = 1$ , so that the kinematic and dynamical scales are indistinguishable in our present experience But where we have experience extending over large tracts of time, as in the coils exhibited by spiral nebulae, or as in the tracing backwards of the history of the solar system, serious differences result In particular, the epoch of "creation"  $t = 0$  on the kinematic scale is measured by  $\tau = -\infty$  on the dynamical scale This is simply a way of saying that an infinite number of a given type of dynamical event has occurred since "creation", for example, the period of oscillation of a simple pendulum, say  $s$  on the kinematic scale and  $\sigma$  on the dynamical scale, is given by  $s = (t/t_0) \sigma$ , where  $\sigma$  is taken as constant Thus on the kinematic scale the period shortens as we recede towards  $t = 0$ , so much so that an infinite number of swings is required to reach  $t = 0$  The epoch  $t = 0$  is, in fact, dynamically inaccessible in time, just as the absolute zero of temperature is thermodynamically inaccessible This is of fundamental evolutionary significance That the "age" of the solar system given by radioactive rocks is approximately equal to the "age" of the universe given by the recession of the nebulae,  $te$ , is equal to the kinematic value of the present epoch, is evidence for the view that a radioactive clock keeps kinematic time  $t$ , not dynamical time  $\tau$ , by rather more complicated arguments, which will be given later, it will be shown that likewise an atomic clock keeps kinematic time,  $te$ , emits a frequency whose measure  $\nu_0$  in kinematic time is a constant This foreshadows a fundamental difference between atomic and nuclear dynamics and macroscopic dynamics, a difference which is the more plausible in that we may expect atoms to be governed by "probability" time, which in turn we should expect to be identical with radioactive kinematic time Again, as a by-product, we resolve the old controversy concerning the "short" or radioactive time-scale for the universe and the "long" or dynamical time-scale, either is valid, according to circumstances Lastly we resolve

\* In this paper, on the whole, I work on the Newtonian plane of approximation, to bring out the essential elements of the situations analysed The departures from this order of approximation which are observable on the large scale will be treated in a separate paper, where it will be shown, for example, that the spiral appearance of the great nebulae is an immediate consequence of the ideas here developed.

the controversy as to whether the red-shifts in the spectra of the extragalactic nebulae imply *motion* or not; the answer is that when lengths or distances are measured on the kinematic scale the nebulae are receding, but when they are measured on the dynamical scale the nebulae are stationary. (A Doppler shift is known to be time-invariant under any transformation of time-scale.\*) An ideal length-measure, rigid on the dynamical scale, is not rigid† on the kinematic scale

6—It will be seen that we thus solve a question raised by de Sitter and we are led, in fact, rationally to his conjectural solution. He wrote:‡ “We can easily relegate the catastrophe (of creation) to the time minus infinity by introducing another time-variable, e.g.,  $cT = \kappa \log y$  which will make  $y = 0$  for  $T = -\infty$ . If for  $\kappa$  we take the present value of  $R_0$  we will have at the present moment  $dT/dt = 1$ . There is nothing in our experience of the physical world that would enable us to distinguish between the times  $T$  and  $t$ . We do not know which of these times it is that we use as independent variable in the equations of celestial mechanics, or by which we measure the rate of progress of radioactive disintegration, or of the evolution of a star, or of any other physical process.” De Sitter overstated the position in saying that there is nothing in our experience of the physical world that would enable us to distinguish between the times  $\tau$  and  $t$ , for it is, in fact, possible to *derive* the laws of dynamics rationally from kinematic considerations alone, without recourse to experience, and then by comparison of these with the empirical laws to identify  $\tau$  and not  $t$  as the independent variable in the empirical laws. It must be realized that the transformation (A) above is the only one which will transform the theoretically derived equation of motion into Newtonian form. It will be seen that we here employ observation in one of its fundamental rôles,§ namely that of identifying in nature an entity which in a different form has appeared in the axiomatic definitions, just as in geometry we use the observed fact that a triangle has its angles adding up to two right angles to identify the two-spread in which it lies as a Euclidean plane. Once the identification is effected, we are entitled

\* Whitrow and Walker, ‘Quart. J. Math.’ (Oxford), vol. 6, p. 257 (1935).

† This gives a complete answer to the criticisms of my procedure made by “A. S. E.” in ‘Nature,’ 27 April (1935), p. 635. Had these investigations not been based on an analysis of the notion of length by means of light-signals, the present results could never have been reached.

‡ “The Astronomical Aspect of the Theory of Relativity”, ‘Univ. Calif. Publ. Math.’ vol. 2, p. 185 (1933).

§ The other fundamental rôle of observation is, of course, that of discovery.

to a belief in the validity of the theorem or law concerned, but it is its relevance to nature, not its truth, which is established by observation.

7—Incidentally, we put the Newtonian laws of dynamics on a purely deductive basis. Our work thus stands in marked contrast to the ideas expressed in Robertson's recent papers,\* where he considers that the deductions from a purely kinematic basis are limited, in some unspecified way, by "the imposition of physical law", whatever that may mean, and that kinematics needs supplementing by some "theory" of gravitation.

General relativity is a fusion of kinematic light-signalling with the Einstein generalizations of the Newtonian laws of dynamics. The former employs the time  $t$ , the latter the time  $\tau$ . Since  $(d\tau/dt)_{t=t_0} = 1$ , general relativity mechanics probably correctly describes all present occurrences, but will require reconsideration when the difference between  $\tau$  and  $t$  becomes appreciable. Hence its inability to deal satisfactorily with spiral nebulae or with the universe as a whole.

8—In what follows, in order not to force the argument, we shall begin by treating the dynamics of a "semi-isolated" system in terms of the variable  $t$  only. The necessity of transforming from  $t$  to  $\tau$ , in order to get agreement with experience, then emerges naturally of itself. It would have been possible to give the fundamental transformation of the original equation of motion at once, but as this is suggested only when the virial theorem has been formulated, I have preferred to adopt the former procedure.

#### THE DYNAMICS OF A "SEMI-ISOLATED" SYSTEM

##### (a) *The Energy Theorem*

9—We take as origin  $O$  any fundamental particle of the substratum or smoothed-out universe. The substratum has then a distribution of particle-density  $n(\mathbf{P}, t) dx dy dz$  given by

$$n(\mathbf{P}, t) = \frac{Bt}{c^3 (t^2 - \mathbf{P}^2/c^2)^{3/2}}, \quad (1)$$

where  $t$  is the conventional epoch at  $P$  measured by the clock in  $O$ 's possession. (The method of rating and synchronizing the clocks possessed by  $O$  and  $P$  on a kinematic basis from the property  $O \equiv P$  has been given in detail elsewhere †) The velocity-distribution of the substratum (1) is given by

$$\mathbf{V} = \mathbf{P}/t. \quad (2)$$

\* 'Astrophys J,' vol 83, p 190 (1936)

† W S, chap 2

In the presence of the substratum (1) and (2), the equation of motion of an additional particle of mass  $m$ , moving under an external force  $\mathbf{F}$ , has been shown\* to be

$$\frac{1}{Y^4} \frac{d}{dt} \left[ m \xi^4 \frac{\mathbf{V}}{Y^4} \right] = \mathbf{F} - m \xi^4 \left( \mathbf{P} - \mathbf{V} \frac{Z}{Y} \right) \frac{1}{X}, \quad (3)$$

where

$$X = t^2 - \mathbf{P}^2/c^2, \quad Y = 1 - \mathbf{V}^2/c^2, \quad Z = t - \mathbf{P} \cdot \mathbf{V}/c^2, \quad \xi = Z^2/XY$$

In (3) the second term on the right-hand side represents the "effect", on the rate of change of momentum, of the general "smoothed-out" distribution of matter in the universe, *i.e.*, of the substratum. The vector  $\mathbf{F}$  includes any applied force and any gravitational force over and above that due to the substratum, *i.e.*, it includes any effect of local aggregations of matter.

For  $|\mathbf{P}|/ct$  small and  $|\mathbf{V}|/c$  small, *i.e.*, within a given galaxy and for low velocities, (3) reduces to†

$$m \frac{d\mathbf{V}}{dt} = \mathbf{F} - m \frac{\mathbf{P} - \mathbf{V}t}{t^3}. \quad (4)$$

In this dynamics, equation (4) with  $\mathbf{F}$  put equal to zero replaces Newton's First Law of Motion, and (4) itself replaces the Second Law. The equation of motion (3) and its approximate form (4) have been derived *rationality* in I, solely as properties of motion in the substratum (1) and (2) derivable from its definition, without appeal to any empirical laws of dynamics‡. Our object is to compare the properties of a "semi-isolated" system obtained from (4) with the empirical Newtonian properties.

10—We apply (4) to each one of a set of particles of masses  $m_i$ , of position-vectors  $\mathbf{P}_i$  and velocities  $\mathbf{V}_i$ . It has been shown in I that kinetic energy and rate of working of external forces must be calculated using the velocity  $(\mathbf{V}_i - \mathbf{P}_i/t)$  of a particle  $P_i$  relative to its immediate cosmical

\* I, equation (43)

† It would only complicate the succeeding analysis unnecessarily to work out the relativistic forms of the theorems which follow, at this stage, the essential thing is to gain insight into the meaning of the approximation (4)

[Note added in proof, 9 December, 1936—The relativistic forms of the theorems here given have since been worked out. In all cases the  $(t, \tau)$  transformation removes the explicit appearance of the gravitational field of the substratum]

‡ As remarked above, the form of the acceleration-function in a substratum, namely  $G(\xi) \equiv -1$  which is required to establish (3), can now be derived purely kinematically. The proof of this will be published elsewhere

surroundings in the substratum, which have a velocity  $\mathbf{P}_s/t$ . We therefore define symbols  $T$  and  $dW/dt$  by

$$T = \sum_i \frac{1}{2} m_i (\mathbf{V}_i - \mathbf{P}_s/t)^2, \quad (5)$$

$$\frac{dW}{dt} = \sum_i \mathbf{F}_i \cdot \left( \mathbf{V}_i - \frac{\mathbf{P}_s}{t} \right) \quad (6)$$

The symbol  $dW/dt$  denotes the rate of working of the external forces in pushing the particles of the system through the substratum. Then from (4) we have

$$\begin{aligned} \frac{dW}{dt} &= \sum_i m_i \left( \mathbf{V}_i - \frac{\mathbf{P}_s}{t} \right) \cdot \left( \frac{d\mathbf{V}_i}{dt} + \frac{\mathbf{P}_s}{t^2} - \frac{\mathbf{V}_i}{t} \right) \\ &= \frac{dT}{dt} \end{aligned} \quad (7)$$

Hence  $dW/dt$  is the time-differential coefficient of a function  $W$  of the positions and velocities, and we have

$$T - W = \text{const} = E, \quad (8)$$

say. This is the approximate form of a theorem already established relativistically in I, §§ 22-24

(b) *The Virial Theorem*

11—Define symbols  $I$  and  $U$  by

$$I = \sum_i m_i \mathbf{P}_i^2, \quad (9)$$

$$U = \sum_i \mathbf{F}_i \cdot \mathbf{P}_i \quad (10)$$

$U$  is the virial of the external forces. From (4) we have

$$U = \sum_i m_i \frac{d\mathbf{V}_i}{dt} \cdot \mathbf{P}_i + \sum_i m_i \frac{\mathbf{P}_i^2}{t^2} - \sum_i m_i \frac{\mathbf{P}_i \cdot \mathbf{V}_i}{t}.$$

By the usual virial transformations,\* this can be put in the form

$$U = \frac{1}{2} \frac{d^2 I}{dt^2} - \frac{3}{2} \frac{1}{t} \frac{dI}{dt} + 2 \frac{I}{t^2} - 2T \quad (11)$$

This suggests making the transformation

$$I = (t^3/t_0^3) I, \quad (12)$$

\* Cf Clausius, 'Phil Mag,' ser 4, vol 40, p 123 (1870)

where  $t_0$  is the present value of  $t$ . Then (11) becomes

$$U = \frac{1}{2} \frac{1}{t_0^3} \left[ t^3 \frac{d^2 i}{dt^2} + t \frac{di}{dt} \right] - 2T \quad (13)$$

This is the theorem of the virial in this dynamics

12—A system for which  $i = \text{const}$  may be called a “steadily expanding” system. Such a system is the analogue in this dynamics of the “steady state” of a classical system. For  $i = \text{const}$  we have by (13)

$$U + 2T = 0 \quad (14)$$

13—*Calculation of the Virial when the Forces are Gravitational*—It was shown in II that in the present dynamics local gravitational forces may be calculated as in Newtonian gravitation, provided the “constant” of gravitation  $\gamma$  is taken to be proportional\* to  $t$ . We may therefore put

$$\gamma = \gamma_0 (t/t_0), \quad (15)$$

where  $t_0$  is the present epoch,  $\gamma_0$  the present value of the Newtonian constant, calculated† as in I and II from the mass  $M_1$  of the fictitious homogeneous universe‡. We have then

$$\mathbf{F}_i = -\gamma_0 \frac{t}{t_0} \sum_k \frac{(\mathbf{P}_i - \mathbf{P}_k) m_i m_k}{|\mathbf{P}_i - \mathbf{P}_k|^3}, \quad (16)$$

whence if the external forces are wholly gravitational

$$\begin{aligned} U &= -\gamma_0 \frac{t}{t_0} \sum_i \sum_k \frac{\mathbf{P}_i \cdot (\mathbf{P}_i - \mathbf{P}_k) m_i m_k}{|\mathbf{P}_i - \mathbf{P}_k|^3} \\ &= -\gamma_0 \frac{t}{t_0} \sum'_{i,k} \frac{m_i m_k}{|\mathbf{P}_i - \mathbf{P}_k|} \\ &= -\phi, \end{aligned} \quad (17)$$

say, where  $\phi$  is the Newtonian potential energy with  $\gamma \propto t$ . Further, under the same conditions

$$\begin{aligned} \frac{dW}{dt} &= -\gamma_0 \frac{t}{t_0} \sum_i \sum_k \frac{(\mathbf{P}_i - \mathbf{P}_k) \cdot (\mathbf{V}_i - \mathbf{V}_k)/t}{|\mathbf{P}_i - \mathbf{P}_k|^3} m_i m_k \\ &= -\gamma_0 \frac{t}{t_0} \sum'_{i,k} \frac{(\mathbf{P}_i - \mathbf{P}_k) \cdot [(\mathbf{V}_i - \mathbf{V}_k) - (\mathbf{P}_i - \mathbf{P}_k)/t]}{|\mathbf{P}_i - \mathbf{P}_k|^3} m_i m_k \\ &= \frac{d}{dt} \left[ \gamma_0 \frac{t}{t_0} \sum'_{i,k} \frac{m_i m_k}{|\mathbf{P}_i - \mathbf{P}_k|} \right] \\ &= \frac{d\phi}{dt} \end{aligned} \quad (17')$$

\* The physical meaning of this variation with  $t$  will be apparent later.

† I, p. 43, II, p. 27.

‡ The formula is  $\gamma_0 = c^2 t_0 / M_1$ .

We may accordingly take  $W = \phi$  in this case, and the theorems of energy and the virial then become

$$T - \phi = E \quad (18)$$

$$2T - \phi = \frac{1}{2} \frac{1}{t_0^2} \left[ t^2 \frac{d^2 t}{dt^2} + t \frac{dt}{dt} \right] \quad (19)$$

It follows that in a steadily expanding system ( $i = \text{const}$ ) we have

$$T = \text{const} = -E, \quad \phi = \text{const} = -2E, \quad (20)$$

and  $E$  is essentially negative

### (c) Angular Momentum Theorems

14—If  $\mathbf{\Gamma}$  is the moment about  $O$  of the system of the external forces, we have

$$\mathbf{\Gamma} = \sum_i \mathbf{P}_i \wedge \mathbf{F}_i \quad (21)$$

If  $\mathbf{H}(O)$  is the angular momentum of the system about  $O$  then

$$\mathbf{H}(O) = \sum_i \mathbf{P}_i \wedge m_i \mathbf{V}_i \quad (22)$$

Hence by (4),

$$\begin{aligned} \mathbf{\Gamma} &= \sum_i \mathbf{P}_i \wedge m_i \left[ \frac{d\mathbf{V}_i}{dt} + \frac{\mathbf{P}_i - \mathbf{V}_i t}{t^2} \right] \\ &= \frac{d\mathbf{H}(O)}{dt} - \frac{\mathbf{H}(O)}{t} \end{aligned} \quad (23)$$

If the external forces always pass through  $O$  (case of central forces), or if they occur in equal and opposite pairs (Newton's Third Law), then  $\mathbf{\Gamma} = 0$ , and the solution of (23) is

$$\mathbf{H}(O) = \mathbf{A}t, \quad (24)$$

where  $\mathbf{A}$  is a vector-constant. Thus angular momentum in this dynamics increases secularly with the time

15—If we define  $\mathbf{H}(P_0)$  to be the angular momentum about some particle  $P_0$  whose motion is known, a similar theorem may be proved about  $\mathbf{H}(P_0)$ . It will be sufficient to consider a single particle  $P$  of mass  $m$  in motion about the particle  $P_0$  of mass  $m_0$ ;  $P_0$  is not necessarily a fundamental particle (This case corresponds to a planet moving round a sun.) Then we may suppose the particle  $P_0$  to be acted on by a force

$m_0 \mathbf{f} - \mathbf{R}$ , the particle  $P$  by a force  $m \mathbf{f} + \mathbf{R}$ ; the force  $\mathbf{f}$  per unit mass then represents the local field,  $\mathbf{R}$  the interaction.\* We have then

$$m_0 \frac{d\mathbf{V}_0}{dt} = m_0 \mathbf{f} - \mathbf{R} - m_0 \frac{\mathbf{P}_0 - \mathbf{V}_0 t}{t^2},$$

$$m \frac{d\mathbf{V}}{dt} = m \mathbf{f} + \mathbf{R} - m \frac{\mathbf{P} - \mathbf{V} t}{t^2},$$

$$\mathbf{H}(\mathbf{P}_0) = (\mathbf{P} - \mathbf{P}_0) \wedge m(\mathbf{V} - \mathbf{V}_0)$$

Hence

$$\frac{d\mathbf{H}(\mathbf{P}_0)}{dt} = m(\mathbf{P} - \mathbf{P}_0) \wedge \left[ \left( \frac{1}{m} + \frac{1}{m_0} \right) \mathbf{R} - \frac{\mathbf{P} - \mathbf{V} t}{t^2} + \frac{\mathbf{P}_0 - \mathbf{V}_0 t}{t^2} \right]$$

If the interaction  $\pm \mathbf{R}$  is along the line joining the two particles, then

$$(\mathbf{P} - \mathbf{P}_0) \wedge \mathbf{R} = 0$$

Accordingly

$$\frac{d\mathbf{H}(\mathbf{P}_0)}{dt} = \frac{(\mathbf{P} - \mathbf{P}_0) \wedge m(\mathbf{V} - \mathbf{V}_0)}{t} = \frac{\mathbf{H}(\mathbf{P}_0)}{t},$$

whence as before

$$\mathbf{H}(\mathbf{P}_0) = \mathbf{A} t \quad (25)$$

16—The angular momentum of a system of particles about their centre of mass follows a similar law. Here

$$\mathbf{H}(\bar{\mathbf{P}}) = \sum_i (\mathbf{P}_i - \bar{\mathbf{P}}) \wedge m_i (\mathbf{V}_i - \bar{\mathbf{V}}), \quad (26)$$

where

$$m_i \frac{d\mathbf{V}_i}{dt} = m_i \mathbf{f} + \mathbf{R}_i - m_i \frac{\mathbf{P}_i - \mathbf{V}_i t}{t^2}, \quad (27)$$

and

$$\sum_i m_i \mathbf{P} = (\sum_i m_i) \bar{\mathbf{P}}, \quad \sum_i m_i \mathbf{V}_i = (\sum_i m_i) \bar{\mathbf{V}} \quad (28)$$

I suppose, as before, that the moment about the centre of mass of the interactions is zero, so that

$$\sum_i (\mathbf{P}_i - \bar{\mathbf{P}}) \wedge \mathbf{R}_i = 0 \quad (29)$$

Then

$$\frac{d\mathbf{H}(\bar{\mathbf{P}})}{dt} = \sum_i (\mathbf{P}_i - \bar{\mathbf{P}}) \wedge m_i \frac{d(\mathbf{V}_i - \bar{\mathbf{V}})}{dt} = \sum_i (\mathbf{P}_i - \bar{\mathbf{P}}) \wedge m_i \frac{d\mathbf{V}_i}{dt}$$

\* I am not here assuming Newton's Third Law. My decomposition of the actual forces  $\mathbf{F}_0$  and  $\mathbf{F}$  on the two particles into  $m_0 \mathbf{f} - \mathbf{R}$  and  $m \mathbf{f} + \mathbf{R}$  serves to define the interaction  $\pm \mathbf{R}$  as  $\pm \frac{1}{2}(\mathbf{F} - \mathbf{F}_0)$ .

Substituting for  $d\mathbf{V}_i/dt$  from (27) and using (28) and (29), we find after a few transformations that

$$\frac{d\mathbf{H}(\bar{\mathbf{P}})}{dt} = \sum_i \frac{(\mathbf{P}_i - \bar{\mathbf{P}}) \wedge m_i (\mathbf{V}_i - \bar{\mathbf{V}})}{t} = \frac{\mathbf{H}(\bar{\mathbf{P}})}{t},$$

whence

$$\mathbf{H}(\bar{\mathbf{P}}) = \mathbf{A}t \quad (30)$$

17—The relativistic form of the simplest of these theorems is worth giving. The momentum  $\mathbf{p}$  is now defined by

$$\mathbf{p} = m\xi^{\frac{1}{2}} \frac{\mathbf{V}}{\bar{Y}^{\frac{1}{2}}}, \quad (31)$$

and angular momentum  $\mathbf{H}(\mathbf{O})$  by

$$\mathbf{H}(\mathbf{O}) = \mathbf{P} \wedge \mathbf{p} \quad (32)$$

Accordingly

$$\begin{aligned} \frac{1}{\bar{Y}^{\frac{1}{2}}} \frac{d\mathbf{H}(\mathbf{O})}{dt} &= \mathbf{P} \wedge \frac{1}{\bar{Y}^{\frac{1}{2}}} \frac{d\mathbf{p}}{dt} = \mathbf{P} \wedge \left[ \mathbf{F} - m\xi^{\frac{1}{2}} \left( \mathbf{P} - \mathbf{V} \frac{Z}{\bar{Y}} \right) \frac{1}{\bar{X}} \right] \\ &= \mathbf{\Gamma} + \mathbf{H}(\mathbf{O}) \frac{Z}{\bar{X}\bar{Y}^{\frac{1}{2}}}. \end{aligned}$$

Since

$$\frac{dX^{\frac{1}{2}}}{dt} = \frac{Z}{\bar{X}^{\frac{1}{2}}},$$

this may be written

$$\xi^{\frac{1}{2}} \left[ \frac{d\mathbf{H}(\mathbf{O})}{dX^{\frac{1}{2}}} - \frac{\mathbf{H}(\mathbf{O})}{X^{\frac{1}{2}}} \right] = \mathbf{\Gamma}$$

When  $\mathbf{\Gamma} = 0$  we have

$$\mathbf{H}(\mathbf{O}) = \mathbf{A}X^{\frac{1}{2}} \quad (33)$$

For  $|\mathbf{P}|/ct$  small, this reduces to the earlier theorems. The physical significance of the secular increase of angular momentum with  $t$  will be discussed later.

#### TRANSFORMATION OF THE TIME-VARIABLE

18—The form of (13) suggests transforming the time-variable from  $t$  to  $\tau$  by Euler's transformation. We put

$$\frac{dt}{t} = \frac{d\tau}{t_0}, \quad (34)$$

where the present value of  $t$ , namely  $t_0$ , is introduced to make  $\tau$  of the physical dimensions of a time and to make

$$\left( \frac{d\tau}{dt} \right)_{t=t_0} = 1 \quad (35)$$

The integral of (34) may be written

$$\tau = t_0 \log (t/t_0) + t_0, \quad (\text{A})$$

which makes  $t$  and  $\tau$  agree at the present time. An epoch measured as  $\tau$  will correspond to some epoch  $t$  which depends on the present epoch  $t_0$ . Thus we should really write

$$\tau = \tau(t; t_0),$$

and for the  $\tau$ -scales corresponding to two different epochs  $t_0$  and  $t_1$  we have

$$\frac{d\tau(t, t_1)}{d\tau(t, t_0)} = \frac{t_1}{t_0} \quad (36)$$

Equation (13) then becomes

$$U = \frac{1}{2} \frac{d^2 t}{d\tau^2} - 2T \quad (37)$$

This is the Newtonian *form* of the theorem of the virial if  $\tau$  is regarded as the time-variable of Newtonian dynamics. But it will only be *identical* with the Newtonian theorem if  $U$ ,  $t$ , and  $T$  are the actual measures of the virial, moment of inertia about  $O$ , and kinetic energy in the units defined by adopting  $\tau$  as the measure of time, for it must be remembered that in the present sequence\* all measures of all physical quantities are fundamentally based on clock-measurements. We propose to re-graduate the numbering of the divisions on our observer's clocks from  $t$  to  $\tau$  and all measures of physical quantities, including "constants", may therefore be altered.† The consequence of this we now investigate.

19.—The transformation (12) suggests that we transform  $\mathbf{P}$  to a vector-variable  $\Pi$  according to the formula

$$\mathbf{P} = \frac{t}{t_0} \Pi. \quad (38)$$

Then the velocity  $\mathbf{V}$  relative to  $O$  is expressed by

$$\mathbf{V} = \frac{d\mathbf{P}}{dt} = \frac{1}{t_0} \left[ \Pi + t \frac{d\Pi}{dt} \right], \quad (39)$$

whence

$$\mathbf{V} - \frac{\mathbf{P}}{t} = \frac{t}{t_0} \frac{d\Pi}{dt} = \frac{d\Pi}{d\tau}. \quad (40)$$

\* See W S, chap. 2

† E.g., the measure of a length is altered by the transformation, and a rod which is "rigid" on the  $\tau$ -scale is not rigid on the  $t$ -scale.

Hence the velocity of a particle relative to its immediate cosmical surrounding,  $\mathbf{V} = \mathbf{P}/t$  on the  $t$ -scale, is equal to the actual velocity relative to  $O$  on the  $\tau$ -scale if  $\Pi$  measures the distance from  $O$  on the  $\tau$ -scale.

But distances are measured by light-signals. If a signal leaves  $O$  at  $t_1$ , is reflected at a particle  $P$ , and returns at time  $t_2$  at  $O$ , then the length  $l$  assigned to  $OP$  is given by

$$\frac{1}{2}c(t_2 - t_1) = l,$$

or say

$$\frac{1}{2}c \Delta t = l \quad (41)$$

Measuring the same length as  $\lambda$  on the  $\tau$ -scale, we have

$$\frac{1}{2}c(\tau_2 - \tau_1) = \lambda,$$

or say

$$\frac{1}{2}c \Delta \tau = \lambda \quad (42)$$

Hence for short distances

$$l = \frac{\Delta t}{\Delta \tau} \lambda,$$

or by the time-transformation law (34)

$$l = \frac{t}{t_0} \lambda \quad (44)$$

This shows by comparison with (38) that for not too large distances  $\Pi$  is the actual measure of  $\mathbf{P}$  on the  $\tau$  scale, and will be regarded as the actual position-vector of  $P$  by an observer at  $O$  using the  $\tau$ -scale of time.

20—We now transform our fundamental equation of motion (4) in the same way. We have by (39)

$$\frac{d\mathbf{V}}{dt} = \frac{1}{t_0} \left[ 2 \frac{d\Pi}{dt} + t \frac{d^2\Pi}{dt^2} \right],$$

whence, using (40), (4) gives

$$\frac{m}{t_0} \left[ t \frac{d^2\Pi}{dt^2} + \frac{d\Pi}{dt} \right] = \mathbf{F}.$$

Applying (34), this gives

$$m \frac{d^2\Pi}{d\tau^2} = \Phi, \quad (45)$$

where

$$\Phi = \frac{t}{t_0} \mathbf{F} \quad (46)$$

Equation (45) is of the *form* of the Newtonian equation of motion of a particle of mass  $m$  under force  $\Phi$ , if  $\tau$  is taken to be the independent

variable measuring line. But  $\Phi$  is, in fact, the measure of the force  $\mathbf{F}$  on the  $\tau$ -scale. For  $m$ , which is an integration constant,\* is independent of the scale of time, and using the notation of dimensional equations the vector  $\Phi$  is given by

$$\Phi = \frac{t}{t_0} \mathbf{F} = \frac{t}{t_0} [m] \frac{[\Delta I]}{[\Delta t]^2} = \frac{t}{t_0} [m] \frac{[(t/t_0) \Delta \lambda]}{[(t/t_0) \Delta \tau]^2} = [m] \frac{[\Delta \lambda]}{[\Delta \tau]^2},$$

and so is the measure of  $\mathbf{F}$  on the  $\tau$ -scale

21—We now recollect that equation (4) and, accordingly, also (45), have been derived by purely abstract reasoning from the properties of the substratum (1) and (2). Comparison of (45) with the empirical Newtonian equation of motion of a particle  $m$  under a force  $\Phi$  now allows us to identify the variable  $\tau$  as the time of dynamics at the present epoch. We shall therefore refer to the  $\tau$ -scale as the *dynamical* scale of time, it being understood that this means the *present* dynamical scale of time, and we shall refer to the  $t$ -scale as the kinematic scale of time. The time  $\tau$  postulated by Newton at the basis of his dynamics as "evenly flowing" is thus shown not to be evenly flowing in comparison with the time  $t$  of kinematics †

The dynamical scale of time is a human, ephemeral, method of time-measurement which has arisen owing to the fundamental laws of dynamics having been discovered empirically in the form (45) and not in the more fundamental form (4). Our ancestors, existing at kinematic time  $t_1$ , would also have recognized (45) as the equation of motion of a free particle. But they would have adopted the transformation

$$\tau(t, t_1) = t_1 \log(t/t_1) + t_1$$

Thus we describe their epoch, on our own scale, not as  $t_1$  (their description) but as  $\tau_{10} \equiv \tau(t_1, t_0) = t_0 \log(t_1/t_0) + t_0$ . And they would have described, on their scale, our present epoch not as  $t_0$  but as

$$\tau_{01} \equiv \tau(t_0, t_1) = t_1 \log(t_0/t_1) + t_1.$$

\* See I, § 12

† It would be inappropriate to embark here on a detailed discussion of the Newtonian natural philosophy in the light of the present results. It may be permissible to mention, however, that the present investigations take into account the two points in which the Newtonian scheme has been criticized, namely its adoption of an undefined "time" and its failure to define uniform motion in the abstract. The substratum provides the set of Galilean frames necessary for Mach's principle to be respected.

We notice that

$$\frac{\tau_{10}}{t_0} + \frac{\tau_{01}}{t_1} = 2,$$

$$\frac{\tau_{10}}{t_0} + 2 \log t_0 = \frac{\tau_{01}}{t_1} + 2 \log t_1$$

22—We proceed to evaluate various dynamical quantities on the  $\tau$ -scale. We have

$$T = \sum_i \frac{1}{2} m_i \left( \mathbf{V}_i - \frac{\mathbf{P}_i}{t} \right)^2 = \sum_i \frac{1}{2} m_i \left( \frac{d\Pi_i}{d\tau} \right)^2, \quad (47)$$

$$U = - \sum_i \mathbf{F}_i \cdot \mathbf{P}_i = - \sum_i \Phi_i \cdot \Pi_i, \quad t = \sum_i m_i \Pi_i^2, \quad (48)$$

$$\frac{dW}{d\tau} = \frac{t}{t_0} \frac{dW}{dt} = \frac{t}{t_0} \sum_i \mathbf{F}_i \cdot \left( \mathbf{V}_i - \frac{\mathbf{P}_i}{t} \right) = \sum_i \Phi_i \cdot \frac{d\Pi_i}{d\tau}, \quad (49)$$

$$\phi = \gamma_0 \frac{t}{t_0} \sum_{i,k}' \frac{m_i m_k}{|\mathbf{P}_i - \mathbf{P}_k|} = \gamma_0 \sum_{i,k}' \frac{m_i m_k}{|\Pi_i - \Pi_k|}, \quad (50)$$

$$\mathbf{H}(O) = \sum_i \frac{t}{t_0} \Pi_i \wedge \frac{m_i}{t_0} \left( \Pi_i + t \frac{d\Pi_i}{dt} \right) = \frac{t}{t_0} \sum_i \Pi_i \wedge m_i \frac{d\Pi_i}{d\tau} = \frac{t}{t_0} \mathbf{h}(O), \quad (51)$$

where in the last relation  $\mathbf{h}(O)$  denotes the angular momentum about  $O$  in the  $\tau$ -scale.

It follows from (47), (48), (50) that the measures of kinetic energy, of the virial and of gravitational potential on the  $t$ -scale, are equal to their measures on the  $\tau$ -scale, when the latter are defined in the usual Newtonian fashion. Such quantities may be called "time-invariants". On the other hand, the rate of working of the forces is not a time-invariant;  $dW/dt$  is, of course, equal to  $(t_0/t) dW/d\tau$ , but  $dW/d\tau$  then comes out by (49) to be precisely the Newtonian definition of rate of working. Similarly the angular momentum  $\mathbf{H}(O)$  is not a time-invariant. The energy  $E$  of equations (6) and (20) is a time-invariant.

The measure of  $\gamma$ , the constant of gravitation, on the  $\tau$ -scale is a constant, namely  $\gamma_0$ . A "steadily expanding" system on the  $t$ -scale is regarded as a "steady system" on the  $\tau$ -scale.

In general, any physical measure on the  $t$ -scale is equal to  $(t/t_0)^n$  times its measure on the  $\tau$ -scale, where  $n$  is the excess of the number of dimensions of length over the number of dimensions of time (for the physical quantity concerned), in the usual  $[m]$ ,  $[l]$ ,  $[t]$  system of dimensions.

23—*Angular Momentum*—From the relations

$$\mathbf{H}(O) = \mathbf{A}t, \quad \mathbf{H}(O) = (t/t_0) \mathbf{h}(O)$$

already established, it follows that for a semi-isolated system under zero external couple,  $\mathbf{h}(O)$ , the angular momentum on the  $\tau$ -scale, is *constant*. This is the usual Newtonian theorem.

Nevertheless, the actual measure of an angular momentum made by contemporary observers using their own  $\tau$ -scale will increase secularly with the time. This is a rather subtle point, which may be made clearer by the following remarks. Let  $\mathbf{h}$  be the angular momentum of a system at time  $t_0$ , measured on the  $\tau$ -scale corresponding to  $t_0$ . Then  $\mathbf{h} = \mathbf{H}$  the value of  $\mathbf{H}(O)$  on the  $t$ -scale at the time  $t_0$ . An observer, continuing to use this same  $\tau$ -scale—the  $\tau$ -scale corresponding to  $t_0$ —and employing Newtonian dynamics, will predict that the angular momentum will remain constant and equal to  $\mathbf{h}$  and will find his measures of the angular momentum to remain constant if he employs a clock which records time  $\tau(t, t_0)$ . But at time  $t_1$  the value of  $\mathbf{H}(O)$  will be  $(t_1/t_0) \mathbf{H}_0 = \mathbf{H}_1$ , say, and an observer at time  $t_1$ , using a clock measuring time  $\tau(t; t_1)$ , will measure the angular momentum as  $\mathbf{H}_1$ . The question then whether the angular momentum measure will, in fact, remain constant or vary with the time reduces to the question whether or not the time-keeper used by the observer keeps the time corresponding to a fixed value  $t_0$ . This question we now examine.

#### TIME-KEEPERS

24—*The Simple Pendulum*—The simplest time-keeper is the simple pendulum. We calculate its period  $s$  from the formula  $s = 2\pi(l/g)^{1/2}$ , where  $g = \gamma M/a^2$  and  $M, a$  are the mass and radius of the earth. If the pendulum and the earth have invariable length-dimensions measured on the  $t$ -scale, *i.e.*, if they are ideal rigid bodies as defined by light-signalling using  $t$ -clocks, this period  $s$  is not constant, but the pendulum measures  $t$ -time. If, however, the pendulum and earth have their length-dimensions measured on the  $\tau$ -scale, and appear to be of constant dimensions measured on this scale by means of light-signals recorded in  $\tau$ -time, then the length and radius will be constants  $\lambda$  and  $\alpha$ , where as before

$$l = (t/t_0) \lambda, \quad a = (t/t_0) \alpha,$$

and  $l$  and  $a$  will then increase with  $t$ . The period on the  $\tau$ -scale is  $\sigma = 2\pi(\lambda\alpha^3/\gamma_0 M)^{1/2}$  and is constant. The period on the  $t$ -scale, since  $\gamma = \gamma_0(t/t_0)$  is now

$$s = 2\pi \left[ \frac{(t/t_0) \lambda (t/t_0)^2 \alpha^3 \gamma^{1/2}}{\gamma_0 (t/t_0) M} \right] = \frac{t}{t_0} \sigma,$$

and increases with  $t$ . We notice that the ratio of  $s$  to  $\sigma$  is equal to  $\Delta t/\Delta \tau$ ,

where  $\Delta t$  and  $\Delta \tau$  are measures of the same (small) interval of time on the two scales, as it must be since  $s$  and  $\sigma$  are precisely a pair of such measures. Thus a simple pendulum, if rigid on the  $\tau$ -scale corresponding to  $t_0$ , will measure  $\tau(t, t_0)$  time, whereas if it is rigid on the  $t$ -scale it will measure  $t$ -time, but not uniformly.

25—From what has been said about angular momentum, it follows that a rotator rigid on the  $\tau$ -scale measures  $\tau$ -time, one rigid on the  $t$ -scale measures  $t$ -time. This can also be verified as follows. An angular velocity,  $w$  on the  $t$ -scale, is measured as  $\omega$  on the  $\tau$ -scale where

$$w = \frac{2\pi}{[\Delta t]} = \frac{2\pi}{[(t/t_0) \Delta \tau]} = \frac{t_0}{t} \omega$$

Hence the angular momentum,  $kI^2w$ , is equal to  $k(t/t_0) \lambda^3 \omega$  or  $(t/t_0)$  times the measure of the angular momentum on the  $\tau$ -scale, in agreement with previous theorems. The rotator measures a time as the number of complete rotations described multiplied by the apparent period,  $2\pi/w$  or  $2\pi/\omega$  and the last numbers, for short intervals, are as  $t$  to  $t_0$ , thus the rotator measures the time on the scale in which it is rigid.

26—A revolving planet measures time similarly. The Kepler-Newton value of the period  $s$  is  $2\pi a^3/(\gamma M)^{1/2}$ , the period  $\sigma$  is  $2\pi \alpha^3/(\gamma_0 M)^{1/2}$  where  $a$ ,  $\alpha$  are the semi-axes major on the two scales. As before,  $a = (t/t_0) \alpha$ ,  $\gamma = (t/t_0) \gamma_0$ , and so  $s/\sigma = t/t_0 = \Delta t/\Delta \tau$ .

27—*Doppler Effect*—A Doppler effect is a time-invariant. This is obvious physically, since a Doppler-shift coefficient is a measure of a change of colour, which must be independent of the scale of time-measurement. The following analytical verification of this is simpler than that due to Whitrow and Walker (*loc cit*). Let a distant emitter emit signals of frequency  $\nu(t')$ , not necessarily constant in  $t'$ , where  $t'$  is the local time at the emitter. Let the signal emitted at local time  $t'$  be received at the observer at his local time  $t_2$  at apparent frequency  $n(t_2)$ . Then since all signals emitted are received, we have  $\nu(t') dt' = n(t_2) dt_2$ . The Doppler shift coefficient  $D(t_2)$  as observed is defined as

$$D(t_2) = \frac{\nu(t_2)}{n(t_2)}, \quad (52)$$

it being supposed that the observer is furnished with a similar emitter as standard of comparison. Hence

$$D(t_2) = \frac{\nu(t_2)}{\nu(t')} \cdot \frac{dt_2}{dt'}. \quad (53)$$

Now let the scale of time-reckoning be changed from  $t$  to  $\tau$  by any arbitrary transformation (not necessarily the kinematic-dynamic transformation). The emitted frequency is then reckoned as  $\bar{v}(\tau')$ , the received one as  $\bar{n}(t_2)$ , and, by a similar calculation,

$$D(\tau_2) = \frac{\bar{v}(\tau_2)}{\bar{v}(\tau')} \cdot \frac{d\tau_2}{d\tau'} \quad (54)$$

But all the signals emitted in the interval  $(t, t + dt)$  are equally emitted inside the interval  $(\tau, \tau + d\tau)$ . Hence

$$v(t) dt = \bar{v}(\tau) d\tau,$$

for any corresponding times  $t, \tau$ . Hence by (54)

$$D(\tau_2) = \frac{v(t_2)}{v(t')} \frac{dt_2}{dt'}, \quad (55)$$

or by (53)

$$D(\tau_2) = D(t_2) \quad (56)$$

This is otherwise obvious since a Doppler-shift coefficient is equivalent to a measure of  $\delta\lambda/\lambda$ ,  $\lambda$  being a wave-length, and this ratio is independent of the definition of the rigid length-scale employed.

28—The question, whether our actual macroscopic time-keepers keep kinematic or dynamical time, appears to depend on whether our standard rigid-length measures are rigid on the kinematic or on the dynamical scale. What we have established is that in Newtonian dynamics the independent variable is dynamical time  $\tau$ . If we take Newtonian dynamics as empirically both true and exact, *i.e.*, for example, that the measure of the angular momentum of a semi-isolated system does, in fact, remain constant, then it follows that our time-keepers keep dynamical time and that the "rigid-body" defined by macroscopic light-signalling is expanding in kinematic time. That atoms keep kinematic time will be made probable later from cosmological considerations. Conversely, if macroscopic time-keepers keep kinematic time, then Newtonian dynamics still holds good, but its predictions must be translated into  $t$ -measures before they will agree with experience over large intervals of time, for such intervals the  $t$ -dynamics, based on (4) and not on (45), should rather be employed.

#### COSMOLOGICAL CONSIDERATIONS

29—To apply these ideas to a receding nebula, which is not necessarily at a distance small compared with  $ct_0$ , more refined analysis is necessary.

Suppose that ideally the distance of such a nebula is determined by light-signalling as  $|\mathbf{P}|$  on the  $t$ -scale at time  $t$  and  $|\Pi|$  on the  $\tau$ -scale at time  $\tau$ . Then in the light-signalling notation previously employed, with the usual conventions for assigning distances and epochs, we have

$$\frac{1}{2}c(t_2 - t_1) = |\mathbf{P}|, \quad \frac{1}{2}c(\tau_2 - \tau_1) = |\Pi|$$

But

$$\frac{1}{2}(t_2 + t_1) = t, \quad \frac{1}{2}(\tau_2 + \tau_1) = \tau$$

$$\tau_1 = t_0 \log(t_1/t_0) + t_0,$$

$$\tau_2 = t_0 \log(t_2/t_0) + t_0$$

Hence, eliminating  $t_1$ ,  $t_2$ ,  $\tau_1$ ,  $\tau_2$ , we have the two relations\*

$$|\Pi| = \frac{1}{2}ct_0 \log \frac{t + |\mathbf{P}|/c}{t - |\mathbf{P}|/c},$$

$$\tau = \frac{1}{2}t_0 \log \frac{t^2 - \mathbf{P}^2/c^2}{t_0^2} + t_0$$

Put

$$d|\Pi|/d\tau = u,$$

$$d|\mathbf{P}|/dt = v,$$

then simple differentiation yields the relation

$$u = \frac{v - |\mathbf{P}|/t}{1 - v|\mathbf{P}|/c^2t} \quad (57)$$

This is similar in form to the Einstein formula for the composition of the radial velocities  $v$  and  $|\mathbf{P}|/t$  but it has a radically different origin.† If the point  $\mathbf{P}$  is quite close to  $O$ , the cosmical velocity  $|\mathbf{P}|/t$  will be very small, and we get  $u \sim v$ , so that for small distances velocity is a time-invariant. The same formula follows to a lower order of approximation from

$$v = \frac{d(\Delta l)}{dt} = \frac{d}{dt} \left( \frac{t}{t_0} \Delta \lambda \right) = \frac{\Delta \lambda}{t_0} + \frac{d(\Delta \lambda)}{d\tau} = \frac{\Delta l}{t} + u$$

For a fundamental particle or receding nebula,  $v = |\mathbf{P}|/t$  and accord-

\* [Note added in proof, 9 December, 1936—This transformation has been given independently by Leontowski (privately communicated), as a useful change of co-ordinates. He also showed that the nebulae are stationary in  $\tau$ -time. Cf. Nuut, "Expansionistischen Kinematik," 'Publ. Obs. astr. Tartu,' vol. 28, No. 4 (1935). The further consequences of this transformation have been communicated in a later paper.]

† We verify that when  $v = c$ , we have also  $u = c$ . Thus the velocity of light is a time-invariant.

ingly  $v = 0$ . Thus  $|\Pi|$  is constant in the  $\tau$  ( $t$ ;  $t_0$ ) scale,\* and the receding nebula appears as if rigidly connected to the observer when rigidity is defined by the  $\tau$ -scale

30—This offers a solution of the much-disputed problem as to whether the universe is “really” expanding or not. It is expanding on the  $t$ -scale, stationary on the  $\tau$ -scale†. We ordinarily, *i.e.*, for short distances, make no distinction between the two scales. If we go to nebular distances, using the empirical Newtonian dynamics and assuming our macroscopic time-keepers to keep dynamical time  $\tau$ , the universe is to be considered as stationary. If we use the rational  $t$ -dynamics, assuming our time-keepers to keep kinematic time  $t$ , the universe is to be considered as expanding. Imagine a nebular nucleus joined to ourselves by a material bar, supposed rigid, would the end of the bar and the nebular nucleus separate? The answer is that they would if the bar is deemed rigid on the kinematic scale but not if the bar is deemed rigid on the dynamic scale.

31—Further consequences can be drawn. We actually observe a red shift. Hence  $D(t_2) > 1$ ,  $D(\tau_2) > 1$ . By (53) and (54), each of these is the product of two factors. On the kinematic scale it is to be expected that an atom keeps a constant frequency  $\nu$ . Hence  $\nu(t_2)/\nu(t') = 1$ , and accordingly by (53)

$$D(t_2) = \frac{dt_2}{dt'} > 1,$$

the usual formula for the Doppler shift as due to motion. In the dynamic scale the nebulae are stationary, and hence  $d\tau_2/d\tau' = 1$ , hence, by (54),

$$D(\tau_2) = \frac{\sqrt{\tau_2}}{(\tau')} > 1$$

Thus on the dynamic scale the characteristic frequency of an atom *increases* with the time, since  $\tau_2 > \tau'$ . This gives an immediate physical interpretation of the red-shift which occurs for a dynamically stationary universe. For the light now received was emitted some time ago, when the characteristic frequency was smaller (on the  $\tau$ -scale). Since frequencies are propagated unchanged, the frequency when received will

\* Cf Synge, ‘Nature,’ vol 138, p 28 (1936). Synge’s construction for “relative stationariness” of two observers breaks down if they part company in the finite experience of each of them, but in the present case the observers part company at  $t = 0$ ,  $\tau = -\infty$ , and our  $(t, \tau)$  transformation illustrates Synge’s result.

† Cf W. K. Clifford’s celebrated question, mentioned, *e.g.*, in Bridgeman’s “Nature of Physical Theory,” p 11 (1936).

be smaller than the then-frequency (on the dynamical scale) of the receiving atom, and a red-shift will be observed.\*

32—The parameter  $w^2/\gamma\rho$  which plays an important part in the theory of rotating fluids, is a time-invariant For

$$\frac{w^2}{\gamma\rho} = \left(\frac{t_0}{t}\omega\right)^2 / \gamma_0 \left(\frac{t}{t_0}\right) \rho_0 \left(\frac{t_0}{t}\right)^3 = \frac{\omega^2}{\gamma_0 \rho_0}$$

Nevertheless, for a given density  $\rho$  on the  $t$ -dynamics,

$$w^2/\gamma\rho \propto (t_0/t)^2/(t/t_0) \propto (t_0/t)^3,$$

and so  $w^2/\gamma\rho$  was much larger at earlier  $t$ . This may account for the prevalence of double stars, on the fission theory of their origin.

Again the number of swings of a pendulum between now and  $t = 0$  is a time-invariant. For it is equal to

$$\int_0^s \frac{dt}{s} = \int_{-\infty}^{\tau_0} \left(\frac{t_0}{t}\frac{1}{\sigma}\right) \frac{t}{t_0} d\tau = \int_{-\infty}^{\tau_0} \frac{d\tau}{\sigma}$$

If for an actual pendulum the dynamical period  $\sigma$  is constant, then this number of swings is infinite, the pendulum swinging faster and faster in kinematic time as  $t \rightarrow 0$ . If, on the other hand,  $s$  is constant, the number is finite, and  $\sigma \rightarrow \infty$  as  $\tau \rightarrow -\infty$ . The number of "beats" of a radioactive clock is, of course, finite, as is known from the geo-physical evidence, but whether a macroscopic clock keeps a time different from that of a radioactive clock cannot be determined at present experimentally.

33—The cosmical consequences of our angular momentum theorems are of some interest. They account for the otherwise mysterious prevalence of angular momentum in the universe at large, a phenomenon to whose surprising occurrence Eddington has repeatedly called attention. Why are most large-scale systems rotating? Spiral nebulae, spindle-shaped nebulae, our own galaxy, multiple-star systems, individual stars, the solar system, all appear endowed with inexplicable stores of angular momentum (globular clusters afford a notable though rare exception). The answer is that angular momentum increases secularly with the epoch. When the systems were born, they may be supposed to have been endowed by chance with some small non-zero angular momentum, in some determinate sense. This will then augment itself secularly, *in the same sense*,

\* It has been shown by Whitrow ('Quart. J. Math. (Oxford),' vol. 7, p. 271 (1936)) that a photon obeys the  $t$ -dynamics and that on this dynamics the energy  $E$  of a photon bears a ratio to its frequency  $\nu$  which is a universal constant.

according to equations of the type  $d\mathbf{H}/dt = \mathbf{H}/t$ , or  $\mathbf{H} \propto t$ . The physical reason is that any particular moving member of a semi-isolated system is not central in the field of the substratum or smoothed-out universe, as reckoned by  $O$  the actual centre of the system, and accordingly the system experiences a couple about  $O$  due to what may loosely be called the "pull" of the smoothed-out universe. The resultant couple is in the sense of the initial  $\mathbf{H}$ , which is therefore magnified secularly. Thus though a small *present* store of angular momentum is a theoretical possibility, in general we shall find local accumulations of angular momentum. These should be distributed at random, as they were initially, but they will occur in large, differing amounts of angular momentum, inasmuch as small initial differences will have become magnified. This seems to correspond to the present distribution of angular momentum in the universe at large, non-spinning systems being comparatively rare, as we see is to be expected. It must be remembered that, even on the dynamical scale, the measure  $\mathbf{h}$  of the angular momentum is always equal to the then value of  $\mathbf{H}$ . Thus the objections levelled at the original nebular hypothesis of Kant, by thinkers from Laplace onwards, on the score of the inability of the supposed random nebula to generate angular momentum of itself, disappear. The consequences of these considerations in predicting equi-angular spiral orbits for large-scale gravitational motions as displayed for our inspection in the heavens will be dealt with elsewhere.

I am indebted to Professor R. H. Fowler, F.R.S., for certain criticisms of an earlier draft of the paper.

#### SUMMARY

34—The theorems of rational dynamics, derived in earlier papers, without recourse to the empirical laws of dynamics or gravitation, were expressed in terms of kinematic time  $t$  as independent variable. It is shown that the equation of motion and all derivative theorems pass into the empirical Newtonian forms when the independent variable  $t$  is transformed to a new variable  $\tau$  given by

$$\tau = t_0 \log (t/t_0) + t_0,$$

where  $t_0$  is the present value of  $t$ , i.e., the age of the universe reckoned from the natural origin of time. When the graduations of a clock keeping kinematic time  $t$  are re-numbered from  $t$  to  $\tau$ , all physical quantities such as position-vectors, forces, angular momenta, the constant of gravitation, which have been defined fundamentally in terms of time-determinations, have new measures on the  $\tau$ -scale, and it is shown that it is the  $\tau$ -measures

which occur in the transformed equations and theorems. It follows, by comparison of rational dynamics with empirical experience, that in classical dynamics the independent variable is  $\tau$ , not  $t$ . We are thus led by rational argument to a conjecture once made by de Sitter. Macroscopic time-keepers such as a pendulum, a rotating earth, or a revolving planet, keep dynamical time  $\tau$  when their parameters are supposed constants on the  $\tau$ -scale, but atoms and radioactive clocks keep kinematic time  $t$ . A variety of dynamical and cosmological consequences are investigated. In particular, the prevalence of angular momentum in the universe at large is explained, and the natural origin of time is shown to be inaccessible by a sequence of dynamical phenomena traced backwards.\*

---

## Explosion Waves and Shock Waves. IV—Quasi-Detonation in Mixtures of Methane and Air

By WILLIAM PAYMAN, D Sc., Ph D., and WILFRED CHARLES FURNESS SHEPHERD, B Sc., Ph D

(Communicated by J. F. Thorpe, F R S—Received 18 June, 1936)

[PLATES 12-16]

### INTRODUCTION

The possibility of detonation in mixtures of methane and air, apart from its theoretical interest, is of practical importance in connexion with the study of explosions in coal mines.

Many attempts have been made experimentally to increase the violence of explosion or the intensity of combustion of mixtures of methane and air to see if speeds of flame and effects of violence comparable with those of detonation could be obtained. Mason and Wheeler† noted that restrictions in the path of an explosion accelerated the flame, and observed that as the flame of a methane-air mixture passed through the second of two restrictions placed in a 30.5-cm. tube "the development of the

\* [Note added in proof, 9 December, 1936—Doubts as to the ultimate validity of the theorem of conservation of angular momentum were independently expressed by Sir James Jeans at the Blackpool meeting of the British Association, September, 1936.]

† 'J. Chem. Soc.', p. 47 (1920).

detonation wave appeared imminent" The experiments were continued by Chapman and Wheeler,\* who obtained a maximum speed of 420 metres per second beyond the restricted section of a tube 5 cm. in diameter. The effect of the restrictions was in their opinion to induce rapid motion in the mixture through which the flame was travelling

Still higher speeds were obtained in mixtures of methane and air by Robinson and Wheeler† in a steel tube, 30.5 cm. in diameter and 32.3 metres long, fitted with restrictions along its middle section. As flame passed through the restricted zone, its speed increased rapidly from 2 to 450 metres per second, afterwards, it fell gradually to about 300 metres per second and then increased again to 600 metres per second over the end portion of the tube. In discussing their results Robinson and Wheeler observed that, despite the high speed at which the flame travelled after it had passed through the restricted zone, a constant regime comparable with that of the detonation wave was not established.

Measurements of the rates of detonation in mixtures of methane, oxygen, and nitrogen give some indication of the limiting composition which will maintain detonation with comparatively simple modes of initiation and of the probable minimum rate of detonation. The lowest recorded rate of detonation in mixtures of methane, oxygen, and nitrogen is 1151 metres per second for the mixture  $\text{CH}_4 + 4\text{O}_2 + 4\text{N}_2$  as determined by Berthelot and Vieille‡. Neither Berthelot and Vieille nor Dixon§ found it possible to detonate mixtures of methane and air.

Payman and Walls|| measured the rate of detonation in a range of methane-oxygen mixtures and found that in the limiting mixture, which contained 11.1% of methane, the rate of detonation was 1678 metres per second. A somewhat lower limit, 10% of methane in oxygen, was found by Campbell, Whitworth, and Littler,¶ but the rate of detonation was not recorded. Dixon (*loc cit*) found that in a mixture containing excess oxygen the substitution of nitrogen for oxygen not only lowered the rate of detonation but at the limit prevented its establishment. Hence it would seem unlikely that the methane-air mixture of the greatest calorific value, containing 9.5% of methane, would be capable of supporting detonation.

Such a mixture is, however, evidently only just beyond the limit of

\* 'J. Chem. Soc.', p. 2139 (1926).

† 'J. Chem. Soc.', p. 758 (1933).

‡ 'C. R. Acad. Sci., Paris,' A vol. 95, p. 151 (1882).

§ 'Phil. Trans.,' A, vol. 184, p. 97 (1893).

|| 'J. Chem. Soc.', p. 420 (1923).

¶ 'J. Chem. Soc.', p. 339 (1932).

detonation, and it would seem possible that the addition of "secondary" energy, for example, in the form of heat, to a methane-air mixture might render it capable of maintaining detonation so long as the secondary energy continued to be supplied. A parallel can be drawn with gas mixtures which in normal circumstances are not capable of supporting self-propagation of flame, and in that sense are non-inflammable. The passage of a powerful electric spark or the introduction of a lamp flame results in inflammation taking place around the source of heat (for example, in the "flame cap" of a miner's lamp), but the inflammation ceases as soon as the energy of the spark is dissipated or the flame is removed. We have found it possible to establish a "detonation" in which the energy necessary to maintain it is not wholly derived from the combustion of the gas mixture. It is not true detonation, and we have therefore termed it "quasi-detonation".

The possibility of the establishment of quasi-detonation was first suggested to us by the fact that the initial rate of detonation in a gas mixture is often appreciably higher than the normal rate attained later. This we regard as being due to the additive effect of secondary energy provided by adiabatic compression and by shock waves from previously inflamed gas mixture. It is particularly noticeable when a blasting detonator is used as the initiator\*. Our first attempts to obtain detonation in methane-air mixtures were therefore made, using blasting detonators as initiators, the gas mixtures being contained in narrow tubes of glass or steel.

A favourable opportunity also presented itself for experiments with methane-air mixtures on a larger scale. Under a cooperative scheme of research between the Safety in Mines Research Board and the United States Bureau of Mines the authors fitted up a wave-speed camera† at the Bureau of Mines Experiment Station at Pittsburgh. The associated apparatus was used primarily for a study of the ignition of methane-air mixtures by mining explosives, and an account of this work has been published‡. Advantage was taken of the facilities available to examine the propagation of flame in methane-air mixtures ignited by sources of varying intensity, including charges of high explosives. The small-scale experiments described in the present paper were carried out at Buxton, the large-scale work at Pittsburgh.

\* Berthelot and Le Chatelier, 'Ann Chem. Phys.', vol 20, p 15 (1900); Payman and Titman, 'Proc Roy Soc', A, vol 152, p 418 (1935).

† Payman and Shepherd, 'Pap Safety Min Res Bd Lond', No 29 (1926); Payman and Woodhead, 'Proc Roy Soc', A, vol 132, p 200 (1931).

‡ Shepherd, 'Bull U S Bur Min', Washington, No 354 (1932).

## SMALL-SCALE EXPERIMENTS

Two types of standard No. 6 detonators were used as means of ignition in the small-scale experiments. lead azide cased in aluminium, and mercury fulminate cased in copper. A single detonator of the former type when fired in a large free volume of a mixture of methane and air will ignite it, whereas a dozen or more fulminate detonators fired in a bunch together will not cause ignition. Since the small-scale experiments were to be made with tubes 2.5 cm. in diameter, a series of experiments was carried out to examine the effect of such confinement on the igniting powers of the two types of detonators.

*Ignition Tests with Methane-Air Mixtures*—When a detonator is fired in a narrow tube filled with a gas mixture, there may be either a general inflammation or a local ignition. The detonator itself produces a large flame the size of which is usually increased when a mixture of methane and air is present in the tube, even when general inflammation does not ensue. In order to distinguish between a local ignition and a general inflammation, the far end of the tube containing the methane-air mixture (9.5% methane) was made to project into a cubical box of 1800-litre capacity containing a mixture of the same composition. Inflammation was deemed to have occurred only if the explosion of the detonator and the combustion of the gas mixture inside the tube ignited the mixture in the box. The tube was of 2.5 cm. internal diameter. The end outside the box was closed with a rubber bung through a hole in which the detonator was inserted.

Experiments were carried out with copper-cased fulminate detonators in steel tubes of different lengths. General inflammation of the gas mixture inside the box did not occur in any experiment, although with tubes less than 100 cm. in length a vivid tongue of flame, about 15 cm. long, was projected into the box. No visible flame was projected from tubes that were more than 120 cm. long. If the tube contained air, flame from the detonator was not projected from a tube more than 75 cm. long.

It was found possible, also, to fire aluminium-cased azide detonators in steel tubes 2.5 cm. in diameter, when the tubes exceeded a certain critical length, without inflaming the mixture in the box. With tubes of lengths up to 125 cm., inflammation of the mixture in the box was accompanied by great violence, with a tube 125 cm. long, inflammation was obtained in two only out of three experiments, whilst in four tests with a tube 150 cm. long there was no inflammation, although bright tongues of flame were projected from the tube.

*Wave-Speed Camera Records*—It was thought desirable to examine the sequence of events within the tube at a considerable distance from the source of ignition. For the first experiments a closed steel tube 147 cm long and 2.5 cm in diameter was used, the last 30 cm being the stainless steel tube used for the wave-speed photography described in Part III. The explosion was recorded over this last 30 cm, and some of the records are reproduced in figs 1 to 5 on Plate 12. The detonator was placed in a rubber bung closing one end of the tube as in the earlier experiments. The far end was closed with a brass plate.

An aluminium-cased detonator fired in free air\* gives rise to a brilliant flame, 25 cm long. The effect of enclosing the detonator in a tube initially containing air is to increase the length of the flame to 50 cm. The brilliance of the flame is largely due to combustion of the fragmented aluminium case, though the flame of the detonating compound itself is luminous. Many of the aluminium particles which have escaped combustion in the flame of the detonator strike the end of the tube, 147 cm from the detonator, and some take fire, causing mild shock waves to be sent back along the tube as a result of their collision and conflagration, fig 1. These particles have travelled ahead of the main shock wave, shown lower down the record as a bright white trace. Their speeds range from 1500 to 1700 metres per second, whilst that of the main shock wave varies in different experiments between 840 and 900 metres per second. In individual records the speed of this wave is almost constant until it meets the flames of the burning particles spreading from the end of the tube. This observation is important, for it shows that up to the meeting point, which is quite close to the end of the tube, there is no appreciable motion of the air ahead of the wave, despite the fact that many particles have passed through it. The shock wave reverses the direction of these flames which are then carried back to the end of the tube, where enhanced combustion is set up. Soon after the main wave has passed, the Schlieren light is completely obscured, partly by the turbulent gases but mainly by the smoke from the explosion of the detonator.

The explosion of a 9.5% methane-air mixture initiated by an azide detonator is shown in fig 2. Flame travels to the end of the tube at a slowly diminishing rate, its mean speed over the end portion of the tube being 1550 metres per second. This is considerably higher than the speed of the shock wave from the detonator in air. When the flame reaches the end of the tube, a wave is sent back at high speed, suggesting

\* Payman, Woodhead, and Titman, 'Proc. Roy. Soc., A', vol 148, p 615 (1935).

that the flame and the shock wave move together and that the shock wave has been reinforced and maintained at its initial high speed by the combustion of the methane. The speed of the flame is but little lower indeed than the rate of detonation, 1680 metres per second, for the mixture containing 11.1% methane in oxygen, and is thus close to the rate anticipated for a mixture containing 9.5% methane in air. Particles of aluminium are seen moving in front of the flame and some of them inflame on collision with the closed end of the tube. They travel at the same speed as the flame.

When the mixture of methane and air is replaced by one of methane and oxygen, a more luminous flame is produced, which travels at a much greater mean speed, 1920 metres per second. A striking feature of the record, shown in fig. 3, is the spontaneous ignition of aluminium particles ahead of the flame. It is rather remarkable that this flame should die out and should not ignite the methane-oxygen mixture. In two repeat experiments the records show the main flame only, unaccompanied by spontaneous ignition of aluminium, and the speed is lower, 1585 metres per second in one experiment and 1625 in the other. In each record the speed is uniform, and there is some indication of the flame being striated, there is no movement of the gas mixture ahead of the flame.

As is shown in fig. 4, particles are far less numerous when a copper-cased fulminate detonator is fired into air. A few particles ahead of the shock wave are observed, but they do not inflame when they strike the end of the tube, and their speed, about 1000 metres per second, is considerably less than that of the aluminium particles from an azide detonator. The speed of the shock wave, 950 metres per second, is slightly higher over this portion of the tube than that of the wave from an azide detonator.

Conditions under which copper-cased fulminate detonators can cause ignition of methane-air mixtures have not been found. Ignition experiments with these detonators have therefore been restricted to mixtures of methane with oxygen. In the explosion of a 9.5% mixture of methane in oxygen initiated by a fulminate detonator, fig. 5, the presence and influence of solid particles are negligible factors. The flame is striated and moves at a uniform rate through mixture previously quiescent. In three repeat experiments the measured rates, in each instance uniform, are 1590, 1595, and 1610 metres per second. The uniform rates of flame in the five mixtures containing 9.5% methane in oxygen yield an average rate of 1600 metres per second, which is in good agreement with the value of 1595 metres per second calculated for the rate of detonation in this

mixture using the Jouguet formula \* Thus it would seem that this methane-oxygen mixture is capable of true detonation

It is evident also that a high speed of flame, comparable with the rate of detonation in the corresponding methane-oxygen mixture, is obtained when a methane-air mixture (9.5% methane) is ignited by an aluminium-cased azide detonator. It cannot be said that the high speed is due entirely to the combustion of the methane, and that the explosion is a true detonation, for it has been shown that, initially, the products of explosion of the detonator (shock wave and flame) and, later, the solid particles therefrom, play an important part in sustaining the flame. This is shown clearly by figs 6, 7, 8, and 9, Plate 12, which were all taken at the open end of a 1-metre glass tube, 2.5 cm in diameter, in such a manner that a direct flame record was obtained of the explosion within the tube and a wave-speed record of the effects projected from the tube. For fig 6 an azide detonator was fired at the closed end of the tube filled with air. For fig 7 the tube contained a 9.5% mixture of methane in air and the flame of the burning methane-air mixture can be seen faintly within the glass tube. It is clear from the greater speed of the projected gases in fig 7 as compared with fig 6 that the influence of the burning methane is considerable. There is, however, a marked difference between this record and those obtained with true detonation in gas mixtures ignited by an electric spark, figs. 8 and 9. Fig. 8 shows the result when electrolytic gas is detonated within the tube at a rate of 2820 metres per second. There are no solid particles and the main shock wave sent out from the end of the tube gives a distinct trace. The front of the gaseous products is also well-defined. That the confusion of effects in fig 7 is not due to any rotatory movement of the flame is shown by comparison with fig 9 for which a mixture  $2\text{CO} + \text{O}_2$ , detonating at a rate of 1760 metres per second, was used. Although inside the tube the flame record is distinctly striated, outside the traces left by the shock wave and gases are similar to those recorded with a non-rotating flame, as in fig 8. The confused effects in fig 7 are evidently due mainly to an association with the combined shock wave and flame front of the products of explosion of the detonator, and a swarm of solid particles. These provide a supply of secondary energy for the maintenance of the flame †

\* "Mécanique des Explosifs," Paris, 1917

† Fig 15 is of further interest in showing that the striations persist in the gas within the tube after detonation has died down, hence they are not an optical effect due to the crossing of slow waves and luminous effects sent out from the wave front, as has been suggested (Bone, Fraser, and Wheeler, 'Phil. Trans.', A, vol. 235, p. 29 (1935)).

## LARGE-SCALE EXPERIMENTS

The apparatus used for the large-scale work has been described in detail elsewhere.\* The explosion gallery was a length of drawn-steel piping 30.5 cm. in diameter and 3.65 metres long, one end of which was permanently closed by a steel plate. The double windows necessary for the Schlieren photography of the explosion within the gallery were made by cutting ten slots, 30.5 cm. long and 6 mm. wide, symmetrically placed along each side of the gallery and covered with cellophane during an experiment. To maintain the strength of the gallery, the first window on each side started 9 cm. from the closed end and neighbouring windows were spaced 2.5 cm. apart. At the far end a length of 29 cm. was left uncut.

The gallery was mounted horizontally on a carriage, and in order to follow the progress of the explosion, it was moved in successive experiments to bring each pair of opposite windows in turn into the illuminating beam of light, for the width of the Schlieren field of view limited each wave-speed record of the explosion to this length of gallery. In passing across the gallery, the illuminating beam converged from 30.5 cm. to 27.7 cm. The lens of the camera was focussed on the axis of the gallery, and the Schlieren field of view was 29.1 cm., a shadow 4.1 cm. wide was cast by the metal left between windows.

The composite photographs shown in this paper are prepared by mounting side by side the records obtained in a series of experiments. A record covering a field of view immediately beyond the end of the gallery has been included on several of the composite photographs. The series of narrow vertical black bands are shadows cast by the metal strips between adjacent windows and the broader black bands correspond with the unslotted end-portions of the gallery.

For all the large-scale experiments, a standard mixture of methane and air, containing  $9.1 \pm 0.2\%$  of methane, was used in the gallery. In order to trace the effects of successive increments in the violence of the source of ignition on the propagation of flame along the gallery, the experimental work was divided into three sections in which the igniting sources were (1) the flame of a methane-air mixture, (2) a detonation wave in an electrolytic gas mixture, and (3) the detonation of a high explosive.

*Ignition by the Flame of a Methane-Air Mixture*—The methane-air mixture used for ignition was contained in a steel tube 2.5 cm. in diameter and 125 cm. long, closed at one end, the other end being open and projecting 9.5 cm. into the gallery through a hole at the centre of the steel

\* Shepherd, 'Bull. U.S. Bur. Min.', Washington, No. 354 (1932).

plate at the closed end. In this position the end of the tube coincided with the edge of the light passing through the first windows. The steel tube was filled with the standard mixture of methane and air, and ignition was by an electric spark passed near the closed end.

Fig. 10, Plate 13, shows a composite photograph of the explosion in the gallery and also of the effects extending 22 cm. beyond the far end, which in this experiment was closed by a waxed paper disk. As flame spreads through the methane-air mixture in the ignition tube, the mixture ahead of the flame is being pushed out of the open end into the gallery. The forerunner of this gas movement is a vortex ring,\* shown faintly as a black and white trace in the top right-hand corner of the record. Flame appears some 7 milliseconds later and ignites the mixture within the gallery. The explosion then proceeds along the gallery. After travelling about 20 cm., the flame slows down and continues at a fairly uniform rate of about 50 metres per second until the fourth window is reached. From this point it accelerates and has a speed of 200 metres per second when it reaches the end of the gallery, its mean speed being 87 metres per second. Shock waves do not appear to be established during the explosion.

The paper disk closing the end of the gallery is blown out about 13 milliseconds after the first appearance of flame in the gallery and about 30 milliseconds before the flame reaches the far end. The torn paper is shown by the inclined black band in the top left-hand corner of fig. 10. At the instant of rupture, a shock wave is sent out into the air at a speed of 340 metres per second, and from the moment of rupture until the arrival of the flame gas mixture is being pushed out of the gallery.

Rupture of the disk so early in the course of the explosion, and in the absence of shock waves, can be due only to increased pressure arising from the early stages of the combustion. The speed of sound in the gallery mixture at atmospheric temperature is about 340 metres per second, and a line drawn on the record backwards from the instant of rupture of the disk with an inclination equivalent to this speed joins the trace of the flame when it is about half-way along the first window. Combustion up to this point must have supplied the pressure required to burst the disk. Pressure developed by the flame beyond this point can have no share in causing the rupture since, in the absence of shock waves, it cannot be dissipated at a rate faster than the speed of sound. Similarly, a line drawn downwards with a declination corresponding to the speed of sound from the same point at the end of the gallery meets the trace of the flame when the latter is passing the fourth window. If this line is

\* Gawthrop, Shepherd, and Perrott, 'J. Franklin Inst.', vol. 211, p. 67 (1931).

regarded as the trace of a wave travelling back along the gallery at the speed of sound, its arrival at any point marks the first instant at which the effect of the now open end can be felt at that point. Thus the flame begins to feel the effect of the open end when it is at the fourth window and it is here, as we have seen, that the flame begins to accelerate. The course of events is shown more clearly in later records where the front of the disturbance ahead of the flame is bounded by a shock wave, the track of which is self-recorded.

*Ignition by Electrolytic Gas*—The electrolytic gas, contained in the ignition tube used in the previous experiments, was ignited by an electric spark. The open end of the tube was sealed by a piece of adhesive rubber tape, which was removed immediately before the spark was passed. Three series of experiments were carried out in order to examine the effect of different conditions at the end of the gallery distant from the source of ignition.

(a)—*Gallery Open at the Far End*—For this series of experiments the far end of the gallery was opened immediately before the igniting spark was passed in the electrolytic gas. Detonation in the electrolytic gas was quickly set up and gave rise at the end of the tube to a main shock wave and to a number of minor waves which can be seen travelling along the gallery, fig 11, Plate 13. The main wave spreads spherically until it reaches the wall of the gallery, during which period its speed steadily diminishes. Thereafter the front of the wave, which proceeds along the gallery as the pioneer effect of the explosion, has a constant velocity of 360 metres per second. As it leaves the gallery and begins to expand spherically, the wave forms a large vortex ring, shown by the composite black and white trace at V. A number of feeble waves are reflected at a small cavity near the open end of the gallery.

The methane-air mixture is ignited as soon as the detonation wave in the electrolytic gas emerges from the ignition-tube, and flame is propagated at gradually diminishing speed until it reaches the third window. It then travels to the seventh window at a fairly uniform speed of 120 metres per second. Thenceforward the flame accelerates, for it is now influenced by the open end of the gallery. The effect of the open end will obviously first be felt by the flame when it meets the feeble waves returning from the open end. These waves are travelling back at a speed approximating to that of sound in the mixture, although their apparent speed is less. Until these waves return, the explosion progresses wholly unaffected by the open end. When they have passed, the effect of the free outlet for the

gases pushed ahead of the flame is felt, and from this point an acceleration of the flame begins and persists until the end of the gallery is reached. The average speed of flame inside the gallery is 178 metres per second, the maximum 512 metres per second. Ten milliseconds after flame leaves the open end, gas is sucked back into the gallery as cooling takes place.

Although the speed of flame was increased by the use of a stronger source of ignition, speeds comparable with that of detonation were not attained. Nevertheless, at the open end of the gallery, the speed of flame is but little less than those recorded by Robinson and Wheeler (*loc cit*) in experiments with a restricted gallery of the same diameter. The high speed attained is due to the current of gas mixture escaping from the gallery ahead of the flame, in which current the flame is itself propagating. Thus the measured speed is only an apparent speed and the true rate of propagation through the gas mixture is much less.

(b)—*Gallery Closed by a Waxed Paper Disk*—When the far end of the gallery is closed by a waxed paper disk, the development of the explosion is not altered appreciably, fig 12, Plate 14. The main shock wave from the detonating gas mixture again travels along the gallery at a speed of 360 metres per second. On impact with the disk, part of the wave is transmitted and part is reflected. Ruptured by the impact, the paper disk casts a black shadow on the record as it moves away from the end of the gallery. The wave, which travels onwards, expands spherically in the air and has a mean speed of 340 metres per second over the first 20 cm after leaving the gallery. The speed of the reflected wave gradually decreases and the mean value relative to the gallery is 290 metres per second. When the reflected wave meets the flame, at the seventh window, a regime of constant speed of flame (125 metres per second), established soon after ignition, is terminated. After a temporary retardation the flame begins to accelerate under the effect of the now open end, and it attains an apparent speed of 520 metres per second on reaching the end of the gallery. This speed and the mean speed of the flame throughout the gallery (170 metres per second) are similar to those observed with the open gallery in the previous experiment.

The reflected wave travels at a mean apparent speed of 290 metres per second. Its true speed, however, must be at least that of sound in the mixture, that is, 340 metres per second, and therefore the gas mixture must be moving forward at a speed of not less than 50 metres per second. This wave is more powerful than the weak reflected waves shown in fig 10, and its arrival at any point marks the first instant at which the effect of the now open end of the gallery can be felt. But in that part of

the gallery not yet reached by this wave, the explosion is developing under steady conditions. Pressure, which rises steadily as combustion proceeds, is being dissipated with at least the speed of sound, the speed of the flame being uniform. Thus the reflected wave as it returns encounters mixture at progressively increased pressure. It is this process of continuous equalization of a steadily rising pressure from a flame travelling at constant speed that imparts movement to the gas layers. From the speeds recorded, each individual layer as it is encountered by the returning wave is moving forward at a speed of about 50 metres per second. After the reflected wave has passed any layer, the behaviour of the latter is immediately changed as the open end of the gallery begins to exert its influence. The pressure along the gallery falls from that of the layer just passed to that of the atmosphere just beyond the open end and a current of mixture is established, because of this pressure gradient. When the flame passes through the reflected wave, the presence of this current is at once made evident by the accelerated motion of the flame. It is illustrated also in the motion of later shock waves which re-enter the gallery after reflexion at the paper disk as it moves away from the end. As they re-enter, their apparent speed is about 170 metres per second, which means that they encounter gas moving in the opposite direction at roughly the same speed. As they approach the flame, their speed falls still more and the speed of the current is calculated to be about 220 metres per second. Since the apparent speed of the flame at this point is 325 metres per second, it follows that the true speed of the flame is 105 metres per second. Still later, waves reflected at the paper are prevented from entering the gallery. They leave parabolic traces on the record beyond the end\*. Hence the mixture must be issuing from the gallery at a rate exceeding the true speed of these later waves. The speed of the current, as calculated from the slope of these traces, is 415 metres per second just in front of the flame. Since the apparent speed of the latter is 520 metres per second, it follows that the true flame speed is 105 metres per second, a value equal to that found for the flame within the gallery. This speed is comparable with that of the constant movement which persisted up to the arrival of the reflected wave.

(c)—*Gallery Closed by a Steel Plate*—The principal effect of closing the far end of the gallery by a steel plate is to retard the flame in the later stages of the explosion, fig 13, Plate 15. The development of the explosion is exactly the same as in the two previous experiments up to the time when

\* Similar behaviour of shock waves in a totally closed vessel have been recorded by Payman and Titman, 'Proc Roy Soc,' A, vol 148, p 615 (1935).

the reflected wave meets the flame. The time is somewhat earlier because here the reflected wave travels back at a higher speed due to its total, instead of partial, reflexion at the end. Driving back the flame front at the end of the sixth window, the wave passes on through the hot gases behind the flame at increased speed. Just before meeting the flame its rate is 310 metres per second, and on entering the hot gases it accelerates to give a mean speed of 475 metres per second over the sixth window. The rate rises to 910 metres per second over the fifth window and thence to the end of the gallery it is 1070 metres per second. After reflexion at the ignition-end, the wave overtakes and passes through the flame, which surges forward. It is again reflected at the far end and once more meets and retards the flame, this process being repeated until the flame has succeeded in traversing the gallery. On the first occasion that the wave reflected from the ignition-end overtakes the flame, it is partly transmitted and partly reflected at the interface of flame and unburnt mixture. The wave reflected back from the flame is clearly shown and the movements of this wave and the stronger parent wave can be followed for many journeys to and fro. Close examination of the record shows that it is the parent wave rather than the waves produced by partial reflexions which controls the flame movement.

The principal vibrations of the flame front are thus traceable to the effect of the main shock wave and also to the pressure changes, occurring at the ends of the gallery, which are heralded by this wave. The frequency of the vibrations increases from 89 to 140 per second as the flame spreads through the gallery and at the same time their amplitude diminishes. The natural frequency of the gallery is determined by the average speed of sound therein, which increases as the mean temperature rises. In other words, the frequency of vibration is fixed by the combined length of the burnt and unburnt gases. This is confirmed by the movement observable in the hot and cold gases, for this synchronizes with the oscillatory motion of the flame.

The first shock wave produced by the detonation of the gas mixture in the ignition-tube has a speed of 363 metres per second. Later, the wave has a speed in the unburnt mixture of between 450 and 500 metres per second. The rise in speed can be caused only by a rise in temperature due to adiabatic compression of the unburnt gases. This heating is probably the cause of the eddies which can be seen in the gases ahead of the flame about 25 milliseconds after ignition and which follow closely the pendulum motion of the flame, within which they are gradually absorbed. The increase in speed of the wave is roughly equivalent to a rise in temperature of  $150^{\circ}\text{C}$ . in the medium. In a few records evidence

has been obtained of auto-ignitions in the methane-air mixture ahead of the flame due to this adiabatic heating supplemented by momentary heating in passing shock waves Fig 14, Plate 15, shows an auto-ignition of the methane-air mixture at a point 14 cm. in advance of the flame.

The mean speed of flame throughout the gallery is about 38 metres per second and the explosion lasts about one-tenth of a second High speeds of flame are not developed except over short distances in isolated experiments, when it sometimes happens that a shock wave emerges from the flame when the latter is about to surge forward in a vibration The shock wave then drags the flame with it at its own speed, but the flame soon lags behind and the two effects separate This combination of wave and flame is shown, to some extent, in the lower portion of fig 14, in which the speed of the shock wave is 500 metres per second \*

*The Effect of Restrictions*—It appeared probable that since high speeds of flame are obtained in a methane-air mixture when restrictions are placed in the path of the flame, or when a strong source of ignition is used, a combination of these would result in still higher speeds With a single restriction placed near the end of the gallery and ignition by detonating electrolytic gas, the speeds of flame in and beyond the restricted zone were not so high as those obtained by Robinson and Wheeler (*loc cit*) With three restrictions, consisting of annular rings, spaced 33 cm apart, which reduced the cross-section of the gallery to one-half, a maximum speed of 420 metres per second was obtained just beyond the restricted zone A speed of 545 metres per second was obtained with three rings which reduced the cross-section to one-quarter When either of these sets of restrictions was used speeds of about 800 metres per second were obtained near the open end of the gallery

Fig 15, Plate 14, shows the composite record of the explosion along the gallery equipped with the three rings which reduced the cross-section to one-quarter The rings were placed midway along the second, third, and fourth windows of the gallery, the far end of which was closed by a paper disk The restrictions presented a narrow edge to the light passing through the gallery, and their positions are shown by the black shadows on the record These shadows have been marked by the letter R on the record.

The main shock wave from the detonation of the electrolytic gas is degraded as it passes through each restriction, and its speed beyond the

\* The diffuse horizontal bands seen very clearly in the flame gases during the first 18 milliseconds in these composite records are of the type discussed in an earlier paper (Shepherd, 'Bull. U S Bur Min.,' Washington, No 354 (1932)).

restricted zone is 345 metres per second as compared with 360 metres per second in a smooth gallery. As this, and each following wave, meets a restriction, part passes through the opening and the rest is reflected from the solid face. As the transmitted portion passes through the restriction and begins to spread afresh to the walls of the gallery, it gives rise to a vortex ring which is recognized by its distinctive composite trace.

As the flame passes through the restricted zone its speed progressively increases and is 545 metres per second on emergence. This speed is maintained only over a distance of about 15 cm, after which it falls to 400 metres per second and then remains constant until the flame passes out of view at the end of the tenth window. Up to this late stage the explosion spreads unaffected by the end of the gallery towards which it is travelling, for no shock wave has as yet reached this end. A period of uniform movement exists, it will be recalled, under similar conditions in the smooth gallery.

An interesting feature of the record is the building up, beyond the restricted zone, of an intense shock wave by the coalescence of lesser waves successively overtaking each other. These waves appear to originate at, or in, the flame front during its travel over the first metre beyond the restrictions, and they have united to form a single wave just as the primary wave is overtaken. The final speed of the combined waves is 575 metres per second. Soon after the intense shock wave has ruptured the disk at the end of the gallery, the phase of uniform movement is disturbed, presumably by the wave reflected from the disk, and acceleration of the flame sets in. Flame issues from the end of the gallery at the high speed of 785 metres per second and the increase in speed from 400 to 785 metres per second occurs over the end 29 cm of the gallery, despite a momentary retardation when the flame collides with the reflected wave. This rapid acceleration of the flame is indicative of the high pressure which exists in the immediate rear of the shock wave and is released when the disk is ruptured. The reflected wave travels back through the hot gases at 890 metres per second.

Although the effect of the restrictions is to increase further the violence of the explosion, the highest speed of flame is attained at the mouth of the gallery and is largely due to the rapid motion of the unburnt mixture. It is not an intrinsic speed of the flame, which has no characteristics of a true detonation wave. During the explosion beyond the restricted zone, the flame proceeds at a uniform rate of 400 metres per second and combustion is so intense that shock waves are emitted from the flame surface, but the flame is unable to maintain itself at the speed of the waves and it lags behind.

*Ignition by High Explosives*—For experiments with high explosives the ignition-tube was replaced by a small steel cannon with a bore-hole 2.5 cm in diameter and 38 cm long. When placed in position, the cannon projected through the end plate of the gallery and the front face came nearly to the boundary of the light passing through the first pair of windows. The cannon was loaded with a charge of explosive pushed to the back of the bore and primed with a No. 6 fulminate detonator inserted in the end of the cartridge nearer to the mouth. Under these conditions a small charge of any high explosive, unstemmed, is sufficient to ignite the 9% mixture of methane and air. The particular explosive used in these experiments was one of the class permitted for use in fiery coal mines and had the following composition: ammonium nitrate, 65%; trinitrotoluol, 14.6%; sodium chloride, 20.3%; and moisture, 0.1% by weight. In preliminary tests a charge of 50 gm was found to cause ignition in five consecutive shots, 30 gm did not cause ignition and intermediate weights gave irregular ignitions. A weight of 50 gm was adopted as the standard charge.

The explosion following ignition by this charge is shown in fig. 16, Plate 16, and it is clear that detonation or something closely resembling it has been established in the methane-air mixture. A steady decrease in the speed of the intense shock wave sent out by the explosive occurs over the first 60 cm of the gallery, but at the third window it becomes apparent that the wave has begun to accelerate. The acceleration is shown in the average speeds past the first, second, third, and fourth windows which are 1450, 1130, 1250, and 1400 metres per second. Since there is no movement of the mixture ahead of the shock wave, this rise in speed must be caused by the addition of energy from some cause acting in or from behind the shock wave itself. With only air in the gallery the decrease in speed of the wave is continued throughout. Initially in close contact with the wave is the primary flame of the explosive, but this does not extend beyond the first window. Products of the detonation, shown as a black area because of their opacity to the light, are also in intimate contact with the shock wave and the flame.

When the wave begins to accelerate at the third window, flame is well established in the rear part of the gallery. Within the products there suddenly appears a second flame, which travels forwards at high speed and overtakes and causes the acceleration of the main wave near the end of the second window. From this point flame and shock wave travel along the gallery with little or no separation. Later, more flames similar in type to the second flame are visible in the products joining the shock wave-flame front at the fourth and later windows of the gallery. The

formation of these flames is ascribed to a sequence of waves formed by repeated reflexion at the gallery wall of the first spherical wave from the detonation \*. These waves, causing re-illumination of the gases in their path, travel along at regular intervals and periodically reinforce the main shock wave and the flame front. Flame exists in the wave front at the fourth window, and this combination persists to the end of the gallery. Acceleration of the front of the explosion is still continuing when, midway along the sixth window, "detonation" is apparently established within the flame. The "detonation" quickly overtakes the wave front and then proceeds to the end of the gallery at a mean rate of 1900 metres per second. Reflexion takes place at the paper disk at this end and the returning wave has a speed which initially is 815 metres per second and later increases to 1060 metres per second. That the paper disk remains intact until struck by the "detonation" is further proof that the methane-air mixture is quiescent until absorbed in the "detonation" wave. At the inception of this "detonation", a "retonation wave" is produced which causes a revival of luminosity in the hot gases in the rear. This "retonation wave" is clear and is distinct from the minor waves visible on many records and caused by reflexion at the end of the wave from the flat ends of the windows cut in the wall of the gallery.

Figs 17 and 18, Plate 16, are separate records of the explosion passing the sixth and eighth windows. In addition to the central Schlieren record, they show flame directly photographed through the adjacent windows and they record the inception of "detonation" and the later propagation of the flame. In fig 18 the flame has a uniform speed of 1950 metres per second. The reduced luminosity and apparent reduced speed of the flame at the extremities of the record illustrate one difficulty of the direct photography of flame in a gallery of this large diameter, for flame is recorded as soon as any part of it enters the diverging field covered by the camera lens. Since this field diverges considerably from front to back of the gallery, the apparent distance travelled by the flame is less than the actual distance, and an error is therefore introduced into the speed measurements. This error may amount to as much as 10% with the optical arrangements used in the present experiments and is shown as an apparent reduction in speed. If speed measurements are confined to the central Schlieren portion of each record the error is much reduced. The frequency of the waves travelling back along the gallery and made visible by re-illumination of the gases in their path in both figs 16 and 17 is about 3000 per second.

\* Shepherd, 'Bull. U S Bur Min,' Washington, No. 354 (1932).

The explosion has been referred to in the foregoing description as "detonation", and in many characteristics it is indistinguishable from detonation. Intense luminosity is developed. The flame travels at a high and uniform speed. Gas ahead of the flame remains undisturbed until absorbed in the wave front. At the inception a "retonation wave" is produced. The explosion is attended by high pressure, for in an early experiment the gallery was split open over five feet along both sides towards the end remote from the cannon.

On the composite record, fig. 16, each section of which was obtained in a separate experiment, the flame travels at a rate of 1900 metres per second. The rates of "detonation" measured on the individual records vary between 1820 and 1950 metres per second, but on any single record the rate is uniform. Different records show that the point of initiation of the "detonation" is variable, for example, it has been observed at the sixth, seventh, and eighth windows. This may mean that the "detonation" is not continuous and that a single record of the whole explosion would reveal intermittent phases of "detonation". Nevertheless, it is true that two points of "detonation" have never been shown on any one record, despite the fact that the full width of the records covers about 70 cm. of the gallery. The records disclose, however, that the main front of the explosion is periodically reinforced by the arrival of shock waves from behind.

Experiments with air in the gallery show that, on the detonation in the cannon of the 50-gm. charge of explosive, a cloud of particles is projected at high speed and that these particles begin to break through the main shock wave at the third window where, in an ignition of a methane-air mixture, acceleration of the explosion front is first noted. The majority of these particles, which are extremely hot as they emerge from the wave into the undisturbed atmosphere ahead, is composed of the inert salts contained in the original explosive and small agglomerates of explosive which have escaped detonation in the cannon. Due to their inertia, the particles maintain their initial high speeds over considerable distances. It is to be expected, therefore, that when the second flame within the products spreads, at the third window, to the wave front and acceleration begins, these particles are entrained. The sustaining influence of hot particles has been illustrated in the experiments with aluminium-cased detonators. The two effects—the following waves and the hot particles—form in the wave front secondary sources of energy which assist the maintenance of the explosion.

Comparatively, it would seem that the magnitude of the secondary energy is less in the large-scale than in the small-scale experiments. Yet

the explosions in the gallery have more characteristics of true detonation than those in the 2.5-cm tube. Thus it is possible that, as the diameter of the explosion chamber increases, the secondary energy required to establish quasi-detonation is reduced. It is clear that 9.1% methane-air mixtures in the 30.5-cm gallery are near to the border line of true detonating mixtures.

Experiments have been carried out with smaller charges of the same explosive. Ignition is occasionally caused by cartridges only 35 gm in weight and the resultant explosion is of a slow type which has been observed exceptionally in one or two tests with the standard 50-gm charge. Similar results are obtained with other kinds of high explosives; with small igniting charges, the rate of inflammation is comparatively slow whilst larger charges give rise to explosion similar to that which has been described as quasi-detonation.

#### SUMMARY

Experiments on a small and on a large scale have been carried out to investigate the possibility of detonation in mixtures of methane and air.

In the small-scale experiments the methane-air mixture was contained in a narrow tube, 2.5 cm in diameter, and aluminium-cased lead azide detonators were used as the source of ignition. The resulting explosion is in many respects similar to detonation, a luminous flame propagates at a high speed through mixture which remains at rest until arrival of the flame, and a high pressure is generated. It is unlike detonation, in that the speed is not uniform and the wave or flame front is partly sustained first by the flame and then by hot particles from the detonator. The explosion is described as "quasi-detonation", since the energy maintaining the wave is not wholly derived from the combustion of the methane.

Copper-cased mercury fulminate detonators do not ignite methane-air mixtures. They ignite and establish immediate detonation in a 9.5% mixture of methane with oxygen. Lead azide detonators set up detonation in this methane-oxygen mixture at a considerably higher rate. This propagation at higher than the normal detonation rate, due to the additive effect of a secondary source of energy, is commonly noted immediately after the inception of detonation in gaseous mixtures with other modes of ignition.

An explosion which is similar to detonation was also established in large-scale experiments in which a 9.1% methane-air mixture was con-



Fig. 1.

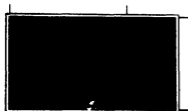


Fig. 2.



Fig. 3.

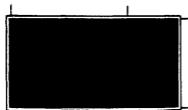


Fig. 4.

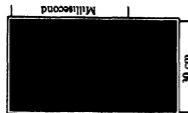


Fig. 5.

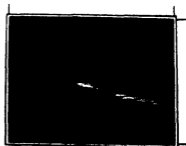


Fig. 6.



Fig. 7.

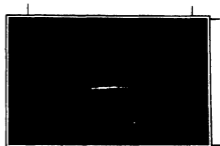


Fig. 8.

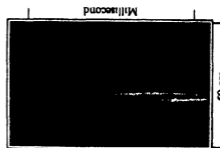


Fig. 9.



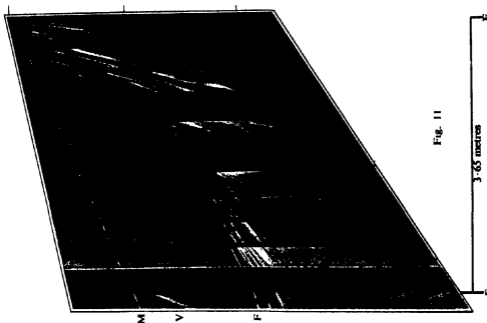


Fig. 11

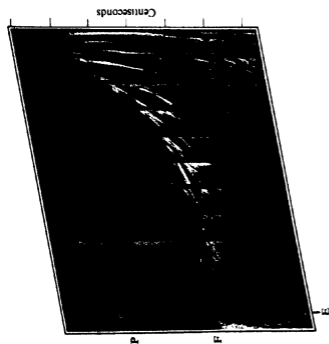


Fig. 10

M — Main wave  
V = Vortex ring  
F = Flame

E End of explosion gallery  
R Restriction  
P = Paper disk



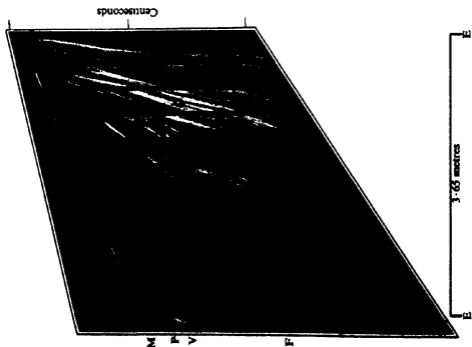


Fig. 12.

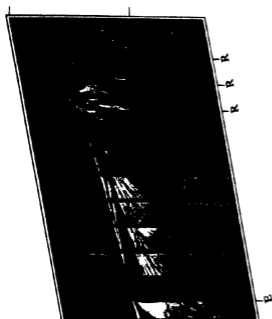


Fig 15

M = Main wave  
V = Vortex ring  
F = Flame

E = End of explosion gallery  
R = Restriction  
P = Paper disk



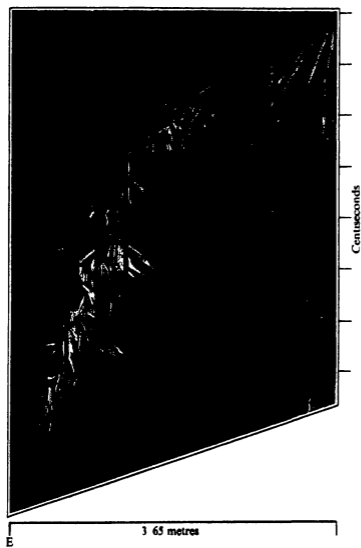


Fig 13

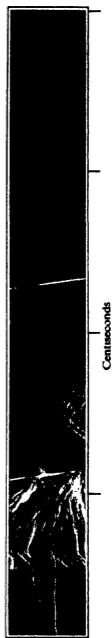


Fig 14



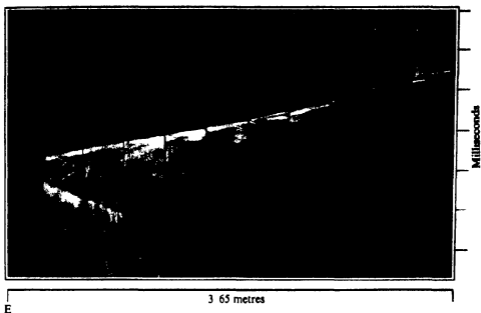


Fig 16



Fig. 17



Fig. 18.



tained in a gallery 30.5 cm. in diameter and ignited by means of a charge of high explosive. This quasi-detonation is propagated through quiescent mixture at a uniform rate of 1900 metres per second and the flame is intensely luminous and accompanied by high pressure

High speeds of flame in methane-air mixtures are also observed in the large gallery when the source of ignition is detonating electrolytic gas,  $2\text{H}_2 + \text{O}_2$ . These high speeds are due to the fact that the flame is propagating through mixture which is itself in rapid motion, and there is no semblance to detonation. The effect may be increased by placing restrictions along the gallery, when speeds of about 800 metres per second are attained and combustion becomes so intense that shock waves are sent out, but the flame is unable to maintain itself at the speed of the waves it emits. When the gallery is securely closed at both ends, an extensive movement of gas mixture ahead of the flame is not possible and much lower speeds are recorded. The shock wave from the igniting source suffers repeated reflexion and imposes vibratory movements on the flame front. The interface between unburnt and burning mixture acts as a partial reflector of waves inside the hot gases. Adiabatic heating of the body of mixture ahead of the flame takes place as pressure inside the closed gallery rises and spontaneous ignition may occur in this heated zone under the added influence of passing shock waves

---

# The Lorentz Transformations in the New Quantum Electrodynamics

By L. INFELD, LW6W

(Communicated by R. H. Fowler, F.R.S.—Received 15 July, 1936)

In the paper "Quantization of the New Field Equations—I," written by Born and Infeld,<sup>†</sup> we tried to give in the last section a proof of the invariance of the commutation rules under Lorentz transformations. The proof given there is not only very intricate, but also, as Feenberg kindly pointed out, not correct in the use of the  $\delta$ -functions. As a formalism analogous to ours was recently used by H. Euler<sup>‡</sup> and may, perhaps, find application in the further development of the theory, it seems desirable to give a simple and strict proof of the Lorentz invariance. This is the problem with which we shall deal in this paper.

## 1—DEFINITIONS AND NOTATIONS

In this section we shall repeat some of the results previously obtained. Using the same notation,  $\mathbf{B}$  and  $\mathbf{D}$  are the fundamental field vectors—

$$\left. \begin{aligned} \mathbf{B} &\rightarrow f^{*14}, f^{*24}, f^{*34}, & \mathbf{E} &\rightarrow f^{*23}, f^{*31}, f^{*12} \\ \mathbf{D} &\rightarrow p_{14}, p_{24}, p_{34}, & \mathbf{H} &\rightarrow p_{23}, p_{31}, p_{12} \\ \mathbf{E} &= \frac{\partial U}{\partial \mathbf{D}}, & \mathbf{H} &= \frac{\partial U}{\partial \mathbf{B}}, & U &= \text{energy density} \end{aligned} \right\} \quad (1.1)$$

The commutation rules<sup>§</sup> are

$$\left[ f, \int G dv \right] = \frac{\partial f}{\partial \mathbf{B}} \cdot \left( \nabla \times \frac{\partial G}{\partial \mathbf{D}} \right) - \frac{\partial f}{\partial \mathbf{D}} \cdot \left( \nabla \times \frac{\partial G}{\partial \mathbf{B}} \right), \quad (1.2)$$

where  $f$  and  $G$  are arbitrary functions of  $x, y, z, t, \mathbf{B}, \mathbf{D}$  || Putting

$$f \rightarrow \mathbf{B}^*, \mathbf{D}; \quad G \rightarrow \delta(x - x') \delta(y - y') \delta(z - z') \mathbf{B},$$

<sup>†</sup> 'Proc. Roy. Soc.,' A, vol. 147, p. 522 (1934), quoted as I.

<sup>‡</sup> 'Ann. Physik,' vol. 26, p. 398 (1936).

<sup>§</sup> 'Proc. Roy. Soc.,' A, vol. 150, p. 141 (1935), quoted as II.

|| II, p. 144.

respectively, we obtain the fundamental commutation rules

$$\left. \begin{aligned} [B_k, B'_l] &= 0, & [D_k, D'_l] &= 0, & [B_k, D'_l] &= 0 \\ [D_1, B'_2] &= -[B_1, D'_2] = \delta(x-x') \delta(y-y') \delta_z(z-z') \\ \delta_s &= \frac{\partial \delta}{\partial z}, & k, l &= 1, 2, 3 \end{aligned} \right\} \quad (13)$$

In II we introduced the tensor†

$$\left. \begin{aligned} M^{ki} &= \int (x^k T^{4i} - x^i T^{4k}) dv \\ T^{4k} &\rightarrow (\mathbf{S}, U), & \mathbf{S} &= \mathbf{D} \times \mathbf{B}, & x^k &\rightarrow x, y, z, t \\ k, l &= 1 & 4 \end{aligned} \right\} \quad (14)$$

and proved that

$$M^{ki} = [W, M^{ki}] + \frac{\partial M^{ki}}{\partial t} = 0, \quad W = \int U dv,$$

i.e.,  $M^{ki}$  are integrals of the motion

## 2—LFMMA

From (12), (14) we obtain

$$\begin{aligned} [p^{i4}, M^{mn}] &= \delta^{4n} p^{im} - \delta^{4m} p^{in} + \delta^{im} p^{4n} - \delta^{in} p^{4m} \\ &\quad + x^m \delta^{4n} \frac{\partial p^{4i}}{\partial x^s} - x^n \delta^{4m} \frac{\partial p^{4i}}{\partial x^s}, \end{aligned} \quad (21)$$

$$\begin{aligned} [f^{*i4}, M^{mn}] &= \delta^{4n} f^{*im} - \delta^{4m} f^{*in} + \delta^{im} f^{*4n} - \delta^{in} f^{*4m} \\ &\quad + x^m \delta^{4n} \frac{\partial f^{*4i}}{\partial x^s} - x^n \delta^{4m} \frac{\partial f^{*4i}}{\partial x^s}, \end{aligned} \quad (22)$$

$$\delta_{11} = \delta^{11} = \delta_{22} = \delta_{33} = \delta^{33} = -1, \quad \delta_{44} = \delta^{44} = +1$$

We shall verify (21) only for one special case, say  $l = 1, m = 1, n = 2$ , as the calculations in the other cases are quite similar. We have

$$\begin{aligned} p^{14} &= -D_1, & M^{12} &= \int (xS_2 - yS_1) dv \\ S_1 &= D_2 B_3 - D_3 B_2, & S_2 &= D_3 B_1 - D_1 B_3 \end{aligned}$$

Using (12) where

$$G = xS_2 - yS_1, \quad f = D_1,$$

† II, p. 154.

we find

$$[D_1, M^{12}] = -\frac{\partial}{\partial y} \frac{\partial G}{\partial B_2} + \frac{\partial}{\partial z} \frac{\partial G}{\partial B_1} = x \frac{\partial D_1}{\partial y} + D_1 + y \frac{\partial D_1}{\partial y} + y \frac{\partial D_1}{\partial z},$$

or, taking account of the field equations  $\operatorname{div} \mathbf{B} = 0$ ,  $\operatorname{div} \mathbf{D} = 0$ ,

$$[D_1, M^{12}] = -y \frac{\partial D_1}{\partial x} + x \frac{\partial D_1}{\partial y} + D_1 = x^1 \frac{\partial p^{41}}{\partial x^2} - x^2 \frac{\partial p^{41}}{\partial x^1} + p^{42},$$

and this is exactly (2.1) for  $l = 1$ ,  $m = 1$ ,  $n = 2$

### 3—THE INFINITESIMALLY SMALL LORENTZ TRANSFORMATION

Let  $x^k$  ( $k = 1 \dots 4$ ) denote the coordinates of a world point in the coordinate system  $\Sigma$  and  $\bar{x}^k$  ( $k = 1 \dots 4$ ) the coordinates of a world point in the coordinate system  $\bar{\Sigma}$ . We shall consider only the following infinitesimally small transformation from  $\Sigma$  to  $\bar{\Sigma}$

$$\bar{x}^m = \delta_n^m x^n + \epsilon_n^m x^n. \quad (3.1)$$

The dot in  $\epsilon_n^m$  denotes the order of the suffixes,  $e, g$ ,

$$\epsilon_2^3 = \delta_{22} \epsilon^{32} = -\epsilon^{23}, \quad \epsilon_{43} = \delta_{44} \epsilon^4_3 = \epsilon^4_3 \quad (3.2)$$

In consequence, we shall neglect in all the following calculations the expressions in which the products of two  $\epsilon_{nm}$  appear

We find from (3.1)

$$x^m = \delta_n^m \bar{x}^n - \epsilon_n^m \bar{x}^n. \quad (3.3)$$

From the invariance of  $x_n x^n$  it follows that

$$\epsilon_{rn} = -\epsilon_{nr} \quad (3.4)$$

When  $r = n$  we have, therefore,  $\epsilon_{rr} = 0$

All results which we shall obtain, assuming an infinitesimally small transformation, are also valid for a finite transformation because of the group character of the Lorentz transformations

Our commutation rules are defined only for the same time  $t$  in the functions  $f$  and  $G$ . In order to find the transformation rules for (1.3), we have to choose two world points with the *same* numerical values of the coordinates in  $\Sigma$  and  $\bar{\Sigma}$ . The transformation formula for  $p^{kt}$  and  $f^{*kt}$  are therefore

$$\left. \begin{aligned} \bar{p}^{kt} &= p^{kt} + p^{n4} \epsilon_n^k + p^{kn} \epsilon_n^4 - \frac{\partial p^{kt}}{\partial x^i} \epsilon_i^1 x^1 \\ \bar{f}^{*kt} &= f^{*kt} + f^{*n4} \epsilon_n^k + f^{*kn} \epsilon_n^4 - \frac{\partial f^{*kt}}{\partial x^i} \epsilon_i^1 x^1 \end{aligned} \right\} \quad (3.5)$$

The last expression on the right-hand side arises from the fact that the two world points in  $\Sigma$  and  $\bar{\Sigma}$  are not identical, but that their coordinates have the same numerical values

We shall show now that it is possible to write (3.5) in the following form

$$\left. \begin{aligned} \bar{p}^{k4} &= p^{k4} + \epsilon [p^{k4}, M] \\ f^{*k4} &= f^{*k4} + \epsilon [f^{*k4}, M] \end{aligned} \right\}, \quad (3.6)$$

where

$$\epsilon M = \frac{1}{2} \epsilon_{rs} M^{rs}, \quad (3.7)$$

and the factor  $\epsilon$  has to remind us that the additional expression in (3.6) is infinitesimally small. To prove (3.6) we have only to use (2.1) and carry out the summation indicated in (3.7). It is important to notice that  $M^{rs}$  does not depend either on space or on time coordinates. We can, therefore, write (3.6) in a still different way—

$$\left. \begin{aligned} \bar{p}^{k4} &= S p^{k4} S^{-1}, & f^{*k4} &= S f^{*k4} S^{-1} \\ S &= 1 - \frac{i}{\hbar} \epsilon M; & S^{-1} &= 1 + \frac{i}{\hbar} \epsilon M \end{aligned} \right\}. \quad (3.8)$$

And as the right-hand sides in equation (1.3) are c-numbers, we see immediately that the relativistic invariance of the fundamental commutation rules (1.3) follows from (3.8), considering the fact that the components of  $\mathbf{D}$  and  $\mathbf{B}$ , appearing in (1.3), are all of the type  $p^{k4}$ ,  $f^{*k4}$ .

[*Note added in proof*, 15 October, 1936—I have just been informed by Mr M. H. L. Pryce that he has independently developed this method in a more general context. This is being published in 'Proc. Roy. Soc.,' A.]

I should like to thank Professor M. Born for drawing my attention to this problem.

#### SUMMARY

The relativistic invariance of the commutation rules (1.3) was proved in a simple way by introducing the tensor  $M^{rs}$ , the components of which are integrals of the motion.

## The Hyperfine Structure and Zeeman Effect of the Resonance Lines of Silver

By D A JACKSON and H KUHN, Clarendon Laboratory, Oxford

(Communicated by F A Lindemann, F R S—Received 18 July, 1936)

[PLATES 17-19]

### INTRODUCTION

In the work described below, the hyperfine structure of the resonance lines of silver was investigated by the method of absorption in an atomic beam \*. The intensities of the observed components were measured, and the structure in a magnetic field was observed, from the results the nuclear spins and magnetic moments of both of the isotopes of silver were determined

### EXPERIMENTAL

#### 1—*The Spectrograph and Interferometer*

The high resolving power instrument used was a Fabry-Pérot interferometer combined with a  $1\frac{1}{2}$ -m spectrograph, fitted with a Cornu quartz prism and quartz rock salt achromatic objectives. The étalon plates were plane to about 1/100 of a wave-length and were coated by evaporation with aluminium. The resolving power of the étalon was about 1/10 of an order for light of wave-length 3100 Å, the plates and separating pieces were made of fused silica. The instrument has been described before

#### 2—*The Light Source*

The light source used to produce the resonance lines of silver in which the absorption of the atomic beam was to be observed was a fused silica discharge tube of the "end-on" type, fitted with external electrodes and excited by a 1/2 kw high frequency oscillator. The tube was filled with Ne-He mixture at 2-3 mm pressure, and the capillary contained a small quantity of silver chloride, which was heated by a current in a nichrome wire. The vapour pressure of the silver chloride could be very exactly controlled by adjusting the heating current. When the pressure was very low, the lines were narrow and free from self-reversal, a partial resolution

\* D A Jackson and Kuhn, 'Proc Roy Soc', A, vol 148, p 335 (1935), vol 154, p. 679 (1936)

of each line can be seen, a wing being visible on the long wave side. At higher temperatures the lines become broadened, the stronger line becoming broad before the weaker line. At still higher temperatures self-reversal occurred.

The accompanying photographs (figs 3-5, Plate 17) show the spectrum of the line  $5^2S_{1/2} - 5^2P_{3/2}$  observed with a 2 cm étalon under the three conditions described above. All these conditions were exactly reproducible, provided the light source was run for about 20 minutes to allow equilibrium to be reached. The condition shown in fig 4, Plate 17, was the most generally used. The intensity of the light was very great, with the étalon in use the time of exposure was between 2 and 5 minutes.

### 3—The Atomic Beam

The atomic beam was produced by heating vacuum melted silver in a tube of fused silica, fitted with an observation chamber, at the upper end; the tube was exhausted by a mercury pump, and heated by means of a platinum furnace; the temperature was determined by means of a Pt-Pt Rh thermocouple. The temperatures used were between  $1050^{\circ}$  and  $1200^{\circ}$  C, corresponding to vapour pressure at the lower end of the tube between  $1/10$  and  $1/100$  mm.

The sharpness of the absorption lines depended on the ratio of the length to the diameter of the atomic beam tube. With étalon paths of 4 cm or greater a collimation of 1 : 10 to 1 : 15 was used, with 3 cm 1 : 7 to 1 : 10 and with the 2 cm étalon 1 : 4 to 1 : 6. It was found that the half-value width of the absorption lines corresponding to a collimation of 1 : 15 was about  $0.01 \text{ cm}^{-1}$ , and that corresponding to a collimation of 1 : 7 about  $0.02 \text{ cm}^{-1}$ . This experimental value of the width is rather greater than that which would be expected theoretically, particularly at small collimations, this can be ascribed to a certain amount of reflexion of atoms at the walls of the silica tube at the lower end, where the temperature is still fairly high. When the sharpest lines were needed, the top of the silica tube was pinched in (in a direction at right angles to the line of sight), its internal diameter being reduced from 12 mm to 5 mm.; this reduced the half-value width of the lines to about half.

### THE STRUCTURE OF THE LINES

The absorption of the atomic beam was observed with étalon separations of 2, 3, 4, 5, 8, and 10 cm. With the 2 cm separation the structure could be resolved into two components, the one of shorter wave-length very

much stronger than the other; the separation of these components was  $0.057 \text{ cm}^{-1}$  for  $5^2S_{1/2} - 5^2P_{3/2}$ , 3281 Å, and  $0.064 \text{ cm}^{-1}$  for  $5^2S_{1/2} - 5^2P_{1/2}$ , 3383 Å. A photograph of the fringes is reproduced in fig. 6, Plate 17. The largest recurrent white space, marked *g*, corresponds to the intervals between the successive orders of the emission line, the two weaker white lines, marked *x* and *y*, are the two lines produced by the absorption of the atomic beam, the line reproduced is  $5^2S_{1/2} - 5^2P_{3/2}$ , the other resonance line appeared very similar.

With the 3 cm étalon the weak component *y* was resolved into two; *b'* and *a'*; the separations of these were  $0.025 \text{ cm}^{-1}$  for  $5^2S_{1/2} - 5^2P_{3/2}$  and  $0.026 \text{ cm}^{-1}$  for  $5^2S_{1/2} - 5^2P_{1/2}$ . These are shown in the reproduction, figs 7 and 8, Plate 17. Here the gap between the successive orders has vanished, for the half-value width of the light source is now very nearly equal to the change in wave-length corresponding to one order ( $0.166 \text{ cm}^{-1}$ ).

The photographs made with the 4 cm étalon were very similar to those with the 3 cm étalon; a reproduction of the line  $5^2S_{1/2} - 5^2P_{3/2}$  is given in fig. 9, Plate 18, a photometer curve in fig. 16, Plate 19.

The 5 cm étalon showed the strong component *x* to be composed of two components separated by  $0.013 \text{ cm}^{-1}$ ; this could be seen better with the 6 cm étalon, a reproduction of this is given (fig. 10, Plate 18); for this étalon separation the light source was kept very cool, so that it corresponded to fig. 3, Plate 17. The étalons of greater plate separation revealed no further structure.

The  $5^2S_{1/2} - 5^2P_{3/2}$  line therefore consists of two doublets, one much stronger than the other, the strong doublet has a separation of  $0.013 \text{ cm}^{-1}$  and the weak  $0.025 \text{ cm}^{-1}$ , the centres of the two are separated by  $0.057 \text{ cm}^{-1}$ ; the structure is therefore 0.000,  $-0.013$ ,  $-0.052$ , and  $-0.077 \text{ cm}^{-1}$ . It was also possible to measure the separation of the component at  $-0.052$  (*b'*) from that of the components 0.000 and  $-0.013$  with the 6 cm étalon; the result is in agreement with that above, for it was found to be  $0.045 \text{ cm}^{-1}$  from the centre of the two strong lines, corresponding to  $0.0515$  from 0.000. With an étalon plate separation of 10 cm, a weak line could be observed separated by  $0.020 \text{ cm}^{-1}$  from the centre of the strong doublet, this corresponds to the next order of the line at  $-0.077$ , giving a value of  $0.020 + 0.050 = 0.070$  for the separation from the centre of the lines 0.000 and  $-0.013$ , corresponding to  $0.0765$  from 0.000; this is again in good agreement with the values found by means of the 4 cm. étalon. The structure 0.000,  $-0.013$ ,  $-0.052$ , and  $-0.077 \text{ cm}^{-1}$  for the line  $5^2S_{1/2} - 5^2P_{3/2}$ , 3281 Å., can therefore be relied upon to an accuracy of about  $\pm 0.001 \text{ cm}^{-1}$ .

The  $5^2S_{1/2} - 5^2P_{1/2}$  line has a similar structure, it consists of a strong doublet

with separation  $0.013 \text{ cm}^{-1}$  and a weak doublet with separation  $0.026 \text{ cm}^{-1}$ , the centres of the two doublets being separated by  $0.064 \text{ cm}^{-1}$ ; this separation was measured with the plates made with 2, 3, and 4 cm separation of the étalon plates, and consistent results were obtained. The separation of the strong components, shown in the plates made with étalon separations greater than 4 cm, was not nearly so clear as that in the other resonance line; this can be explained by the structure of the level  $^2P_{1/2}$  (which is always about twice as great as that of the  $^2P_{3/2}$  level) beginning to appear. The structure of the line  $^2S_{1/2} - ^2P_{1/2}$ ,  $3281 \text{ Å}$ , is therefore  $0.000$ ,  $-0.013$ ,  $-0.058$  and  $-0.084 \text{ cm}^{-1}$ , the accuracy of these measurements is not quite so great as that for the line  $^2S_{1/2} - ^2P_{3/2}$ ; it is

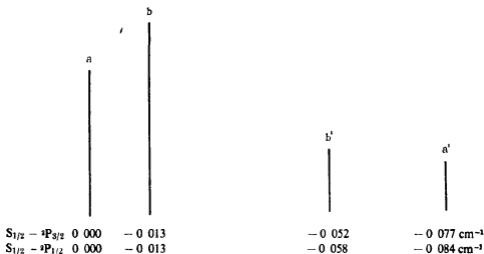


FIG. 1

about  $\pm 0.002 \text{ cm}^{-1}$ . The structure of the lines is shown diagrammatically in fig. 1.

#### DETERMINATION OF INTENSITIES

A quantitative determination of the intensity ratio of the lines  $a$  and  $b$  to the lines  $b'$  and  $a'$  was made for the  $^2S_{1/2} - ^2P_{3/2}$  resonance line. It had been found that the components  $a$  and  $b$  were of nearly equal intensity, and very much stronger than  $b'$  and  $a'$ , which were also of nearly equal intensities. The two isotopes 107 and 109 of silver are present in nearly equal proportion, it can therefore be assumed that one strong line and one weak line belongs to each element, and the ratio of the intensities of the strong to the weak lines enables the value of the nuclear spin to be determined. The best way of determining this ratio is to use a very small collimation of the atomic beam so that the half-value width of the lines is

greater than the separation of the close doublets; it is also necessary to use an étalon of 2 cm plate separation, so that the resonance lines in which the absorption is observed do not overlap at all in adjacent orders, it is then possible to measure the intensity with and without absorption and thus determine the intensity ratio of the strong doublet ( $a + b$ ) to the weak doublet ( $b' + a'$ )

The light source was obtained in a steady state by letting it run under fixed conditions of excitation and heating of the capillary for at least 1/4 hour, its intensity then remained very accurately constant. The silver in the atomic beam tube was then brought to the required temperature, the collimation being 1/4, under these conditions the half-value width of the lines is about  $0.035 \text{ cm}^{-1}$ . The furnace was then removed, and a photograph made of the light source, the furnace was then brought into position and a photograph made of the light source with the absorption of the atomic beam, the furnace was then again removed and a second photograph was made of the light source. The exposures were exactly 2 minutes in all the photographs, and were made on the same plate. The total duration of the experiment was only 11 minutes, the second photograph of the light source was started only one minute after the photograph of the absorption of the atomic beam was completed. An intensity scale was then made on a part of the plate near to the first exposures. The plate was put into a Hilger E 2 quartz spectrograph, this was illuminated with a continuous hydrogen spectrum obtained by excitation with the 1/2 kw oscillator of a silica tube with external electrodes filled with hydrogen. Five exposures were made all of duration 2 minutes, but of slit widths varying by steps of 2 from 0.03 to 0.5 mm. As the light source was continuous the intensity of the illumination was proportional to the width of slit opening. A density range was used in which there is a linear relationship between the log of the intensity and the log of the darkening of the plate.

The plate was then put through a photometer, the use of which was very kindly permitted by Professor Plaskett. The photometer curves are shown on figs 17 and 18, Plate 19. It was found that the change in intensity between the light source photograph taken before the absorption photograph and that taken afterwards was very small; the change during the very much shorter time between the absorption and second light source photograph could therefore be neglected. A cross-wire attached to the lower end of the spectrograph slit enabled the position of the absorption lines in the emission to be exactly determined, from this the amount of absorption in each line could be directly measured.

The mean value of the ratio of the absorption coefficients is thus 2.2.

This, however, requires a correction. The half-value width of the absorption lines is about  $0.035 \text{ cm}^{-1}$ , and the separation of the two components is only  $0.057 \text{ cm}^{-1}$ , assuming an exponential drop in intensity, the intensity in the centre of one line of the absorption due to the other will be

$(\frac{1}{2})^{\frac{0.035}{0.057}}$  or  $\approx 1/10$  In this case a true intensity ratio of  $X$  will be observed as  $\frac{X + \frac{1}{10}}{1 + \frac{X}{10}}$ , so that  $2.2 = \frac{X + \frac{1}{10}}{1 + \frac{X}{10}}$ .  $X$  is equal to 2.7 The

calculation of this correction is somewhat crude, but it suffices to show that the observed intensity ratio of 2.2 corresponds to a true intensity ratio of about 2.7 It was assumed that the intensity falls exponentially outside the lines; this is more likely to be too rapid than too slow so that the correction is liable to be too small

TABLE I

Fringe	2	3	4	5
Log <sub>10</sub> of intensity of light source at point $x$	0.70	0.66	0.59	0.54
Log <sub>10</sub> of intensity in absorption at point $x$	0.28	0.26	0.28	0.20
Difference* (Abs. coeff.)	0.42	0.40	0.31	0.34
Log <sub>10</sub> of intensity of light source at point $y$	0.63	0.55	0.52	0.50
Log <sub>10</sub> of intensity in absorption at point $y$	0.42	0.39	0.38	0.34
Difference* (Abs. coeff.)	0.21	0.17	0.14	0.16
Ratio $x : y$	2.0	2.3	2.2	2.1

\* It can be seen that the absorption coefficient decreases by about one-quarter from fringe 2 to fringe 5, this is because the width of the atomic beam has increased from 1 cm. to about 1.3 cm. in a distance of 1 cm., the separation of fringes 2 and 5

Another source of error is the limited resolving power of the étalon. (about  $0.025 \text{ cm}^{-1}$  for a 2 cm. étalon) This would tend to make the intensity ratio appear smaller, for the intensity of the background surrounding the weak line is smaller than that surrounding the strong line. The influence of this effect was tested by making intensity determinations with a collimation of 1:6 corresponding to a half-value width of about  $0.025 \text{ cm}^{-1}$ . It was found that the observed intensity ratio was appreciably smaller (the value found was 2.0) than that with the collimation 1:4; this is not unexpected, for the narrower the absorption lines the greater will be the effect of the limited resolving power in making the absorption of the stronger line too weak.

A third possible source of error is that the separation of the two weaker lines (0.025) is greater than that of the two stronger lines (0.013). This

would tend to make the stronger lines appear too strong, for the half-value width ( $\approx 0.035$ ) is not very large compared with the width of the resolved doublets, nevertheless the fact that the relative intensity of the stronger lines is smaller with the greater collimation shows that this effect must be more than balanced by the effect of limited resolving power of the étalon, just described

The intensity determinations therefore show that the intensity ratio of the strong lines to the weak lines must be greater than 2.2; a conservatively estimated correction gives the value 2.7.

The photometer curves of the absorption made with the 3 and 4 cm. étalons show that the line  $b'$  is somewhat stronger than the line  $a'$ . Photographs made with the 5 cm. étalon also show that  $b$  is somewhat stronger than  $a$ , but this is not easy to measure on account of the closeness of the lines. The photographs made with the 6 cm. étalon showed  $a$  and  $b$  very much more clearly resolved, but here the intensities are confused because the line  $a'$  in the next order lies within  $0.006 \text{ cm}^{-1}$  of the line  $a$ .

Silver consists of two isotopes 107 and 109, in proportion of about 1.3 to 1. From this it follows that the lines  $b$  and  $b'$  belong to Ag 107 and  $a$  and  $a'$  belong to Ag 109. The intensity ratio for each isotope is the same, being about  $2.7 \pm 1$ , this is in very good agreement with the value 3.1 required for a spin of  $1/2$ . The next lower value, corresponding to a spin of 1, is 2.1, this is definitely excluded by the results of the measurements.

The separation between the lines of Ag 107 ( $0.039$ ) is almost exactly half of that between the lines of Ag 109 ( $0.077$ ). There is a difference of  $0.004 \text{ cm}^{-1}$  in the position of the centres of gravity, the lines of Ag 107 having the smaller frequency.

#### THE STRUCTURE OF THE LINE $5^2S_{1/2} - 5^2P_{3/2}$ IN A MAGNETIC FIELD

The effect of magnetic fields on the structure of the line 3281 Å ( $5^2S_{1/2} - 5^2P_{3/2}$ ) was investigated with a 4 cm. étalon, at field strengths between 750 and 1500 gauss, only the  $\pi$  components were observed. The arrangement used was similar to that used for the investigation of the hyperfine structure, the collimation of the atomic beam was 1.13, the upper end of the tube being constricted, but the observation chamber was placed between the poles of an electromagnet capable of giving fields up to 1500 gauss. The fields were measured by observing the throw in a ballistic galvanometer. The light was polarized by means of a silica plate which was set up at almost grazing incidence in front of the slit, and

also by the prism of the spectrograph. The polarization was very nearly complete, any residual  $\sigma$  polarized light would only have the effect of causing general fog, the  $\sigma$  absorption lines being outside the wave-length range of the light source.

The hyperfine structure of the lines was profoundly changed (see fig. 11, Plate 18), the two Zeeman components observed were each seen to be single lines, their width was found to be between 0.025 and 0.030  $\text{cm}^{-1}$ ; that is, between 1/5 and 1/4 of an order with the 4 cm étalon. The photometer curves at four different field strengths are shown in figs. 12-15, Plate 18. In Table II are given the separations at various field strengths.

TABLE II

Field in gauss	760	920	1250	1450
Observed separation in $\text{cm}^{-1}$	0.029	0.037	0.039	0.045
$H \times 4.7 \times 10^{-3} \times \frac{1}{2}$	0.024	0.029	0.040	0.045

In the last line is given the calculated separation between the  $\pi$  components of the  $^2S_{1/2} - ^2P_{3/2}$  line.

It can be seen that at the highest field strength both lines are of equal intensity and their separation agrees with the theoretical value. At lower field strengths, the value is rather too great and the two components are not of quite equal intensity.

In a strong magnetic field (when the Zeeman effect is large compared with the hyperfine structure) a doublet structure due to a  $^2S_{1/2}$  term, with a 3:1 ratio of the intensities corresponding to a nuclear spin of 1/2, should still be observed in each Zeeman component as a doublet structure, but the lines should be of equal intensity, and their separation reduced to 1/3. Here therefore the structure 0.000, -0.013, -0.052, and -0.077 should become 0.000, -0.010, -0.023, and -0.026 (the centre of gravity of the lines of Ag 107 being shifted by -0.004). As the separation of the closest lines which can be resolved by the 4 cm. étalon is about 0.015  $\text{cm}^{-1}$ , this structure could not be resolved but would appear as a single line of width 0.026  $\text{cm}^{-1}$ . This is in extremely good agreement with the observation, the width of the lines observed is not greater than 0.030  $\text{cm}^{-1}$ ; the small difference is due to the residual half-value width of the lines (about 0.006  $\text{cm}^{-1}$ ).

If the spin of the nuclei were 1, the corresponding structure would consist of three lines, equally spaced, with a total width of 0.039  $\text{cm}^{-1}$ ; the instrumental width and Doppler width of the lines would bring this up to at least 0.045  $\text{cm}^{-1}$ , corresponding to over 1/3 of an order; this

is clearly impossible, for the lines are still resolved when the separation of the centres is only  $0.029 \text{ cm}^{-1}$  or  $1/4$  of an order.

It also shows that the components  $a$  and  $a'$  belong to one isotope and  $b$  and  $b'$  to the other, for the other arrangement would require a structure of  $0.000$  and  $0.021$  for one element and  $0.000$  and  $0.017$  for the other, with an isotope shift of  $0.014 \text{ cm}^{-1}$ , that is to say a structure  $0.000$ ,  $0.014$ ,  $0.017$ ,  $0.035 \text{ cm}^{-1}$ . This would require a width of at least  $0.040 \text{ cm}^{-1}$  when the residual Doppler width and instrumental width are considered; which again is far too great for the observed value  $0.025$  to  $0.030 \text{ cm}^{-1}$ .

The too great separation of the Zeeman components at low field strengths indicates that the Paschen-Back effect is not quite complete; at the highest field strengths the agreement between the observed separation and that required by theory is perfect, so it may be taken that the Paschen-Back effect is complete. The separation of the two  $\pi$  components is here  $0.045 \text{ cm}^{-1}$  so that that of the outer  $\sigma$  components would be  $0.23 \text{ cm}^{-1}$ , that is to say about three times greater than the hyperfine structure, at the lowest field strength the Zeeman splitting of the outer  $\sigma$  components is only 50% greater than the hyperfine structure, it is therefore not unexpected that the Paschen-Back effect is not complete.

#### DISCUSSION

The observed hyperfine structure was almost the same for both of the resonance lines, it is therefore ascribed to the common level  $5^2S_{1/2}$ ; the small differences are due to the small structure of the  $^3P_{1/2}$  and  $^3P_{3/2}$  levels. The two isotopes of silver 107 and 109 are present in the proportion of  $1:3$ , for this reason each isotope must give rise to one strong line and one weak line, the two inner lines  $b$  and  $b'$  (fig. 1) are ascribed to the isotope 107 and the two outer lines  $a$  and  $a'$  to the isotope 109. The intensity ratio of about  $3:1$  for the strong lines  $a$  and  $b$  to the weak lines  $b'$  and  $a'$  shows that the value of the spin is  $1/2$  for both isotopes. The observation of the structure of the lines in the magnetic field gave an independent proof of the value  $1/2$  for the spin, it also provided additional evidence that the two outer components belong to one isotope and the two inner components to the other.

From the observed  $b - b'$  splittings of  $0.039 \text{ cm}^{-1}$  for the line  $^3S_{1/2} - ^3P_{3/2}$  and  $0.045$  for the line  $^3S_{1/2} - ^3P_{1/2}$  it follows that the  $^3S_{1/2}$  level of the isotope 107 is split into two levels separated by  $0.041 \text{ cm}^{-1}$ , assuming the normal ratio  $5:3$  between the splitting of a  $^3P_{1/2}$  and a  $^3P_{3/2}$  level. For the isotope 109 the corresponding separations  $a - a'$  were  $0.077$  and

FIG 3



FIG 4



FIG 5



Light source with 2 cm etalon  
( $S_{1/2} \dots P_{3/2}$ )

$\lambda \rightarrow$

FIG 6



FIG 7



FIG 8



Absorption  
FIG 6—2 cm etalon ( $S_{1/2} \dots P_{1/2}$ )  
FIG 7—3 cm etalon ( $S_{1/2} \dots P_{3/2}$ )  
FIG 8—3 cm etalon ( $S_{1/2} \dots P_{1/2}$ )



FIG 9



FIG 10



FIG 11

# Absorption

FIG 9—4 cm etalon ( $S_{1/2} - P_{1/2}$ )

FIG 10—6 cm etalon ( $S_{1/2} - P_{1/2}$ )

FIG 11—Zeeman effect 920 gauss - components,  
4 cm etalon ( $S_{1/2} - P_{1/2}$ )



FIG 12

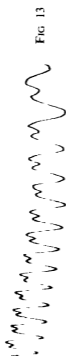


FIG 13



FIG 14



FIG 15

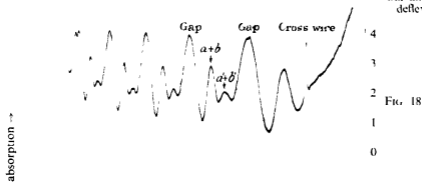
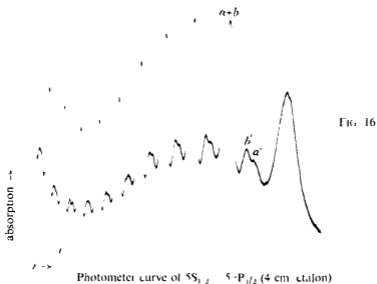
# Photometer curves of Zeeman effect 4 cm etalon - components

FIG 12—760 gauss

FIG 13—920 gauss

FIG 14—1250 gauss

FIG 15—1450 gauss



$\lambda \rightarrow$   
Photometer curves with and without absorption of  $5S_{1/2} - 5P_{1/2}$  (2 cm étalon)



$0.084 \text{ cm}^{-1}$ . From this it follows that the  $^3\text{S}_{1/2}$  level is here split into two levels separated by  $0.079 \text{ cm}^{-1}$ .

The magnetic moments of the nuclei can be calculated from these splittings by means of Goudsmit's formula, the result is  $-0.10$  nuclear magneton for Ag 107 and  $-0.19$  for Ag 109. The absolute accuracy of these values depends on the accuracy of Goudsmit's\* formula; but the ratio of the magnetic moments must be exactly equal to the ratio of the splittings, *i.e.*,  $79/41 = 1.93$ . This is well within the experimental error equal to 2 : 1.

The isotope shift can be found with considerable accuracy, its value depends on the accuracy with which the separations of the two strong lines, *a*, *b* and the two weak lines *a'*, *b'* were determined. The relative accuracy, particularly for the line  $^3\text{S}_{1/2} - ^3\text{P}_{3/2}$ , is very great; for the separation of the weak lines, which is twice that of the strong lines, was measured with a 3 cm étalon and a 1.7 collimation, while that of the strong line was measured with a 6 cm étalon and a 1.15 collimation. The systematic uncertainty in measuring the separation of two close lines was thus proportionately equal in both doublets. The isotope shift of  $-0.004 \text{ cm}^{-1}$  for Ag 107 can therefore be regarded as certain to  $\pm 0.001 \text{ cm}^{-1}$ . This is of considerable interest, as the centre of gravity shift would be equal to  $-0.003 \text{ cm}^{-1}$ .

Hill,† working with a water-cooled hollow cathode, observed a structure of two lines one at  $0.000$  and the other at  $0.056 \text{ cm}^{-1}$ , these, of course, correspond to *a* and *b* observed as one line and *b'* and *a'* observed as the other. The intensity ratio he measured was  $1.74 : 1$ . Now assuming the only width of his line was the Doppler width, the half-value width is equal to  $0.04 \text{ cm}^{-1}$ , and therefore, assuming an exponential decrease the true intensity ratio, *I*, is given by

$$\frac{I + \left(\frac{1}{2}\right)^{\frac{0.056}{0.04}}}{1 + I \times \left(\frac{1}{2}\right)^{\frac{0.056}{0.04}}} = \frac{I + 0.16}{1 + 0.16 \times I} = 1.74$$

This gives *I* equal to  $2.3 : 1$ . The correction here is certainly too small; the effect of the limited resolving power of the étalon tends to make the apparent intensity ratio low; and there is also a certain amount of self-absorption bound to be present. If these sources of error are considered, Hill's measurements are in good agreement with the value  $3 : 1$  required by a spin of  $1/2$ . Fig. 2 shows Hill's photometer curves; it can at once

\* 'Phys. Rev.', vol 43, p. 636 (1933)

† 'Phys. Rev.', vol 48, p. 233 (1935)

low temperatures is too small. For the metal platinum, in particular, the measurements of de Haas and de Boer† show that between 0° K and 20° K the resistance can be represented by the formula

$$R = \text{const } G\left(\frac{\Theta}{T}\right) + 1.5 \times 10^{-6} R_0 \cdot T^2, \quad (2)$$

where  $R_0$  is the resistance at 0° C. This is shown in fig. 1 where we plot  $\log(R/R_0)$  against  $\log T/\Theta$ . Curve I gives the observed values, curve II the observed values with the second term in (2) subtracted, and curve III the values based upon the Gruneisen function  $G(\Theta/T)$  with  $\Theta = 225$ .

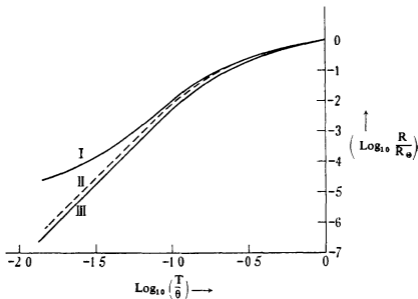


FIG. 1—Resistance of platinum. I, observed (de Haas and de Boer), II, observed resistance with  $T^2$  term subtracted, III, theoretical Gruneisen curve with  $\Theta = 225$ , fitted at  $T = \Theta$ .

The purpose of this paper is to calculate the contribution to the resistance due to the interaction of one electron with another, which is neglected in Bloch's work. We find that this additional resistance is, in fact, proportional to  $T^2$ , and therefore predominant at low temperatures. We shall, however, show that for monovalent metals it is negligible even at 1° K. The condition for a large contribution is found to be that the "effective mass" of some of the conduction electrons shall be large. This is the case for the transition metals and leads to high paramagnetism and large electronic specific heat.

† 'Phys. Lab. Leiden,' No. 231c (1934)

In our subsequent work we shall, by making certain simplifying assumptions, obtain a quantitative estimate of the extra resistance, and shall compare our results with experiment for the transition metals, nickel, palladium, and platinum

2—It is obvious that, if the electrons in a metal behave as if they were free, collisions between them could not alter the current, since momentum is conserved and the current is proportional to the momentum. We shall therefore expect the  $T^2$  term in the resistance of such metals as the alkalis, in which the electrons are believed to behave almost as free electrons,<sup>†</sup> to be very small. An upper limit is given below

A simple model, which has been used by Mott<sup>‡</sup> to estimate the "normal" resistance of transition metals, will therefore be adopted. We shall assume that *two* Brillouin zones (which we may refer to as the *s*- and *d*-zones) are responsible for the conduction. Near the bottom of the *s*-zone, in the region of occupied states, we shall write for the energy  $E$  in terms of the wave number  $k$

$$E(k) = \hbar^2 k^2 / 2m_1 \quad (3)$$

Near the top of the *d*-zone, which we may assume to be nearly full, we shall write

$$E(j) = E_0 - \hbar^2 j^2 / 2m_2, \quad (4)$$

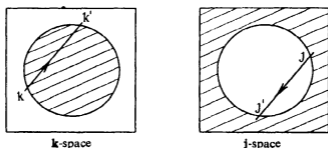


FIG. 2—*k*-space for a transition metal, with occupied states shaded

where  $j$  is the wave number. The "effective masses"  $m_1$ ,  $m_2$  appearing in (3) and (4) may be estimated for certain metals from a knowledge of the specific heats at low temperatures (*see below*)

The unoccupied states in the *d*-band will be referred to as "positive holes". The occupied states in *k*-space and *j*-space are shown in fig. 2. It may be seen as follows that a collision between an electron and a

<sup>†</sup> Cf. Wigner and Seitz, 'Phys. Rev.', vol. 43, p. 804 (1933)

<sup>‡</sup> 'Proc. Roy. Soc.', A, vol. 47, p. 571 (1935), vol. 153, p. 699 (1936)

positive hole will affect the current if the  $s$ -electron jumps from a state  $\mathbf{k}$  to a state  $\mathbf{k}'$  and the  $d$ -electron from a state  $\mathbf{j}$  to a state  $\mathbf{j}'$  then by the conservation of momentum

$$\mathbf{k} - \mathbf{k}' + \mathbf{j} - \mathbf{j}' = 0$$

Such a pair of transitions is shown in fig 2. Since the current corresponding to a state  $\mathbf{k}$  is  $e\hbar\mathbf{k}/m_1$ , and that corresponding to a state  $\mathbf{j}$  is  $-e\hbar\mathbf{j}/m_2$ , the change produced in the current is

$$e\hbar\left(\frac{\mathbf{k} - \mathbf{k}'}{m_1} - \frac{\mathbf{j} - \mathbf{j}'}{m_2}\right) = e\hbar\left(\frac{1}{m_1} + \frac{1}{m_2}\right)(\mathbf{k} - \mathbf{k}')$$

This is just the change in the current obtained by treating the positive holes in the  $d$ -shell as having physical reality, mass  $m_2$  and velocity  $\hbar\mathbf{j}/m_2$ .

In the discussion of the transition metals given by Mott it is deduced from their high paramagnetism that  $m_2 \gg m_1$ , and hence almost all the current is carried by the  $s$ -zone. We have thus to calculate the probability per unit time that, owing to its interaction with a positive hole, an  $s$ -electron is scattered through an angle  $\theta$  into a solid angle  $d\omega$ . If we denote this probability by  $S(\theta) d\omega$ , the term in the resistance due to these collisions is given by†

$$R = \frac{m_1}{ne^2} \frac{1}{\tau} \quad (5)$$

$$\frac{1}{\tau} = \int S(\theta) (1 - \cos \theta) d\omega, \quad (6)$$

where  $n$  is the number of  $s$ -electrons per unit volume.

In order to calculate  $S(\theta)$  we require a formula for the potential energy of interaction of an  $s$ -electron and a positive hole at a distance  $r$  from each other. The simplest assumption would be to take this equal to  $-e^2/r$ , this, however, gives an infinite resistance. We shall therefore take for the potential energy

$$U(r) = -e^2 e^{-ar}/r \quad (7)$$

The physical meaning of the screening term is that the field around any positive hole will be screened by all the other electrons. An estimate has been given by Mott‡ of the screening around any (static) point charge in

† Cf Mott and Jones, "The Theory of the Properties of Metals and Alloys," Oxford, 1936.

‡ Mott, 'Proc Camb Phil Soc,' vol. 32, p. 289 (1936).

a metal, which gives  $q \sim 2 \times 10^8 \text{ cm}^{-1}$ . Since the positive holes are, in fact, heavy compared with the  $s$ -electrons, this estimate may be used tentatively

In calculating the collision between an  $s$ -electron and a positive hole, we shall take the wave functions to be plane waves, then it may easily be shown that when we have two beams of unit intensity (one particle crossing unit area per unit time) composed of particles of masses  $m_1, m_2$  moving in opposite directions with velocities  $u_1, u_2$  such that  $m_1 u_1 = m_2 u_2$ , the number of particles of mass  $m_1$  per unit volume scattered into the solid angle  $d\omega$  per unit time is

$$\left( \frac{e^2}{2m^*} \right)^2 \frac{d\omega}{u_2 (\gamma'^2 \sin^2 \frac{1}{2}\theta + \gamma^2)^2}, \quad (8)$$

where

$$\left. \begin{aligned} m^* &= m_1 m_2 / (m_1 + m_2) \\ \gamma' &= m_1 u_1 / m^* \\ \gamma &= \hbar q / 4\pi m^* \end{aligned} \right\} \quad (9)$$

We shall employ this formula later to deduce the scattering probability for any velocities by referring our scattering to moving axes

3—To carry out the calculation of the interaction between the electrons we shall consider them to be distributed in velocity space rather than wave number space. Let then  $V_1, V_2$  denote the velocities of the electrons at the Fermi surfaces and  $m_1, m_2$  the effective masses for the  $s$ -zone and  $d$ -zone respectively. Since the number of holes is equal to the number of  $s$ -electrons, it follows that

$$m_1 V_1 = m_2 V_2$$

Further, let the velocity of an electron in the  $s$ -zone be represented by  $u$  and in the  $d$ -zone by  $v$ . The Fermi distribution functions giving the probability that a given state  $u$  or  $v$  is occupied are then

$$\left. \begin{aligned} f_1(u) &= \frac{1}{1 + \exp \left\{ \frac{m_1}{2kT} (u^2 - V_1^2) \right\}} \\ f_2(v) &= \frac{1}{1 + \exp \left\{ \frac{m_2}{2kT} (v^2 - V_2^2) \right\}} \end{aligned} \right\} \quad (10)$$

Let us consider, then, the scattering of  $s$ -electrons from a state representing a velocity  $u$  in the  $z$ -direction into a solid angle  $d\omega$  in a direction inclined at an angle  $\theta$  to that axis by collisions with  $d$ -electrons. We shall

denote the velocity after the collision by  $\rho$  and the initial and final velocities of a colliding  $d$ -electron by  $v, v'$  respectively. When  $u, \rho$ , and  $\theta$  are fixed the fact that energy and momentum must be conserved during the collision requires that  $\mathbf{v}$  lies on a plane in  $\mathbf{v}$ -space given by

$$v_x(u - \rho \cos \theta) - v_x \rho \sin \theta + \left\{ \frac{\rho^2}{2} \left( 1 + \frac{m_1}{m_2} \right) - \frac{u^2}{2} \left( 1 - \frac{m_1}{m_2} \right) - \frac{m_1}{m_2} u \rho \cos \theta \right\} = 0 \quad (11)$$

This plane is called the  $\rho$ -plane, if we wish to consider the scattering with speeds  $\rho$  to  $\rho + d\rho$  we must sum over all velocities of the colliding  $d$ -electron lying between the planes  $\rho$  and  $\rho + d\rho$ .

We first calculate  $P(u, \rho, \theta) d\rho d\omega$  defined as the probability of scattering into the solid angle  $d\omega$  for electrons with the initial velocity  $u$  scattered with velocities  $\rho$  to  $\rho + d\rho$ , the required function  $S(\theta)$  is then given by

$$S(\theta) = \int P(u, \rho, \theta) d\rho \quad (12)$$

First it is convenient to introduce a function  $F(\mathbf{v})$  defined thus consider the interaction of two beams of particles each of unit intensity. Let us suppose that when the particles of the one beam having velocity  $u$  along the  $z$ -axis and mass  $m_1$  interact with those of the other beam having velocity  $\mathbf{v}$  and mass  $m_2$ , then the number of particles of the former beam scattered per unit volume per unit time into the solid angle  $d\omega$  is  $F(\mathbf{v}) d\omega$ . The required scattering probability of electrons with initial velocity  $u$  in the  $z$ -direction is now easily specified when we multiply by various factors arising as follows

I—The volume  $\Omega$  of the crystal

II—A factor giving the number of electrons in the initial states. If there were one electron in each of the states  $u, v$ , then the intensities of the beams would have to be taken as  $\Omega^{-1}u$  and  $\Omega^{-1}v$  respectively, and, since the actual probabilities of an electron being in these states are  $f_1(u), f_2(v)$ , the second factor is  $\Omega^{-2}uv f_1(u) f_2(v)$

III—A factor representing the probabilities that the states into which scattering occurs are unoccupied this is  $\{1 - f_1(\rho)\} \{1 - f_2(v')\}$

Thus the scattering probability  $P(u, \rho, \theta) d\omega$  is given by

$$\Sigma V^{-1} uv f_1(u) f_2(v) \{1 - f_1(\rho)\} \{1 - f_2(v')\} F(\mathbf{v}) d\omega, \quad (13)$$

where the summation extends over all states  $\mathbf{v}$  lying between the planes  $\rho$  and  $\rho + d\rho$ . Finally this expression may be written as an integral,

since the number of states in the element  $dv_x dv_y dv_z$  is  $\frac{\Omega m^3}{h^3} dv_x dv_y dv_z$ ; whence we have

$$P(u, \rho, \theta) = \frac{m^3}{h^3} u f_1(u) \{1 - f_1(\rho)\} \int v f_2(v) \{1 - f_2(v')\} F(\mathbf{v}) dv_x dv_y dv_z \quad (14)$$

The scattering function  $F(\mathbf{v})$  may be obtained from (8) by referring the scattering to moving axes  $Ox', Oy', Oz'$  relative to which the beams have velocities  $\mathbf{u}_1, \mathbf{u}_2$  satisfying the equation  $m_1 \mathbf{u}_1 + m_2 \mathbf{u}_2 = 0$ . The velocity of these moving axes will then be  $\alpha = (m_1 \mathbf{u} + m_2 \mathbf{v}) / m_1 + m_2$  whilst  $\mathbf{u}_1 = \mathbf{u} - \alpha$  and  $\mathbf{u}_2 = \mathbf{v} - \alpha$ .

Relative to the new axes  $\chi$  denotes the angle of scattering of particles  $m_1$ , and  $d\omega'$  the new solid angle. Hence on taking into account the fact that the new intensities are  $u_1/u$  and  $u_2/v$ , the scattering relative to  $Ox', Oy', Oz'$  per unit volume and unit time is, by (8) equal to

$$\left(\frac{e^2}{2m^*}\right)^2 \frac{u_1 u_2}{uv} \frac{d\omega'}{u_2 (\gamma'^2 \sin^2 \frac{1}{2}\chi + \gamma^2)^2} \quad (15)$$

If  $\lambda$  denotes the angle between the direction of scattering relative to to  $Oxyz$  and that with respect to  $Ox'y'z'$  then

$$d\omega' = \frac{\rho^2 d\omega}{u_1^2 |\cos \lambda|},$$

so that

$$F(\mathbf{v}) = \left(\frac{e^2}{2m^*}\right)^2 \frac{\rho^2}{uu_1 v} \frac{1}{|\cos \lambda| (\gamma'^2 \sin^2 \frac{1}{2}\chi + \gamma^2)^2}, \quad (16)$$

where

$$\left. \begin{aligned} \cos \lambda &= (\rho^2 + u_1^2 - \alpha^2) / 2\rho u_1 \\ \eta &= m_1 u_1 / m^* \\ (m_1 + m_2) u_1^2 \cos \chi &= -m_2 (\mathbf{v} \cdot \alpha) + m_2 u (\rho \cos \theta + \alpha_x) \\ &\quad - m_2 \rho (v_x \sin \theta \cos \phi + v_y \sin \theta \sin \phi + v_z \cos \theta) \end{aligned} \right\} \quad (17)$$

The desired scattering probability with velocities  $\rho$  to  $\rho + d\rho$  is therefore given by

$$P(u, \rho, \theta) d\omega d\rho = \left(\frac{e^2}{2m^*}\right)^2 \frac{m^3}{h^3} d\omega f_1(u) \rho^2 \{1 - f_1(\rho)\} \times \int \frac{f_2(v) \{1 - f_2(v')\} dv_x dv_y dv_z}{u_1 \cos \lambda (\gamma'^2 \sin^2 \frac{1}{2}\chi + \gamma^2)^2}, \quad (18)$$

where the integration extends between the planes  $\rho$  and  $\rho + d\rho$  in  $\mathbf{v}$ -space. The form of the Fermi functions occurring in (18) ensures that the integrand is important only when  $u, \rho \approx V_1$  and  $v, v' \approx V_1$ , i.e., the important

values of  $\mathbf{v}$  are those in the domain of the circle in which the plane  $\rho = V_1$  (when also  $u = V_1$ ) meets the sphere  $v = V_2$  in  $\mathbf{v}$ -space. This plane is given by

$$v_s - v_e \cot \frac{1}{2}\theta + m_1 V_1 / m_2 = 0 \quad (19)$$

Approximations based upon these considerations are now introduced into (18) in the following manner. We consider the integration over the  $\mathbf{v}$ -space between the planes  $\rho$  and  $\rho + d\rho$  taking first the contribution from between the spheres  $v, v + dv$

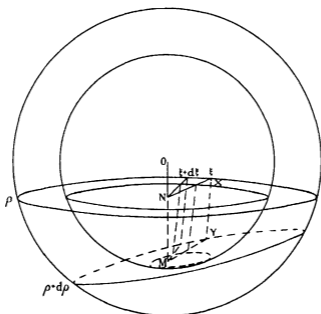


FIG. 3

We split up the velocity space between the planes  $\rho$  and  $\rho + d\rho$  by first considering that part of this space lying between the spheres  $v, v + dv$ . This part is then further subdivided into volume elements specified by  $\xi, \xi + d\xi$  where  $\xi$  is an angular coordinate measured around the perpendicular  $ON = p$  to the  $\rho$ -plane.  $ON$  meets the plane  $\rho + d\rho$  in  $M$  and  $\xi$  actually specifies a plane through  $OM$  (see figs 3 and 4). This volume element of  $\mathbf{v}$ -space is easily seen to be given by  $v dv d\xi$ .  $XY$  Referring to fig. 4 we denote by  $b$  the inclination of the  $\rho$ -plane to the plane, and set  $v_s = 0$ ,  $\delta = \angle NOX$ ,  $\delta' = \angle NOY$ ,  $\angle XOY = \delta - \delta' = \epsilon$ , so that  $XY = v\epsilon$ . We have then

$$\left. \begin{aligned} p + NM &= (p + d\rho) \sec(db) \\ (p + NM) \sec(db) &= v \cos \delta' = v \sin \delta' \cos \xi \cdot \tan(db) \end{aligned} \right\}, \quad (20)$$

which yield

$$XY = v \left\{ \frac{1}{(v^2 - p^2)^{1/2}} \frac{dp}{d\rho} - \frac{d\alpha}{d\rho} \cos \xi \right\} d\rho, \quad (21)$$

and a volume element

$$dv_x dv_y dv_z = v^2 \left\{ \frac{1}{(v^2 - p^2)^{1/2}} \frac{dp}{d\rho} - \frac{d\alpha}{d\rho} \cos \xi \right\} d\rho dv d\xi, \quad (22)$$

so that we obtain

$$P(u, \rho, 0) d\rho d\omega = \left( \frac{e^2}{2m^*} \right)^2 \frac{m_2^3}{h^3} d\omega f_1(u) \rho^2 \{1 - f_1(\rho)\} d\rho \\ \times \int v^2 f_2(v) \{1 - f_2(v')\} dv \int \frac{\left\{ \frac{1}{(v^2 - p^2)^{1/2}} \frac{dp}{d\rho} - \frac{d\alpha}{d\rho} \cos \xi \right\} d\xi}{u_1 \cos \lambda (\gamma^{1/2} \sin^2 \frac{1}{2} \chi + \gamma^2)^2}, \quad (23)$$

involving integrations over the coordinates  $\xi$  and  $v$

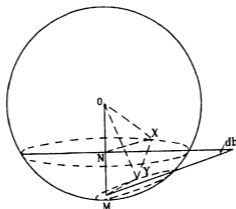


FIG. 4

To carry out the  $\xi$ -integration, we note that as an approximation all parts of (23) except the Fermi distribution functions  $f$  may be evaluated for  $u, \rho = V_1, v = V_2$ . Then for the  $\xi$ -integral we have

$$\int_0^{2\pi} \frac{\left\{ \frac{1}{(v^2 - p^2)^{1/2}} \frac{dp}{d\rho} - \frac{d\alpha}{d\rho} \cos \xi \right\}}{u_1 \cos \lambda (\gamma^{1/2} \sin^2 \frac{1}{2} \chi + \gamma^2)^2} d\xi = \frac{1 + m_2/m_1}{V_1^2 \sin \theta} \frac{2\pi L}{(L^2 - M^2)^{1/2}}, \quad (24)$$

where

$$\left. \begin{aligned} L &= \gamma^2 + V_2^2 \{ (\beta^2 + 3\beta) \sin^2 \frac{1}{2} \theta + 1 - \beta \} \\ M &= V_2^2 (\beta - 1) \cos^2 \frac{1}{2} \theta \\ \beta &= m_2/m_1 = V_1/V_2 \end{aligned} \right\} \quad (25)$$

The integration over  $v$  is now  $\int_p^\infty v^2 f_2(v) \{1 - f_2(v')\} dv$ . Since

$v'^2 = v^2 + m_1/m_2 (u^2 - \rho^2)$ , the integrand is important only for values of  $v$  near  $V_2$  and, since it is therefore permissible to replace the lower limit of the integral by zero, the integral becomes approximately

$$\frac{kT}{m_2 V_2} V_2^2 \frac{\Gamma}{1 - e^{-1}},$$

with

$$\Gamma = \frac{m_1}{2kT} (u^2 - \rho^2) \quad (26)$$

Accordingly we now have

$$P(u, \rho, \theta) d\rho d\omega =$$

$$\left(\frac{e^2}{2m^*}\right)^2 \frac{m_2^3}{h^3} \left(\frac{kT}{m_2 V_2}\right) \left[ \frac{2\pi V_2^2 (1 + \beta) L d\omega}{V_1^2 \sin \theta (L^2 - M^2)^{1/2}} \right] \frac{f_1(u) \rho^2 \{1 - f_1(\rho)\} \Gamma d\rho}{1 - e^{-\Gamma}}, \quad (27)$$

where  $\rho$  appears in the form  $\rho^2 \{1 - f_1(\rho)\}/1 - e^{-\Gamma}$ , which is of the nature of a  $\delta$ -function with its maximum near  $\rho = V_1$ . A result of this type is to be expected, as  $\rho$  must lie within a small interval  $kT/m_1 V_1$  of the Fermi surface  $V_1$ . By integrating over  $\rho$  we now derive the required scattering function  $S(u, \theta) d\omega$  in the form

$$S(u, \theta) d\omega = d\omega \int_0^\infty P(u, \rho, \theta) d\rho = \left(\frac{e^2}{2m^*}\right)^2 \frac{m_2^3}{h^3} \left(\frac{kT}{m_2 V_2}\right) f_1(u) \\ \times \left[ \frac{2\pi V_2^2 (1 + \beta) L d\omega}{V_1^2 \sin \theta (L^2 - M^2)^{1/2}} \right] \int_0^\infty \frac{\rho^2 \{1 - f_1(\rho)\} \Gamma d\rho}{1 - e^{-\Gamma}},$$

which gives approximately on evaluating the  $\rho$ -integral

$$S(u, \theta) d\omega = \left(\frac{e^2}{2m^*}\right)^2 \frac{m_2^3}{h^3} \left(\frac{kT}{m_1 V_1 V_2}\right)^2 \left[ \frac{2\pi V_2^4 (1 + \beta) L d\omega}{\sin \theta (L^2 - M^2)^{1/2}} \right] \frac{e^\Delta (\pi^2 + \Delta^2)}{2(e^\Delta + 1)^2}, \quad (28)$$

where

$$\Delta = \frac{m_1}{2kT} (u^2 - V_1^2) \quad (29)$$

It follows that

$$\frac{1}{\tau} = \int S(\theta) (1 - \cos \theta) d\omega = \left(\frac{e^2}{2m^*}\right)^2 \frac{m_2^3}{h^3} \left(\frac{kT}{m_1 V_1 V_2}\right)^2 \\ \times \left[ \int_0^\pi \frac{4\pi^2 V_2^4 (1 + \beta) L (1 - \cos \theta) d\theta}{(L^2 - M^2)^{1/2}} \right] \frac{e^\Delta (\pi^2 + \Delta^2)}{2(e^\Delta + 1)^2},$$

which upon integrating over  $\theta$  becomes

$$\frac{1}{\tau} = \left(\frac{e^2}{2m}\right)^2 \frac{m_s^3}{h^3} \left(\frac{kT}{m_1 V_1 V_2}\right)^2 \times \left[ \frac{8\pi^2 V_2 (1 + \beta)}{\gamma \{ \gamma^2/V_2^2 + (1 + \beta)^2 \}^{3/2}} F \left\{ \frac{V_2}{\gamma} \sqrt{2\beta - 2} \right\} \right] \frac{e^4 (\pi^2 + \Delta^2)}{2 (e^4 + 1)^2}, \quad (30)$$

where  $F(K)$  denotes the elliptic integral

$$\int_0^{\pi/2} \frac{d\phi}{\sqrt{(1 - K^2 \sin^2 \phi)}}.$$

We shall write our formula for  $\tau$  in the more convenient form

$$\left. \begin{aligned} \frac{1}{\tau} &= \left(\frac{e^2}{2m_1}\right)^2 \frac{m_s^3}{h^3} \left(\frac{kT}{\zeta_1}\right)^2 \frac{e^4 (\pi^2 + \Delta^2)}{2 (e^4 + 1)^2} H(\beta, q) \\ H(\beta, q) &= \frac{8\pi^2 V_2}{\gamma} \frac{\beta^3 (\beta + 1)^3}{\{ \gamma^2/V_2^2 + (1 + \beta)^2 \}^{3/2}} F \left\{ \frac{V_2}{\gamma} \sqrt{2\beta - 2} \right\} \end{aligned} \right\} \quad (31)$$

It is now easy to estimate the resistance due to electron interaction at temperatures so low that we may neglect the lattice resistance. By our approximations we have calculated  $\tau(u)$  for values of  $u$  near  $V_1$ , the velocity at the Fermi surface. When  $u = V_1$  ( $i.e.$ ,  $\Delta = 0$ ) we have, writing  $m, \zeta$  instead of  $m_1, \zeta_1$

$$\frac{1}{\tau} = \left(\frac{e^2}{2m}\right)^2 \frac{m^3}{h^3} \left(\frac{kT}{\zeta}\right)^2 \frac{\pi^2}{8} H(\beta, q), \quad (32)$$

so that, using the formula  $\sigma = ne^2\tau/2m$  where the factor 2 occurs because  $\tau$  has been calculated for collisions with  $d$  electrons with one spin only, we derive an estimate of the resistance  $R = 1/\sigma$  in the form

$$R = \frac{2m}{ne^2} \left(\frac{e^2}{2m}\right)^2 \frac{m^3}{h^3} \left(\frac{kT}{\zeta}\right)^2 \frac{\pi^2}{8} H(\beta, q),$$

reducing to

$$R = \frac{\pi^2 e^2 m^2}{16 n h^3} \left(\frac{kT}{\zeta}\right)^2 H(\beta, q) \quad (33)$$

In the formula (33),  $n$  denotes the number of  $s$ -electrons per unit volume,  $m$  the electronic mass,  $\zeta$  the breadth of the  $s$ -band,  $\beta = m_s/m_1$ ,  $q$  the screening constant, and  $H(\beta, q)$  is given by (31)

To discuss the dependence of the resistance  $R$  upon the mass-ratio  $\beta$  and the screening constant  $q$ , we may write

$$R \propto H(\beta, aq),$$

where  $a$  denotes the lattice constant

Table I gives the values of  $H/16\pi^2$  calculated for the two cases  $q^{-1} = \frac{2}{3} \times 10^8$  cm and  $q^{-1} = \frac{1}{2} \times 10^8$  cm for several values of  $\beta$ , assuming that  $a = 3.85 \times 10^{-8}$  cm as for palladium

TABLE I

$\beta = m_2/m_1$	$H/16\pi^2$	
	$q^{-1} = \frac{2}{3} \times 10^8$ cm	$q^{-1} = \frac{1}{2} \times 10^8$ cm
1	0.3	0.2
2	1.9	0.9
4	9.4	4.2
5	15.0	7.4
8	39.4	18
10	62	32
13.5	113	53

$R$  is thus an increasing function of  $\beta$ , but decreases with  $q$

Our conclusion that the extra resistance is proportional to  $T^2$  may be explained qualitatively as follows: we are interested in the probability that an  $s$ -electron lying near the surface of the Fermi distribution should jump to any other state. In the transition the  $s$ -electron cannot lose energy greater than about  $kT$  since it must jump into an unoccupied state. Therefore the  $d$ -electron with which it makes a collision cannot gain more energy than  $kT$ . It follows that this  $d$ -electron must, *both before and after the collision*, be in a state lying in a range  $kT$  at the surface of the Fermi distribution. Thus if  $\zeta_2$  is the Fermi energy for the  $d$ -electrons we may say roughly that, out of all the possible collisions with  $d$ -electrons, only a fraction  $(kT/\zeta_2)^2$  is allowed by the exclusion principle. We thus see why the resistance is proportional to  $T^2$ , and, since

$$\zeta_2 = \frac{h^2}{8m_2} \left( \frac{3n}{\pi} \right)^{1/3},$$

why it increases roughly with the ratio  $(m_2/m_1)^2$

#### 4—COMPARISON WITH EXPERIMENT

We have seen that the resistance increases rapidly with the ratio  $m_2/m_1$ . If we consider the case  $m_1 = m_2$ , we obtain the order of magnitude of the resistance due to collisions for an element such as copper if the deviations from spherical symmetry are large. Putting  $m_1 = m_2$ , formula (33) gives for copper with  $q = 1.8 \times 10^8$  cm $^{-1}$  at  $4.2^\circ$  K,  $R = 6.0 \times 10^{-13}$  ohm/cm compared with a value of  $1.4 \times 10^{-9}$  ohm the lowest of the values for the total resistances of several specimens of

copper given by de Haas, de Boer, and den Berg † The effect of electron collisions is thus quite negligible

The resistance will be largest for the transition metals where  $m_2/m_1$  is large  $m_2$  may be estimated from the atomic heat at helium temperatures which has been measured for palladium‡ and nickel§ The formula for the atomic heat is

$$\frac{2\pi^2 k^2}{3} T \frac{4m_2}{h^2} (1 - 8\pi^2)^{1/2} \frac{L}{J n_A} \text{ cal/degree,}$$

where  $L$  denotes the number of atoms per gm atom and  $J$  the number of ergs per cal Assuming that  $m_1$  is the electronic mass, we deduce  $m_2/m_1 = 13.5$  for palladium and  $m_2/m_1 = 9.3$  for nickel

Let us then use this value of  $m_2/m_1$  and formula (33) to estimate the resistance of the transition element palladium at  $4.2^\circ \text{K}$  by inserting the values

$$n = 0.6 n_A = \frac{(0.6) 4}{3 \cdot 85^3} \times 10^{24}, \quad \beta = \frac{m_2}{m_1} = 13.5, \quad \zeta = 4.15 \text{ e-v,}$$

(the breadth of the  $s$ -band deduced from the free electron picture) Then we obtain

$$R (\text{ohm/cm}) = 6.5 \times 10^{-14} \times H(\beta, q)$$

compared with the experimental value  $1.07 \times 10^{-9}$  ohm of Meissner and Voigt|| We deduce  $H(\beta, q)/16\pi^2 = 104.5$  so that, from the above table of values, we find approximately  $q = 1.5 \times 10^8 \text{ cm}^{-1}$  Such a value of the screening constant is of the same order as that obtained by Mott¶ by an application of the Thomas-Fermi method Thus theory indicates a resistance due to electron collisions varying as  $T^2$  and, for palladium, of the same order of magnitude as that required by experiment For nickel a similar calculation with  $\beta = 9.3$  yields  $q = 1.3 \times 10^8 \text{ cm}^{-1}$

For the element platinum, however, no measurements of the atomic heat are available††, but if we assume, as for palladium, that  $q = 1.5 \times 10^8$

† 'Comm Phys Lab Leiden,' No 233b (1934)

‡ Simon and Pickard, unpublished results

§ Keesom and Clark, 'Physica,' vol 2, p 513 (1935)

|| 'Handb Exp Physik,' vol 11, p 57 (1935)

¶ 'Proc Camb Phil Soc,' vol 32, p 289 (1936)

†† [Note added in proof, 21 September, 1936—The atomic heat of platinum at liquid helium temperatures has recently been measured by Kok and Keesom ('Physica,' vol 3, to appear shortly) The linear term in the atomic heat is  $0.001607 T$ , corresponding to an effective mass  $m_2/m_1 = 6.9$  in close agreement with the value  $6.5$  deduced in this paper from the electrical resistance at the same temperatures I am indebted to Professor Mott, and hence to Professor Keesom, for allowing me to see these results before publication]

$\text{cm}^{-1}$  we may deduce from the observed resistance that  $\beta = 6.5$ . Thus the effective mass  $m_2$  of a  $d$ -electron in platinum is about one-half that for palladium, in agreement with the fact that Pt is less paramagnetic than Pd. The estimates 0.42 e-volts and 0.35 e-volts of Mott and Jones† for the energy interval at the top of the  $d$ -zone, deduced from the thermoelectric power and resistance at high temperatures respectively, lead to the values 10.1 and 12.1 for the effective mass  $m_2/m_1$  in platinum.

I wish to express my thanks to Professor N. F. Mott for suggesting the problem, and to him and to Dr. H. Jones for their advice and encouragement.

#### SUMMARY

The contribution to the electrical resistance of metals from collisions between the conduction electrons is discussed. It is shown that these collisions contribute an extra term proportional to  $T^2$ . This term is shown to be negligibly small for normal metals down to less than  $1^\circ \text{K}$ , but for the transition metals Pd and Pt it is the predominating term at helium temperatures, in agreement with experiment.

† "The Theory of the Properties of Metals and Alloys," Oxford, 1936.

---

## The Exchanges of Energy Between a Platinum Surface and Hydrogen and Deuterium Molecules

By W B MANN and W C NEWELL, Departments of Physics and Chemistry, Imperial College of Science, London

(Communicated by A O Rankine, FRS—Received 28 July, 1936)

The results obtained by Strachan\* suggested that it might be of interest to determine the accommodation coefficients of hydrogen and deuterium relative to the same platinum surface after that surface had been cleaned by prolonged heating at a high temperature. By determining the rates of increase of the accommodation coefficients with time, after flashing and lowering to normal temperatures, both for hydrogen and deuterium, it was hoped that some indication as to the relative times of life of hydrogen and deuterium molecules on a platinum surface would also be forthcoming. It is very doubtful, however, if the process of contamination is due only to adsorption of hydrogen and deuterium molecules on the surface, evidence has, indeed, been obtained which indicates that the quantity of gas taken up by the platinum is far too great to be attributed only to surface effects.

### APPARATUS

The apparatus employed was similar to that previously described,† the only essential differences being that a McCleod gauge was used to measure pressures and the accommodation coefficients were determined by measuring the heat loss from a platinum wire about 40 cm. long, 0.026 mm. diameter, hanging in a loop inside a pyrex glass sheath of 5 cm. diameter. By means of a 2-inch ground joint at its upper end this sheath was easily placed in position around the loop of platinum wire. A well-stirred bath of transformer oil served to maintain the glass sheath at a constant temperature.

### THE PREPARATION OF THE DEUTERIUM

Considerable attention was given to the preparation of the deuterium from the deuterium oxide available. The reactions of water with aluminium amalgam, with an electrically heated magnesium wire spiral,

\* 'Proc Roy Soc,' A, vol 150, p 456 (1935)

† 'Proc Roy Soc,' A, vol 146, p 776 (1934)

and also with sodium were investigated. The aluminium amalgam was found to be extremely difficult to handle owing to its ease of reaction with oxygen, and its necessarily large bulk. The electrically heated magnesium wire spiral was found to become covered with a protective film, and further reaction took place only when the magnesium was on the point of melting.

The reaction between sodium and water has been thoroughly investigated by Halla and Tompa,\* who found that, in addition to the primary reaction,

(I)  $2\text{Na} + 2\text{H}_2\text{O} \rightarrow 2\text{NaOH} + \text{H}_2$ , two alternative further reactions take place on warming with excess of sodium, namely

(II)  $\text{NaOH} + 2\text{Na} \rightarrow \text{Na}_2\text{O} + \text{NaH}$ , and

(III)  $2\text{NaOH} + 2\text{Na} \rightarrow 2\text{Na}_2\text{O} + \text{H}_2$ , reaction (III) being favoured by lowering the pressure of hydrogen. Similar reactions take place with deuterium substituted for hydrogen, but at different rates†. Now with water containing both hydrogen and deuterium, it would strictly be necessary to carry the reactions (I) and (III) to completion, in order that the gaseous product should have the same proportions of these isotopes as the original water. This complete decomposition is, however, unnecessary if the water used is nearly pure deuterium oxide. With water containing 99.95% of deuterium oxide, such as we have used, reaction (I) would, even in the extreme case of separation, result in the proportion of deuterium in the gas evolved being not less than 99.90%. The implied upper limit of hydrogen impurity (0.1%) is insufficient to affect the results, having regard to the experimental accuracy attainable. Accordingly, the preparation of the deuterium has been based on reaction (I) only.

The apparatus used in the preparation of the deuterium is shown in fig. 1. The cleaned sodium was placed in a nickel crucible contained in the modified liquid air trap B, which was quickly fused to the rest of the apparatus consisting of the trap A, containing glass-wool, and the tube C which was to contain the water for decomposition. The apparatus was evacuated and degassed by heating. The tap N was closed, dry air admitted to C, about 0.5 gm. of water inserted, and the tube sealed. The water was frozen, using liquid nitrogen, the tap N was opened and the whole apparatus re-evacuated. The tap N was again closed and the ice in C allowed to melt and then to boil by warming, in order to remove any traces of dissolved air. With the tap N still closed the sodium was heated to about 350°C., until there was no further evolution of gas.

\* 'Z. anorg. Chem.', vol. 219, p. 321 (1934).

† Rollefson, 'J. Chem. Phys.', vol. 2, p. 144 (1934), also Abel, Bratu, and Redlich, 'Z. phys. Chem.', vol. 173, p. 353 (1935).

The water was re-cooled in liquid nitrogen, the tap N was opened, and the apparatus pumped to a hard vacuum

After some time the tap M was closed and the liquid nitrogen transferred from C to B. The water in C was distilled over forming ice upon the sodium. On removing the liquid nitrogen, the water upon liquefaction began to react with the sodium. The gas formed was passed through the liquid air trap A in order to remove any water vapour.

The reaction could easily be retarded or stopped by re-cooling the contents of the sodium tube B in liquid nitrogen. In carrying out this preparation, precautions were taken against a possible explosion which might take place should the sodium tube crack.

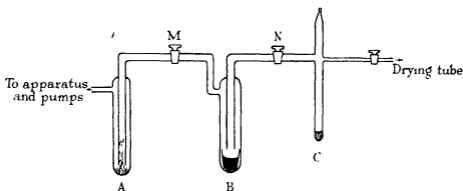


FIG. 1

The hydrogen used was prepared by electrolysis and its purity checked using a thermal conductivity meter. The specimen of deuterium was also compared with another specimen, prepared by the same sodium method, using the conductivity meter. Its purity was also kindly checked by Mr. C. T. Archer by comparison of its absolute thermal conductivity with other specimens of deuterium which had been prepared by decomposition of 99.95% deuterium oxide both by magnesium and by sodium.

In each case 1 litre of gas, at a pressure of about 15 cm. of mercury, was prepared, the appropriate pressure for the accommodation coefficient measurements was obtained by expansion from a suitable gas pipette.

## RESULTS AND DISCUSSION

After mounting, the temperature of the wire was raised to red heat in air to remove strain. Preliminary results were now obtained without further heat treatment for hydrogen, deuterium, and spectroscopically

pure helium. Relative to the wire in this condition, the accommodation coefficients for these gases were respectively equal to 0.239, 0.303, and 0.289. These results were obtained with the wire at a mean temperature of about  $100^{\circ}\text{C}$ , the temperature of the surroundings being maintained at about  $16^{\circ}\text{C}$ . For deuterium, in calculating the theoretical heat loss by molecular conduction from the wire, the ratio of the specific heats was taken equal to that for hydrogen over the same range of temperature.\*

These results having been obtained for a normal contaminated platinum wire, the apparatus was evacuated and the mean temperature of the wire was raised to  $1000^{\circ}\text{C}$ . The wire was maintained at this temperature in a vacuum for a period of about twenty-four hours. At the end of this

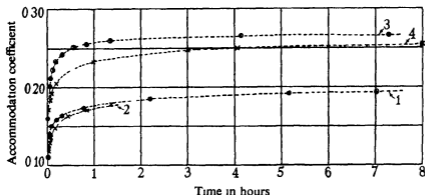


FIG. 2—Subsequent values of accommodation coefficients ( $\alpha$ ) 1, hydrogen, 22 hours  $\alpha = 0.199$ , 2, 23 hours  $\alpha = 0.200$ , 2, hydrogen, 16 hours  $\alpha = 0.198$ , 24 hours  $\alpha = 0.199$ , 3, deuterium, 7 hours  $\alpha = 0.266$ , 19 hours  $\alpha = 0.264$ , 4, deuterium, 8 hours  $\alpha = 0.255$ , 48 hours  $\alpha = 0.258$

time the mean temperature of the wire was lowered to  $100^{\circ}\text{C}$ , and hydrogen admitted to a pressure of about 100 dynes per  $\text{cm}^2$ . The mean temperature of the wire was maintained constant and the variation of accommodation coefficient with time determined. Results for this and for subsequent determinations, using both hydrogen and deuterium, are shown in fig. 2. Each set of readings was taken after a preliminary heating of the wire to  $1000^{\circ}\text{C}$  for twenty-four hours in a vacuum. The zero of time corresponds to the time of admission of the charge of gas, extrapolation to this time giving the value of the accommodation coefficient relative to a clean platinum surface. For hydrogen this value of the accommodation coefficient came to between 0.10 and 0.11 and for deuterium to about 0.16. The former is in good agreement with the value of

\* Farkas, A. and L., 'Proc Roy Soc,' A, vol 144, p 468 (1934)

0.11 previously obtained for hydrogen,\* the wire then having been cleaned by heating at  $800^{\circ}\text{C}$ , not in a vacuum, but in the hydrogen itself

Values of the accommodation coefficient for helium relative to the wire, after two different twenty-four hour periods of cleaning, came to 0.047 and 0.038 for mean temperatures of the wire equal to  $1018^{\circ}$ , and  $1162^{\circ}\text{C}$ . These results are in good agreement with the values, 0.058, and 0.045 at  $1000^{\circ}$  and  $1200^{\circ}\text{C}$ , previously obtained \*

The extrapolated values of the accommodation coefficients for hydrogen and deuterium, relative to a clean wire, were obtained, using only those

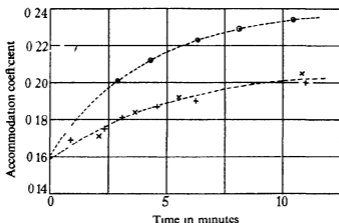


FIG. 3—O 1st set, x 2nd set, + 3rd set

readings taken within the first ten or fifteen minutes after admitting the gas and lowering the mean temperature of the wire to  $100^{\circ}\text{C}$ . Such extrapolations, for three sets of readings in deuterium, are shown in fig. 3

The rise in the accommodation coefficient was followed for some sixteen or twenty hours until the wire became fully saturated and a steady state was attained. The accommodation coefficients, relative to the saturated wire, for hydrogen, deuterium, and for helium were then determined. The results are shown in Table I

These values of the accommodation coefficients show an independence of the gas in which the saturation occurs, a result which was not anticipated. The consistency of these results, together with the good agreement, already mentioned, of the accommodation coefficients of hydrogen

\* Mann, 'Proc. Roy. Soc.', A, vol. 146, p. 776 (1934).

relative to a clean platinum surface for two specimens of platinum of quite different origin,\* suggest that the data in Table I may safely be applied to platinum filaments in general use, so long as these have been cleaned by flashing in a vacuum for a considerable time beforehand †

TABLE I—ACCOMMODATION COEFFICIENTS RELATIVE TO THE SATURATED WIRE

	Condition of wire	Hydrogen	Deuterium	Helium
1	Saturated in $H_2$	0.200	—	0.242
2	" $H_2$	0.199	0.264	0.247
3	" $D_2$	0.197	0.265	0.245
4	" $D_2$	0.201	0.258	0.242

A remarkable feature of the curves shown in fig. 2 is the comparatively long time required for saturation to become complete, both for hydrogen and deuterium. That this is a real effect and is not due to resistance drift of the wire was shown by a blank experiment in which the mean temperature of the wire was lowered from  $1000^\circ$  to  $100^\circ$  C. in a vacuum. The wire immediately settled down to a constant condition.

This delay in the attainment of saturation is probably due to penetration of the gas into the body of the wire. It was found that, after saturation, evacuation and heating resulted in the slow evolution of quantities of gas surprisingly large in comparison with the volume of the wire, the volume of hydrogen evolved, measured at room temperature and atmospheric pressure, was of the order of seventy times the volume of the wire. Assuming the surface of the wire to be smooth and exposing, say, (100) planes, this volume would correspond, if the hydrogen were merely adsorbed, to about two thousand hydrogen atoms to every exposed platinum atom in the surface. It seems likely, therefore, that both the hydrogen and deuterium are first adsorbed and then diffuse slowly into the platinum in much the same way as has been observed by Roberts‡ for oxygen and tungsten. This would account for the very slow rate at which saturation is attained.

In conclusion, we wish to thank Professor Rankine for his kind advice regarding the presentation of this communication.

\* The platinum wire used in the present experiments was supplied by Messrs Johnson, Matthey of London, that used in the previous work by Messrs W. C. Heraeus.

† It should be mentioned that preliminary heat treatment of platinum is also very necessary to remove strain, in order to obtain a reproducible value of the electrical resistance, invariable both with respect to time and to subsequent treatment.

‡ Roberts, 'Proc. Roy. Soc. A', vol. 152, p. 464 (1935).

#### SUMMARY

The exchange of energy between hydrogen and deuterium molecules and the same platinum surface have been investigated. Values of the accommodation coefficients relative to the cleaned wire at a mean temperature of 100° C, the surroundings being at room temperature, are respectively equal to 0.11 and 0.16 for hydrogen and deuterium. The accommodation coefficient of helium relative to the same surface is of the order of 0.05.

A development of the sodium method of preparation for deuterium is described. Its advantages are discussed with respect to the simplicity of the apparatus required, the ease with which the reaction may be controlled, and the consistent purity of the final product.

---

## The Dielectric Polarization of *n*-Long Chain Ketones Near their Melting Points

BY ALEX MÜLLER

(Communicated by Sir William Bragg, O M, F R S—Received 28 July, 1936)

#### INTRODUCTION

A series of normal long chain paraffins has been investigated in two previous papers\* with the object of gaining insight into the structure changes of the crystal lattices at temperatures approaching the melting points.

It is found that in a range of 15 to 20° C below the melting points, the lattices expand rapidly with the temperature, and that with certain members of the series reversible changes take place accompanied by a large increase of volume. Simultaneously the lattices tend to become more symmetrical.

It seems as though the directional forces normal to the chains vanish and that the molecules become free to turn round their long axes. It is important to test this conclusion in every possible way, and one of the

\* 'Proc. Roy. Soc.' A, vol. 127, p. 417 (1930); vol. 138, p. 514 (1932).

tests is the measurement of the dielectric polarization. The present paper deals with an investigation of this kind of two typical representatives of the long chain series.

The paraffin molecule itself has no permanent dipole and is therefore not suited for this investigation. The normal mono-ketone, *i.e.*, the paraffin in which a pair of hydrogen atoms is replaced by an oxygen atom, lends itself well for this purpose. It is not to be expected that the substitution of two hydrogen atoms by oxygen should alter the crystal structure appreciably if the chains are sufficiently long. X-ray analysis shows, indeed, that the two structures are almost identical. The oxygen atom is bound to the chain by chemical forces and the nature of the binding is such that the oxygen atom is not free to rotate independently round the chain axis of the molecule. The only possible rotation of the dipole is the one in which the molecule as a whole turns round its axis. This freedom of rotation must have a marked effect upon the dielectric polarization except when the dipole axis happens to coincide with the chain axis, which is not the case with these ketones. If, as is found in the present work, the polarization of the solid increases with rising temperature, the conclusion must be that the chain molecules become more and more free to orient themselves in the electric field by turning round their long axes.

A similar investigation on a chain compound has been made by Buckingham.\* Buckingham measures the dielectric polarization of ethyl behenate and observes that the transformation of the crystal lattice near the melting point and the corresponding changes in the polarization go exactly parallel to each other. He also comes to the conclusion that the phenomena which he observes must be interpreted as an increased mobility of the molecules round the chain axes. The ketones chosen in the present work have a simpler structure than the ethyl behenate and the position of the dipole in the molecule is known with the least ambiguity. There are no transformations near the melting point, which again simplifies the interpretation. For the task set in this work the ketones can be regarded as the most convenient objects for investigation.

#### APPARATUS

The apparatus consists of a small electric oscillator and a loosely coupled resonance circuit containing the condenser with the substance. This substance condenser is in a thermostat which is kept at any tempera-

\* 'Trans. Faraday Soc.', vol. 30, p. 377 (1934).

ture between 20 and 90° C. In the resonance circuit is a variable capacity in parallel with the substance condenser. The dielectric constants are measured by readings on the scale of the variable capacity when the resonance circuit is in tune with the transmitter.

Most of the measurements are made with an oscillating circuit of 8.9 metre wave-length, as measured on a Lecher system. Measurements with approximately double this wave-length give identical results; and a few measurements made at room temperature with a wave length of 2 metres show that there are no anomalous effects in this range. The apparatus is built on conventional lines. It is very simple and just a few words may be said about its design. The oscillator, of 8.9 metre wave-length, has a single loop of copper wire of gauge No. 16, the diameter of the loop being about 45 cm. One end of this loop is connected to the anode of an Osram H2 valve, the other, with the interception of a small block condenser of 0.0003 mf, to the grid of the valve. The grid leak resistance is 5000 ohms. The anode battery is connected to a point about half-way from the ends of the loop. The anode voltage is 60 to 80 volts and the current 5 to 7 milliamps. The two other wave-lengths are obtained with similar apparatus, one with a very small loop, the other with a loop of several turns.

The resonance circuit is 10 to 15 inches away from the transmitter. The variable measuring capacity is of the sliding cylindrical type. The position of the moving cylinder is read on a caliper scale attached to the instrument. The capacity of the condenser is proportional to the readings on the caliper scale except for the extreme position in which the inner cylinder is nearly withdrawn from the outer tube. The inner and outer diameter of the condenser cylinders are  $D_1 = 1.89_4$  cm, and  $D_2 = 2.06_3$  cm. The capacity change corresponding to 1 cm displacement of the cylinder is therefore

$$C = \frac{1}{2 \ln D_2/D_1} = 5.85_0$$

The substance condenser is connected in parallel to the measuring condenser. Most of the measurements are made with a small condenser consisting of two concentric iron cylinders. The inner of the two has a bore large enough to hold the bulb of a mercury thermometer. The outer cylinder is separated from the inner by short pieces of quartz rod. The capacity of the substance condenser measured directly is  $1.538 \pm 0.006$ , the capacity of 1 scale division ( $= 1$  cm) of the variable condenser being taken as the unit. The relative calibration with benzene  $\epsilon = 2.283$  and ether  $\epsilon = 4.335$  gives  $1.533 \pm 0.011$ . This value is taken as the

effective capacity in all the following calculations. The arrangement of the resonance circuit and a diagram of the substance condenser are shown in figs. 1 and 2. The self-inductance of the resonance circuit is a single loop of 8.5 cm diameter of stout copper wire. Several loops of other sizes are used for calibration. The substance condenser is placed in a

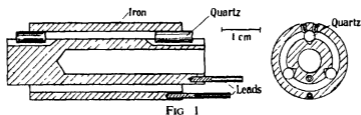


FIG 1

double-walled glass vessel. Water is circulated between the glass walls with the aid of two small motor driven toy pumps. This water is drawn from a Dewar flask and is heated by an immersion heater to any temperature between 20° and 90° C. The temperature is read on a mercury thermometer, the bulb of which is placed in the hole in the substance condenser. The immersion heater is connected to an auto-transformer

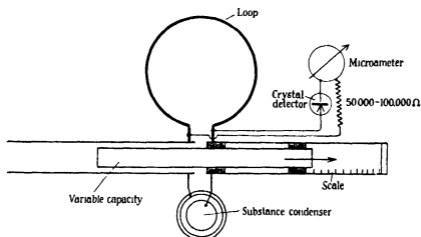


FIG 2

with many tapings, thus allowing the temperature to be varied by sufficiently small steps. The temperature can be kept constant to 1/10 of a degree for any length of time. The heat developed in the immersion heater compensates the heat losses in the system. The constancy of the heating current is watched on an ammeter with mirror scale. The arrangement is shown in fig. 3.

The constancy of the oscillator is checked by a second loosely coupled resonance circuit. The maximum variations of the  $\lambda^2$  taken from observations on several successive days do not exceed  $\frac{1}{2}\%$ . The errors introduced by these variations are negligible here.

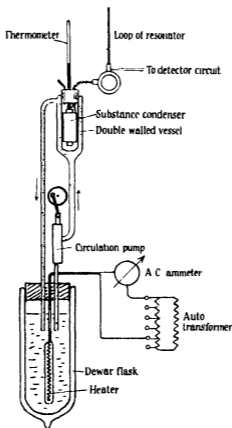


FIG. 3

#### RUN OF AN EXPERIMENT

The resonance circuit is first tuned in with the empty substance condenser, by adjusting the variable capacity, until a maximum current is reached in the detector circuit. The caliper scale is then read giving a value  $r_0$ .

The substance is poured into the glass vessel containing the condenser, and air bubbles are removed by exhausting the vessel. The temperature is adjusted with the aid of the heating circuit while the water is kept circulating during the whole experiment. When the temperature has

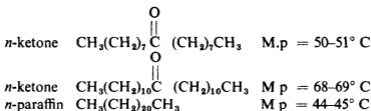
reached a stationary value the resonator circuit is again tuned in and a second reading is made,  $r_t$ , corresponding to the temperature  $t$ . The dielectric capacity of the substance is

$$\epsilon_t = 1 + \frac{r_0 - r_t}{1533},$$

1533 being the capacity of the empty substance condenser expressed in scale divisions of the variable capacity. At the end of a series of experiments with one substance, usually repeated on several successive days, the condenser is emptied and the zero is again read. A few more points about these experiments will be discussed later on.

### MATERIALS

The substances whose dielectric properties are investigated are



*i.e.*, two normal symmetrical ketones with 17 and 23 carbon atoms and a normal paraffin with 22 carbon atoms.

The  $\text{C}_{17}$  ketone was made from pelargonic acid. The starting material for both the  $\text{C}_{23}$  ketone and the  $\text{C}_{22}$  paraffin was lauric acid. The writer wishes to express his thanks to Dr. Oldham for the careful preparation of these substances.

### EXPERIMENTS WITH THE PARAFFIN $\text{C}_{22}\text{H}_{46}$

The errors in the measurement of dielectric capacities which are due to the incomplete filling of the condenser after solidification of the dielectric are estimated in the present work from measurements on a pure paraffin. It is assumed that the absolute magnitude of this error is the same with the ketones. This assumption is justified by the already emphasized similarity of both ketones and paraffins.

Observations made with the pure paraffin show the following facts. The dielectric capacity at temperatures above the melting point remains practically constant in the range of 45° to 90° C. At the melting point there is usually a small increase which in most experiments is of the order

of 2% and on rare occasions rises to 5 to 6%. Below the melting point the dielectric capacity remains again constant down to room temperature. Previous X-ray measurements (*loc cit*) show that there is a considerable contraction when the paraffin becomes solid. A certain amount of substance enters between the two cylinders of the condenser when this contraction takes place, and this increase in density produces a rise in the dielectric capacity. The actual amount of this rise depends upon the gap between the cylinders, the viscosity of the substance at the melting point, and the position of the spot in the condenser at which the crystallization starts. With the present apparatus no control is possible over all these factors. It is therefore not surprising that the above mentioned variations should occur. The essential point is that they are negligible compared with the large changes which take place at the melting points of the ketones.

#### EXPERIMENTS WITH THE KETONES $C_{17}H_{34}O$ AND $C_{23}H_{46}O$

Measurements with ketones taken on different days reproduce within a few per cent of the absolute value of the dielectric constant  $\epsilon$ . The relative measurements referring to the difference  $\Delta\epsilon$  of the dielectric capacity at room temperature and a temperature  $t$  show even smaller variations, except those in the immediate vicinity of the melting point. Provided a temperature equilibrium is reached after each temperature adjustment, there is no appreciable difference between the heating and the cooling curves. The diagram shows three typical curves obtained with the two ketones and the paraffin. The arrows indicate the melting points.

The figures ( $\Delta\epsilon = \epsilon_t - \epsilon_{\text{room } t=\text{mp}}$ ) corresponding to these curves are tabulated on p. 411 and also the maximum values of  $\Delta\epsilon_{\text{max}} = \epsilon_{\text{max}} - \epsilon_{\text{room } t=\text{mp}}$  and the values of the dielectric constant at room temperature. Both these and the  $\Delta\epsilon_{\text{max}}$  represent averages taken from all the observations.

#### DISCUSSION OF THE RESULTS

Comparing the dielectric constants of the two ketones and the paraffin, it is found that the polarizations of these substances at room temperature differ not more than about 10%. This follows directly from the figures given in the table and is to be expected because the molecular volume, referred to a unit length of chain, is very nearly the same for all three substances. The existing differences of polarization are outside the limits of experimental error and may either be due to a residual mobility

of the chains at room temperature or to a characteristic vibration in the region of shorter wave-length. The results which Cartwright and Errera\* obtain from the investigation of acetone in the far infra-red suggest very strongly that this difference of polarization is due to a characteristic frequency between  $150\ \mu$  and 2 metres, in accordance with a conclusion at the end of this paper. This important point will be discussed in a continuation of this work.

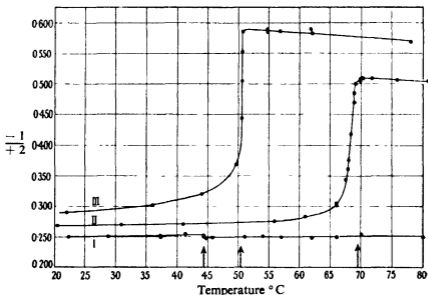
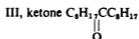
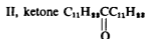


FIG 4—Observed  $\frac{\epsilon - 1}{\epsilon + 2}$  of I, paraffin  $C_{31}H_{64}$ .



As the temperature increases, the polarizations of both ketones begin to rise, first slowly and then more and more rapidly until they reach a maximum at the melting point or at least very close to it. The polarization of the paraffin remains practically constant. One of the main results of this investigation is the fact that the rise in polarization becomes quite appreciable at temperatures well away from the melting point. This shows that already an appreciable number of molecules in the solid becomes free to orient itself in the external field. The nature of this

\* \* Proc Roy Soc., A, vol 154, p. 138 (1936).

freedom is a rotation round the chain axes. The present work leads, therefore, to the conclusion already arrived at by structure analysis

$\Delta\epsilon$  AS FUNCTION OF THE TEMPERATURE (TYPICAL SERIES OF OBSERVATIONS),  
 $\Delta\epsilon_{\max}$  AND  $\epsilon$  AT ROOM TEMPERATURE (AVERAGES)

Paraffin $C_{23}H_{48}$ (cooling curve)		Ketone $C_{17}H_{34}O$ (cooling curve)		Ketone $C_{23}H_{46}O$ (heating curve)	
Temperature °C.	$\Delta\epsilon$	Temperature °C	$\Delta\epsilon$	Temperature °C	$\Delta\epsilon$
86	- 0 008	78	2 711	18	$\pm 0$
82	-0 005	70	2 960	31	0 008
70	+0 029	62	3 056	41	0 014
66	-0 002	61 8	3 045	56	0 045
62	-0 009	56 8	2 993	61	0 085
57	-0 001	54 8	3 059	66	0 200
54	+0 005	50 7	3 007	67 5	0 476
51	-0 002	50 6	2 472	67 8	0 596
45 8	-0 006	50 6	1 820	68 0	0 698
44 8	-0 013	50 5	1 167	68 3	1 049
44 3	-0 001	49 6	0 516	68 8	1 550
44 3	+0 013	44	0 189	68 8	1 717
41 3	+0 029	36	0 072	69 1	1 901
37 3	+0	22	$\pm 0$	69 8	1 945
37 3	+0 013			69 9	2 002
28 8	+0 006			70 3	2 005
22 3	$\pm 0$			70 1	2 023
				71 8	2 018
				75 8	1 974
				80 8	1 945
				84 8	1 911
				86 8	1 881
				88 8	1 861
				90 3	1 869
		Temp near m p. (50-51° C)	$\Delta\epsilon_{\max}$ 3 16 $\pm$ 0 06	Temp near m p (68-69° C)	$\Delta\epsilon_{\max}$ 2 074 $\pm$ 0 034
Room temp	$\epsilon$ 2 00	Room temp	$\epsilon$ 2 222 $\pm$ 0 018	Room temp	$\epsilon$ 2 10

No attempt is made in this paper to account numerically for the shape of the curves shown in the diagram. A satisfactory solution of this problem requires obviously the knowledge of the Hamiltonian of the system, and owing to the particularly simple structure of the substances

it seems not unlikely that such a solution will be found. Attempts in this direction are being made in this laboratory.

It is easy to make an estimate of the maximum polarization which would be observed if all the molecules were free to follow the external field by turning round a fixed axis. If at the same time all these axes are distributed at random a simple calculation shows that the resulting polarization due to these dipoles is equal to

$$\frac{\mu^2 \sin^2 \sigma}{3\kappa T},$$

$\mu$  = dipole moment and  $\sigma$  = the angle between the dipole axis and the axis of the molecule (rotation axis). From structure considerations it seems not unlikely that this angle is  $90^\circ$  or nearly  $90^\circ$  in the present case of the symmetrical ketones. The dipole polarization becomes, therefore,  $\frac{\mu^2}{3\kappa T}$ , i.e., identical with that which would occur if all the molecules were completely free as in the liquid. It is impossible to draw any conclusions from the observations made in the immediate neighbourhood of the melting point, but from the form of the curve it seems that gradually all the molecules become free to follow the external electrical vibrations.

The increase in polarization at the melting point being due to a free motion of the dipole, the difference between the maximum polarization and that at room temperature, or even better the polarization of the paraffin, should give an approximate figure for the dipole moment. This procedure would not be correct in the general case. In substances with high dipole concentration there is far too much mutual influence between the dipoles, and saturation could not be reached with normal fields. In the present case the situation is different. Owing to the large size of the chain molecules, the dipole concentration in these substances is quite small, i.e., the molten substance is similar to a solution of moderate concentration so far as the dipoles are concerned. The calculation should therefore give an approximate value for the dipole moment, as is shown in the following. We have

$$\frac{\mu^2}{3\kappa T} = \frac{3}{4\pi} \left\{ \left( \frac{\epsilon - 1}{\epsilon + 2} \right)_{\text{max}} \cdot v_{\text{ket}} - \left( \frac{\epsilon - 1}{\epsilon + 2} \right)_{\text{paraf}} v_{\text{paraf}} \right\},$$

$v_{\text{ket}} = v_{\text{paraf}} = v$  = molecular volumes of corresponding ketone and paraffin, which differ by not more than 1% from each other. We find for  $C_{17}$ ,  $v = 520 \times 10^{-24}$  cc and for  $C_{23}$ ,  $v = 690 \times 10^{-24}$  cc. These volumes are observed at a temperature near the melting point of the ketones.

$\mu$  = dipole moment in electrostatic units,  $\kappa = 1.37 \times 10^{-16}$  ergs./degree C.,  $T$  = melting points (absolute);  $\left(\frac{\epsilon - 1}{\epsilon + 2}\right)_{\max}$  obtained from the present measurements and given in the table,  $\left(\frac{\epsilon - 1}{\epsilon + 2}\right)_{\text{paraff}}$  independent of the chain length of the paraffin, *i.e.*, the same for  $C_{17}$ ,  $C_{22}$ ,  $C_{23}$  and given in the table

With these data the following figures for the dipole moments are obtained

$$\text{Ketone } C_{17}H_{34}O \quad \mu = 2.38 \times 10^{-18} \text{ el stat units}$$

$$\text{Ketone } C_{23}H_{46}O \quad \mu = 2.48 \times 10^{-18} \quad , ,$$

It is to be expected that they should be smaller than those corresponding to the dipole in dilute solution. Two series of experiments in which the ketone  $C_{17}$  is dissolved in heptane confirm this. The dipole moment is again calculated from the difference between the dilute solution and the pure paraffin. The dipole moments found in the two series of experiments are  $\mu = 2.85$  and  $2.72 \times 10^{-18}$ , *i.e.*, an average of  $\mu = 2.78 \times 10^{-18}$ .

This figure is, within the limits of experimental error, identical with the value of the dipole moment in acetone  $\mu = 2.760 \times 10^{-18}$  and a number of other ketones\*.

The fact that the dipole moments calculated from the pure molten substances are smaller than those obtained from the diluted solution shows that there is an interaction between the dipoles. It should be possible to get an estimate of the energy due to this interaction in the crystal lattice. This problem is under investigation.

With the aid of the present material, it is possible to give at least a qualitative picture of the phenomena which precede the melting of these long chain ketones and other similar chain compounds. Starting from low temperatures, the lattice expands first slowly until the temperature comes to within 15 to 20° C of the melting point. In this range the lattice begins to expand rapidly. The directional forces which at lower temperatures keep the chains in definite positions relative to each other become weaker and the molecules acquire the freedom to turn round their axes. The dissymmetry of the cross-section of the chain is smoothed out by this rotation, the crystal becomes symmetrical relative to the chain axes, and at the melting point the directional forces are overbalanced by the forces due to the thermal agitation.

\* Table of dipole moments, 'Trans. Faraday Soc.', vol. 30, Appendix (1934)

It has already been mentioned that the dielectric properties are independent of the wave-length in the range of 2 to 18 metres. Calculations made in connexion with a previous paper on the lattice energies of chain compounds\* show that an anomalous effect is to be expected in the neighbourhood of about 1 cm wavelength. Experiments to test this point are in preparation

The writer wishes to thank Dr R. Eisenschitz for many valuable discussions and to express his appreciation to Mr C H Jenkinson for the excellent workmanship shown in the making of the standard variable capacity. He also wishes to thank the Director and the Managers of the Royal Institution for the opportunities given to him for carrying out this work at the Davy Faraday Laboratory

#### SUMMARY

The dielectric capacity of each of two symmetrical normal long chain ketones is measured at different temperatures near the melting point of the substance. Considerable increase of the D.C. is observed in a range of 15° to 20° C below the melting points. The phenomenon is interpreted as an increase of rotational mobility of the chain molecules round the chain axes in a state where the substances are still solid. This confirms the conclusion previously drawn from structure analysis of similar substances near their melting points.

An appreciable mutual influence of the dipoles is observed in the pure molten substances. Observations on dilute solutions yield a dipole moment which is identical with that found in acetone and similar ketones.

\* 'Proc Roy Soc,' A, vol 154, p 624 (1936)

---

# The Influence of Pressure on the Spontaneous Ignition and Limits of Inflammability of Ether-Air Mixtures

By D T A TOWNEND, D Sc., and E A C CHAMBERLAIN, Ph D

(Communicated by W A Bone, F R S—Received 30 July, 1936)

## INTRODUCTION

As part of a wider investigation into the influence of pressure on the spontaneous ignition of inflammable gas-air media generally, some time ago we studied the behaviour of diethyl ether and found it to simulate that of the higher paraffins, in that at low pressures ignition occurs in a high temperature system and at higher pressures in a low temperature system, which develops in the range where normally only cool flames are propagated\*. We were also impressed with the analogy between our own observations and those on the limits of inflammability of ether-air mixtures made in 1927 by A G White† who discovered that at low pressures there are two ranges of explosive mixtures which can propagate flame, one for normal and another for cool flames, separated by a range of mixtures through which no flame can be propagated, with increase of pressure these explosive ranges become superposed. We decided to examine the matter more closely because it seemed likely that an explanation of the analogy referred to would throw light on the whole problem. Moreover, the subject is of practical importance, having in mind the risks inherent in certain circumstances in the use of ether as an anaesthetic, and it was hoped that our results might also be of some service in this connexion.

A likely interpretation could be based on the thermal theory of flame propagation. This applies to the slow initial stages of gaseous explosions and was developed by Mallard and Le Chatelier‡ who proposed the following well-known equation for the velocity,  $V$ , of the "uniform movement"—

$$V = \frac{L}{C} \frac{(T - t)}{(t - \theta)} f(Tt),$$

where  $T$  = the temperature attained in the combustion,  $t$  = the ignition

\* Cf previous papers on this subject, 'Proc Roy Soc.' A, vol 141, p 484 (1933), vol 143, p 168 (1933), vol 146, p 133 (1934), vol 154, p 95 (1936).

† 'J chem Soc.' p 498 (1927)

‡ 'Annals des Mines,' vol 8, p 274 (1883).

temperature of the mixture,  $\theta$  = the initial temperature,  $L$  = the thermal conductivity of the unburnt gas,  $C$  = its mean heat capacity between  $\theta$  and  $t$ , and  $f(Tt)$  = a function taking into account the change of  $L$  and  $C$  with temperature. Other modifications have been proposed, but discussion has usually centred round the above equation, and although it is not possible to apply it quantitatively, owing to the insuperable difficulties involved in determining the precise values of the various terms concerned and lack of knowledge concerning the amount of combustion occurring in the flame front and energy losses, etc., it lends itself well to the qualitative interpretation of the effect of the various factors controlling initial slow flame speeds. For example, Mason and Wheeler\* showed that with mixtures of like thermal conductivity the speed is proportional to  $(T - t)$ , and inversely proportional to  $(t - \theta)$ . Moreover, with combustible-air/oxygen media the mixture giving rise to the maximum flame speed contains an excess of combustible corresponding, owing to the suppression of  $\text{CO}_2$ —and  $\text{H}_2\text{O}$ —dissociation, with that developing the highest temperature, indeed, Bone and Bell† have recently shown that with  $\text{CO-O}_2$  media the flame speed-composition curve exhibits two maxima corresponding with the suppression of  $\text{CO}_2$  dissociation by excess of either  $\text{CO}$  or  $\text{O}_2$ .

While it is not difficult to demonstrate the correspondence between  $(T - t)$  and flame speed, any variation with mixture composition of the ignition temperature factor  $(t - \theta)$  is usually not sufficiently great for any marked change in flame speed to be anticipated. Recently, however, it has been shown with higher paraffin hydrocarbon-air media that, on the attainment of a critical pressure, the ignition temperature falls from a higher system above  $500^\circ\text{C}$  to a lower system at about  $300^\circ\text{C}$ ,‡ and in conformity, while at certain pressures the ignition temperatures of excess-air mixtures are in the upper system, those of mixtures richer in hydrocarbon are in the lower system. Gusev and Neumann, appreciating the importance of these observations as a means of testing the general application of the Le Chatelier theory, have proved its essential validity by demonstrating that with pentane-air mixtures initially at 7 atmospheres pressure and  $175^\circ\text{C}$ , the flame speed curve is composite, the speeds through mixtures containing more than a critical proportion of pentane being relatively greater than those through mixtures containing a smaller proportion §

\* 'J. chem. Soc.', p. 1044 (1917).

† 'Proc. Roy. Soc.,' A, vol. 143, p. 1 (1933).

‡ *Loc. cit.*

§ 'C.R. Acad. Sci. U.S.S.R.', vol. 2, p. 377 (1935).

Moreover, according to the Le Chatelier theory, the mixture at the limit of inflammability is that in which the heat developed in the flame front is just adequate to raise to the ignition point the explosive mixture ahead of it. Any change, therefore, in the physical condition of the medium responsible for an abrupt change in the ignition temperature should effect a corresponding abrupt variation in the composition of the mixture at the limit of inflammability, and this might well account for the correspondence between the two sets of observations with ether-air mixtures.

On the other hand, the recognition in recent years of chain processes in the initial isothermal stages of gaseous combustion has led to some discussion as to the likelihood of their occurrence in flames.\* Hot molecules or chemically reactive species may be considered as functioning as chain carriers either (a) during the direct transfer of energy from the inflamed to the reactant molecules, or, if very rapid heat transfer be assumed, (b) during the subsequent initial combustion leading to the development of the ignition of the medium ahead of the flame.†

Our experiments seem to indicate that while the thermal view may, generally speaking, apply in the case of normal flames, with cool flames chain processes appear to predominate.

#### A—IGNITION TEMPERATURES

*Previous Investigations*—Perusal of the literature‡ shows the ignition points of ether-air mixtures at atmospheric pressure to have been located either above 400° C. or at about 200° C., usually depending upon the method employed, the values for ether-oxygen mixtures are invariably located at the lower of these temperatures. The influence of pressure on the ignition points was studied in his concentric tube apparatus by H. B. Dixon,§ who found for determinations relative to a constant time lag of 0.5 sec. a progressive fall from 665° to 248° as the pressure was raised from 75 to 1770 mm. At higher pressures from 2 to 18 atmospheres the values calculated from determinations in his adiabatic compression machine fell from about 280° to 250° C.

\* Cf. Garner and Pollard, 'J. chem. Soc.', p. 144 (1935), Semenov, 'Z. phys. Chem.', B, vol. 28, p. 43 (1935), Egerton and Gates, 'Proc. Roy. Soc.', A, vol. 116 p. 516 (1927), Thompson, 'Z. phys. Chem.', B, vol. 48, p. 219 (1932), Coward, 'J. Soc. chem. Ind.', vol. 55, p. 175 (1936).

† Cf. Sokolik and Voronkov, 'Nature', vol. 137, p. 534 (1936), Rivin and Sokolik, 'Acta Phys. Chim.', vol. 4, p. 301 (1936).

‡ "Flame and Combustion in Gases," p. 483.

§ See Coward, 'J. chem. Soc.', p. 1936 (1934).

As regards cool flames in ether-air mixtures, White and Price\* found in a static system "sub-ignition" temperatures between  $178^{\circ}$  and  $188^{\circ}$  C, which varied somewhat with change in the reduced pressures employed. Also Prettre,† using a flow system at atmospheric pressure, observed cool flames at  $200$ – $230^{\circ}$  which gave place to true ignition at  $240$ – $250^{\circ}$  C

*Experimental*—The ether used throughout the investigation was a specially prepared dry sample uncontaminated with aldehydes or peroxides and stored in an atmosphere of nitrogen.

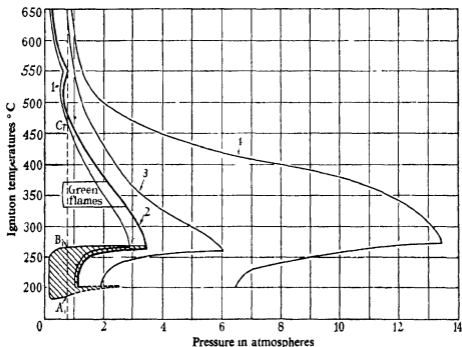


FIG. 1—Ether-air mixtures. Percentage mixtures for the curves 1 = 10, 2 = 5, 3 = 2, 4 = 1. Silica liner in use. Shaded area defines temperature and pressure limits for cool flames with 5% mixture.

The method employed in determining the ignition temperatures was essentially that described in a previous paper,‡ it consisted in rapidly admitting the mixture under investigation into an explosion vessel provided with a silica lined cylindrical cavity 15 cm.  $\times$  3.75 cm, capacity = 165 cc, and maintained at the experimental temperature. By varying

\* 'J. chem. Soc.', p. 1462 (1919).

† 'Bull. Soc. chim.', vol. 51, p. 1132 (1932).

‡ 'Proc. Roy. Soc.', A, vol. 141, p. 484 (1933).

the initial pressure of the mixture two pressures usually separated by not more than 0.05 atmosphere were ultimately determined, at the lower of which ignition did not occur and at the higher of which it did, the ignitions being recorded both by the kick imparted to a Bourdon gauge and by visual observations of the "flash" seen through a window fitted to the explosion vessel. The ignition point curves reproduced in fig. 1 were obtained by plotting the means of the pressures so determined over the whole temperature range.

No difficulty was ever experienced in reproducing the results very closely.

*Results*—We have determined the influence of pressure on the ignition points of four representative ether-air mixtures containing 1, 2, 5, and 10% of ether, respectively, curves 4, 3, 2, and 1. For clarity the detail of the cool flame area (shaded), etc. is restricted to the 5% mixture (heavy line).

Generally speaking, the curves simulate those determined for the higher paraffin hydrocarbons (*qv*), for two distinct ignition systems (an upper and a lower) were observed, the lower developing with increase of initial pressure in the temperature range within which cool flames are normally observed. There were, however, certain new features found in the behaviour of ether-air mixtures, and attention is specially directed to the following.

1—Whereas the temperature range in which cool flames propagate and the lower true ignition system develops has hitherto always been found between about 280° and 410° C, \* with ether-air mixtures it is much lower and lies between approximately 180° and 270° C.

2—At all temperatures above the cool flame upper limit until either (*a*) the explosion vessel attains a red heat and thus destroys visual observation, or (*b*) true ignition occurs, a blue luminescence is apparent in the mixture immediately after its admission.

3—Between about 330° C. and 365° C. a zone was found in which a new phenomenon was observed, namely, the propagation of green flames which differed markedly both from the slow travelling pale blue cool flames and the true ignitions which gave rise to a bright white or yellowish emission. These green flames travelled with a high velocity, as when true ignition occurred and gave rise to the development of a pressure much greater than the small pulse observed with a cool flame and more

\* This applies not only to the higher paraffins but also to the higher olefines and primary aldehydes (250°–350° C), our observations on which have not yet been published.

akin to the kick characteristic of true ignition; they were never observed outside such limits of temperature and pressure as are shown for the 5% ether-air mixture and as far as we are aware are peculiar to ether-air mixtures

4—In confirmation of the observation of White and Price,\* the ignition points for cool flames at reduced pressures were found to reach a minimum value with increase of pressure, this is recognized as the phenomenon now known as "low pressure ignition limits"

5—A striking feature of the true ignitions in the low temperature range was that although with all four mixtures the ignition points were easily determined at 200° C, if the temperature were lowered even by 1° C, ignition was quite impossible even if the pressure were raised to 15 atmospheres. We have little doubt, therefore, that "ignition limits" occur with the true ignitions as with cool flames and the ignition point curve, if determinable, would therefore be somewhat as shown by the dotted line (No. 2)

6—Another interesting observation was that, with the two mixtures containing an excess of ether (Nos. 1 and 2), the ignition point curves are not smooth in the upper system, ignition being effected at lower pressures at about 500° C than at 50° higher

7—The time lags were always very much shorter than, but showed the same general variation with temperature as, those observed with the hydrocarbons. They were about 2 seconds at 550° C, gradually becoming shorter as the temperature fell, until in the lower system they were only about 2/5 sec, at 200° C, however, they had increased to 4/5 sec

No attempt has yet been made to study quantitatively the processes involved in the oxidation of ether over the temperature range covered in the present investigation; as far as the ignition points are concerned, the violence of the ignitions of mixtures undiluted with nitrogen precludes their investigation under our present method of procedure. As regards the general interpretation of the main upper and lower ignition systems, in previous papers relating to the higher hydrocarbons, we have tentatively put forward the view that ignition in the upper system pertains mainly to the thermal decomposition of intermediate oxygenated bodies, while ignition in the lower range occurs when temperature and pressure conditions favour their survival and further oxidation. While this explanation was based on thermal grounds, it is not inconsistent with the survival of (say) aldehydes giving rise to some chain mechanism as, for example, might result from the formation of per-acids during their secondary

oxidations The view held by supporters of the peroxide theory of hydrocarbon combustion is that the low temperature system arises from chain propagation resulting from the formation of primary peroxides and an apparent negative temperature coefficient of reaction velocity sets in at temperatures above that at which such peroxides are relatively long lived \*

Recently Aivazov and Neumann† have also put forward a view based on the theory of interacting chains that cool flames arise when some intermediate product reaches a critical concentration and that its maximum concentration falls with increase of temperature owing to its instability

#### B—LIMITS OF INFLAMMABILITY

*Previous Investigation*—Reference need only be made here to the extensive researches of A G White,‡ who has made a comprehensive study of the limits of inflammability of explosive mixtures of many inflammable gases and vapours under a wide range of experimental conditions His curves showing the influence of varying pressures up to 1 atmosphere on these limits for ether-air mixtures, and relating to horizontal propagation of flame in a 5 l cm glass tube 1.5 metres in length, are reproduced in fig 3, top inset There are two ranges of inflammable mixtures, that on the left pertaining to ordinary flames and that on the right (with richer mixtures) to cool flames, separated by a range of non-inflammable mixtures which narrows with increase of pressure and finally disappears as the two inflammable ranges merge at about 550 mm pressure Care had to be exercised to use the appropriate means of ignition in each particular case, a high tension spark being employed for ordinary flames and an electrically heated helix of platinum wire for the cool flames

The main purpose of our extended study of the problem was to investigate whether, with increase of pressure, the range for ordinary flames would become superposed on the cool flame range, in much the same way as with spontaneous ignition a true ignition system is imposed on the cool flame range on the attainment of an adequately high pressure, in this our anticipation was fulfilled

*Experimental*—In order to experiment at pressures between 1 and 5 atmospheres and at the same time ensure close observation of the flames,

\* Egerton and Ubbelohde, 'Nature,' vol. 135, p. 927 (1935)

† 'Acta Phys. Chim.,' U.S.S.R., vol. 4, p. 575 (1936)

‡ 'J. chem. Soc.,' p. 1462 (1919), pp. 1244, 1688, 2561 (1922), p. 2387 (1924), pp. 48, 672 (1925), p. 498 (1927)

a stout glass tube 2.5 cm in diam and 1 metre long was supported in a mild steel tube, A, fig 2, with a slit 1 cm wide milled along one side. The tube was contained in a large light-tight chamber, provided with an observation aperture, and connected to a pressure filling system, the gas-tight joints at the ends of the tube being as illustrated in the inset. Experiments were carried out at three temperatures, namely 20°, 60°, and 100° C, the heating being effected electrically by means of insulated resistance wire wound round the mild steel tube.

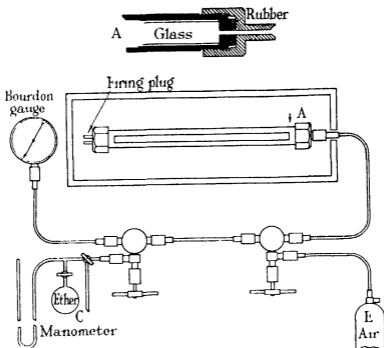


FIG 2

The method of making a mixture in the tube was (a) first of all to evacuate it, then (b) admit ether vapour to the required partial pressure from the bulb C containing the liquid, and (c) admit compressed air from the cylinder E to the desired total pressure. Proper mixing was ensured by allowing glass marbles to roll up and down the tube by means of a rocking device for 15 minutes, and before firing the mixture any gas pressure in excess of that desired was released. The observations were generally easily reproducible.

**Results**—In order to illustrate our results, we have given, in fig 3, curves showing the influence of varying initial pressure up to 5 atmo-

spheres on the limits for each type of flame propagation, the mixtures being maintained at an initial temperature of  $100^{\circ}\text{C}$ . It should be stated that the procedure adopted by White in regard to methods of

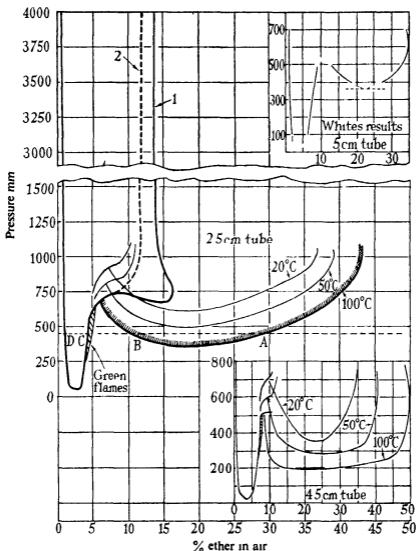


FIG 3

ignition was followed in the present investigation. At low pressures where the two ranges of inflammability were separate a high tension spark gave sharp limits for normal flames but failed to initiate cool flames; on the other hand, a heated platinum helix though successful in

initiating cool flames, gave rise to surface combustion when used with mixtures in the normal flame range

The criterion adopted for inflammability with both types of flame was complete propagation throughout the length of the tube

At pressures where the two ranges became superposed difficulty was experienced, in the first place, in deciding upon a criterion for the propagation of the normal flame (upper limit). It made its appearance at first as a development of the cool flame some distance along the tube from the source of ignition; the higher the ether content of the mixture the greater was this distance and eventually the transition failed to occur. The outer curve, 1, pertains to mixtures in which the change over from cool to normal flame occurred halfway along the tube. It was not always easy to decide the limiting composition of mixtures which would propagate the normal flame *ab initio*, for it was found that occasionally at these pressures even a high tension spark might give rise to a cool flame, the inner dotted curve, 2, shows these limits approximately, however, the accuracy being within about 0.5% in the ether content of the mixtures.

Another observation of importance was that at pressures just below that at which the two composition ranges merged, a narrow and ill-defined range of mixtures with ether-contents above the limit for normal flames was located, in which green flames, identical in appearance with those discovered in the ignition temperature experiments, were propagated. The approximate limits for these mixtures are shown by the diagonally shaded area, the green flames were never observed at pressures outside the range shown. These flames were much less easily reproducible than either the normal or the cool flames.

*The Analogy Between the Spontaneous Ignition Points and Limits of Inflammability*—As already indicated, according to the thermal view of flame propagation, the mixture at the limit of inflammability is that in which the heat developed in the flame is just adequate to raise the unburnt medium ahead of it to its ignition temperature. If such be the case it would be supposed that change in pressure should exert a corresponding influence on both these constants. It is only possible to obtain a general comparison, however, for (a) the ignition temperatures applying to flame propagation, would be relative to constant very short lags, and (b) the ignition temperatures vary somewhat with change in mixture composition. With regard to (a) fortunately the lags observed in the ignition temperature determinations were short and the characteristics of the curves obtained would not vary greatly for constant shorter lags;

and with regard to (b) the general influence of pressure on spontaneous ignition was much the same for all ether-air mixtures.

To facilitate an understanding of the possible thermal interpretation of the analogy between the two constants, we have dotted across each diagram (figs. 1 and 3) a line at 450 mm on the pressure scale, lettering the four composition limits at this pressure A, B, C, and D (fig. 3) and the corresponding ignition temperature limits  $A_1$ ,  $B_1$ , and  $C_1$  (fig. 1). In brief, the mixture at the limit A would, on inflammation, develop sufficient heat to raise the unburnt medium to the ignition temperature  $A_1$  requisite to propagate a cool flame. With increase in oxygen content of the mixtures more heat would be liberated in the flame and at the limit B the flame temperature would be such that the life of some material essential to its propagation would be inadequate, this would correspond with the upper temperature limit for cool flames  $B_1$ , and mixtures of composition between B and C would on this account be non-inflammable, corresponding with the range of non-ignitibility between the two ignition systems, *i.e.*, between  $B_1$  and  $C_1$ . Mixtures of greater potential heat content than that at C, however, would give rise to normal flames, for these would be capable of raising the unburnt media above the ignition temperature for normal flames,  $C_1$ . Finally, a maximum heat evolution would be developed with approximately the theoretical mixture (3.5% ether content) and the mixture D containing an excess of air would again be just capable of liberating the heat necessary to attain the ignition point  $C_1$ .

Further, it will be observed (fig. 3) that, (i) at about 750 mm the limit of inflammability for normal flames widens abruptly, passing over into the cool flame range in much the same way as the ignition temperatures for true ignition pass at a critical pressure from the higher to the lower system (fig. 1), (ii) the composition limits for mixtures which give rise to the green flames (fig. 3) are intermediate between those for the normal and the cool flames as would be predicted from the location of the temperature limits within which their occurrence was located in the spontaneous ignition observations (fig. 1), and (iii) just as the minimum ignition temperatures both for cool flames and true ignition were found to be raised with increase of pressure following the pressure limit phenomenon (p. 420 and fig. 1), so the limits of inflammability both for cool and normal flames were found to narrow as the initial pressure was raised much above 1 atmosphere. The analogy was therefore striking and support apparently forthcoming for the general application of the Le Chatelier thermal view.

In order to test the matter still further, however, we decided to carry

out some determinations on the limits of inflammability of cool flames at varying initial temperatures, for if the view outlined were correct then it would be supposed that while the limits A, C, and D would be widened with increasing initial temperature of the mixtures, that at B would be narrowed, for the increased initial heat provided the limit mixture would render it non-inflammable owing to its now falling in the non-ignition range between  $B_1$  and  $C_1$  (fig. 1) \*. The curves for the cool flame limits at 20° and 50° C. are shown in fig. 3 (thin lines), from which it will be seen that this anticipation was not fulfilled, both the limits A and B being narrowed progressively with reduction in initial temperature.

As also according to the thermal view, the cool flame speeds would become greater progressively as the air contents of the mixtures were increased between the limits A and B, we decided to investigate this aspect of the matter; for it now seemed likely that a maximum speed might be obtained with a mixture located within this range. Determinations were therefore made in a 4.5 cm. tube over a wide range of initial temperatures and pressures (see lower inset fig. 3), the cool flame velocities being very slow, they were measurable by means of a stop watch. Rather to our surprise, as will be seen from the following figures, it was found that the velocities of the cool flames were constant within the error of experiment and independent of mixture composition, initial temperature, and pressure.

*Cool Flame Velocities in Glass Tube, 4.5 cm. Diameter*  
*cm/sec*

(Values are for various representative mixtures in the range of inflammability at the initial temperatures and pressures stated.)

Temperature ° C	Pressure (mm)					
	240	300	450	550	600	700
20	—	—	22.5	24	23	27
	—	—	22.5	24	25	24
	—	—	22.5	24	24	27
	—	—	—	23	26	24
	—	—	—	23	24	24
50	—	—	—	—	—	24
	—	—	—	—	—	24
	—	—	—	—	—	23

\* We were very greatly indebted to Dr. A. G. White, with whom we discussed our results and their implications, for the information that he had found in his experiments that widening the explosion tube employed had widened the limit B. On this account we carried out the further experiments here described.

*Cool Flame Velocities in Glass Tube 4.5 cm Diameter*  
cm/sec —(continued)

Temperature ° C	Pressure (mm)					
	240	300	450	550	600	700
100	24	24	24	—	23	23.5
	24	24	24	—	23	—
	24	24	24	—	24	—
	22	23	22	—	—	—
150	—	—	—	—	—	24
	—	—	—	—	—	24
	—	—	—	—	—	24
	—	—	—	—	—	24
160	—	—	—	—	—	24
	—	—	—	—	—	23

Taking into account all the factors concerned, it now appeared as though (i) the cool flame range is concerned with an initial reaction between ether and oxygen, the most reactive mixtures being in molecular proportion between 1:1 and 2:1 (*i.e.*, 18% and 29% ether in air), and (ii) on account of the constant flame velocity the flame temperature for all mixtures is probably limited and approximately constant (corresponding with the upper temperature limits for cool flames  $C_1$ ) and no doubt determined by the dissociation of an intermediate product.

On extending our investigation of the cool flame speeds to determinations in narrower tubes, we found them to be markedly lowered as the following figures relative to a tube, 2.5 cm in diameter, show

*Cool Flame Velocities in Glass Tube, 2.5 cm Diameter*  
cm/sec

Temperature ° C	Pressure (mm)	
	600	700
20	13.5	13.5
	13.5	13.5
	13.5	13.5
	—	13.5
50	13.5	13.5
	13	13
	13	13
	—	13

In view of the fact that while a wide variation in initial temperature had been without apparent effect on the velocities, whereas change in

tube diameter had considerably influenced them, it seemed doubtful whether cool flames can be considered in the light of the simple thermal theory and their propagation is probably directly concerned with a chain mechanism. A few determinations in a tube of intermediate diameter, 3.5 cm, gave speed values of approximately 21.5 cm per sec, and taking the mixture used for them we found Semenov's relation  $pd^n = \text{const}$ , where  $p$  = the limiting pressure for ignition and  $d$  = the diameter of the tube to hold good,  $n$  being equal approximately to unity, assuming the relation to be applicable in such circumstances this might be taken as indicating a mechanism with the breaking of chains on the walls of the vessel. Other factors needing consideration, however, are the low heat contents of the flames, the influence of convection,\* as well as the character and area of the flame envelope†. We are therefore following up this aspect of the matter more closely.

In order not to complicate our diagram (fig. 3), we have shown only a limited portion at about 1 atmosphere pressure of the curves indicating the upper limit for normal flames at 20° and 50° C. It should be stated, however, that at lower pressures these limits at all three temperatures were almost coincident but showed a definite tendency to narrow with increasing temperature. It is not unlikely that this effect is connected with the irregularity in the ignition points found with mixtures of corresponding composition at low pressures referred to on p. 420. We are also hoping to investigate this observation still further.

In conclusion, we desire to express our thanks to the Gas Light and Coke Company for their Research Fellowship, which has enabled one of us (E. A. C. C.) to devote his whole time to the work, to Dr. A. G. White who in private communication gave us the benefit of his wide experience of the subject, and to Dr. R. H. Sapiro, to whom we were indebted for the special sample of ether used in the investigation.

#### SUMMARY

The influence of varying initial pressure on the spontaneous ignition of ether-air mixtures has been found to be much the same as that observed with the higher paraffin hydrocarbons. There are two temperature ranges of spontaneous ignition, location in a higher range occurring at low pressures and at higher pressures in a lower range where normally only cool flames are propagated. The lower range with ether (180°–

\* Cf. White, *loc. cit.*

† Cf. Coward and Hartwell, 'J. chem. Soc.', p. 2676 (1932).

270°) was much below that observed with higher hydrocarbons (280°–410°).

An analogy was observed between the influence of pressure on spontaneous ignition and limits of inflammability, for at low pressures there are two ranges of inflammable mixtures, one for normal and the other for cool flames, separated by a range of mixtures which do not propagate flame, with increase of pressure the inflammable ranges become superposed in much the same way as do the spontaneous ignition ranges.

While, generally speaking, the analogy may with the normal flames be interpreted on the basis of the Le Chatelier thermal view of flame propagation, the mixture of limit composition being assumed to develop just enough heat to raise the unburnt medium to its ignition point, this is doubtful in the case of the cool flames which seem to require an interpretation based on a chain mechanism

---

## Spectrographic Studies of the Explosive Combustion of Methane

By J. BELL, Ph.D. (Beit Research Fellow)

(Communicated by William A. Bone, F.R.S.—Received 30 July, 1936)

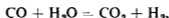
[PLATES 20–23]

The combustion of the simpler hydrocarbons has been studied over a wide range of conditions and many analytical and kinetic data have been accumulated. Although several spectroscopic investigations have been made, all have been confined within narrow experimental limits and none accompanied by detailed chemical analyses. The majority have dealt with the radiation from the inner cone of a hydrocarbon flame, usually maintained in some form of flame separator. Although under such conditions the hydrocarbon burns substantially to carbonic oxide, hydrogen, and water, further interactions between these products occur during the cooling period. This is seen from the following analyses of the interconal gases from a methane-air and an ethylene-air flame

*Mixture Burned in the Inner Cone—*(i)  $\text{CH}_4 + 1.3 [\text{O}_2 + 3.76\text{N}_2]$ , (ii)  $\text{C}_2\text{H}_4 + 2.0 [\text{O}_2 + 3.76\text{N}_2]$ .

Interconal gases—	(i)	(ii)
$\text{CO}_2$	8.5	4.9
$\text{O}_2$	0.6	0.2
$\text{CO}$	12.9	15.1
$\text{C}_n\text{H}_n$	0.0	0.3
$\text{H}_2$	11.5	9.5
$\text{N}_2$	66.3	70.0

These show that in each case combustion had been about two-thirds completed in the inner cone, and that secondary reactions, such as



were also taking place. Hence it is doubtful whether any evidence derived from the spectra of such inner conal flames can have much relevance in regard to the primary combustion processes.

Previous investigations\* have, however, established the presence, in such inner conal flame spectra, of

- (i) OH-bands at 2608 Å, 2811 Å, 3064 Å
- (ii) CH-bands at 3143 Å, 3900 Å, 4300 Å
- (iii)  $\text{C}_2$ -bands at 4737 Å, 5165 Å, 5635 Å

Vaidya† has also identified a band system, extending from 4100 Å to 2500 Å, which he designated as the "ethylene flame"-bands and rather arbitrarily ascribed to the "CHO" group. Moreover, the characteristic banded and continuous CO radiation has usually been observed.

In view of the difficulty of drawing definite conclusions from such evidence, because of the lack of any relevant analytical data, it was suggested to me by Professor W. A. Bone that a more systematic spectrographic investigation of flames traversing homogeneous explosive media of progressively graded composition, accompanied by chemical analyses, might elucidate the matter. Accordingly such an investigation was undertaken in his laboratory and the present paper deals with the flame spectra of explosions of various methane-oxygen media. Such mixtures were exploded over a wide range of composition and initial pressures, and

\* Laurer, 'Z. Phys.', vol. 82, p. 178 (1933), Bonhoeffer and Haber, 'Z. phys. Chem.', A, vol. 137, p. 243 (1928).

† 'Proc. Roy. Soc.', A, vol. 147, p. 513 (1934).

detailed analytical and spectrographic observations were made. It soon became evident that the analytical data could best be explained on the supposition of methyl alcohol being the initial explosion product and, as will be shown later, both methyl alcohol and formaldehyde were actually isolated from the explosion products when oxygen was in considerable defect.

Finally, the scope of the investigation was extended to continuous flames of methane, methyl alcohol, and formaldehyde burning under widely varying conditions of pressure and mixture composition.

### 1—SPECTROGRAPHIC INVESTIGATIONS OF METHANE-OXYGEN EXPLOSION FLAMES

A graded series of methane-oxygen mixtures was exploded in a cylindrical steel explosion vessel, fitted at each end with quartz windows, and spectrograms of the radiation were obtained. Simultaneously, also, pressure measurements and analyses of the initial mixture and the final gaseous products were made, and from the resulting data, carbon-hydrogen-oxygen balances were drawn up. In every case the resulting analytical data (Tables I, II, III) were practically identical with those of D. T. A. Townend,\* who had already investigated chemically the combustion of such mixtures. It should be noted that over the  $\text{CH}_4 + \text{O}_2$

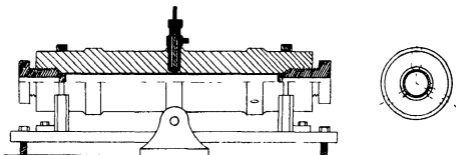


FIG. 1.

to  $2\text{CH}_4 + \text{O}_2$  mixture-composition range the proportion of the total hydrogen appearing as water in the final products passed through a well-defined minimum at about the  $3\text{CH}_4 + 2\text{O}_2$  point, and with any particular mixture was a maximum at the lowest initial pressure and reached a minimum at some definite higher pressure.

(a) *The Explosion Vessel*—A cylindrical explosion vessel (fig 1), 1 metre long and external diameter 20 cm, closed at each end, was employed.

\* 'Proc. Roy. Soc.,' A, vol. 116, p. 640 (1927).

TABLE I—CH<sub>4</sub>-O<sub>2</sub> EXPLOSIONS AT P<sub>i</sub> = 6 ATM

Approximate mixture	CH <sub>4</sub> + O <sub>2</sub>		4CH <sub>4</sub> + 3O <sub>2</sub>		3CH <sub>4</sub> + 2O <sub>2</sub>		2CH <sub>4</sub> + O <sub>2</sub>	
	P <sub>i</sub> (atm)	P <sub>f</sub> /P <sub>i</sub>	P <sub>i</sub> (atm)	P <sub>f</sub> /P <sub>i</sub>	P <sub>i</sub> (atm)	P <sub>f</sub> /P <sub>i</sub>	P <sub>i</sub> (atm)	P <sub>f</sub> /P <sub>i</sub>
*Original mixture—	CH <sub>4</sub>	50.0	56.6	59.2	6.03	66.0	6.07	
	O <sub>2</sub>	50.0	43.4	40.8	8.61	34.0	6.60	
*Gaseous products—	CO <sub>2</sub>	5.8	3.3	2.8	0.1	3.5	0.1	
	O <sub>2</sub>	1.8	0.1	0.1	34.2	24.1	24.1	
	CO	40.4	35.6	61.4	56.6	56.6	56.6	
	H <sub>2</sub>	49.9	60.5	1.5	15.7	15.7	15.7	
	CH <sub>4</sub>	2.0	0.5					
Units in—	C	50.0	56.6	59.2	66.0	66.0	66.0	
	H <sub>2</sub>	100.0	113.2	118.4	132.0	132.0	132.0	
Original mixture	O <sub>2</sub>	50.0	43.4	40.8	34.0	34.0	34.0	
	C	50.2	56.6	54.9	47.1	47.1	47.1	
Gaseous products	O <sub>2</sub>	29.0	29.8	27.7	17.0	17.0	17.0	
	C	—	—	—	—	—	—	
Difference	H <sub>2</sub>	43.8	26.4	26.5	36.3	36.3	36.3	
	O <sub>2</sub>	21.0	13.6	13.1	18.9	18.9	18.9	
Per cent.	C	—	—	7.3	28.7	28.7	28.7	
	O <sub>2</sub>	43.8	23.3	22.4	27.5	27.5	27.5	

\* N<sub>2</sub> free

TABLE II— $4\text{CH}_4 + 3\text{O}_2$  EXPLOSIONS

Approximate mixture	$\text{CH}_4 + \text{O}_2$	$4\text{CH}_4 + 3\text{O}_2$	$3\text{CH}_4 + 2\text{O}_2$	$2\text{CH}_4 + \text{O}_2$
Pi (atm)	1 00	6 01	11 00	20 01
Pf (atm)	1 35	8 46	15 90	29 09
Pf/Pi	1 35	1 41	1 45	1 46
*Original mixture—				
CH <sub>4</sub>	56 1	56 6	56 7	56 6
O <sub>2</sub>	43 9	43 4	43 3	43 4
*Gaseous products—				
CO <sub>2</sub>	3 1	3 3	3 5	4 0
O <sub>2</sub>	0 5	0 1	0 4	0 5
CO	36 9	35 6	35 4	34 6
H <sub>2</sub>	58 3	60 5	60 5	59 5
CH <sub>4</sub>	1 2	0 5	0 2	1 4
Units in—				
Original mixture	C H <sub>2</sub> O <sub>2</sub>	C H <sub>2</sub> O <sub>2</sub>	C H <sub>2</sub> O <sub>2</sub>	C H <sub>2</sub> O <sub>2</sub>
Gaseous products	56 1 112 2 43 9 55 8 82 1 29 9	56 6 113 2 43 4 56 6 86 8 29 8	56 7 113 4 43 3 56 7 88 4 31 4	56 6 113 2 43 3 57 0 91 0 31 8
Difference	— 30 1 14 0	— 26 4 13 6	— 25 0 11 9	— 22 2 11 5
Per cent	— 29 4 31 9	— 23 3 31 4	— 21 8 27 5	— 19 6 26 5
Ratio $\frac{\text{CO} \times \text{OH}_2}{\text{CO}_2 \times \text{H}_2}$ in products	4 5	3 3	2 9	2 2

\* N<sub>2</sub>-free

TABLE III— $3\text{CH}_4 + 2\text{O}_2$  EXPLOSIONS

Approximate mixture	$\text{CH}_4 + \text{O}_2$	$4\text{CH}_4 + 3\text{O}_2$	$3\text{CH}_4 + 2\text{O}_2$	$2\text{CH}_4 + \text{O}_2$
Pi (atm)	6.03	10.02	25.00	50.10
Pf (atm)	8.61	14.50	36.30	67.20
Pf/Pi	1.43	1.45	1.45	1.34
*Original mixture—				
CH <sub>4</sub>	59.2	59.3	58.8	58.8
O <sub>2</sub>	40.8	40.7	41.2	41.2
*Gaseous products—				
CO <sub>2</sub>	2.8	2.9	3.3	5.6
O <sub>2</sub>	0.1	0.1	0.1	0.4
CO	34.2	33.9	34.0	32.2
H <sub>2</sub>	61.4	61.3	60.6	55.7
CH <sub>4</sub>	1.5	1.8	2.0	6.1
Units in—				
Original mixture	C	C	C	C
Gaseous products	H <sub>2</sub>	H <sub>2</sub>	H <sub>2</sub>	H <sub>2</sub>
	O <sub>2</sub>	O <sub>2</sub>	O <sub>2</sub>	O <sub>2</sub>
Difference	59.2	59.3	58.8	58.8
	118.4	118.6	117.6	117.6
	40.8	40.7	41.2	41.2
	54.9	56.0	57.1	58.8
	91.9	94.2	93.9	91.2
	13.2	11.9	11.7	11.6
	26.5	24.4	23.7	26.4
	7.3	5.6	2.9	—
Per cent	3.7	3.2	2.8	2.0
Ratio $\frac{\text{CO} \times \text{OH}_2}{\text{CO}_2 \times \text{H}_2}$ in products				

\*N<sub>2</sub>-free

The explosion chamber, 75 cm. long and 5 cm. internal diameter, was fitted with a highly polished, stainless steel lining which remained perfectly clean throughout the experiments. Its length could be reduced by inserting a tightly fitting stainless steel plug of variable length. Along the chamber were three side openings, one in the middle and the others about 10 cm. from each end. An ignition plug, a blank plug, or a filling valve could be screwed into any of these according to experimental requirements.

The windows, made from perfectly clear natural quartz, were 2.5 cm. thick, and 1.25 or 2.5 cm. in diameter. Each was ground with a slight taper and then lapped into a similarly tapered end plug where it was held in place by a steel retaining ring. It was found that although such windows would withstand explosion pressures of 500 atm. without fracture or leakage, provided the pressure rise was comparatively slow, in more violent explosions they were liable to develop surface cracks at much lower pressures.

The explosive media were ignited by the fusion of a platinum wire, so arranged that the flame travelled towards the slit of the spectrograph. A Hilger "E2" quartz spectrograph, having a dispersion of 20 Å per mm. at 3110 Å, was used throughout the experiments. The slit of the instrument was placed some distance from the end plug, and a quartz lens was used to focus the radiation on to the slit. For reference purposes an iron arc spectrum was superimposed on each plate.

(b) *Procedure*—To avoid disturbing the alignment of the apparatus, the gaseous mixtures were not made up in the explosion chamber itself but to a predetermined pressure in another vessel, which could be rotated so as to ensure good mixing, and they were afterwards admitted to the evacuated explosion chamber as required. The usual filling system of valves and gauges was employed, the gases being passed from storage cylinders through tubes of redistilled phosphorus pentoxide. Between each two successive explosions the bomb was dismantled and dried out and its windows cleaned and dried, after which it was evacuated in readiness for the next explosion.

Ilford "Monarch" and "Special Rapid Panchromatic" plates were used, and owing to the low intensity of the radiation from such explosions it was necessary to carry out many successive experiments with each medium before a good photo-spectrogram could be obtained.

(c) *Results*—(1) Since the investigation has been largely concerned with the role of hydroxyl radicals in flame reactions, it was necessary first of all to determine the sensitivity of the apparatus and method em-

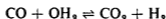
ployed with regard to the hydroxyl radiation. For this purpose a series of explosions were made with hydrogen-oxygen and carbonic oxide-hydrogen-oxygen mixtures at an initial pressure of 5 atm. and under conditions identical with those of the subsequent methane-oxygen explosions. The results showed that the combustion of approximately 4 litres of hydrogen was needed to ensure the obtaining of a distinct photographic record of the 3064 Å OH-bands in the resulting spectrograms.

*Explosions of a CH<sub>4</sub> + O<sub>2</sub> Mixture at Varying Initial Pressures*  
(Plate 20)

An equimolecular CH<sub>4</sub> + O<sub>2</sub> mixture was exploded at initial pressures between 1 and 6 atm., in some cases as many as 30 explosions were made in which 50 litres of mixture were burned. It was found impracticable to work at higher pressures because the quartz windows developed surface cracks. In all cases approximately the same quantity of methane was burned; but, as will be shown later, small adjustments were made to ensure that under all conditions the same quantity of water survived in the gaseous products. The resultant products corresponded with the empirical equation



with subsequent adjustment of the equilibrium



during the cooling period.

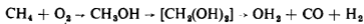
The resulting spectrograms (Plate 20, *a* to *d* inclusive) comprised a continuous radiation extending from about 5000 Å to 2300 Å on which were superimposed OH-bands at 2811 Å and 3064 Å. Neither CH-bands, nor C<sub>2</sub>-bands, nor yet any so-called "ethylene flame"-bands were visible. It was found impossible entirely to eliminate iron lines from the spectrograms.

As the initial explosion pressure was increased the intensities of the OH-bands rapidly diminished. Thus when 8 litres of methane were burned at an initial pressure of 1 atm., both the 2811 Å. and 3064 Å. band systems were present, but at an initial pressure of 6 atm. neither was visible. Even when 23 litres of methane were burned at the latter pressure the 3064 Å. bands only were visible and even these very faintly.

The analytical data showed that the percentage of the total hydrogen appearing as water in the final products steadily diminished as the initial

pressure was raised. Hence for the survival of the same quantity of water in all the experiments increasing amounts of methane had to be burned as the initial explosion pressure was raised.

Reference to the sensitivity tests and also to later experimental data showed that at the same initial pressures the OH-band intensities were much less in the case of a  $\text{CH}_4 + \text{O}_2$  explosion than in either a  $\text{H}_2 - \text{O}_2$  or a  $\text{CO} - \text{H}_2 - \text{O}_2$  explosion in which the same amount of water was produced and a lower maximum flame temperature developed. Such a result is consistent with the view that in the combustion of a  $\text{CH}_4 + \text{O}_2$  medium the  $\text{H}_2\text{O}$  is not directly formed, but only indirectly through the decomposition of intermediate oxidation products, *e.g.*,



(3) *Explosions of Mixtures Ranging in Composition from  $\text{CH}_4 + \text{O}_2$  to  $4\text{CH}_4 + 3\text{O}_2$*  (Plate 21)

Explosions of mixtures containing approximately 52, 54, and 56% of methane were next investigated. As the methane content of the medium was increased, at any given pressure, the intensities of the OH-bands diminished until, with a  $4\text{CH}_4 + 3\text{O}_2$  mixture, they were absent at all initial pressures between 1 and 20 atm. Moreover, with any given mixture the effect of increasing the initial pressure was rapidly to diminish the OH-band intensities. Such a result harmonizes with the view that the OH emitters accrue from the thermal decomposition of  $\text{CH}_3\text{OH}$  and/or  $\text{CH}_2(\text{OH})_2$ , the stabilities of which would be influenced by pressure.

(4) *Summary of Spectrographic Data for  $\text{CH}_4 + \text{O}_2 - 2\text{CH}_4 + \text{O}_2$  Media*

The spectrographic data obtained for this range of mixture composition are summarized in Table IV, the intensities given being estimated by visual examination of the negatives.

(5) *Explosion of a  $\text{CH}_4 + 8\text{O}_2$  Mixture*

A  $\text{CH}_4 + 8\text{O}_2$  mixture was exploded at varying initial pressures between 1 and 10 atm. The resulting spectrograms (Plate 20, *e* and *f*) showed, in addition to the continuous spectrum and the OH-bands already observed in the  $\text{CH}_4 + \text{O}_2$  explosions, the CO banded radiation. So large an excess of oxygen was employed in order both to mitigate the

violence of the explosion and to obtain a maximum mean flame temperature comparative with the  $\text{CH}_4 + \text{O}_2$  to  $2\text{CH}_4 + \text{O}_2$  media

TABLE IV

P <sub>i</sub> (atm)	% CH <sub>4</sub> in medium	CH <sub>4</sub> burned (litres)	H <sub>2</sub> O produced (litres)	OH-band intensities	
				3064 Å	2811 Å
1	49.2	8.0	7.7	8	3
2	49.8	9.8	9.4	5	1.5
3	49.3	10.2	9.5	4	1
5	49.7	10.8	9.4	2	0
6	49.8	10.8	9.0	0	0
6	50.6	23.0	18.9	1	0
1	52.6	11.4	9.5	2	0
3	52.2	11.0	9.3	1.5	0
5	52.1	11.0	9.9	Extremely faint	0
1	53.9	15.3	9.6	Extremely faint	0
3	53.9	16.0	9.8	0	0
1	57.1	21.1	10.5	—	Not visible at any pressure
6	57.6	28.4	10.6	—	
11	57.7	19.5	8.2	—	
20	57.6	19.1	8.4	—	

As the initial pressure was raised the intensities of the OH-bands gradually diminished (Table V), such diminution was much smaller than in any of the  $\text{CH}_4 + \text{O}_2$  to  $2\text{CH}_4 + \text{O}_2$  explosions. It should also be noted that the maximum explosion temperature was slightly lower than in the corresponding  $4\text{CH}_4 + 3\text{O}_2$  explosion in which the OH-bands were not observed.

TABLE V

P <sub>i</sub> (atm)	% CH <sub>4</sub> in medium	CH <sub>4</sub> burned (litres)	OH-band intensities 3064 Å.
1	11.7	4.5	3
6	11.9	4.5	2
10	11.8	4.5	2

A comparison of these results with those of the  $\text{CH}_4 + \text{O}_2$  series at corresponding initial pressures showed that, on burning 4.5 litres, only,

of methane as a  $\text{CH}_4 + 8\text{O}_2$  mixture, the intensities of the OH-bands were approximately twice as great as when even as much as 23.7 litres of methane were burned as a  $\text{CH}_4 + \text{O}_2$  mixture. This difference in intensity, and also the differing effect of pressure on the OH-band intensities in the  $\text{CH}_4 + \text{O}_2$  to  $2\text{CH}_4 + \text{O}_2$  and in the  $\text{CH}_4 + 8\text{O}_2$  explosions, should especially be noted, for it would seem that the OH emitters were produced differently in the two cases.

#### (6) Explosions of a $3\text{CH}_4 + 2\text{O}_2$ Mixture

Having found that carbon deposition is first observable in a  $3\text{CH}_4 + 2\text{O}_2$  explosion, a mixture containing 62.1% of methane was exploded at initial pressures up to 10 atm, 8.3% of the original carbon being deposited at the highest pressure. Also, a mixture containing 60.9% of methane was exploded at initial pressures up to 6 atm, 4.4% of the original carbon being deposited at the highest pressure.

In these experiments as much as 70 litres of methane were burned, but no OH-bands, CH-bands, or  $\text{C}_2$ -bands were ever detected. A continuous spectrum only was obtained in all cases similar to that resulting from a  $4\text{CH}_4 + 3\text{O}_2$  explosion (Plate 21, d). This continuous radiation was probably due to the separation of aggregated carbon.

### II—EXPLOSION OF METHANE-OXYGEN MEDIA WITH RAPID COOLING OF THE REACTING GASES

A successful attempt was made to isolate intermediate oxidation products transiently formed during such explosions by suddenly chilling the reacting medium at a predetermined instant during the explosion period before the attainment of maximum pressure.

The apparatus consisted (fig. 2) of an explosion chamber separated by a metal disk from a much larger expansion chamber. The explosion chamber, which was hemispherical in shape and of 2 litres capacity, was provided with three openings into which a Petavel manometer, an inlet valve, and an ignition plug could be screwed. It was separated from the expansion chamber by a metal "bursting disk" held in recesses in the bodies of the explosion and expansion chambers. These were held together by two semi-circular clamps, the joint being made gas tight by "Klingerite" washers. The expansion chamber was a cylindrical iron casting and its volume was 38.4 times that of the explosion chamber.

The experimental procedure was similar to that previously employed by Townend and Outridge.\*

The methane and oxygen were separately admitted to the explosion chamber, from storage cylinders through vessels containing redistilled phosphorus pentoxide. After mixing and adjustment of the initial pressure, the mixture was exploded and a pressure-time record, up to the time when the disk burst, taken by means of a Petavel manometer in the usual way. On the disk bursting, the reacting gases were suddenly released and cooled to room temperature in less than 0.005 sec. in the expansion chamber. After sampling the final products they were released through vessels containing water and externally cooled in ice.

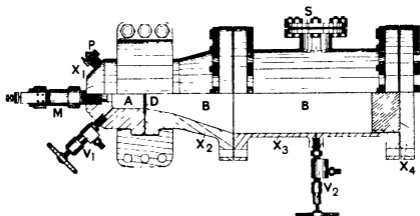


FIG. 2

*Results*—In Table VI are shown, side by side, the results of two experiments at initial pressures of 10.9 and 42.7 atm. respectively in which the disk burst at a point three- to four-fifths along the rising pressure curve, and also two control experiments in which the disk did not burst.

On examination, the washings were found to contain methyl alcohol and formaldehyde. No trace of peroxides could be detected with titanous sulphate solution. Considerable quantities of carbon were, however, deposited during the explosions, particularly at the lower pressures.

Formaldehyde was identified by its characteristic coloration with Schiff's reagent in the presence of sulphuric acid, methyl alcohol was isolated and identified by converting it into methyl 3,5-dinitro-benzoate, melting point 107.5° C.

In quantitative experiments formaldehyde was estimated colorimetrically with Schiff's reagent in the presence of sulphuric acid and, after

\* 'Proc. Roy. Soc.,' A, vol. 139, p. 74 (1933)

TABLE VI

	Disk burst			Control experiment			Disk burst			Control experiment		
	Disk burst			Disk unburst			Disk burst			Disk unburst		
$P_1$ (atm.)	10	90		10	90		42	70		42	70	
$P_{\max}$ (atm.)	92	0		98	4		32	0		39	0	
$t_b$ sec.)	0	16		0	20		0	16		0	26	
*Original mixture—												
CH <sub>4</sub>	67	6		67	1		73	0		72	5	
O <sub>2</sub>	32	4		32	9		27	0		27	5	
*Gaseous products—												
CO <sub>2</sub>	0	0		3	1		0	2		3	7	
O <sub>1</sub>	5	1		0	5		4	7		0	4	
CO	25	2		26	9		23	0		24	0	
H <sub>2</sub>	59	2		60	0		37	2		49	7	
CH <sub>4</sub>	10	5		9	5		34	9		22	2	
Units in—												
Original mixture	C	H <sub>2</sub>	O <sub>2</sub>	C	H <sub>2</sub>	O <sub>2</sub>	C	H <sub>2</sub>	O <sub>2</sub>	C	H <sub>2</sub>	O <sub>2</sub>
Gaseous products	67	6	135	67	1	134	73	0	146	72	5	145
	49	9	112	53	8	107	73	0	135	68	0	128
	—	—	—	—	—	—	—	—	—	—	—	—
Difference	17	7	23	13	3	26	—	—	10	4	5	16
	—	—	—	—	—	—	—	—	8	6	7	6
	26	2	17	19	9	19	—	—	7	6	2	11
Per cent.	—	—	—	—	—	—	—	—	4	—	—	—
Per cent. in products—												
CH <sub>3</sub> OH	0	10		Nil			0	13		Nil		
HCHO	0	02		Nil			0	03		Nil		

\* N<sub>2</sub>-free

removing the formaldehyde by distillation with aniline and phosphoric acid, the methyl alcohol was oxidized to formaldehyde which was estimated colorimetrically

The results showed that appreciable quantities of both methyl alcohol and formaldehyde were present in the reacting mixture. The percentage of these products appeared to increase with the initial pressure, and it will be seen in each case that methyl alcohol is present in the rapidly cooled products in much greater amounts than formaldehyde. Also, whereas there was very little carbon dioxide in the rapidly cooled gases, much more of it was found in the slowly cooled products, a circumstance doubtless due to the reversible water-gas reaction which in the rapidly cooled products would be frozen out at a very high temperature

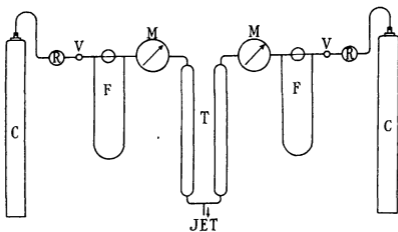


FIG. 3.

### III—SPECTROGRAPHIC INVESTIGATIONS OF STEADY FLAMES OF METHANE, METHYL ALCOHOL, AND FORMALDEHYDE

Steady flames of methane, methyl alcohol, and formaldehyde, burnt with the admixture of an oxygen-nitrogen supporter, were investigated over a wide range of mixture composition and, in the case of methane, over a wide range of pressures also

The apparatus employed at atmospheric pressure is shown diagrammatically in fig 3. The gases, stored in the cylinders C, were delivered to the system at a constant pressure of 1.5 atm. by the reducing valves R. The rates of gas flow, measured by the variable orifice flow meters F, were controlled by the valves V, and the total amount of gas flowing during any experiment measured by the meters M. The gases were

separately dried by passage over redistilled phosphorus pentoxide, contained in the tubes T, and were then mixed and passed to the silica jet J at which the flame was maintained. This jet, fig. 4, the diameter of which could be varied as required, was enclosed in a cylindrical glass tube BB fitted with quartz windows, which were electrically heated to prevent condensation. Samples of the initial mixture and gaseous products were obtained through the tubes  $T_1T_2$ . With this arrangement it was possible to maintain a flame of known composition for any length of time without any appreciable variation in the composition of the initial mixture. In taking the spectrograms, the radiation from the flame was focussed on to the slit of the spectrograph.

In experiments with methane the apparatus was used without any external heating, but in other cases this was necessary. The highly purified methyl alcohol, contained in a steel pressure vessel, was maintained at a constant vapour pressure in a thermostatically controlled bath at 100–105° C and delivered to the flow-meter system through an electrically heated reducing valve. The formaldehyde vapour was obtained from the monomeric liquid prepared according to Spence and Wilde's method\*. The whole of the flowmeter system and the silica jet itself were wound with nickel-chrome resistance wire and heated, in the case of methyl alcohol to 100° C and in the case of formaldehyde to 150° C.

In studying the flames at higher pressures, a special apparatus was designed in which any desired mixture could be burned at pressures up to 100 atm. Considerable difficulty was encountered in measuring accurately widely varying gas velocities over this pressure range, but finally a variable orifice flowmeter was designed. The latter consisted (fig. 5) of a high pressure valve O so constructed that the orifice of the valve opened linearly, the degree of opening being measured on a circular scale. The pressure drop across this orifice was measured by a manometer, consisting of an aperture S fitted with conical glass windows and

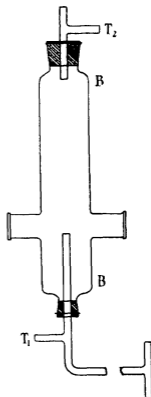


FIG. 4.

\* 'J. chem. Soc.', p 238 (1935).

connected to the liquid reservoir R. The liquid level, observed in S, was maintained constant at varying rates of gas flow by varying the degree of opening of the orifice valve. The pressure in the flowmeter system, measured on gauge  $G_1$ , was maintained at any desired value by manipulation of valve  $V_1$ , whilst the rate of gas flow was controlled by valve  $V_2$ . With this system rates of flow varying from 1 to 50 cu ft per hour may be measured at pressures varying from 1 to 100 atm.

In operating the apparatus, the gases, contained in cylinders  $CC_1$ , were passed through the flowmeter systems to the mixing chamber M.

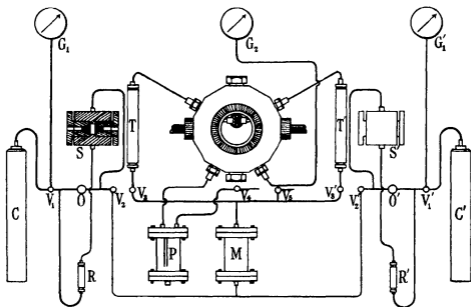


FIG 5

The gaseous mixture was drawn off through the valves  $V_3V_3^1$  and after flowing through the drying tubes  $TT^1$  containing redistilled phosphorus pentoxide was passed to the combustion chamber. This consisted (fig 6) of a cavity 4.5 inches diameter and 1 inch deep enclosed by a steel ring AA to which were bolted two end plates B and C. The ring carried the two inlet connexions D, E and two quartz window plugs F, G. Each of the cover plates also carried a window plug H, K and various outlet connexions. The burners consisted of multitubular silica jets fitted with silica washers 1 inch diameter, the flame being maintained between these disks.

The pressure in the combustion chamber, measured by gauge  $G_2$ , was controlled by regulating the flow of the gaseous products through valve

$V_4$ . The liquid products were collected in the catch pot P which was provided with a draw-off valve. The combustion chamber was also provided with a valve, through which samples of the gaseous products could be drawn off, whilst provision was made for sampling the initial mixture at valve  $V_6$ . It was necessary to heat the window plugs electrically in order to prevent condensation on the windows

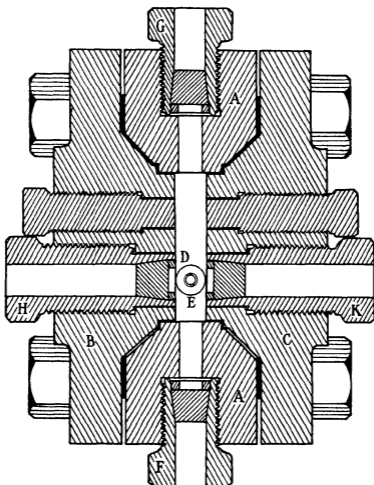


FIG. 6.

By suitable manipulation it was possible to maintain a flame of any desired composition at pressures from 1 to 100 atm., the velocity of the mixture through the jets being regulated by valves  $V_3V_5$ ,<sup>1</sup> so that the flame was maintained in the form of a vertical disk midway between the jets without touching either of them. A slightly enlarged image of this

flame was focussed on the slit of the spectrograph, so that any continuous black body radiation from the hot silica fell clear of the slit. Ilford "Zenith 650" and "Special Rapid Panchromatic" plates have been used with the Hilger E2 quartz spectrograph

*Methane-Oxygen-Nitrogen Flames at Atmospheric Pressure*

These flames have been studied over a range of mixture composition between the limits  $2\text{CH}_4 + \text{O}_2 + 2\text{N}_2$  and  $\text{CH}_4 + 2(\text{O}_2 + 2\text{N}_2)$ . In all cases the same quantity of methane was burned and the resulting spectrograms are shown in Plate 22, *a* to *d*

The spectrum of a  $\text{CH}_4 + 2.3[\text{O}_2 + 2.2\text{N}_2]$  flame (*a*) consisted of: (i) a faint continuous radiation, extending from about 5000 Å. to 2300 Å., upon which is superimposed faintly the characteristic CO banded spectrum. These features, although easily discernible in the original negatives, are scarcely visible in the reproductions, (ii) OH-bands at 2608 Å., 2811 Å., and 3064 Å., (iii) CH-bands at 3872 Å. and 4315 Å., (iv)  $\text{C}_2$ -bands at 4381 Å. and 4737 Å.; (v) a faint system of bands, scarcely visible in the reproduction, degraded to the red with successive heads at 3645, 3427, 3458, 3506, 3588, 3645, 3676, 3750, and 3824 Å.

TABLE VII

Band intensities

Mixture composition	Band intensities					
	OH		CH		$\text{C}_2$	
	2811 Å	3064 Å.	3872 Å.	4315 Å	4381 Å	4737 Å
1 $88\text{CH}_4 + \text{O}_2 + 2.2\text{N}_2$	0	very faint	0	1	0	0
1 $11\text{CH}_4 + \text{O}_2 + 2.2\text{N}_2$	0	2	very faint	2	very faint	0
$\text{CH}_4 + 1.16[\text{O}_2 + 2.2\text{N}_2]$	2	10	1	8	1	1.0
$\text{CH}_4 + 2.30[\text{O}_2 + 2.2\text{N}_2]$	2	10	1	8	2	1.5
2 $20\text{CH}_3\text{OH} + \text{O}_2 + 2.2\text{N}_2$	very faint	1	0	0	0	0
$\text{CH}_3\text{OH} + 1.20[\text{O}_2 + 2.2\text{N}_2]$	1	3	0	0.5	0	0
$\text{CH}_3\text{OH} + 1.50[\text{O}_2 + 2.2\text{N}_2]$ ..	2	6	1	1	very faint	0

These corresponded with a band system first observed by Vaidya in ethylene flames; they were designated by him the "ethylene flame"-bands, and ascribed to the CHO group, but on insufficient evidence

Variations in the composition of the initial mixture result in great changes in the intensities of these band systems (Table VII).

The intensities of all these band systems diminished as the percentage of methane in the initial mixture was increased. As might be expected,

the CO-bands were not present with mixtures containing more than the equimolecular proportion of methane. The so-called "ethylene flame"-bands appeared extremely faintly in the  $\text{CH}_4 + 2.3[\text{O}_2 + 2.2\text{N}_2]$  flame and were not at all visible in flames containing more than the equimolecular proportion of methane.

This diminution in intensity with increasing methane content, was most noticeable in the case of the  $\text{C}_2$ -bands, and to a less extent in the CH-bands and OH-bands. The great difference between the intensities of the OH-bands in the  $\text{CH}_4 + 1.16[\text{O}_2 + 2.2\text{N}_2]$  and the  $1.1\text{CH}_4 + \text{O}_2 + 2.2\text{N}_2$  flame spectrograms was especially noteworthy.

#### *Methyl Alcohol-Oxygen-Nitrogen Flames at Atmospheric Pressure*

The spectra of methyl alcohol flames were very similar to those of corresponding methane flames, and typical examples are shown in Plate 22e, f. In  $\text{CH}_3\text{OH} + 1.5[\text{O}_2 + 2.2\text{N}_2]$  flame spectra, not only were the CO banded and continuous radiations visible, but also OH-bands at 3064 Å, 2811 Å, and 2608 Å, CH-bands at 4315 Å, and 3872 Å, and  $\text{C}_2$ -bands at 4318 Å and 4737 Å, as well as the so-called "ethylene flame"-bands. A comparison with a methane-oxygen-nitrogen flame of approximately the same molecular composition burning under the same conditions showed that whereas the intensities of the OH-bands and the CH-bands were not greatly different in the two cases, the  $\text{C}_2$ -bands were relatively much fainter in the methyl alcohol flame.

As the methyl alcohol content of the media was increased the intensities of all these band systems diminished, as in the case of methane, until with the  $2.2\text{CH}_3\text{OH} + \text{O}_2 + 2.2\text{N}_2$  flame only the 2811 Å, and 3064 Å OH-bands were visible (Table VII).

#### *Formaldehyde-Oxygen-Nitrogen Flames at Atmospheric Pressure*

A typical spectrogram of a  $\text{CH}_2\text{O} + 2[\text{O}_2 + 2.2\text{N}_2]$  flame is shown in Plate 22, g. It consisted of (i) a continuous background extending from about 5000 Å to 2300 Å, upon which was superimposed the CO-banded spectrum, (ii) OH-bands at 2608 Å, 2811 Å, and 3064 Å.

Neither  $\text{C}_2$ -bands, nor CH-bands, nor yet any "ethylene flame"-bands have been detected in these flame spectra under any conditions.

The spectra of flames containing an excess of formaldehyde over the equimolecular proportion differed from those containing an excess of oxygen only in that the intensities of the OH-bands were slightly diminished.

*Methane-Air Flames at High Pressures*

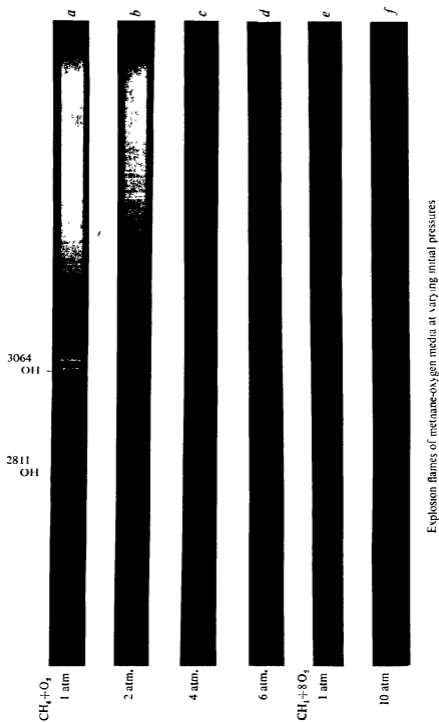
These experiments were undertaken with a view to studying the effects of pressure upon steady flames. The flames of (i)  $1 \cdot 2\text{CH}_4 + \text{O}_2 + 3 \cdot 76\text{N}_2$ , and (ii)  $\text{CH}_4 + 1 \cdot 2[\text{O}_2 + 3 \cdot 76\text{N}_2]$  mixtures were investigated at various pressures up to 30 atm, the resulting spectrograms being shown in Plate 23.

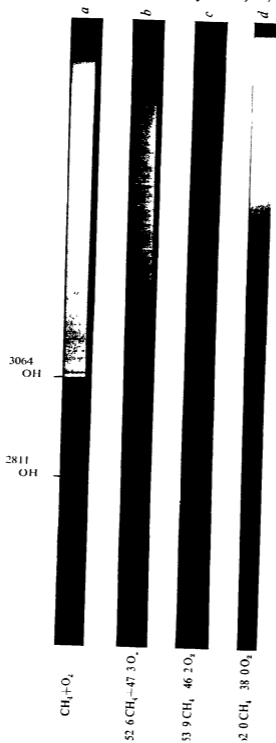
(i)—The spectrum of a  $1 \cdot 2\text{CH}_4 + \text{O}_2 + 3 \cdot 76\text{N}_2$  flame, burning at 2 atm, consisted of (a) a faint continuous background extending from 5000 Å to about 2300 Å, (b) very faintly, "ethylene flame"-bands; (c)  $\text{C}_2$ -bands at 4381 Å and 4737 Å, (d) CH-bands at 3872 Å and 4315 Å, (e) OH-bands at 2811 Å and 3064 Å.

As the pressure was increased all these band systems rapidly diminished in intensity. Thus at 5 atm the "ethylene flame"-bands were never visible, at 10 atm the  $\text{C}_2$ -bands had become very faint, at 20 atm both the  $\text{C}_2$ -bands and the CH-bands had disappeared and only the 3064 Å OH-bands remained visible. At the same time the intensity of the continuous radiation increased.

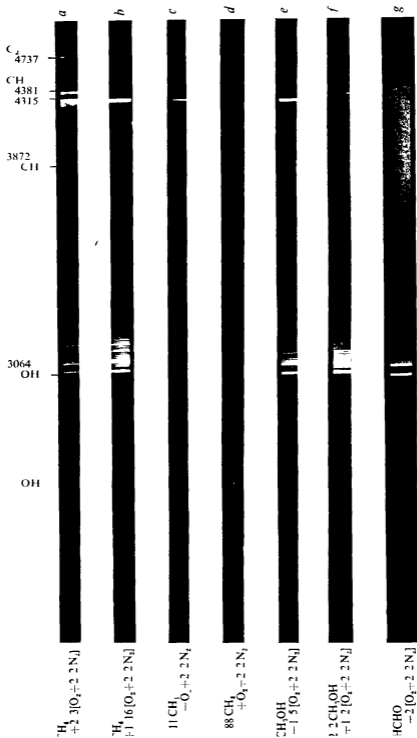
(ii)—Comparison of the  $\text{CH}_4 + 1 \cdot 2[\text{O}_2 + 3 \cdot 76\text{N}_2]$  flame with the  $1 \cdot 2\text{CH}_4 + \text{O}_2 + 3 \cdot 76\text{N}_2$  flame, at 2 atm showed that in the former case all the band systems were more intense, and in addition CO flame bands were faintly visible. In this case also the intensities of the  $\text{C}_2$ -bands and CH-bands diminished with increasing pressure until at 30 atm they were no longer visible. The intensities of the OH-bands, on the other hand, were not greatly influenced by pressure, for there was a relatively small diminution in intensity over the whole pressure range investigated. Moreover, the intensity of the CO banded and continuous spectrum was increased by this increase in pressure.

The analytical data for the  $1 \cdot 2\text{CH}_4 + \text{O}_2 + 3 \cdot 76\text{N}_2$  flames are given in Table VIII. It will be seen that approximately 50% of the carbon in the original mixture was unaccounted for in the gaseous products, and that the ratio of hydrogen to oxygen in the liquid products was approximately 4:1. At the conclusion of each experiment the apparatus was dismantled but in no case could any carbon deposition be detected. Finally it should be noted that the percentage of carbon in the liquid products increased as the pressure was raised.

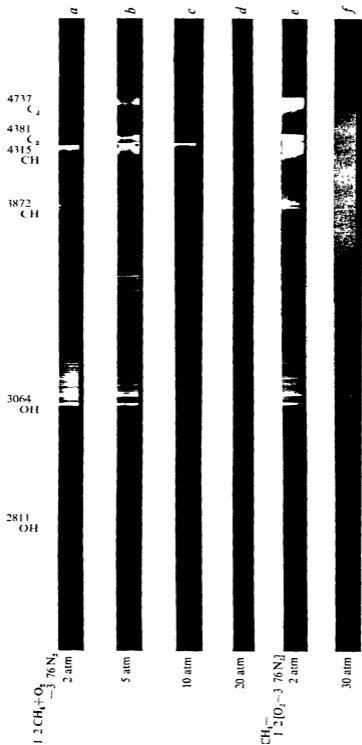




Explosion flames of methane-oxygen media at atmospheric pressure



Continuous flames burning at atmospheric pressure



Continuous flames of methane-air media burning under pressure

TABLE VIII

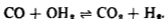
Pressure (atm )	2.0	5.0	10.0	20.0		
Original mixture—						
CH <sub>4</sub>	20.5	20.5	20.4	20.4		
O <sub>2</sub>	16.7	16.7	16.8	16.8		
N <sub>2</sub>	62.8	62.8	62.8	62.8		
Gaseous products—						
CO <sub>2</sub>	7.7	7.6	7.5	7.1		
CO	5.0	4.7	4.2	3.9		
H <sub>2</sub>	2.8	2.9	3.1	3.1		
CH <sub>4</sub>	0.6	0.5	0.4	0.5		
N <sub>2</sub>	83.9	84.3	84.8	85.4		
Units in—						
Original mixture	C	H <sub>2</sub>	O <sub>2</sub>	C	H <sub>2</sub>	O <sub>2</sub>
	20.5	41.0	16.7	20.4	40.8	16.8
Gaseous product	10.0	3.1	7.7	8.9	2.9	7.1
Difference	10.5	37.9	9.0	11.5	37.9	9.7
Per cent	51.2	92.4	53.8	56.3	92.8	57.7

## DISCUSSION

As is well known, the combustion of an equimolecular methane-oxygen mixture takes place almost entirely according to the stoichiometric equation,



although secondary reactions occur during the cooling period. Of these the most prominent is the reversible water gas reaction,



The explosion spectra obtained at initial pressures of 1 atm showed that over the composition range  $\text{CH}_4 + \text{O}_2$  to  $4\text{CH}_4 + 3\text{O}_2$  the OH radiation was emitted in considerable quantity and that its intensity was diminished by the progressive additions of methane to the explosive medium, until with the  $4\text{CH}_4 + 3\text{O}_2$  mixture it could not be detected. Moreover, with any given mixture the intensity of this radiation was rapidly diminished by increasing the initial explosion pressure. The maximum explosion temperature was, of course, rapidly diminished by the progressive addition of methane to the explosive medium, and increased, on the other hand, with the initial explosion pressure, although over the pressure range employed this increase was not great.

In explosions of media containing more oxygen than the equimolecular proportion, the combustion of the carbonic oxide and hydrogen initially formed came into play. In such cases a corresponding increase in the initial pressure resulted in very much smaller diminutions in the intensities of the OH-bands. This was also the case in the hydrogen-oxygen and carbonic oxide-hydrogen-oxygen explosions, which, under comparable conditions, always emitted OH radiation much more strongly than the equimolecular methane-oxygen explosions although they resulted in a much lower maximum explosion temperature. This evidence would seem to indicate that, although the OH radiation is emitted during both stages of the combustion, the emitters are produced in different manners during the initial and final stages.

Since it is now thought that hydroxyl radicals play a major role in the combustion of hydrogen and in the combustion of carbonic oxide-hydrogen mixtures, the absence of any marked pressure effect is readily understandable in such cases. As, however, in equimolecular methane-oxygen explosions, either a decrease in the flame temperature or an increase in the pressure eventually suppressed the formation of the OH radicals, it would seem that in such cases these radicals were mainly produced

by the thermal decomposition of some intermediate oxidation product, although to a minor extent they might arise from the thermal decomposition of water

Considering now the analytical data, the following results of explosions of media varying in composition between  $5\text{CH}_4 + 2\text{O}_2$  and  $\text{CH}_4 + \text{O}_2$  should be noted

- (i) Large quantities of carbon were deposited in the case of mixtures containing more than 60% of methane
- (ii) Increase of the initial pressure or of the oxygen content of the medium greatly diminished, or even completely suppressed, this carbon deposition
- (iii) The proportion of the original oxygen appearing as water in the explosion products was greatest at the lowest initial pressure, decreased as the pressure was increased, and reached a minimum at some definite higher pressure

Bone and Gardner\* have recently shown that the slow combustion of methane may be accurately represented by a hydroxylation scheme. Since the final oxidation products are substantially the same in both the slow and the explosive combustion, such a scheme presumably also represents the course of the explosive combustion, which has been described by Bone as a "non-stop run" in which the intermediate products have only a transient existence. Thermal decompositions, both of the original methane and of the intermediate products, are, of course, much more likely in the explosive combustion than in the slow combustion.

According to this scheme, methyl alcohol is the initial oxidation product under all conditions. Criticisms† of this view have been advanced in which it is contended that formaldehyde is usually the initial oxidation product and that the primary production of methyl alcohol is to be regarded as a limiting condition at high pressures. Bone and Gardner, after a comparative study of the oxidation of methane, methyl alcohol, and formaldehyde, showed that methyl alcohol is undoubtedly the initial methane oxidation product, but that it is so rapidly further oxidized to formaldehyde and steam that its presence is usually so completely masked by that of the formaldehyde as to render its detection difficult except

\* *Proc. Roy. Soc., A*, vol 154, p 297 (1936).

† Norrish, *Proc. Roy. Soc., A*, vol 150, p 36 (1935).

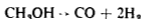
under special conditions, such as were attained by Newitt and Gardner \*

The experiments described here show that methyl alcohol and formaldehyde are successively formed, and may be isolated during the explosive combustion of methane. Moreover, the proportion of these intermediates present appears to increase with the pressure, a result which is in complete agreement with the work of Newitt and Szego †. Hence all the available experimental evidence indicates that, in the explosive combustion of methane, methyl alcohol is the initial oxidation product. This primary reaction is rapidly succeeded, not only by further hydroxylation stages, but also by thermal decompositions.

According to Bone and Davies‡ the thermal decomposition of methyl alcohol may be representable at low temperatures by the equation



and at high temperatures by the equation



Hence it might be expected that as the proportion of oxygen in the explosive media was progressively diminished, with consequent diminution of the maximum explosion temperature, the percentage of the total oxygen appearing as water in the final products would first of all decrease and, after reaching a minimum, begin to increase on account of low temperature decomposition of the primarily formed alcohol beginning to predominate. Actually the water formation was found to be a minimum with a mixture approximating to the composition  $3\text{CH}_4 + 2\text{O}_2$ .

Again, it might be anticipated that, as the decomposition of the unburned methane would be partially suppressed at the higher explosion pressures, and also as the methyl alcohol decomposition into carbonic oxide and hydrogen would predominate at these high temperatures, increase of pressure would result in diminished carbon deposition, which was, in fact, actually observed. Thus all the evidence, spectrographic and otherwise, obtained from these explosions indicates that the reaction may be represented as a series of hydroxylation stages accompanied by thermal decompositions. Supporting evidence is afforded by the pressure flame results, for the carbon-hydrogen-oxygen balances drawn up for such experiments indicate that a large proportion of the original carbon

\* 'Proc Roy Soc,' A, vol 154, p 329 (1936)

† 'Proc Roy Soc,' A, vol 147, p 555 (1934)

‡ 'J Chem Soc,' vol 105, p 1691 (1914)

survived in the liquid products, and it is significant that this proportion increased with the pressure

In considering the spectrographic evidence derived from the continuous flames, it should be noted that whereas their spectra contained the CH-bands, the  $C_2$ -bands, and the so-called "ethylene flame"-bands, none of these was ever detected in the explosion spectra, although the main course of the combustion is undoubtedly the same in both cases. The intensities of these bands varied with the flame temperature. They were all most intense in flames containing an excess of oxygen over the equimolecular proportion, and rapidly diminished in intensity as the flame temperature was progressively reduced by the addition of methane to the initial mixture. Moreover, they were diminished in intensity, and were finally suppressed, as the pressure was raised. This would appear to indicate that the band emitters arose from some thermal decomposition of intermediate oxidation products, which would be gradually suppressed by either increasing pressure or decreasing temperature. The conditions in these steady flames are such as would be more likely to give rise to thermal decompositions than those prevailing in the corresponding explosion flames.

The origins of the  $C_2$ -bands and the CH-bands are well known, but in the case of the so-called "ethylene flame"-bands they are extremely doubtful. Vaidya has arbitrarily ascribed them to the CHO group, but from the present evidence they may be more reasonably ascribed to the  $CH_2$  group, particularly as they are always associated with a strong CH emission.

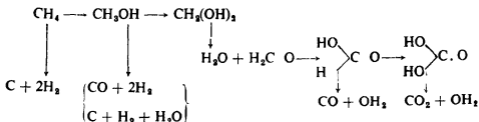
The CH-bands and the  $C_2$ -bands were present in the methane and methyl alcohol but not in the formaldehyde flame spectra. Since the analytical data indicate that there must be an appreciable concentration of methyl alcohol in the methane flame, it is not unreasonable to assume that the band emitters are produced by the low temperature decomposition of the methyl alcohol, according to the equation



These spectrographic results also showed that the intensities of the OH bands were greater in the  $CH_4 + 1/2 [O_2 + 3/76 N_2]$  than in the  $1/2 CH_4 + O_2 + 3/76 N_2$  flame spectra. Moreover, these intensities were diminished, either by diminishing the flame temperature or by increasing the pressure, thus confirming the evidence adduced from the explosion experiments.

As a whole, therefore, the results of this investigation support the view

that, apart from secondary reactions during the cooling period, the explosive combustion of methane may be represented by the scheme.—



which, apart from the thermal decompositions of methane and methyl alcohol, also represents the course of the slow combustion

In conclusion, my best thanks are due to Professor W A Bone, at whose suggestion and in whose laboratories this investigation has been carried out, for his constant guidance and advice

#### SUMMARY

Detailed analytical and spectrographic investigations of explosion flames of homogeneous methane-oxygen media, burning under widely varying conditions of pressure and mixture composition, have been made. It has been shown that in the combustion of an equimolecular methane-oxygen mixture to water, carbonic oxide, and hydrogen, this water is produced by the thermal decomposition of intermediate oxidation products and not directly by the combustion of hydrogen. Moreover, by rapid cooling of the reacting media both methyl alcohol and formaldehyde have been isolated from these explosions.

The steady flames of methane, methyl alcohol, and formaldehyde have been investigated spectrographically over a wide range of mixture composition and, in the case of methane, over a wide range of pressure also. The various band systems present in these spectra, the intensities of which varied both with the mixture composition and the pressure, have been shown to arise by thermal decompositions of intermediate oxidation products.

The results, as a whole, have shown that the explosive combustion of methane may be represented by a hydroxylation scheme, which, apart from thermal decompositions, is identical with that representing the course of the slow combustion

## The Spectrum of Trebly-Ionized Lead, Pb IV

By M F CRAWFORD, A. B. McLAY,\* and A M CROOKER,† McLennan Laboratory, University of Toronto

(Communicated by O W Richardson, F R S—Received 30 July, 1936)

Carroll,‡ Smith,§ Rao and Narayan|| and Schoepfle¶ have established terms of the one-electron configurations of Pb IV. Schoepfle, whose analysis is the most complete, has identified the  $6s$ ,  $7s$ ,  $8s$ ,  $6p$ ,  $7p$ ,  $6d$ ,  $7d$ ,  $5f$  doublets, and in addition assigned a number of terms to the many-electron configurations that have as limit the  $5d^9 6s$  configuration of Pb V.

The Au I *iso-electronic* sequence, especially the configurations involving the  $5d^9$  core, has been under investigation in this laboratory for some time. The analysis of Au I\*\* and of Hg II†† have been published and that of Pb IV is presented here. The investigation of Tl III is practically completed and will be published soon, Bi V is partially analysed. The state of our work on Tl III and Bi V is mentioned here because certain terms of these spectra and the corresponding terms of Pb IV have been established mainly by the regularity of the Moseley curves for these terms throughout the sequence Au I to Bi V. Thus the analysis of one spectrum has been facilitated and confirmed by a knowledge of the others. It is certain that some of the terms of Pb IV would not have been found except by such a method.

The experimental data were obtained by photographing the spectrum from 400 Å. to 9000 Å. A three-metre, normal incidence, vacuum grating was used for the region below 2100 Å. The region from 1350 Å. to 2200 Å. was also investigated with a fluorite and a small quartz spectrograph to record the faint lines and to segregate the first and second order lines observed on the grating spectrograms. Hilger quartz and glass E<sup>1</sup>

\* Associate Professor of Physics, McMaster University, Hamilton, Ontario, Canada

† Holder of Fellowship awarded by National Research Council of Canada in 1934-35, and 1851 Exhibition Scholar at King's College, University of London, in 1935-36

‡ 'Phil. Trans.', A, vol. 225, p. 357 (1926)

§ 'Phys. Rev.', vol. 36, p. 1 (1930)

|| 'Z. Physik', vol. 61, p. 149 (1930)

¶ 'Phys. Rev.', vol. 47, p. 232 (1935)

\*\* McLennan and McLay, 'Proc. Roy. Soc.', A, vol. 134, p. 35 (1932)

†† McLennan, McLay, and Crawford, 'Proc. Roy. Soc.', A, vol. 134, p. 41 (1932).

spectrographs were used for the region 2100 Å–8000 Å, supplemented with a constant deviation spectrograph for the region 6000 Å–9000 Å. The spectrum was also photographed from 2100 Å–6600 Å with a 21-foot concave grating focussed to record the  $n\lambda$  region 12,700 Å–21,000 Å, where  $n$  is the order, in one exposure.

The lines were excited by an electrodeless discharge in Pb vapour. The source was similar to that used in the investigation of Bi.\* Over the entire region series of spectrograms were taken for different excitation conditions in the source. The variation of intensity of a line with excitation usually showed quite definitely to which spectrum of Pb it belonged.

The more intense lines in the region 2100 Å–6600 Å appeared on the 21-foot grating spectrograms and were measured relative to Fe standards. These wave-lengths, which are marked with an asterisk in Table II, are accurate to within 0.01 Å. The other lines above 2100 Å were measured on the prism spectrograms relative to Fe, Cu, and Ne standards. These wave-lengths, except for the very faint lines, are estimated to be accurate to within 0.05 Å. The wave-lengths measured on the 21-foot grating plates served as internal standards to check the precision of the wave-lengths determined from the prism spectrograms. The wave-lengths below 2100 Å were measured on the vacuum grating spectrograms relative to C, O, N lines which appeared as impurities. Our measurements below 1440 Å checked in both the first and second orders to within a few one-hundredths of an Angstrom with Arvidsson's †. In view of this, Arvidsson's values have been used for the region below 1440 Å. The intensities were determined by visual inspection of the spectrograms; on account of the range of the spectrum and the variety of instruments used, they can be considered only as rough estimates.

Our data on the excitation characteristics of the lines below 1440 Å, in general, are in agreement with Arvidsson's. A few of the fainter lines assigned to Class 5 by Arvidsson are relatively more intense on our plates. Our highest excitation corresponded to Arvidsson's Class 5, the lines of Class 6 were not excited.

All the terms of Pb IV that were identified by others and confirmed by us and those established for the first time in this investigation are listed in Table I. The term values are relative to the most stable term,  $6s^2S_1$ , which is assigned the value zero. The wave-lengths of the lines by which the terms were established are listed with their intensities, wave-numbers, and classifications in Table II.

\* Crawford and McLay, 'Proc. Roy. Soc., A', vol. 143, p. 540 (1934).

† 'Ann. Physik,' vol. 12, p. 787 (1932).

The simple doublet notation has been retained for all one-electron terms that are in isolated energy positions, and which are therefore comparatively free from perturbation by terms of the complex configurations. Of these doublet terms  $5g\ ^2G$  and the three  $^2H^0$  are new, the others were reported by previous investigators\*. The  $5g$  doublet separation is resolved in the  $^2G - ^2H^0$  transitions and the relative intensities of the components show that  $5g\ ^2G$  is inverted. The  $^2H^0$  intervals are not resolved.

TABLE I—TERMS OF Pb IV

Configuration	Term	Value cm <sup>-1</sup>	Configuration	Term	Value cm <sup>-1</sup>
6s	$^1S_0$	0		$14_{\frac{1}{2}}^0$	208524 0
6p	$^3P_1^0$	76158		$15_{\frac{1}{2}}^0$	209051 1
6p	$^1P_1^0$	97219	$5d^9_{\frac{1}{2}}6s_16p_{1\frac{1}{2}}$	$16_{\frac{1}{2}}^0$	209788 4
$5d^9_{\frac{1}{2}}6s^2$	$1_{\frac{1}{2}}^0$	101252	and	$17_{\frac{1}{2}}^0$	210369 7
$5d^9_{\frac{1}{2}}6s^2$	$2_{\frac{1}{2}}^0$	122568	$5d^9_{\frac{1}{2}}6s_16p_{\frac{1}{2}}$	$18_{\frac{1}{2}}^0$	213519 2
$5d^9_{\frac{1}{2}}6s_16p_{\frac{1}{2}}$	$1_{\frac{1}{2}}^0$	166369	and	$19_{\frac{1}{2}}^0$	214842 1
	$2_{\frac{1}{2}}^0$	172667	$5d^9_{\frac{1}{2}}6s_16p_{1\frac{1}{2}}$	$20_{\frac{1}{2}}^0$	214891 8
	$3_{\frac{1}{2}}^0$	173248	and	$21_{\frac{1}{2}}^0$	217216
	$4_{\frac{1}{2}}^0$	175388	7p	$22_{\frac{1}{2}}^0$	217851 9
6d	$^3D_{1\frac{1}{2}}$	184558 8	and	$23_{\frac{1}{2}}^0$	219461 0
7s	$^1S_0$	185103 0	5f	$24_{\frac{1}{2}}^0$	221716 1
6d	$^1D_{1\frac{1}{2}}$	186816 8		$25_{\frac{1}{2}}^0$	231013
	$5_{\frac{1}{2}}^0$	188759		$26_{\frac{1}{2}}^0$	232638
	$6_{\frac{1}{2}}^0$	*		$27_{\frac{1}{2}}^0$	235565†
	$7_{\frac{1}{2}}^0$	193776	8s	$^1S_0$	249634 5
$5d^9_{\frac{1}{2}}6s_16p_{1\frac{1}{2}}$	$8_{\frac{1}{2}}^0$	193855†	7d	$^1D_{1\frac{1}{2}}$	250401 6
and	$9_{\frac{1}{2}}^0$	193954	7d	$^3D_{1\frac{1}{2}}$	251419 5
$5d^9_{\frac{1}{2}}6s_16p_{\frac{1}{2}}$	$10_{\frac{1}{2}}^0$	194147	5g	$^1G_{\frac{1}{2}}$	270496
	$11_{\frac{1}{2}}^0$	197024	5g	$^3G_{\frac{1}{2}}$	270498
	$12_{\frac{1}{2}}^0$	200021	6h	$^1H^0$	292543
	$13_{\frac{1}{2}}^0$	201460	7h	$^1H^0$	305516
$5d^{10}$ of Pb V	$^1S_0$	341350‡	8h	$^1H^0$	313939

\* Predicted by extrapolation from Au I, Hg II

† Not too well established by term combinations, but position fits Moseley curve of Au I, Hg II, and Tl III

‡ Value obtained by assuming  $nh\ ^2H^0$  hydrogenic

The odd terms designated  $1^0$  to  $5^0$  and  $7^0$  to  $27^0$  include the two  $7p$  levels, the two  $5f$  levels, and twenty-two of the twenty-three levels predicted for  $5d^96s6p$ . As there undoubtedly are large perturbations between the terms arising from these overlapping odd configurations, the individual terms

\* Carrol, 'Phil. Trans.', A, vol. 225, p. 357 (1926), Smith, S., 'Phys. Rev.', vol. 36, p. 1 (1930), Rao and Narayan, 'Z. Physik', vol. 61, p. 149 (1930), Schoepfle, 'Phys. Rev.', vol. 47, p. 232 (1935)

TABLE II—CLASSIFIED WAVE-LENGTHS OF Pb IV

Intensity	$\lambda$ (Å)	$\nu$ cm <sup>-1</sup>	Classification
1	8749.7	11426	$4i_1^0$ — $6d^1D_{3/2}$
3	6111.95	16356.9	$7s^1S_0$ — $13i_1^0$
5	5915.11	16901.2	$6d^1D_{3/2}$ — $13i_1^0$
4	5627.69	17764.3	$26s_1^0$ — $7d^1D_{3/2}$
2	5156.13	19389.2	$25i_1^0$ — $7d^1D_{3/2}$
8	4605.54*	21706.9	]- $6d^1D_{3/2}$ — $14s_1^0$
16	05.43	21707.4	
10	4534.93*	22044.9	$5g^1G_{3/2}$ — $6h^1H^0$
15	4534.46*	22047.2	$5g^1G_{3/2}$ — $6h^1H^0$
8	4496.34*	22234.1	]- $6d^1D_{3/2}$ — $15i_1^0$
16	96.25	22234.5	
7	4174.56*	23947.9	]- $7s^1S_0$ — $15i_1^0$
13	74.49	23948.3	
8	4081.8	24493	$6d^1D_{3/2}$ — $15i_1^0$
30	4049.84*	24685.4	$7s^1S_0$ — $16i_1^0$
20	3962.49	25229.5	$6d^1D_{3/2}$ — $16i_1^0$
2	3956.66	25266.7	$7s^1S_0$ — $17i_1^0$
4	3943.88*	25348.6	]- $6p^1P_{3/2}^0$ — $2i_1$
8	43.71	25349.7	
5	3873.25	25810.8	$6d^1D_{3/2}$ — $17i_1^0$
2	3567.23*	28025.0	]- $6d^1D_{3/2}$ — $19i_1^0$
4	67.16	28025.5	
6	3560.91*	28074.7	]- $6d^1D_{3/2}$ — $20s_1^0$
9	60.85	28075.2	
1	3452.04*	28960.1	]- $6d^1D_{3/2}$ — $18s_1^0$
2	51.97	28960.7	
6	3365.64*	29703.5	$24s_1^0$ — $7d^1D_{3/2}$
4	3361.60*	29739.2	$7s^1S_0$ — $19i_1^0$
2	3301.2	30283.4	$6d^1D_{3/2}$ — $19i_1^0$
1	3288.6	30399	$6d^1D_{3/2}$ — $21i_1^0$
10	3231.06*	30940.7	$23i_1^0$ — $7d^1D_{3/2}$
40	3221.22*	31035.2	$6d^1D_{3/2}$ — $22i_1^0$
8	3145.47*	31782.6	$22i_1^0$ — $8s^1S_0$
3	3128.1	31959	$23s_1^0$ — $7d^1D_{3/2}$
8	3071.33*	32549.7	$22i_1^0$ — $7d^1D_{3/2}$
10	3062.43*	32644.3	$6d^1D_{3/2}$ — $23i_1^0$
3	3061.27	32656.7	$6d^1D_{3/2}$ — $21i_1^0$
30	3052.66*	32748.8	$7s^1S_0$ — $22i_1^0$
15	3002.76*	33293.0	$6d^1D_{3/2}$ — $22i_1^0$
25	2978.20*	33567.6	$22i_1^0$ — $7d^1D_{3/2}$
10	2873.32*	34792.8	$19i_1^0$ — $8s^1S_0$ (a)
20	2864.55*	34899.3	$6d^1D_{3/2}$ — $24s_1^0$
20	2864.31*	34902.2	$6d^1D_{3/2}$ — $23s_1^0$
3	2854.86	35017.8	$5g^1G_{3/2}$ — $7h^1H^0$
4	2854.66	35020.2	$5g^1G_{3/2}$ — $7h^1H^0$

TABLE II—continued

Intensity	$\lambda$ (Å)	$\nu$ cm <sup>-1</sup>	Classification
3	2811 36	35559 5	19 <sub>11</sub> <sup>0</sup> — 7d <sup>3</sup> D <sub>11</sub>
8	2736 9	36527	20 <sub>21</sub> <sup>0</sup> — 7d <sup>3</sup> D <sub>21</sub>
12	2733 16	36576 9	19 <sub>11</sub> <sup>0</sup> — 7d <sup>3</sup> D <sub>21</sub>
1	2710 6	36881	18 <sub>21</sub> <sup>0</sup> — 7d <sup>3</sup> D <sub>11</sub>
15	2640 5	37860	26 <sub>21</sub> <sup>0</sup> — 5g <sup>3</sup> G <sub>21</sub>
8	2637 74	37900 0	18 <sub>21</sub> <sup>0</sup> — 7d <sup>3</sup> D <sub>21</sub> (b)
4	2545 9	39267	17 <sub>1</sub> <sup>0</sup> — 8s <sup>3</sup> S <sub>1</sub>
12	2508 85	39846 9	16 <sub>1</sub> <sup>0</sup> — 8s <sup>3</sup> S <sub>1</sub>
7	2497 17	40033 2	17 <sub>1</sub> <sup>0</sup> — 7d <sup>3</sup> D <sub>11</sub>
6	2463 3	40584	15 <sub>11</sub> <sup>0</sup> — 8s <sup>3</sup> S <sub>1</sub>
20	2461 51*	40613 2	16 <sub>1</sub> <sup>0</sup> — 7d <sup>3</sup> D <sub>11</sub>
8	2417 7	41349	15 <sub>11</sub> <sup>0</sup> — 7d <sup>3</sup> D <sub>11</sub>
15	2359 55	42368 0	15 <sub>11</sub> <sup>0</sup> — 7d <sup>3</sup> D <sub>21</sub>
6	2330 45	42897 0	14 <sub>21</sub> <sup>0</sup> — 7d <sup>3</sup> D <sub>21</sub>
6	2301 38	43439 5	5g <sup>3</sup> G <sub>21</sub> — 8h <sup>3</sup> H <sup>0</sup>
8	2301 25	43441 2	5g <sup>3</sup> G <sub>41</sub> — 8h <sup>3</sup> H <sup>0</sup>
2	2282 34	43801.2	2 <sub>11</sub> — 1 <sub>21</sub> <sup>0</sup>
4	2181 71	45821	6d <sup>3</sup> D <sub>21</sub> — 26 <sub>21</sub> <sup>0</sup>
5	2177 45	45911	7s <sup>3</sup> S <sub>1</sub> — 25 <sub>1</sub> <sup>0</sup>
5	2154 06*	46409 3	]—
10	54 01	46410 4	
3	2152 00	46454	6d <sup>3</sup> D <sub>11</sub> — 25 <sub>1</sub> <sup>0</sup>
7	2079 25	48079	6d <sup>3</sup> D <sub>11</sub> — 26 <sub>21</sub> <sup>0</sup>
3	2075 20	48173	13 <sub>1</sub> <sup>0</sup> — 8s <sup>3</sup> S <sub>1</sub>
7	2049 37	48780	24 <sub>21</sub> <sup>0</sup> — 5g <sup>3</sup> G
5	2042 65	48940	13 <sub>1</sub> <sup>0</sup> — 7d <sup>3</sup> D <sub>11</sub>
(I. vac)			
1	1981 64	50463	7s <sup>3</sup> S <sub>1</sub> — 27 <sub>11</sub> <sup>0</sup>
8	1973 14	50681	2 <sub>11</sub> — 3 <sub>21</sub> <sup>0</sup>
20	1959 32	51038	23 <sub>21</sub> <sup>0</sup> — 5g <sup>3</sup> G
5	1893 22	52820	2 <sub>11</sub> — 4 <sub>11</sub> <sup>0</sup>
3	1798 44	55604	20 <sub>21</sub> <sup>0</sup> — 5g <sup>3</sup> G
0	1777 71	56252	10 <sub>1</sub> <sup>0</sup> — 7d <sup>3</sup> D <sub>11</sub>
3	1613 66	61971	14 <sub>21</sub> <sup>0</sup> — 5g <sup>3</sup> G
12	1535 70	65117	1 <sub>21</sub> — 1 <sub>21</sub> <sup>0</sup>
8	1510 76	66192	2 <sub>11</sub> — 5 <sub>11</sub> <sup>0</sup>
Arv (c)			
1	12	1404 34	2 <sub>11</sub> — 7 <sub>21</sub> <sup>0</sup>
6	15	1400 26	1 <sub>21</sub> — 2 <sub>21</sub> <sup>0</sup>
2	8	1397.03	2 <sub>11</sub> — 10 <sub>1</sub> <sup>0</sup>
5	12	1388.97	1 <sub>21</sub> — 3 <sub>21</sub> <sup>0</sup>
6	12	1348 87	1 <sub>21</sub> — 4 <sub>11</sub> <sup>0</sup>
4	10	1343 09	2 <sub>11</sub> — 11 <sub>21</sub> <sup>0</sup>

TABLE II—continued

Intensity		$\lambda$ (I vac)	$\nu$ cm <sup>-1</sup>	Classification	
Arv. (c)					
40	50	1313 06	76158	6s <sup>2</sup> S <sub>1/2</sub>	— 6p <sup>2</sup> P <sub>1/2</sub> <sup>o</sup>
2	10	1291 08	77454	2 <sub>1/2</sub>	— 12 <sub>1/2</sub> <sup>o</sup>
2	6	1267 52	78894	2 <sub>1/2</sub>	— 13 <sub>1/2</sub> <sup>o</sup>
—	2	1156 29	86483	2 <sub>1/2</sub>	— 15 <sub>1/2</sub> <sup>o</sup>
0	3	1146 45	87226	2 <sub>1/2</sub>	— 16 <sub>1/2</sub> <sup>o</sup> (d)
6	10	1144 95	87340	6p <sup>2</sup> P <sub>1/2</sub> <sup>o</sup>	— 6d <sup>2</sup> D <sub>1/2</sub>
1	3	1138 94	87801	2 <sub>1/2</sub>	— 17 <sub>1/2</sub> <sup>o</sup>
7	10	1137 86	87884	6p <sup>2</sup> P <sub>1/2</sub> <sup>o</sup>	— 7s <sup>2</sup> S <sub>1/2</sub>
7	9	1116 08	89599	6p <sup>2</sup> P <sub>1/2</sub> <sup>o</sup>	— 6d <sup>2</sup> D <sub>1/2</sub>
1	5	1099 46	90954	2 <sub>1/2</sub>	— 18 <sub>1/2</sub> <sup>o</sup>
3	9	1080 80	92524	1 <sub>1/2</sub>	— 7 <sub>1/2</sub> <sup>o</sup>
2	7	1079 88	92603	1 <sub>1/2</sub>	— 8 <sub>1/2</sub> <sup>o</sup>
0	1	1078 75	92701	1 <sub>1/2</sub>	— 9 <sub>1/2</sub> <sup>o</sup>
2	4	1056 54	94649	2 <sub>1/2</sub>	— 21 <sub>1/2</sub> <sup>o</sup>
—	1	1049 50	95283	2 <sub>1/2</sub>	— 22 <sub>1/2</sub> <sup>o</sup>
3	7	1044 14	95773	1 <sub>1/2</sub>	— 11 <sub>1/2</sub> <sup>o</sup>
3 <sup>o</sup>	6	1032 06	96894	2 <sub>1/2</sub>	— 23 <sub>1/2</sub> <sup>o</sup>
30	20	1028 61	97219	6s <sup>2</sup> S <sub>1/2</sub>	— 6p <sup>2</sup> P <sub>1/2</sub> <sup>o</sup>
3	6	1012 47	98768	1 <sub>1/2</sub>	— 12 <sub>1/2</sub> <sup>o</sup>
10	7	932 18	107275	1 <sub>1/2</sub>	— 14 <sub>1/2</sub> <sup>o</sup>
7	9	927 62	107803	1 <sub>1/2</sub>	— 15 <sub>1/2</sub> <sup>o</sup>
10	9	922 49	108402	6p <sup>2</sup> P <sub>1/2</sub> <sup>o</sup>	— 6d <sup>2</sup> D <sub>1/2</sub>
2	4	922 12	108466	2 <sub>1/2</sub>	— 25 <sub>1/2</sub> <sup>o</sup> (d)
7	6	917 89	108946	6p <sup>2</sup> P <sub>1/2</sub> <sup>o</sup>	— 7s <sup>2</sup> S <sub>1/2</sub>
6	5	908 51	110070	2 <sub>1/2</sub>	— 26 <sub>1/2</sub> <sup>o</sup>
8	8	890 72	112269	1 <sub>1/2</sub>	— 18 <sub>1/2</sub> <sup>o</sup>
6	5	884 98	112997	2 <sub>1/2</sub>	— 27 <sub>1/2</sub> <sup>o</sup>
1	5	879 98	113639	1 <sub>1/2</sub>	— 20 <sub>1/2</sub> <sup>o</sup>
6	6	862 34	115964	1 <sub>1/2</sub>	— 21 <sub>1/2</sub> <sup>o</sup>
7	5	857 65	116598	1 <sub>1/2</sub>	— 22 <sub>1/2</sub> <sup>o</sup>
3	3	845 96	118209	1 <sub>1/2</sub>	— 23 <sub>1/2</sub> <sup>o</sup>
7	8	830 11	120466	1 <sub>1/2</sub>	— 24 <sub>1/2</sub> <sup>o</sup>
2	2	656 09	152418	6p <sup>2</sup> P <sub>1/2</sub> <sup>o</sup>	— 8s <sup>2</sup> S <sub>1/2</sub>
2	2	648 50	154202	6p <sup>2</sup> P <sub>1/2</sub> <sup>o</sup>	— 7d <sup>2</sup> D <sub>1/2</sub>
2	3	584 51	173482	6p <sup>2</sup> P <sub>1/2</sub> <sup>o</sup>	— 8s <sup>2</sup> S <sub>1/2</sub>
2	2	576 43	174246	6p <sup>2</sup> P <sub>1/2</sub> <sup>o</sup>	— 7d <sup>2</sup> D <sub>1/2</sub>
6	6	570 16	175389	6s <sup>2</sup> S <sub>1/2</sub>	— 4 <sub>1/2</sub> <sup>o</sup>
4	4	529 78	188758	6s <sup>2</sup> S <sub>1/2</sub>	— 5 <sub>1/2</sub> <sup>o</sup>
1	0	515 58	193956	6s <sup>2</sup> S <sub>1/2</sub>	— 9 <sub>1/2</sub> <sup>o</sup>
5	3	515 08	194145	6s <sup>2</sup> S <sub>1/2</sub>	— 10 <sub>1/2</sub> <sup>o</sup>
9	4	499 95	200020	6s <sup>2</sup> S <sub>1/2</sub>	— 12 <sub>1/2</sub> <sup>o</sup>
8	4	496 37	201463	6s <sup>2</sup> S <sub>1/2</sub>	— 13 <sub>1/2</sub> <sup>o</sup>
8	3	478 355	209050	6s <sup>2</sup> S <sub>1/2</sub>	— 15 <sub>1/2</sub> <sup>o</sup>

TABLE II—(continued)

Intensity		$\lambda$ (I.vac.)	$\nu$ cm <sup>-1</sup>	Classification
Arv. (c)				
— 1		476 68	209784	6s <sup>4</sup> S <sub>1/2</sub> — 16 <sub>1</sub> <sup>0</sup>
7 3		475 36	210367	6s <sup>4</sup> S <sub>1/2</sub> — 17 <sub>1</sub> <sup>0</sup>
7 3		465 450	214846	6s <sup>4</sup> S <sub>1/2</sub> — 19 <sub>1</sub> <sup>0</sup>
6 2		459 04	217846	6s <sup>4</sup> S <sub>1/2</sub> — 22 <sub>1</sub> <sup>0</sup>
3 0		432 880	231011	6s <sup>4</sup> S <sub>1/2</sub> — 25 <sub>1</sub> <sup>0</sup>

\* Wave-length determined from 21-foot grating measurements

(a) Also classified in Pb I

(b) Also classified in Pb III

(c) Data from Arvidsson's, 'Ann Physik,' vol 12, p 787 (1932)

(d) Also classified as transitions between questionable terms of Pb V by Mack and Fromer, 'Phys Rev,' vol 48, p 357 (1935)

from 5<sup>0</sup> to 27<sup>0</sup> have not been uniquely assigned to configurations. The predicted term 6<sub>41</sub><sup>0</sup> has not been found, since the only established even term with which it can combine by the J rule is 5g <sup>2</sup>G. Its position between 5<sup>0</sup> and 7<sup>0</sup> is predicted by extrapolation from the known values of the corresponding terms of Au I and Hg II. The terms 16<sub>1</sub><sup>0</sup> and 22<sub>1</sub><sup>0</sup> were previously identified by Smith† and Schoepfle‡ as 7p <sup>2</sup>P<sub>1/2</sub>, and the term 24<sub>31</sub><sup>0</sup> was designated 5f <sup>3</sup>F<sub>3/2</sub> by Schoepfle. In our analysis these three terms are not segregated but grouped with the terms 5<sup>0</sup> – 27<sup>0</sup>, these twenty-three terms are assigned to the configurations 7p, 5f, 5d<sup>0</sup>6s6p, since it is doubtful if a unique assignment is significant when the terms intermingle as they do here.

Schoepfle also established three other terms 3, 9<sup>0</sup>, 10<sup>0</sup>, in his notation, which correspond to three terms 1, 15<sup>0</sup>, 17<sup>0</sup>, respectively, established by us. He gave no configuration assignment for the first level which in our analysis is one of the terms of the important 5d<sup>0</sup>6s<sup>2</sup> configuration. The second two he assigned to 5d<sup>0</sup>5s6p in agreement with our allocation, but gave J = 1½ for 10<sup>0</sup>, whereas this term, 17<sup>0</sup> in our analysis, has J = ½. In Schoepfle's analysis the value J = 1½ for 10<sup>0</sup> depends upon the correctness of the classification of  $\lambda$  4245 08 as 6d <sup>2</sup>D<sub>3/2</sub> – 10<sub>1</sub><sup>0</sup>. This line on our plates shows Pb II excitation characteristics and has been classified by Earls and Sawyer§ as a transition in Pb II. Further, the frequency of this line differs by 3 cm<sup>-1</sup> from the frequency predicted from our term values for the transition 6d <sup>2</sup>D<sub>3/2</sub> – 17<sup>0</sup>. The rejection of Schoepfle's classification of  $\lambda$  4245 08 leaves J = ½ for this term.

† 'Phys Rev,' vol 36, p 1 (1930)

‡ *Ibid*, vol 47, p 232 (1935)

§ 'Phys Rev.,' vol 47, p 115 (1935)

A number of terms reported by Scheopfle\* appear to be unreal in view of the results of this investigation; they are, in his notation:  $^3D_{11}, ^3_2$  of  $5d^96s^2$ ; 1, 2, and 4, without configuration assignment; 5 to 7 of  $5d^96s6d$ ,  $1^0$  to  $8^0$ ,  $11^0$  and  $12^0$  of  $5d^96s6p$ , and  $5f^3F_{31}^0$ .

Each of the terms  $2_{31}^0$  and  $8_{31}^0$  in our analysis is established by a single transition. The approximate positions of these terms were determined by Moseley curves drawn for the corresponding terms of Au I, Hg II, Tl III, and Bi V, these terms are well established by a number of combinations in both Au I and Hg II. Using the approximate term value of  $2_{31}^0$  obtained from the Moseley curve, the transition  $1_{31}-2_{31}^0$  is predicted in the region 71,300–71,500  $\text{cm}^{-1}$ .  $\lambda 1400.26$  has been selected as this transition since it is the only unclassified line with the right excitation and intensity in this region. A similar procedure locates the transition  $1_{31}-8_{31}^0$  in the region 91,600–93,600  $\text{cm}^{-1}$ . There are two lines in this region,  $\lambda 1079.88$  and  $\lambda 1084.18$ , with suitable excitations and intensities.  $\lambda 1079.88$  was selected because it is more intense than  $\lambda 1084.18$  on our plates. The other choice, however, is not precluded, it gives 193,488  $\text{cm}^{-1}$  as the alternative term value of  $8_{31}^0$ .

The remaining terms are established by at least two transitions having the proper excitation characteristics. In addition, the relative mean energies of the configurations and their multiplet separations are substantiated by Moseley curves for the sequence Au I to Bi V, and are also consistent with the separations in the other spectra of Pb.

The correctness of our analysis is also confirmed for a number of terms by hyperfine structure observations. The bracketed wave-lengths listed in Table II with eight of the transitions are isotopic hyperfine structures. The weaker component of each pair is emitted by  $\text{Pb}^{208}$  the stronger by  $\text{Pb}^{206}$ , both isotopes have  $I = 0$ . It is to be noted that the lines showing isotope shifts are classified as transitions between terms arising from configurations involving a different number of  $6s$  electrons. In discussing isotope shifts it must be kept in mind that the term systems of different isotopes are quite independent. Thus it is always necessary to state which levels have been arbitrarily brought into coincidence to form a datum for assigning relative shifts to the other levels. Arbitrarily assuming that  $5d^{10}7d$  levels of both  $\text{Pb}^{206}$  and  $\text{Pb}^{208}$  coincide, then the isotopic hyperfine structures of the eight lines can be consistently interpreted on the basis that the  $5d^96s^2, 2_{11}$  level of  $\text{Pb}^{206}$  is 1  $\text{cm}^{-1}$  more stable than the same level of  $\text{Pb}^{208}$ , and the  $5d^96s6p$  levels,  $14^0, 15^0, 18^0, 19^0, 20^0$  of  $\text{Pb}^{206}$  are 0.5  $\text{cm}^{-1}$  more stable than the corresponding levels of  $\text{Pb}^{208}$ .

\* Phys. Rev., vol 47, p 232 (1935)

Thus, for our configuration assignments the observed isotope shifts lead to a term displacement of  $0.5 \text{ cm}^{-1}$  per  $6s$  electron per two nuclear mass units, with the levels of the lighter isotope more stable than those of the heavier isotope. This is consistent with Breit's\* theory of isotope shifts for the heavy elements, and with the shifts observed in Pb III.†

In conclusion, the authors wish to thank Professor E. F. Burton, Director of the McLennan Laboratory, for his encouraging interest and for the facilities placed at our disposal. Our thanks are also due to Professor O. W. Richardson for the use of a calculating machine lent by the Royal Society.

#### SUMMARY

The spectrum of Pb IV has been photographed in the region from 400 Å. to 9000 Å. An analysis of the data has permitted the establishment of the terms from the one-electron configurations  $6s$ ,  $7s$ ,  $8s$ ,  $6p$ ,  $7p$ ,  $6d$ ,  $7d$ , and  $5f$ , which have been tentatively identified by other workers. In addition to these terms, we have found the  $5g$   $^2G$  and three  $^4H$  terms, the two terms from the inverted doublet  $5d^9 6s^2$   $^3D$  and twenty-two of the twenty-three levels predicted for the  $5d^9 6s 6p$  configuration. The ionization limit of  $314,350 \text{ cm}^{-1}$ , corresponding to an ionization potential of 42.11 volts, was obtained by assuming the sequence  $n h$   $^2H$  to be hydrogenic. The analysis is in agreement with the doublet laws, the excitation data, and the observed intensities.

Hyperfine structure, due to the relative displacement of the terms of the lead isotopes  $\text{Pb}^{206}$  and  $\text{Pb}^{208}$ , is resolved in eight lines. These lines are all classified as transitions between terms arising from configurations involving a different number of  $6s$  electrons. The observed shifts may be explained consistently by assigning to a term a displacement of  $0.5 \text{ cm}^{-1}$  for each  $6s$  electron present, with the levels of the lighter isotope more stable than those of the heavier isotope. This explanation is consistent with Breit's theory of isotope shifts for the heavy elements and with the shifts observed in these spectra by other investigators.

\* 'Phys. Rev.', vol. 42, p. 348 (1932)

† Crooker, 'Can. J. Res.' (in press)

## Temperature Coefficients in the Anion Catalysed Decomposition of Nitramide

By E C BAUGHAN and R P BELL

(Communicated by C N Hinshelwood, F R S—Received 6 August, 1936)

### INTRODUCTION

The decomposition



has been extensively studied by Brönsted and his collaborators and shown to be a simple case of general basic catalysis. Brönsted and Pedersen\* showed that the reaction is unimolecular with respect to nitramide and that in solutions of strong acids the rate is independent of the acid used and of its concentration; this "spontaneous" rate  $k_0$  is therefore attributed to catalysis by water. In solutions of weak acids the rate was found to be given by

$$k = k_0 + \sum k_r C_A, \quad (1)$$

where  $C_A$  is the concentration of any anion, and  $k_r$  the catalytic constant for that anion. The weaker the acid, the stronger is the anion as a catalyst, and the  $k_r$ 's were found to obey the relation

$$\log k_r = \log G - \alpha \log K, \quad (2)$$

where  $K$  is the dissociation constant of the acid, and  $G$  and  $\alpha$  are empirical constants. A relation of the same type was found to hold for non-aqueous solvents and other types of base, the values of  $G$  and  $\alpha$  varying with the solvent and with the charge-type of the catalyst †

All reactions so far investigated which exhibit general acid-base catalysis obey equations of the same type,‡ while formally similar expressions

\* 'Z phys. Chem.', vol 108, p 185 (1924)

† Brönsted and Duus, 'Z phys. Chem.', vol 117, p 299 (1925) (neutral amine bases), Brönsted and Volqvartz, *ibid*, vol 155, p 211 (1929) (amine bases with two positive charges), Brönsted and Vance, *ibid*, vol 163, p 240 (1933) (neutral bases and univalent anions in isoamyl alcohol), Brönsted, Nicholson, and Tovborg-Jensen, *ibid*, vol 169, p 379 (1934) (similar bases in *m*-cresol)

‡ For a review, see Kilpatrick and Kilpatrick, 'Chem. Rev.', vol 10, p 213 (1932), also Bell, 'Proc. Roy. Soc. A', vol 143, p 377 (1934)

apply to many other types of reaction, *e.g.*, oxidation reduction systems, reactions involving the transfer of methyl groups, etc.\*

The theoretical basis of these equations is, however, still uncertain Brönsted† showed that equation (2) could be plausibly derived from the assumptions (a) that the difference between the dissociation energies for dissociation and catalysis respectively is independent of the catalyst, and (b) that the factor A in the Arrhenius equation

$$k_e = Ae^{-E/RT} \quad (3)$$

is constant for a series of catalysts Polanyi and Horiuti‡ have derived the same equation more directly from a simple picture of proton transfer. In this derivation also it is assumed that the change in velocity from catalyst to catalyst is entirely due to change in the activation energy E, and the method of treatment implies that the constant  $\alpha$  in the Brönsted equation should be independent of temperature

Information on these points could be obtained from measurements of the temperature coefficients of reactions showing general acid-base catalysis Existing data in this field rarely extend over a sufficiently wide range of catalysts or temperatures Smith§ has shown that for the acetone-iodine reaction E is practically constant for a number of catalysts (equation (2) being obeyed), while several cases have been found in which there is simultaneous variation of A and E over a set of catalysts, with a rough tendency for A to increase with increasing E ||

Such measurements might also throw light on another problem It has been pointed out by Hinshelwood¶ that examination of the A and E factors of the Arrhenius equation for a series of similar reactions may help to decide whether quantum-mechanical theories (*e.g.*, non-classical passage of energy barriers) are required for the explanation of reaction velocities A statistical survey by Hinshelwood and Winkler\*\* would make it appear that E-variation is the more important in most of such

\* See Hammett, 'Chem. Rev.', vol 17, p 125 (1935), Burkhardt, Ford, and Singleton, 'J. Chem. Soc.', p 17 (1936)

† 'Chem. Rev.', vol 5, p 231 (1928)

‡ 'Acta Physicochim. U.S.S.R.', vol 2, p 505 (1935), *cf. also* Bell, 'Proc. Roy. Soc. A', vol 154, p 414 (1936)

§ 'J. Chem. Soc. Lond.', p 1744 (1934)

|| Hinshelwood and Legard, 'J. Chem. Soc. Lond.', pp. 587, 1588 (1935), Burkhardt, Ford, and Singleton, 'J. Chem. Soc. Lond.', p 17 (1936), Pedersen, 'J. Phys. Chem.', vol 38, p 501 (1934)

¶ 'J. Chem. Soc. Lond.', p 1111 (1935), 'Bull. Soc. chim. Fr.', vol 2, p 1786 (1935)

\*\* 'J. Chem. Soc. Lond.', p. 371 (1936)

series, as a classical treatment would predict. However, few data are included for catalytic reactions, and it has been shown\* that the effects of non-classical behaviour would be particularly prominent in acid-base reactions on account of the low mass of the proton

In investigating the validity of equation (2) at different temperatures it is necessary to know the temperature variation of the dissociation constants. Recent work by Harned and his collaborators† provides accurate data for a number of carboxylic acids between 0° and 60°, and anions of

TABLE I—THE "SPONTANEOUS" REACTION  $k_0$ 

Temperature °	Solution	$k_0 \times 10^{-5}$	$k_0 \times 10^{-5}$ (mean value)
15	0.057N HCl	35.5	38.3
	0.0057N HCl	40.0	
	0.0136N HClO <sub>4</sub>	40.0	
	0.05N benzene-sulphonic acid	37.9	
25	0.057N HCl	123.5	122.5
	0.0057N HCl	122.0	
	0.0150N HClO <sub>4</sub>	124.5	
	0.05N benzene-sulphonic acid	120.0	
35	0.057N HCl	393	392
	0.0136N HClO <sub>4</sub>	386	
	0.005N HCl	380	
	0.05N benzene-sulphonic acid	408	
45	0.06N HCl	1108	1112
	0.012N HCl	1105	
	0.107N HClO <sub>4</sub>	1110	
	0.15N benzene-sulphonic acid	1125	

this type were therefore used as catalysts in the present work. Measurements were made on catalysis by water (the "spontaneous" rate) and by the anions of acetic, formic, benzoic, salicylic, and *o*-nitrobenzoic acids at 15°, 25°, 35°, and 45°, and by the anions of trimethylacetic, monochloroacetic, and dichloroacetic acids at three of these temperatures. The values of the dissociation constants at 25° range from  $9.77 \times 10^{-6}$  for trimethylacetic acid to  $5.5 \times 10^{-2}$  for dichloroacetic. The water catalysed reaction was measured in solutions of various strong acids (to eliminate hydroxyl ion catalysis, see Table I). The anion catalysed reaction was measured in solutions of suitable alkali metal salts containing

\* Bell, 'Proc. Roy. Soc., A', vol. 139, p. 466 (1933), vol. 148, p. 241 (1935)

† J. Amer. Chem. Soc., vol. 56, p. 1050 (1934)

known amounts of free acid, the actual anion concentration being calculated from the composition of the solution and the dissociation constant of the acid.

#### EXPERIMENTAL

The reaction was followed by measuring the pressure of nitrous oxide evolved at constant volume. The apparatus was essentially that used by Pedersen\* modified by bending the connexion from the reaction vessel to the mercury manometer so that the manometer itself was inside the thermostat. Preliminary experiments on the evolution of carbon dioxide showed that a regular banging of the clamped reaction flask was more efficient than shaking, for eliminating supersaturation. The initial time interval during which the results are affected by supersaturation† was found to diminish greatly with increasing temperature, being about 20 minutes at 15° and less than two minutes at 45°. The solutions were de-aerated by exhausting and banging for a few minutes before each experiment. The thermostats were electrically regulated to within  $\pm 0.02^\circ \text{C}$  and their temperatures set by thermometers standardized by the N.P.L. Ground surfaces were greased with vaseline rubber mixture at 15°, and at higher temperatures with a high temperature bearing grease (FE 3) kindly supplied by Shell Mex Ltd. It was found that vaseline-rubber and "Apiezon" greases were useless under these conditions.

Nitramide was prepared from urethane and ethyl nitrate by the method of Thiele and Lachmann.‡ In the last stage of the preparation, the ether extraction was carried out by freezing out the whole of the water phase by adding a mixture of ether and solid carbon dioxide, as recommended by Marlies and La Mer§. Three extractions by this method were found sufficient. The nitramide obtained by evaporating off the ether was dissolved in a little dry ether and precipitated by adding ligroin. The net yield was usually 10–20%, and was not improved by using ether specially freed from peroxides and alcohol.

Benzoic, salicylic, and *o*-nitrobenzoic acids were recrystallized from water, and monochloroacetic acid from benzene. Formic and dichloroacetic acids were fractionally distilled and came over within  $0.2^\circ \text{C}$ . Acetic acid was frozen and the first crop of crystals collected. Trimethylacetic acid was prepared from pinacolone and purified by vacuum distillation followed by fractional freezing.

\* 'J. Amer. Chem. Soc.', vol. 53, p. 19 (1931).

† Cf. Pedersen, 'J. Amer. Chem. Soc.', vol. 49, p. 2687 (1927).

‡ 'Liebig's Ann.', vol. 288, p. 267 (1895).

§ 'J. Amer. Chem. Soc.', vol. 56, p. 2008 (1935).

Lithium benzoate and sodium formate were crystallized from water, potassium *o*-nitrobenzoate and sodium salicylate from ethyl alcohol, and potassium mono- and di-chloracetate from methyl alcohol. All these were anhydrous salts and were dried in a vacuum desiccator for at least a week before use. Sodium acetate was used as the trihydrate without further purification. No convenient solid trimethylacetate could be found, and the solutions of this ion were made by dissolving an excess of the acid in solutions of sodium hydroxide free from carbonate.

### RESULTS

All the unimolecular velocity constants were calculated by the method of Guggenheim\* and no systematic deviations were observed. The number of readings taken in a single experiment was 30–60, and the half times varied from about 3 minutes to about 12 hours. The values obtained for the unimolecular constants  $k$  and the catalytic constants  $k_c$  (defined in equation (1)) are given in Tables I and II. Decadic logarithms have been used, and the units of time and concentration are minutes and gram molecules per 1000 grams respectively. It will be seen that the values of  $k_c$  show no variation with the anion concentration or (for acetates and formates) with the hydrogen ion concentration. Table III shows a comparison of our results at 15° with those of Brønsted and Pedersen at the same temperature†. The agreement is satisfactory.

Assuming the Arrhenius equation to be obeyed, the best values of the constants  $A$  and  $E$  (see equation (2)) were calculated for each catalyst by the method of least squares from the individual observations on  $k_c$ . The probable errors in  $E$  were evaluated in the usual way,  $1/T$  being regarded as a known coefficient. The results for  $A$  and  $E$  are given in Table IV, and Table V shows a comparison between the values of  $k_c$  calculated by inserting these results in the Arrhenius equation, and the mean values of  $k_c$  actually observed. The discrepancies are in most cases well within the probable error of the mean (given by  $\sqrt{\frac{\sum d^2}{n(n-1)}}$

where the  $d$ 's are the deviations from their mean of the  $n$  individual points), and in no case greater than three times this. We may therefore conclude that the reactions studied obey the Arrhenius equation within the accuracy of the present work.

In testing the Brønsted equation the dissociation constants of acetic, formic, and monochloroacetic acids were taken from recent accurate work

\* 'Phil. Mag.', (7), vol. 2, p. 540 (1926).

† 'Z. phys. Chem.', vol. 108, p. 185 (1924).

TABLE II—THE ANION-CATALYSED REACTIONS\* VALUES OF  $k_s$ 

At 15°						
Catalyst	C <sub>cat</sub>	C <sub>acid</sub>	C <sub>anion</sub>	k × 10 <sup>-3</sup>	k <sub>r</sub>	k <sub>e</sub> (mean value)
Tri-methyl- acetate	0 01735	0 01038	0 0174	1547	0 870	0 822
	0 0107	0 00660	0 0107	920	0 824	
	0 00858	0 0049	0 00859	716	0 793	
	0 00471	0 0029	0 00471 <sub>s</sub>	415	0 801	
Acetate	0 01583	0 0126	0 01584	800	0 481	0 492
	0 00958	0 0169	0 00961	526	0 503	
	0 00484	0 0338	0 00497	234	0 493	
	0 00347	0 0146	0 00355	212	0 490	
Benzoate	0 0378	0 0034	0 0378	720	0 185	0 189
	0 0271	0 0024	0 0271	521	0 179	
	0 0189	0 0016	0 0189	368	0 175	
	0 0141	0 0012	0 0141	312	0 190	
	0 0141	0 0012	0 0141	308	0 188	
Formate	0 0484	0 0664	0 0486	426	0 0798	0 0804
	0 0474	0 0607	0 0477	420	0 0805	
	0 0341	0 0855	0 0343	317	0 0806	
	0 0274	0 0308	0 0276	260	0 0803	
Salicylate	0 0946	0 0045	0 0946	238	0 0218	0 0209
	0 0745	0 0036	0 0745	185	0 0196	
	0 0474	0 0024	0 0474	130	0 0192	
	0 0269	0 0013	0 0269	101	0 0227	
o-Nitrobenzoate	0 202	0 002	0 202	119 0	0 00400	0 00420
	0 117	0 002	0 117	91 0	0 00437	
	0 0880	0 001	0 0880	79 5	0 00449	
	0 0585	0 001	0 0585	63 5	0 00402	
At 25°						
Tri-methyl acetate	0 00686	0 00426	0 00686	1700	2 30	2 30
	0 00471	0 00293	0 00472	1255	2 40	
	0 00364	0 00226	0 00364	955	2 32	
	0 00219	0 00136	0 00220	598	2 19	
Acetate ..	0 00790	0 0277	0 00799	1322	1 50	1 48
	0 00691	0 00250	0 00691	1150	1 49	
	0 00644	0 00368	0 00645	1051	1 44	
	0 00287	0 00138	0 00288	548	1 48	

TABLE II—(continued)

At 25°						
Catalyst	$C_{alt}$	$C_{acid}$	$C_{anion}$	$k \times 10^{-3}$	$k_e$	$k_o$ (mean value)
Benzoate	0 02335	0 005	0 02338	1407	0 550	0 550
	0 01604	0 003	0 01606	1010	0 553	
	0 01245	0 0002	0 01245	804	0 548	
Formate	0 0503	0 0305	0 0504	1300	0 240	0 255
	0 0346	0 0126	0 0347	1036	0 264	
	0 0274	0 00525	0 0274	811	0 253	
	0 0143	0 0142	0 0144	486	0 252	
Salicylate	0 1375	0 0085	0 1375	1025	0 0672	0 0665
	0 0941	0 0030	0 0941	735	0 0652	
	0 0894	0 0020	0 0894	721	0 0660	
	0 0539	0 0015	0 0539	488	0 0678	
Mono-chlor- acetate	0 1762	0 0027	0 1762	898	0 0438	0 0465
	0 1079	0 0108	0 1081	626	0 0467	
	0 0649	0 0057	0 0652	423	0 0461	
	0 0441	0 032	0 0442	340	0 0492	
<i>o</i> -Nitrobenzoate	0 239	0 003	0 239	516	0 0167	0 0167 <sub>o</sub>
	0 125	0 002	0 125	321	0 0164	
	0 077	0 001	0 077	250	0 0166	
	0 074	0 001	0 074	251	0 0170	
Di-chloracetate	0 417	0 012	0 419	250 <sub>o</sub>	0 00250	0 00239
	0 300	0 022	0 305	193 <sub>7</sub>	0 00233	
	0 285	0 049	0 292	195 <sub>4</sub>	0 00249	
	0 247	0 001	0 247	181 <sub>4</sub>	0 00237	
	0 157	0 033	0 171	161 <sub>o</sub>	0 00225	
At 35°						
Tri-methyl- acetate	0 00364	0 00226	0 00364	2880	6 85	6 44
	0 00347	0 00105	0 00347	2605	6 39	
	0 00272	0 00083	0 00272	2160	6 53	
	0 000634	0 00040	0 000695	800	5 96	
Acetate	0 00653	0 0261	0 00664	3215	4 26	4 28
	0 00581	0 00317	0 00582	2785	4 12	
	0 00358	0 0535	0 00389	2155	4 47	
	0 00164	0 00795	0 00174	1083	4 00	
Benzoate	0 0160	0 0005	0 0160	2808	1 51	1 57
	0 0141	0 0004	0 0141	2790	1 69	
	0 00830	0 0003	0 00830	1610	1 50	
	0 00749	0 0002	0 00749	1585	1 59	

TABLE II—(continued)

At 35°						
Catalyst	$C_{alt}$	$C_{acid}$	$C_{anion}$	$k \times 10^{-5}$	$k_c$	$k_o$ (mean value)
Formate	0.0346	0.0126	0.0347	3005	0.752	0.728
	0.0274	0.0308	0.0278	2350	0.720	
	0.0259	0.0050	0.0259	2208	0.702	
	0.0144	0.0264	0.0148	1490	0.740	
Salicylate	0.1375	0.0083	0.1375	3140	0.201	0.205
	0.0946	0.0045	0.0946	2315	0.203	
	0.0946	0.0045	0.0946	2305	0.202	
	0.0474	0.0024	0.0474	1346	0.204	
	0.0269	0.0013	0.0269	978	0.218	
Mono-chlor-acetate	0.267	0.0063	0.267	3790	0.128	0.133
	0.187	0.0190	0.188	2975	0.138	
	0.125	0.0076	0.125	1978	0.131	
	0.0609	0.0032	0.0609	819	0.135	
o-Nitrobenzoate	0.2022	0.002	0.2022	1382	0.0490	0.0518
	0.1167	0.002	0.1167	1014	0.0533	
	0.0880	0.001	0.0880	850	0.0532	
	0.0585	0.001	0.0585	696	0.0520	
Di-chloracetate	0.424	0.008	0.424	720	0.00790	0.00828
	0.332	0.009	0.333	700	0.00940	
	0.276	0.012	0.278	590	0.00734	
	0.191	0.025	0.196	550	0.00836	
	0.117	0.018	0.124	490	0.00838	
At 45°						
Acetate	0.00271	0.00069	0.00272	4475	12.4	11.4
	0.00201	0.00044	0.00202	3090	9.8	
	0.001535	0.00127	0.00155	2950	11.8	
	0.00124	0.00083	0.00125	2500	10.0	
	0.000813	0.000462	0.000822	2205	13.1	
Benzoate	0.00796	0.00135	0.00798	4600	4.38	4.36
	0.00620	0.00105	0.00621	3895	4.48	
	0.00451	0.00082	0.00451	3010	4.21	
Formate	0.0213	0.008	0.0214	5300	1.95	1.92
	0.0144	0.0072	0.0145	3760	1.84	
	0.0102	0.0033	0.0103	3030	1.86	
	0.00744	0.0045	0.0076	2695	2.10	

TABLE II—(continued)

Catalyst	$C_{\text{salt}}$	$C_{\text{acid}}$	At 45° $C_{\text{anion}}$	$k \times 10^{-3}$	$k_e$	$k_e$ (mean value)
Salicylate	0.0969	0.005	0.0969	6390	0.544	0.545
	0.0684	0.002	0.0684	4560	0.508	
	0.0472	0.002	0.0472	3910	0.593	
	0.0247	0.001	0.0247	2430	0.535	
Mono-chlor- acetate	0.1762	0.0027	0.1762	8080	0.395	0.371
	0.1079	0.0108	0.1081	5080	0.367	
	0.0881	0.0126	0.0883	4290	0.360	
	0.0406	0.0035	0.0407	2687	0.387	
	0.0258	0.0080	0.0263	2027	0.348	
<i>o</i> -Nitrobenzoate	0.180	0.009	0.180	4110	0.166 <sub>a</sub>	0.167 <sub>a</sub>
	0.143	0.007	0.143	3550	0.170 <sub>a</sub>	
	0.0774	0.004	0.077	2395	0.166 <sub>a</sub>	
	0.0592	0.003	0.059	2100	0.167 <sub>a</sub>	
Di-chloracetate	0.510	0.004	0.510	2555	0.0283	0.0277
	0.435	0.011	0.436	2260	0.0270	
	0.300	0.022	0.305	1930	0.0269	
	0.280	0.0074	0.282	1905	0.0282	
	0.201	0.0099	0.203	1665	0.0276	
	0.180	0.0104	0.184	1635	0.0285	

TABLE III—COMPARISON OF THESE RESULTS WITH THOSE OF BRÖNSTED AND PEDERSEN AT 15° C

Catalyst	This work $38.3 \times 10^{-3}$	Bronsted and Pedersen $38.3 \times 10^{-3}$
$k_e$		
Acetate	0.492	0.504
Benzoate	0.183	0.189
Formate	0.0804	0.0822
Salicylate	0.0209	(0.0206)*

\* Salicylate value from one single experiment

TABLE IV—VALUES OF A, E IN THE ARRHENIUS EQUATION

Catalyst	A	E (calories)	Probable error in E (cals.)
"Spontaneous rate"	$1.90 \times 10^{13}$	20,680	150
Tri-methyl acetate	$7.48 \times 10^{13}$	18,400	210
Acetate	$1.77 \times 10^{14}$	19,180	180
Benzoate	$7.69 \times 10^{13}$	19,260	100
Formate	$4.08 \times 10^{13}$	19,370	80
Salicylate	$3.67 \times 10^{13}$	20,080	150
Mono-chloracetate	$1.95 \times 10^{13}$	19,940	220
<i>o</i> -Nitrobenzoate	$3.83 \times 10^{14}$	22,320	150
Di-chloracetate	$5.43 \times 10^{14}$	23,670	200

TABLE V—COMPARISON OF OBSERVED CATALYTIC CONSTANTS WITH THOSE CALCULATED FROM THE EQUATIONS IN TABLE IV

Catalyst		15°	25°	35°	45°
"Spontaneous" $k_0$	(obs)	$38.3 \times 10^{-4}$	$122.5 \times 10^{-4}$	$386 \times 10^{-4}$	$1112 \times 10^{-4}$
	(calc)	$37.3 \times 10^{-4}$	$125.0 \times 10^{-4}$	$389 \times 10^{-4}$	$1125 \times 10^{-4}$
Tri-methyl acetate	(obs)	0.822	2.30	6.44	—
	(calc)	0.802	2.35	6.46	—
Acetate	(obs)	0.492	1.48	4.28	11.4
	(calc)	0.483	1.48	4.25	11.4
Benzoate	(obs)	0.189	0.550	1.57	4.36
	(calc)	0.181	0.556	1.60	4.32
Formate	(obs)	0.0804	0.255	0.728	1.92
	(calc)	0.0804	0.249	0.721	1.95
Salicylate	(obs)	0.0209	0.0665	0.205	0.545
	(calc)	0.0207	0.0668	0.201	0.565
Mono-chloracetate	(obs)	—	0.0465	0.133	0.371
	(calc)	—	0.0451	0.135	0.375
o-Nitrobenzoate	(obs)	0.00420	0.0167	0.0518	0.168
	(calc)	0.00428	0.0157	0.0537	0.169
Di-chloracetate	(obs)	—	0.00239	0.00828	0.0277
	(calc)	—	0.00229	0.00840	0.0284

on cells without liquid junctions \*. The values for benzoic, salicylic, o-nitrobenzoic, and trimethyl acetic acids were taken from Landolt-Börnstein's tables. The results for the first three of these acids obey the empirical equation found by Harned and Embree to express the variation of dissociation constant with temperature, and hence are probably reliable. For trimethylacetic acid values at 25° only are available. Only one unconfirmed value for the dissociation constant of dichloroacetic acid is recorded, and the results for this anion have not been taken into account in testing the Brönsted equation.

The values of the dissociation constants and catalytic constants for the remaining anions were treated by the method of least squares to obtain the best values of the constants  $G$  and  $\alpha$  in equation (2). The results are given in Table VI, and Table VII shows the comparison between the values of  $k_c$  calculated from these equations and the observed

\* Harned and Ehlers, 'J. Amer. Chem. Soc.', vol. 55, p. 652 (1933) (acetic acid); Harned and Embree, *ibid.*, vol. 56, p. 1042 (1934) (formic acid), Wright, *ibid.*, vol. 56, p. 314 (1934) (monochloroacetic acid).

mean values. In nearly all cases the deviations are not significantly greater than the probable errors in  $k_e$ . For the monochloracetate ion, however, the deviations amount to 8–14%, and are thus considerable. It is difficult to decide how far this represents a real departure from Brønsted's equation since, although the value given by Wright for the dissociation

TABLE VI—VALUES OF  $G$  AND  $\alpha$  IN THE EQUATION  
 $\log k_e = \log G - \alpha \log K$

Temperature °	$G$	$\alpha$
15	$8.44 \times 10^{-3}$	0.79 <sub>4</sub>
25	$3.69 \times 10^{-4}$	0.75 <sub>4</sub>
35	$1.03_4 \times 10^{-3}$	0.76 <sub>4</sub>
45	$2.79 \times 10^{-3}$	0.76 <sub>4</sub>

TABLE VII—COMPARISON OF OBSERVED CATALYTIC CONSTANTS WITH THOSE CALCULATED FROM THE EQUATIONS IN TABLE VI

Catalyst		15°	25°	35°	45°
Tri-methyl acetate	obs	0.822	2.30	6.44	—
	calc	0.822	2.28	6.80	—
Acetate	obs	0.492	1.48	4.28	11.4
	calc	0.507	1.47	4.38	11.9
Benzoate	obs	0.189	0.550	1.57	4.36
	calc	0.169	0.546	1.56	4.14
Formate	obs	0.0804	0.255	0.728	1.92
	calc	0.0813	0.255	0.755	2.12
Salicylate	obs	0.0209	0.0665	0.205	0.545
	calc	0.0206	0.0662	0.180	0.500
<i>o</i> -Nitrobenzoate	obs	0.00420	0.0167	0.0518	0.167
	calc	0.00421	0.0171	0.0562	0.174
Mono-chloracetate	obs	—	0.0465	0.133	0.371
	calc	—	0.0540	0.150	0.404

constant of monochloracetic acid at 25° ( $1.38 \times 10^{-3}$ ) agrees well with that obtained by Saxton and Langer\* by a different method ( $1.40 \times 10^{-3}$ ), Lewis and Schutz† in a recent paper give a value ( $1.71 \times 10^{-3}$ ) which would completely remove the discrepancy with the Brønsted equation.

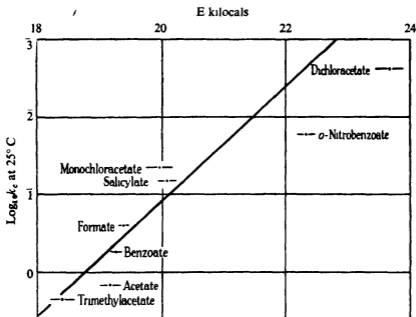
The general agreement with equation (2) is not nearly so good if the

\* 'J. Amer. Chem. Soc.', vol. 55, p. 3638 (1933).

† 'J. Amer. Chem. Soc.', vol. 56, p. 1913 (1934)

temperature variation of the dissociation constant is not taken into account. The increased accuracy is particularly noticeable for *o*-nitrobenzoate, the change in dissociation constant being large—from  $7.28 \times 10^{-3}$  at  $15^\circ\text{C}$  to  $4.42 \times 10^{-3}$  at  $45^\circ\text{C}$ . The assumption that the same equation is valid for the dichloracetate ion leads to the following values for the dissociation constant:  $8.47 \times 10^{-3}$  at  $25^\circ$ ,  $6.54 \times 10^{-3}$  at  $35^\circ$ , and  $4.95 \times 10^{-3}$  at  $45^\circ$ .

As regards the variation of the two factors  $G$  and  $\alpha$  with temperature (Table VI), we see that  $\alpha$  is nearly independent of temperature between  $25^\circ$  and  $45^\circ$ , but that at  $15^\circ$  it is higher by an amount (4%) which certainly represents a real effect.  $G$ , on the other hand, varies considerably with temperature, but does not obey a simple equation of the Arrhenius type.



### DISCUSSION

The relative importance of changes in the two factors  $A$  and  $E$  of the Arrhenius equation is shown by fig. 1, in which the values of  $E$  for different catalysts are plotted against the corresponding values of  $\log_{10} k_c$  at  $25^\circ$ . The straight line drawn has the slope  $2.303 RT$ , which is the theoretical value for constant  $A$ . Horizontal lines through the points indicate the probable errors in  $E$  (as calculated from the least squares treatment). It is clear that although there is a rough parallelism between

$E$  and  $k_e$ , the variations in  $A$  involve a factor of about 30 and are well outside the experimental error. It is therefore hardly satisfactory to base a theoretical derivation on the Brönsted relation on the assumption that  $A$  is constant,\* especially as this relation is obeyed to within a few per cent in the present case

According to the extended collision picture of bimolecular reactions, the factor  $A$  may be regarded as the product of the collision number  $Z$  and an *ad hoc* factor  $P$ . Although the exact value of  $Z$  for reactions in solution may be a matter of some doubt, it can hardly vary by a factor of more than about two for the anions studied here. The observed variations in  $A$  will thus be interpreted mainly as variations in the factor  $P$ , which are in some way related to structural variations in the reacting molecules. The agreement with Brönsted's equation necessitates that these structural variations should have a parallel effect on  $P$  and on the dissociation constant of the acid, this is difficult to envisage.

TABLE VIII—COMPARISON OF HEATS OF IONIZATION OF ACIDS AND ACTIVATION-ENERGIES

Catalyst	Heat of ionization (cals)	$E_{(cal)}$
Acetate	— 100	19 180
Formate	— 10	19,260
Benzoate	+ 450	19,370
Mono-chloracetate	— 1240	19,950
Salicylate	+ 950	20,080
<i>o</i> -Nitrobenzoate	— 2720	22,320

On the transition state theory† variations in  $A$  represent variations in the entropy of formation of the critical complex, which again would depend on structural factors. In this case we might anticipate a parallelism between the entropy of formation of the critical complex and the entropy of ionization of the corresponding acid, and hence (on account of the Brönsted relation) between  $E$  and  $H$ , the heat of ionization of the acid ‡. In Table VIII the values of  $E$  are compared with the values of  $H$

\* Cf. Horiuti and Polanyi, 'Acta Physicochim. U.S.S.R.', vol 2, p 505 (1935)

† Eyring, 'J. Chem. Phys.', vol 3, p 107 (1935), Evans and Polanyi, 'Trans. Faraday Soc.', vol 31, p 875 (1935)

‡  $H$  is here the actual heat of ionization of the acid in water at the temperature in question, and bears no simple relation to the quantity  $Q$  occurring in the theoretical treatments of Horiuti and Polanyi and of Bell ('Proc. Roy. Soc.', A, vol 154, p 414 (1936)) which represents the energy of removing a proton at absolute zero under idealized conditions

at 25° (calculated from the temperature variation of the dissociation constants); no correlation is apparent

It may be noted that a correlation of this kind can be derived formally from equations (2) and (3) under certain conditions. Differentiating both equations with respect to temperature, we have for the difference in activation energy between two catalysts

$$\begin{aligned} \Delta E &= -\alpha RT^2 \Delta \left( \frac{\partial \log K}{\partial T} \right) - RT^2 \Delta (\log K) \frac{\partial \alpha}{\partial T} \\ &= \alpha \Delta H - RT^2 \Delta (\log K) \frac{\partial \alpha}{\partial T} \end{aligned} \quad (4)$$

Hence if  $\alpha$  is independent of temperature (as assumed in the treatment of Polanyi and Horuti),

$$\Delta E = \alpha \Delta H \quad (5)$$

Actually we have found that  $\alpha$  varies with temperature (Table VI), and although the variation is small it is sufficient to destroy completely the simple correlation expressed by (5). If both  $K$  and  $\alpha$  are independent of temperature, equation (4) becomes

$$\Delta E = 0, \quad (6)$$

i.e.,  $E$  should be constant for a series of catalysts. This is what has actually been found by Smith\* for the acetone-iodine reaction, and in confirmation of the above deduction we may note that  $H$  is very small for all the catalysts used, and  $\alpha$  has the same value at 0° and at 25°.

The behaviour of the values of  $A$  and  $E$  observed in the present paper suggests strongly that they only approximately represent physically separable quantities. This might arise theoretically in several ways, e.g., if the probability of decomposition of the critical complex is a function of its energy,† or if the proton transfer involved is appreciably non-classical in nature. In the latter case it has been shown that‡ non-classical behaviour may lead to large deviations from a simple relation between  $\log_{10} k_c$  and  $E$  without introducing observable departures from the Bronsted equation or the Arrhenius equation. (Thus in the present case the observed variations in  $A$  would only involve a variation of apparent activation energy of about 200 cal. over the temperature range investigated, and the corresponding deviations from the Brönsted equation

\* 'J Chem Soc Lond,' p 1744 (1934)

† Cf. LaMer, 'J Chem Phys,' vol 1, p 789 (1933)

‡ Bell, 'Proc Roy Soc.' A, vol 154, p 414 (1936)

would be less than 10%) An explanation of the present results might thus be sought along these lines, which would also allow for a variation of  $\alpha$  with temperature On the other hand, non-classical proton transfer can only account for values of  $A$  smaller than the collision number Converting the observed data into the ordinary units  $\log_e$ , seconds<sup>-1</sup>, we obtain values for  $A$  ranging from  $1.41 \times 10^{11}$  for monochloracetate to  $39 \times 10^{11}$  for dichloracetate The average value for the comparable collision number in the gas phase is about  $2.8 \times 10^{11}$ , so that the prediction of a small  $P$ -factor is not fulfilled It is therefore probable that other factors must be considered before it is possible to give a complete explanation of the observed  $A$  and  $E$  values

#### SUMMARY

The velocity of decomposition of nitramide in aqueous solution has been studied at 15°, 25°, 35°, and 45°, the catalysts used being water (the "spontaneous" reaction), and the anions of trimethylacetic, acetic, benzoic, formic, salicylic, monochloracetic, *o*-nitrobenzoic, and dichloracetic acids

Brönsted's equation relating catalytic constant to dissociation constant is valid at each temperature, and holds more accurately if the dissociation constants used relate to the same temperature as the catalytic constants

The Arrhenius equation  $k = Ae^{-E/RT}$  is obeyed by each catalyst The change in velocity from one catalyst to another is largely determined by changes in  $E$ , but the variations in  $A$  amount to many times the experimental error There is no parallelism between the value of  $E$  for a given anion and the heat of ionization of the corresponding acid

Possible theoretical interpretations of these facts have been discussed, and it is concluded that in this and similar cases the observed values of  $A$  and  $E$  only approximately represent physically separable quantities. The facts can be partially accounted for by assuming a non-classical proton transfer, but it is unlikely that this hypothesis can afford a complete explanation

For the anion catalysts, the average value of  $A$  is of the order of magnitude of a collision number

---

## Royal Society Expedition to Montserrat, B.W.I. Preliminary Report on Seismic Observations

By C F POWELL

(Communicated by Sir Gerald Lennox-Conyngham, F R S—Received  
28 September, 1936)

[PLATES 24 AND 25]

The following preliminary report deals briefly with the observations made during my residence in Montserrat from 24 March to 24 July, 1936, and with the main conclusions to be drawn from them.

The Royal Society Expedition is greatly indebted to the representatives of His Majesty's Government, to His Excellency Sir Gordon Lethem, Governor of the Leeward Islands, and to the Commissioner and Acting Commissioners of Montserrat for much kindness and assistance. We are also indebted for the most generous and liberal assistance rendered to the expedition by officials, representatives of organizations, and private individuals in ways too numerous to be described in detail. The members of the Expedition had the fullest support from the Government and the citizens of the island.

I am greatly indebted to Mr F A Perret who kindly allowed me to erect a concrete pillar in his hut at the Gages Soufrière for the support of a Jagger shock recorder, and who gave me the advantage of his experience in these West Indian islands in a number of discussions during his visit to Montserrat from 16 to 19 May, 1936.

### I—SEISMIC OBSERVATIONS

The Expedition was equipped with the following instruments: four horizontal Jagger shock recorders, one Kew-Jagger vertical shock recorder, and one two-component horizontal Wiechert seismograph with stationary mass of two hundred kilograms. In addition, sound ranging equipment was kindly lent by the War Office, to be operated in conjunction with specially designed shock meters employing hot wire microphones.

The reports of individual observers, living at different points in the island, of their impressions of some of the most serious of the earthquakes

in the period from May, 1934, to December, 1936, and the distribution of the damage done by different earthquakes suggested that most of the shocks were highly local in origin, the foci probably lying under the island. The same conclusion was drawn by Perret from the measurements made during the severe earthquakes of November, 1935, with the three-directional seismometer erected by him at the estate house at Gages.

Two main problems presented themselves for solution. It was first necessary to attempt to determine the location of the earthquake foci with more precision than is possible by comparing the accounts of individual observers living at different points in the island. The second problem was to determine the variation with time of the general seismic activity in order to detect any association of this activity with such factors as rainfall, barometric pressure, lunar and solar gravitational influences which may exist. The solution of the first problem would enable us to say whether the foci were associated closely with any of the numerous volcanic centres in the island. The detection of a relationship between the seismic activity and other factors would give us one method of determining and isolating some of the complex of factors which together determine the occurrence of the earthquakes.

The chart supplied by the Curator of the Botanical Station, Mr Gomez, showing the daily variation in the number of earthquakes, figs. 1 and 2, strongly suggests the existence of a six monthly rhythm in the earthquake activity, the times of most pronounced disturbance, both as regards the daily number of observed shocks and in the magnitude of the worst individual shocks for the years 1934 and 1935, being the months of May and November or December. The use of instruments makes it possible to examine the variation of the seismic activity with time with more precision.

Of the earthquakes which have occurred in Montserrat during the past three past years, by far the most serious, from a world point of view, was that on 10 November, 1935, at about 18 hours 28 minutes G M T \*. This earthquake was recorded at stations all over the world, at Kew, at Manila, and at many stations in the U S A, amongst others. It is likely that the energy released during this earthquake was of a different order of magnitude from that in any other of the individual shocks, although these may have produced equally serious effects at some points in Montserrat. It will be observed that previous to 10 and 11 November the general tendency had been for the seismic activity to increase and that subsequently there was a marked decrease.

\* I am greatly indebted to Dr. Lee, of Kew Observatory, for information about this earthquake.

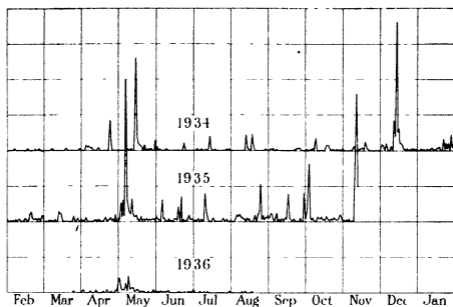


FIG 1—Daily number of tremors for 1934, 1935, 1936

The data for the period from 12 November, 1935, to 24 March, 1936, were not available when this figure was drawn. The seismic activity during this period was small.

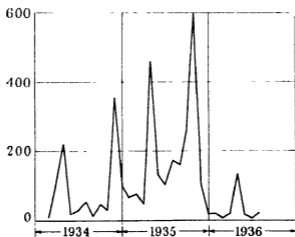


FIG 2—Number of tremors per month

## 2—THE SHOCKS ARE LOCAL IN ORIGIN

One method used in conventional seismology for determining the distance of the focus of an earthquake from the observatory depends on the following considerations. The disturbance of the earth's crust at the place where the earthquake originates leads to the radiation from this focus of a complex system of elastic waves in the elastic-solid crust. Among the waves of different types which spread outwards are (a) a longitudinal compressional wave, essentially similar in type to sound waves, and known as the P wave, and (b) a transverse wave motion known as the S wave. These are the two wave motions radiating from the focus which move with the greatest speed, the P waves having a greater velocity than the S. As a result of the difference in velocity of the two waves, they arrive at any observing station at different instants, the difference in the arrival times being greater the farther the point of origin of the waves from the observing station. If the speed of the two waves through the crust is known, then, from the time interval between the arrival of the P and S waves, the distance of the observing station from the point of origin can be calculated.

An example of a record obtained on the Wiechert seismograph as a result of a distant earthquake is shown in fig 3, Plate 24. It was obtained in Montserrat on 13 July, 1936, and was due to the earthquake in Chile on that date.

In contrast with those given by distant earthquakes, figs 4, 5, 6, and 7, Plate 24, are typical examples of the records produced by earthquakes which produce sensible movements in Montserrat. Fig 4 was produced by a shock which occurred somewhere in the sea between Montserrat and Antigua. It will be seen that the P-S\* separation time is very much shorter than with the really distant earthquake but that the P and S waves are clearly resolved. Figs. 5 and 7 are typical of the great majority of those which have occurred during my stay in the island, and it will be seen that there is practically no resolution of the P and S waves. In some cases the P wave cannot be distinguished from the larger movements associated with the arrival of the S waves. In other cases the P wave is represented by a small spur preceding the main movement. We must assume that in such cases the focus is within a few miles of the observing station and we conclude that the foci of the majority of the

\* We shall assume that the two wave motions which can be distinguished in fig 4 are to be identified with the P and S waves of conventional seismology. This assumption is not, however, essential to the argument.

shocks occurring during the period of residence of the members of the expedition were highly local

### 3—DISTRIBUTION OF THE FOCI

Since the shocks are so highly local in origin, it becomes impossible to locate the foci by the methods of conventional seismology. The most simple of these methods depends upon the measurement of the P-S separation times produced by a given shock on instruments at three separate stations, and hence the deduction of the distance of the focus from these three points. The time scale of the conventional seismographs is of the order of an inch to a minute, and it has been shown that on such a scale the P and S waves are not sufficiently resolved for accurate measurements of the P-S separation times to be made in highly local shocks.

#### *a—The Sound Ranging Equipment*

It was to meet such a situation as this that the expedition was supplied with the sound ranging equipment and the hot wire shock recorders. In this instrument the time scale is very extended compared with that of the ordinary seismograph and shock recorders, a second being represented by about an inch and measurements are possible to a hundredth of a second. The instrument is, however, expensive to run. Before the time of departure of the expedition from England the latest news available showed that the shocks were occurring sometimes at the rate of two hundred a day, and in these conditions it would have been possible to run the instrument to great advantage. After the decrease in seismic activity which followed the earthquake "swarm" in the first half of May, 1936, the shocks never occurred sufficiently frequently to make it possible to use this equipment except with a very large expenditure of photographic paper. Other methods had therefore to be devised for determining the foci of the comparatively rare shocks which occurred in this period.

#### *b—The Jagger Shock Recorders*

With distant earthquakes it is possible to deduce the bearing of an earthquake focus from a given station by observations of the horizontal movements at the station in two perpendicular directions. This determination depends on a comparison of the initial movement associated with the arrival of the P wave and not on any measure of the general amplitude of the wave motion which follows. Deductions from this

amplitude could be made only if the waves were plane polarized, whereas in actual fact the movements are extremely complicated, as a result of the complex of reflected and refracted waves arriving at the station. With the shocks similar to that shown in fig. 4, the bearing of the focus can be deduced by this method, but such shocks are comparatively rare. With the more local shocks the frequency of the wave motion is much higher than that with more distant shocks and the initial movement can rarely be distinguished. Examples of the records of shocks on a Jaggarr instrument are shown in figs. 8 and 9, Plate 25, and it will be seen that the time scale is such that the trace appears as an unresolved mark on the surface of the chart. It is therefore not possible to deduce the position of the epicentre of the local shocks by observations at two stations each equipped with two shock recorders mounted on two walls at right angles to one another.

The method adopted was to determine the distribution of the amplitude of the earth movements produced by a given tremor at different points in the island, by means of the Jaggarr shock recorders. We define the amplitude of a tremor as equal to the maximum deflexion in millimetres in the trace recorded on the shock recorder at the station. The Jaggarr instruments record the earth movements in one direction only whereas, for the complete determination of the earth movement at any point, it is necessary to make measurements in three mutually perpendicular directions. Preliminary experiments indicated, however, that a fairly good measure of the horizontal amplitude at any point could be obtained with a single horizontal shock recorder. The records obtained on two such instruments mounted at the same place one on each of two walls at right angles were found to be very nearly equal as a result of the passage of a single shock. This equality between the traces on the two instruments was maintained for shocks of widely different intensity. This result must be associated with the fact mentioned above that the horizontal earth movements at any point are so extremely complex, a compound of many waves variously orientated. Only four horizontal Jaggarr instruments were available, and it was considered that the advantages of having amplitude measurements at four points were to be preferred to the more complete observations possible at the two stations only.

The horizontal Jaggarr shock recorders were finally established with equal sensitivity at the following points: Gages, Bethel, St John's, and Olveston, the vertical Kew-Jaggarr at Paradise and the Wiechert seismograph (with a sensitivity about ten times that of the Jaggarr instruments) at the Grove Botanical Station.

The amplitude distribution among these stations produced between

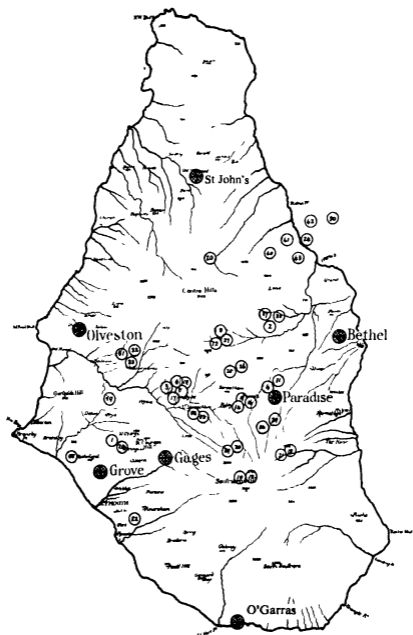


FIG 10—Map showing positions of Jaggar stations and suggested epicentres Jaggar station shown thus ⊕, epicentres thus ⊕

11 May and 30 June by about fifty separate tremors was determined. It should be noticed that the distribution of amplitude for shocks coming from the same focus should always be constant and independent of any

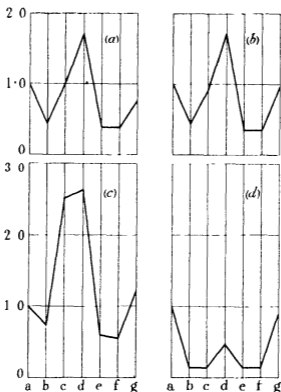


FIG. 11—Distribution in amplitude amongst stations equipped with Jagger shock recorders. Station *a*, Gages—taken as unity, *b*, Olveston, *c*, St John's, *d*, Bethel, *e* and *f*, two components of Wiechert seismograph at Grove Botanical Station, *g*, Paradise. Distance of any point in the patterns above the base line represents the amplitude of the shock at the corresponding station relative to that at Gages.

Shock (a) occurred on 22nd June at 21 hours 52.3 minutes. Amplitude 0.75 mm.

Shock (b) occurred on 22 June at 21 hours 53.3 minutes. Amplitude 0.65 mm.

Shock (c) occurred on 30 June at 23 hours 31 minutes. Amplitude 2.6 mm.

Shock (d) occurred on 8 June at 10 hours 6 minutes. Amplitude 0.9 mm.

(a) and (b) must have occurred at almost the same focus.

directional properties of the instruments. In fig 11a and b, the distribution of amplitude produced by two shocks which followed one another at an interval of a minute are shown pictorially. It will be seen that the two distributions are almost exactly similar and we deduce that these

two shocks originated at the same focus. By plotting the amplitude distribution for all the shocks, it was found that a number of different points or regions were involved as foci for the occurrence of earthquakes. Further, the large changes of relative amplitude amongst the different stations suggested that the foci were distributed throughout the island. This is shown, for example, by the contrast in the distribution of amplitude represented by figs 11*a*, *c*, and *d*, and the contrast of these figures with those for other shocks. In many instances earthquakes recurred at foci which had been active some time previously, earthquakes from new foci having occurred in the interim. The large variations in the figures representing the distribution of amplitude for different shocks further suggests that in some instances the foci are close to the surface compared with the distance between stations, for otherwise we should expect the amplitude to be nearly equal at different stations.

In order to determine the position of the focus to which a given amplitude distribution corresponds, it is necessary to make certain simplifying assumptions. The earth movement at any point as a result of an earthquake at a given focus must, in actual fact, depend on a number of factors of which it is difficult to estimate the influence, such as the nature of the rocks forming the crust between the focus and the station, the details of the local topography, etc. For simplicity we assume, however, that the amplitude of the waves produced by an earthquake decreases inversely with the distance from the focus, and that no disturbance is introduced by the nature of the buildings on which the instrument is mounted. It is then possible to make estimates of the position of the focus corresponding to any amplitude distribution. This procedure has been followed for all the shocks on which measurements have been made. The results are shown in the map in fig 10 in which the epicentres corresponding to the suggested foci for shocks which occurred between 11 May and 30 June are plotted as circles. The enclosed numbers give the order in which the shocks occurred. The epicentre is the point in the surface of the earth vertically above the focus.

The distribution of epicentres represented in fig 10 should be regarded as provisional only, since further experience and the additional results, which may be expected with the instruments now maintained in Montserrat, may lead to modifications. It is considered unlikely, however, that the results are seriously in error since there are relationships between the patterns corresponding to different foci which must be observed; the final allocation of epicentres must, in fact, satisfy the condition that there is no sudden change in the amplitude distribution in going from one to another of two neighbouring foci, and this condition must be

observed for the whole complex of suggested foci. The final result is therefore likely to be much more reliable than if no relationships were to be observed between the different foci, and it is probable that future revision will not seriously modify the general conclusions.

It will be seen that the epicentres of the earthquakes which occurred during the period March-July, 1936, lie in a broad belt running across the middle of the island in a direction N.E., between the Centre Hills and the Soufrière Hills. The epicentres show no tendency to cluster in the immediate neighbourhood of any of the active soufrières.

The accounts of individual observers and the distribution of damage suggests that the earthquake of 10 November, 1935, did not originate under the island.

#### 5—THE NATURE OF THE FOCI AND THE ORIGIN OF THE EARTHQUAKES

Hitherto we have treated the foci as points, and it remains to inquire to what extent this treatment is justified. The very large variations in the distribution of intensity of the tremors throughout the island during the whole of the present period of seismic activity show that we are dealing for the most part with what are technically described as "volcanic" earthquakes. The results suggest that the focal regions are restricted in comparison with the distance between stations. It would require a larger number of stations equipped with Jagger shock recorders than are at present in operation to prove this point definitely, but it is the view that is most probable and the one in best accord with the observations.

The accounts of individual observers and the experimental observations both demonstrate that the intensity of the shocks has varied over a large range during the present series. During the worst of the shocks it seems likely that vertical accelerations greater than that of gravity have occurred. In some volcanic regions such as Hawaii, earthquake "swarms" are generally associated with magma falling in the volcanic cone. On the other hand, the history of the seismo-volcanic events in the West Indian Islands suggests that in this region earthquakes generally occur at times when the magmatic pressure is increasing. It is therefore natural to assume that the earthquakes are to be associated in the present instance with magmatic intrusion at various points under the island. A final pronouncement on this point would be possible only after the seismic phenomena had been correlated with other observations such as those obtained with tilt meters.

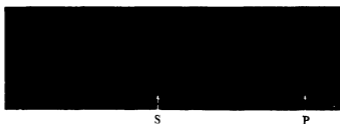


FIG. 3—Chile earthquake of 13 July, 1936



FIG. 4—Earthquake under sea between Montserrat and Antigua



FIG. 5—Local shocks. No resolution of S and P waves



FIG. 6—Shock similar to fig. 4



FIG. 7—Small spur representing P wave

Records from Wiechert Seismograph

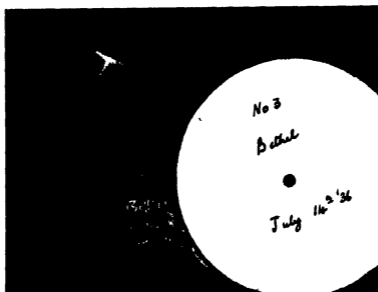


FIG 8—Single shock nearly full size



FIG 9—Complete record showing many shocks About 1/5 natural size

Records from Jaggar shock recorders

It is possible that at a certain point in the history of any one of the volcanoes in this region intrusion of magma may lead to a general strengthening of the volcanic edifice by a kind of "grouting" process, so that subsequently it is better able to resist the incidence of magmatic pressure. Such effects would explain the existence of several volcanic centres in the restricted area presented by the island of Montserrat. It may be pointed out here that the fact that the present foci are not exclusively and immediately associated with any old volcanic centre is no guarantee in itself that a new outbreak will not take place in or near the island. Since the island is made up of at least six old volcanoes, at least on five occasions an eruption has taken place from a new centre (see Mr. Macgregor's report)\* Mr. Macgregor informs me, however, that the outbreak of a new centre must be regarded as a very rare event compared with an eruption from an old one.

#### 6—VARIATION OF SEISMIC ACTIVITY WITH TIME

The variation with time in the daily number of observed tremors as recorded by the Curator at the Grove Botanical Station, fig 2, shows clearly the existence of the six monthly cycle, the times of increased activity in May being especially prominent.

A more detailed impression of the variation in activity can be obtained by making use of the results from the Jaggard shock recorders. In the curve showing the daily number of tremors no account is taken of the magnitude of the individual shocks, so that shocks varying in intensity several hundred-fold are represented in the same way. This difficulty can be overcome by plotting a quantity, the total daily seismic amplitude, instead of the daily number of recorded tremors. This quantity is defined as the sum of the amplitudes of the individual shocks occurring at a given station in a twenty-four hour period, the definition of amplitude being that given previously.

Such a curve is shown in fig. 12, and it will be seen that the increase in activity in the early part of May, 1936, is more marked than in figs 1 and 2. To judge from the accounts of the local observers, it is certain that in previous years also the shocks of greatest intensity occurred during times of greatest activity as measured by the daily number of shocks. Hitherto it has not been found possible to associate the variations in the seismic activity with any natural forces varying in intensity with a period of six months.

\* 'Proc Roy Soc,' B, vol 121, pp. 232-252 (1936).

## 7—CONCENTRATION OF SULPHUROUS GASES IN THE ATMOSPHERE

Estimates of the concentration of sulphur dioxide in the atmosphere at Plymouth, Montserrat, using a wet method depending on passing air through a solution of hyperol and estimating any resulting acid by titration against a standard alkali, gave negative results. The concentration of this gas in the atmosphere during the time of residence of members of the expedition must have been negligible.

The concentration of sulphuretted hydrogen at a variety of points was measured by a stain comparison method using lead acetate papers and

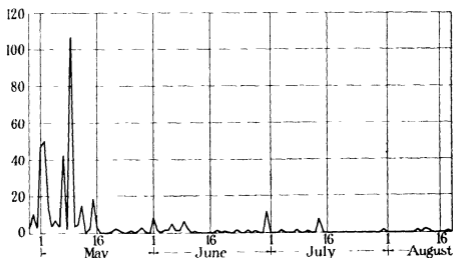


FIG. 12—Curve showing variation of daily seismic intensity with time

an air pump. A weekly routine of observations was established whereby the concentration of this gas at a number of defined points at different distances from the Gages Soufrière was measured. At the present time, the concentration increases as the soufrière is approached until, in the immediate neighbourhood of the gas and steam vents, it reaches a value of about one in five thousand. According to observations made by Perret, the rate of emission of gas is now much less than it was as recently as November, 1935. The decrease in the concentration as one recedes from the soufrière shows that the vents are now the only important source of the gas in this neighbourhood.

The marked odour which is sometimes perceived in Plymouth is not due to diffusion from the soufrière but results from the transport of "pockets" of highly charged air in relatively calm weather. It is thus that regions contaminated by gas are observed to be very localized. Even when the

odour of the gas is very pronounced in Plymouth, the concentration of the gas is sometimes less than one in ten million. In the neighbourhood of the *soufrières* the odour is not that which one usually associates with sulphuretted hydrogen. This may be due to the high concentration and the resulting fatigue in the olfactory organs.

#### 8—TEMPERATURE MEASUREMENTS

The temperature of the gases issuing from the region of the main vent at the Gages *Soufrière* have been continuously recorded on the Bristol thermograph installed by Mr Perret. Certain parts of this instrument have now been seriously affected by the continuous action of the hot gases, and the instrument has been put out of action. It is greatly to be hoped that it will be possible for Mr Perret to arrange for the replacement of these parts. In the meantime the temperatures of the gas vents are measured by hand thermometers during the weekly visit to the *soufrière*. During my residence in Montserrat the temperatures at these points remained close to the normal boiling point corresponding to the barometric pressure.

#### 9—GENERAL DISCUSSION

The decline in the seismic activity and the decrease in the rate of emission of gas from the Gages *Soufrière* following the severe earthquake of 10 November, 1935, suggest that the seismo-volcanic episode which has occurred in Montserrat during the past few years is now drawing to a close. Unless there is a marked recurrence in activity, the history of the whole episode will present many features in common with previous earthquake "swarms" both in this island and elsewhere. Thus, according to the reports of residents in Nevis, there were earthquakes in that island from February to June of 1930. The impressions of residents and the distribution of damage to buildings suggest that in this case also the earthquakes were very local in origin. The most disturbed regions were in the neighbourhood of Bath Village, near Charlestown, where there are hot springs and fumaroles with sulphur deposits. Previous to the eruption of Mt. Pelée and the *Soufrière* of St Vincent in 1902, there was an earthquake swarm in Montserrat which started in 1902 and ended at the time of the eruptions, but the descriptions of local residents suggest that in this case the foci were not situated immediately under the island. In the twelve months previous to the eruption of Mt. Pelée in 1851 there were many earthquakes in Guadeloupe. Thus although earthquake swarms in any island have not in

general been followed immediately by volcanic disturbance in that island, yet in several instances seismic disturbance at one point has been associated with volcanic disturbance elsewhere. The limited history of the Lesser Antilles of which we have record therefore suggests that the occurrence of earthquake swarms is evidence for the existence of unstable conditions in a common magma underlying the whole group, which may or may not lead to volcanic disturbance at some point or points in the chain.

The information which has been obtained during the present expedition has not been sufficient to enable us to make any prediction as to the likelihood or otherwise of the present earthquakes being followed in the near future by a volcanic event in Montserrat or elsewhere. Such a prediction could only legitimately be made on the basis of a real knowledge of the complex of interacting processes and conditions which together determine the occurrence of such events. Such knowledge can only be obtained by extended observations at a number of points in the Caribbean arc. I am in agreement with Mr Macgregor that the general decline in activity is reassuring and that there is probably no immediate cause for alarm, that whilst it is certain that the volcanic history of this region is not yet completed, so that an outbreak is likely to take place at some point at some indefinite time in the future, yet such an event is unlikely to occur without premonitory symptoms of which, at the present time in Montserrat, there is no evidence.

The general decline in activity, whilst reassuring, should not be allowed to lead to a too easy optimism. The French expedition to Mt Pelée following the eruption in 1851 stated that unless future eruptions of the volcano were on a much larger scale than the last the town of St. Pierre was in no danger. In their conclusion they state "Summing up, Mt. Pelée appears to be merely one more interesting curiosity added to the natural history of Martinique, a curiosity which foreigners will wish to visit and which, with fitting industry on the part of the natives, may be made a source of health and wealth."

Similar and disastrous predictions were made, Dr Jaggar informs me, during the course of the series of eruptions of Mt Pelée in 1902.

Our present knowledge of the seismo-volcanic phenomena in these islands is so limited that the establishment of a quite modest equipment of observing instruments might well lead to discoveries of considerable value. The organization which has been established in Montserrat could be regarded as a first step in the establishment of instruments at a number of points in the island chain and as an experiment in the maintenance of instruments in the hands of untrained observers and volunteers. The

establishment of such routine observations, even on the smallest scale, might well lead to the recognition of symptoms of any crisis earlier than would otherwise be possible and would provide important information for those responsible for the social organization necessary to meet such a crisis. Further, it is an excellent thing for the leading citizens to take an active and intelligent part, as volunteer operators of instruments, in the general organization of the scientific observations. The fruits of such observations may not be reaped for many years, but eventually they may lead to the saving of many hundreds of lives.

I am greatly indebted to Sir Gerald Lenox-Conyngham, Dr T. Jaggard, and Mr A G MacGregor for a number of discussions, and to Dr Whipple and members of the staff at Kew Observatory for advice on the erection and maintenance of the various seismographs. It was made possible for me to join the Expedition by the generous granting of leave of absence and financial assistance from the University of Bristol.

#### 10—SUMMARY

The decline in the seismic intensity which has followed the severe earthquake of 10 November, 1935, and the contemporary decrease in the rate of emission of gas from the Gages Soufrière, suggest that the seismo-volcanic episode in Montserrat during the last three years is now drawing to a close.

During 1934-36 there has been a marked tendency for times of pronounced activity, both in respect of the daily number of shocks and in the intensity of the worst shocks, to occur at approximately six monthly intervals, the months of greatest activity being May and November or December.

The earthquakes which took place in Montserrat between April and July, 1936, were highly local in origin, the foci in many cases being near the surface. They are properly described as "volcanic" earthquakes. There was a tendency for several earthquakes to originate at the same or at closely neighbouring foci. A preliminary analysis suggests that the epicentres corresponding to the foci lie in a broad belt running across the middle of the island in a N.E. direction and embracing St. George's Hill and parts of the Centre Hills and of the Soufrière Hills. Although there is no evidence that the earthquakes showed a tendency to originate in the immediate neighbourhood of any one of the active soufrières, yet almost all the foci were within a few kilometres of one or other of them. There is

thus a belt running across the island which shows evidence of both seismic and *soufrière* activity.

The present earthquake "storm" in Montserrat, whilst severe, is by no means a novel event in the geological history of the islands comprising the Caribbean arc. The earthquake "storm" in Nevis in 1930 presented many features in common with the present series in Montserrat although of much smaller intensity and of much shorter duration. The limited knowledge of these islands which has been accumulated during historic times suggests that an earthquake storm in one island is not in general followed by a volcanic outbreak in that island. Nevertheless, history suggests that such a storm is an indication of unstable magmatic conditions beneath the group as a whole and that this instability may lead to disturbance at some particular point or points.

The decline in seismic activity is reassuring, but predictions as to the likelihood or otherwise of the occurrence of earthquakes or volcanic events can only be made on the basis of a knowledge and understanding of the complex processes and conditions involved. At the present time our knowledge is rudimentary. I am in agreement with Mr Macgregor that there is probably no immediate cause for alarm; that it is unlikely that a volcanic outbreak would occur without premonitory symptoms, of which at the present time there is no evidence in Montserrat.

The knowledge necessary for a real understanding of the fundamental processes which are occurring can only be obtained by extended observations at a number of points in the Caribbean arc. Valuable information could be obtained in the first instance by a quite modest investigation. If the experiment of leaving the instruments in the care of untrained observers in Montserrat is successful, then similar equipment might be installed in other British islands in this region. In this way an organization could be built up which might, in time, be able to predict the nature and extent of any threatening catastrophe and which would make important contributions to the science of geophysics

---

## On the Thermal Decomposition of Methyl Nitrite

By A. G. CARTER, B Sc., and MORRIS W. TRAVERS, F R.S., Chemistry Department, University of Bristol.

(Received 7 September, 1936)

Steacie and Shaw\* have made a study of the thermal decomposition of a series of alkyl nitrites at temperatures between 170° and 240°. Their results are contained in the series of papers to which reference is made; but of these only the first is at present significant, for in it they consider the decomposition of methyl nitrite, and give their reasons for the conclusions which they arrive at regarding the nature of the decomposition process, which they assume to be common to the whole series. Their results led them to the conclusion that the decomposition process proceeds in accordance with the equation,



the process being of the first order. Assuming that this was so, the critical increment calculated from the temperature coefficient was found to be 36.4 kcal.

If the decomposition process really does take place in accordance with the equation written above, the conclusion that the process is unimolecular is confusing rather than helpful. It appeared possible that a study of the problem by methods more detailed than that applied by Steacie and Shaw might throw further light upon it, and with that object in view the present work was undertaken.

Steacie and Shaw's method consisted in heating the vapour of the nitrite in a pyrex bulb at constant temperature and measuring the rate of change of pressure. Certain samples were heated for such a time as was required for complete decomposition, when it was found that secondary reactions had taken place, an important by-product being carbon monoxide. They did not observe that nitrous oxide is also a by-product. A factor derived from these analytical results was used to correct the pressure observations.

The method used in this investigation, referred to as the *method of detailed analyses*, has been described in a series of papers published from this laboratory. An accurately measured quantity of the pure gas is

\* 'Proc. Roy. Soc.,' A, vol. 146, p. 388 (1934, a), 'J. Phys. Chem.,' vol. 2, p. 345 (1934, b); *ibid.*, vol. 3, p. 344 (1934, c), 'Proc. Roy. Soc.,' A, vol. 151, p. 658 (1935).

condensed in a reaction tube, which is of silica, and has been heated overnight to 500° C while full of hydrogen, and is then sealed. Preliminary experiments with pyrex glass tubes were found to give inconsistent results. After heating a tube for a definite time, and quenching it, the contents were analysed in the following manner.

The tube was connected through the apparatus for removing the contents\* with the Töpler pump. Mercury was used as a seal. After exhausting the apparatus, and allowing it to stand for half an hour for the absorption of traces of moisture, the tube containing pentoxide of phosphorus was cut out from the system, so that, on breaking off the point of the reaction tube, the gases did not come into contact with the pentoxide, which absorbs methyl nitrite. The gaseous content of the tube was then taken off in two fractions, the first while the tube was cooled with liquid oxygen and the second while it was cooled in solid carbon dioxide. Fraction I contained the whole of the carbon monoxide, and most of the nitric oxide, and fraction II a little of the nitric oxide, nitrous oxide, methyl nitrite, and probably some carbon dioxide. The second fraction was then condensed in the bulb of an apparatus for the fractionation of gaseous mixtures of the usual type, and condensed at liquid oxygen temperature. On connecting the bulb with the Töpler pump, a little more nitric oxide was removed, and added to the first fraction. This operation was repeated a considerable number of times, when, as a check experiment showed, the nitric oxide and carbon monoxide could be separated completely from the other gases.

The first fraction was measured, and then allowed to remain in contact with a mixture of metallic copper and copper oxide at 500° C for some hours, after which the gas was again measured, the carbon dioxide absorbed, and the residual nitrogen was measured. The analytical results showed that the gas was a mixture of carbon monoxide and nitric oxide, with not more than a very small trace of hydrogen, if any. We did not succeed in making an exact analysis of the second fraction, for we could find no reagent which would remove any one of the constituents and leave the others unchanged. Methyl nitrite is absorbed by a slightly acid solution of ferrous sulphate, and by repeated treatment with small quantities of the reagent, and with caustic soda, a small quantity of nitrous oxide was separated, but the solubility of this gas rendered quantitative separation by this method impossible. Quantities of methyl nitrite were treated for varying times at temperatures up to 100° C with solutions of caustic alkali, potassium permanganate, acid and potassium chromate, hydriodic acid, etc. However, it was found that when the

\* Sedden and Travers, 'Proc. Roy. Soc., A', vol. 156, p. 241 (1936).

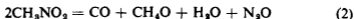
nitrite was attacked to any material extent, nitrous oxide was always formed. It was therefore only possible to burn the gas in the tube containing copper and copper oxide, and to determine the carbon and nitrogen content of the mixture.

Only one series of experiments was carried out with the silica tube, for these serve to demonstrate the nature of the changes taking place. The temperature was 200° C, which is in the middle of the range of Steacie and Shaw's experiments, and the initial concentration of the methyl nitrite was 0.02 gm. molecules per litre. The results are expressed in terms of gram atoms of carbon or nitrogen per litre.

The results are set down in Table I.

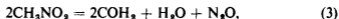
Time	Fraction I		Fraction II		
	C as CO	N as NO	C	N	Excess N as N <sub>2</sub> O
10	0.00002	0.00084	0.01849	—	—
12½	4	156	1773	0.01809	0.00036
15	7	298	1611	1665	54
20	13	362	1554	1633	74
22½	12	418	1398	1502	—
25	11	465	1383	1514	—
27	20	547	1322	1342	—
30	45	791	1195	1198	—
40	22	891	998	1085	—
45	33	952	860	1057	—
50	36	1090	672	920	—
60	38	1203	661	834	—
80	31	1496	406	490	—

The results are plotted in fig. 1. The form of the graph representing the rate of formation of nitric oxide is similar to that representing a number of similar thermal decomposition processes, the process being initially accelerated, and then coming momentarily to a standstill. The form of the graph representing the change of concentration of carbon monoxide in the gas, which is relatively very small, is peculiar, but may be accounted for by assuming that the compound suffers oxidation. The carbon monoxide may be formed either by the oxidation of formaldehyde, or, more probably, by a process represented by



However, if it is assumed that in the early stages of the process the only constituents of fraction II are methyl nitrite and nitrous oxide, the nitrous

oxide present (column 6) is much more than is necessary to account for the carbon monoxide formed, and it is necessary to assume that another process,



operates.

Even by detailed analysis, using the methods which we have described, it is not possible to do more than indicate the general course of the

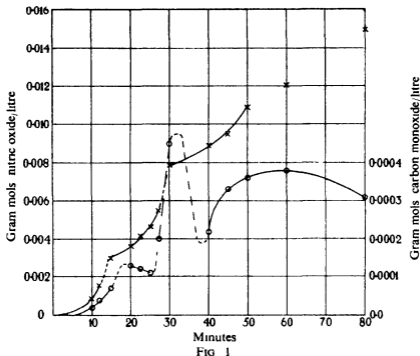


FIG. 1

processes involved in the thermal decomposition of methyl nitrite. The decomposition process seems to belong to a class of reactions in which the rates of decomposition are initially accelerated, the  $x-t$  graphs showing breaks of the kind indicated. In the sub-class to which the thermal decomposition of methyl nitrite belongs there seems generally to be two products, probably derived from a single short-lived intermediate, by reactions represented by equations (1) and (3) \*.

No useful purpose would be served in continuing a very difficult piece of work beyond the stage at which the general nature of the processes involved can be indicated, and at which it can be shown that there is no justification for the statement that it involves a first order reaction.

\* Travers and Sedden, 'Nature,' vol. 137, p. 906 (1936), Travers, 'Nature,' vol. 138, p. 26 (1936).

## Mechanism of the Production of Small Eddies from Large Ones

By G. I. TAYLOR, F.R.S., and A. E. GREEN, B.A.

(Received 12 October, 1936)

### INTRODUCTION

The connexion between the statistical representation of turbulence and dissipation of energy has been discussed\* in relation to the decay of the isotropic turbulence which is produced in a wind tunnel by means of regular grids. It was shown that a length  $\lambda$  can be defined which may be taken as a measure of the scale of the small eddies which are responsible for dissipation. This  $\lambda$  can be found by measuring the correlation  $R_y$  between the indications of two hot wire anemometers set at a distance  $y$  apart on a line perpendicular to the axis of the tunnel. Then

$$\frac{1}{\lambda^2} = \lim_{y \rightarrow 0} \frac{1 - R_y}{y^2},$$

and the mean rate of dissipation of energy per unit volume is

$$\bar{W} = 15 \mu \bar{u^2} / \lambda^2, \quad (1)$$

where  $\bar{u^2}$  is the mean of the square of one component of velocity.

When turbulence is generated in a wind stream by a grid of regularly spaced bars it may be expected to possess a definite scale proportional to the linear dimensions of the grid. In any complete statistical description of turbulence this scale must be implicitly or explicitly involved. One way in which the scale can be defined is to measure the distance  $y$  apart by which the two hot wires must be separated before the correlation between the indications disappears. Another way is to define the scale as

$$l_s = \int_0^y R_y dy \quad (2)$$

It is to be expected that if the turbulence is entirely produced by a regular grid (i.e., there is no turbulence in the stream before it reaches

\* Taylor, 'Proc. Roy. Soc.', A, vol. 151, p. 421 (1935)

the grid)  $l_2$  and  $y$  will be proportional to  $M$ , the mesh-length of the grid. In one set of experiments with a square-mesh grid it was found that

$$l_2 = 0.195M. \quad (3)$$

In these experiments,  $R_v$  was not determined accurately when its value was small, but the  $R_v$  curve seems to cut the axis  $R_v = 0$  at\*

$$y = \frac{1}{2}M. \quad (4)$$

It has not yet been shown experimentally whether these figures apply generally.

If the speeds all over a turbulent field are increased in the ratio  $m:1$  the Reynolds stresses increase in the ratio  $m^2:1$ , so that the rate of dissipation of energy increases in the ratio  $m^3:1$ . Now

$$\bar{W} = 15\mu\bar{u}^2/\lambda^2, \quad (5)$$

so that  $1/\lambda^2$  must increase in the ratio  $m:1$ . This result can be expressed by the formula

$$\frac{\lambda}{L} = \text{const} \sqrt{\frac{\nu}{u'L}}, \quad (6)$$

where  $L$  is a length representing the scale of the turbulence and  $u'^2 = \bar{u}^2$ . It has, in fact, been found in a large number of experiments on the rate of dissipation of energy in a stream behind regular square-mesh grids that

$$\frac{\lambda}{M} = 2.0 \sqrt{\frac{\nu}{u'M}}, \quad (7)$$

and if  $y = \frac{1}{2}M$  this may be written

$$\frac{\lambda}{y} = 1.41 \sqrt{\frac{\nu}{u'y}}, \quad (8)$$

or if  $l_2 = 0.195M$

$$\frac{\lambda}{l_2} = 0.88 \sqrt{\frac{\nu}{u'l_2}}. \quad (9)$$

Of these equivalent formulae (7) seems to be firmly established, but (8) and (9) depend on only one set of measurements.

\* See Taylor, 'Proc. Roy. Soc.' A, vol. 151, p. 445 (1935), Pt. II, fig. 1, where it will be seen that  $R_v$  tends to zero at  $y = 0.45$  inches when  $M = 0.9$  inches.

# OBJECT OF THE PRESENT WORK

The theory outlined above represents in a satisfactory manner the dissipation of energy in turbulent flow. The alternative formulae (7), (8), or (9) which relate the scale of the small scale turbulence to the main scale of turbulence are, however, quite empirical. They are merely the formulae which are necessary in order that the observed square law of resistance in turbulent fields may hold. They represent the effect of the fundamental process in turbulent flow, namely the grinding down of eddies produced by solid obstructions (and on a scale comparable with these obstructions) into smaller and smaller eddies until these eddies are of so small a scale that they die away owing to viscosity more rapidly than they are produced by the grinding down process.

To explain this process is, perhaps, the fundamental problem in turbulent motion. It seems clear that it is intimately associated with diffusion. Suppose that eddying motion of some definite scale is generated in a non-viscous fluid. Consider two particles A, B situated on the same vortex line in a turbulent field of flow and separated initially by a small distance  $d_0$ .

If the turbulence is diffusive, in the sense that a concentrated collection of particles spreads into a diffuse cloud (and turbulence is always found to be diffusive), the average distance  $d$  between pairs of particles like A and B increases continually.

If the fluid were non-viscous the continual increase in the average value of  $d^2$  would necessarily involve a continual increase in  $\omega^2$ ,  $\omega$  being the resultant vorticity at any point. In fact, the equation for conservation of circulation in a non-viscous fluid is

$$\frac{\omega}{d} = \frac{\omega_0}{d_0} \quad \text{or} \quad \frac{\omega^2}{d^2} = \frac{\omega_0^2}{d_0^2}, \quad (10)$$

where  $\omega_0$  is the initial resultant vorticity when  $d = d_0$ . Hence  $\omega^2$  increases continually as  $d^2$  increases.

The mean rate of dissipation of energy in a viscous fluid is

$$\bar{W} = \mu (\bar{\epsilon}^2 + \bar{\eta}^2 + \bar{\zeta}^2) = \mu \bar{\omega}^2, \quad (11)$$

so that if turbulence is set up in a slightly viscous fluid by the formation of large scale eddies (e.g., as in a wind tunnel when the wind meets a large scale obstruction) we may expect first an increase in  $\bar{\omega}^2$  in accordance with (10).

When  $\bar{\omega}^2$  has increased to some value which depends on the viscosity,

it is no longer possible to neglect the effect of viscosity in the equation for the conservation of circulation, so that (10) ceases to be true. Experiment shows, in fact, that in a wind tunnel  $\bar{W}$  reaches the definite value indicated by (5) and (6).

It is difficult to express these ideas in a mathematical form without assuming some definite form for the disturbance, but it is almost impossible to suggest an initial form which has the characteristics of the statistical isotropic turbulent motion to which (5) and (6) apply. Accordingly, we have searched for types of initial motion which have a definite scale and also have some of the properties of statistically uniform isotropic turbulence with a view to tracing the subsequent motion and finding out whether anything analogous to the process of the grinding down into smaller and smaller eddies occurs.

At the outset the extreme limitations of mathematical methods are very evident, for it is only in special cases where the initial motion is such that one of the essential features of turbulent motion (*i.e.*, extension along vortex lines) is absent that the subsequent motion has so far been calculated. By far the largest class of fields of flow which has been analysed mathematically is two-dimensional. Since the vortex lines are then perpendicular to the plane of motion, they are not extending, and this essential characteristic of turbulent flow is therefore absent.

The largest class of three-dimensional motions which has been solved is the irrotational motions of a non-viscous fluid. Here again there are no vortex lines, so that no motions of this type are significant in connexion with turbulence. Another class of motions which can be treated by existing methods is deviations from states of rest or steady motion. Such motions are only significant in discussing the first beginning of turbulence arising in a steady flow.

#### DECAY OF A SPECIAL CLASS OF VORTICES

It appears that nothing but a complete solution of the equations of motion in some special case will suffice to illustrate the process of grinding down of large eddies into smaller ones. In the following pages an attempt is made to trace the subsequent motion of a viscous incompressible fluid when the initial motion is represented by

$$\left. \begin{aligned} u &= A \cos ax \sin by \sin cz \\ v &= B \sin ax \cos by \sin cz \\ w &= C \sin ax \sin by \cos cz \end{aligned} \right\} \quad (12)$$

These equations are consistent if

$$Aa + Bb + Cc = 0 \quad (13)$$

One equation of motion is

$$-\frac{\partial u}{\partial t} = u \frac{\partial u}{\partial x} + v \frac{\partial u}{\partial y} + w \frac{\partial u}{\partial z} + \frac{1}{\rho} \frac{\partial P}{\partial x} - \nu \nabla^2 u, \quad (14)$$

if, therefore,  $\partial P / \partial x$  is known when the initial velocity components are known, the initial value of  $\partial u / \partial t$  is known, and it is possible to take the first step in a step-by-step solution

Eliminating  $\partial u / \partial t$ ,  $\partial v / \partial t$ ,  $\partial w / \partial t$  between the three equations of motion and the equation of continuity,

$$-\frac{1}{\rho} \nabla^2 P = \left( \frac{\partial u}{\partial x} \right)^2 + \left( \frac{\partial v}{\partial y} \right)^2 + \left( \frac{\partial w}{\partial z} \right)^2 + 2 \left( \frac{\partial v}{\partial x} \frac{\partial u}{\partial y} + \frac{\partial w}{\partial y} \frac{\partial v}{\partial z} + \frac{\partial u}{\partial z} \frac{\partial w}{\partial x} \right) \quad (15)$$

Hence, substituting for  $\partial u / \partial x$ ,

$$-\frac{1}{\rho} \nabla^2 P = \frac{1}{2} \sum_{xyz} A^2 a^2 (\cos 2by \cos 2cz - \cos 2ax) \quad (16)$$

The periodic solution of (16) is

$$\frac{P}{\rho} = \frac{1}{8} \sum_{xyz} A^2 \left( \frac{a^2}{b^2 + c^2} \cos 2by \cos 2cz - \cos 2ax \right) \quad (17)$$

Substituting for  $u$ ,  $v$ ,  $w$  and  $P$  from (12) and (17) in (14) gives the initial value of  $\partial u / \partial t$  as

$$\begin{aligned} \frac{\partial u}{\partial t} = & -\theta \nu A \cos ax \sin by \sin cz + \frac{A_2}{a} \sin 2ax \cos 2by \\ & - \frac{A_2}{a} \sin 2ax \cos 2cz, \end{aligned} \quad (18)$$

where

$$\theta = a^2 + b^2 + c^2 \quad (19)$$

and the constants  $A_2$ ,  $A_3$  are obtained by cyclic permutation of the letters  $a$ ,  $b$ ,  $c$  from a constant  $A_1$  where

$$A_1 = \frac{b}{4} \left( A^2 b \frac{a^2}{b^2 + c^2} + ABa \right) = -\frac{c}{4} \left( A^2 c \frac{a^2}{b^2 + c^2} + ACa \right) \quad (20)$$

The initial values of  $\partial v / \partial t$ ,  $\partial w / \partial t$  are obtained from (18) by simultaneous cyclic permutation of the letters  $a$ ,  $b$ ,  $c$  and  $x$ ,  $y$ ,  $z$ .

## FIRST APPROXIMATION

The first approximation to the value of  $u$  after time  $t$  is obtained from (18) by a simple integration. It is

$$u = A (1 - \theta \nu t) \cos ax \sin by \sin cz + \frac{A_1}{a} t \sin 2ax \cos 2by - \frac{A_2}{a} t \sin 2ax \cos 2cz \quad (21)$$

with corresponding values for  $v, w$ .

## SUCCESSIVE APPROXIMATIONS

Since all the terms in  $u$  given by (21) are the same type as those in the original  $u$ , namely

$$\left\{ \begin{matrix} \cos \\ \sin \end{matrix} \right\} l a x \left\{ \begin{matrix} \cos \\ \sin \end{matrix} \right\} m b y \left\{ \begin{matrix} \cos \\ \sin \end{matrix} \right\} n c z, *$$

the same process may be applied to find  $u$  to a second approximation when the value of  $u$  is taken to be that given by (21) instead of the original  $u$ . By successive repetitions the complete solution could be obtained for the motion which ensues when the flow represented by (12) is established at time  $t = 0$ . The resulting expressions for  $u, v, w$  will consist entirely of terms of the type

$$\left\{ \begin{matrix} \cos \\ \sin \end{matrix} \right\} l a x \left\{ \begin{matrix} \cos \\ \sin \end{matrix} \right\} m b y \left\{ \begin{matrix} \cos \\ \sin \end{matrix} \right\} n c z,$$

multiplied by a power series of the type  $A_0 + A_1 t + A_2 t^2 + \dots$ . In fact, if a solution of the type

$$\begin{pmatrix} u \\ v \\ w \end{pmatrix} = \begin{pmatrix} {}_0A_{lmn}^{CAC} + {}_1A_{lmn}^{CAC} t + {}_2A_{lmn}^{CAC} t^2 + \dots \\ {}_0B_{lmn}^{CAC} + {}_1B_{lmn}^{CAC} t + {}_2B_{lmn}^{CAC} t^2 + \dots \\ {}_0C_{lmn}^{CAC} + {}_1C_{lmn}^{CAC} t + {}_2C_{lmn}^{CAC} t^2 + \dots \end{pmatrix} \left\{ \begin{matrix} \cos \\ \sin \end{matrix} \right\} l a x \left\{ \begin{matrix} \cos \\ \sin \end{matrix} \right\} m b y \left\{ \begin{matrix} \cos \\ \sin \end{matrix} \right\} n c z \quad (22)$$

is assumed and  $\partial u / \partial t, \partial v / \partial t, \partial w / \partial t$  are calculated as explained above, and equated to the values obtained by differentiating (22) with respect to  $t$ , the coefficients of

$$t^r \left\{ \begin{matrix} \cos \\ \sin \end{matrix} \right\} l a x \left\{ \begin{matrix} \cos \\ \sin \end{matrix} \right\} m b y \left\{ \begin{matrix} \cos \\ \sin \end{matrix} \right\} n c z$$

\*  $l, m, n$ , integers.

on the two sides can then be equated and the coefficients  $\rho A_{lmn}^{csc}$  determined. The upper suffices  $c, s, c$  are used to show which of the two alternatives sine or cosine occurs in the Fourier term, and the meaning of the other suffices is obvious. Thus the coefficient of

$$t^r \cos lax \sin mby \cos ncz$$

would be  $\rho A_{lmn}^{csc}$ .

## SECOND APPROXIMATION

The above process will now be examined in more detail. The first approximation to  $u$  is already given in (21). The second application of the process gives the following expression for  $u$  as a second approximation, namely

$$\begin{aligned} u = & \delta_1 \cos ax \sin by \sin cz + \frac{x_3}{a} \sin 2ax \cos 2by - \frac{x_2}{a} \sin 2ax \cos 2cz \\ & + \frac{\alpha_1}{3} \cos 3ax \sin by \sin cz + \gamma_2 \cos ax \sin 3by \sin cz \\ & + \beta_3 \cos ax \sin by \sin 3cz + \frac{y_3}{a} \cos 3ax \sin 3by \sin cz \\ & - \frac{y_2}{a} \cos 3ax \sin by \sin 3cz + \frac{L_1}{2} \sin 4ax \cos 2by \cos 2cz \\ & + N_2 \sin 2ax \cos 4by \cos 2cz + M_3 \sin 2ax \cos 2by \cos 4cz \end{aligned} \quad (23)$$

As before,  $v, w$  are obtained from  $u$  by simultaneous permutation of  $a, b, c; x, y, z$ , and the suffices 1, 2, 3. The coefficients are

$$\left. \begin{aligned} \delta_1 &= A \left( 1 - \theta vt + \frac{1}{2} \theta^2 v^2 t^2 \right) - \frac{1}{2a} (CcA_3 - BbA_2) \left( \frac{1}{2} t^2 - \frac{1}{3} \theta vt^3 \right) \\ x_1 &= A_1 \left( t - \theta vt^2 + \frac{1}{3} \theta^2 v^2 t^3 \right) - 2A_1 (b^2 + c^2) vt^2 \\ &\quad - \frac{A_2 A_3}{3} \left( \frac{b^2 - c^2}{b^2 + c^2} \right) t^3 \\ y_1 &= \frac{1}{2} \left( \frac{1}{2} t^2 - \frac{1}{3} \theta vt^3 \right) A_1 A_a \\ \frac{\alpha_1}{3} &= - \left( \frac{1}{2} t^2 - \frac{1}{3} \theta vt^3 \right) \left( \frac{6a \{ A_3 (Aa - Bb) + A_2 (Cc - Aa) \}}{9a^2 + b^2 + c^2} \right. \\ &\quad \left. - AA_3 + AA_2 - \frac{1}{2} A_2 \frac{Cc}{a} + \frac{1}{2} A_3 \frac{Bb}{a} \right) \\ \beta_1 &= - \left( \frac{1}{2} t^2 - \frac{1}{3} \theta vt^3 \right) \left( \frac{2b \{ A_3 (Aa - Bb) + A_2 (Cc - Aa) \}}{9a^2 + b^2 + c^2} \right. \\ &\quad \left. + \frac{1}{2} \frac{a}{b} AA_3 + \frac{1}{2} BA_2 \right) \end{aligned} \right\} \quad (24)$$

$$\left. \begin{aligned} \gamma_1 &= -\left(\frac{1}{2}t^2 - \frac{1}{3}\theta vt^3\right) \left( \frac{2c\{A_3(Aa - Bb) + A_2(Cc - Aa)\}}{9a^2 + b^2 + c^2} \right. \\ &\quad \left. - \frac{1}{2}\frac{a}{c}AA_2 - \frac{1}{2}CA_3 \right) \\ \frac{L_1}{2} &= -\frac{1}{3}t^3 \left( \frac{4a}{4a^2 + b^2 + c^2} - \frac{2}{a} \right) A_2A_3 \\ M_1 &= -\frac{1}{3}t^3 \left( \frac{2b}{4a^2 + b^2 + c^2} + \frac{1}{b} \right) A_2A_3 \\ N_1 &= -\frac{1}{3}t^3 \left( \frac{2c}{4a^2 + b^2 + c^2} + \frac{1}{c} \right) A_2A_3 \end{aligned} \right\} \begin{array}{l} (24) \\ (\text{cont}) \end{array}$$

the coefficients with suffices 2, 3 being obtained by cyclic permutation of the letters  $a, b, c$ . These coefficients are not all independent but are connected by the following relations

$$a\delta_1 + b\delta_2 + c\delta_3 = 0 \quad (25)$$

$$a\alpha_1 + b\beta_1 + c\gamma_1 = 0, \quad (26)$$

with two similar relations obtained by cyclic permutation, and

$$aL_1 + bM_1 + cN_1 = 0, \quad (27)$$

with two similar relations as before

We have obtained the third approximation for  $u, v, w$  in the general case, but it is too long to set out here. In order to give some idea of the length of the work, it is sufficient to say that the expression for  $u$  consists of 518 terms of the type

$$P(t) \left( \frac{\cos}{\sin} \right) l_1 ax \pm \left( \frac{\cos}{\sin} \right) l_2 ax \left( \frac{\cos}{\sin} \right) m_1 by \pm \left( \frac{\cos}{\sin} \right) m_2 by \\ \times \left( \frac{\cos}{\sin} n_1 cz \pm \left( \frac{\cos}{\sin} \right) n_2 cz \right),$$

where  $l_1, l_2, m_1, m_2, n_1, n_2$  are integers or zero and  $P(t)$  is a power series in  $t$ . At this stage it seems impossible to obtain significant results in the general case when the initial motion is represented by (12), so attention is now confined to a special case

#### SPECIAL CASE

The special case which is considered is when  $a = b = c$ ,  $A = -B$ , and  $C = 0$ . Equation (13) is then satisfied, while (19) and (20) give

$$\theta = 3a^2, \quad A_1 = -A_2 = -\frac{1}{8}A^2a^2; \quad A_3 = 0. \quad (28)$$

The expressions in (24) reduce to

$$\left. \begin{aligned} \delta_3 = x_3 = y_3 = \alpha_3 = L_1 = M_1 = N_1 = L_2 = M_2 = N_2 = 0 \\ \delta_1 = -\delta_2 = A \left( 1 - 3a^2vt + \frac{9}{2}a^4v^2t^2 \right) + \frac{1}{2}AA_1 \left( \frac{1}{2}t^2 - a^2vt^3 \right) \\ x_1 = -x_2 = A_1 \left( t - 7a^2vt^2 + 3a^4v^2t^3 \right) \\ \frac{1}{2}\alpha_1 = -\frac{1}{2}\alpha_2 = -\beta_1 = -\gamma_1 = \beta_2 = \gamma_2 = \frac{15}{22}AA_1 \left( \frac{1}{2}t^2 - a^2vt^3 \right) \\ -\beta_3 = \gamma_3 = \frac{y_1}{a} = \frac{y_2}{a} = \frac{1}{2}AA_1 \left( \frac{1}{2}t^2 - a^2vt^3 \right) \\ -\frac{1}{2}L_3 = M_3 = N_3 = \frac{4}{9}\frac{A_1^2}{a}t^3 \end{aligned} \right\} \quad (29)$$

Before proceeding any further, it is necessary to recall that we are seeking an expression for the mean rate of dissipation of energy  $\bar{W}$  and

$$\frac{\bar{W}}{\mu} = \bar{\xi}^2 + \bar{\eta}^2 + \bar{\zeta}^2, \quad (30)$$

where  $\xi$ ,  $\eta$ ,  $\zeta$  are the components of vorticity and the mean value is taken throughout each cubical volume in which the initial motion lies. The only terms which contribute to this mean value are those of the type  $\left\{ \frac{\cos^2}{\sin^2} \right\} \lambda ax \left\{ \frac{\cos^2}{\sin^2} \right\} mby \left\{ \frac{\cos^2}{\sin^2} \right\} ncx$ , which have a mean value of  $1/8$ . The mean value of each of the "cross terms" in  $\bar{\xi}^2$ ,  $\bar{\eta}^2$ ,  $\bar{\zeta}^2$  is zero. Now, it can be seen that the first application of the above process for finding  $\partial u/\partial t$ ,  $\partial v/\partial t$ ,  $\partial w/\partial t$  or, in other words, the first approximation to  $u$ ,  $v$ ,  $w$  at time  $t$ , gives  $u$ ,  $v$ ,  $w$  correct to the first power of  $t$ . The second approximation gives  $u$ ,  $v$ ,  $w$  correct to  $t^2$  and so on. In general the  $r$ th repetition of the process or the  $r$ th approximation gives  $u$ ,  $v$ ,  $w$  correct to  $t^r$ . So that after the third approximation we can at once obtain the value of  $\bar{W}$  correct to  $t^3$ . If, however, the expression (23) for  $u$  is examined, it will be seen that the terms whose coefficients are  $L_1$ ,  $M_1$ ,  $N_1$ , have  $t^3$  as the lowest power of  $t$ , and, further, that any terms, besides those given in (23), which are introduced during the third and succeeding approximations will not contain powers of  $t$  less than  $t^3$ . The first eight terms in the expressions for  $u$ ,  $v$ ,  $w$  are therefore the only terms which contribute to  $\bar{W}$  when developed as far as terms in  $t^6$ . However, in order to obtain  $\bar{W}$  to this approximation, it is not necessary to obtain all of these eight terms correct to  $t^6$ . It is sufficient to obtain the first term of  $u$ ,  $v$ ,  $w$  correct to  $t^6$ , the next two terms correct to  $t^4$ , and the next five terms correct to  $t^3$ .

After the third approximation, the first eight terms are known correct to  $t^8$ , and it would appear that two further repetitions of the process are necessary in order to obtain the first three terms to the required order. It will be shown in the following pages that it is not necessary to do this owing to the fact that only the first eight terms of  $u, v, w$  as set forth in (23) make any contribution to the first term, to the order  $t^6$ , and to the next two terms, to the order  $t^4$ , however many repetitions of the process are made.\*

After the third approximation, let the coefficients which are given in (29) be represented by the same letters with dashes,  $e.g.$ ,  $\delta_1$  now becomes  $\delta'_1$ . These new coefficients are then given by the following expressions

$$\left. \begin{aligned} \frac{d\delta'_1}{dt} &= -\frac{d\delta'_2}{dt} = \frac{1}{2} \delta_1 x_1 - \lambda_1 (\gamma_2 + \frac{1}{2} \beta_4) - \theta v \delta_1 \\ \frac{dx'_1}{dt} &= -\frac{dx'_2}{dt} = -\frac{1}{8} a^2 \delta_1^2 - a^2 \delta_1 \left( \frac{y_2}{4a} + \frac{\alpha_1}{12} + \frac{\gamma_2}{4} \right) + 8a^2 v x_2 \end{aligned} \right\} \quad (31)$$

and

$$\left. \begin{aligned} \frac{1}{2} \alpha'_1 &= -\frac{1}{2} \alpha'_2 = -\beta'_1 = -\gamma'_1 = \beta'_2 = \gamma'_2 \\ &= \frac{15}{22} A A_1 \left( \frac{1}{2} t^2 - \frac{31}{6} a^2 v t^3 \right) \\ -\beta'_3 &= \gamma'_3 = \frac{1}{2} A A_1 \left( \frac{1}{2} t^2 - \frac{31}{6} a^2 v t^3 \right) \\ \gamma'_1 &= \gamma'_2 = \frac{1}{2} A A_1 a \left( \frac{1}{2} t^2 - \frac{13}{2} a^2 v t^3 \right) \end{aligned} \right\} \quad (32)$$

The coefficients  $\delta_3, x_3, y_3, \alpha_3$  remain zero throughout. Substituting the expressions (29) in (31) and integrating it is found that

$$\begin{aligned} \delta'_1 = -\delta'_2 &= A \left\{ 1 - 3a^2 v t + \frac{1}{2} t^2 \left( 9a^4 v^2 - \frac{1}{16} A^2 a^2 \right) \right. \\ &\quad \left. - \frac{1}{3} t^3 \left( \frac{27}{2} a^6 v^3 - \frac{23}{32} a^4 v A^2 \right) \right. \\ &\quad \left. + \frac{1}{4} A_1 t^4 \left( \frac{A^2 a^2}{88} + \frac{63}{4} a^4 v^2 \right) - \frac{1}{8} t^5 \left( \frac{9}{88} a^4 v A^2 + \frac{81}{4} a^6 v^3 \right) \right\} \end{aligned} \quad (33)$$

\* Contributions to the first three terms arise from the product terms in the equations of motion. The last three terms of (23), together with any further terms that arise during the third and succeeding approximations, either give no term of the required type when forming products with the first eight terms of (23) or if they give terms of the required type their coefficients are of a higher order of  $t$  than is required. This is true for the general case as well as in the particular case we are considering.

and

$$x'_1 = -x'_2 = A_1 \left\{ t - 7a^2vt^2 + \frac{74}{3}a^4v^2t^3 - \frac{43}{44 \cdot 12}A^2a^2t^3 + \frac{5}{44} \frac{43}{16}A^2a^4vt^4 - \frac{51}{4}a^6v^3t^4 \right\} \quad (34)$$

In (33) powers of  $t$  above  $t^5$  are neglected and in (34) powers of  $t$  above  $t^4$  are neglected, but in both cases the expressions are only correct as far as  $t^3$ .

Now let the coefficients  $\delta'_1, \delta'_2, x'_1, x'_2$  be denoted by  $\delta''_1, \delta''_2, x''_1, x''_2$  after the fourth approximation. Expressions for these latter coefficients can then be obtained by adding a dash to each coefficient in the relations (31). If now the expressions (32), (33), and (34) be substituted in the right-hand side of the resulting equations and one integration is performed, we obtain

$$\begin{aligned} \delta''_1 = -\delta''_2 = A \left\{ 1 - 3a^2vt + \frac{1}{2}t^2(9a^4v^2 - \frac{1}{16}A^2a^2) \right. \\ \left. - \frac{1}{3}t^3(\frac{27}{2}a^6v^3 - \frac{23}{32}a^4vA^2) \right. \\ \left. + \frac{1}{4}t^4(\frac{31}{132}\frac{A^4a^4}{64} - \frac{185}{48}A^2a^6v^2 + \frac{27}{2}a^8v^4) \right. \\ \left. + \frac{1}{5}A_1t^5\frac{39}{44}\frac{39}{32}A^2a^4v - \frac{1171}{16}a^6v^3 \right\}, \quad (35) \end{aligned}$$

and

$$x''_1 = -x''_2 = A_1 \left\{ t - 7a^2vt^2 + \frac{74}{3}a^4v^2t^3 - \frac{43}{44 \cdot 12}A^2a^2t^3 + \frac{43}{44}A^2a^4vt^4 - \frac{175}{3}a^6v^3t^4 \right\} \quad (36)$$

The coefficients  $x''_1, x''_2$  are now obtained to the required order, but we must go one step further with  $\delta''_1, \delta''_2$ . Let the fifth approximation to these latter coefficients be noted by  $\delta'''_1, \delta'''_2$ . These are obtained from  $\delta''_1, \delta''_2$  in exactly the same way as  $\delta''_1, \delta''_2$  were obtained from  $\delta'_1, \delta'_2$ . The values of  $\delta'''_1, \delta'''_2$ , which are correct to the order  $t^5$ , are

$$\begin{aligned} \delta'''_1 = -\delta'''_2 = A \left\{ 1 - 3a^2vt + \frac{1}{2}t^2(9a^4v^2 - \frac{1}{16}A^2a^2) \right. \\ \left. - \frac{1}{3}t^3(\frac{27}{2}a^6v^3 - \frac{23}{32}a^4vA^2) \right. \\ \left. + \frac{1}{4}t^4(\frac{31}{132}\frac{A^2a^4}{64} - \frac{185}{48}A^2a^6v^2 + \frac{27}{2}a^8v^4) \right. \\ \left. - \frac{1}{3}t^5(\frac{555}{44}\frac{39}{32}\frac{A^4a^4v}{8} - \frac{2575}{192}A^2a^6v^3 + \frac{81}{8}a^{10}v^5) \right\}. \quad (37) \end{aligned}$$

The final expressions for  $u, v, w$  which will give the value of the mean rate of dissipation of energy  $\bar{W}$  correct to the order  $r^6$  are

$$u = \delta'''_1 \cos ax \sin ay \sin az - \frac{x''_3}{a} \sin 2ax \cos 2az \\ + \frac{\alpha'_1}{3} \cos 3ax \sin ay \sin az + \gamma'_2 \cos ax \sin 3ay \sin az \\ + \beta'_3 \cos ax \sin ay \sin 3az - \frac{y'_3}{a} \cos 3ax \sin ay \sin 3az \quad (38)$$

$$v = \delta'''_2 \sin ax \cos ay \sin az + \frac{x''_1}{a} \sin 2ay \cos 2az \\ + \frac{\alpha'_2}{3} \sin ax \cos 3ay \sin az + \gamma'_3 \sin ax \cos ay \sin 3az \\ + \beta'_1 \sin 3ax \cos ay \sin az + \frac{y'_1}{a} \sin ax \cos 3ay \sin 3az, \quad (39)$$

and

$$w = \frac{x''_2}{a} \cos 2ax \sin 2az - \frac{x''_1}{a} \cos 2ay \sin 2az \\ + \gamma'_1 \sin 3ax \sin ay \cos az + \beta'_2 \sin ax \sin 3ay \cos az \\ + \frac{y'_2}{a} \sin 3ax \sin ay \cos 3az - \frac{y'_1}{a} \sin ax \sin 3ay \cos 3az, \quad (40)$$

the coefficients being given by (32), (36), and (37)

#### RESULTS IN NON-DIMENSIONAL FORM

It is now convenient to express the velocity components in a non-dimensional form Put

$$T = Aat \quad R = A/av, \quad (41)$$

then  $R$  is a Reynolds number and

$$\left. \begin{aligned} \frac{1}{2} \alpha'_1 = -\frac{1}{2} \alpha'_2 = -\beta'_1 = -\gamma'_1 = \beta'_2 = \gamma'_2 \\ = -\frac{15}{176} A \left( \frac{1}{2} T^2 - \frac{31}{6} \frac{T^3}{R} \right) \\ -\beta'_3 = \gamma'_3 = -\frac{1}{16} A \left( \frac{1}{2} T^2 - \frac{31}{6} \frac{T^3}{R} \right) \\ y'_1 = y'_2 = -\frac{1}{16} Aa \left( \frac{1}{2} T^2 - \frac{13}{2} \frac{T^3}{R} \right) \end{aligned} \right\} \quad (42)$$

$$x''_1 = -x''_2 = -\frac{1}{8} Aa \left\{ T - \frac{7T^2}{R} + \left( \frac{74}{3R^2} - \frac{43}{44} \frac{1}{R} \right) T^3 \right. \\ \left. - \left( \frac{175}{3R^2} - \frac{43}{44} \right) \frac{T^4}{R} \right\}, \quad (43)$$

and

$$\begin{aligned} \delta''_1 = -\delta''_2 = A \left\{ 1 - \frac{3T}{R} + \left( \frac{9}{R^2} - \frac{1}{16} \right) \frac{T^2}{2} - \left( \frac{27}{2R^3} - \frac{23}{32} \right) \frac{T^3}{3R} \right. \\ \left. + \left( \frac{31}{132} - \frac{185}{48R^2} + \frac{27}{2R^4} \right) \frac{T^4}{4} \right. \\ \left. - \left( \frac{555}{44} - \frac{32}{32} - \frac{2575}{192R^2} + \frac{81}{8R^4} \right) \frac{T^5}{5R} \right\} \quad (44) \end{aligned}$$

The formula (1) is true for isotropic turbulence. In our present problem, where the turbulence is not isotropic, it seems reasonable to replace  $\overline{u^2}$ , which is the mean value of the square of one component of velocity in the case where all three are equal, by

$$\overline{u_1^2} = \frac{1}{3} (\overline{u^2} + \overline{v^2} + \overline{w^2}) \quad (45)$$

Using expressions (38), (39), and (40) for  $u, v, w$  where the coefficients of the terms are given by (42), (43), and (44), we obtain, after some calculation,

$$\frac{\overline{W}}{\mu} = \frac{3A^2 a^2}{4} W', \quad (46)$$

where

$$\begin{aligned} W' = 1 - \frac{6T}{R} + \left( \frac{5}{48} + \frac{18}{R^2} \right) T^2 - \left( \frac{5}{3} + \frac{36}{R^2} \right) \frac{T^3}{R} \\ + \left( \frac{50}{99} - \frac{64}{9} + \frac{1835}{16R^2} + \frac{54}{R^4} \right) T^4 \\ - \left( \frac{361}{44} - \frac{761}{12R^2} + \frac{324}{5R^4} \right) \frac{T^5}{R}. \quad (47) \end{aligned}$$

The expression for  $W'$  is correct to  $T^5$ . In the same way the value of  $\overline{u_1^2}$  can be obtained correct to the order  $T^5$ . It is, however, possible to obtain  $\overline{u_1^2}$  correct to  $T^6$  by making use of the energy equation

$$\overline{W} = -\frac{1}{2\rho} \frac{d\overline{u_1^2}}{dt}$$

which can be expressed as

$$\frac{\overline{W}}{\mu} = -\frac{3}{2} a^2 R \frac{d\overline{u_1^2}}{dT}. \quad (48)$$

From (46), (47), and (48) the value of  $\overline{u_1^2}$  correct to  $T^6$  is given by

$$\overline{u_1^2} = \frac{A^2}{12} u'^2, \quad (49)$$

where

$$\begin{aligned}
 u'^2 = & 1 - \frac{6T}{R} + \frac{18T^2}{R^2} - \left( \frac{5}{24} + \frac{36}{R^2} \right) \frac{T^3}{R} + \left( \frac{5}{2R^2} + \frac{54}{R^4} \right) T^4 \\
 & - \left( \frac{5}{44} - \frac{12}{24R^2} + \frac{367}{24R^3} + \frac{4}{5R^4} \right) \frac{T^5}{R} \\
 & + \left( \frac{361}{44} - \frac{32}{32} + \frac{761}{12R^2} + \frac{324}{5R^4} \right) \frac{T^6}{R^2}
 \end{aligned} \quad (50)$$

A check on the work is provided by the fact that the first five terms in (50) agree with those obtained by direct calculation of  $u_1'^2$ . Also for a non-viscous fluid where  $1/R = 0$  it is at once verified that  $u_1'^2$  remains constant for all time

#### NUMERICAL DISCUSSION

The equations (47) and (50) contain the information which is required. They express, in fact, the way in which  $\bar{W}$  and  $\bar{u}_1'^2$  change with time when the eddies represented by (12) are started at time  $T = 0$ . Since, however, (47) and (50) contain only terms up to  $T^5$  and  $T^6$  respectively, they cease to be valid representations of the flow when  $T$  is too great. In the following tables the terms in (47) and (50) have been calculated for increasing values of  $T$  for the following values of  $R$ —20, 50, 100, 200, 300.

The values of  $W'$  and  $u'^2$ , so far as they are represented by the approximations (47) and (50), are given in Tables I–V. These tables are not carried beyond the values of  $T$  for which the approximation is likely to be reasonably good, but calculations were made using the approximate expressions (47) and (50) beyond the limit of  $T$ , at which they can be regarded as reasonably accurate, because it is thought that the results may have at least a qualitative interest.

In fig. 1 the values of  $W'$  for increasing values of  $T$  are shown by means of five curves, one for each of the chosen values of  $R$ . Each curve is marked with a full line as far as the terms are given in Tables I–V and a broken line for the higher values of  $T$ , for which the approximation of (47) and (50) may be taken as of qualitative value only.

Initially  $W'$  begins to decrease, but when  $R \geq 100$  this decrease is very small and  $W'$  subsequently increases. The broken line indicates that at a time which depends on  $R$ ,  $W'$  reaches a maximum and afterwards begins to decrease. This decrease is, no doubt, due to the fact that  $u'^2$ , *i.e.*, the total energy of the eddies, is decreasing continually from the start, so that even though  $\lambda$ , the scale of the smallest eddies, may be

TABLE I\*

R = 300

$$W' = 1 - 0.02T + 0.10436T^2 - 0.0055568T^3 + 0.0080329T^4 \\ - 0.00085702T^5$$

$$u'^2 = 1 - 0.02T + 0.0002T^2 - 0.0006957T^3 + 0.000027784T^4 \\ - 0.000032132T^5 + 0.0000028567T^6$$

T	Values of individual terms						Total W'
	0.02T	T <sup>2</sup>	T <sup>3</sup>	T <sup>4</sup>	T <sup>5</sup>		
0.5	0.01	0.02609	0.0007	0.0005	—		1.0159
1.0	0.02	0.1043	0.0055	0.0080	0.0008		1.0859
1.5	0.03	0.2348	0.0187	0.0407	0.0065		1.2202
2.0	0.04	0.4175	0.0444	0.1285	0.0274		1.4341
2.5	0.05	0.6523	0.0868	0.3138	0.0837		1.7455
3.0	0.06	0.9393	0.1500	0.6507	0.2082		2.1717
3.5	0.07	1.2785	0.2382	1.2055	0.4501		2.7256

T	0.02T	T <sup>2</sup>	T <sup>3</sup>	T <sup>4</sup>	T <sup>5</sup>	T <sup>6</sup> *	u' <sup>2</sup>	λa/π
0.5	0.01	—	—	—	—	—	0.9899	0.4055
1.0	0.02	0.0002	0.0007	—	—	—	0.9795	0.3905
1.5	0.03	0.0004	0.0023	0.0001	0.0002	—	0.9680	0.3660
2.0	0.04	0.0008	0.0055	0.0004	0.0010	0.0002	0.9548	0.3352
2.5	0.05	0.0012	0.0109	0.0011	0.0031	0.0007	0.9390	0.3015
3.0	0.06	0.0018	0.0189	0.0022	0.0078	0.0021	0.9195	0.2675
4.0	0.08	0.0032	0.0445	0.0071	0.0329	0.0117	0.8645	0.2068
5.0	0.10	0.0050	0.0869	0.0173	0.1005	0.0446	0.7795	0.1597
6.0	0.12	0.0072	0.1502	0.0360	0.2500	0.1333	0.6563	0.1242

\* The coefficients of T<sup>2</sup> to T<sup>6</sup> at the head of the columns of figures are omitted. The upper set of figures are the values of the terms of W' for various values of T, the lower set of figures are the values of the terms of u'<sup>2</sup>.

decreasing or constant  $\bar{W} = 15\mu\bar{u}^2/\lambda^2$  decreases. It will be seen in fig. 1 that if  $R < 50$ , W' is never greater than its initial value 1.0.

#### COMPARISON BETWEEN CALCULATED $\lambda$ AND THAT OBSERVED IN TURBULENT FLOW

The value of  $\lambda$  may be calculated from (1), but in order to express it in a non-dimensional form so that it may be comparable with that which

TABLE II

R = 200

$$W' = 1 - 0.03T + 0.104616T^2 - 0.00833783T^3 + 0.0082099T^4 \\ - 0.0012899T^5$$

$$u'^2 = 1 - 0.03T + 0.00045T^2 - 0.00104616T^3 + 0.0000625337T^4 \\ - 0.00004926T^5 + 0.0000064496T^6$$

T	0.03T	T <sup>2</sup>	T <sup>3</sup>	T <sup>4</sup>	T <sup>5</sup>	W'
0.2	0.006	0.0042	0.0001	—	—	0.9975
0.4	0.012	0.0167	0.0005	0.0002	—	1.0044
1.0	0.030	0.1046	0.0083	0.0082	0.0013	1.0732
1.5	0.045	0.2354	0.0281	0.0415	0.0098	1.1940
2.0	0.060	0.4185	0.0667	0.1313	0.0413	1.3819
2.5	0.075	0.6539	0.1303	0.3207	0.1260	1.6433
3.0	0.090	0.9416	0.2251	0.6650	0.3134	1.9780

T	0.03T	T <sup>2</sup>	T <sup>3</sup>	T <sup>4</sup>	T <sup>5</sup>	T <sup>6</sup>	u' <sup>2</sup>	λa/π
1.0	0.030	0.0004	0.0010	0.0001	—	—	0.9694	0.3910
1.5	0.045	0.0010	0.0035	0.0003	—	—	0.9527	0.3671
2.0	0.060	0.0018	0.0084	0.0010	0.0015	0.0004	0.9333	0.3379
2.5	0.075	0.0028	0.0163	0.0024	0.0048	0.0016	0.9107	0.3060
3.0	0.090	0.0041	0.0282	0.0051	0.0119	0.0047	0.8836	0.2748
4.0	0.120	0.0072	0.0669	0.0160	0.0504	0.0264	0.8122	0.2214
5.0	0.150	0.0112	0.1308	0.0391	0.1540	0.1008	0.7163	0.1854

occurs in the turbulence produced by a grid of regular bars of mesh-length  $M$ , for which  $\lambda$  has been measured, it is necessary to consider how the wave-length of the periodic disturbance (12) may be expected to compare with the mesh-length  $M$  of the grid which produces the turbulence. One obvious standard of comparison is the distance apart of two points where the correlation between the velocities is zero. In the case of the periodic eddies (12), this is obviously one-quarter of the wave-length, *i.e.*,  $\pi/2a$ , while in the case of the turbulence produced by a regular grid of mesh-length  $M$  it is  $\frac{1}{2}M$ \*. Thus we may take

$$\frac{\pi}{2a} = \frac{M}{2} \text{ or } M = \pi/a, \quad (51)$$

\* See (4), p. 500

TABLE III

R = 100

$$W' = 1 - 0.06T + 0.10596T^2 - 0.0167T^3 + 0.009166T^4 - 0.002627T^5$$

$$u'^2 = 1 - 0.06T + 0.0018T^2 - 0.002119T^3 + 0.0002505T^4 - 0.00011T^5 + 0.00002627T^6$$

T	0.06T	T <sup>2</sup>	T <sup>3</sup>	T <sup>4</sup>	T <sup>5</sup>	W'
0.6	0.036	0.0381	0.0036	0.0012	0.0002	0.9995
1.0	0.060	0.1059	0.0167	0.0091	0.0026	1.0358
1.5	0.090	0.2384	0.0564	0.0464	0.0199	1.1185
2.0	0.120	0.4238	0.1336	0.1467	0.0841	1.2328
2.5	0.150	0.6622	0.2610	0.3581	0.2566	1.3527
3.1	0.186	1.0181	0.4976	0.8465	0.7522	1.4288

T	0.06T	T <sup>2</sup>	T <sup>3</sup>	T <sup>4</sup>	T <sup>5</sup>	T <sup>6</sup>	u' <sup>2</sup>	λa/π
1.0	0.060	0.0018	0.0022	0.0003	0.0001	—	0.9399	0.3915
1.5	0.090	0.0041	0.0071	0.0013	0.0008	0.0003	0.9077	0.3705
2.0	0.120	0.0072	0.0168	0.0040	0.0035	0.0017	0.8726	0.3460
2.5	0.150	0.0113	0.0328	0.0098	0.0107	0.0064	0.8339	0.3228
3.1	0.186	0.0173	0.0626	0.0231	0.0315	0.0233	0.7836	0.3043
3.6	0.216	0.0233	0.0980	0.0421	0.0665	0.0572	0.7421	0.3072
4.0	0.240	0.0288	0.1344	0.0641	0.1126	0.1076	0.7134	0.3405

TABLE IV

$$W' = 1 - 0.12T + 0.11136T^2 - 0.033621T^3 + 0.012997T^4 - 0.0056355T^5$$

$$u'^2 = 1 - 0.12T + 0.0072T^2 - 0.0044546T^3 + 0.0010086T^4 - 0.00031193T^5 + 0.00011271T^6$$

T	0.12T	T <sup>2</sup>	T <sup>3</sup>	T <sup>4</sup>	T <sup>5</sup>	W'
0.6	0.072	0.0401	0.0073	0.0017	0.0004	0.9621
1.0	0.120	0.1113	0.0336	0.0130	0.0056	0.9651
1.5	0.180	0.2505	0.1135	0.0658	0.0428	0.9801
1.6	0.192	0.2851	0.1377	0.0852	0.0591	0.9815
2.0	0.240	0.4454	0.2690	0.2080	0.1803	0.9641

T	0.12T	T <sup>2</sup>	T <sup>3</sup>	T <sup>4</sup>	T <sup>5</sup>	T <sup>6</sup>	u' <sup>2</sup>	λa/π
0.6	0.072	0.0026	0.0009	0.0001	—	—	0.9298	0.4040
1.0	0.120	0.0072	0.0044	0.0010	0.0003	0.0001	0.8837	0.3930
1.5	0.180	0.0162	0.0150	0.0051	0.0024	0.0013	0.8252	0.3770
1.6	0.192	0.0184	0.0182	0.0066	0.0032	0.0019	0.8135	0.3743
2.0	0.240	0.0288	0.0356	0.0161	0.0100	0.0072	0.7665	0.3665
2.4	0.284	0.0415	0.0616	0.0335	0.0248	0.0215	0.7261	0.3745

TABLE V

$$R = 20$$

$$W' = 1 - 0.3T + 0.14916T^2 - 0.08783T^3 + 0.040086T^4$$

$$- 0.020767T^5$$

T	0.3T	T <sup>2</sup>	T <sup>3</sup>	T <sup>4</sup>	T <sup>5</sup>	W'
0.2	0.06	0.0059	0.0007	—	—	0.9453
0.6	0.18	0.0537	0.0189	0.0052	0.0016	0.8583
1.0	0.30	0.1492	0.0878	0.0401	0.0207	0.7806
1.5	0.45	0.3356	0.2963	0.2028	0.1577	0.6344

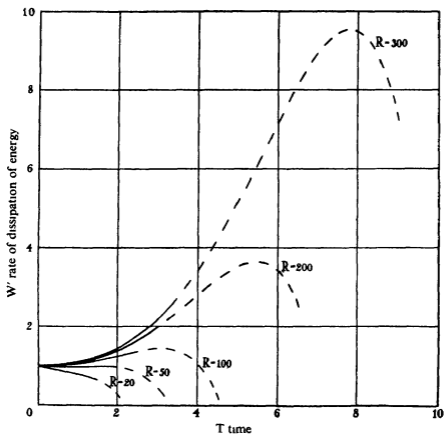


FIG. 1

and we may therefore compare  $\lambda/M$  measured in a wind tunnel with the calculated values of  $\lambda a/\pi$ .

The calculated values of  $\lambda a/\pi$  are given in Tables I-IV, and they are shown graphically in fig. 2. The initial value of  $\lambda a/\pi$  is 0.41 whatever the value of  $R$  may be. For very low values of  $R$  the decay of energy would be exponential,\* corresponding to the constant value of

$$\lambda a/\pi = 0.41$$

For larger values of  $R$ ,  $\lambda a/\pi$  decreases with the time, but the indications of the broken lines, particularly in the cases of  $R = 50$  and  $R = 100$ , seem to suggest that  $\lambda a/\pi$  would not decrease indefinitely

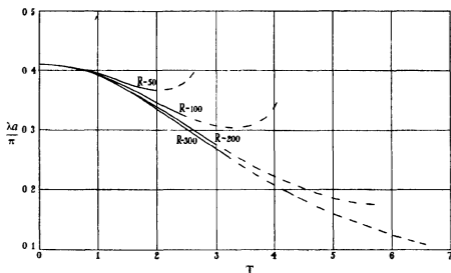


FIG. 2

For comparison with observation, it must be remembered that  $\lambda/M$  has been found experimentally to be  $2.0 \sqrt{\frac{\nu}{M \nu \bar{u}^3}}$ . To compare the observed rate of dissipation with that calculated, it is necessary to compare  $\lambda/M$  with  $\lambda a/\pi$  when the total energy of the turbulence is the same in the two cases, i.e.,  $\bar{u}^2$  in the wind tunnel must be taken as  $\bar{u}_1^2 = \frac{A^2}{12} \bar{u}^2$ †. Then, since  $M$  is comparable with  $\pi/a$  and  $R = A/a\nu$ , we must compare

\* This is easily shown by using (5) with the energy equation.

† See (45) and (49).

$\frac{\nu}{M\sqrt{u^2}}$  with  $\frac{\sqrt{12}}{\pi R u'}$ . The ordinates of the curve (fig 3) in which the comparison between observation and the present calculations is made may be taken as

$$\left. \begin{aligned} R' &= \frac{\pi R}{\sqrt{12}} u' \text{ for the calculated points} \\ \text{or} \quad R' &= \frac{M\sqrt{u^2}}{\nu} \text{ for the observed points} \end{aligned} \right\} \quad (52)$$

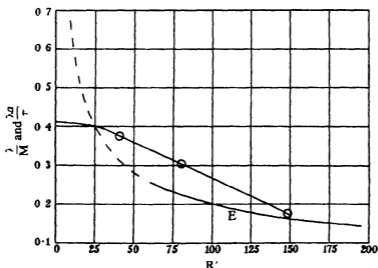


FIG 3—E, experimental curve, O, calculated points.

and then the experimental formula (7) for  $\lambda/M$  becomes

$$\frac{\lambda}{M} = 2.0 \sqrt{\frac{\nu}{M\sqrt{u_1^2}}} = 2.0 (R')^{-1}.$$

The calculated values of  $\lambda a/\pi$  corresponding to the maximum  $\bar{W}$  are shown in fig 3. It will be seen that provided  $R' > 25$  the calculated values of  $\lambda a/\pi$  are in good agreement, so far as order of magnitude is concerned, with the formula deduced from observation.

#### LOWER LIMIT OF APPLICATION OF (7)

In the work on dissipation it was suggested that formula (7) would only hold provided  $\frac{M\sqrt{u^2}}{\nu}$  is less than 60. The corresponding value of  $R'$  is

60, and the part of the observed curve which falls below this is marked by a broken line

#### UPPER LIMIT OF $R$ FOR EXPONENTIAL DECAY OF TURBULENCE

The lower limit below which formula (7) may be expected to hold is necessarily above the highest value of  $R$  for which  $\lambda$  does not appreciably decrease after the motion is started, i.e., it is above the range for which the decay is exponential.

To find this limit the rate of decay may be calculated on the assumption that  $\lambda a/\pi$  has its initial value 0.41. If  $W'_{\max}$  is the maximum value of

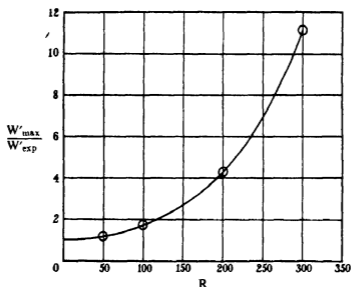


FIG. 4

$W'$ , as shown in fig 1, we may calculate  $W'_{\max} / W'_{\exp}$  where  $W'_{\exp}$  is the value which  $W'$  would have, assuming exponential decrement at the time corresponding with  $W'_{\max}$ . The increase of  $W'_{\max} / W'_{\exp}$  above its value for  $R \rightarrow 0$ , namely 1.0, then represents, qualitatively at any rate, the effect we are discussing, namely the decrease in  $\lambda$  due to increase in the mean square of the vorticity.

The values of  $W'_{\max} / W'_{\exp}$  are shown in fig 4. It will be seen that up to  $R = 50$  the effect is very small, the increase being only 19% at  $R = 50$ . Above  $R = 50$  the effect rapidly increases

## LOCAL INCREASE IN VORTICITY

The progressive increase in the mean square of the vorticity which the present investigation reveals is due to comparatively large local increases in vorticity in certain parts of the field. One region where the vorticity increases is along the axis  $y = 0, z = 0$ . Taking the case when  $1/R = 0$ , i.e., the fluid is non-viscous, we may take the component  $\xi$  where  $\xi = \frac{\partial w}{\partial y} - \frac{\partial v}{\partial z}$ .

If we use the formula correct to  $T^3$ , then

$$\frac{\xi}{Aa} = \left(1 + \frac{3}{32} T^2\right) \sin ax - \frac{T^2}{32} \sin 3ax$$

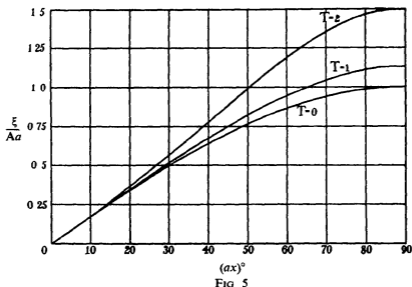


FIG. 5

The values of  $\xi/Aa$  are shown in fig. 5 as functions of  $ax$  for various values of  $T$ . It will be seen that at  $ax = \frac{1}{2}\pi$  the value of  $\xi/Aa$  increases 50% between  $T = 0$  and  $T = 2$ .

## APPENDIX

In the text only those terms necessary for calculation of  $\bar{W}$  and  $\bar{u}_1^2$  are given.

The complete expressions for  $u, v, w$  for the particular case considered were, however, calculated correct to  $T^3$ . They are

$$\begin{aligned}
 u = & \delta'''_1 \cos ax \sin ay \sin az + \frac{x''_3}{a} \sin 2ax \cos 2ay - \frac{x''_2}{a} \sin 2ax \cos 2az \\
 & + \frac{\alpha'_1}{3} \cos 3ax \sin ay \sin az + \gamma'_2 \cos ax \sin 3ay \sin az \\
 & + \beta'_3 \cos ax \sin ay \sin 3az + \frac{y'_3}{a} \cos 3ax \sin 3ay \sin az \\
 & - \frac{y'_2}{a} \cos 3ax \sin ay \sin 3az + \frac{L'_1}{2} \sin 4ax \cos 2ay \cos 2az \\
 & + N'_2 \sin 2ax \cos 4ay \cos 2az + M'_3 \sin 2ax \cos 2ay \cos 4az \\
 & + z_1 \sin 2ax \cos 2ay \cos 2az + \frac{u_3}{a} \sin 4ax \cos 4ay \\
 & - \frac{u_2}{a} \sin 4ax \cos 4az + \frac{2G_3}{a} \sin 2ax \cos 4ay - \frac{G_2}{a} \sin 4ax \cos 2az \\
 & + \frac{H_3}{a} \sin 4ax \cos 2ay - \frac{2H_2}{a} \sin 2ax \cos 4az \\
 & + \frac{J_3}{a} \sin 4ax \cos 4ay \cos 2az - \frac{J_2}{a} \sin 4ax \cos 2ay \cos 4az,
 \end{aligned}$$

with two similar expressions for  $v, w$  obtained by cyclic permutation of  $x, y, z$  and the suffices 1, 2, 3. In addition to the coefficients already defined and evaluated in (24), (29), etc., the following values complete the solution correct to  $T^3$ .

$$\begin{aligned}
 L'_1 = L'_2 &= -\frac{AT^3}{99}, & M'_1 = N'_2 &= \frac{49AT^3}{66 \cdot 24 \cdot 8}, \\
 M'_2 = N'_1 &= \frac{79AT^3}{66 \cdot 24 \cdot 8}, \\
 \frac{1}{2}L'_3 &= -M'_3 = -N'_3 = -\frac{AT^3}{96}, \\
 z_1 = z_2 &= -\frac{1}{2}z_3 = -\frac{19AT^3}{396 \cdot 8}, \\
 u_1 = -u_2 &= -\frac{AaT^3}{192}, & u_3 &= 0, \\
 H_1 = -G_2 &= \frac{27AaT^3}{440 \cdot 8}, \\
 H_2 = H_3 = -G_1 &= -G_3 = \frac{AaT^3}{384}, \\
 J_1 = -J_2 &= -\frac{AaT^3}{384}, & J_3 &= 0.
 \end{aligned}$$

## Motion of an Infinite Elliptic Cylinder in Fluids with Constant Vorticity

By MANOHAR RAY, M.Sc., Research Scholar, Calcutta University

(Communicated by M. N. Saha, F.R.S.—Received 20 August, 1936)

### 1—INTRODUCTION

An extension of Kirchhoff's theory of the motion of solid bodies in irrotationally moving liquids to the case of motion in liquids in which a vorticity is present does not exist. Only a few isolated cases of such motion are known. Bearing on the consideration of this paper, there is an important work by Taylor\* which expresses the additional pressure effect on a system of cylinders moving in a perfect liquid without rotation when the whole system is rotated uniformly about an axis. Taylor's theory reduces the problem of such motion to one of irrotational motion. In the present paper the motion of a perfect liquid having constant vorticity, and in which a cylinder of any cross-section is moving in any manner, has been considered. The pressure integral can be obtained in a simple form, referred to axes fixed in the body, which is very suitable for calculation. It is shown, whenever the pure potential motion of the liquid for the rotation of the cylinder and the solution of a definite potential problem or the corresponding Green's function can be found, the formula can be applied to calculate the motion of the cylinder in liquids with constant vorticity. Two important cases of constant vorticity are uniform shear motion along a direction and uniform rotation about an axis. In the present paper the former case is considered in detail for an elliptic cylinder. The case of uniform rotation being covered by Taylor's result it is only verified that the present method gives the same result as Taylor's formulae. There are some simple free motions of an elliptic cylinder in a liquid with uniform shear motion which have been discussed in the paper.

### 2—EQUATIONS OF MOTION REFERRED TO AXES FIXED IN THE BODY AND THE PRESSURE INTEGRAL

It is first necessary to write down the equations of motion referred to a system of axes fixed in the body having both translation and rotation. These equations are obtained below following a method of Taylor

\* 'Proc. Roy. Soc.' A, vol. 93, p. 99 (1917)

Let  $(x_0, y_0)$  be the coordinates relative to fixed axes  $OX_0, OY_0$  through  $O$  a fixed origin, of a point  $C$  of the cross-section at any instant,  $Cx, Cy$  be the positions of the axes in the body at that instant. Let  $(xy)$  be the coordinates of any point  $P$  of the fluid relative to  $Cx, Cy$  so that if  $x', y'$  be the coordinates of  $P$  relative to  $OX_0, OY_0$  then

$$\left. \begin{aligned} x' &= x_0 + x \cos \theta - y \sin \theta, \\ y' &= y_0 + x \sin \theta + y \cos \theta, \end{aligned} \right\} \quad (1)$$

where  $\theta$  is the angle between  $Cx$  and  $OX_0$  at that instant. Let  $(uv)$  be the velocity of the fluid at  $P$  relative to  $Cx, Cy$ . Now if  $v_x$  represents the component of velocity of the fluid at  $P$  in the direction  $\chi$  referred to fixed axes  $OX_0, OY_0$ , then the equation of motion is

$$-\frac{1}{\rho} \frac{\partial p}{\partial s_x} = \frac{Dv_x}{Dt}, \quad (2)$$

where  $ds_x$  represents an element of length in the direction  $\chi$  and

$$v_x = x_0 \cos \chi + y_0 \sin \chi + u \cos (\chi - \theta) + v \sin (\chi - \theta) \quad (3)$$

Now  $Dv_x/Dt$  may be written as

$$\frac{\delta v_x}{\delta t} + (x_0 + u \cos \theta - v \sin \theta) \frac{\partial v_x}{\partial x'} + (y_0 + u \sin \theta + v \cos \theta) \frac{\partial v_x}{\partial y'},$$

where  $\delta v_x/\delta t$  represents the rate of change in  $v_x$  at a point fixed in space.

From (1) we have

$$\frac{\partial}{\partial x'} = \cos \theta \frac{\partial}{\partial x} - \sin \theta \frac{\partial}{\partial y}, \quad \frac{\partial}{\partial y'} = \sin \theta \frac{\partial}{\partial x} + \cos \theta \frac{\partial}{\partial y} \quad (4)$$

Also if  $\delta x, \delta y$  are the changes in coordinates of a fixed point in time  $\delta t$

$$\frac{\delta v_x}{\delta t} = \frac{\partial v_x}{\partial t} + \frac{\partial v_x}{\partial x} \frac{\delta x}{\delta t} + \frac{\partial v_x}{\partial y} \frac{\delta y}{\delta t}, \quad (5)$$

where  $\partial v_x/\partial t$  represents the rate of change of  $v_x$  at a point fixed relative to the moving axes.

Now

$$\frac{\delta x}{\delta t} (= \dot{x}), \quad \frac{\delta y}{\delta t} (= \dot{y}),$$

are the rates of change in  $x$  and  $y$  due to the motion of the moving axes  $Cx, Cy$  and can be obtained by differentiating (1) and putting  $x'$  and  $y'$  zero.

That is

$$x_0 + x \cos \theta - x \sin \theta \theta - y \sin \theta - y \cos \theta \theta = 0,$$

$$y_0 + x \sin \theta + x \cos \theta \theta + y \cos \theta - y \sin \theta \theta = 0,$$

whence

$$-(x_0 \cos \theta + y_0 \sin \theta) = x - y\theta, \quad -(y_0 \cos \theta - x_0 \sin \theta) = y + x\theta.$$

Thus

$$\begin{aligned} \frac{\delta v_x}{\delta t} = \frac{\partial v_x}{\partial t} - (x_0 \cos \theta + y_0 \sin \theta - y\theta) \frac{\partial v_x}{\partial x} \\ + (x_0 \sin \theta - y_0 \cos \theta - x\theta) \frac{\partial v_x}{\partial y} \end{aligned} \quad (6)$$

From (4) and (6) we have

$$\frac{DV_x}{Dt} = \frac{\partial v_x}{\partial t} + (u + y\theta) \frac{\partial v_x}{\partial x} + (v - x\theta) \frac{\partial v_x}{\partial y}, \quad (7)$$

and using (3) we get finally

$$\begin{aligned} \frac{DV_x}{Dt} = x_0 \cos \chi + y_0 \sin \chi + \frac{\partial u}{\partial t} \cos (\chi - \theta) + u\theta \sin (\chi - \theta) \\ + \frac{\partial v}{\partial t} \sin (\chi - \theta) - v\theta \cos (\chi - \theta) \\ + (u + y\theta) \left\{ \frac{\partial u}{\partial x} \cos (\chi - \theta) + \frac{\partial v}{\partial x} \sin (\chi - \theta) \right\} \\ + (v - x\theta) \left\{ \frac{\partial u}{\partial y} \cos (\chi - \theta) + \frac{\partial v}{\partial y} \sin (\chi - \theta) \right\} \end{aligned} \quad (8)$$

The equations of motion referred to axes fixed in the body can now be obtained from (2) and (8) by putting  $\chi = \theta$  and  $\theta + \frac{\pi}{2}$  as follows,

$$\left. \begin{aligned} -\frac{1}{\rho} \frac{\partial p}{\partial x} &= x_0 \cos \theta + y_0 \sin \theta + \frac{\partial u}{\partial t} - v\theta + (u + y\theta) \frac{\partial u}{\partial x} + (v - x\theta) \frac{\partial u}{\partial y}, \\ -\frac{1}{\rho} \frac{\partial p}{\partial y} &= -x_0 \sin \theta + y_0 \cos \theta + \frac{\partial v}{\partial t} + u\theta + (u + y\theta) \frac{\partial v}{\partial x} + (v - x\theta) \frac{\partial v}{\partial y}. \end{aligned} \right\} \quad (9)$$

To integrate these equations we take along with them the equation of continuity

$$\frac{\partial u}{\partial x} + \frac{\partial v}{\partial y} = 0, \quad (10)$$

which is satisfied by

$$u = -\frac{\partial \psi}{\partial y}, \quad v = \frac{\partial \psi}{\partial x}, \quad (11)$$

where  $\psi$  is the stream-function.

Again, if  $\zeta$  be the vorticity

$$\zeta = \frac{\partial v}{\partial x} - \frac{\partial u}{\partial y}, \quad (12)$$

and if  $\zeta$  be absolutely constant

$$\frac{\partial}{\partial x} \left( \frac{\partial v}{\partial t} \right) - \frac{\partial}{\partial y} \left( \frac{\partial u}{\partial t} \right) = 0$$

Thus

$$-\frac{\partial u}{\partial t} = \frac{\partial}{\partial x} \left( \frac{\partial \phi}{\partial t} \right) \quad \text{and} \quad -\frac{\partial v}{\partial t} = \frac{\partial}{\partial y} \left( \frac{\partial \phi}{\partial t} \right), \quad (13)$$

where  $\partial \phi / \partial t$  is a certain function of  $x, y, t$ , so that from (11) and (13)

we at once see that  $\frac{\partial}{\partial t} (\phi + iy\psi)$  is a function of the complex variable

$x + iy^*$ . This consideration determines  $\partial \phi / \partial t$  when  $\psi$  is known

With the above substitutions we can at once integrate (9) and get

$$\begin{aligned} \frac{p}{\rho} = \frac{\partial \phi}{\partial t} - (x_0 \cos \theta + y_0 \sin \theta) \lambda - (y_0 \cos \theta - x_0 \sin \theta) y \\ - \frac{1}{2} q^2 + \zeta \psi - \frac{1}{2} \zeta \theta (x^2 + y^2) + \theta \left( x \frac{\partial \psi}{\partial \lambda} + y \frac{\partial \psi}{\partial y} \right), \end{aligned} \quad (14)$$

where  $q$  is the velocity

A form\* of this integral referred to fixed axes is known, but the present one is far more suitable for calculation

The next step in the solution is the determination of the stream-function  $\psi$ , and in all cases where this function can be found further progress can be made in the way of determining the pressure and the motion of the body.

### 3—SOME TYPICAL APPLICATIONS

It is of some interest to consider if there is any connexion of this  $\psi$  function with the  $\psi$  function for the irrotational motion when the cylinder is moving in analogous manner in the liquid at rest at infinity. As the axes are fixed in the body if  $\theta$  be the instantaneous angular rotation of the cylinder the  $\psi$  function will have to satisfy

$$\nabla^2 \psi = 2\pi, \quad (15)$$

\* Lamb, "Hydrodynamics," 6th ed., p. 233.

everywhere in the liquid, on the cylinder

$$\psi = \frac{1}{2}\theta (x^2 + y^2) + \text{const}, \quad (16)$$

and at infinity  $\psi$  should satisfy the given condition of motion. If we call  $\psi_3$  the stream-function satisfying this last condition at infinity, then since the vorticity is uniform we must have

$$\nabla^2 \psi_3 = 2\omega. \quad (17)$$

If the boundary of the cylinder at the instant be  $f = 0$ , let  $\psi_3$  on  $f = 0$  at the instant be called  $\psi_3'$ . Let  $\psi_1$  be the stream-function for the irrotational motion of the liquid referred to our axes when the cylinder has only angular rotation  $\theta$ . Then  $\nabla^2 \psi_1 = 0$  in the liquid,

$$\psi_1 = \frac{1}{2}\theta (x^2 + y^2) + \text{const}$$

on  $f = 0$ , and  $\psi_1 = 0$  at infinity

Now consider the two-dimensional space outside  $f = 0$ . Take the potential function  $\psi_2$  which satisfies the equation

$$\nabla^2 \psi_2 = 0,$$

in the region outside the cylinder has the value  $-\psi_3'$  on  $f = 0$  and vanishes at infinity

$\psi_2$  is thus made to depend on the Green's function for the corresponding potential problem

The solution of our problem satisfying the conditions (15) and (16) is

$$\psi = \psi_1 + \psi_2 + \psi_3, \quad (20)$$

since this satisfies (15) and (16) on  $f = 0$  on account of (18) and also the given condition of motion at infinity. Hence the stream-function of our problem is obtained by the superposition of the stream-functions of the given motion (at infinity), of the irrotational motion due to instantaneous rotation only of the cylinder and of the potential function of the above boundary problem

#### 4—STREAM-FUNCTION FOR AN ELLIPTIC CYLINDER IN CASES OF UNIFORM SHEAR

Let us now consider an elliptic cylinder moving in a liquid whose undisturbed motion is a laminar one parallel to  $OX_0$  with constant vorticity  $2\omega$ . Let  $C$  be the centre of the elliptic cross-section and the axes of the ellipse be chosen axes fixed in the body. Let the orientation

of these axes in space be given by the angle  $\theta$  which the major axis of the ellipse makes with the fixed axis  $OX_0$ . The stream-function for the undisturbed motion found at a great distance from the cylinder, relative to the instantaneous positions of the moving axes at C is given by, taking the direction of shear to be in the negative  $x$ -direction,

$$\begin{aligned}-\frac{\partial \psi_0}{\partial y} &= -2\pi y' \cos \theta - (x_0 \cos \theta + y_0 \sin \theta) \\ &= -2\pi (y_0 \cos \theta + x \sin \theta \cos \theta + y \cos^2 \theta) \\ &\quad - (x_0 \cos \theta + y_0 \sin \theta), \\ \frac{\partial \psi_0}{\partial x} &= 2\pi (y_0 \sin \theta + x \sin^2 \theta + y \sin \theta \cos \theta) - (y_0 \cos \theta - x_0 \sin \theta),\end{aligned}$$

this is satisfied by

$$\begin{aligned}\psi_0 &= 2\pi y_0 (y \cos \theta + x \sin \theta) + \pi (y \cos \theta + x \sin \theta)^2 \\ &\quad + (x_0 \cos \theta + y_0 \sin \theta) y - (y_0 \cos \theta - x_0 \sin \theta) x \\ &= \frac{1}{2}\pi (x^2 + y^2) + \frac{1}{2}\pi (y^2 - x^2) \cos 2\theta + 2\pi xy \sin \theta \cos \theta \\ &\quad + 2\pi y_0 (y \cos \theta + x \sin \theta) + (x_0 \cos \theta + y_0 \sin \theta) y \\ &\quad - (y_0 \cos \theta - x_0 \sin \theta) x\end{aligned}\quad (21)$$

Introducing elliptic coordinates by means of the substitution

$$x + iy = c \cosh (\xi + i\eta), \quad (22)$$

we find the following form for  $\psi_0$ ,

$$\begin{aligned}\psi_0 &= \frac{1}{4}\pi c^2 (\cosh 2\xi + \cos 2\eta) - \frac{1}{4}\pi c^2 (\cosh 2\xi \cos 2\eta + 1) \\ &\quad + \frac{1}{4}\pi c^2 \sinh 2\xi \sin 2\eta \sin 2\theta \\ &\quad + c (x_0 \cos \theta + y_0 \sin \theta + 2\pi y_0 \cos \theta) \sinh \xi \sin \eta \\ &\quad + c (x_0 \sin \theta - y_0 \cos \theta + 2\pi y_0 \sin \theta) \cosh \xi \cos \eta.\end{aligned}\quad (23)$$

For the disturbed motion, considering that the ellipse at the same time revolves about its centre C with angular velocity  $\theta$ , the stream-function relative to the moving point C, when  $\xi = \xi_0$  gives the elliptic boundary of the cross-section of the cylinder, is

$$\begin{aligned}\psi &= \frac{1}{4}\pi c^2 \{ \cosh 2\xi + \cos 2\eta - e^{2(\xi-\xi_0)} \cos 2\eta \} - \frac{1}{4}\pi c^2 \cos 2\theta \\ &\quad - \frac{1}{4}\pi c^2 \cos 2\theta \{ \cosh 2\xi - \cosh 2\xi_0 e^{2(\xi-\xi_0)} \} \cos 2\eta \\ &\quad + \frac{1}{4}\pi c^2 \sin 2\theta \{ \sinh 2\xi - \sinh 2\xi_0 e^{2(\xi-\xi_0)} \} \sin 2\eta \\ &\quad + c (x_0 \cos \theta + y_0 \sin \theta + 2\pi y_0 \cos \theta) (\sinh \xi - \sinh \xi_0 e^{2(\xi-\xi_0)}) \sin \eta \\ &\quad + c (x_0 \sin \theta - y_0 \cos \theta + 2\pi y_0 \sin \theta) (\cosh \xi - \cosh \xi_0 e^{2(\xi-\xi_0)}) \cos \eta \\ &\quad + \frac{1}{4}c^2 \theta e^{2(\xi-\xi_0)} \cos 2\eta,\end{aligned}\quad (24)$$

for this satisfies  $\nabla^2 \psi = 2\omega$ , makes  $\psi = \text{const.} + \frac{1}{4}c^2\theta \cos 2\eta$  on  $\xi = \xi_0$ , and agrees with (23) when  $\xi$  increases indefinitely

### 5—CALCULATION OF FORCE AND COUPLE ON THE CYLINDER

The component forces parallel to  $Cx$ ,  $Cy$  which act on the cylinder due to fluid pressure are given by

$$F_x = - \int p l \, ds, \quad F_y = - \int p m \, ds, \quad (25)$$

and the couple tending to rotate the cylinder is

$$G = \int (p l y - p m x) \, ds, \quad (26)$$

where all the integrals are taken round the transverse section, ( $lm$ ) being the direction-cosines of the outward normal. Now from (24) we get by differentiation

$$\begin{aligned} \frac{\partial \psi}{\partial t} = & \frac{1}{2}\omega c^2\theta \sin 2\theta (\cosh 2\xi - \cosh 2\xi_0 e^{2(\xi_0 - \xi)}) \cos 2\eta \\ & + \frac{1}{2}\omega c^2\theta \cos 2\theta (\sinh 2\xi - \sinh 2\xi_0 e^{2(\xi_0 - \xi)}) \sin 2\eta \\ & + c \{ (x_0 + 2\omega y_0 + y_0\theta) \cos \theta + (y_0 - x_0\theta - 2\omega y_0\theta) \sin \theta \} \\ & \times (\sinh \xi - \sinh \xi_0 e^{(\xi_0 - \xi)}) \sin \eta \\ & + c \{ (-y_0 + x_0\theta + 2\omega y_0\theta) \cos \theta + (x_0 + 2\omega y_0 + y_0\theta) \sin \theta \} \\ & \times (\cosh \xi - \cosh \xi_0 e^{(\xi_0 - \xi)}) \cos \eta + \frac{1}{4}c^2\theta e^{2(\xi_0 - \xi)} \cos 2\eta, \end{aligned}$$

omitting terms not containing  $\eta$ , since they will ultimately vanish in the integrals (25) and (26).

The corresponding function conjugate to this will have the form

$$\begin{aligned} \frac{\partial \phi}{\partial t} = & -\frac{1}{2}\omega c^2\dot{\theta} \sin 2\theta (\sinh 2\xi + \cosh 2\xi_0 e^{2(\xi_0 - \xi)}) \sin 2\eta \\ & + \frac{1}{2}\omega c^2\dot{\theta} \cos 2\theta (\cosh 2\xi + \sinh 2\xi_0 e^{2(\xi_0 - \xi)}) \cos 2\eta \\ & + c \{ (x_0 + 2\omega y_0 + y_0\theta) \cos \theta + (y_0 - x_0\theta - 2\omega y_0\theta) \sin \theta \} \\ & \times (\cosh \xi + \sinh \xi_0 e^{(\xi_0 - \xi)}) \cos \eta \\ & - c \{ (-y_0 + x_0\theta + 2\omega y_0\theta) \cos \theta + (x_0 + 2\omega y_0 + y_0\theta) \sin \theta \} \\ & \times (\sinh \xi + \cosh \xi_0 e^{(\xi_0 - \xi)}) \sin \eta + \frac{1}{4}c^2\dot{\theta} e^{2(\xi_0 - \xi)} \sin 2\eta. \end{aligned}$$

Thus for  $\xi = \xi_0$ ,

$$\begin{aligned} \left( \frac{\partial \phi}{\partial t} \right)_{t=t_0} &= \frac{1}{2} \varpi c^2 \theta (\sinh 2\xi_0 + \cosh 2\xi_0) (\cos 2\theta \cos 2\eta - \sin 2\theta \sin 2\eta) \\ &\quad + c \{ (x_0 + 2\varpi y_0 + y_0 \theta) \cos \theta + (y_0 - x_0 \theta - 2\varpi y_0 \theta) \sin \theta \} \\ &\quad \times (\cosh \xi_0 + \sinh \xi_0) \cos \eta \\ &\quad - c \{ (-y_0 + x_0 \theta + 2\varpi y_0 \theta) \cos \theta + (x_0 + 2\varpi y_0 + y_0 \theta) \sin \theta \} \\ &\quad \times (\sinh \xi_0 + \cosh \xi_0) \sin \eta + \frac{1}{2} c^2 \dot{\theta} \sin 2\eta \end{aligned} \quad (27)$$

Again, from (24) we get on  $\xi = \xi_0$

$$\begin{aligned} \left( \frac{\partial \psi}{\partial \xi} \right)_{t=t_0} &= \frac{1}{2} \varpi c^2 (\sinh 2\xi_0 + \cos 2\eta) \\ &\quad + \frac{1}{2} \varpi c^2 (\sinh 2\xi_0 + \cosh 2\xi_0) (\sin 2\theta \sin 2\eta - \cos 2\theta \cos 2\eta) \\ &\quad + c (x_0 \cos \theta + y_0 \sin \theta + 2\varpi y_0 \cos \theta) (\sinh \xi_0 + \cosh \xi_0) \sin \eta \\ &\quad + c (x_0 \sin \theta - y_0 \cos \theta + 2\varpi y_0 \sin \theta) (\sinh \xi_0 + \cosh \xi_0) \cos \eta \\ &\quad - \frac{1}{2} c^2 \dot{\theta} \cos 2\eta, \end{aligned} \quad (28A)$$

$$\left( \frac{\partial \psi}{\partial \eta} \right)_{t=t_0} = -\frac{1}{2} c^2 \dot{\theta} \sin 2\eta. \quad (28B)$$

From these values of the differentials

$$q^2 = \frac{2}{c^2 (\cosh 2\xi - \cos 2\eta)} \left\{ \left( \frac{\partial \psi}{\partial \xi} \right)^2 + \left( \frac{\partial \psi}{\partial \eta} \right)^2 \right\}, \quad (29)$$

and

$$x \frac{\partial \psi}{\partial x} + y \frac{\partial \psi}{\partial y} = \frac{2}{\cosh 2\xi - \cos 2\eta} \left( \sinh \xi \cosh \xi \frac{\partial \psi}{\partial \xi} - \sin \eta \cos \eta \frac{\partial \psi}{\partial \eta} \right), \quad (30)$$

can be calculated on  $\xi = \xi_0$ .

Thus in (14) every term on the right-hand side is known on the cylinder so that  $p$  can now be calculated.

On substitution of this value of  $p$  in the integrals (25) we get after some calculation using

$$a = c \cosh \xi_0, \quad b = c \sinh \xi_0,$$

$$\begin{aligned} -F_1 &= \pi \rho [b^2 (x_0 \cos \theta + y_0 \sin \theta) + 2\varpi y_0 b (a + b) \cos \theta \\ &\quad - 2\varpi (x_0 \sin \theta - y_0 \cos \theta + 2\varpi y_0 \sin \theta) a (a + b) \sin^2 \theta \\ &\quad - \varpi (x_0 \cos \theta + y_0 \sin \theta + 2\varpi y_0 \cos \theta) b (a + b) \sin 2\theta \\ &\quad + \dot{\theta} (x_0 \sin \theta - y_0 \cos \theta + 2\varpi y_0 \sin \theta) (a^2 - b^2)], \end{aligned} \quad (31A)$$

$$\begin{aligned}
-F_3 = & \pi \rho [a^2 (y_0 \cos \theta - x_0 \sin \theta) - 2\pi y_0 a (a+b) \sin \theta \\
& - 2\pi (\dot{x}_0 \cos \theta + y_0 \sin \theta + 2\pi y_0 \cos \theta) b (a+b) \cos^2 \theta \\
& - \pi (x_0 \sin \theta - y_0 \cos \theta + 2\pi y_0 \sin \theta) a (a+b) \sin 2\theta \\
& - \dot{\theta} (x_0 \cos \theta + y_0 \sin \theta + 2\pi y_0 \cos \theta) (a^2 - b^2)] \quad (31B)
\end{aligned}$$

The force-components parallel to  $OX_0$ ,  $OY_0$  are

$$\begin{aligned}
F'_1 = & -\pi \rho [(b^2 \cos^2 \theta + a^2 \sin^2 \theta) x_0 \\
& - (a^2 - b^2) \sin \theta \cos \theta y_0 + 2\pi y_0 (a+b) (a \sin^2 \theta + b \cos^2 \theta) \\
& + (a^2 - b^2) \theta \{(x_0 + 2\pi y_0) \sin 2\theta - y_0 \cos 2\theta\}], \quad (32A)
\end{aligned}$$

$$\begin{aligned}
F'_2 = & -\pi \rho [(a^2 \cos^2 \theta + b^2 \sin^2 \theta) y_0 \\
& - (a^2 - b^2) \sin \theta \cos \theta x_0 - 2\pi y_0 \sin \theta \cos \theta (a^2 - b^2) \\
& - 2\pi (x_0 \sin \theta - y_0 \cos \theta + 2\pi y_0 \sin \theta) a (a+b) \sin \theta \\
& - 2\pi (x_0 \cos \theta + y_0 \sin \theta + 2\pi y_0 \cos \theta) b (a+b) \cos \theta \\
& - (a^2 - b^2) \theta \{(x_0 + 2\pi y_0) \cos 2\theta + y_0 \sin 2\theta\}] \quad (32B)
\end{aligned}$$

Similarly the couple can be calculated from (26) as

$$\begin{aligned}
G = & -\frac{\pi}{8} \rho (a^2 - b^2)^2 \theta \\
& - \frac{\pi}{4} \rho \pi (a^2 - b^2) \sin 2\theta \{2(a-b)(a+3b)\theta - \pi(a+b)^2\} \\
& + \pi \rho (a^2 - b^2) (x_0 \cos \theta + y_0 \sin \theta + 2\pi y_0 \cos \theta) \\
& \times (x_0 \sin \theta - y_0 \cos \theta + 2\pi y_0 \sin \theta) \quad (33)
\end{aligned}$$

If we put  $a = b$  we find that the force-components are independent of  $\theta$  and  $\dot{\theta}$  and the couple is zero. In fact, we get in that case

$$\left. \begin{aligned}
F_1 = & -\pi \rho a^2 (x_0 + 4\pi y_0), \\
F_2 = & -\pi \rho a^2 (y_0 - 4\pi x_0 - 8\pi^2 y_0), \\
G = & 0.
\end{aligned} \right\} \quad (34)$$

These results agree completely with those found by Taylor.\*

## 6—MOTION OF THE CYLINDER

The equations of motion of the cylinder can now be written easily. If  $\rho'$  be the density of the cylinder,  $(X, Y)$  and  $G'$  the external force and

\* 'Proc. Roy Soc.,' A, vol 93, p. 99 (1917)

couple per unit length of the cylinder, the equations of motion are (dropping the zero suffixes)

$$\begin{aligned} \pi \rho' abx + \pi \rho [(b^2 \cos^2 \theta + a^2 \sin^2 \theta) x - (a^2 - b^2) \sin \theta \cos \theta y \\ + 2\pi y (a + b) (b \cos^2 \theta + a \sin^2 \theta) \\ + (a^2 - b^2) \theta \{(x + 2\pi y) \sin 2\theta - y \cos 2\theta\}] = X, \end{aligned} \quad (35A)$$

$$\begin{aligned} \pi \rho' aby + \pi \rho [(a^2 \cos^2 \theta + b^2 \sin^2 \theta) y \\ - (a^2 - b^2) \sin \theta \cos \theta x - 2\pi y (a^2 - b^2) \sin \theta \cos \theta \\ - 2\pi (x \sin \theta - y \cos \theta + 2\pi y \sin \theta) a (a + b) \sin \theta \\ - 2\pi (x \cos \theta + y \sin \theta + 2\pi y \cos \theta) b (a + b) \cos \theta \\ - (a^2 - b^2) \theta \{(x + 2\pi y) \cos 2\theta + y \sin 2\theta\}] = Y, \end{aligned} \quad (35B)$$

and

$$\begin{aligned} \pi \rho' ab \frac{a^2 + b^2}{4} \theta = -\frac{\pi}{8} \rho (a^2 - b^2)^2 \theta \\ - \frac{\pi}{4} \rho \pi (a^2 - b^2) \sin 2\theta \{2(a - b)(a + 3b) \theta - \pi(a + b)^2\} \\ + \pi \rho (a^2 - b^2) (x \cos \theta + y \sin \theta + 2\pi y \cos \theta) \\ \times (x \sin \theta - y \cos \theta + 2\pi y \sin \theta) + G' \end{aligned} \quad (35C)$$

These equations are too complicated for general integration

Certain simple cases of motion are discussed below

(a) For *free motion*  $X = Y = G' = 0$ . As a particular case we note that the first two equations in (35) can be satisfied by  $x + 2\pi y = 0$  and  $y = 0$ . These give

$$x = -2\pi h, \quad y = h = \text{const.} \quad (36)$$

The motion of the centre is thus the same as that of the liquid particle it displaces for uniform shear motion

The couple equation has the form

$$\begin{aligned} \{\rho' (a^2 + b^2) ab + \frac{1}{2} \rho (a^2 - b^2)^2\} \theta \\ = -\rho \pi (a^2 - b^2) \sin 2\theta \{2(a - b)(a + 3b) \theta - \pi(a + b)^2\}. \end{aligned} \quad (35C')$$

Hence the cylinder can move *freely* with constant velocity in the fixed  $x_0$  direction, the velocity of its centre being the same as that of the fluid particle it displaces, and the rotation about the axis being given by (35C'). One obvious solution of (35C'), in addition to  $\theta = 0$ , is

$$\theta = \text{constant} = \frac{\pi(a + b)^2}{2(a - b)(a + 3b)}. \quad (37)$$

Hence free motion is possible parallel to the line of shear, with the centre having the uniform velocity of the undisturbed liquid, and the cylinder having constant angular rotation about the axis of amount given by (37), or no rotation; in the latter case the major axis will be directed permanently in the direction of shear. It is to be noted that the limit of this uniform rotation when the ellipse approaches a circle does not exist. Another simple case of free motion is given below

(b) Turning to the particular case when the major axis of the elliptic section is kept parallel to the shear, we get as equations of motion

$$\pi \rho' a b x + \pi \rho \{b^2 x + 2 \omega b (a + b) y\} = X, \quad (38A)$$

$$\pi \rho' a b y + \pi \rho \{a^2 y - 2 \omega b (a + b) (2 \omega y + \dot{x})\} = Y, \quad (38B)$$

$$G + G' = 0, \quad (38C)$$

where

$$G = -\pi \rho (a^2 - b^2) (2 \omega y + x) y$$

(i) To find the possible paths under an external couple only, the major axis remaining parallel to the line of shear, we put in (38)

$$X = Y = 0,$$

$$x = A e^{i \lambda \omega t}, \quad y = i B e^{i \lambda \omega t}$$

The equation for  $\lambda$  is, after discarding a factor  $\lambda^2$ ,

$$(a \rho' + b \rho) (a \rho + b \rho') \lambda^2 + 4 \rho (\rho' - \rho) b (a + b) = 0 \quad (39)$$

When  $\rho > \rho'$ , the two roots of  $\lambda$  are real and equal to  $\pm \lambda$  say, so that, when  $\rho > \rho'$ , putting

$$x = A_1 e^{i \lambda \omega t} + A_2 e^{-i \lambda \omega t},$$

$$y = i (B_1 e^{i \lambda \omega t} + B_2 e^{-i \lambda \omega t}),$$

we get

$$\frac{B_2}{A_2} = -\frac{B_1}{A_1} = \frac{(\rho' a + \rho b) \lambda}{2 \rho (a + b)} = \alpha, \quad (40)$$

where  $\alpha < 1$

These paths are similar ellipses

When  $\rho < \rho'$ , the values of  $\lambda$  are imaginary and we put in this case conveniently

$$x = A e^{\lambda \omega t}, \quad y = B e^{\lambda \omega t}$$

This gives on substitution

$$x = A_1 e^{\lambda \omega t} + A_2 e^{-\lambda \omega t},$$

$$y = B_1 e^{\lambda \omega t} + B_2 e^{-\lambda \omega t},$$

where  $\lambda$  and the ratio  $B/A$  are determined by the same equation as before, but now  $\alpha > 1$ .

These paths are similar hyperbolas

Thus when  $\rho > \rho'$ , the paths with the major axis of the elliptic section remaining parallel to the line of shear, which can be maintained by a couple only, are similar ellipses with axes having the ratio  $\alpha$  and major axis parallel to the line of shear. Similarly when  $\rho < \rho'$ , the paths are hyperbolas of corresponding orientation

In these cases we can easily calculate the requisite couple. Thus for an elliptic path

$$x = A \cos \lambda \omega t, \quad y = B \sin \lambda \omega t, \\ G = \pi \rho (a^2 - b^2) (A \lambda - 2B) \lambda \omega^2 \frac{xy}{A} \quad (41)$$

(ii) Next we consider the motions with major axis permanently in the direction of the shear, which can be maintained by a force only. The couple  $G$  can vanish in one or other of two ways. These possibilities are

$$y = 0, \quad X = \pi b (\rho b + \rho' a) x, \quad Y = -2\pi \rho \pi b (a + b) (2\pi y + x), \quad (42A)$$

and

$$x + 2\pi y = 0, \quad X = 2\pi \omega ab (\rho - \rho') y, \quad Y = \pi a (\rho a + \rho' b) y \quad (42B)$$

Free motion with the centre of the ellipse moving like the fluid particle it displaces is, of course, possible. It should be noted that  $\theta = 0$  is a solution of (35c'). Another *free motion* is possible when  $\rho = \rho'$  for  $y = c = \text{const}$  and  $x = -2\pi c$ . The corresponding path of the centre is a *parabola* of which the axis is parallel to the line of shear. The motion is analogous to that of the free fall of a particle under gravity. The major axis of the elliptic section maintains its direction along the line of shear in this case.

All cases of motion under a single force are given by (42A) and (42B). Two interesting cases are,

$$x = \text{const}, \quad y = \text{const},$$

*i.e.*, any uniform motion parallel to the line of shear, which can be maintained by a *constant force perpendicular to the direction of uniform motion* given by (42A) and

$$y = 0, \quad x + 2\pi y = 0,$$

*i.e.*, a parabolic motion with the axis of the parabola along the direction of shear, which is capable of being maintained (only for  $\rho \neq \rho'$ ) by a

constant force (proportional to  $\rho - \rho'$ ) parallel to the line of shear given by (42B)

### 7—UNIFORM ROTATION

Let us next consider the case when the undisturbed motion of the fluid is one of uniform rotation  $\varpi$  about the fixed point O

The stream-function for the motion will be given by

$$\begin{aligned}\psi = & \frac{1}{4}\varpi c^2 \{ \cosh 2\xi + \cos 2\eta - e^{2(\xi-\eta)} \cos 2\eta \} \\ & + c \{ \varpi (x_0 \cos \theta + y_0 \sin \theta) - (y_0 \cos \theta - x_0 \sin \theta) \} \\ & \times (\cosh \xi - \cosh \xi_0 e^{t-t_0}) \cos \eta + c \{ \varpi (y_0 \cos \theta - x_0 \sin \theta) \\ & + (x_0 \cos \theta + y_0 \sin \theta) \} (\sinh \xi - \sinh \xi_0 e^{t-t_0}) \sin \eta \\ & + \frac{1}{2}\varpi \{ (x_0 \cos \theta + y_0 \sin \theta)^2 + (y_0 \cos \theta - x_0 \sin \theta)^2 \} \\ & + \frac{1}{4}c^2 \theta e^{2(t-t_0)} \cos 2\eta, \quad (43)\end{aligned}$$

for this satisfies  $\nabla^2 \psi = 2\varpi$ , makes  $\psi = \text{const} + \frac{1}{4}c^2 \theta \cos 2\eta$  on  $\xi = \xi_0$ , and the condition of rotation at infinity

Proceeding as for uniform shear, we can calculate the component forces and the couple acting on the cylinder. The results of the calculation are given below

$$\begin{aligned}-F_1 = & \pi\rho [b^2 (x_0 \cos \theta + y_0 \sin \theta) \\ & + (y_0 \cos \theta - x_0 \sin \theta) \{ (b^2 - a^2) \theta + (a+b)^2 \varpi \} \\ & - \varpi (x_0 \cos \theta + y_0 \sin \theta) \{ (b^2 - a^2) \theta + a(a+b) \varpi \}], \quad (44A)\end{aligned}$$

$$\begin{aligned}-F_2 = & \pi\rho [a^2 (y_0 \cos \theta - x_0 \sin \theta) \\ & - (x_0 \cos \theta + y_0 \sin \theta) \{ (a^2 - b^2) \theta + (a+b)^2 \varpi \} \\ & - \varpi (y_0 \cos \theta - x_0 \sin \theta) \{ (a^2 - b^2) \theta + b(a+b) \varpi \}] \quad (44B)\end{aligned}$$

That is,

$$\begin{aligned}F_1 = & -\pi\rho [b^2 A_x + \{ (b^2 - a^2) \theta + (a+b)^2 \varpi \} V_x \\ & - \varpi \{ (b^2 - a^2) \theta + a(a+b) \varpi \} D_x], \quad (45A)\end{aligned}$$

$$\begin{aligned}F_2 = & -\pi\rho [a^2 A_y - \{ (a^2 - b^2) \theta + (a+b)^2 \varpi \} V_y \\ & - \varpi \{ (a^2 - b^2) \theta + b(a+b) \varpi \} D_y], \quad (45B)\end{aligned}$$

where  $(A_x, A_y)$  are the components of the acceleration,  $(V_x, V_y)$  the components of the velocity of the centre of gravity of the ellipse parallel to its axes, and  $(D_x, D_y)$  are the projections of OC on the pair of axes through O also parallel to the axes of the ellipse.

The couple is given by

$$G = -\frac{\pi}{8} \rho (a^2 - b^2)^2 \dot{\theta} + \pi \rho (a^2 - b^2) \{ (\omega x_0 - y_0) \cos \theta + (\omega y_0 + x_0) \sin \theta \} \{ (\omega y_0 + x_0) \cos \theta + (y_0 - \omega x_0) \sin \theta \}, \quad (46A)$$

or in terms of the vectors  $V$ ,  $D$ ,

$$\begin{aligned} G &= -\frac{\pi}{8} \rho (a^2 - b^2)^2 \dot{\theta} + \pi \rho (a^2 - b^2) (\omega D_x - V_y) (\omega D_y + V_x) \\ &= -\frac{\pi}{8} \rho (a^2 - b^2)^2 \dot{\theta} - \pi \rho (a^2 - b^2) (V_y^{(\omega)} - V_y) (V_x^{(\omega)} - V_x), \end{aligned} \quad (46B)$$

where  $(V_x^{(\omega)}, V_y^{(\omega)})$  are the velocities parallel to the axes of the ellipse, of the centre  $C$  in a circular path round  $O$ , described with angular velocity  $\omega$

These results, (44), (46), are found to be identical with those obtained from Taylor's general formulae when the section is an ellipse, after some necessary transformation of axes

[*Note added in proof, 5 January, 1937*—Since writing the paper I have attempted a numerical solution of equation (35c) in order to study the nature of the unique rotational velocity (37), for which free motion of the elliptic cylinder along a current with shear motion is possible. It has been found that this unique rotation sharply divides all motions into two types, such that a motion with rotational velocity *at any time less than this* unique velocity can have at no subsequent instant a rotation at any time *greater than* this unique velocity will subsequently always possess this property. The free motion with uniform rotation is unstable.]

In conclusion, I want to thank Professor N. R. Sen for help in this work.

## The Polarization of Radio Echoes

By D. F. MARTYN, D.Sc., A.R.C.Sc., J. H. PIDDINGTON, M.Sc., B.E., and  
G. H. MUNRO, M.Sc., Research Physicists, Australian Radio Research  
Board

(Communicated by Lord Rutherford, O.M., F.R.S.—Received 3 July,  
1936)

[PLATE 26]

### 1—INTRODUCTION

The study of the polarization of downcoming radio waves has become increasingly important during the last few years. The early theoretical work of Appleton\* and of Nichols and Schelleng† showed that the earth's magnetic field was likely to influence radio waves profoundly during their passage through the ionized upper regions of the earth's atmosphere. The upgoing wave entering these regions would be split into two components of opposite senses of polarization, and each component would experience different attenuations and different group velocities during its passage. These views were supported by the experimental work of Appleton and Ratcliffe,‡ who found that downcoming waves of broadcasting frequencies in England were nearly circularly polarized, the sense of polarization being left-handed to an observer looking along the direction of propagation of the wave, which was chosen practically to coincide with the positive direction of the earth's magnetic field. Appleton and Ratcliffe showed that such a result was to be anticipated, since one of the two downcoming waves (the *extraordinary* component) would be much more strongly absorbed in the ionized regions than the other, the *ordinary* component. The essential correctness of these views was strikingly confirmed by Green§ in Australia, working under conditions almost identical with those of Appleton and Ratcliffe, but receiving downcoming waves travelling *against* the positive direction of the earth's field. Green found that the waves received under these conditions were approximately circularly polarized in the *right-handed* sense.

\* 'Proc. Phys. Soc.,' vol. 37, p. 22D (1925)

† 'Bell Syst. Tech. J.,' vol. 4, p. 215 (1925)

‡ 'Proc. Roy. Soc.,' A, vol. 117, p. 576 (1928)

§ 'Bull. Coun. sci. industr. Res. Aust. No. 59,' 1932

Thus far, experimental work on the subject had been confined to broadcasting frequencies, the frequency change device of Appleton and Barnett\* being employed in the measurement of the polarizations. Theoretical considerations showed, however, that for short radio waves, of frequencies above the critical gyromagnetic frequency of about  $10^7$  radians per second, it might be possible to receive both the ordinary and the extraordinary components with comparable intensities. These two components were identified experimentally for the F region by Appleton and Bulder,† who used the pulse or echo method originally due to Breit and Tuve,‡ at a frequency of 3.75 mc/sec. Subsequent intensive examination of the ionosphere by the pulse method on short wave-lengths revealed great complexities. At least four regions capable of reflecting radio waves have been discovered, and each of these regions may give rise to multiple echoes, not only for the reasons given above but also because of multiple reflexions between the ground and each region, and between the regions themselves. For these reasons the pulse method of ionospheric exploration has largely superseded the frequency change method in the last few years, since elaborate harmonic analysis is necessary if the latter method be employed when several downcoming waves are present.

With the development of automatic photographic recording of the echo pattern by the pulse method, the provision of means for the proper identification of each echo trace became of importance. In particular, it was important to identify the two or more magneto-ionic components which might be receivable from any one region, since failure to so do would lead to serious confusion in the identification of the number and positions of the reflecting regions present. Such identification has been largely achieved by Ratcliffe and E. L. C. White,§ who have developed an aerial system capable of responding only to circularly polarized downcoming waves of either right- or left-handed sense, such sense being capable of alteration at will by a simple switch.

Nevertheless, as has been shown theoretically by Baker and Green,|| downcoming waves on leaving the ionosphere should acquire a limiting polarization which will, in general, be elliptic. Detailed calculations by Martyn¶ have shown that the degree of ellipticity may be pronounced.

\* 'Proc. Roy. Soc.,' A, vol. 109, p. 621 (1925).

† 'Proc. Phys. Soc.,' vol. 45, p. 208 (1933).

‡ 'Phys. Rev.,' vol. 28, p. 571 (1926).

§ 'Phil. Mag.,' vol. 16, p. 125 (1933).

|| 'Bull. Coun. sci. industr. Res. Aust.,' No. 60, 1932.

¶ 'Phil. Mag.,' vol. 19, p. 376 (1935).

It is therefore desirable that a complete study of the ellipticity of the downcoming echoes should be made. An apparatus for this purpose has been developed by Appleton and Watson Watt,\* who have extended the range of the cathode ray direction finding technique into the short wave region, where they have used pulse emissions. The polarization of each echo is delineated as a rotating trace on a cathode ray oscillograph screen. Unfortunately, an apparatus of this type is necessarily complicated in construction and very sensitive in adjustment. This happens mainly because it is necessary to keep in alignment the radio frequency phases in two independent receiving amplifiers, a problem which is exceptionally difficult of solution at frequencies of several megacycles per second. This difficulty does not occur in the original method of polarization measurement used by Appleton and Ratcliffe, and Martyn and Green† have shown that it is possible, by a modification of the former authors' technique, to determine polarization by comparing the amplitudes and phases of the *low frequency* outputs of two separate receiving systems. The present paper describes how these ideas have been applied to the development of a relatively simple polarimeter which combines the advantages of the frequency-change technique, and its freedom from radio-frequency difficulties, with the superior resolving power of the pulse method in the presence of multiple downcoming echoes.

The paper also gives results which have been obtained by this method, and discusses their bearing on the structure of the ionosphere.

## 2—EXPERIMENTAL METHOD

### (2.1) *Theory of Method*

In the original polarization measurements of Appleton and Ratcliffe, the downcoming wave was allowed to combine with the ground wave successively in three separately oriented loop aerial systems. A frequency change of the emitted wave was made in each case, and the polarization was calculated from the amplitude of the interference fringes obtained from each aerial system. In view of the time interval required for the successive frequency changes with each aerial system, it was only possible to make measurements at times when the polarization was steady, as was found to be the case in the early morning just before sunrise. This

\* 'Wireless World,' vol. 17 (8 July, 1932).

† 'Proc. Roy. Soc.,' A, vol. 109, p. 621 (1925).

method was modified by Martyn and Green,\* who observed the interference fringes *simultaneously* on separate aerial systems. By comparing the relative amplitudes and phases of the fringes obtained with three separate aerial systems, which consisted of two vertical loops and one vertical antenna, they were able to measure not only the polarization but also the angle of lateral deviation, and consequently the true angle of incidence of the downcoming wave

Unfortunately, although simple in application, these methods of measurement are applicable only when a single downcoming wave is being received. An attempt was therefore made to combine the above principles of polarization measurement with the emission of short radio-frequency pulses, which naturally affords temporal separation when more than one echo is received. We have achieved this end by employing a pulse emitter, whose frequency is controlled by a low power master oscillator in the manner originally developed by Hafstad and Tuve† for the purpose of examining the phase of downcoming echoes.

Powerful pulses of 500 watts peak power, and of duration  $2 \times 10^{-4}$  secs. were emitted at intervals of 1/50 sec (the supply mains period), and were received, together with the downcoming echoes, simultaneously on two vertical mutually perpendicular loop aerials located some 300 yards from the emitter, each at angles of  $45^\circ$  to the line of propagation. At the same time a weak continuous radio-frequency wave was allowed to radiate from the master oscillator. This wave was much too weak to give perceptible reflexion from the ionosphere, but when received directly by the ground path was several times stronger than the downcoming pulse echoes. Each loop aerial was connected to a radio-frequency amplifier and detector, and the outputs from each detector were respectively applied to the two pairs of opposite plates of a cathode ray oscillograph, which were so placed as to be capable of deflecting the beam either vertically or horizontally. A semi-elliptical time base, of frequency 50 c./sec., was applied magnetically to the cathode ray beam. A rectifier was employed with one of the two transformers producing the time base, so that the pattern traced on the screen of the oscillograph was a semi-ellipse cut across the major axis. The phase of the pulse emissions was adjusted so that the ground pulse and principal echoes gave a stationary pattern on this major axis, which was oriented horizontally. When now the amplifier connected to the vertically deflecting plates  $X_1$ ,  $X'_1$  was switched on, an echo pattern similar to that normally obtained by the simple pulse method appeared on the screen, but with this important

\* \* Proc. Roy. Soc., A, vol. 148, p. 104 (1935)

† Proc. Inst. Rad. Eng., vol. 17, p. 1786 (1929)

difference, that whereas the ground pulse appeared as usual as a large downward deflexion over the appropriate small interval of the time base, the downcoming echoes, on the other hand, appeared as deflexions *either* upwards or downwards, the amplitudes of these deflexions depending not only on the echo amplitude but also on the phase difference between the echo and the continuous ground wave. These echo patterns were therefore not stationary in size or in disposition, but oscillated up and down in accordance with the naturally occurring fluctuations in the optical paths of the echoes. When next the second amplifier was switched on and adjusted to give equal amplification with the first, the deflexion due to the ground pulse was now at an angle of  $45^\circ$  to the vertical, while the deflexions due to each echo appeared at random angles to the vertical. As optical path variations occurred, the direction of these deflexions began to rotate in such a fashion that the extremity of each deflexion turned out an ellipse.

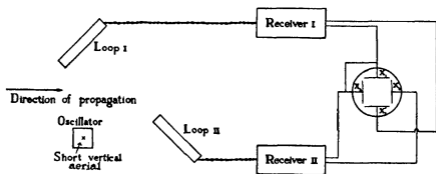


FIG. 1—Schematic arrangement of apparatus for measuring polarization of echoes.

It can be shown that each such ellipse gives the polarization of each echo. It is readily found (*cf* Martyn and Green (*loc cit*)) that

$$E_1 = \frac{H_0}{\sqrt{2}} [\sin pt + \sqrt{a^2 - 2ab \cos \xi + b^2} \sin (pt + \theta + \epsilon_1)] \quad (1)$$

$$E_2 = \frac{H_0}{\sqrt{2}} [\sin pt + \sqrt{a^2 + 2ab \cos \xi + b^2} \sin (pt + \theta + \epsilon_2)], \quad (2)$$

where

$E_1, E_2$  are the E M F s in loops I and II respectively (fig. 1),

$H_0$  is the magnetic force in the (continuous) ground wave,

$H_1$  and  $H'_1$  are the normally and abnormally polarized components of the magnetic force in the vertically downcoming pulse;

$p$  is the angular (radio) frequency of the wave (and pulse);

$\xi$  is the phase difference between the normal and abnormal components of the pulse;

$\theta$  is the phase difference between the normal component of the downcoming pulse and the ground wave,

$$a = 2H_1/H_0, \quad b = 2H'_1/H_0;$$

$$\tan \epsilon_1 = -b \sin \xi / (a - b \cos \xi),$$

and

$$\tan \epsilon_2 = b \sin \xi / (a + b \cos \xi)$$

It follows that if  $x_1$  be the maximum vertical displacement of the oscillograph spot due to the echo received in aerial I, and  $x_2$  the corresponding maximum horizontal displacement produced by the second amplifier, then when the echo amplitude is small compared with the ground wave  $H_0$  we have

$$x_1 = k \sqrt{H_1^2 - 2H_1H'_1 \cos \xi + H_1'^2} \cos(\theta + \epsilon_1)$$

and

$$x_2 = k \sqrt{H_1^2 + 2H_1H'_1 \cos \xi + H_1'^2} \cos(\theta + \epsilon_2),$$

where  $k$  is a constant of the amplifiers

It follows that as  $\theta$  changes, the extremity of the deflexion of the spot traces out a figure which is, in general, an ellipse, and, further, that the polarization constants  $H_1$ ,  $H'_1$ ,  $\xi$  may be deduced directly from the shape, size, and orientation of this ellipse

By inspection of equations (1) and (2), it may be seen that precisely the same ellipse would have been obtained, in the absence of the ground wave  $H_0$ , if  $E_1$  and  $E_2$  had been amplified and applied directly to the plates of the oscillograph, provided care had been taken to preserve the correct relative phases of the radio frequency oscillations during amplification. In this event the ellipse would be traced out at the radio frequency  $p/2\pi$ . Such is essentially the method of polarization measurement due to Appleton and Watson Watt, which has already been mentioned above

We have found it inconvenient in practice to wait for the ellipse to be traced out by naturally occurring variations in  $\theta$ , and, moreover, have found it desirable to remove our receiving aerials to a better site, free from surrounding conductors, and located 25 km. from the emitter. At this distance the continuous ground wave, necessarily only feebly emitted, is much too weak to give perceptible interference with the downcoming echo pulses. We have overcome both of these inconveniences by supplying the ground wave locally at the receiving site, from a separate oscillator.

By arranging that the frequency of this wave is slightly different from that of the pulse emitter, we ensure that each successive echo arrives in a different phase relationship to the ground wave, so that the ellipse is delineated sufficiently rapidly to be photographed complete in a fraction of a second

### (2.2) *Arrangement of Apparatus*

The loop aerials (fig. 1) are placed 12 feet apart, this separation being found adequate to avoid mutual coupling. The oscillator supplying the artificial "ground wave" is placed symmetrically at the intersection of two imaginary horizontal lines passing through the centre of each loop at an angle of  $45^\circ$  to the plane of the loop. This oscillator is supplied by batteries, and is carefully screened. It radiates by means of a small vertical wire 3 inches long. The receivers are of the superheterodyne type, and are capable of tuning over the range from 0.5 to 30 mc/sec. The intermediate frequency transformers in the first receiver are tuned to 450 kc/sec, and those in the second receiver to 470 kc/sec. This ensures that the beat oscillator of one receiver is unable to cause audible interference in the other by heterodyning with the external oscillator. Each receiver is capable, when adjusted to full amplification, of giving an output of 100 volts across  $1/4$  megohm when a modulated E.M.F. of 5 microvolts and 30% modulation is received. They are designed to amplify equally the band of frequencies contained in the pulse, and test measurements show a change of amplification of only 4 decibels over a frequency band of 14 kc/sec when the receivers are tuned. Each receiver is placed below its loop aerial and 4 feet away. The loops are connected to the receivers by loosely twisted low capacity leads of equal length. This arrangement is found adequate to prevent appreciable mutual couplings between the aerials through the receiver chassis. Tests show that a sharp and very small minimum signal is received from the ground pulse when each loop is rotated into a position with its plane at right angles to the direction of propagation.

The amplifications of each receiver are conveniently adjusted to equality by observation of the ground pulse on the screen of the oscillograph. When this becomes a deflexion at  $45^\circ$  to the vertical, correct adjustment has been made, and the ellipses due to each echo give the polarization faithfully. A typical photograph of the resulting pattern is shown in fig. 2a, Plate 26, which was taken at 18.50 hours on 26 March, 1936. For purposes of illustration, it is more convenient to have the ground pulse at right angles to the time base. This is simply achieved by rotating the cathode-ray tube clockwise through  $45^\circ$ , while leaving the magnetic

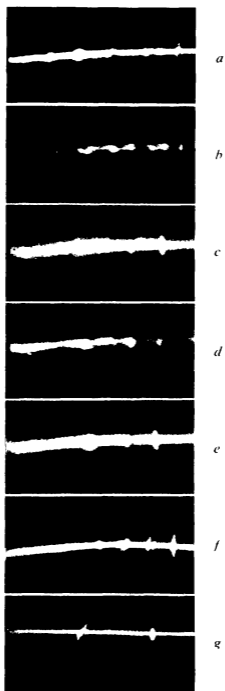


FIG. 2.



deflecting coils of the time base *in situ*. All the ellipses reproduced in this paper have been rotated clockwise by this amount.

In the figure the ground pulse appears on the right. Passing to the left there appears first an elliptical echo from the E region of the ionosphere. Next to that appears a large ellipse, which is identified, from its position on the time axis, to come from the F region. Next appears a small ellipse due to an "M" reflexion\* between the E and F regions, and finally a small ellipse arising from an echo which has been twice reflected between the F region and the ground.

### (2.3) *Determination of Sense of Rotation*

The specification of the polarization of each echo is not complete without a knowledge of the direction of the rotation of the magnetic vector in the ellipse of polarization. It has been possible to find this by slightly de-tuning the intermediate amplifier in one of the two receivers, in a manner somewhat analogous to that employed in the method of Appleton and Watson Watt. The sense of rotation of the magnetic vector can then be obtained by careful observation of the resulting change of shape of the ellipse on the oscillograph screen.

We have found this method complicated in practice, since it is undesirable to interfere with the tuning of the intermediate frequency amplifier once this has been adjusted. Moreover, we have found it exceptionally difficult to detect the small changes thus produced in the ellipse, in the presence of the often rapid and marked changes which are occurring continuously because of fluctuations in the ionosphere itself.

A method free from these objections has been developed by one of us (G. H. M.) It is arranged that the low frequency voltage output from receiver II, besides being applied to the deflecting plates of the oscillograph  $X_1X'_1$  (fig. 1), is also applied, after being retarded in phase by approximately  $90^\circ$ , to the focussing cylinder of the cathode ray tube, in such a way that the cathode ray beam is defocussed when this voltage adds positively to the normal voltage on the cylinder, but remains in focus over the negative half-cycle of the oscillatory voltage. The effect of this arrangement on a circularly polarized echo pattern is shown in fig. 3. If we assume that the direction of rotation of the trace which sweeps out the circle ABCD is clockwise, then as the voltage across  $X_1X'_1$  becomes positive, the extremity of the trace is passing A. The trace does not become defocussed, however, until it reaches B, owing to

\* Ratcliffe and White, 'Phil. Mag.', vol 16, p 125 (1933).

the  $90^\circ$  phase lag which has been introduced before application of the voltage to the focussing cylinder. Over the whole shaded semicircle BCD the trace remains out of focus, and only becomes visible again in passing from D to B. It follows that only one-half of the circle is in focus and therefore visible, and three-quarters of this semicircle lies *above* the time base line TT'.

If now we suppose that the trace rotates in anticlockwise fashion, then it follows, from similar reasoning, that the other hemisphere BAD is now defocussed, and so three-quarters of the visible hemisphere DCB lies *below* the time base line. In practice it has been found that the defocussing properties of individual cathode ray tubes vary considerably, and it has been possible, by a careful selection of tube, to arrange that

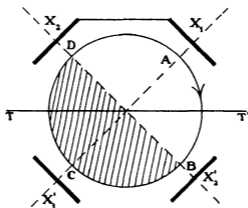


FIG. 3—The determination of the sense of rotation of the polarization vectors

the circle (or ellipse) is defocussed almost completely, either above or below the time base line, according as the sense of the polarization in the downcoming echo is left- or right-handed respectively.

It will be observed that in the above description of the operation of the sense device we have assumed for simplicity that each pulse was of sufficient duration to permit of at least one complete revolution of the trace defining the ellipse. In practice this is not so, since the duration of the pulse is less than the period of the beat frequency between the pulse and the artificial ground wave. In other words, each individual echo does not persist over a complete cycle of the low frequency E.M.F. produced at the detector. The arrival of subsequent echoes occurs at different phases of the oscillatory cycle, however, so that the complete pattern appears to be continuous when viewed by the eye or by a photographic exposure of not less than about 0.5 sec.

The application of the sense device is illustrated in fig 2, Plate 26. At *a* is shown the echo pattern already described. Immediately after this photograph was taken, the sense device was switched on and another exposure *b* was made. It is seen that at this particular time all the echoes were of right-handed polarization. At *c* is shown a photograph of the echo pattern at 23 12 hours on the 26 March, 1936. It is seen that two strong echoes of elliptical polarization are present. These have been identified, by their position on the time axis, to come from the E and F regions respectively. At *d* and *e* are shown two photographs taken a few seconds later, after the application of the sense device. It is seen that in this case the polarization of the echo from the E region is left-handed, while that from the F region is right-handed.

At *f* and *g* are shown examples of echoes of almost linear polarization obtained respectively from the E and F regions. In such cases, as is to be expected, the application of the sense device produces no appreciable change in the visible pattern, since a linearly polarized echo may be regarded as compounded of two equal circularly polarized echoes having opposite senses of rotation.

### 3—EXPERIMENTAL RESULTS AND CONCLUSIONS

#### (3.1) *The Normal Diurnal Course of Polarization Changes*

Observations have been made, on two or three evenings a week, over the period from December, 1935, to March, 1936. These have been made at the receiving site at Liverpool, 25 km. west of the emitter, which is located in the P. N. Russell School of Electrical Engineering in the University of Sydney. During these observations, which have been made on a frequency of 3 mc/sec., it has been found that the diurnal variations of the polarizations of the downcoming echoes exhibit characteristic features, as follows—

- (1) 10 00–14 00 (Eastern Australian Standard Time)—Over this period echoes are too weak to be observed.
- (2) 14 00–17 00—An echo appears from the E region. It is elliptical and is right-handed. It gradually increases in intensity and is soon accompanied by a second, doubly reflected echo from the same region. These echoes increase in intensity until 17 00, when they decrease in size and ultimately disappear.
- (3) 17 00–18 00—Almost simultaneously with their disappearance an echo appears from the F region. At first this echo also has elliptical right-handed polarization. Within an hour, however, it

begins to undergo rapid changes, varying from an almost circular to a linear state in a few seconds, while at the same time the major axis of the ellipse rotates

- (4) 18 00–20 00—An echo from the E region reappears, of left-handed elliptical polarization. The echo from the F region soon becomes a relatively stable and fat ellipse of right-handed polarization. Later the F region echo disappears and that from the E region becomes unstable, changing rapidly in eccentricity and rotating.
- (5) 20 00–23 00—The E region echo decreases gradually in amplitude, while remaining unstable in polarization, and finally disappears. Shortly afterwards the F region echo returns, at first with stable right-handed elliptical polarization, but later with rapidly rotating almost linear polarization.
- (6) 23 00–04 00—At irregular intervals during this period the sequence of events described in (4) and (5) may be repeated.

### (3.2) *The Nature of the Ionization of the E Region*

It is possible to draw several conclusions from the above observations. The ionized upper atmosphere is rendered doubly refracting by the earth's magnetic field, and Appleton and Builder\* have shown that the densities of ionization  $N$  required just to reflect, at vertical incidence, the two components into which the upgoing wave or pulse is split, are given by

$$N_0 = mp^2/4\pi e^2, \quad (3)$$

and

$$N_x = m(p^2 - pp_H)/4\pi e^2, \quad (4)$$

where

$m$ ,  $e$  are the mass and charge of an ion (or electron)

$$p_H = He/mc,$$

$H$  is the total value of the earth's magnetic field in the region,

$c$  is the velocity of light *in vacuo*,

and the subscripts 0 and  $x$  refer to the ordinary and extraordinary components respectively. It follows that a lesser density of ionization is required to reflect the extraordinary than the ordinary component.

Appleton and Builder have found clear evidence of the existence of two separate reflected components from the F region, and by varying the frequency ( $p/2\pi$ ) of the emitter until each component in turn just ceased to be reflected, they have shown, with the aid of equations (3) and (4),

\* 'Proc Phys Soc.', vol 45, p 208 (1933)

that the magnitude of  $e/m$  is consistent with the assumption that the ionization consists mainly of free electrons. This view is further supported by their observations of the sense of polarization of each component, their results showing that the sign of  $e$  is negative.

No such definite evidence exists concerning the ionization of the E region. F W G White\* finds two components reflected from this region, and deduces from observations of their diurnal intensity variations that they are the magneto-ionic components. Appleton and Naismith† also find two components from this region, but the frequency separation between the waves required just to penetrate the region successively is not nearly so clearly defined as for the F region. Kirby and Judson‡ in America find no evidence at all of magneto-ionic effects, and conclude that the E region consists of heavy ions. Appleton,§ summing up the evidence, finds it inconclusive ||

We find that our observations afford proof of magneto-ionic effects in the E region, and that they permit an explanation only if electrons are mainly responsible. As described above, we find numerous occasions on which echoes are simultaneously reflected from the E and F regions, the sense of the former echoes being left-handed and of the later right-handed. At such times the polarization of each echo is a fat ellipse, of remarkably constant characteristics, and this condition may persist for many minutes. An example of such an occasion is illustrated in fig. 2c, d, and e, Plate 26. We further find that such occasions are always preceded or succeeded by conditions where an echo comes only from the E region, and that when this happens the polarization is unstable, and may even become linear. These facts receive a simple explanation if we suppose that two components exist and that in the former case the ordinary component has penetrated to the F region, while in the latter case both components are reflected from the E region, but with so small a temporal separation that they overlap, the combination giving an unstable resultant polarization which must change rapidly with small fluctuations in the optical paths of each component. The essential correctness of this view is confirmed by observation of the doubly reflected echoes from the E region. The temporal separation of the components in these echoes would be twice that existing in the first echo, and we have indeed found

\* 'Proc. Phys. Soc.', vol 46, p 91 (1934)

† 'Proc. Roy. Soc., A', vol 150, p 685 (1935)

‡ 'Bur. Stand. J. Res. Wash.', vol 14, p 469 (April, 1935)

§ 'Rep. Prog. Phys., Phys. Soc. Lond.', vol 2, p 153 (1935)

|| See also in this connexion, Ratcliffe and White, 'Phil. Mag.', vol 16, p 125 (1933)

that when the first echo is unstable in polarization, it is often possible to detect two components in the second echo. An example of this is reproduced in fig 2*f* for a case when the first echo was nearly linear. For all of these reasons we conclude that magneto-ionic splitting of echoes in the E region does normally occur.

Now equation (4) shows that a density of approximately  $10^6$  electrons, or  $2 \times 10^9$  ions, per cc must be present if the extraordinary component is to be downwardly refracted for a frequency of 3 mc/sec. If the ordinary component is to be refracted downwards as well, then these numbers must be increased to  $2 \times 10^6$  electrons, or  $2 \cdot 0001 \times 10^9$  ions per cc. Let us consider a condition where the E region has just sufficient density to return the extraordinary component. If now the effective carriers be electrons, then an increase of density of 100% is necessary in order to return the ordinary component as well, but if the carriers be ions, then an increase of density of  $5 \times 10^{-3}$  % would be sufficient to give the same result. Now we have found in the course of previous measurements\* that the value of  $N$  for the E region undergoes pronounced and rapid changes throughout the night. We conclude that it is impossible for  $N$  to remain constant to within  $5 \times 10^{-3}$  % over the many intervals of several minutes during which we have observed the E region to be in the critical condition in which it returns the extraordinary but not the ordinary component. No such difficulty arises if electrons are responsible for the refraction of the echoes, since a change of 100% in  $N$  normally does take several minutes to occur.

We conclude that electrons are mainly responsible for the influence of the E region on radio waves.

The interpretation of the diurnal changes described in the previous section appears now to be clear, and is as follows —

- (1) 10 00–14 00—All echoes are heavily attenuated by absorption.
- (2) 14 00–17 00—The ordinary component is returned from the E region, the extraordinary component being still heavily attenuated, as theory predicts†. Gradually the absorption decreases, but before the extraordinary component can become detectable the ordinary component penetrates to the F region.
- (3) 17 00–18 00—At first the ordinary component alone is returned from the F region and the polarization is therefore steady. Later the extraordinary component becomes strong enough to be detect-

\* Martyn and Pulley, 'Proc Roy Soc,' A, vol 154, p 455 (1936).

† Martyn, 'Phil Mag,' vol 19, p 376 (1935).

able, and by overlapping the ordinary component it produces unstable polarization

- (4) The "evening concentration" of electrons in the E region sets in, at first in sufficient strength to return the extraordinary component, while allowing the ordinary component to penetrate to the F region. Further concentration in the E region results in the ordinary component being returned from this region, with a consequent recurrence of unstable polarization.

The sequence of events from 20 00 to 04 00 can be readily deduced along the same lines

On a very few exceptional occasions (fig 2a, b, Plate 26) we have observed the simultaneous return from the E and F region of echoes both of right-handed polarization. It appears to us that this can occur on occasions when the E region is exceptionally shallow. Under such circumstances, a ray theory of refraction, such as has been used implicitly throughout this work, may break down. The occurrence of these anomalies therefore lends support to the views of Appleton and Naismith\* on the occasional existence of such thin strata at the levels of the E region

### (3.3) *The Limiting Polarization of Echoes*

Baker and Green† have shown theoretically that the polarization of a wave leaving the ionized regions tends to a limiting value. Some doubt exists, however, concerning the manner in which this limit should be calculated. Thus Martyn,‡ assuming that the ionization tends to zero at low values of  $\nu$ , the collision frequency of an electron with the air molecules, finds pronounced degrees of ellipticity, while Green and Builder,§ following the same procedure, have been able to explain the anomalies of long wave signal reception discovered by Hollingworth||. On the other hand, M. Taylor¶ calculates a circular limiting polarization on all wave-lengths, and Ratchliffe\*\* reaches a similar conclusion by taking the limiting polarization at high values of  $\nu$ .

No experimental measurements on this point have yet been published.

From the results obtained by the present method, we have been able to reach certain conclusions. For this purpose it is necessary to consider

\* 'Proc Roy Soc,' A, vol 150, p 685 (1935)

† 'Bull Coun sci industr Res Aust,' No 60 (1932)

‡ 'Phil Mag,' vol 19, p 376 (1935)

§ 'Proc Roy Soc,' A, vol 145, p 145 (1934)

|| 'Proc Roy Soc,' A, vol 119, p 444 (1928)

¶ 'Proc Phys. Soc,' vol 46, p. 408 (1934).

\*\* 'Wireless Eng.,' vol 10, p 358 (1933).

measurements made only at times when the components are clearly temporally separated. Examination of all such cases reveals that it is quite exceptional for the polarization to become circular. Calculation of the ratio major/minor axis of the ellipses in 15 such cases gives a mean value of 1.2. This is to be compared with the value of 1.1 calculated from the theory. Unfortunately, a comparison of this nature is not quite reliable, since the observed polarization is liable to be disturbed by the existence of lateral deviation of the echoes from the vertical plane of propagation of the ground pulse. Such lateral deviation, which has been measured previously by Martyn and Green,\* may be considerable, and is certainly sufficient to upset any accurate quantitative test. The method is at present being extended to take account of these deviations from the vertical path, and it is hoped that a test on these lines will soon be made. It is possible, however, to arrive at the conclusion that the limiting polarization is not circular. Lateral deviation, even of the largest amount already measured, would be quite insufficient to produce the observed average ratio of 1.2 in the axes of the polarization ellipses, if the downcoming echoes were circularly polarized.

This work has been carried out as part of the programme of the Radio Research Board of the Commonwealth Council for Scientific and Industrial Research, to which the authors are indebted for permission to publish. The authors are indebted to Dr O. O. Pulley for considerable assistance and discussion, to W. G. Gordon, B.Sc., for supervising the emitting station, to Miss E. Martyn for mathematical assistance, to Professor O. U. Vonwiller for the provision of facilities in the Department of Physics, and finally to Professor J. P. V. Madsen, Chairman of the Board, for his constant help and encouragement.

#### SUMMARY

The paper describes a relatively simple and flexible method of determining the polarization ellipse of downcoming radio echoes. The method employs pulse emissions, and is therefore applicable when more than one echo is receivable, but avoids the difficulty of radio-frequency phase instability by a partial employment of the frequency change technique of Appleton and Ratcliffe, as modified by Martyn and Green. A simple method of determining the sense of rotation of the vectors in the polarization ellipse, employing defocussing of the cathode ray beam, is described.

\* 'Proc. Roy. Soc.' A, vol. 148, p. 104 (1935)

The results obtained afford strong evidence of magneto-ionic effects in the E region of the ionosphere. These effects are found to be due to electrons and not to heavy ions. Further evidence is obtained of the occasional presence of a thin layer of electrons at the level of the E region.

It is found that the polarizations of echoes are elliptical, in accordance with Baker and Green's theory of limiting polarization.

---

## The Theory of the Continuous Absorption Spectrum of Bromine

By N. S. BAYLISS, Department of Chemistry, University of Melbourne, Australia

(Communicated by Sir David Masson, F.R.S.—Received 30 July, 1936)

The discovery of the complex nature of the visible continuous absorption spectrum of bromine by Acton, Aickin, and Bayliss† made it interesting to investigate the continuum theoretically, since the interpretation of the two components that they found to be present is still uncertain‡. The investigation also provides another application of the potential energy functions and eigenfunctions that were used by Gibson, Rice, and Bayliss§ in their treatment of the continuous absorption spectrum of chlorine, although the theory has been slightly modified. The experimental data with which the theory is to be compared consist of values at a number of wave-lengths of  $\epsilon_0$  and  $\epsilon_1$ , the absorption coefficients appropriate to the vibrational states  $v'' = 0$  and 1 respectively, which were determined by an analysis of the temperature variation of the observed absorption coefficient  $\epsilon$ . For bromine, the curve of  $\epsilon_0$  against wave number was shown to consist of the sum of the  $\epsilon_0$  curves of two overlapping continua, which arise from separate electronic transitions from the ground state ( $^1\Sigma_g^+$ ), and which were temporarily designated as A ( $\lambda_{\max} = 4150 \text{ \AA}$ ) and B ( $\lambda_{\max} = 4950 \text{ \AA}$ ).

Dirac|| has shown that the probability per second of the absorption of

† 'J. Chem. Phys.', vol. 4, p. 474 (1936).

‡ Mulliken, 'J. Chem. Phys.', vol. 4, p. 620 (1936).

§ 'Phys. Rev.', vol. 44, p. 193 (1933).

|| "Quantum Mechanics," 2nd Edit., Oxford, pp. 180, 245.

radiation by an atom from a beam of photons whose intensity is one photon/unit frequency range/cm<sup>2</sup>/second is

$$k = (8\pi^3\nu/3hc) |(\alpha' | \mathbf{D} | \alpha'')|^2 \quad (1)$$

$\mathbf{D}$  is the electric displacement of the system,  $\nu$  is the absolute frequency, and the absorption will equal that of a classical electric dipole of moment  $\mathbf{D}^2 = |(\alpha' | \mathbf{D} | \alpha'')|^2$ . A slight modification of the above expression enables it to be used for absorption by a molecule. Denoting the electronic coordinates by  $n$ , and using spherical coordinates  $r, \theta, \phi$  (where  $r$  is the nuclear separation) for the nuclei, the eigenfunction of the molecule is expressed as being separable into the product of the electronic, vibrational, and rotational eigenfunctions  $\psi(n), R(r)/r$ , and  $Y(\theta, \phi)$  respectively. The operation  $(\alpha' | \mathbf{D} | \alpha'')$  may then be written.

$$\iiint \psi' R'/r Y' \mathbf{D} \cdot \psi'' R''/r Y'' r^2 \sin \theta \, dn \, dr \, d\theta \, d\phi \quad (2)$$

Furthermore,  $k$  represents the probability of transition to a single upper state  $\alpha'$ , but since the dissociated atoms that are produced by continuous absorption must have their translational motion quantized, the upper state  $\alpha'$  has a large but finite number of energy levels. If the number of these is such that  $Z(\nu)$  transitions per unit frequency range may arise from the lower state  $\alpha''$ , the transition probability that is appropriate to the present discussion is  $kZ(\nu)$ .

In order to simplify equation (2), it is assumed that the electric displacement  $\mathbf{D}$  is independent of the nuclear coordinates, an assumption that has been examined by Coolidge, James, and Present,<sup>†</sup> who found it to be not quite accurate for a light molecule such as  $\text{H}_2$ , but probably to be a good one for heavy diatomic molecules. It has also been shown by Gibson, Rice, and Bayliss<sup>‡</sup> that, for chlorine, molecular rotation has a negligible effect on the vibrational eigenfunctions  $R(r)$ , and their arguments also apply to bromine, so that the integration of (2) over  $r$  may be carried out separately. Now the integration  $\iint Y' Y'' \sin \theta \, d\theta \, d\phi$  is a constant for a given electronic transition, for if one considers the molecule to be in a weak field that is sufficient to remove the  $(2J+1)$ -fold degeneracy of the rotational levels, the total rotational matrix component that applies to all the possible transitions from a given level of quantum numbers  $J''M''$  ( $\Delta J = \pm 1, 0$ ;  $\Delta M = \pm 1, 0$ ) may be calculated by

<sup>†</sup> 'J Chem Phys,' vol 4, p 193 (1936)

<sup>‡</sup> 'Phys Rev,' vol 44, p 193 (1933)

summation from the rotational matrix components of Rademacher and Reiche† This total matrix component is independent of both  $J$  and  $M$ , and hence may be regarded as a constant for the present problem; but it depends on the electronic quantum numbers  $\Lambda'$  and  $\Lambda''$  One may therefore write

$$(\alpha' | \mathbf{D} | \alpha'') = \iiint \psi' Y' \mathbf{D} \psi'' Y'' \sin \theta \, d\theta \, d\phi \int R'/r \cdot R''/r \, r^2 dr \\ = \text{constant} \times \int R' R'' \, dr \quad (3)$$

$R'$  and  $R''$  have been represented as real quantities, to conform with the subsequent calculations, and it will be shown later that the value of the constant is such that

$$|(\alpha' | \mathbf{D} | \alpha'')|^2 = D^2 \left( \int R' R'' \, dr \right)^2, \quad (4)$$

where  $D$  is the moment of the classical dipole that has the same total absorption coefficient as the molecule This is not quite equivalent to the assumption‡ that is sometimes made, that  $D$  can be identified with the integral  $|\int \psi' \mathbf{D} \psi'' \, dn|^2$ , since the rotational matrix component discussed above does not always have the value unity, for example, it equals  $\frac{1}{2}$  for a  $\Pi \leftarrow \Sigma$  transition

The vibrational eigenfunctions  $R(r)$  are solutions of the equation

$$d^2 R/dr^2 + \kappa^2 [E - U(r)] R = 0 \quad (5)$$

in which  $U(r)$  is the potential energy function,  $\kappa^2 = 8\pi^2 \mu/h^2$ , and  $\mu$  is the reduced mass of the molecule The potential energy functions that were found suitable for the ground state of the molecule in the region near the potential minimum, and for the upper state in the region of dissociation, are§

$$U''(r) = \beta/(r - r_0)^2 - \gamma/(r - r_0) \quad (6)$$

$$U'(r) = U'_\infty + (n^2 - \frac{1}{2})/\kappa^2 r^2, \quad (7)$$

$\beta$ ,  $\gamma$ ,  $r_0$ ,  $U'_\infty$ , and  $n$  being constants The solution of (5) and (6) gives the energy levels

$$E''_v = \frac{-\kappa^2 \gamma^2}{4m^2 (1 + v''/m)^2}, \quad (8)$$

† 'Z. Physik,' vol 41, p 453 (1927), see also Weizel, "Bandenspektren," 'Handbuch der Exp. Physik, Erg.,' vol 1, p 165

‡ Gibson, Rice, and Bayliss, 'Phys. Rev.,' vol 44, p 193 (1933); Condon and Morse, "Quantum Mechanics" (McGraw Hill, 1929), p 169

§ Gibson, Rice, and Bayliss, 'Phys. Rev.,' vol. 44, p 193 (1933)

where  $v''$  is the vibrational quantum number, and the normalized eigenfunctions for  $v'' = 0$  and 1 are

$$R''_0(r) = \frac{(2a_0)^{m+\frac{1}{2}}}{\{\Gamma(2m+1)\}^{\frac{1}{2}}} \rho^m e^{-a_0 \rho} \quad (9)$$

$$R''_1(r) = \frac{(2a_1)^{m+\frac{1}{2}}}{\{(2m+2)\Gamma(2m+1)\}^{\frac{1}{2}}} \rho^m e^{-a_1 \rho} \left(1 - \frac{a_1 \rho}{m}\right), \quad (10)$$

where  $\kappa^2 \beta = m(m-1)$ ,  $\kappa^2 \gamma = 2a_0 \cdot (v'' + m)$ , and  $\rho = r - r_0$ .

The solution of (5) and (7) gives the following as the normalized eigenfunction of a state of energy  $E'$

$$R'(r) = N' r^{\frac{1}{2}} J_n(\lambda r), \quad (11)$$

where  $N'$  is the normalizing factor and

$$\lambda^2 = \kappa^2 (E' - U'_\infty) \quad (12)$$

$Z(v)$  and the normalization of  $R'(r)$  both involve the size of the containing vessel in such a way that

$$Z(v) \lambda'^2 = h\kappa^2/2 \quad (13)$$

It now remains to derive the expression for the absorption coefficient and to justify equation (4).  $\epsilon_0$  may be interpreted as the absorption coefficient of a gas at a temperature that is low enough for all its molecules to be in the lowest vibrational state. The arguments that will be developed for such a gas take on a more complex form for a gas whose molecules are distributed in thermodynamical equilibrium amongst the states  $v'' = 0, 1, 2$ , etc., but the results will be the same, *mutatis mutandis*, as may be shown easily if it is remembered that  $\sum N_{v''} \epsilon_{v''} = \epsilon$ , where  $N_{v''}$  is the fraction of the molecules that are in the state  $v''$ . For instance, it is immaterial whether  $\epsilon_0$  or  $\epsilon$  be used to calculate  $D$  in equation (17). Consider a beam of photons consisting of  $I_0$  photons/unit frequency range/cm<sup>2</sup>/second to be incident on such a gas of concentration  $C$  mols./litre, and let  $I$  be the intensity after the beam has traversed  $x$  cm. of the gas. A layer of gas of thickness  $dx$  contains  $CN/1000$  molecules/cm<sup>3</sup>,  $N$  being Avogadro's number. Then from the definition of  $kZ(v)$ ,  $dI = -I kZ(v) CN dx/1000$ , whence  $\log(I_0/I) = kZ(v) CNx/(1000 \ln 10)$ . Since the absorption coefficient  $\epsilon_0$  for the gas is defined by the relation  $\log(I_0/I) = \epsilon_0 Cx$ , one has

$$\epsilon_0 = NkZ(v)/(1000 \ln 10) \quad (14)$$

and combining this with (1), (4), (9), (11), (13),

$$\epsilon_0 = \frac{N}{1000 \ln 10} \cdot \frac{8\pi^2\nu}{3hc} \frac{h\kappa^2}{2} D^2 \left\{ \int R''_0(r) r^3 J_n(\lambda r) dr \right\}^2 \quad (15)$$

and the relation between  $\lambda$  and the frequency  $\nu$  to which  $\epsilon_0$  refers is obtained from (12)

$$h\nu = E' - E''_0 = U'_\infty + \frac{\lambda^2}{\kappa^2} - E''_0 \quad (16)$$

(The equations for  $\epsilon_1$  are obtained by replacing  $R''_0(r)$  by  $R''_1(r)$  in (15) and  $E''_0$  by  $E''_1$  in (16))

The classical equation for the relation between the electric dipole moment and the absorption coefficient is  $D^2 = (3h^2/8\pi^3) \int B d\nu$ , and the relation between  $B$ , the Einstein coefficient, and our absorption coefficient leads to the following expression† to be used in calculating  $D$  from the experimental data

$$D^2 = (3hc/8\pi^3 N) 1000 \ln 10 \int \epsilon_0 d\nu/\nu \quad (17)$$

A comparison of equations (17) and (15), remembering that  $Z(\nu) N'^2 = \frac{1}{2} h \kappa^2$ , shows that they involve identical values of  $D$  provided that

$$\int Z(\nu) \left\{ \int R''_0(r) R'(r) dr \right\}^2 d\nu = 1. \quad (18)$$

Without proving (18) mathematically, its correctness may be demonstrated by a consideration of its physical meaning. Since the normalized eigenfunctions  $R'(r)$  refer to a number of discrete states at intervals  $\Delta\nu = 1/Z(\nu)$ , (18) may be expressed as

$$\Sigma \left\{ \int R''_0(r) R'(r) dr \right\}^2 = 1,$$

where the summation is to be extended over all possible transitions from the level  $\nu'' = 0$  that belong to the given electronic transition. Its meaning is therefore that for the gas whose molecules are all in the lowest vibrational state, all the transitions that belong to a given electronic displacement must end on one or other of the levels whose eigenfunctions are  $R'(r)$ . With this interpretation, (18) is obviously true, and the use of the classical value of  $D$  in equation (15) is justified.

† Tolman, 'Phys. Rev.', vol. 23, p. 693 (1924)

## THE CALCULATIONS

The constants needed for the calculation of  $R''_0(r)$  and  $R''_1(r)$  were determined unambiguously from the spectroscopic data† for the  $^1\Sigma_g^+$  state of bromine, (a) by making the few lowest energy levels of equation (8) fit the observed vibrational levels, and (b) by making the minimum of  $U'(r)$  in (6) coincide with the known value of  $r''_e$  (2.28 Å). To calculate  $R'(r)$ ,  $n$  and  $U'_\infty$  could be chosen arbitrarily so that the calculations gave the best fit with the experimental data. The values of the various constants that were used in calculating the A and B continua are given in Table I. For all other constants, the values given by Birge‡ were used, and the calculations were carried out for the molecule  $\text{Br}^{79}\text{Br}^{81}$ .

TABLE I†

Constants for $R''(r)$ and $U''(r)$				Constants for $R'(r)$ and $U'(r)$	
$m$	452	$\beta$	$1.6795 \times 10^{-47}$	A	B
$a_0$	$4.1642 \times 10^{10}$	$\gamma$	$3.1016 \times 10^{-19}$	$n$	775
$a_1$	$4.1550 \times 10^{10}$	$r_0$	$1.20 \times 10^{-8}$	$U'_\infty$ (cm <sup>-1</sup> )	-24200
$\mu$ for $\text{Br}^{79}\text{Br}^{81} = 65.89 \times 10^{-24}$				$D/e$ (cm)	$0.107 \times 10^{-8}$
					$0.0676 \times 10^{-8}$

† All constants are expressed in absolute c.g.s. units unless indicated otherwise.

The calculation of the Bessel function  $J_n(\lambda r)$  over the range of  $r$  in which  $R''(r)$  is appreciable was done by using the Meissel approximations for the regions  $\lambda r > 1$ ,  $\lambda r < 1$ ,§ and the Debye approximation for the region  $\lambda r \approx 1$ ||. The integration in equation (15) was conveniently replaced by the summation

$$\sum_r R''(r) r^{\frac{1}{2}} J_n(\lambda r) \Delta r$$

which was extended over the range for which both the eigenfunctions were appreciable, at intervals  $\Delta r = 0.005$  Å. This method of performing the integration was found in practice to be more rapid than the analytical method used by Gibson, Rice, and Bayliss.  $D$  was found by applying (17) to the experimental data of Acton, Aickin, and Bayliss on the A and B continua. The calculated curves of  $\epsilon_0$  are shown in fig. 1, where their sum is compared with the experimental data. In fig. 2, the curves of  $\epsilon_1$  are similarly compared. The agreement for  $\epsilon_0$  is excellent, and although

† Brown, 'Phys. Rev.', vol. 39, p. 777 (1932).

‡ 'Rev. Mod. Phys.', vol. 1, p. 1 (1929).

§ Watson, "Theory of Bessel Functions" (Cambridge, 1922), p. 227.

|| Jahnke and Emde, "Funktionentafeln" (1923), p. 103.

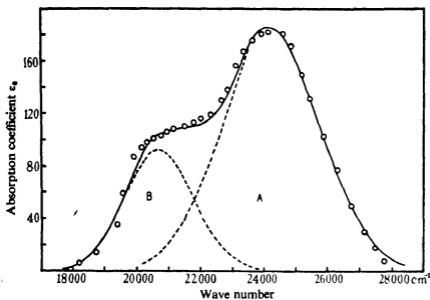


FIG. 1

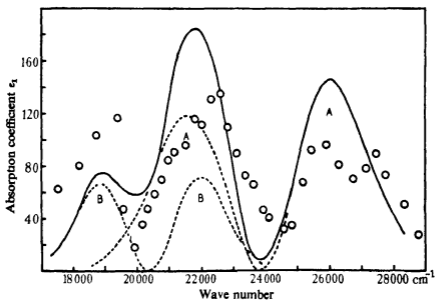


FIG. 2.

the fit for  $\epsilon_1$  is not good, yet it must be regarded as satisfactory, since there are great experimental difficulties in the determination of  $\epsilon_1$  for bromine, where even at room temperature an appreciable fraction of the molecules are in vibrational levels higher than the second

The calculations, which involve as arbitrary constants only  $n$  and  $U'_\infty$ , may be regarded as a method of determining the  $U'(r)$  curves of the upper states of the two continua. In the units necessary to give them in wave numbers and Angstrom units, the potential energy curves thus derived are

$$\begin{aligned} A \quad U'(r) &= -24200 + 600625/2 \cdot 3822r^2 \\ B \quad U'(r) &= -13340 + 422500/2 \cdot 3822r^2 \end{aligned} \quad (19)$$

where the zero of the energy scale is the level  $v'' = 0$  of  $^1\Sigma_g^+$ . In fig 3, these curves are compared with the Morse curve of the  $^3\Pi_{o+u}$  state of bromine, plotted from the data of Brown†. The potential energy curve belonging to the B continuum is a very good extrapolation of the Morse curve, which is evidence in favour of the assignment of the B continuum by Acton, Aickin, and Bayliss to the  $^3\Pi_{o+u} \leftarrow ^1\Sigma_g^+$  transition, and of the A continuum to  $^1\Pi_u \leftarrow ^1\Sigma_g^+$ . As Mulliken has pointed out,‡ this assignment probably means that the B continuum is itself complex, being a mixture of the transitions  $^3\Pi_{o+u} \leftarrow ^1\Sigma_g^+$  and  $^3\Pi_{1u} \leftarrow ^1\Sigma_g^+$ , the complexity not being obvious from the experimental data because the  $U(r)$  curves of  $^3\Pi_{o+u}$  and  $^3\Pi_{1u}$  run close together in the region concerned. If such is the case, our  $U(r)$  curve for B must be regarded as a mean of the two. The method is capable of fixing the slope of the potential energy curves very precisely, since if the curve B in fig 3 were replaced by a curve of the same slope as A, the calculated absorption curve would be more than twice as wide as the experimental one.

The calculations of Gibson, Rice, and Bayliss§ on the continuous absorption of chlorine are not in agreement with equation (15), since their value of the moment, which was chosen to make the theoretical and experimental values coincide, was shown by Mulliken|| to be different from the classical value. However, a recalculation of their integral for a single value of the frequency has shown that a constant numerical error must have entered into their results, and that the value of  $D/e$  that is necessary to fit their calculations to the experimental data is 0.076 A.,

† 'Phys. Rev.', vol 39, p 777 (1932).

‡ 'J. Chem. Phys.', vol 4, p. 620 (1936).

§ 'Phys. Rev.', vol 44, p 193 (1933).

|| 'Phys. Rev.', vol 46, p 549 (1934).

which is in good agreement with the classical value, instead of 0.016 Å, the value quoted in their paper.†

#### AN EMPIRICAL METHOD OF DETERMINING $U(r)$ CURVES

The progress of the work just described was hastened by the discovery of an empirical rule. If the curve of  $R''_0(r)$ , plotted as in fig. 3 as a function

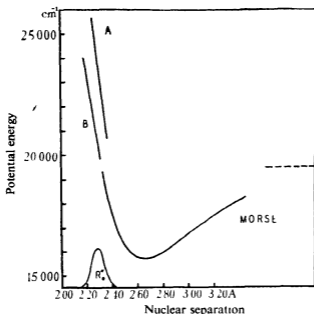


FIG. 3

of  $r$ , is reflected from the curve of  $U'(r)$  on to the frequency axis, the resulting curve accurately describes the variation of the integral

$$\int R''_0(r) r^4 J_n(\lambda r) dr$$

with the transition frequency. Thus, if this curve is squared and multiplied by  $\nu$ , one obtains, except for a constant factor, the calculated values of  $\epsilon_0$  as a function of frequency. In this way, the applicability of a given  $U'(r)$  curve can be tested very rapidly, since the calculation of  $R''_0(r)$  is not difficult. A mathematical proof of the rule was not found, but during the calculations it was found to hold within 1% for points well spread over the curve, and for the several values of  $n$  in the neighbourhood of

† Added to proof. See also Gibson and Rice, 'Phys. Rev.', vol. 50, p. 380 (1936).

700 that were used in the preliminary trials. In his early treatment of continuous absorption, Condon† used this method to explain approximately the observed widths of the halogen continua, but he apparently did not realize that it is capable of a quantitative application. This method of finding the potential energy curve of the upper state of a given continuum is preferable to the method used by Goodeve and Taylor,‡ since by using the expression (6) for  $U''(r)$ , the anharmonic nature of the vibrating molecule is taken into account. In addition, their assumption that  $R''_0(r)$  may be regarded as constant in the region in which  $R'(r)$  is appreciable is incorrect, although their further approximation in omitting the factor  $v$  is probably without much influence on the potential energy curve.

Unless the experimental data include values of  $\epsilon_0$  for the continuum, the above rule will lead to  $U'(r)$  curves that are too steep, since the curve of  $\epsilon$  against frequency is always wider than that of  $\epsilon_0$ . The error that is introduced by using the ordinary absorption coefficients  $\epsilon$  will be greater the smaller is the value of  $\omega_0$  for the ground state of the molecule. Most of the work on continuous spectra has been done at room temperature only, so that in general the data necessary to find  $\epsilon_0$  are not available. However, one can make a rough estimation of  $\epsilon_0$  as follows. At the maximum of the observed continuous absorption, the absorption is due almost wholly to the molecules in the state  $v'' = 0$ , since  $\epsilon_1$  is practically zero at this point, and since there will be relatively few molecules in states  $v'' > 1$ . One may therefore put  $\epsilon_{0(\max)} = (1/N_0) \epsilon_{(\max)}$ , where  $N_0$  is the fraction of the molecules that are in the state  $v'' = 0$ . At the wave-lengths for which  $\epsilon = \frac{1}{2} \epsilon_{(\max)}$ , the absorption coefficient is almost independent of the temperature for the substances investigated (chlorine and bromine), and one may therefore approximate by putting  $\epsilon_0 = \epsilon$  at these points. In this way, the half-width of the  $\epsilon_0$  curve of a given continuum could be estimated from data at room temperature only, and the half-width is the principal factor that determines the slope of the potential energy curve of the upper state.

In conclusion, I wish to express my thanks to Professor R. S. Mulliken for helpful correspondence, to Mr E. H. S. Burhop for kindly criticism, and to Mr R. G. Aickin for assistance with the calculations.

\* 'Phys. Rev.', vol. 32, p. 858 (1928).

† 'Proc. Roy. Soc.', A, vol. 152, p. 221 (1935).

#### SUMMARY

The wave mechanical theory of the continuous absorption spectrum of a diatomic molecule is presented in such a way that the calculation of absorption coefficients involves only two arbitrary constants, which determine the potential energy curve of the upper state concerned in the absorption

The theory is compared with the experimental data for bromine, which has a complex continuum consisting of two well-marked components. The potential energy curve calculated for the upper state of the long wave-length component ( $\lambda_{\max} = 4950 \text{ \AA}$ ) agrees well with the Morse curve of the  $^3\Pi_{o+u}$  state of bromine, while that of the short wave-length major component ( $\lambda_{\max} = 4150 \text{ \AA}$ ) lies some 3000 wave numbers above.

An empirical relation is discussed, which enables one to determine rapidly the course of the potential energy curve of the upper state of a continuous absorption from a knowledge of the absorption coefficients and the spectroscopic constants of the ground state

# The Spectrum of Ionized Tellurium—Extension of Te III

By S G KRISHNAMURTY, M A., Research Scholar, and K R RAO, D Sc ,  
Andhra University, Waltair

(Communicated by A Fowler, F R S—Received 12 August, 1936)

## INTRODUCTORY

In a former communication\* to the Royal Society, a partial analysis of the spectrum of Te III was reported, wherein the terms and the term combinations of the  $5p$ ,  $5d$ , and  $6p$  configurations were recorded. The multiplets in the quartz region, embodying the combinations of the  $6d$ ,  $sp^3$ , and  $7s$  terms could not be brought out with sufficient intensity on the

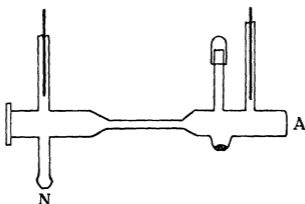


FIG 1—Quartz discharge tube A → to spectrophotograph, N → to pump

photographic plates, owing to the difficulty of maintaining an adequate supply of tellurium vapour in the discharge tube. The melting and boiling points of tellurium being very high, the heating necessary for this purpose was so great that discharge tubes made even of pyrex glass were found to collapse during the experiment. In these later experiments, therefore, a discharge tube made of quartz, and of the design indicated in fig. 1, was used. The end A remained closed permanently, a quartz window being fused to it. This facilitated strong heating of a considerable portion of the tube including the capillary, the capillary itself being kept filled with the vapour of tellurium metal by continuous evacuation of the tube throughout the time of the exposure. This device was found to be very

\* Krishnamurty, 'Proc Roy Soc,' A, vol 151, p. 178 (1935).

effective, the desired multiplets appearing with sufficient intensity on the photographic plates. The instrument used in photographing the spectrum was the Hilger large Littrow type  $E_1$ . The discharge was maintained by a  $\frac{1}{2}$ -kilowatt transformer, used in conjunction with a condenser of capacity of 0.02 mf. The exposures lasted for two or three hours.

#### PREDICTED TERMS

Of the terms in Te III, predicted by Hund's theory, those due to the  $5p$ ,  $5d$ , and  $6p$  configurations were identified in the previous work. The remaining terms, *i.e.*, those due to higher configurations only, are given in Table I.

TABLE I

Term prefix	Terms					
$6p$	$^3D$	$^3P$	$^3S$	$^1D$	$^1P$	$^1S$
$7s$			$^3P$	$^1P$		
$6d$	$^3F$	$^3D$	$^3P$	$^1F$	$^1D$	$^1P$
$sp^3$	$^3S$	$^3S$	$^3D$	$^3P$	$^1D$	$^1P$

All the terms given in Table I have been identified in the present work, with the exception of  $^3S$  and  $^3S$  terms arising from the  $sp^3$  configuration. These terms, however, have not as yet been identified in any of the spectra homologous with Te III.

#### ANALYSIS

All the newly identified multiplets are set out in Table III. The assignments of various terms are not claimed as absolutely certain, because, in this work, comparison could only be made with the analysis of Se III,\* the corresponding data in the iso-electronic spectra of Sn I and Sb II being yet unknown. It is gratifying to note, however, that, from the values ascribed to the  $6d$  terms in the present work, the frequencies of their possible combinations with the  $5p$  terms could be calculated, and the lines were actually observed on plates taken with a large dispersion Siegbahn vacuum grating spectrograph.

The present work has revealed two important characteristic features concerning the terms due to an inner electron transition. (1) According to Hund,† terms arising from a configuration consisting of less than half the number of electrons in a completed sub-group are usually normal (smallest " $J$ " lowest) and those from a configuration consisting of more than half are usually inverted. When such an inversion occurs, the

\* Rao and Krishnamurty, 'Proc. Roy. Soc. A', vol. 145, p. 684 (1934).

† "Linienspektren," p. 198.

normal interval rule might be expected to break down, or at least a considerable departure might occur. In spite of this large departure in Te III, there seems to exist a kind of definite regularity in the intervals of the  $^3P$  as well as the  $^3D$  terms of the above configuration, as is evident from Table II. This table shows only a comparison among similar spectra of the same vertical group.

TABLE II

Spectrum	$sp^3 \ ^3P_0-^3P_1$	$^3P_1-^3P_2$	$^3D_1-^3D_2$	$^3D_1-^3D_3$
O III	-16	unresolved	unresolved	-28
S III	unresolved	-19	28	51
Se III	109	-76	1632	3825
Te III	507	-1550	1082	6941

(2) The second predominant feature is with respect to the magnitudes of the terms themselves. It was observed by Rao,\* in the course of his work on As I and Se III, that the values of such inner electron transition terms relative to those of the first " $s$ " or " $d$ " terms show a marked increase with increasing ionization, when we consider a row of iso-electronic spectra. This would lead to a very interesting consequence, for, though in the arc spectrum of an element,  $eg$ , Ge I, the so-called resonance lines correspond to the transition  $s^2p^2\ ^3P-s^2ps\ ^3P$ , still when we pass on to the iso-electronic spark spectrum of Se III, this resonance transition will be  $s^2p^2\ ^3P-sp^3\ ^3P$ , etc., but not the above. The same occurs with Te III. This would perhaps explain why in some of the arc spectra,  $eg$ , in Sn I, the  $sp^3$  terms have not been located, for these must be expected to give combinations which exist in a region very much below that investigated, while in Te III these have been identified.

The " $ms$ " terms may next be considered. It is seen that though the interval ratios of the  $ms\ ^3P$  terms are large, yet the total interval exhibits a slow and general progression towards the limiting value  $9223\text{ cm}^{-1}$  of  $(5p\ ^3P_1-^3P_{11})$  in Te IV.

$6s\ ^3P_0$		$7s\ ^3P_0$	
	255.6		686.4
$^3P_1$		$^3P_1$	
	7698.3		7827.5
$^3P_2$		$^3P_2$	
	-1206.1		-3913.4
$^1P_1$		$^1P_1$	

\* 'Proc. Roy. Soc.,' A, vol. 125, p. 243 (1929); vol. 140, p. 387 (1933).

According to theoretical consideration  $ms^3P_2$ ,  $^1P_1$ , and  $ms^3P_1$ ,  $^3P_0$  levels should converge to  $mp^3P_{11}$  and  $^2P_1$  respectively of the next higher ion, *i.e.* Te IV. This holds good in C I, Si I, and Ge I-like spectra, but in Sn I-like spectra a slight departure appears to exist, if  $^1P_1$  levels have been correctly identified. For, in Sb II\* and Te III, the interval  $^3P_1$ — $^3P_2$  no doubt increases, but the level  $^1P_1$  tends to approach  $^3P_1$  with the result that the following rule of limits might be operating

$$\begin{aligned} s^3P_2 &\rightarrow p^3P_{11} \\ s^1P_1 \quad ^3P_1 \quad ^3P_0 &\rightarrow p.^2P_1. \end{aligned}$$

TABLE III—MULTIPLETS IN Te III

$\swarrow$ 5p		$^3P_0$	$^3P_1$	$^3P_2$	$^1D_2$
		246955	4751 242204	3434 238790	229577
$sp^3D_1$	164069 3	82890 (10)	78133 (0)	74725 (1)	
	10820 6				
$^3D_2$	153248 7		88955 (2)	85540 (1)	
	6940 7				
$^3D_3$	146308 0			92482 (10)	
$^1D_2$	146491 6		95706 (2)	92304 (10)	
$^3P_0$	150887 3		91307 (10)		
	506 7				
$^3P_1$	150380 6	96579 (10)	91828 (8)	88415 (5)	
	—1549 8				
$^3P_2$	151930 4		90285 (7)	86864 (10)	77674 (1)
$6d^3F_4$	84217 2		157987 (2)		
$^3D_1$	83630 1	163326 (0)			
$^3D_3$	75893 1			162895 (0)	153704 (0)
$7s^3P_1$	76371 6			162420 (0)	153223 (0)
<i>a</i>	145806 0	101142 (2)	96396 (2)	92993 (2)	
<i>b</i>	154654 1	92304 (10)			
<i>c</i>	124833 8		117366 (7)	113951 (3)	

\* Krishnamurty: Unpublished results.

TABLE III—(continued)

	$6p$	$^3P_0$	$^3P_1$	$^3P_2$	$^3S_1$	$^1P_1$
		114692 6	105152 0	107290 5	108665 3	118337 1
$sp^2$	$^1D_1$ 164069 3	49376 (1)			55402 (00)	45735 (0)
	$^1D_2$ 153248 7					34911 9 (2)
	$^1D_3$ 146308 0					
	$^1D_2$ 146491 6		41340 3 (9)	39199 6 (5)	37826 8 (7)	28155 9 (8)
	$^3P_0$ 150887 3					
	$^3P_1$ 150380 6	35689 5 (4)	45227 6 (3)	43088 9 (1)	41715 1 (5)	
	$^3P_2$ 151930 4			44639 1 (3)	43265 1 (5)	
$7s$	$^3P_0$ 77058 0		28094 0 (1)			
	$^3P_1$ 76371 6		28781 1 (2)	30919 1 (8)	32294 1 (6)	41965 7 (1)
	$^3P_2$ 68544 1				40121 4 (10)	
	$^1P_1$ 72457 5	42235 0 (3)	32694 8 (1)		36206 9 (4)	
$c$	124833 8		19682 3 (3)			
$d$	137948 9		32797 7 (0)	30657 5 (10)	29284 5 (7)	
$e$	74066 2			33226 7 (4)		44270 9 (2)
$6d$	$^1D_1$ 83630 1	31061 8 (10)	21524 0 (1)		25036 7 (1)	34707 4 (5)
	$^1D_2$ 74992 6		30159 4 (9)	32298 1 (5)		
	$^1D_3$ 75893 1			31397 5 (10)		
	$^1D_2$ 80343 6					37993 6 (6)
	$^3P_0$ 84607 6					
	$^3P_1$ 85762 4	28930 3 (3)		21529 1 (1)		
	$^3P_2$ 76942 8			30347.6 (9)		
	$^1P_1$ 73385 2			33904 7 (3)		44950.0 (1)

TABLE III—(continued)

	$6p$	$^3D_1$	$^3D_2$	$^3D_3$	$^1D_2$
		114838 3	114625 9	107005 3	103973 0
$sp^3\ ^3D_1$	146491 6		31867 4 (5)	39486 5 (2)	42518 7 (6)
$^3P_0$	150887 3	36049 0 (6)			
$^3P_1$	150380 6		35754 5 (4)		
$^3P_2$	151930 4	37092 5 (3)	37305 0 (8)		
$7s\ ^3P_0$	77058 0	37780 3 (1)			
$^3P_1$	76371 6		38352 6 (2)		27602 6 (3)
$^3P_2$	68544 1			38461 1 (8)	
$^1P_1$	72457 5	42378 6 (0)			31515 7 (4)
$b$	154654 1	39816 2 (2)	40027 8 (1)		
$c$	124833 8				20860 8 (6)
$d$	137948 9			30942 6 (3)	
$e$	74066 2	40772 2 (3)			
$6d\ ^3F_1$	84217 2	30621 1 (10)	30408 7 (5)	22789 6 (2)	
$^3F_2$	83228 6		31397 5 (9)	23776 5 (1)	
$^3F_4$	78411 3			28594 0 (10)	
$^1F_3$	78883 1		35742 4 (10)		25090 3 (10)
$^3D_1$	83630 1	31208 3 (6)	30995 6 (4)		
$^3D_2$	74992 6			32012 6 (6)	
$^3D_3$	75893 1			31112 1 (10)	
$^1D_2$	80343 6				23629 4 (2)
$^3P_0$	84607 6	30230 7 (10)			
$^3P_1$	85762 4	29075 5 (3)	28863 9 (7)		
$^3P_2$	76942 8			30061 8 (10)	27031 1 (3)
$^1P_1$	73385 2				30587 1 (4)

## TERM VALUES

The term values given in the previous paper\* were derived from two members of the sharp series. A number of pairs belonging to other series are available from the present work, but in no case are there found more than two members, hence it is preferred to retain the value of the ground term  $5p^3P_0$  adopted in the previous paper, and the new terms presented in Table IV are determined on this basis.

Finally, in Table V, the lines newly ascribed to Te III, and classified in the present work, are listed. In addition to these, there are still a large number of lines which are to be attributable to the doubly ionized atom of tellurium. But the publication of these is withheld, pending the completion of the analysis of Te II, which will be described in a future communication.

TABLE IV—CATALOGUE OF CLASSIFIED LINES IN Te III

$\lambda$ I A (int.)	$\nu$ vac	Classification	$\lambda$ I A (int.)	$\nu$ vac	Classification
6401 34 (3)	15617 4	$5d^3P_1-6p^3D_1$	3287 58 (5)	30408 7	$^3D_1-^3F_1$
5079 31 (3)	19682 3	$c-6d^3P_1$	3268 41 (4)	30587 1	$^1D_1-^1P_1$
4792 35 (3)	20860 8	$c-^1D_1$	3264 78 (10)	30621 1	$^3D_1-^3F_1$
4644 68 (1)	21524 0	$6p^3P_1-^3D_1$	3260 91 (10)	30657 5	$d-6p^3P_1$
4643 42 (1)	21529 8	$^3P_1-^3P_1$	3233 32 (8)	30919 1	$6p^3P_1-7s^3P_1$
4386 74 (2)	22789 6	$^3D_1-^3F_1$	3230 86 (3)	30942 6	$d-6p^3D_1$
4230 83 (2)	23629 4	$^1D_1-^1D_1$	3225 33 (4)	30995 6	$6p^3D_1-6d^3D_1$
4204 65 (0)	23776 5	$^3D_1-^3F_1$	3213 26 (10)	31112 1	$^3D_1-^3D_1$
3993 01 (3)	25036 7	$^3S_1-^3D_1$	3203 35 (6)	31208 3	$^3D_1-^3D_1$
3984 48 (10)	25090 3	$^1D_1-^1F_1$	3184 05 (0)	31397 5	$^3D_1-^3F_1$
3698 39 (5)	27031 1	$^1D_1-^3P_1$	3172 11 (4)	31515 7	$^1D_1-7s^1P_1$
3621 81 (3)	27602 6	$^1D_1-7s^3P_1$	3137 10 (5)	31867 4	$sp^3^1D_1-6p^3D_1$
3558 47 (1)	28094 0	$^3P_1-^3P_1$	3122 87 (5)	32012 6	$6p^3D_1-6d^3D_1$
3550 64 (8)	28155 9	$sp^3^1D_1-6p^3P_1$	3095 64 (6)	32294 8	$^3S_1-7s^3P_1$
3496 23 (10)	28594 0	$6p^3D_1-^3F_1$	3095 26 (5)	32298 1	$^3P_1-6d^3D_1$
3473 51 (2)	28781 1	$^3P_1-^1D_1$	3057 70 (1)	32694 8	$^3P_1-7s^3P_1$
3463 55 (7)	28863 9	$^3D_1-6d^3P_1$	3048 11 (0)	32797 7	$d-6p^3P_1$
3455 59 (3)	28930 3	$^3P_1-^3P_1$	3008 75 (4)	33226 7	$6p^3P_1-c$
3438 33 (3)	29075 5	$^3D_1-^3P_1$	2948 59 (3)	33904 7	$^3P_1-6d^3P_1$
3413 80 (7)	29284 5	$d-^3S_1$	2880 38 (5)	34707 4	$^3P_1-^3D_1$
3325 52 (10)	30061 8	$6p^3D_1-^3P_1$	2863 51 (2)	34911 9	$sp^3^3D_1-6p^3P_1$
3314 77 (9)	30159 4	$^3P_1-^3D_1$	2801 16 (4)	35689 5	$^3P_1-^3P_1$
3313 81 (10)	30168 1	$5d^3F_1-6p^3D_1$	2797 97 (10)	35742 4	$6p^3D_1-6d^3F_1$
3307 02 (10)	30230 7	$6p^3D_1-6d^3P_1$	2796 03 (4)	35754 5	$sp^3^3P_1-6p^3D_1$
3294 21 (5)	30347 6	$^3P_1-^3P_1$	2773 18 (6)	36049.0	$^3P_0-^3D_1$

\* *Idem*, 'Proc. Roy. Soc.,' A, vol. 151, p 178 (1935).

TABLE IV—(continued)

$\lambda$ I A. (int)	$\nu$ vac	Classification	$\lambda$ vac.	$\nu$ vac	Classification
2761 09 (4)	36206 9	$6p\ ^3S_1-7s\ ^1P_1$	2025 20 (1)	49376	$sp^3\ ^3D_1-6p\ ^3P_0$
2695 04 (4)	37094 2	$5d\ ^3F_4-6p\ ^3P_1$	1805 00 (0)	55402	$^3D_1-^3S_1$
2679 81 (2)	37305 8	$sp^3\ ^3P_2-^3D_3$	1338 23 (1)	74725	$5p\ ^3P_2-sp^3\ ^3D_1$
2646 12 (0)	37780 3	$6p\ ^1D_1-7s\ ^3P_0$	1287 44 (1)	77674	$^1D_2-^3P_2$
2642 84 (5)	37826 8	$sp^3\ ^1D_2-6p\ ^3S_1$	1279 86 (0)	78133	$^3P_1-^3D_1$
2631 24 (8)	37993 6	$6p\ ^1P_1-6d\ ^1D_2$	1206 42 (10)	82890	$^3P_0-^3D_1$
2613 42 (2)	38252 6	$^3D_3-7s\ ^3P_1$	1169 04 (1)	85540	$^3P_3-^3D_3$
2599 25 (7)	38461 1	$^3D_5-^3P_1$	1151 23 (10)	86864	$5p\ ^3P_2-sp^3\ ^3P_2$
2550 28 (5)	39199 6	$sp^3\ ^1D_2-6p\ ^3P_2$	1131 02 (5)	88415	$^3P_2-^3P_1$
2531 75 (2)	39486 5	$^1D_2-^3D_3$	1124 16 (2)	88955	$^3P_1-^3D_3$
2510 78 (2)	39816 2	$b\ -6p\ ^3D_1$	1107 60 (7)	90285	$^3P_2-^3P_3$
2497 51 (1)	40027 8	$b\ -6p\ ^3D_2$	1095 21 (10)	91307	$^3P_1-^3P_0$
2491 68 (10)	40121 4	$6p\ ^3S_1-7s\ ^3P_2$	1088 99 (8)	91828	$^3P_1-^3P_1$
2451 96 (3)	40772 2	$^3D_1-e$			$\begin{cases} ^3P_0- b \\ ^3P_2-^1D_2 \end{cases}$
2418 21 (9)	41340 3	$sp^3\ ^1D_2-6p\ ^3P_1$	1083 38 (10)	92304	$^3P_2-^3D_2$
2396 48 (5)	41715 1	$^3P_1-^3S_1$	1081 29 (10)	92482	$^3P_2-^3D_2$
2382 17 (1)	41965 7	$6p\ ^1P_1-7s\ ^3P_1$	1075 35 (2)	92993	$^3P_2- a$
2366 98 (3)	42235 0	$^3P_0-^1P_1$	1044 87 (2)	95706	$^3P_1-^1D_2$
2358 96 (0)	42378 6	$^3D_1-^1P_1$	1037 39 (2)	96396	$^3P_1- a$
2351 19 (6)	42518 7	$sp^3\ ^1D_2-6p\ ^1D_2$	1035 79 (7)	96545	$^3P_2-5d\ ^3F_4$
2320 07 (1)	43088 9	$^3P_1-^3P_2$	988 71 (2)	101142	$^3P_0- a$
2310 59 (3)	43265 6	$^3P_2-^3S_1$	877 57 (5)	113951	$^3P_2- c$
2258 12 (2)	44270 9	$6p\ ^1P_1-e$	852 04 (7)	117366	$^3P_1- c$
2239 48 (3)	44639 1	$sp^3\ ^3P_2-6p\ ^3P_2$	652 64 (0)	153223	$^1D_2-7s\ ^3P_1$
2223 99 (10)	44950 0	$6p\ ^1P_1-6d\ ^1P_1$	650 60 (0)	153704	$^1D_2-6d\ ^3D_2$
2210 35 (3)	45227 6	$sp^3\ ^3P_1-6p\ ^3P_1$	632 96 (2)	157987	$^3P_1-^3F_2$
2186 52 (1)	45735 0	$^3D_1-^3S_1$	615 69 (0)	162420	$^3P_2-7s\ ^3P_1$
			613 89 (0)	162895	$^3P_2-6d\ ^1D_2$
			612 27 (0)	163326	$^3P_0-^3D_1$

## SUMMARY

With a view to extend the analysis of Te III previously undertaken by the authors, further experiments with suitably modified discharge tubes have been conducted, and the results obtained have led to the identification of the terms due to the  $sp^3$ ,  $6d$ , and  $7s$  configurations. More than a hundred lines have newly entered the scheme for Te III. Interesting deviations from the normally expected characteristics are recorded

TABLE V—NEW TERMS IN Tc III

Term	Term value		Term	Term value	
<i>sp</i> <sup>3</sup> D <sub>1</sub>	164069 3		6 <i>d</i> <sup>3</sup> F <sub>4</sub>	84217 2	
<sup>3</sup> D <sub>2</sub>	153248 7	10820 6	<sup>3</sup> F <sub>3</sub>	83228 6	988 6
<sup>3</sup> D <sub>3</sub>	146308 0	6940 7	<sup>3</sup> F <sub>2</sub>	78411 3	4817 3
<sup>1</sup> D <sub>2</sub>	146491 0		<sup>1</sup> F <sub>3</sub>	78883 1	
<sup>3</sup> P <sub>0</sub>	150887 3		<sup>3</sup> D <sub>1</sub>	83630 1	
<sup>3</sup> P <sub>1</sub>	150380 6	506 7	<sup>3</sup> D <sub>2</sub>	74992 6	8637 5
<sup>3</sup> P <sub>2</sub>	151930 4	—1549 8	<sup>3</sup> D <sub>3</sub>	75893 1	—900 5
7 <i>s</i> <sup>3</sup> P <sub>0</sub>	77058 0		<sup>1</sup> D <sub>2</sub>	80343 6	
<sup>3</sup> P <sub>1</sub>	76371 6	686 4	<sup>3</sup> P <sub>0</sub>	84607 6	
<sup>3</sup> P <sub>2</sub>	68544 1	7827 5	<sup>3</sup> P <sub>1</sub>	85762 4	—1154 8
<sup>1</sup> P <sub>1</sub>	72457 5		<sup>3</sup> P <sub>2</sub>	76942 8	8819 6
<i>a</i>	145806 0		<sup>1</sup> P <sub>1</sub>	73385 2	
<i>b</i>	154654 1		<i>e</i>	74066 2	
<i>c</i>	124833 8				
<i>d</i>	137948 9				

---

## On the Absolute Intensities of the Strong $\beta$ -Ray Lines of Ra (B + C), Th (B + C), and Ac (B + C)

By K T LI, of Emmanuel College, Cambridge

(Communicated by C D Ellis, F R S—Received 18 August, 1936)

### I—INTRODUCTION

It is now well established that the homogeneous  $\beta$ -ray groups emitted by radioactive bodies arise by internal conversion of the  $\gamma$ -rays. The ratio of the number of electrons emitted to the number of associated  $\gamma$ -ray quanta is called the internal conversion coefficient and is a quantity of considerable theoretical interest.

An accurate knowledge of the absolute intensities of the  $\beta$ -ray groups is of great importance in determining the internal conversion coefficient in cases where from other evidence the  $\gamma$ -ray intensity is known, or conversely for finding the intensity of the  $\gamma$ -rays by assuming theoretical or empirical values for the internal conversion coefficient.

Relative intensities, even of weak  $\beta$ -ray lines, can be determined fairly easily. In order to know the absolute intensities of all  $\beta$ -ray lines, we need only an absolute determination of the number of electrons per disintegrating atom for one or more of the strong lines. This measurement was carried out by Gurney for RaB\* and ThB† and his values have been universally accepted, although there has been no independent verification.

In the present experiment a direct repetition of Gurney's work was not attempted, but first the relative intensities of the RaB lines were re-measured photographically and secondly the relative intensities of the F line of ThB to the three strong lines of RaB were determined on the basis of equal numbers of disintegrating atoms.

The general result obtained confirms some values of Ellis and Aston‡ for the three RaB lines and also Gurney's value for the ratio of the H line of RaB to the F line of ThB. Further, a critical examination of the data, taking these facts into account, suggests that Gurney's absolute values of the H line of RaB and the F line of ThB are probably dependable, and that his values of the lines G and F of RaB were in error.

\* 'Proc Roy Soc.,' A, vol 109, p. 540 (1925).

† *Ibid*, vol 112, p. 380 (1926)

‡ 'Proc Roy Soc.,' A, vol 129, p. 180 (1930)

The absolute intensities of the lines from  $\text{Ac}(\text{B} + \text{C})$  have never been determined, and therefore, in the course of the present experiments, the relative intensities of the strong line of  $\text{AcC}$  to the strong lines of  $\text{ThB}$  have been compared on the basis of equal numbers of disintegrating atoms. Accepting the absolute intensity of the  $\text{F}$  line of  $\text{ThB}$  determined by Gurney, this gives the absolute intensities of all the lines from  $\text{Ac}(\text{B} + \text{C})$ .

In § 2 we shall describe the method and the apparatus used. The results of the experiments will be given in § 3. Finally in § 4, the intensities of the  $\gamma$ -rays from  $\text{AcC}$  and  $\text{AcC}''$  are discussed and level schemes for these two nuclei suggested.

## 2—METHOD AND APPARATUS

In order to obtain the relative intensities of  $\beta$ -ray groups from different products for equal numbers of disintegrating atoms, two distinct measurements must be made. These are the measurement of the strength of the source and of the number of electrons in each group. For the latter, the photographic method of recording was used. For the former, we had to choose between the  $\alpha$ -ray activity and the  $\gamma$ -ray activity as a measure of the number of disintegrating atoms. There are two difficulties in using the  $\gamma$ -ray activity. First, the ratio of the  $\gamma$ -ray activity from  $\text{Ac}(\text{B} + \text{C})$  to that from  $\text{Ra}(\text{B} + \text{C})$  for equal numbers of disintegrating atoms is not known. Secondly, the deposit on the source may not be uniform, the  $\gamma$ -ray measurement of the source as a whole would not then indicate the strength of that portion used for the photograph. We therefore decided to compare the strength of different sources by measuring the  $\alpha$ -radiation.

### *a—Measurement of the Strength of Source*

A Lindemann electrometer connected to a parallel plate ionization chamber was used to measure the ionization current by the normal compensation method. The design of the ionization chamber was as follows. Two parallel circular electrodes were fixed at the ends of a copper cylinder. The collecting electrode was insulated with a quartz tube and surrounded by a guard ring earthed through the outer cylinder. The  $\alpha$ -particles entered through a rectangular window which was covered by a piece of mica of 4 mm stopping power. This window was sufficiently large to receive all the rays coming through the defining slit from the source. It is of prime importance to use the same portion of the source for measuring the activity and for taking the photograph. To satisfy this con-

dition, the ends of the wire source were waxed to the top of a U-shaped holder, and both this holder and the defining slit were kept fixed rigidly on an aluminium frame during both measurements. Two identical supports, one under the ionization chamber and the other in the  $\beta$ -ray spectrograph, were used to hold this frame and to keep it in the same position for all measurements. Further, to ensure that the source had not been disturbed, the whole frame was slipped into another holder and examined under a travelling telescope before and after the experiment. From an analysis of the semi-circular focussing it can be easily shown that it is not exactly the top half of a circular wire source which contributes to the  $\beta$ -ray line. If we refer to the cross-section of a wire as shown in fig 1, it is not the arc AB but the arc CD that builds up the line. The portion actually used in  $\alpha$ -ray measurement is the arc AB

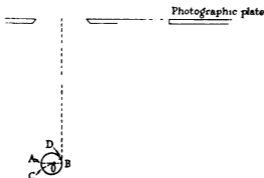


FIG 1

Since the arcs AB and CD are equal to a high order of approximation, the only error that can occur is when the amount of active deposit on AC is not the same as that on DB. But the arcs AC and DB are only 5% of the portion used, and, even if the source is not well distributed, the difference of the total radiation from the arcs AB and CD is within the experimental error.

The distance from the source to the collecting electrode was adjusted in such a way that only the last 1.2 cm. of the range of the  $\alpha$ -particles were effective in producing ions. The holder was so fixed as to make the 6.87 cm.  $\alpha$ -particles of RaC' satisfy this condition. This was verified by observing the variation in the ionization when mica sheets of different stopping power were inserted. It was found that an absorption equivalent to 1.2 cm. of air just reduced the current to zero. In measuring the strength of the Th (B + C) sources, the 8.53 cm.  $\alpha$ -particles from

\* This is the mean range at 15° C, 760 mm.

ThC' were used. In order to produce the same ionization current for each  $\alpha$ -particle, the same portion of the range should be used. It was undesirable to lower the source in the holder since this would have altered the solid angle for photographing the  $\beta$ -ray lines, instead, a mica sheet of approximately 1.65 cm air-equivalent, supported on an aluminium frame, was interposed between the source and the chamber. The frame was fixed to a rod which could be rotated until the actual path of the  $\alpha$ -particle in the mica was equivalent to 1.66 cm of air, giving an emergent range equal to that of RaC'  $\alpha$ -particles. The reliability of this adjustment was tested by taking a reading with and without this piece of mica. The ratio was found to be exactly that expected from the number of ions produced in different parts of the path of an  $\alpha$ -particle.

For the measurement of the Ac (B + C) sources, we could only use the 5.4 cm  $\alpha$ -particles from AcC. The source holder was raised so as to allow again the last 1.2 cm of the  $\alpha$ -particle range to enter in between the electrodes. As before, comparison experiments were carried out with Th (B + C) sources in the same position as the Ac (B + C) sources and with sufficient mica to reduce the emergent range of the 8.53 cm  $\alpha$ -particles to 5.4 cm. A smaller defining slit was used in this case in order to give the same sharp spectrum and nearly the same solid angle.

As a further check, the  $\gamma$ -ray activities of Ra (B + C) and Th (B + C) sources were also determined and on the occasions when the deposit was reasonably uniform, as found by  $\alpha$ -ray measurement, the ratio of the  $\gamma$ -ray activity to the  $\alpha$ -ray activity agreed fairly well with Shenstone and Schlundt's\* measurements.

#### *b—Measurement of Intensity of $\beta$ -ray Lines*

The usual semicircular focussing arrangement was employed, using a large permanent magnet†. The active deposit was collected on a platinum wire 0.25 mm in diameter. The lines were registered on X-ray plates, and the densities measured by a recording photoelectric photometer.

In each set of photographs taken, a separate plate was exposed to a constant source of  $\beta$ -particles for different times and was developed together with the other plates. In this way a characteristic curve for dependence of the blackening on the exposure could be obtained, and this was used to convert the photographic densities to electron densities.

\* 'Phil Mag.', vol 43, p. 1038 (1922).

† Cockcroft, Ellis, and Kershaw, 'Proc. Roy. Soc.', A, vol 135, p. 628 (1932).

The correction for the variation of photographic action with the energy of the electrons was based on the curve given by Ellis \*. The reliability of this curve will be discussed later. The correction for the solid angle with the radius of curvature of the path of electrons was based on calculations made by the writer.†

For Ac (B + C), only a very weak source of a few hundredths of a millicurie was available. To obtain measurable density on the plate, it was necessary to use some twenty sources for each photograph, and the measurement would have been impossible without the use of a permanent magnet. The field remained remarkably constant, and with care in inserting the successive sources the B line of AcC was obtained with reasonable sharpness. The field was usually checked by taking a photograph of the I line of ThB before and after each Ac photograph; no appreciable shift could be noted in the photographs after an interval of ten days.

### 3—RESULTS AND DISCUSSION

For each photograph the exposure could be expressed in arbitrary units by means of the  $\alpha$ -ray measurements. On the other hand, the photometric density, after correction for the photographic action, the characteristic curve of the plate, and the solid angle, gave the true electron density also in arbitrary units. The experimental results are shown in fig. 2 where the electron density is plotted against the exposure for each of the lines investigated. It will be seen that all the points fall on a series of straight lines, the relative slopes of which give the relative intensities of the lines. Since in these experiments both the magnetic field and the exposures were varied, the linear relation shows that the correction applied for the characteristic of the plate and varying solid angle were reasonably accurate.

The final results are shown in the column I of the next table expressed in number of electrons per disintegration, by assuming the value of the F line of ThB being equal to Gurney's value of 0.25. Column II shows Gurney's value and column III those of Ellis and Aston for RaB.

In the first place, we notice that the present experiment confirms the relative photographic measurement of Ellis and Aston and also the relative values of Gurney for RaB H and ThB F. We think that there can be no doubt that Gurney's value for the G and F lines of RaB are in error. As pointed out by Ellis and Aston, this experiment was particularly difficult in this region of low energy owing to the uncertainty in separating

\* 'Proc Roy Soc.' A, vol 138, p 318 (1932).

† Li, 'Proc Camb Phil Soc' (*in the press*).

TABLE I

Line	H $\rho$	I (Li)	II (Gurney)	III (Ellis and Aston)
RaB H	1938	0.0545	0.053	0.053
G	1677	0.0487	0.039	0.048
F	1410	0.0432	0.024	0.042
ThB F	1385	0.250	0.25	
I	1751	0.0353		
AcC B	1946	0.0162		

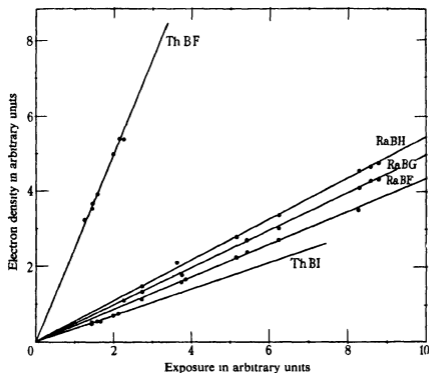


FIG. 2

the groups from the rapidly descending continuous spectrum. This was not so for the F line of ThB because of the different shapes of the continuous spectrum and of the high intensity of the line. It should be mentioned that Ellis and Aston's value can be taken not only as a relative measurement but also as a reasonably accurate absolute determination, and, therefore, the agreement for the H line of RaB is an independent

confirmation. Our final conclusion is that the figures shown in column I represent reasonable values for the absolute intensities of these  $\beta$ -ray groups

As regards the general accuracy of the photographic work, it may be of interest to quote several independent measurements for the relative intensities of the two strong lines of F and I of ThB. These are shown in Table II

TABLE II

Worker Method	Ellis*	Arnoult†	Wang‡	Li
	Photographic	Photographic	Electric	Photographic
F	250	250	250	250
I	35 3	35 4	33 4	35 3

\* 'Proc. Roy. Soc.,' A, vol. 138, p. 318 (1932)

† 'C. R. Acad. Sci. Paris,' vol. 198, p. 1603 (1934)

‡ 'Z. Physik,' vol. 87, 9-10, p. 633 (1934)

An important point in all these measurements is the correction for the variation of the photographic action of  $\beta$ -particles of different speeds. In the present experiment the empirical curve of Ellis\* for this particular type of plates was used. No fresh measurements were made on this point, but the agreement noted above between the relative intensities of the lowest energy line F of ThB and the highest energy line H of RaB by photographic methods seems to indicate the essential validity of this correction

#### 4—DISCUSSION OF THE TRANSITIONS $AcC$ , $C''$ AND $AcB$ , $C$

From the measurement of the intensity of the B line of  $AcC$  we can derive the absolute intensities of the other  $\beta$ -ray lines by using the latest determination of their relative intensities by Surugue†. These values are given in Table III. It will be seen from the table that the various  $\beta$ -ray groups can be associated with five  $\gamma$ -ray transitions and are due to conversion in the various electronic levels as indicated. To obtain the intensities of the  $\gamma$ -rays, we have to assume values for the internal conversion coefficients. The theoretical curves calculated by Hulme,‡ Taylor and Mott,§ and Fisk|| did not agree completely with the experimental results, but the fact that most of the internal conversion coefficients

\* 'Proc. Roy. Soc.,' A, vol. 138, p. 330 (1932)

† 'C. R. Acad. Sci. Paris,' vol. 202, p. 410 (1936)

‡ 'Proc. Roy. Soc.,' A, vol. 138, p. 643 (1932)

§ Taylor and Mott, *ibid.*, vol. 138, p. 665 (1932), vol. 142, p. 215 (1933).

|| *ibid.*, vol. 143, p. 674 (1934)

did lie smoothly on two curves led these writers to derive two empirical\* curves by taking into account all the data available at present. The "empirical conversion coefficients" quoted in the column VI of Table III are taken from these curves. We consider the disintegrations  $\text{AcC} \cdot \text{C}'$  and  $\text{AcB} \cdot \text{C}$  separately as follows.

(i)  $\text{AcC} \cdot \text{C}'$ —It is known that the transition  $\text{AcC} \cdot \text{C}'$  is an  $\alpha$ -disintegration. The two groups of  $\alpha$ -rays from  $\text{AcC}$  have an energy difference equal to the energy of the  $\gamma$ -ray emitted. The relative abundance of these two groups has been measured by Rutherford, Wynn-Williams, and Lewis,† and by Rosenblum, Guillot, and Perry‡ with concordant results and found to be 0.84 of the long range group. This means that the total probability of excitation is 0.16, so that writing  $p(1 - \alpha)$  for the probability of  $\gamma$ -ray emission,  $p\alpha$  for the intensity of the  $\beta$ -ray group, it is clear that  $p$  is 0.16. The present experiment has shown that  $p\alpha = 0.016$  giving a value of  $\alpha$  equal to 0.10.

By referring to the entry in column VI of Table III against  $\gamma\text{B}$ , it is obvious that this transition cannot be dipole. The experimental value 0.10 agrees with the quadrupole value from the empirical curve, which, however, lies considerably above the theoretical curve. In fact, the theoretical value for the electric quadrupole radiation of this frequency would be 0.052. This confirms the conclusion already reached by Hulme and his colleagues (*loc cit*) that many of the internal conversion coefficients of the soft  $\gamma$ -rays have values considerably greater than can be accounted for by quadrupole radiation. It is interesting to remember that these authors tentatively suggested that these soft  $\gamma$ -rays correspond to transitions between the states of a nuclear multiplet.

(ii)  $\text{AcB} \cdot \text{C}$ —The transition  $\text{AcB} \cdot \text{C}$  differs from the  $\text{RaB} \cdot \text{C}$  and  $\text{ThB} \cdot \text{C}$  transitions in that the intensities of all the  $\beta$ -ray groups are extremely low and much less than that of  $\text{C} \cdot \text{C}'$  transition. Direct investigation of the  $\gamma$ -rays by absorption methods indicates that they are of a reasonable intensity, and it therefore seems probable that the  $\text{AcB} \cdot \text{C}$  transitions are mainly dipole in nature and are much less converted. As a tentative solution of this problem, it is suggested that  $\gamma\text{C}$  and  $\gamma\text{D}_2$  are dipole transitions. The quantum energies of the  $\gamma$ -rays lead to a level system as shown in fig. 3, and it therefore is simplest to assume  $\gamma\text{E}$  to be a quadrupole transition. The corresponding intensities of these  $\gamma$ -rays are printed in heavy type in Table III, column VII, and are used to calculate the excitations shown in fig. 3.

\* Hulme, Mott, Oppenheimer, and Taylor, *ibid.*, vol. 155, p. 315 (1936).

† 'Proc. Roy. Soc., A', vol. 133, p. 351 (1931).

‡ 'C.R. Acad. Sci. Paris,' vol. 202, p. 1274 (1936).

TABLE III  
AcB C

Line	Hp	II Energy in e-volts	III Energy of $\gamma$ -ray in e-volts	IV Shell	V Intensity		VI Experimental internal conversion coeff for K shell		VII $\gamma$ -ray intensity (calc from cols V & VI)	
					Rel	Abs (electron/ disint.)	Quadrupole	Dipole	Quadrupole	Dipole
$\gamma$ A A <sub>a</sub> A <sub>b</sub> A <sub>c</sub>	763.2	48.90	65.22	L <sub>I</sub>	20	0.0032	—	—	—	—
	768.5	49.56	65.22	L <sub>II</sub>	2	0.0003	—	—	—	—
	858.8	61.22	65.23	M <sub>I</sub>	5	0.0008	—	—	—	—
	881.3	64.29	65.23	N <sub>I</sub>	1	0.0002	—	—	—	—
$\gamma$ C D <sub>c</sub>	2157	313.4	403.8	K	25	0.0041	0.062	0.017	0.065	0.238
	2522	387.5	403.8	L <sub>I</sub>	3	0.0005	—	—	—	—
$\gamma$ D <sub>a</sub> D <sub>b</sub> D <sub>c</sub>	2250	335.2	425.6	K	20	0.0032	0.052	0.016	0.062	0.202
	2544	409.4	425.7	L <sub>I</sub>	5	0.0008	—	—	—	—
	2602	421.7	425.7	M <sub>I</sub>	5	0.0008	—	—	—	—
$\gamma$ E E <sub>a</sub>	3805	739.0	829.4	K	10	0.0016	0.012	0.004	0.135	0.400
	4075	813.2	829.4	L <sub>I</sub>	2	0.0003	—	—	—	—
AcC C''										
$\gamma$ B D <sub>1</sub> D <sub>a</sub> D <sub>b</sub>	1946	264.6	349.7	K	100	0.0162	0.100	0.025	—	—
	2247	334.4	349.7	L <sub>I</sub>	40	0.0065	—	—	—	—
	2295	346.0	349.7	M <sub>I</sub>	5	0.0008	—	—	—	—
	2306	348.8	349.7	N <sub>I</sub>	1	0.0002	—	—	—	—

The total  $\gamma$ -ray emitted per disintegration by AcB C becomes with these assumptions  $3 \times 10^5$  e-volts, and the same quantity for the transition AcC C'' must be  $0.56 \times 10^6$  e-volts by direct deduction from the  $\alpha$ -ray results

In conclusion, the writer wishes to express his thanks to Lord Rutherford for his interest in this work, and to Dr C D Ellis for suggesting the problem and for his helpful advice, also to Mr G R Crowe for preparing the radioactive sources

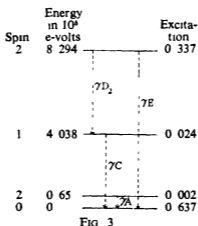


FIG. 3

## SUMMARY

The intensities of the strong  $\beta$ -ray lines of Ra (B + C), Th (B + C), and Ac (B + C) have been measured by the photographic method on the basis of equal numbers of disintegrating atoms

The results of the measurements confirm some values of Ellis and Aston for the three RaB lines and also Gurney's value for the ratio of the H line of RaB to the F line of ThB

By comparing the relative intensities of the strong lines in ThB and AcC the absolute intensities of all the  $\beta$ -ray lines of Ac (B + C) were obtained. Using the values of the internal conversion coefficients from the empirical curves of Hulme, Mott, Oppenheimer, and Taylor, the  $\gamma$ -ray intensities from Ac (B + C) could be calculated. For the strong  $\gamma$ -ray line from AcC it is possible to obtain values for the internal conversion coefficient by making use of the measured intensity of the  $\alpha$ -ray groups. The value obtained is more than twice the theoretical quadrupole curve and lies on the empirical curve referred to above.

## Studies of Cosmic-Ray Showers by Quintuple Coincidences

By HU CHIEN SHAN, Birkbeck College, London

(Communicated by P M S Blackett, F R S—Received 18 August, 1936)

### 1—METHOD AND APPARATUS

In the past, most of the investigations of cosmic-ray showers by means of counters have been made by using a triple coincidence method. In the present experiments a quintuple coincidence method is used. It offers the following advantages. The casual coincidence rate is greatly reduced by adding two more counters, so that the correction for casual rate can be omitted altogether.

If the five counters are given the pentagonal arrangement shown in figs 1 and 3, then at least three rays are required to operate all the counters to cause a coincidence wherever the rays come from. Thus all showers counted contain at least three rays each. Although in Gilbert's three-counter arrangement\* the lead plate is limited so that a shower produced in the lead is only counted if it contains three or more particles, two rays are sufficient to cause a triple coincidence, if they come not from the lead but from the air or from the surrounding materials. In the quintuple coincidence pentagonal arrangement, there is no need to limit the size of the shower-producing material. Thus more material can be used and so the rate of the shower production can be raised. The sheets used to produce showers are bent into semi-cylindrical form (fig 1). In this arrangement, all the shower particles which cause a coincidence have roughly an equal path in the shower-producing material.

Recently an arrangement of four counters has been used by Auger,† Leprince-Ringuet, and Ehrenfest. Though this responds to two rays from certain directions, it does not respond to two rays diverging from a single point in the absorber. Thus it does not count simple secondaries and so it effectively only counts showers.

Quintuple coincidences have already been used for studying cosmic-ray showers by Funfer,‡ but the arrangement of counters was different. One counter was placed closely below the shower-producing lead, the

\* 'Proc Roy Soc,' A, vol 144, p 560 (1934)

† Auger, Leprince-Ringuet, and Ehrenfest, 'J Phys Rad.,' vol. 7, p. 58 (1936).

‡ 'Z. Phys.,' vol. 83, p. 92 (1933).

other four were placed below the first, lying almost all in a horizontal plane. By using this arrangement, he was able to show the similarity in the shape of the air-lead transition curves obtained by quintuple and by triple coincidence counting.

The amplifier circuit is constructed as recommended by Fussell and Johnson,\* and by Barasch†. All leads connecting counters to the amplifier were carefully shielded to avoid pick-up. The resolving time is of the order of  $10^{-3}$  second.

For the work reported in § 2, the measurements were made with brass counters of 0.96 cm internal diameter and 30 cm effective length. For

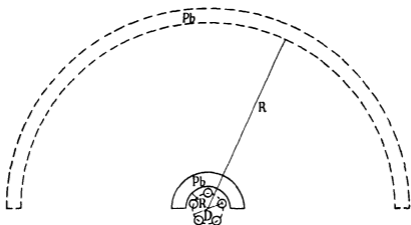


FIG. 1—The arrangement of counters and shower-producing material for transition curve measurement

the work reported in §§ 3 and 4, glass counters of 1.6 cm diameter and 30 cm length were used. All counters are filled with 20% air and 80% argon, at a total pressure of about 20 cm Hg, so as to give a high efficiency of counting cosmic-ray electrons. A high efficiency is important, since the number of quintuple coincidences counted is proportional to the fifth power of the efficiency of a single counter.

## 2—TRANSITION CURVES FOR WIDE AND FOR NARROW ANGLE SHOWERS PRODUCED IN LEAD

It is known that a free electron initially at rest will be projected at an angle  $\theta$  by the impact of a high speed electron,‡ where  $\tan \theta = (2mc^2/E)^{1/2}$ ,

\* 'J. Franklin Inst.', vol. 217, p. 517 (1934).

† 'Proc. Phys. Soc.', vol. 47, p. 824 (1935).

‡ W. Heisenberg, 'Ann. Physik', vol. 13, p. 430 (1932).

where  $m$  is the rest mass of the electron,  $c$  is the velocity of light, and  $E$  the kinetic energy of the secondary electron after collision. However, the actual mechanism of shower production is certainly not mainly of the type of simple collision with an electron but is probably more of the nature of multiple electron-positron pair-production\*.

According to the theoretical calculations of Bethe and Heitler,† the average angle  $\bar{\theta}$  between the direction of the incident photon and that of the created electrons of energy  $E$  is of the order of  $mc^2/E$ . Thus, if we assume that simple pair-production is the chief mechanism of shower formation, we should expect the mean angle  $\bar{\theta}$  of a shower whose particles have a mean energy  $\bar{E}$  to be of the order of  $mc^2/\bar{E}$ . Since Anderson‡ has shown that  $\bar{E}$  for shower particles is of the order of  $15 \times 10^6$  e.v., we may expect the value of  $\bar{\theta}$  to be of the order of  $2^\circ$ . The cloud photographs appear to show a rather greater mean speed.

If, however, showers are due to the production of multiple pairs at a single process—whether such processes occur is still uncertain—it is not possible to calculate the angular distribution, since no theory of such processes exists. But it is reasonable to assume that a relation of the type  $\bar{\theta} \propto mc^2/\bar{E}$  should still hold, though possibly with an additional factor depending on the number of particles in the shower.

So, whatever the actual mechanism, one would expect the mean divergence of a shower to decrease as the mean energy of the particles increases, and some evidence that this is true can be obtained from shower photographs. It follows that the maximum range of the particles should be greater the narrower the shower. Though recent experimental results§ throw considerable doubt on the simple Rossi-Gilbert interpretation of the transition curve, which identifies the thickness of the absorber corresponding to the maximum of the curve, as giving the range of the shower particles, it seemed probable that the maximum of the transition curve would depend to some extent on the energy of the shower particles. Thus, we should expect some difference between the maxima of the transition curves for showers of different angular spread.

In view of these considerations the transition curve for lead has been investigated with counters arranged to record showers of varying angle.

The five counters of diameter 0.95 cm. are arranged as shown in

\* P. M. S. Blackett and G. P. S. Occhialini, 'Proc. Roy. Soc.,' A, vol. 139, p. 699 (1933).

† 'Proc. Roy. Soc.,' A, vol. 146, p. 83 (1934).

‡ 'Int. Conf. Phys., London,' October, 1934.

§ Clay, 'Physica,' vol. 3, p. 352 (1935); C. G. and D. D. Montgomery, 'Phys. Rev.,' vol. 49, p. 705 (1936).

fig 1 The diameter  $D$  of the circle on the circumference of which the centres of all the counters lie is about 3.4 cm. Two different arrangements of shower-producing lead are used. One has an inner radius  $R$  of 2.3 cm and the other of 20 cm. If we define the angle  $\theta$  of divergence of a shower as the average of the angles of all the shower particles measured from the central axis of the shower, then, with the arrangement  $R = 20$  cm, we can say approximately that showers of all angles are recorded except the very narrow ones ( $\theta < 3^\circ$ ), while with the arrangement  $R = 2.3$  cm only wide showers having  $\theta > 15^\circ$  are recorded. The

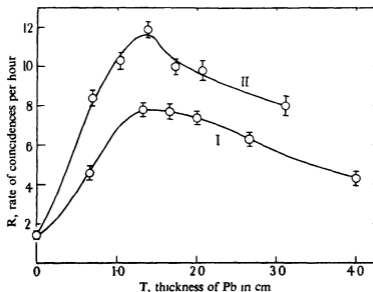


FIG. 2—The transition curves for showers from lead for different angular spread of the showers

results of the measurements are plotted in fig. 2. Curve I is the transition curve for showers of all angles and Curve II that for wide showers alone. It is seen that the maximum of Curve I is very flat, indicating possibly a lack of homogeneity in the energy of the shower particles associated with the wide range of angles, while that of Curve II is very sharp, indicating a more homogeneous energy. The position of the maximum of Curve I is about 1.5 cm lead, and that of Curve II about 1.4 cm. lead, but this difference is less than the experimental error. Thus these results do not confirm our expectation that the position of the maximum varies with the mean angular spread of the showers. Nor is it possible, at present, to give a precise interpretation of the difference between the shapes of transition curves for the wide and narrow angle showers.

### 3—VARIATION OF NUMBER OF RECORDED SHOWERS WITH THE SPACING OF THE COUNTERS

The difference between the transition curves for wide and narrow showers reported in the preceding section led us to study the frequency of occurrence of showers of different angle. The method used was to count the showers with five counters arranged in regular pentagons of

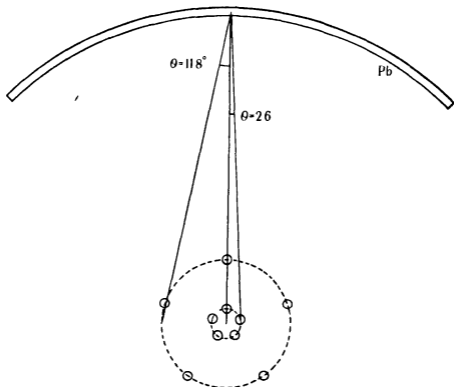


FIG. 3—The experimental arrangement for determining the variation of number of recorded showers with spacing of counters

different sizes, using the same absorber. Lead sheets of  $70 \times 80 \text{ cm}^2$  area and a total thickness of about  $1.4 \text{ cm.}$  were used to produce showers. They were bent to form an arch over the counters with mean radius  $R$  of about  $54 \text{ cm.}$  The centre of the counter pentagon coincides with the centre of curvature of the lead arch (fig. 3). The diameter  $D$  of the circle, on the circumference of which all five counters lie, was varied from  $5 \text{ cm.}$  to  $22.5 \text{ cm.}$  Thus the angle  $\theta$  defined by  $\tan \theta = D/2R$  was varied from  $2.6^\circ$  to  $11.8^\circ$ . The results are plotted in fig. 4.

The experimental curve in fig 4 does not give directly the true frequency-angle distribution of the showers, since the probability that the counter system records a shower, changes when the size of the counter pentagon is changed. An unsuccessful attempt was made to find a method of deducing the true distribution from the observed curve. The only simple conclusion that can be drawn at present is that for the counters used the number of recorded showers is greatest when their distance apart is least. It is probable that the real distribution of showers will show a maximum at an angle of a few degrees, but further measurements and analysis will be necessary before this can be established.

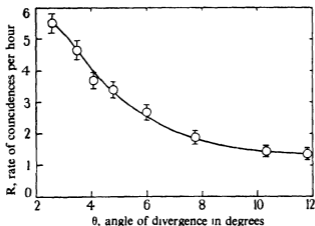


FIG 4—The variation of coincidence with mean angular separation of the counter

#### 4—THE INITIAL PART OF THE TRANSITION CURVES AND THE RELATIVE PROBABILITY OF QUINTUPLE COINCIDENCES CAUSED BY SHOWERS PRODUCED IN DIFFERENT ELEMENTS

Morgan and Nielsen\* pointed out in a note that the initial part of the transition curves for different elements obtained by the triple coincidence method was not linear, but was concave upward. They also showed that the departure from linearity decreased with decreasing atomic number of the shower-producing material, and that for lead the shower rate seemed to increase proportionally to the square of the thickness of the lead, for thicknesses up to 5 mm. This curvature is so interesting and important for a better understanding of the complicated phenomena of the shower production that we decided to investigate the point by the quintuple coincidence method.

\* 'Phys. Rev., vol 48, p 773 (1935)

Using an arrangement similar to that shown in fig 1 with  $D = 5$  cm.,  $R = 4.5$  cm., and the diameter  $d$  of the counters equal to 1.6 cm., the initial parts of the shower transition curves for lead, tin, zinc, and aluminium have been obtained in a laboratory covered with a thin plaster roof. Since shower production is a nuclear phenomenon, the thin sheets of shower-producing material used were spaced so as to give

TABLE I—SHOWERS PRODUCED IN LEAD

gm/sq cm	0	1.9	3.8	5.7
$n$ , number of atoms per cm <sup>2</sup>	0	$5.6 \times 10^{21}$	$11.1 \times 10^{21}$	$16.7 \times 10^{21}$
N, total number of coincidences	41	126	241	512
T, total time in hours	96	68.1	70.9	82.2
$R \pm \Delta R$ , rate per hour	$0.40 \pm 0.07$	$1.85 \pm 0.16$	$3.30 \pm 0.22$	$6.23 \pm 0.27$
$n \cdot Z^2$	0	$377 \times 10^{23}$	$746 \times 10^{23}$	$1123 \times 10^{23}$

TABLE II—SHOWERS PRODUCED IN TIN

gm/sq cm	0	2.48	3.96	5.94	7.92
$n$	0	$12.6 \times 10^{21}$	$25.2 \times 10^{21}$	$37.8 \times 10^{21}$	$50.4 \times 10^{21}$
N	41	88	166	347	401
T	96	61.2	60.5	68.1	66.9
$R \pm \Delta R$	$0.40 \pm 0.07$	$1.44 \pm 0.15$	$2.74 \pm 0.21$	$5.1 \pm 0.27$	$6.0 \pm 0.3$
$n \cdot Z^2$	0	$315 \times 10^{23}$	$630 \times 10^{23}$	$945 \times 10^{23}$	$1260 \times 10^{23}$

TABLE III—SHOWERS PRODUCED IN ZINC

gm/sq cm	0	2.5	5.0	7.5	10
$n$	0	$23 \times 10^{21}$	$46 \times 10^{21}$	$69 \times 10^{21}$	$93 \times 10^{21}$
N	41	76	111	170	268
T	96	63.2	67.3	67.2	74
$R \pm \Delta R$	$0.40 \pm 0.07$	$1.20 \pm 0.14$	$1.65 \pm 0.16$	$2.53 \pm 0.19$	$3.64 \pm 0.22$
$n \cdot Z^2$	0	$207 \times 10^{23}$	$414 \times 10^{23}$	$621 \times 10^{23}$	$837 \times 10^{23}$

roughly equal atomic density. The results are given in Tables I, II, III, and IV. By plotting the shower rate  $R$  against the thickness of the shower-producing elements, expressed as the number  $N$  of atoms per square cm., and comparing the slopes of the different transition curves thus obtained, we find that the number of quintuple coincidences caused by cosmic-ray showers produced by different elements is roughly proportional to the square of the atomic number. This implies that, if the

TABLE IV—SHOWERS PRODUCED IN ALUMINIUM

gm /sq cm	0	1.94	3.68
$n$	0	$43.5 \times 10^{21}$	$87 \times 10^{21}$
N	41	45	67
T	96	83.7	78.3
$R \pm \Delta R$	$0.40 \pm 0.07$	$0.54 \pm 0.08$	$0.85 \pm 0.11$
$n Z^2$	0	$73.5 \times 10^{22}$	$147 \times 10^{22}$

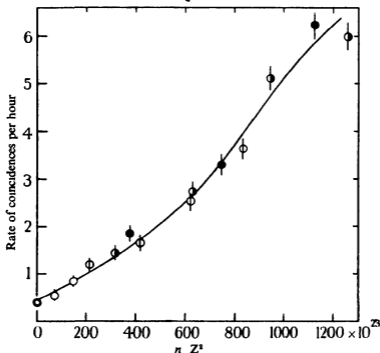


FIG. 5—The initial part of transition curves for lead ●, tin ◐, zinc ○, and aluminium ○

size (number of rays per shower) of the showers is the same for all shower-producing elements, the relative probability of shower production by the incident shower-producing radiation in different elements is also proportional to  $Z^2$ . To show this result clearly we have plotted in fig 4 the shower rate  $R$  against  $n Z^2$  for the different elements, where  $n$  is the number of atoms per sq. cm. of absorber. In fig 5 we see that all the curves seem to coincide with one another on the  $n Z^2$  scale. Thus we can conclude not only that the number of quintuple coincidences caused by showers produced by different nuclei is closely proportional to the square of the atomic number, but that the initial parts of the transition

curves have nearly the same shape for all elements examined. It is interesting to note that though the curves are slightly concave upwards, the initial slope is definitely not zero, as suggested by the results of Morgan and Nielson.

Alocco and Drigo\* have also compared the relative frequency of the shower production by different elements, and reached the qualitative conclusion that the frequency of showers increased with the atomic number of the shower-producing element.

No full explanation of the initial part of the curve can be given till a quantitative theory of the whole transition curve is available. But the slight concavity could be explained qualitatively either on the original theory of Rossi and Gilbert or on that given by Auger. According to the former theory, the photons which are assumed to produce the showers in the shower-producing materials over the counters come mainly from the air. The concavity upwards must then be due to the property of a shower being able to produce secondary showers. That this does occur is known from the cloud photographs of Blackett and Occhialini, and has been brought into special prominence by the photographs of Stevenson and Street,† of Anderson,‡ and of Ehrenfest and Auger.§ Swann|| has also discussed some consequences of this effect. Owing to this property, though the frequency of showers may perhaps increase linearly with the thickness of the absorber, their size also increases, so that the probability of a shower being recorded by a counter system also increases. Hence the number of recorded showers increases more rapidly than linearly with the thickness of absorber.

In Auger's view the photons producing the showers are mainly produced by the primary particles in the absorbing material over the counters. The upward concavity of the transition curve would then be explained directly in terms of the absorption coefficients of the photons and of the shower particles themselves.

Although, as has been stated, it is not possible yet to give a complete theory of the transition curve, the *initial slope* has, on any theory, a very simple interpretation. For it must represent the probability of shower production by the incident radiation from the air and the surrounding buildings, uncomplicated by the subsequent absorption of the shower particles. What part of this radiation consists of photons and what of

\* 'Ric Sci,' 5-1, p. 112 (1934)

† 'Phys Rev,' vol 48, p. 464 (1935), vol 49, p. 425 (1936)

‡ 'Phys Rev,' vol 45, p. 352 (1934)

§ 'J Phys Rad,' vol 8, p. 65 (1936)

|| 'J Franklin Inst,' vol 218, p. 173 (1934)

electrons it is not yet possible to say. In either case, the above result shows that it is the electric field of the nuclei of the absorbing material and not their internal structure which is responsible for shower production.

The author here wishes to express his heartiest thanks to Professor P M S Blackett, F R S, under whose direction and encouragement the present work was carried out, also to Dr W Ehrenberg and Dr H J J. Braddick for their general advice and frequent discussions

#### SUMMARY

Experiments were carried out to study the cosmic-ray showers produced in lead. Five Geiger-Muller tube-counters in a regular pentagon arrangement were connected in parallel to form a quintuple coincidence system. The advantages of the quintuple coincidence method are that the casual coincidence correction is negligible, that the coincidence rate for zero thickness of shower-producing material is very low, and that there is no need to limit the solid angle subtended by the shower-producing material from the counter system.

A—The effect of the angle of divergence of showers on the transition curve has been studied by using two arrangements of shower-producing lead. By using arrangement I, showers of all angles greater than  $3^\circ$  are recorded, by using arrangement II, showers of all angles greater than  $15^\circ$  are recorded. The result is that the transition curve obtained by using arrangement II has a sharp maximum at 1.4 cm Pb and that obtained by using arrangement I has a much flatter maximum at nearly the same thickness. This result does not support the expectation that the angle of a shower is larger when the average range of the shower rays is smaller.

The variation of quintuple coincidences with spacing of the counters was also measured.

B—The initial part of transition curves for lead, tin, zinc, and aluminium has been studied. It was found that the number of quintuple coincidences caused by showers produced in the different elements studied is closely proportional to the square of the atomic number. If the rate of coincidences  $R$  is plotted against  $n Z^2$ ,  $n$  being the number of atoms per unit surface of shower-producing material, the initial parts of the transition curves for different elements seem to be nearly the same. The common curve has an upward concavity with a finite initial slope different from zero.

---

## The Interaction of Atoms and Molecules with Solid Surfaces

### IX—The Emission and Absorption of Energy by a Solid

By C STRACHAN, Department of Natural Philosophy, University of Aberdeen

(Communicated by J E Lennard-Jones, F R S)

(Received 31 August, 1936)

As in the earlier papers† of this series, the interaction of an adsorbed atom and a surface atom of a crystal is represented by a potential field of the type suggested by Morse ‡ Only motion in the direction perpendicular to the surface of the crystal is considered So far, however, the approximation which was used limited the possible energy changes of the solid to those in which only one quantum of energy was absorbed or emitted in any transition The following discussion shows the effect of many-quantum transitions and extends the field of application of the earlier papers §

#### TRANSITION PROBABILITIES

The potential energy function is as before||

$$De^{-2\kappa(u-z)} - 2De^{-\kappa(u-z)}, \quad u - z = h, \quad \dots$$

and may be written

$$V + V_1,$$

where

$$V = D(e^{-2\kappa u} - 2e^{-\kappa u})$$

$$V_1 = D\{e^{-2\kappa u}(e^{2\kappa z} - 1) - 2e^{-\kappa u}(e^{\kappa z} - 1)\},$$

† Lennard-Jones and Strachan, 'Proc Roy Soc,' A, vol 150, p 442 (1935); Strachan, *ibid*, p 456 (referred to as I, II in the sequel), Lennard-Jones and Devonshire, *ibid*, vol 156, pp 6, 29, 37 (1936)

‡ 'Phys Rev,' vol 34, p 57 (1929)

§ Cf also Herzfeld and Göppert Mayer ('Z phys Chem,' "Bodenstein Festband," p. 669 (1931)), where the communication of energy to the internal vibrations of an adsorbed molecule is discussed The problem is different from that considered here and a less general type of interaction is used by these authors

|| The symbols have been defined in I, p. 444

and  $V_1$  is treated as a perturbation. The transition probability is given by (cf I, equation (5))

$$\Gamma_{p,rs}(t) = 2 |(rs|V_1|p)|^2 \frac{1 - \cos(W_r + E_s - W_p - E_t)t/\hbar}{(W_r + E_s - W_p - E_t)^2},$$

where, for a transition between two states in the discrete spectrum for the above field  $V$ ,

$$(rs|V_1|p) = D \left[ \int_{-\infty}^{\infty} \phi_s^* e^{-i\epsilon u} \phi_t du \quad (r|e^{2\epsilon Z} - 1|p) \right. \\ \left. - 2 \int_{-\infty}^{\infty} \phi_s^* e^{-i\epsilon u} \phi_t du \quad (r|e^{\epsilon Z} - 1|p) \right],$$

and, for a transition from a state in the discrete spectrum to one in the continuous spectrum,  $i.e.$ , corresponding to evaporation of the adsorbed atom,

$$(rE|V_1|p) = D \left[ \int_{-\infty}^{\infty} N^*(E) \phi^*(E, u) e^{-i\epsilon u} \phi_t du \quad (r|e^{2\epsilon Z} - 1|p) \right. \\ \left. - 2 \int_{-\infty}^{\infty} N^*(E) \phi^*(E, u) e^{-i\epsilon u} \phi_t du \quad (r|e^{\epsilon Z} - 1|p) \right]$$

Here  $\phi_t$  and  $\phi(E, u)$  are the wave-functions for the discrete and continuous spectra respectively†. Both cases will be included by the notation

$$(rs|V_1|p) = A(r|e^{2\epsilon Z} - 1|p) - 2B(r|e^{\epsilon Z} - 1|p),$$

the matrix elements  $(r|e^{2\epsilon Z} - 1|p)$ , etc., referring to the energy states of the solid. Since the initial and final states  $p$  and  $r$  of the solid are different, this becomes

$$A(r|e^{2\epsilon Z}|p) - 2B(r|e^{\epsilon Z}|p)$$

In the following, the suffixes  $f, j$ † will be used to specify the oscillators corresponding to the normal modes of vibration of the crystal instead of  $f, g, h, j$ . By I, equation (6), we may, for a lattice of simple cubic or face-centred cubic type, write

$$(r|e^{2\epsilon Z}|p) = \prod_{f,j} \int_{-\infty}^{\infty} \chi_{rf,j}(a_{f,j}) \exp[2\kappa(\mathbf{u}_{f,j})_z a_{f,j} \cos(\xi, f)] \chi_{pf,j}(a_{f,j}) da_{f,j} \\ \times \prod_{f,j} \int_{-\infty}^{\infty} \chi_{rf,j}(b_{f,j}) \exp[2\kappa(\mathbf{u}_{f,j})_z b_{f,j} \sin(\xi, f)] \chi_{pf,j}(b_{f,j}) db_{f,j},$$

† Defined in I, equation (11), and II, p. 457

‡ Cf I, equation (1).

where the  $\chi$  are the normalized wave-functions of the harmonic oscillator,  $a_{f,j}$  and  $b_{f,j}$  are normal coordinates of the lattice, while  $(\xi, f)$  is a function of the numbers which specify the oscillator,  $f, g, h$ , and of the coordinates  $\xi, \eta, \zeta$  of the particular (surface) atom whose displacement is  $Z$ . Its value may be taken as

$$2\pi(f\xi + g\eta + h\zeta)/\bar{N}^{\frac{1}{2}}, \quad -\frac{1}{2}\bar{N}^{\frac{1}{2}} < f, g, h \leq \frac{1}{2}\bar{N}^{\frac{1}{2}},$$

for a simple cubic lattice (I), or†

$$2\pi\{\xi(f + \frac{1}{2}) + \eta(g + \frac{1}{2}) + \zeta(h + \frac{1}{2})\}/(2\bar{N})^{\frac{1}{2}} - \pi(\xi + \eta + \zeta),$$

for a face-centred-cubic lattice,  $\bar{N}$  being in each case the number of atoms in the lattice. The unit vector  $\mathbf{u}_{f,j}$  is in the direction of the normal to the elastic wave front for  $j = 1$ , and in a transverse direction for  $j = 2, 3$ . The initial and final quantum numbers for the oscillators are  $p_{f,j}, r_{f,j}$ , respectively. Thus‡

$$\chi_n(a) = N_n^{-1} e^{-\frac{1}{2}\alpha a^2} H_n(\sqrt{\alpha}a),$$

where

$$\alpha = 2\pi M_0 \nu / \hbar, \quad M_0 = \frac{1}{2} M \bar{N}, \quad N_n = (2^n n! \sqrt{(\pi/\alpha)})^{-1},$$

$\nu$  being the frequency of the oscillator

For simplicity we consider first the case  $\xi = \eta = \zeta = 0$ . Later we shall show that this choice does not affect the result. Then only the terms in the  $a_{f,j}$  occur and§

$$\begin{aligned} \int_{-\infty}^{\infty} \chi_r(a) e^{2\pi i (a_{f,j})_z a} \chi_p(a) da &= \frac{1}{N_r N_p} \int_{-\infty}^{\infty} H_r(x) H_p(x) e^{-x^2 + 2\pi i (a_{f,j})_z x / \sqrt{\alpha}} \frac{dx}{\sqrt{\alpha}} \\ &= \frac{1}{N_r N_p} \sqrt{\left(\frac{\pi}{\alpha}\right)} \exp\left\{\kappa^2 (\mathbf{u}_{f,j})_z^2 / \alpha\right\} \begin{cases} \frac{2^r p!}{(p-r)!} \left(\frac{2\kappa (\mathbf{u}_{f,j})_z}{\sqrt{\alpha}}\right)^{p-r}, & p \geq r \\ \frac{2^p r!}{(r-p)!} \left(\frac{2\kappa (\mathbf{u}_{f,j})_z}{\sqrt{\alpha}}\right)^{r-p}, & r \geq p \end{cases} \end{aligned}$$

Higher powers of  $2\kappa (\mathbf{u}_{f,j})_z / \sqrt{\alpha}$  have been neglected since

$$\frac{\kappa^2}{\alpha} = \frac{\kappa^2 \hbar}{2\pi M_0 \nu},$$

† See Appendix 1. The range of values of  $f, g, h$ , is given there.

‡ The  $H_n$  are the Hermite polynomials. The symbol  $a$ , occurring as the argument of  $\chi$  and representing any  $a_{f,j}$ , should not be confused with the lattice constant  $a$  in equation (4), etc.

§ It can be shown that

$$\int_{-\infty}^{\infty} e^{-x^2 + \lambda x} H_m(x) H_n(x) dx = \sqrt{\pi} e^{\lambda^2/4} 2^n m! \lambda^{m-n} \sum_{r=0}^n \frac{n! C_r (\lambda^2/2)^r}{(m-n+r)!} \quad (m \geq n).$$

and, from equation (3), the minimum value of  $v$  is

$$(c/a) \bar{N}^{-1/2} \quad \text{or} \quad (3^{1/2}c/2^{1/2}a) \bar{N}^{-1/2},$$

so that the maximum value of  $\kappa^2/\alpha$  is of order

$$\frac{10^{16} \times 10^{-27}}{\pi \bar{N} (100 \times 10^{-24}) (10^5/10^{-8}) \bar{N}^{-1/2}} = O\left(\frac{1}{100 \bar{N}^{1/2}}\right),$$

and we suppose that  $\bar{N}$  may be taken to be indefinitely large. Thus

$$\begin{aligned} |(rs | V_1 | pl)|^2 &= \left| A \prod_{j,j} \left\{ \exp(\lambda_{jj}^2) \left( \frac{p_{jj}!}{r_{jj}!} \right)^{1/2} \frac{(\lambda_{jj} \sqrt{2})^{p_{jj}-r_{jj}}}{(p_{jj}-r_{jj})!} \right\} \right. \\ &\quad \left. \prod_{j,j} \left\{ \exp(\lambda_{jj}^2) \left( \frac{r_{jj}!}{p_{jj}!} \right)^{1/2} \frac{(\lambda_{jj} \sqrt{2})^{r_{jj}-p_{jj}}}{(r_{jj}-p_{jj})!} \right\} \right. \\ &\quad \left. - 2B \prod_{j,j} \left\{ \exp(\lambda_{jj}^2/4) \left( \frac{p_{jj}!}{r_{jj}!} \right)^{1/2} \frac{(\lambda_{jj}/\sqrt{2})^{p_{jj}-r_{jj}}}{(p_{jj}-r_{jj})!} \right\} \right. \\ &\quad \left. \prod_{j,j} \left\{ \exp(\lambda_{jj}^2/4) \left( \frac{r_{jj}!}{p_{jj}!} \right)^{1/2} \frac{(\lambda_{jj}/\sqrt{2})^{r_{jj}-p_{jj}}}{(r_{jj}-p_{jj})!} \right\} \right|^2, \end{aligned}$$

where

$$\lambda_{jj} = \kappa \hbar^{1/2} (\mathbf{u}_{jj})_z / \sqrt{(\pi M \bar{N} v_{jj})},$$

the first part of each term arising from oscillators emitting quanta, the second from those absorbing quanta. This may be written

$$\begin{aligned} |A' - 2B' 2^{-1/2} \exp(-r_{jj})|^2 &\prod_{j,j} \left\{ \frac{p_{jj}!}{r_{jj}! [(p_{jj}-r_{jj})!]^2} (2\lambda_{jj}^2)^{p_{jj}-r_{jj}} \right\} \\ &\times \prod_{j,j} \left\{ \frac{r_{jj}!}{p_{jj}! [(r_{jj}-p_{jj})!]^2} (2\lambda_{jj}^2)^{r_{jj}-p_{jj}} \right\}, \quad (1) \end{aligned}$$

where

$$\begin{aligned} A' &= A \exp \left\{ \sum_{jj} \lambda_{jj}^2 \right\} \\ B' &= B \exp \left\{ \sum_{jj} \frac{1}{2} \lambda_{jj}^2 \right\} \end{aligned} \quad (2)$$

and are independent of the number of quanta emitted or absorbed. (It should be noted that the above expression for the square of the matrix element contains a factor for each oscillator whether  $p_{jj} - r_{jj}$  is different from zero or not.)

We now sum the transition probabilities over all states of the crystal different from the initial state. The factor

$$4 \sin^2 (W_r + E_s - W_p - E_i) t / 2\hbar = (W_r + E_s - W_p - E_i)^2,$$

emphasizes those states in summation for which energy is approximately conserved. We have a distribution of  $\bar{N}/8\pi^3$  or  $2\bar{N}/8\pi^3$  phase points† per unit volume of the phase-cube or phase-figure for simple or face-centred cubic lattices respectively. Also as an approximation we take

$$v_{fj} = \frac{c_j \tau}{2\pi}, \quad (3)$$

where

$\tau = \frac{1}{a} \times$  radius vector in the phase-figure,  $c_j$  being the velocity of the elastic wave of type  $j$ .

Because of the lower limit

$$c_j \bar{N}^{1/3} a \quad \text{or} \quad \sqrt{3} c_j / 2 \bar{N}^{1/3} a,$$

for  $v_{fj}$ ,  $\tau$  has a lower limit which may be taken as

$$2\pi / \bar{N}^{1/3} a \quad \text{or} \quad \sqrt{3} \pi / 2 \bar{N}^{1/3} a \quad (4)$$

This is of importance in integrating negative powers of  $\tau$  since a lower limit of zero would give a spurious divergence of the integral corresponding to an oscillator of zero frequency which is, of course, meaningless. Consider all transitions for which

$$q_1, q_2, \quad , \quad q'_1, q'_2, \quad ,$$

quanta are emitted by any set of oscillators while

$$q''_1, q''_2, \quad , \quad q'''_1, q'''_2, \quad ,$$

are absorbed by a different set.  $q, q''$  correspond to  $j = 1$ ,  $q', q'''$  to  $j = 3$ . Then the total transition probability for changes of this type may be written as a multiple integral over the phase-figure. Using the notation of I, II, and substituting the suffix  $k$  for the triad  $f, g, h$  for each value of  $j$  so that  $\tau_k^2 d\tau_k d\Omega_k$  is the element of volume of the phase-figure at the point  $f, g, h$ , we have, since

$$(\mathbf{u}_{fj})_k^2 = \begin{cases} \cos^2 \theta_{fj}, & (j = 1) \\ \sin^2 \theta_{fj}, & (j = 3) \end{cases} \quad (\mathbf{u}_{f2})_k^2 = 0,$$

$\tau$ ,  $\theta$ ,  $\phi$  being polar coordinates in the phase-figure,

$$\begin{aligned}
 & |A' - 2B' \cdot 2^{-\frac{1}{2}(q+q'+q''+q''')}|^2 \cdot \int \cdot \int \frac{4 \sin^2(W_r + E_s - W_p - E_l) t / 2\hbar}{(W_r + E_s - W_p - E_l)^2} \\
 & \times \prod_k \left\{ \frac{\bar{N} a^3}{8\pi^3} \frac{p(\tau_k)!}{(p(\tau_k) - q_k)! (q_k!)^2} \left( \frac{4\kappa^2 \hbar \cos^2 \theta_k}{\bar{M} \bar{N} c_1 \tau_k} \right)^{q_k} \tau_k^2 d\tau_k d\Omega_k \right\} \\
 & \times \prod_k \left\{ \frac{\bar{N} a^3}{8\pi^3} \frac{p(\tau'_k)!}{(p(\tau'_k) - q'_k)! (q'_k!)^2} \left( \frac{4\kappa^2 \hbar \sin^2 \theta'_k}{\bar{M} \bar{N} c_3 \tau'_k} \right)^{q'_k} \tau'^2_k d\tau'_k d\Omega'_k \right\} \\
 & \prod_k \left\{ \frac{\bar{N} a^3}{8\pi^3} \frac{(p(\tau''_k) + q''_k)!}{p(\tau''_k)! (q''_k!)^2} \left( \frac{4\kappa^2 \hbar \cos^2 \theta''_k}{\bar{M} \bar{N} c_1 \tau''_k} \right)^{q''_k} \tau''^2_k d\tau''_k d\Omega''_k \right\} \\
 & \times \prod_k \left\{ \frac{\bar{N} a^3}{8\pi^3} \frac{(p(\tau'''_k) + q'''_k)!}{p(\tau'''_k)! (q'''_k!)^2} \left( \frac{4\kappa^2 \hbar \sin^2 \theta'''_k}{\bar{M} \bar{N} c_3 \tau'''_k} \right)^{q'''_k} \tau'''^2_k d\tau'''_k d\Omega'''_k \right\}.
 \end{aligned} \tag{5}$$

The range of integration for each  $\tau$  may be taken as  $(0, \tau_{\max})$  if we replace the phase figure by the phase sphere of equal content, or, if the integrand becomes infinite at  $\tau = 0$ , as  $(\tau_{\min}, \tau_{\max})$ †. The multiple integral is correct as it stands if all the  $q$ 's are different, all the  $q'$ 's different, etc. If some of the  $q$  or the  $q'$  are the same, then we shall have to divide by the appropriate factor which will make the contribution smaller, e.g., if  $\tau, \tau'$  correspond to a value of  $q$  which occurs twice we may integrate over the whole range for both variables, instead of the range  $\tau \leq \tau'$ , provided we divide by 2! In general, if  $m, m'$  of the  $q, q'$  were the same we should divide by  $m!, m'!$ .

We assign its mean statistical value to  $p(\tau)$ , that is

$$p(\tau) = \frac{1}{e^{\hbar\tau/kT} - 1} = \frac{1}{e^{\hbar c_j \tau / \lambda T} - 1}.$$

In the neighbourhood of  $\tau = 0$  this becomes  $kT/\hbar c_j \tau$ . The range of integration for  $\tau$  is  $(0, k\Theta_j/\hbar c_j)$  where  $\Theta_j$  is the characteristic temperature of the crystal corresponding to  $c_j$ . This is finite‡, so that, when any  $q$  is greater than one, a negative power of  $\bar{N}$  occurs in the corresponding integrand. Thus the only part of the range of integration which is of any importance is the lower end where negative powers of  $\tau$  will introduce positive powers of  $\bar{N}$ . Since the factor before the products in the inte-

† For the justification of this, see Appendix 2. The actual value of  $\tau_{\max}$  is given in Appendix 1.

‡ Of the order  $(0, 10^4 \Theta)$

grand of (5) is less than  $4 (t/2\hbar)^2$ , we over-estimate the value of the integral in (5) if we use this value and take the contribution of each  $\tau_k$  to be

$$\left. \begin{aligned} & 4\pi \frac{\bar{N}a^3}{8\pi^3} \int \frac{p(\tau_k)!}{(p(\tau_k) - q_k)! (q_k!)^2} \left( \frac{4\kappa^2 \hbar}{M \bar{N} c_j \tau_k} \right)^{q_k} \tau_k^3 d\tau_k \\ \text{or} & 4\pi \frac{\bar{N}a^3}{8\pi^3} \int \frac{(p(\tau_k) + q_k)!}{p(\tau_k)! (q_k!)^2} \left( \frac{4\kappa^2 \hbar}{M \bar{N} c_j \tau_k} \right)^{q_k} \tau_k^3 d\tau_k \end{aligned} \right\} \quad (6)$$

In each case the factor involving  $p(\tau_k)$  and  $q_k$  is of order  $\tau_k^{-q_k}$  at most near the lower limit of integration. Thus it follows from (4) that if  $q \geq 2$  the result of integration at the lower limit (where the integrand may be treated as a power of  $\tau_k$ )† is a negative power of  $\tau_k$ . Taking (4) into account, this still leaves a negative power of  $\bar{N}$  and therefore the contribution from the lower end of the range is negligible. We have already seen that, when  $q \geq 2$ , the remainder of the range of integration gives a negligible contribution. Thus we need only consider the emission or absorption of one quantum at a time by any oscillator, at any rate in so far as we deal with the first order perturbation.

Consider all changes in which—

$S_1$  oscillators of type  $j = 1$  emit one quantum each,

$S_3$  „ „  $j = 3$  „ „

$S'_1$  „ „  $j = 1$  absorb „ „

$S'_3$  „ „  $j = 3$  „ „

Then the total transition probability for such changes is, using the phase

† The integrals (5) become, in fact, near the lower limit

$$\text{const } \bar{N}^{-(q_k-1)} \int \frac{d\tau_k}{\tau_k^{2q_k-2}} \sim \text{const } \bar{N}^{-(q_k-1)} \frac{1}{(2q_k-1)}$$

In discussing the first order perturbation we are not entitled to demand valid results from the theory when the total number of quanta emitted or absorbed becomes very large. However, even if we use the crude inequalities we have obtained and take the transition probability for the net emission or absorption of  $Q$  quanta (individual oscillators emitting or absorbing) to be of order  $(\beta \bar{N}^{-1})^{\frac{1}{2}} |q_k|$ , where  $\beta$  is a constant and  $\Sigma |q_k|$  implies summation only for those values of the individual  $q_k$  which are greater than 1 or less than -1, it is easy to construct a partition function to show that the sum of the probabilities of all possible transitions for all possible values of  $Q$  from 2 to the maximum number available at a given temperature is negligible when  $\bar{N}$  is sufficiently large, for all transitions in which at least one of the  $q_k$  has magnitude greater than unity. This does not take into account that the number of quanta available from a given oscillator decreases as  $\tau$  increases, a factor which would make the sum still smaller.

sphere and integrating over the angular coordinates, *i.e.*, for the range of values  $0 \leq \phi \leq 2\pi$ ,  $0 \leq \theta \leq \pi/2$ ,†

$$\begin{aligned} & \frac{4}{S_1! S_3! S_1'! S_3'!} |A' - 2B' 2^{-(s_1+s_3+s_1'+s_3')}|^2 \\ & \times \left( \frac{\kappa^2 a^3 \hbar}{3\pi^2 M} \right)^{s_1+s_3+s_1'+s_3'} \left( \frac{1}{c_1} \right)^{s_1+s_3'} \left( \frac{2}{c_3} \right)^{s_1+s_3} \\ & \times \int \int \frac{\sin^2 t}{2\hbar} \{ \hbar c_1 \Sigma (-\tau_k + \tau''_k) + \hbar c_3 \Sigma (-\tau'_k + \tau'''_k) + E_s - E_t \} \\ & \times \int \frac{\{ \hbar c_1 \Sigma (-\tau_k + \tau''_k) + \hbar c_3 \Sigma (-\tau'_k + \tau'''_k) + E_s - E_t \}^2}{\{ \hbar c_1 \Sigma (-\tau_k + \tau''_k) + \hbar c_3 \Sigma (-\tau'_k + \tau'''_k) + E_s - E_t \}^2} \\ & \times \prod_k \{ \tau_k p(\tau_k) d\tau_k \} \prod_k \{ \tau'_k p(\tau'_k) d\tau'_k \} \\ & \times \prod_k \{ \tau''_k (p(\tau''_k) + 1) d\tau''_k \} \prod_k \{ \tau'''_k (p(\tau'''_k) + 1) d\tau'''_k \} \quad (7)^\ddagger \end{aligned}$$

The factors  $S_1!$ , etc., allow integration over all values of  $\tau$ , as mentioned above. The result for the face-centred cubic lattice is obtained by multiplication by  $2^{s_1+s_3+s_1'+s_3'}$ , on account of the difference in the expression for the density of phase-points in terms of  $\bar{N}$ . Writing

$$E_s - E_t = \Delta E, \quad \hbar c_j \tau / kT = x, \text{ etc.},$$

this becomes

$$\begin{aligned} & \frac{4}{S_1! S_3! S_1'! S_3'!} |A' - 2B' 2^{-(s_1+s_3+s_1'+s_3')}|^2 \\ & \times \left( \frac{\kappa^2 a^3 \hbar^2 T^2}{3\pi^2 M} \right)^{s_1+s_3+s_1'+s_3'} \left( \frac{1}{c_1} \right)^{s_1+s_3'} \left( \frac{2}{c_3} \right)^{s_1+s_3} \\ & \times \left[ \frac{1}{k^2 T^2} \right]_0^{\infty} \int_0^{\infty} \prod_k \left( \frac{x_k dx_k}{e^{x_k} - 1} \right) \prod_k \left( \frac{x'_k dx'_k}{1 - e^{-x'_k}} \right) \left[ - \int_0^{\infty} \prod_k \left( \frac{x''_k dx''_k}{e^{x''_k} - 1} \right) \prod_k \left( \frac{x'''_k dx'''_k}{1 - e^{-x'''_k}} \right) \right. \\ & \times \frac{\sin^2 t \left( \frac{kT}{2\hbar} \right) \left\{ \Sigma (-x_k + x''_k - x'_k + x'''_k) + \frac{\Delta E}{kT} \right\}}{\left\{ \Sigma (-x_k + x''_k - x'_k + x'''_k) + \frac{\Delta E}{kT} \right\}^2} \quad (\varpi = 1, 2) \quad (8) \end{aligned}$$

For given values of  $S_1$ , etc., this gives the probability of the transition  $I \rightarrow s$  for the adsorbed atom, or, if we replace  $E_s$  by  $E$  in the above and use the appropriate values of  $A$ ,  $B$ , it gives the transition probability per

† See I, p. 451, footnote

‡ The same suffix  $k$  is used for  $\tau$ ,  $\tau'$ , etc., although the range of values of  $k$  is not necessarily the same for  $\tau$ ,  $\tau'$ , etc.

unit energy range from state  $l$  to a state in the continuous spectrum,  $\nu e$ , corresponding to desorption with kinetic energy  $E$

Now, if we do not take  $\xi = \eta = \zeta = 0$ , we shall introduce terms corresponding to the normal coordinates  $b_{jj}$ . These will not affect the argument giving the relative importance of transitions for various values of the  $q_k$ . We may thus restrict consideration to the case where all the  $q$  are unity. The values of  $A'$ ,  $B'$  are not affected since in (2) we merely replace each  $\lambda_{jj}^2$  by  $\lambda_{jj}^2 \{\cos^2(\xi, f) + \sin^2(\xi, f)\}$ . When we come to evaluate the transition probabilities corresponding to a given set of  $S_1, S_3, S'_1, S'_3$ , integrals arising from the  $b_{jj}$  must now be included. Thus, returning to (5) and putting all the  $q$  equal to unity, the result is that each factor  $4\kappa^2 \frac{\cos^2}{\sin^2} \theta_k$  is replaced by the sum of two terms equal to that factor multiplied by  $\cos^2(\xi, f)$  and  $\sin^2(\xi, f)$  respectively. This, however, does not alter the result.

It is to be noticed that the factor

$$\frac{\kappa^2 a^3 k^2}{3\pi^2 \hbar M c_j},$$

in (8) is of order  $10^{-8}$ . We shall therefore expect that this factor will have an important effect in making the contributions for small values of  $S_1$ , etc., the most important.

From (2) we have

$$\left. \begin{aligned} A' &= A \exp \left\{ \frac{\pi \kappa^2 \hbar a^3}{4\pi^3 M} \left[ \frac{1}{c_1} \int \tau d\tau d\Omega \cos^2 \theta + \frac{1}{c_3} \int \tau d\tau d\Omega \sin^2 \theta \right] \right\} \\ &= A \exp \left\{ \frac{\pi \kappa^2 k^2 a^3}{24\pi^2 \hbar M} \left( \frac{\Theta_1^2}{c_1^3} + \frac{2\Theta_3^2}{c_3^3} \right) \right\} \\ B' &= B \exp \left\{ \frac{\pi \kappa^2 k^2 a^3}{96\pi^2 \hbar M} \left( \frac{\Theta_1^2}{c_1^3} + \frac{\Theta_3^2}{c_3^3} \right) \right\} \end{aligned} \right\}, \quad (9)$$

and the factor

$$\frac{\kappa^2 k^2 a^3}{24\pi^2 \hbar M} \left( \frac{\Theta_1^2}{c_1^3} + \frac{2\Theta_3^2}{c_3^3} \right) = O \left( \frac{10^{16} \times (2 \times 10^{-32}) \times (27 \times 10^{-24})}{24\pi^2 \times 10^{-27} \times (100 \times 10^{-24})} \cdot \frac{3(300)^2}{(4 \times 10^3)^2} \right),$$

is small. Hence

$$A' = A, \quad B' = B, \quad (9')$$

approximately. When only one oscillator makes a transition and, say,

emits energy, then  $S_1 = 1$ ,  $S_3 = 0$ , or  $S_1 = 0$ ,  $S_3 = 1$ ,  $S'_1$ ,  $S'_3$  being zero in both cases. The transition probability is then

$$4 |A' - B'|^2 \frac{\pi \kappa^2 a^2}{3\pi^2 \hbar M} \cdot \left\{ \frac{1}{c_1^3} \int_0^{\Theta_1/T} \frac{x}{e^x - 1} \frac{\sin^2 \frac{\hbar k T}{2\hbar} \left( -x + \frac{\Delta E}{kT} \right)}{\left( -x + \frac{\Delta E}{kT} \right)^2} dx \right. \\ \left. + \frac{2}{c_3^3} \int_0^{\Theta_3/T} \frac{x}{e^x - 1} \frac{\sin^2 \frac{\hbar k T}{2\hbar} \left( -x + \frac{\Delta E}{kT} \right)}{\left( -x + \frac{\Delta E}{kT} \right)^2} dx \right\},$$

which, by (9), agrees with the results of the simpler theory of I, II

#### DISCUSSION OF THE FORMULA (8)

The consideration of some special cases will throw light on the significance of (8)

Consider first the absorption of energy by the solid. In the following we shall simplify the results by taking  $c_1 = c_3 = c$ , and  $\Theta_1 = \Theta_3 = \Theta$ . Suppose the amount of energy satisfies one of the following conditions:

- (i) is greater than the maximum quantum which the solid can absorb or emit and is less than two such quanta, *i.e.*,

$$\frac{\Theta}{T} < -\frac{\Delta E}{kT} < \frac{2\Theta}{T}.$$

- (ii) is greater than two such quanta and less than three, *i.e.*,

$$\frac{2\Theta}{T} < -\frac{\Delta E}{kT} < \frac{3\Theta}{T}.$$

- (iii)

$$\frac{3\Theta}{T} < -\frac{\Delta E}{kT} < \frac{4\Theta}{T}.$$

Then, for transitions in which each oscillator absorbs energy, (8) gives, after summation over the possible values of  $S'_1$ ,  $S'_3$  ( $S_1 = S_3 = 0$ ), putting

$$\beta = -\Delta E/kT, \quad U = \frac{\pi \kappa^2 a^2 k^2 T^2}{3\pi^2 \hbar M c^3},$$

$$(i) \frac{18}{k^2 T^2} \left| A' - \frac{B'}{2} \right|^2 U^2 \int_0^{\Theta/T} \int_0^{\Theta/T} dx dy \frac{xy}{(1-e^{-x})(1-e^{-y})} \frac{\sin^2 \frac{\hbar k T}{2\hbar} (x+y-\beta)}{(x+y-\beta)^2} \quad (10)$$

$$\begin{aligned}
 \text{(ii)} \quad & \frac{18}{k^2 T^2} \left| A' - \frac{B'}{4} \right|^2 U^3 \iiint_0^{\Theta/T} dx dy dz \frac{xyz}{(1-e^{-x})(1-e^{-y})(1-e^{-z})} \frac{\sin^2 \frac{tkT}{2h} (x+y+z-\beta)}{(x+y+z-\beta)^3} \\
 \text{(iii)} \quad & \frac{27}{2k^2 T^2} \left| A' - \frac{B'}{8} \right|^2 U^4 \\
 & \times \iiint_0^{\Theta/T} \iiint_0^{\Theta/T} dx dy dz du \frac{xyz u}{(1-e^{-x})(1-e^{-y})(1-e^{-z})(1-e^{-u})} \frac{\sin^2 \frac{tkT}{2h} (x+y+z+u-\beta)}{(x+y+z+u-\beta)^3}
 \end{aligned}$$

(10)---(continued)

Had we considered emission of energy by the solid it would be necessary merely to replace  $(1 - e^{-x})$  by  $(e^x - 1)$ , etc., and to define  $\beta$  as  $\Delta E/kT$ .

As mentioned above, the factor  $U$  will be of great importance in determining the relative magnitudes of the probability of various types of transition. The last factor in the integrands which implies conservation of energy attains a maximum of  $(tkT/2h)^2$ . If we include transitions in which some oscillators emit and some absorb energy, terms of both types  $(1 - e^{-x})$  and  $(e^x - 1)$  will occur in the integrands. The factors  $x/(1 - e^{-x})$ ,  $x/(e^x - 1)$ , etc., are of the order of a few units provided  $\Theta/T$  is not too large so that we may draw the following conclusions

(We must consider the exchange of only a few quanta since the theory is only an approximation.) Because of the smallness of  $U$

(a)—The transition probability will be determined almost entirely by the term involving the minimum number of quanta which provides energy easily sufficient for the change

(b)—Transitions which involve the emission of energy by some oscillators and absorption by others are of little importance as the energy can always be provided by fewer quanta when the oscillators make transitions all in the same sense

(c)—These conclusions are upset in such cases as the following. Suppose that in (i), for example,  $\beta$  is just less than  $2\Theta/T$ . For values of  $t$  which are not too small the last factor in the integrand of (i) makes the integrand appreciable only near the line  $x + y = \beta$ , and, if  $\beta$  and  $2\Theta/T$  are very nearly equal, very little of this line will lie in the square domain of integration and the integral will be very small

#### THE EVAPORATION OF HYDROGEN MOLECULES FROM COPPER

In II numerical results were given for the relative probabilities of evaporation of the molecules  $H_2$ ,  $HD$ , and  $D_2$  from the surface of copper.

The above conclusions throw light on the modifications of these results necessitated by the multiple emission of quanta by the solid. An examination of equations (2) and (3) of II shows that the part of the transition probability which depends on the wave-functions of the adsorbed particle decreases as the kinetic energy of evaporation,  $E$ , increases. The factor  $U$  above is of the order  $10^{-8} T^2$ . Thus, where one quantum provides sufficient energy, the previous results will not be appreciably affected, while, for greater energies of desorption, both the smallness of  $U$  and the decrease of the matrix element (3) of II make the probability of evaporation smaller. Thus the results given in II and III† will not be affected to a great extent by multiple emissions. The second order perturbation may also be expected to modify the result for large  $E$ . It seems reasonable to expect that, in evaporation from each state, one-quantum emissions determine the probability almost entirely, provided that in each case the quantum can provide sufficient energy.

#### APPLICATION TO SURFACE MIGRATION

It is of interest to evaluate some times associated with the interaction of an atom in a state of migration and the underlying metal. Let us suppose that the atom migrates along the sides of intergranular fissures in the metal until it makes a transition to a state in the surface field of the metal in which it has insufficient energy to cross the "col" between adjacent energy minima in the periodic surface field‡. Thus, if  $l$  be the number of the first state in which the energy  $E_l$  of the atom is greater than that required for migration, the inverse of the probability per unit time of the transition  $l \rightarrow l-1$  will give the order of magnitude of the lifetime of an atom in a state of migration.

For the purposes of illustration, numerical results may be taken from a study of the sorption of hydrogen and deuterium by copper and palladium by Melville and Rideal§. Although it is not implied that the diffusion of hydrogen in palladium has the simple mechanism just suggested, the parameters of the surface field may be evaluated and used to find the consequences of such a process of migration.

The values 52.2 and 52.7 kg cal per gram atom (M R, p. 91) for the energy required to remove hydrogen and deuterium from inside palladium give the values

$$\kappa \approx 1.07 \times 10^8 \text{ cm}^{-1}, \quad D = 3.72 \times 10^{-12} \text{ ergs}$$

† Lennard-Jones and Devonshire, 'Proc Roy Soc,' A, vol 156, p. 6 (1936).

‡ See I, § 6 and p. 453, footnote.

§ 'Proc Roy Soc,' A, vol 153, p. 77 (1935) (referred to as M R).

From M R , pp 92 and 101,† the true energies of activation for migration may be taken as 16.17 and 17.31 kg. cal per gram atom for hydrogen and deuterium respectively. For palladium

$$a = 1.93 \times 10^{-8} \text{ cm} ; \quad c = 3.165 \times 10^5 \text{ cm /sec.}$$

It is then found that the maximum energy of a quantum (using the phase-sphere) is  $5.27 \times 10^{-14}$  ergs, and that the transitions  $6 \rightarrow 5$ ,  $8 \rightarrow 7$ , the deactivating transitions for hydrogen, deuterium, require absorption by the solid of at least four and three quanta respectively on account of the wider spacing of the energy levels for hydrogen. At a temperature of  $500^\circ \text{ K}$ , we find that the average time intervals between successive deactivations are of the order of  $10^{-7}$  and  $10^{-11}$  seconds for hydrogen, deuterium respectively. These results do not give the ratio of the average times spent on migration since these depend on the frequency of activation of the atoms.

In conclusion, it is a pleasure to express appreciation of discussion of this problem with Professor Lennard-Jones, to whom I am indebted for suggesting it.

#### SUMMARY

The interchange of energy between a crystal and an atom adsorbed on its surface is considered with special reference to exchanges in which a number of quanta are derived from, or communicated to, the heat motion of the solid.

It appears that, within the limits of application of first-order perturbation theory, any change in which more than one quantum is emitted or absorbed by the oscillator corresponding to any normal mode of vibration of the crystal is very improbable. Other exchanges are governed by a factor which makes the probability of any energy interchange almost entirely dependent on that of the transition involving the minimum number of quanta which can provide the necessary energy.

This is of importance in determining the validity of previous results relating to the desorption of the isotopic molecules of hydrogen from a metal surface. The theory is also applied to estimate the average time intervals between successive deactivations of atoms of hydrogen and deuterium from a state of migration on the surface of a metal.

† A slight error has to be corrected here. Clearly 0.4 is to be replaced by  $2.50/2$  and  $1.72/2$ .

## APPENDIX 1

It is convenient for this discussion to formulate the dynamics of the face-centred cubic lattice in a manner somewhat different from that given by Born and others† in the general theory of crystal lattices. The rectangular coordinates of an atom may be written  $(l_1a, l_2a, l_3a)$ , where  $a$  is a constant length and  $l_1, l_2, l_3$  are of the forms  $(2m_1, 2m_2, 2m_3), (2m_1 + 1, 2m_2 + 1, 2m_3 + 1), (2m_1 + 1, 2m_2, 2m_3 + 1), (2m_1 + 1, 2m_2 + 1, 2m_3), m_1, m_2, m_3$  being positive or negative integers or zero. The equations of motion are obtained in the usual form in terms of the displacement  $u^i$  of the atom  $(l_1, l_2, l_3)$

It is found‡ that the following standing waves are possible

$$u^i = \frac{C_j}{\sqrt{m}} \cos(l, \phi) e^{-i\omega_j t},$$

$$u^i = \frac{C_j}{\sqrt{m}} \sin(l, \phi) e^{-i\omega_j t} \quad j = 1, 2, 3,$$

where  $m$  is the mass of an atom, the  $C_j$  are vectors normalized in the usual way,† and the circular frequencies  $\omega_j$  are obtained from the well-known determinantal equation. Also

$$(l, \phi) = l_1\phi_1 + l_2\phi_2 + l_3\phi_3 = \tau(s, l_1a_1 + l_2a_2 + l_3a_3)$$

The unit vector  $s$  is in the direction of the wave-normal,  $a_1, a_2, a_3$  are vectors of length  $a$  in the direction of the axes, and the wave-length of the vibration is given by

$$\lambda = 2\pi/\tau$$

The restriction on the possible values of  $l_1, l_2, l_3$  makes it necessary to consider only values of  $\phi_1, \phi_2, \phi_3$  for which

$$\pm \phi_1 \pm \phi_2 \pm \phi_3 < 3\pi/2$$

Thus the phase-figure is no longer a cube but becomes a fourteen-sided figure bounded by the planes

$$\phi_1 = \pm \pi, \quad \phi_2 = \pm \pi, \quad \phi_3 = \pm \pi, \quad \pm \phi_1 \pm \phi_2 \pm \phi_3 = 3\pi/2.$$

In this figure phase-points are distributed at the points

$$\phi_1 = (f + \frac{1}{2}) \frac{2\pi}{(2N)^{\frac{1}{3}}} - \pi, \quad f = 0, 1, \quad (2N)^{\frac{1}{3}} - 1; \text{ etc.},$$

† Born, 'Enc. Math. Wiss.', vol. 5, part 3, p. 527, Waller, 'Uppsala Univ. Arsskr.' (1925)

‡ A detailed account of this investigation will be published elsewhere.

$\bar{N}$  being the number of atoms in the crystal. Only the points lying inside the phase-figure are, of course, relevant. This can be shown to produce the normal and orthogonal relations associated with normal coordinates. By definition

$$\tau a = \sqrt{(\phi_1^2 + \phi_2^2 + \phi_3^2)},$$

so that  $\tau_{\min}$  and  $\tau_{\max}$ , which are proportional respectively to the minimum distance of any phase point from the centre of the phase-figure and the radius of the phase-sphere of content equal to that of the phase-figure, are given by

$$\sqrt{3\pi}/(2\bar{N})^{1/2}a, \quad (3\pi^2)^{1/2}/a$$

With the usual approximation the frequency of any normal vibration is given by

$$\nu = \frac{c}{\lambda} = \frac{c\tau}{2\pi},$$

where  $c$  is the velocity of the corresponding wave. The surfaces of constant frequency are spheres, a result which simplifies the calculation of the total transition probability. The phase-sphere is a closer approximation to this phase-figure than to a phase-cube.

## APPENDIX 2

It is necessary to justify the replacement of the sum of the values of the transition probability at the phase-points by the integral of the values over the phase-figure. Since the density of phase-points is extremely large, difficulty will arise only near  $\tau = 0$ . In fact, the difference between sum and integral will be appreciable only for a certain, not large, number of points near  $\tau = 0$ , i.e., for values of  $\tau < \tau_1$  such that  $\bar{N}\tau_1^3$  is not large. The sum has no contribution from points inside  $\tau_{\min}$  (which is of order  $\bar{N}^{-1/2}$ ). According to (5), (6), the function we are concerned with is of order  $\bar{N}^{-q}\tau^{-2q}$  near  $\tau = 0$ . Hence the sum is of the order of the value of the function at  $\tau_{\min}$  multiplied by the number of points, i.e., of

$$\bar{N}^{-q}(\bar{N}^{-1/2})^{-2q} \times \text{finite} = \bar{N}^{-1/2} \times \text{finite}.$$

The integral, on the other hand, is of the order

$$\bar{N}^{1-q} \int_{\tau_{\min}}^{\tau_1} \tau^{2-2q} d\tau \sim \bar{N}^{1-q} (\bar{N}^{-1})^{2-2q} \bar{N}^{-1/2} \times \text{finite}$$

Thus, both being negligible for  $q \gg 1$ , their difference is also negligible.

## The Effect of the Fitzgerald-Lorentz Contraction on the Frequency of Longitudinal Vibration of a Rod

By A B WOOD, D Sc, Admiralty Research Laboratory and G A TOMLINSON, D Sc, and L ESSEN, B Sc, National Physical Laboratory

(Communicated by Sir Frank Smith, Sec R S—Received 30 September, 1936)

### INTRODUCTION

By A B WOOD, D Sc

The failure of the Michelson-Morley experiment to detect ether-drift led Fitzgerald in 1892 to suggest that the framework which supported the interferometer mirrors was distorted by its motion through the ether in such a way that the expected ether-drift effect was exactly neutralized. Later experiments by Morley and Miller, in 1903, using different materials for the framework led substantially to the same result. Fitzgerald's hypothesis received the support of Lorentz in 1895, and as recently as 1921 the latter remarks "There can be no question about the reality of this change of length". Lorentz considered that the change of length produced by motion was just as real as that produced by change of temperature\*.

According to the Fitzgerald-Lorentz theory, a moving body contracts in the direction of motion in the ratio

$$1 \text{ to } \left(1 - \frac{v^2}{c^2}\right)^{\frac{1}{2}}, \quad (1)$$

where  $v$  is the velocity of translation of the body and  $c$  is the velocity of light. The velocity of the earth's orbital motion is approximately 30 km/sec, and the velocity of light is 300,000 km/sec. A body carried by the earth is therefore subject to a contraction of 5 parts in  $10^9$  of its length as it is oriented from a direction at right angles to a direction along the line of the earth's orbital motion†.

If this change of length is real, as Lorentz supposes, an interesting problem arises for a rod vibrating longitudinally. The fundamental

\* 'Nature,' vol 106, p 793 (1921)

† This disregards the rotational motion of the earth about its N.S. axis, the velocity of a point on the equator being only 0.46 km./sec. Other motions of the earth apart from the orbital motion in the solar system are also disregarded.

frequency  $N$  of such a vibration for a rod of length  $l$ , elasticity  $E$ , density  $\rho$ , and sound velocity  $u$ , is given by

$$N = \frac{u}{2l} - \frac{1}{2l} \sqrt{\frac{E}{\rho}} = \frac{1}{T}. \quad (2)$$

If the length only is affected by motion we should expect a change of frequency of 5 parts in  $10^9$  as the rod is turned from a direction at right angles to a direction along the line of the earth's orbital motion. In the Michelson-Morley experiment an attempt was made to observe a change in the apparent velocity of light as the apparatus was rotated. The failure to detect the change led to the assumption regarding the change of length of the apparatus. The vibrating rod experiment now proposed differs in one important particular. If, as we might suppose, there is no observable change of frequency of the rod as it is rotated, the neutralization of the change of length must be due to a change in some other physical characteristic of the rod. This has no counterpart in the Michelson-Morley experiment.

Relativity theory predicts the result of the Michelson-Morley experiment and states, further, that it is impossible by means of an experiment to detect uniform motion relative to the ether. This being so we should not expect to detect a change of frequency of the vibrating rod as it is rotated. This implies not only a change of length of the rod but also a change of elasticity and/or density. It seems unlikely that the density will change, for the motion would probably affect the density of the rod equally whether broadside or end-on to the ether drift. Zero change of frequency would therefore imply a change of elasticity which exactly compensates for the change of length assumed by Fitzgerald and Lorentz.\* On this basis, expression (2) for the frequency indicates a *decrease of elasticity* in the ratio

$$1 \text{ to } 1 - \frac{v^2}{c^2}. \quad (3)$$

which neutralizes the *decrease of length* in the ratio

$$1 \text{ to } \left(1 - \frac{v^2}{c^2}\right)^{\frac{1}{2}}.$$

That is to say, the length of the rod will change by 5 parts in  $10^9$  and the elasticity by 10 parts in  $10^9$  due to the earth's orbital motion.

\* The alternative explanation, that neither length nor elasticity change would, of course, be completely at variance with the Fitzgerald-Lorentz theory and would require a stationary ether.

During the last few years very accurate methods have been devised for comparison of standards of frequency. The National Physical Laboratory, has an elinvar rod and a quartz oscillator which can be relied on to maintain a constant frequency with an accuracy of  $\pm 1$  part in  $10^9$  for an hour or more. Standard quartz oscillators in use at the Physikalisch-Technische Reichsanstalt, Berlin, are stated to be capable of maintaining an accuracy of the same order. The frequency stability of these oscillators is determined by means of slow beats obtained between two oscillators of nearly equal frequencies, the time required to give a definite number of beats being accurately measured.\* Quartz rod oscillators are particularly suitable for the vibrating rod experiment. If an appreciable change of frequency occurs whilst one rod is rotated, a second "reference" rod remaining stationary, then a change of beat frequency between the two rods† will be observed.

The errors arising in the Michelson-Morley interferometer experiment are due mainly to the relatively large dimensions of the interferometer arms, 4 or 5 metres long. Minute changes of separation of the interferometer mirrors might be caused by temperature variations, magnetic and centrifugal effects, yielding of supports, flexure of the arms in rotation, etc. The elimination of these errors presents a formidable problem when a search is being made for a change of 5 parts in  $10^9$ . With a rod of quartz a few centimetres long, however, such troubles are almost entirely absent and the accuracy of the final result must therefore be greatly increased.

The possibilities of carrying out such an experiment with quartz rods were discussed with Mr J. E. Sears and Dr G. A. Tomlinson, in February, 1935. Sir Arthur Eddington very kindly advised on the relativity aspect of the matter, and it is desired to take this opportunity of thanking him for his very helpful comments on the proposed experiments. The Director of the Laboratory, the late Sir Joseph Petavel, agreed to have the experiment made, and the work has been carried out by Dr. G. A. Tomlinson and Mr. L. Essen who, in their respective Departments of the Laboratory, have much experience of accurate time and frequency standards.

\* Sheibe and Adelsberger, 'Ann Physik,' vol 18, p 1 (1933)

† The beats occur, of course, between the electrical circuits containing the two rods

## EXPERIMENTAL INVESTIGATION

By G. A. TOMLINSON, D Sc., and L. ESSEN, B Sc.

The experiment suggested is clearly one that demands an extremely high degree of precision in the frequency measurements involved, if it is to be completely successful. Oscillators in use at The National Physical Laboratory as frequency standards had been maintained at a constant frequency for a period of an hour to within 1 part in  $10^9$ ; two oscillators of different types, controlling phonic motor clocks, had maintained relatively correct time to within 0.001 second for ten days. Even this high order of precision was considered to be hardly adequate for this experiment in which one must, if successful, discriminate decisively between an effect of magnitude such as 5 parts in  $10^9$  and no effect at all. To improve on the precision already attained, with the added complication that the oscillator under observation must be rotated, presented a problem beset with difficulties. Nevertheless, a careful consideration of all the factors affecting the experiment led us to think that it might be attempted with a reasonable chance of success.

The experiment with sound waves, as contrasted with the use of light waves in the Michelson-Morley experiment, appeared to have certain inherent advantages. The wave path, for example, needs to be only a few centimetres in length, and it appeared possible that the frequency measurements could be made with sufficiently high precision to yield a definite result in a single experiment, eliminating the necessity for resort to a statistical analysis of a large number of observations.

There is not at present an entirely satisfactory agreement amongst those who have worked at great length and with great care on the Michelson-Morley experiment. Although the experiment is always cited as proving that there is no ether drift, it is interesting to note that this has never been claimed by the original experimenters themselves. Michelson and Morley concluded from their experiments that the effect was not more than one-fourth of that anticipated, or that the relative motion did not exceed one-fourth of the earth's orbital velocity. The whole of these observations, and those of later experiments conducted by Morley and Miller, have more recently been analysed by Miller,\* who finds that they are in striking agreement, giving a relative velocity of about 9 km/sec. On the other hand, the experiment has been repeated by a number of

\* 'Rev. Mod. Phys.', vol. 5, p. 203 (1933).

other observers among whom are Kennedy,\* A. Piccard and Stahel,† Michelson, Rease, and Pearson,‡ and Joos,§ and they all report a null effect within the limit of accuracy of their measurements which is usually of the order of 1 km/sec

These considerations made it appear particularly desirable to undertake the similar experiment on the velocity of sound, especially as the total experimental evidence of other kinds, mainly astronomical, in support of the theory of relativity is so limited

#### GENERAL SCHEME OF THE EXPERIMENT

The oscillators previously established at the Laboratory consisted of a ring type of quartz crystal and a metre bar of elinvar in a vertical position. The former is obviously of unsuitable form for the purpose of this experiment and the latter would lead to a very unwieldy piece of apparatus. It was therefore decided to set up two closely similar quartz oscillators of bar shape, one of these being stationary and the other mounted on a rotating table. The frequency selected as suitable was 100 kilocycles per second and the two oscillators were tuned to have a frequency difference of approximately 3 cycles per second. The frequencies are compared by making an accurate measurement of their mutual beat frequency by means of a high precision chronograph. Comparisons of the two frequencies were made with six different positions of the rotating plate in steps of 60°. The length of the crystal having the above frequency is 54 mm, which leads to a complete assembly of apparatus of very reasonable dimensions.

The success of the experiment depends largely on two factors, the possibility of measuring the beat frequency with sufficient precision in a reasonably short time such as from two to five minutes, and the attainment of a sufficiently stable frequency over the duration of the experiment. The problem of measurement, with the equipment already available, has proved fairly straightforward, but various difficulties have been encountered with frequency stability, on account of the very high degree of constancy required.

These difficulties arise to some extent from the fact that an electrically maintained oscillator of any kind does not vibrate exactly at its free

\* 'Proc Nat Acad Sci Wash,' vol 12, p 621 (1926), 'Astrophys J,' vol 68, p 367 (1928)

† 'C R Acad Sci, Paris,' vol 183, p 420 (1926), and vol 185, p 1198 (1927), 'Naturwiss,' vol 14, p 935 (1926), and vol. 16, p 25 (1928)

‡ 'Nature,' vol 123, p. 88 (1929).

§ 'Ann. Physik,' vol 537, p 385 (1930)

acoustical frequency, but at a frequency slightly modified by the associated electrical circuit. The frequency is also affected by changes in physical conditions such as temperature and pressure. Precautions were therefore taken to ensure that all the conditions that affect the frequency were maintained as constant as possible continuously day and night. These features of the experiment are described in more detail in the sections which follow.

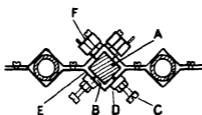
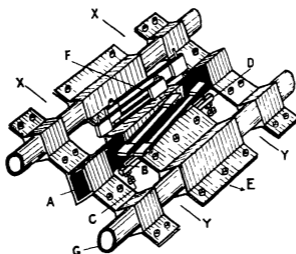
#### DESCRIPTION OF THE QUARTZ BARS AND THE ASSOCIATED ELECTRICAL CIRCUITS

For the purposes of this experiment the requirements were not quite the same as for the usual standard of frequency. The long period stability of the oscillator was not so important, since a complete set of observations occupied only two hours, but it was desired, if possible, to reduce the random fluctuations of the order of 1 part in  $10^8$  which have hitherto been found to occur in the most stable standards known. To achieve this a considerable amount of preliminary investigation was necessary. Bars of different dimensions were cut to attain a temperature coefficient of frequency of as low a value as possible at a suitable temperature of operation. They were tested as resonators to ensure that no other unwanted modes of vibration were present, and that the logarithmic decrement was low, and the position of the nodes was carefully determined by this means. Experiments were made with a number of different types of mounting and with different circuit conditions. This work was, however, pursued only so far as to give an oscillator of the desired stability, and we shall here merely give a brief description of the final form adopted. The type of frequency standard developed at the Physikalisch-Technische-Reichsanstalt appeared very suitable for the purpose in view and was accordingly used for the investigations.

The bars are 54.3 mm long in the direction of the electric axis and of square section, the sides of the square being of length 7.5 mm. in the directions of the optic and third axes. They vibrate longitudinally in their first overtone mode at a frequency of 100 kc/sec, and are supported rigidly at the two nodes. They were cut in the optical workshop of the Laboratory and the frequency was adjusted by the authors by grinding one of the end faces with a fine abrasive.

The method adopted for supporting the quartz crystal at its nodal points is shown in fig. 1. The bar A rests on four points B with its diagonal directions horizontal and vertical, the points bearing at the centre of two adjacent faces. Each point is formed on the end of an adjustable screw

C carried by a rigid bar D which is soldered to the centre electrode E. The contact point is actually in the form of a spherical cap made by polishing the apex of a conical end turned on the screw. To prevent any movement of the bar that might be caused by vibration, it is held against each point by a light pressure applied by a similar point on the opposite face, this point being attached to the end of a cantilever spring



Section XY

FIG 1

F of phosphor bronze strip To minimize any tangential force at the point of contact, the springs are made of two parallel strips of phosphor bronze soldered to small brass separating blocks at each end. One block is used to attach the spring by a screw to the electrode and the other carries the contact point, a short piece of phosphor bronze wire. With this system of springs the contact approaches the surface of the quartz bar closely in the normal direction.

The frequency is directly affected by any alteration of the air gap

between the bar and the electrodes, and it is therefore important to keep this dimension constant. To this end each electrode is extended in both directions perpendicular to the bar and is clamped, as shown in the illustration, to two pieces of silica tube *G* which lie parallel to the quartz bar. This construction has ample rigidity and provides high insulation resistance between the electrodes.

The circuit used to maintain the oscillations and provide an output at 100 kc/sec is shown in fig. 2. It is similar to the circuit used at the Laboratory for maintaining the vibration of the frequency standards, previously described by one of the authors\*. Special precautions have been taken, however, to ensure that there is no reaction on the frequency

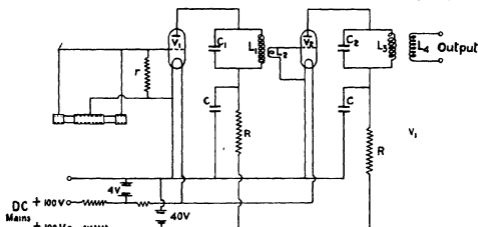


FIG. 2— $V_1, V_2$ , LS7 valves,  $L_1, L_2$ , 1 mH (approx),  $C_1$ , 0.0023  $\mu$ F,  $C_2$ , 0.0028  $\mu$ F,  $C_3$ , 2  $\mu$ F,  $r$ , 2 megohms,  $R$ , 20,000 ohms

by the load taken from the amplifier valve and that there is no coupling with any outside circuits. All the coils used are toroids, and are screened by copper cases. The primary coil  $L_1$  consists of 300 turns, over which the secondary winding  $L_2$ , consisting of 10 turns is symmetrically disposed. This is connected to the grid of the amplifier valve.  $L_3$  of 300 turns and  $L_4$  of 100 turns are the primary and secondary of a toroid in the amplifier valve circuit.

The low- and high-tension supplies to the driving and amplifier circuits were provided by accumulators which were continuously trickle-charged from the D.C. mains. Under these conditions the voltage rises to about 2.15 volts per cell and then remains very constant in spite of small fluctuations in the voltage of the mains. Large condensers were connected across the batteries to smooth out the more rapid variations.

\* Essen, 'Proc Roy Soc.,' A, vol 155, p. 498 (1936).

The general result of the preliminary work showed that the oscillator, with the electrode system and method of mounting described above, possessed satisfactory characteristics in nearly all respects. The coefficients of frequency change with changes in the various external conditions were small, having the following values —

- 3 in  $10^{10}$  for a 0.1% increase in L T voltage.
- 3 in  $10^{10}$  for a 0.1% increase in H T voltage
- +1.5 in  $10^{10}$  for a 0.01% increase in anode (tuned circuit) capacitance
- 8 in  $10^{10}$  for a 0.001  $\mu\mu\text{F}$  increase in grid-cathode capacitance
- +1 in  $10^{10}$  for a 0.001° C increase in temperature (Bar 1)
- 1 in  $10^{10}$  for a 0.001° C increase in temperature (Bar 2)
- 1.6 in  $10^{10}$  for a 0.01 mm increase in pressure.

On the other hand, the frequency of this type of oscillator, probably owing to some ageing effect, was invariably found to be subject to continuous drift in one direction from day to day. The rate of change steadily diminishes but the frequency was not constant after several months under very constant conditions. The rate of drift throughout any day was liable to vary slightly, probably owing to small changes of temperature. These changes, however, were quite slow, and as the oscillators had proved to be very satisfactory with regard to random fluctuations of frequency it was decided to proceed with the experiments and make a suitable correction for the drift observed in the course of each experiment.

#### THE MEASUREMENT OF THE BEAT FREQUENCY

The comparison of the relative frequency involves simply an accurate measurement of the frequency of the beats set up between the two oscillators. For this purpose the outputs of the two amplifiers shown in fig. 2 were connected through screened leads to the grids of two valves  $V_1$  and  $V_2$  in the circuit shown in fig. 3. The combined output was amplified in two resistance capacity coupled stages, so that in the anode circuit of the last valve the current varied sinusoidally between about 0 and 4 milliamperes at the frequency of the beat, about 3.5 cycles per second. These current pulses were recorded on a high precision chronograph\* designed and made at the Laboratory.

To attain a precision in the frequency comparison of 1 part in  $10^{10}$  requires a precision of about 3 parts in  $10^6$  in the actual measurement of the beat frequency, or in a period such as 5 minutes the beats require to

\* Sears and Tomlinson, 'J. Sci. Instr.', vol. 8, p. 21 (1931)

be recorded with an error not exceeding 0.001 second. It would clearly be very difficult to do this with a direct record of a sinusoidal current of such a low frequency, and various methods were investigated for recording the beats. In one of these methods an additional circuit followed the amplifier to produce an impulse in the form of a condenser discharge, which was recorded directly on the chronograph with the precision required. In another method the beat current controlled a multivibrator at the frequency of the beat and the impulsive current supplied by this circuit was recorded. The method finally adopted, on account of its simplicity and reliability, involves the use of a reed armature relay\* designed by one of the authors.

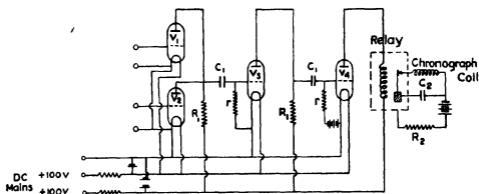


FIG. 3—Circuit arrangements for recording the beats.  $V_1$ ,  $V_2$ ,  $V_3$ , PM2DX valves,  $V_4$ , PM21A valve.  $R_1$ , 60,000 ohms,  $R_2$ , 100,000 ohms,  $r$ , 2 megohms,  $C_1$  0.1  $\mu$ F,  $C_2$ , 1  $\mu$ F.

The armature of this relay is a stiff reed of stalloy, clamped rigidly at one end, carrying a platinum contact point at the free end. The movement of the reed follows the changes in the current almost instantaneously, the lag being not more than 0.0001 second. There is no friction in the movement of the reed and consequently the input current required to deflect the reed sufficiently to make contact is very constant. If, therefore, the relay is adjusted so that the operating value of the current is reached during the steep portion of the sinusoidal current supply, a very satisfactory precision in the timing of the contact is obtained. The relay on making contact discharged a condenser through the coil of one of the two chronograph markers, as shown by the circuit diagram of fig. 3. When the relay contact is broken the condenser is charged again, in readiness for the next beat signal, through a resistance of 100,000 ohms.

\* Tomlinson, 'J. Sci. Instr.', vol. 10, p. 204 (1933).

by a dry battery. In this manner the slowly varying current of the beat wave was converted into an abrupt pulse in the chronograph marker, and the uniformity of operation of the relay proved to be very satisfactory. A series of successive beat signals would be recorded uniformly on the chronograph to well within a millisecond.

Variations in the speed of the chronograph were effectively eliminated by recording accurate seconds signals from a high precision clock on the other marker. The observed duration between the first and last beats in the period measured thus consisted of an integral number of seconds obtained directly in terms of the clock, with only a fraction of a second to be measured on the chronograph and therefore dependent on the uniformity of its speed.

The calculation of the change in frequency of the rotating oscillator relative to that of the fixed oscillator is a simple one. If  $n$  and  $m$  are the respective frequencies, the beat frequency is

$$f = n - m = \frac{N}{t}$$

if  $t$  seconds is the measured time for  $N$  beats. If  $t$  is found to vary by a small amount  $\delta t$ , due to a change  $\delta n$  in the frequency of the rotating oscillator, we have

$$\frac{\delta t}{t} = - \frac{\delta f}{f} \approx \pm \frac{\delta n}{f}$$

and therefore

$$\frac{\delta n}{n} = \pm \frac{f}{n} \frac{\delta t}{t} \quad (2)$$

A numerical example will show more clearly the high degree of precision attainable in the frequency measurement. In one of the actual observations the time for 880 beats was measured, the duration being almost exactly 250 seconds. If for  $\delta t$  we insert the value 0.0005 sec, which represents the probable error in the measurement of  $t$ , the expression  $\delta n/n$  then represents the error in the frequency measurement, and it has the value

$$\begin{aligned} \frac{\delta n}{n} &= \pm \frac{880}{250} \times \frac{1}{100,000} \times \frac{0.0005}{250} \\ &= \pm 0.7 \times 10^{-10}. \end{aligned}$$

#### TEMPERATURE CONTROL

The two oscillators were installed in a small room which was constructed for use as a cold store. This room is very effectively lagged with

granulated cork and is fitted with double doors and internal shutters to the windows. The lower half of the room is below the ground level. The room is thus very suitable for close temperature control. For this purpose a toluene thermostat was used to operate a relay for switching two heater lamps on or off. A fan directed a stream of air on to the wall at a point between the two lamps and so circulated two streams of warmed air in opposite directions. The fan was supported from the ceiling by rubber cords to minimize the effects of its vibration.

Each quartz oscillator was enclosed at a pressure of 20 mm. in a sealed glass vessel A about 4 inches in diameter, as seen in fig. 4 which shows the arrangement of apparatus used for the rotating oscillator. The vessel is placed on three cork supports inside a massive brass cylinder B with thick brass end covers. The air space between the glass vessel and the metal cylinder is loosely filled with cotton wool. The cylinder B is again completely surrounded by a second larger brass cylinder C covered externally with  $\frac{1}{2}$ -inch felt D and again with cotton wool in the interspace. The circuit E for maintaining the crystal in vibration is placed alongside the outer cylinder and an earthed copper cover F lined externally with felt G is lowered over the whole.

The heavy thermal insulation is intended to prevent the residual fluctuations in the room temperature from penetrating to the quartz oscillators to any significant extent. The alternative and more usual method of temperature control by a thermostat and heating element suitably placed inside the apparatus was not adopted on account of possible electrical disturbance of the regularity of the beats by the on and off operation of the heating current. The temperature of the apparatus has been found to vary very slightly from day to day, probably due to gradients in the room. This is not of great importance, however, as we are concerned only with changes in the relative frequency of the two oscillators over the duration of any individual experiment. The arrangements in the case of the fixed oscillator were similar in all essential respects.

#### DESCRIPTION OF THE ROTATING TABLE

It is necessary that the moving oscillator, its amplifier, thermal insulating vessels, and the earthed screen should all rotate together to avoid any changes of capacitance in the amplifier circuits. With this in view all the apparatus is placed on a double circular slab of gaboon board H (fig. 4) which itself rests on the face of a special type of rotating plate J that is used in the Metrology Department of the Laboratory for a variety of purposes. This consists of a fixed circular base plate K, resting on

three levelling screws, and a rotating upper plate L. The bearing surface of each plate is a highly finished horizontal plane face M in the form of an annular ring about 7 inches in diameter and  $\frac{1}{8}$ -inch in width. The bearing

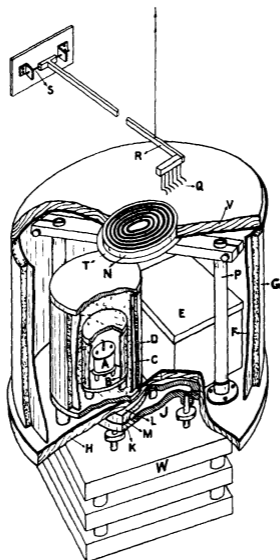


FIG 4

was filled with a heavy grease to carry the weight of the apparatus and the table was found to turn very smoothly like a well-greased tap. It was originally intended to design a more elaborate means of rotation in which the apparatus would be floated in a bath of liquid, and the rotating

table was used in the first place as a temporary method only. It proved to be so satisfactory, however, that it has been retained throughout the experiments.

The driving circuit of the rotating oscillator must be provided with leads for the low- and high-tension supplies, which could not be housed conveniently in the enclosure, and for the output current. For this purpose six concentric circular mercury troughs turned in the face of a thick disk N of teak are used. The teak disk is supported by two brass columns P screwed to the base-board. Contact with the rotating mercury troughs is made by means of a comb Q of six insulated amalgamated copper wires bent to suit the curvature of the troughs, with a length of about two inches submerged in the mercury. These contact wires are carried by an arm R which is supported on a pivot S in such a way that the arm can be hauled upwards to enable the copper cover to be removed when necessary.

The proper functioning of the dipping contacts was regarded as of considerable importance since the frequency is affected by the low tension voltage to the extent of 1 part in  $10^{10}$  per millivolt. An experiment was therefore made in which leads were taken from the apparatus to a potentiometer and careful observations of the voltage actually supplied to the amplifier were made while the apparatus was being rotated. The potentiometer was sensitive to within 0.1 millivolt, but no variation of voltage could be observed.

The outer screening cover of copper is cylindrical in shape and has a circular hole cut in the top face, large enough to pass over the teak disk. To complete the electrical screening the teak disk is lined beneath with a copper disk T about an inch larger than the hole in the cover which rests on and overlaps the copper disk when lowered into place. The top of the cover is not exposed to the air but is covered with a loose disk V turned from thick gaboon board, and on this is placed a graduated scale for measuring the angle of rotation.

The rotating plate rests on a built-up pedestal consisting of slabs of stone W separated by blocks of cork.

#### ADJUSTMENT OF THE PLANE OF ROTATION

It was observed during the preliminary experiments that the frequency was slightly affected by any change in the inclination of the oscillator. Such a change would occur in the course of a revolution if the plane of rotation was not truly horizontal. The magnitude of the effect was examined by producing known changes in the inclination of the crystal

by means of the levelling screws of the rotating table. In this way it was possible to tilt the oscillator about each of two horizontal axes, one of these being the geometrical axis of the rod and the other a line at right angles to this. In each case the oscillator was tilted by equal amounts in each direction from its normal position, and the frequency was measured by a direct comparison with that of the fixed oscillator. Table I shows the results obtained, the sign allotted to the angle being arbitrary.

TABLE I

	Angle of tilt	Frequency change
Rotation about the geometrical axis of the bar	+1°	+24 in 10 <sup>14</sup>
	-1°	-25 in 10 <sup>14</sup>
Rotation about an axis perpendicular to the axis of the bar	+1°	+7 in 10 <sup>14</sup>
	-1°	-4 in 10 <sup>14</sup>

Although these changes are small, it is necessary to consider them in a little more detail, since their effect in the actual experiment is of importance as it involves the introduction of a small periodic frequency variation. The immediate cause of the change in frequency is probably the alteration in the distribution of the weight of the quartz bar between the four supporting points. It had been found in the preliminary work that the frequency was directly affected by the pressure applied to the points. As the centre of gravity of the bar is a little above the supporting points, a tilt will increase the pressure on two of the points and reduce it on the others. This change of pressure will be quite different in the two kinds of tilt applied to the bar, being considerably greater when the rotation occurs about the axis of the bar. This is in agreement with the measured frequency changes.

It will be seen from the table that the change of frequency was found to be continuous in one direction over the total angle of tilt applied. This may be due to some initial lack of symmetry in the pressure on the four points. The total pressure on the supporting points was several times the actual weight of the bar, owing to the pressure of the phosphor bronze springs, the change produced by tilting could easily have been smaller than the probable initial differences of pressure arising from unequal adjustment of the springs. Furthermore, it was for various reasons impracticable to adjust either the long axis or the diagonal axis of the bar to be exactly horizontal. An ideally mounted bar would be expected to change in frequency by identical amounts for a given tilt in either direction, the actual behaviour is probably explained correctly as a result of the various kinds of asymmetry that may occur.

The rotating plate was initially adjusted by means of a sensitive level to turn in a horizontal plane, and after the apparatus had been assembled on the plate it was readjusted with the level, and observations were made of the deviations from the horizontal plane on rotating the plate. The measured variation in the inclination of the level during a revolution was found to be within  $\pm 30''$ . From the results of Table I the frequency change caused by this deviation does not exceed 2 parts in  $10^{11}$ . Furthermore, the table indicates that there should be one maximum and one minimum value of the frequency per revolution, and that these should be approximately the same amount above and below the mean frequency. The periodic effect introduced has, therefore, one complete cycle in  $360^\circ$  and it is nearly symmetrical.

In the ultimate experiments on the possible periodic effect caused by the Fitzgerald-Lorentz contraction, the frequency variation in two successive half-revolutions were virtually added, to derive a mean value of the effect. In this process, any periodic change having one cycle per revolution was eliminated altogether if it was symmetrical. We may thus conclude that the final results of the experiment were not affected to any significant extent by the small periodic effect of magnitude  $\pm 2$  in  $10^{11}$  which was expected to occur as the result of residual errors in levelling. It may be of interest to mention here that an experiment is described later in the paper in which we rotated the oscillator in a plane deliberately set not quite horizontal, and observed the frequency variations. The result appears in fig. 12 and is a well-defined periodic having a  $360^\circ$  cycle, confirming the above conclusions.

It has been mentioned that the quartz rod itself was not placed with any precision in a horizontal plane. This was not considered to be of importance provided the plane of rotation was horizontal, as this ensured that the rod would rotate with an invariable inclination.

#### GENERAL EXPERIMENTAL PROCEDURE

The procedure adopted in an experiment was as follows. One of us took charge of the chronograph and the other made the series of rotations of the oscillator. As these were in different buildings a timed schedule was always prepared and adhered to. In each angular position of the oscillator the total time of a number of beats, such as 880, for example, was measured, but only the beats in the initial and final ten seconds were actually recorded. This was done to economize as regards the space used on the chronograph for each observation, and enabled four successive complete rotations, with a total of 25 frequency measurements,

to be recorded easily on one plate. The time allowed for each frequency measurement was usually from 3 to 5 minutes with an interval of about a minute for the rotation to the next position. Although most of the beats were not recorded, there was no doubt about the total number between the first and last beats measured, as a preliminary fully recorded trial was always made.

Generally speaking, the precision attained in the measurement of the frequency has exceeded the residual variations in actual frequency of the oscillators, which is a desirable condition. Two beats and two seconds signals were usually measured each time and the average of these taken. This was found to give a sufficiently precise measurement, although there were about 35 beats recorded in the 10 seconds, all of which were available for measurement if it had been necessary.

Early experiments in which the oscillator made only a single rotation showed at once that there was no periodic change of frequency at all comparable in magnitude with the Fitzgerald-Lorentz contraction as usually estimated. At the same time these experiments showed that the erratic variations in frequency and those which are due to the slow drift already mentioned might easily conceal a very small periodic effect when only a single rotation is made. The erratic changes may also in one rotation lead to an incorrect estimate of the true amount of drift, for which a correction is ultimately made. It was therefore considered advisable to turn the oscillator through several complete revolutions in succession and examine the average variations in frequency. This procedure in a large measure eliminates the effects of the erratic variations and yields a more correct value of the mean frequency drift per cycle.

#### RESULTS OF THE EXPERIMENT

The result obtained in an experiment comprising four complete rotations in steps of  $60^\circ$  is shown in fig. 5 and the numerical results are given in Table II. The ordinates represent the proportional change of frequency  $\delta n/n$  in parts in  $10^{10}$  throughout the experiment. The frequency drift is clearly shown with the erratic variations superimposed. In the course of the experiment, which took 96 minutes, some variation in the rate of drift has also occurred, due to a small slow temperature cycle.

In one revolution the oscillator is twice disposed transversely and longitudinally to the horizontal component of its velocity in space, so that  $180^\circ$  constitutes a complete cycle as regards modification of its length or of the velocity of sound along it. The curve has therefore been divided into 8 sections of  $180^\circ$  and the average ordinates of these sections

TABLE II—2 JUNE, 1936. TIME 7.18 P M

	Measured time of 670 beats Unit 1 sec.				Change in relative frequency Unit 1 in $10^{10}$			
	0°	60°	120°	180°	0°	60°	120°	180°
1st cycle	189 9683	189 9686	189 9679	189 9674	0	+ 0 5	- 0 7	- 1 7
2nd "	189 9674	189 9646	189 9641	189 9635	- 1 7	6 8	- 7 8	- 8 9
3rd "	189 9635	189 9612	189 9606	189 9609	- 8 9	-13 1	-14 2	-13 7
4th "	189 9609	189 9594	189 9596	189 9589	-13 7	-16 5	-16 1	-17 4
5th "	189 9589	189 9573	189 9557	189 9543	-17 4	-20 4	-23 3	-25 9
6th "	189 9543	189 9557	189 9510	189 9515	25 9	-23 1	-32 0	-31 0
7th "	189 9515	189 9488	189 9473	189 9443	-31 0	-36 0	38 8	-44 5
8th "	189 9443	189 9430	189 9414	189 9405	44 5	-46 8	-50 0	-51 7
Mean of 8 cycles					-17 9	-20 3	22 9	-24 4
Values relative to 0° position					0	2 4	- 5 0	- 6 5

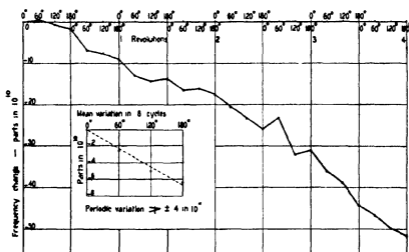


FIG 5

have been plotted to twice the scale of the complete curve, as shown by the inset graph. The irregularities are greatly reduced by the averaging process and a reasonable mean straight line has been drawn through the points, representing the mean progressive frequency change throughout the experiment. The deviations from this line of the actual points represent the maximum amount of any periodic effect due to the rotation of the oscillator. These deviations do not exceed a range of  $\pm 4$  parts in  $10^{10}$ .

In all the experiments that have been made a very similar result is obtained. The results of some other experiments are shown in the same way in figs 6, 7, and 8, and in Tables III, IV, and V. The deviations of frequency from the straight line representing the mean drift are found to be  $\pm 4$  in  $10^{11}$ ,  $\pm 5$  in  $10^{11}$ , and  $\pm 3.5$  in  $10^{11}$ . It is of interest to com-

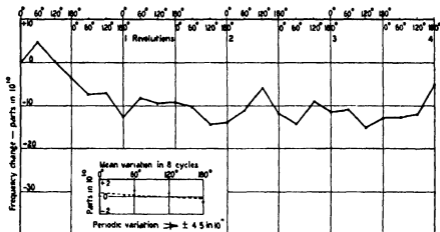


FIG. 6.

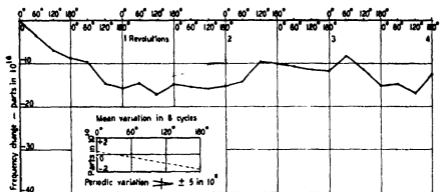


FIG. 7

pute the mean periodic frequency variation of the above four experiments. In Table VI the mean frequency change in the cycle is given for each experiment, as abstracted from the previous tables. The mean of these values for each angular position is shown in the fifth line and the progressive variation in these is linear to within limits  $\pm 2.5$  parts in  $10^{11}$ .

There is always a possibility that at some particular hour of the day the motion of the oscillator may be perpendicular to the plane of rotation,

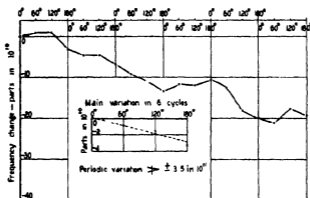


FIG 8

TABLE III—30 MAY, 1936 TIME 5 50 A M

	Measured time of 670 beats Unit 1 sec				Change in relative frequency Unit 1 in $10^{10}$			
	0°	60°	120°	180°	0°	60°	120°	180°
1st cycle	189 9641	189 9666	189 9643	189 9620	0	+ 4 6	+ 0 4	- 3 5
2nd "	189 9620	189 9601	189 9603	189 9573	- 3 5	- 7 4	- 7 0	-12 6
3rd "	189 9573	189 9597	189 9590	189 9591	-12 6	- 8 1	- 9 4	- 9 2
4th "	189 9591	189 9586	189 9563	189 9566	- 9 2	-10 2	-14 4	-13 8
5th "	189 9566	189 9582	189 9610	189 9576	-13 8	-10 9	- 5 7	-12 0
6th "	189 9576	189 9564	189 9592	189 9579	-12 0	-14 2	- 9 0	-11 5
7th "	189 9579	189 9583	189 9560	189 9572	-11 5	-10 7	-15 0	-12 8
8th "	189 9572	189 9572	189 9595	189 9614	-12 8	-12 8	-12 2	- 5 0
Mean of 8 cycles					- 9 4	- 8 7	- 9 0	-10 0
Values relative to 0° position					0	+ 0 7	+ 0 4	- 0 6

TABLE IV—25 MAY, 1936 TIME 10 15 P M

	Measured time of 740 beats Unit 1 sec				Change in relative frequency Unit 1 in $10^{10}$			
	0°	60°	120°	180°	0°	60°	120°	180°
1st cycle	209 8583	209 8562	209 8542	209 8531	0	- 3 5	- 6 9	- 8 7
2nd "	209 8531	209 8525	209 8498	209 8489	- 8 7	- 9 7	-14 7	-15 8
3rd "	209 8489	209 8497	209 8481	209 8496	-15 8	-14 5	-17 1	-14 6
4th "	209 8496	209 8491	209 8489	209 8493	-14 6	-15 4	-15 8	-15 1
5th "	209 8493	209 8499	209 8526	209 8523	-15 1	-14 1	- 9 6	-10 1
6th "	209 8523	209 8520	209 8515	209 8513	-10 1	-10 6	-11 5	-11 7
7th "	209 8513	209 8534	209 8515	209 8493	-11 7	- 8 2	-11 5	-15 1
8th "	209 8493	209 8495	209 8483	209 8511	-15 1	-14 6	-16 8	-12 1
Mean of 8 cycles					-11 4	-11 3	-13 0	-12 9
Values relative to 0° position					0	+ 0 1	- 1 6	- 1 5

TABLE V—20 MAY, 1936. TIME 9 50 P. M.

	Measured time of 880 beats Unit 1 sec				Change in relative frequency. Unit 1 in 10 <sup>10</sup>			
	0°	60°	120°	180°	0°	60°	120°	180°
1st cycle	249 9800	249 9807	249 9808	249 9779	0	+ 1 0	+ 1 0	- 2 9
2nd "	249 9779	249 9768	249 9768	249 9753	- 2 9	- 4 5	- 4 5	- 6 6
3rd "	249 9753	249 9735	249 9722	249 9705	- 6 6	- 9 1	- 10 9	- 13 3
4th "	249 9705	249 9718	249 9714	249 9726	- 13 3	- 11 5	- 12 0	- 10 4
5th "	249 9726	249 9712	249 9671	249 9658	- 10 4	- 12 3	- 18 0	- 19 9
6th "	249 9658	249 9650	249 9676	249 9663	- 19 9	- 21 0	- 17 4	- 19 2
Mean of 6 cycles					- 8 8	- 9 6	- 10 3	- 12 0
Values relative to 0° position					0	- 0 8	- 1 5	- 3 2

TABLE VI

	Mean frequency change in one cycle Unit 1 in 10 <sup>10</sup>			
	0°	60°	120°	180°
Experiment 1	- 17 9	- 20 3	- 22 9	- 24 4
" 2	- 9 4	- 8 7	- 9 0	- 10 0
" 3	- 11 4	- 11 3	- 13 0	- 12 9
" 4	- 8 8	- 9 6	- 10 3	- 12 0
Mean of 4 values	- 11 87	- 12 48	- 13 80	- 14 82
Relative to 0° position	0	- 0 61	- 1 93	- 2 95

and in this event no modification of any of its properties would be expected. The experiments have therefore been made at various times to investigate any difference of effect that might be due to this cause. As the results show, there is no difference in this respect within the limits of accuracy attained. This is confirmed by other experiments in which several shorter trials were made at intervals on the same day. These also yielded a null result in all cases, though with a slightly less precision than the longer experiments already described.

We have also considered the further possibility that the cosmical and orbital velocities of the earth were equal and opposite at the time the experiments were made. The probability of such an occurrence seems very small, as astronomical observations lead to an estimate of the cosmical velocity which is considerably greater than the orbital velocity. The question of the cosmical velocity, however, is inevitably so uncertain, both as to its estimated magnitude and as regards the system of reference, that we have repeated the experiments after an interval of four months. In this time the change in direction of the orbital velocity will have caused a material change in the resultant velocity of the oscillator irrespective

of any consideration of the magnitude of the cosmical velocity. Simple reasoning shows that, whatever the magnitude and direction of the cosmical velocity, the oscillator cannot have no velocity at both the periods when the experiments were made, and must, in fact, have a velocity of at least the same order as the orbital velocity on at least one of the occasions.

The later experiments were again carried out at different hours of the day and the results are shown in Tables VII, VIII, and IX and figs 9, 10, and 11. The maximum periodic effect of rotation on the frequency in these experiments is found to be  $\pm 4$  in  $10^{11}$ ,  $\pm 3$  in  $10^{11}$ , and  $\pm 3$  in  $10^{11}$  and the mean variation of the three experiments amounts to not more than  $\pm 1$  in  $10^{11}$ . The results thus show that the prediction of the theory of relativity, that the frequency should be unaffected by motion relative to the ether, is proved experimentally to be correct within very narrow limits.

In an experiment of this kind, in which at most only a small effect of the order 1 in  $10^8$  could be expected, and which actually yields a null result, it is natural to wonder whether the methods employed would have accurately picked out a small periodic variation in frequency if this had occurred. It has been possible to test this by artificially introducing a small periodic change by tilting the plane of rotation of the oscillator slightly out of the horizontal plane. One of the levelling screws supporting the rotating plate was turned round once, making the plane of rotation inclined to the horizontal by about  $0.5^\circ$ . The effect of a small alteration in the inclination of the oscillator has already been discussed.

An experiment was carried out similar in all respects to those previously described, and in this case a pronounced periodic variation of frequency was found, having an amplitude of about  $\pm 9$  parts in  $10^{10}$  and giving a complete cycle in  $360^\circ$  of rotation. The result of this experiment is given in fig. 12 which demonstrates in a satisfying way that the methods and apparatus were quite capable of measuring a very minute periodic effect had such an effect existed.

Some further experiments were made to prove that a real periodic variation of frequency was not all the time being cancelled out by an equal and opposite effect introduced without our knowledge by other causes inherent in the apparatus. The probability of this happening is not large and, moreover, such a periodic error arising from any of the causes mentioned below would be expected to have a full cycle in every  $360^\circ$  of rotation, and would therefore disappear, if symmetrical, in the subdivision of the rotation into sections of  $180^\circ$ .

The only further possible causes of a periodic effect that we can imagine are (1) the rotation of the apparatus in the earth's magnetic field, (2)

TABLE VII—15 SEPTEMBER, 1936 TIME 11 A.M.

	Measured time of 1020 beats Unit 1 sec				Change in relative frequency Unit 1 in $10^{10}$			
	0°	60°	120°	180°	0°	60°	120°	180°
1st cycle	260 1665	260 1692	260 1702	260 1662	0	+ 4 1	+ 5 6	- 0 4
2nd "	260 1662	260 1675	260 1711	260 1738	- 0 4	+ 1 5	+ 6 9	+11 0
3rd "	260 1738	260 1755	260 1767	260 1774	+11 0	+13 6	+15 4	+16 5
4th "	260 1774	260 1738	260 1716	260 1721	+16 5	+11 0	+ 7 7	+ 8 5
5th "	260 1721	260 1736	260 1754	260 1766	+ 8 5	+10 7	+13 4	+15 2
6th "	260 1766	260 1766	260 1756	260 1743	+15 2	+15 2	+13 7	+11 8
Mean of 6 cycles					+ 8 47	+ 9 35	+10 45	+10 43
Values relative to 0° position					0	+ 0 88	+ 1 98	+ 1 96

TABLE VIII—21 SEPTEMBER, 1936 TIME 6 A.M.

	Measured time of 934 beats Unit 1 sec				Change in relative frequency Unit 1 in $10^{10}$			
	0°	60°	120°	180°	0°	60°	120°	180°
1st cycle	239 9833	239 9841	239 9867	239 9855	0	+ 1 3	+ 5 5	+ 3 5
2nd "	239 9855	239 9850	239 9846	239 9850	+ 3 5	+ 2 7	+ 2 1	+ 2 7
3rd "	239 9850	239 9856	239 9882	239 9884	+ 2 7	+ 3 7	+ 7 9	+ 8 2
4th "	239 9884	239 9868	239 9878	239 9894	+ 8 2	+ 5 7	+ 7 3	+ 9 9
5th "	239 9894	239 9909	239 9907	239 9903	+ 9 9	+12 3	+12 0	+11 3
6th "	239 9903	239 9906	239 9896	239 9904	+11 3	+11 8	+10 2	+11 5
Mean of 6 cycles					+ 5 93	+ 6 25	+ 7 5	+ 7 85
Values relative to 0° position					0	+ 0 32	+ 1 57	+ 1 92

TABLE IX—24 SEPTEMBER, 1936 TIME 8 35 P.M.

	Measured time of 934 beats Unit 1 sec				Change in relative frequency. Unit 1 in $10^{10}$			
	0°	60°	120°	180°	0°	60°	120°	180°
1st cycle	239 8840	239 8839	239 8823	239 8837	0	- 0 2	- 2 7	- 0 5
2nd "	239 8837	239 8818	239 8808	239 8799	- 0 5	- 3 6	- 5 2	- 6 6
3rd "	239 8799	239 8799	239 8800	239 8816	- 6 6	- 6 6	- 6 5	- 3 9
4th "	239 8816	239 8828	239 8833	239 8848	- 3 9	- 1 9	- 1 1	+ 1 3
5th "	239 8848	239 8857	239 8876	239 8873	+ 1 3	+ 2 7	+ 5 8	+ 5 3
6th "	239 8873	239 8888	239 8873	239 8867	+ 5 3	+ 7 8	+ 5 4	+ 4 4
Mean of 6 cycles					- 0 73	- 0 30	- 0 72	0
Values relative to 0° position					0	+ 0 43	+ 0 01	+ 0 73

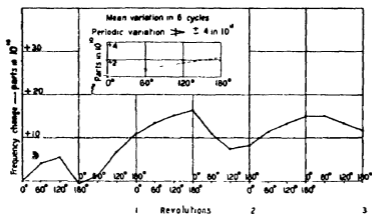


FIG 9

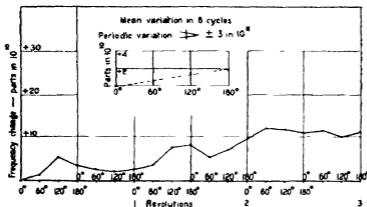


FIG 10

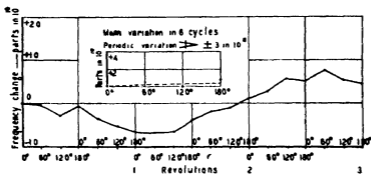


FIG 11.

electrical coupling between the two oscillators, and (3) capacitance changes between the rotating mercury troughs and the fixed comb of contact wires

To examine the possible effect of a magnetic field, two large Helmholtz coils were set up one on each side of the rotating apparatus to produce a magnetic field half-way between the coils in the North and South direction of about 10 times the magnitude of the earth's horizontal field. The frequency of the oscillator was measured in different angular positions, and no alteration at all could be detected due to the magnetic field. It was not possible to place the coils at the standard Helmholtz

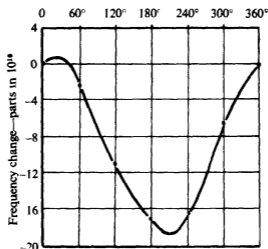


FIG. 12

distance and the field was therefore not uniform. As a completely null result was obtained, this was not considered to be essential.

To test the second possibility, a large sheet of stalloy was placed between the two oscillators, firstly in a vertical position and insulated, and secondly in a horizontal position and connected to earth. These two arrangements would introduce considerable disturbances in the amount of coupling, if any, due to magnetic and electric fields respectively. Consecutive frequency measurements were made with the normal arrangement of apparatus, then with the sheet of stalloy in place, and again with the sheet removed. The results showed nothing more than the usual random changes of 1 to 2 parts in 10<sup>10</sup>, proving that the screening of the oscillators is effective in preventing any significant amount of coupling. There is good independent evidence that the coupling between the fixed and moving oscillators is negligible, although the two are comparatively near. In

the course of the preliminary work, the fifth harmonic of the Laboratory standard crystal oscillator, of frequency 20 kilocycles per second, was used for comparison purposes. This crystal is situated at a distant part of the building and could have no coupling influence on the two 100 kilocycle oscillators. It was found that when one of these was completely switched out of action there was no measurable change in the frequency of the other relative to that of the standard.

The effect of capacitance changes due to the rotation of the mercury troughs was examined in a direct manner by comparing the frequency with and without a  $50\text{ }\mu\text{F}$  condenser connected in turn across the low tension and output, the low tension and high tension, and the high tension and output. Although this added capacitance is many times greater than any periodic change that can be caused by any relative movement of the leads during the rotation, its effect on the frequency was less than 4 parts in  $10^{10}$ .

The rotation of the oscillator will give rise to a periodic contraction in the width of the crystal differing in phase by  $180^\circ$  from the contraction in length. It was anticipated that such a change in one of the cross-sectional dimensions might produce a secondary change in the frequency of longitudinal vibration. This was investigated during the course of grinding the quartz, when there was an opportunity of measuring the frequency with a progressively diminishing width of rod. It was found that a proportional change in the width produced an effect on the frequency of about 1% of the effect produced by the same proportional change in the length of the bar. The effect of a periodic lateral contraction is therefore negligible, in view of the general magnitude of the observed effects.

#### DISCUSSION OF THE RESULT OF THE EXPERIMENT

The experiment, on every occasion it has been made, has yielded a null result, showing that the frequency of the oscillator is unaffected by its orientation with respect to the direction of its motion. The possibility of encountering a condition in which the velocity of the oscillator has a zero component in the plane of rotation has been eliminated by making the experiment at different times of the day. Such a condition is unique and can only occur once in the day. The variation in the inclination of the horizontal plane is a large angle equal to twice the latitude of London, so that in at least some of the experiments it is certain that there is a large component of the velocity in the plane of rotation. The more unlikely possibility of the oscillator having zero or a very small resultant velocity has been met by making the experiment at two different

points in the earth's orbit. Again there can be only one place in the orbit where this condition could occur, and if this were in May, for example, the velocity in September would be approximately  $\sqrt{3}$  times the earth's orbital velocity.

It is of some practical interest that the experiments demonstrate that any form of longitudinal oscillator or tuning fork used as a frequency standard is not subject to a diurnal periodic effect on account of the rotation of the earth, or to any annual effect due to the change in direction of the orbital velocity of the earth.

The result of the experiment is a decisive verification of the prediction of the theory of relativity, which affirms that the experiment must of necessity fail to show by a change of frequency whether the bar is moving relatively to the ether. Mathematicians might be prepared to accept this prediction as a result of abstract reasoning, and the chief interest of the result lies, perhaps, in its physical implications. From the point of view of physics, the complete compensation of the Fitzgerald-Lorentz contraction by a modification of the elasticity is so remarkable that the experimental proof of this should be welcome to the physicist who is convinced by the Michelson-Morley experiment that the oscillator alters in length.

The deduction that the elasticity of matter is modified by motion relative to the ether invites interesting speculation in itself, and the further deduction that this modification exactly compensates the modification in another physical property greatly enhances the interest in the physical phenomena involved. That both the length and elasticity of a body are affected by the ether stream is quite intelligible, as both these perceptible physical properties must be reducible ultimately to the operation of atomic forces, which implies electric or magnetic forces. The compensating property of the two modifications appears to suggest that there may be some close connexion between the physical causes which determine the length and the elasticity respectively. The possibility of such a connexion is evident, without any reference to the present experiment, if we regard the dimensions of a body as being determined by the atomic distance, when the atomic forces are in equilibrium, and the elasticity as a direct result of the operation of the same atomic forces under conditions of disturbed equilibrium.

Further than these simple considerations, which suggest that there may be a physical interpretation of the deduction from the theory of relativity, we do not propose to digress into the region of speculation, but prefer to leave this paper as a record of experimental work.

We have pleasure in acknowledging our indebtedness to Mr. J. E. Sears and Dr. E. H. Rayner who have encouraged us very materially with their support and interest. We have to thank the Research Committee of the Laboratory for the opportunity to carry out the experiment. We should also like to record our appreciation of the great interest taken in the experiment by the late Sir Joseph Petavel, which was maintained throughout his fatal illness.

#### SUMMARY

An experiment somewhat analogous to the Michelson-Morley experiment is suggested. In this experiment a rod in longitudinal vibration is rotated in a horizontal plane so that its length varies periodically by reason of the Fitzgerald-Lorentz contraction. Accurate measurements are made of the vibration frequency, which should vary with the length, if the length only is affected. Relativity theory, however, predicts that no change of frequency should be observed and that there should be a complete compensation of the contraction in length by a modification of the velocity of sound according to the orientation of the bar with respect to the direction of its motion.

The experiment has been carried out with two similar longitudinal piezo-electric quartz oscillators, one rotating and one stationary, the relative frequency being measured. The methods adopted to attain the necessary degree of precision are described.

The results fully confirm the prediction of the theory of relativity. The experiment yielded a null result within narrow limits of uncertainty of about  $\pm 4$  parts in  $10^{11}$ , or less than 1% of the estimated contraction due to the earth's orbital motion.

---

## The Ultra-Violet Absorption Spectra of Some Complex Aromatic Hydrocarbons—II

By W V MAYNEORD, and E M F ROE (International Cancer Research Foundation Scholar), Research Institute and Physics Department of the Royal Cancer Hospital (Free), London

(Communicated by E L Kennaway, F R S.—Received 7 September, 1936)

[PLATE 27]

### INTRODUCTION

The results of the study of the absorption spectra of a number of complex aromatic hydrocarbons, some of which are of considerable biological importance, were described in a previous paper (Part I) \* The present paper contains results of similar experimental investigations, together with an account of quantitative measurements at low temperatures For general theoretical relationships, nomenclature, and technique at room temperatures, reference should be made to Part I, the results here described being obtained as before with a "Spekker" photometer The only experimental change is the substitution of a transformer for the induction coil outfit previously employed

### PURITY OF MATERIALS

With few exceptions, all of the compounds studied were prepared synthetically in this Institute by methods described in the original memoirs to which reference is made The specimens employed for spectroscopic purposes were the original highly purified analytical samples or else specimens which had been specially prepared and purified for examination

The method of preparation and other sources of material were as follows —

Benzene—Supplied by British Drug Houses, Ltd, "extra pure for molecular weight determinations"

Naphthalene—Supplied by British Drug Houses, Ltd., "extra pure for molecular weight determinations"

Anthracene—Dehydration of pure 9 10-dihydroanthraquinol, prepared by the reduction of synthetic anthraquinone

\* Mayneord and Roe, 'Proc Roy Soc,' A, vol. 152, p 299 (1935)

- Phenanthrene—Platinum dehydrogenation of *as*-octahydrophenanthrene, Cook and Hewett ('J Chem. Soc.', p. 1098 (1933)).
- Oestradiol—Supplied by Dr A Girard (compare Girard, Sandulesco, and Fridenson, 'C R Soc Biol, Paris,' vol 112, p 964 (1933)).
- Oestrone—Supplied by Dr. A Girard Isolated from mares' urine.
- Equilin—Supplied by Dr A Girard Isolated from mares' urine
- Hexahydrophenanthrone—the crystalline stereoisomeride, m p 95–96°C. Cook, Hewett, and Lawrence ('J Chem Soc.', p 77 (1936))
- 9·9:10 10-Tetramethyl-9 10-dihydro-1 2 5 6-dibenzanthracene. Synthesized by J W Cook (*unpublished*)
- Cholanthrene—Cook, Haslewood, and Robinson ('J Chem Soc.', p 667 (1935))
- 6-*iso*Propyl-1 2-benzanthracene — Cook ('J Chem Soc.', p 463 (1932))
- Fluorene—Catalytic hydrogenation of fluorenone oxime (compare Cook and Hewett, 'J Chem Soc.', p 65 (1936))
- 1 2-Benzfluorene—Cook, Hewett, Mayneord, and Roe ('J Chem. Soc.', p 1736 (1934))
- 3 4-Benzfluorene—Cook, Dansi, Hewett, Iball, Mayneord, and Roe ('J Chem Soc.', p 1322 (1935))
- 1 2 5 6-Dibenzfluorene—Cook, Dansi, Hewett, Iball, Mayneord, and Roe ('J Chem Soc.', p 1325 (1935))
- 3 4-Benzphenanthrene—Cook ('J Chem Soc.', p 2524 (1931))
- 1'·2'-Naphtha-2 3-fluorene—Cook, Dansi, Hewett, Iball, Mayneord, and Roe ('J Chem Soc.', p 1323 (1935))

#### EXPERIMENTAL RESULTS

For convenience in description we have retained the somewhat arbitrary division into groups used in Part I

*Benzene Group*—A single benzenoid ring is present in a number of polycyclic compounds which may be included in this group. In Part I the experimental results of neoergostatriene, -tetraene, and -pentaene were reported. Equilin, oestrone, oestradiol, and 9-keto-1:2 3.4:11·12-hexahydrophenanthrone have since been examined (figs 1 and 2). Although the equilin molecule contains one more double bond than oestrone, the two spectra are very similar. It was concluded, therefore, that this additional double bond is separated from the benzene ring in equilin by at least one CH<sub>2</sub> group. This suggestion, together with the chemical evidence, led to its assignment to the 7:8-position of the ring

adjacent to the aromatic ring (*cf.* Cook and Roe\*), as shown in the formula (fig. 1)

For both these compounds, an increase in the intensity of the benzene ring absorption is observed, due to the introduction of a —OH group in

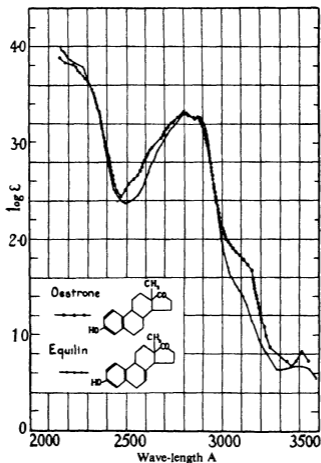


FIG. 1

the aromatic nucleus, ( $\log \epsilon = 3.3$  as a maximum in the region of 2800 Å), *cf.* the spectra of the cresols (Wolf and Herold)† It is interesting to compare the spectrum of oestradiol (fig. 2) with that of oestrone (fig. 1). The two spectra are very similar, so that it is evident that the keto group in oestrone exerts very little influence on the absorption

\* 'J. Soc. Chem. Ind.', vol. 54, p. 501 (1935).

† 'Z. phys. Chem.', B, vol. 13, p. 201 (1931).

spectrum The 2800 Å band, apparently due mainly to the phenol nucleus, is about 10% more intense in oestrone than in oestradiol A weak absorption region is present between 3100–3500 Å in both compounds Our results may be compared with those of Callow \* The hexahydrophenanthrene (fig 2) shows a very intense absorption at about 2500 Å, presumably due to the aromatic ring conjugated to a C=O

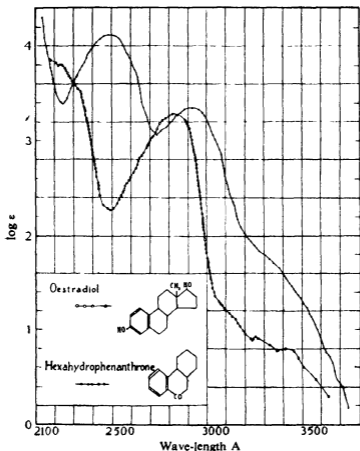


FIG 2

group, as well as a strong ketone band at 2920 Å. The spectrum is similar to that of ethyl benzoylacetate in alcohol (Morton) †

*Naphthalene Group*—The only additional compound in this group which has been examined is 9·9·10·10-tetramethyl-9·10-dihydro-

\* Callow, 'Biochem. J.', vol. 30, p. 906 (1936)

† Morton, 'J. Chem. Soc.', p. 893 (1934)

1:2:5:6-dibenzanthracene (fig. 3), which gives further evidence of the simplification of the absorption spectrum of 1:2:5:6-dibenzanthracene when the central ring is saturated in the 9:10-positions. The similarity of this spectrum to that of naphthalene is even more marked than in the *cis*- and *trans*-9:10-dimethyl-9:10-dihydro-derivatives previously re-

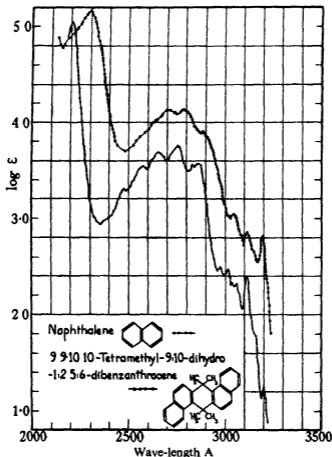


FIG. 3.

ported, possibly owing to the heavier weighting of the central ring. It is interesting to note that the absolute value of the extinction coefficient is now approximately twice that of naphthalene, presumably owing to the double naphthalenic system present in the molecule.

**Anthracene Group**—The additional compounds examined in this group are cholanthrene and 6-isopropyl-1:2-benzanthracene (fig. 4), both of which show the typical benzanthracene absorption spectrum. The

spectrum of 6-isopropyl-1,2-benzanthracene is very similar to that of its 6-methyl-analogue, both as regards the positions and the intensities of bands (*cf* Part I, p 313). There is, however, rather more resolution of bands in the far ultra-violet region of the spectrum of the isopropyl-compound.

Cholanthrene may be compared with 5,6-cyclopenteno-1,2-benzanthrene (Part I, p 315), for both compounds are 5-substituted benz-

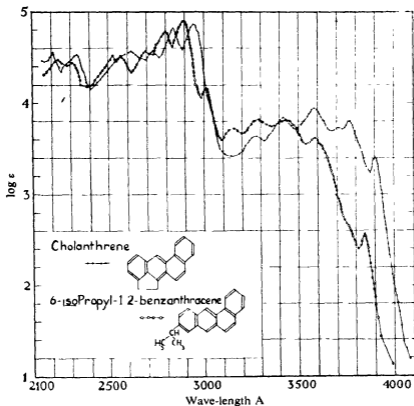


FIG 4

anthracenes and are also strongly carcinogenic. The spectrum of cholanthrene is shifted to the ultra-violet compared with 5,6-cyclopenteno-1,2-benzanthracene, and its far and middle ultra-violet bands are situated at shorter wave-lengths even than in 1,2-benzanthracene. The band intensities are in general similar in the two compounds, the distinctive 3000 Å benzanthracene band being reduced to a barely perceptible shoulder in both spectra. This band is moderately

intense in the 6-isopropyl-derivative, and the reduction in its intensity may be related to substitution at the 5-position of the benzantracene molecule

**Fluorene Group**—The close chemical relationship between the compounds of this group and the naphthafluorenes (closely related to Diels's hydrocarbon " $C_{25}H_{18}$ " from cholesterol), and the fact that 1,2,5,6-dibenzfluorene is weakly carcinogenic, led to an examination of the

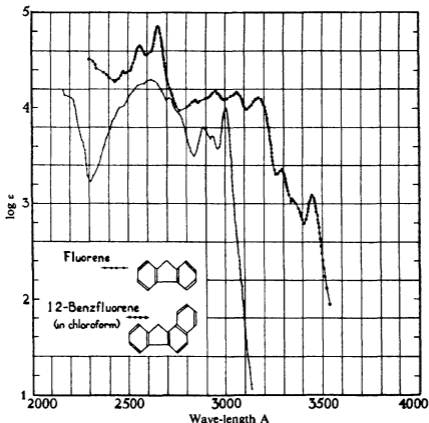


FIG. 5

absorption spectra of fluorene, 1,2-benzfluorene, 3,4-benzfluorene, and 1,2,5,6-dibenzfluorene (figs 5 and 6).

The spectrum of fluorene has been investigated by a number of workers, but owing to the fact that some of the samples used were evidently impure, divergent results were obtained. The results shown in fig. 5 are in agreement with those of Ramart-Lucas\* and Askew,† who stated that

\* 'Bull. Soc. Chim.', vol. 2, p. 1376 (1935).

† 'J. Chem. Soc.', p. 512 (1935).

the bands between 3000 Å. and 4000 Å. in fluorene reported by Capper and Marsh\*, and Menczel† were due to impurities. The spectrum of pure fluorene is essentially similar in form to that of diphenylmethane (examined by Ramart-Lucas,‡ Castille,§ Titeica,||), the cyclization of the central part of the diphenylmethane molecule giving rise to increased absorption, and a shift towards the visible in the fluorene spectrum.

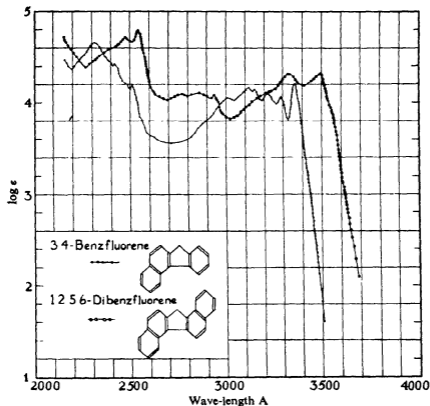


FIG. 6

The addition of a benzene ring to the 1, 2- or 3, 4-positions of fluorene causes an extension of the ultra-violet absorption limit from about 3200 Å to 3500 Å. There is, however, a notable difference between the

\* 'J. Chem. Soc.,' p. 724 (1926)

† 'Z. phys. Chem.,' vol. 125, p. 161 (1927)

‡ 'Bull. Soc. Chim.,' vol. 2, p. 1376 (1935)

§ 'Bull. Acad. Belg. Cl. Sci.,' vol. 12, p. 498 (1926)

|| 'C. R. Acad. Sci. Paris,' vol. 199, p. 458 (1934)

form of the two benzfluorene curves. Evidently the position of the additional benzene ring with respect to the methylene group of fluorene is important. The 1,2-benzfluorene spectrum somewhat resembles that of 1,2-benzanthracene (Part I, p. 312) in the arrangement and relative intensities of the absorption systems.

The 1,2,5,6-dibenzfluorene molecule can be regarded as a benz-derivative of either 1,2- or 3,4-benzfluorene, but its absorption spectrum

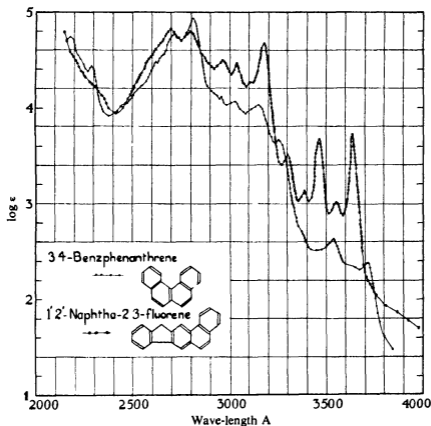


FIG. 7

(fig. 6) does not bear any close resemblance to those of either of these compounds. The spectrum consists of three groups of rather diffuse bands, with an absorption limit at about 3700 Å.

*Phenanthrene Group*—3,4-Benzphenanthrene and 1',2'-naphtha-2,3-fluorene are the only additional substances examined in this group (fig. 7). The former compound was, until recently, the only substance, not derived from 1,2-benzanthracene, known to possess carcinogenic activity.

Both of these derivatives give a spectrum of the phenanthrene type although the 3·4-benzphenanthrene spectrum shows wider divergences than any other compound previously examined in this group. Whereas the 1' 2'-naphtha-2 3-fluorene spectrum shows the principal phenanthrene band-systems, with a strongly-marked alternation in the intensities of the long wave-length bands (as in *cyclopentenophenanthrene*, Part I, p 317), the 3·4-benzphenanthrene band-groups are less sharply differentiated. The characteristic, sharp, long wave-length phenanthrene peaks are here represented by broader and weaker bands. Thus, the addition of a benzene ring to the 3·4-position of phenanthrene has modified the phenanthrene spectrum even more than in picene and chrysene (1 2-benzphenanthrene) (Part I, p 319). The spectrum of 1' 2'-naphtha-2 3-fluorene shows, however, the dominating influence of the phenanthrene portion of the molecule, although the band systems below 3200 Å in the naphthfluorene somewhat resembles the fluorene spectrum.

#### LOW TEMPERATURE EXPERIMENTS

In order to provide further data for an attack on the theoretical interpretation of these absorption spectra and to provide a technique capable of dealing with substances unstable at ordinary temperatures, measurements have been carried out at temperatures down to  $-120^{\circ}\text{C}$ . The experimental technique developed for this work is described below.

The apparatus (fig. 8) consists essentially of a Dewar vessel having a detachable metal-glass upper portion A, which is used as a liquid oxygen container. To the lower end of the latter is screwed a brass block B, into which are fitted the metal absorption cells containing the solvent and solution to be examined.

The detachable portion of the apparatus consists of a modified Philips's demountable X-ray tube of soda-glass sealed to a chrome-iron alloy. The brass block containing the absorption cells takes the place of the anode. Fortunately, even direct contact with liquid oxygen does not crack the metal-glass seal. Two pairs of quartz windows D are sealed by means of picein into the opposite sides of the rectangular brass box which forms the outer wall of the vacuum vessel, and are in alignment with the absorption cells. A rubber washer (1 mm thick, and slightly greased) is used between the upper and lower portions of the apparatus so that the whole is easily demountable. The apparatus is evacuated by means of a rotatory oil pump through a side-tube in the lower metal portion, the vacuum attained being normally of the order of 0.01 mm.

mercury. Under these conditions, condensation and crystallization of water vapour and  $\text{CO}_2$  on the quartz windows are completely avoided.

It was soon found that the simple, cylindrical type of absorption cell as used with the Hilger rotating sector photometer is not suitable for measurements at low temperatures. Large bubbles formed by contraction of the alcohol interfere with the passage of the light beam through

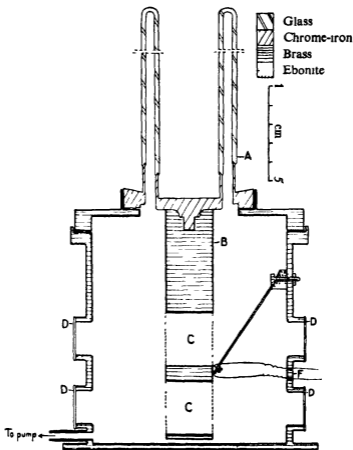


FIG 8.

the apparatus. The provision of side-arms with ground-in stoppers appeared to overcome this difficulty, but the problem of adequate thermal contact with the cooling block still remained. It was found that cells made entirely of quartz cooled far too slowly, even when packing materials such as copper-amalgam, lead shavings, and aluminium powder were employed between cell and block. It was thought that metal cells would be preferable, and a final form was devised as shown in fig. 9. The body

and side-arms were constructed of brass with carefully ground steel stoppers, while the quartz end-plates and brass faces were optically polished, the plates being clamped into position with brass screw caps using lead washers 0.1 mm thick

The apparatus is mounted on a base astride the photometer platform and may be adjusted to optical alignment by means of levelling screws

Owing to the large heat capacity of the original block containing the absorption cells, the temperature of the solution still falls very slowly at low temperatures and a hollow block, conveying liquid oxygen much

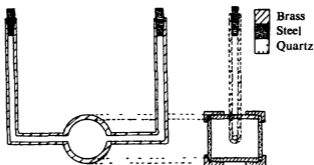


FIG. 9

closer to the absorption cells, has therefore been constructed for use below  $-120^{\circ}\text{C}$

The temperature of the block was estimated by means of a copper-constantan thermocouple (in series with a pointer galvanometer) mounted on a springy ebonite strip which presses one junction against the block when the latter is lowered into position. The holes through which the thermocouple leads pass to the exterior were made vacuum-tight with picein wax. The thermocouple was calibrated at the melting-points of water ( $0^{\circ}\text{C}$ ), pyridine ( $-42^{\circ}\text{C}$ ), methyl alcohol ( $-94.9^{\circ}\text{C}$ ), carbon disulphide ( $-112^{\circ}\text{C}$ ), ethyl alcohol ( $-114.9^{\circ}\text{C}$ ), *n*-pentane ( $-131.5^{\circ}\text{C}$ ), and the boiling-point of liquid oxygen ( $-182.9^{\circ}\text{C}$ ). Temperatures can be read to  $0.5^{\circ}\text{C}$ , although in practice the temperature of the block is only constant to about  $5^{\circ}\text{C}$  while a series of exposures is made.

It is obviously important to find a solvent which does not crystallize at low temperatures but sets to a glassy solid. Contrary to the experience of some previous observers, we have found that ethyl alcohol almost invariably crystallizes at low temperatures and is therefore unsuitable. However, a mixture of ethyl and methyl alcohols (five to one by volume) is entirely satisfactory. The absorption spectrum of benzene in this

mixed solvent at room temperature is identical, within the experimental error, with that in ethyl alcohol

In practice the cells are carefully filled and the ground stoppers (slightly greased) firmly inserted in the side-arms. The brass block and cells are then cooled on ice and inserted into the apparatus. This is evacuated for about two minutes before liquid oxygen is pumped into the glass-metal upper portion

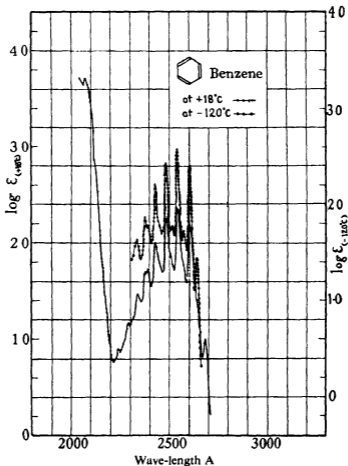


FIG 10

## EXPERIMENTAL RESULTS

*Benzene*—Benzene is the only compound whose spectrum we have so far examined quantitatively at low temperatures. Measurements have

been made at  $18^{\circ}\text{C}$ ,  $-22^{\circ}\text{C}$ ,  $-55^{\circ}\text{C}$ ,  $-85^{\circ}\text{C}$ , and  $-120^{\circ}\text{C}$ . The results are shown in figs 10 and 11. No allowance has been made for changes in concentration owing to contraction.

The most obvious result of temperature reduction is the considerable increase in the extinction coefficient at the maxima of the bands, with the single exception of the longest wave-length peak at  $2679\text{ \AA}$ . The apparent sharpening of the bands is to some extent not real, for at a given extinction coefficient the band-width is often increased at the lower temperature. Greater resolution is obtained, however, as may be seen in the separation into definite peaks of the room temperature "shoulders" on the long wave-length slopes of the main bands. It is interesting to observe that the minima between the bands are not appreciably affected by a reduction of temperature.

The increase in the extinction coefficients at the maxima of various bands on decreasing the temperature is shown in fig 12. It will be seen that in general there is an increase of some 50% but that the bands at  $2387\text{ \AA}$  and  $2679\text{ \AA}$  are anomalous. The small increase in intensity in the former has the effect of reversing the relative intensities of the pair of bands  $2387\text{ \AA}$ . and  $2376\text{ \AA}$ , while the  $2679\text{ \AA}$  band decreases in intensity as the temperature is lowered and finally disappears at about  $-120^{\circ}\text{C}$ . It is interesting to note that the latter band shows an anomalous frequency

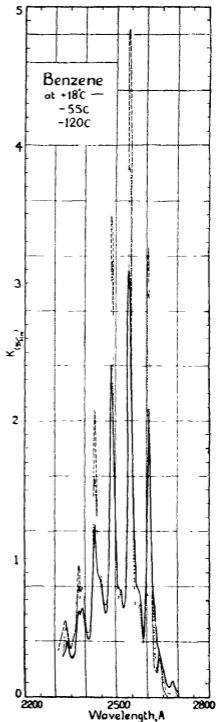


FIG. 11.

separation from its neighbour of  $1120\text{ cm.}^{-1}$ , the normal frequency difference for the main benzene bands being  $925\text{ cm.}^{-1}$ .

The positions of the band maxima for benzene solutions remain remarkably constant down to  $-120^\circ\text{C}$ , the lowest temperature reached. In the course of studies of benzene crystals at  $-180^\circ\text{C}$ ., Croup,\* and Kronenberger and Pringsheim† found band-shifts to shorter wave-lengths as the temperature fell

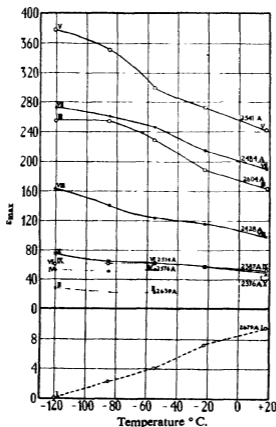


FIG. 12.

#### PRELIMINARY QUALITATIVE INVESTIGATIONS

Qualitative investigations have been made of naphthalene, anthracene, and phenanthrene. The results are preliminary, however, and were derived from visual inspection of continuous spectra obtained with a hydrogen tube as source.

\* 'Phys. Rev.', vol. 40, p. 345 (1932).

† 'Z. Physik,' vol 40, p. 75 (1926); vol 63, p. 494 (1930).

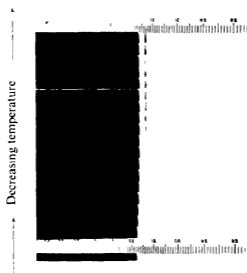


FIG. 13 -Portion of absorption spectrum of naphthalene in ethyl alcohol, using hydrogen tube as source, showing effect of decreasing temperature



*Naphthalene*—Multiplication and increasing sharpness of bands was noticed as the temperature decreased, while wave-length shifts were observed varying in magnitude with the positions of the band-groups. The middle ultra-violet group (2350–2900 Å.) moves about 10 Å. towards the visible while the long wave-length band-group (2900–3200 Å.) apparently remains stationary as the temperature is decreased. It is interesting to note (fig. 13, Plate 27) that the longest wave-length band of naphthalene (3200 Å.) gradually disappears, though its adjacent “shoulder” at 3150 Å. grows more pronounced (cf. results for benzene).

*Anthracene*—On cooling a solution of anthracene apparent multiplication of bands occurs, both the long wave-length (2850–3850 Å.) and middle ultra-violet (2250–2600 Å.) band-groups moving about 15–20 Å. towards the visible. It must be emphasized that the shift here considered is that of the long wave-length edge of the band, for the positions of the maxima have not yet been obtained.

*Phenanthrene*—The changes observed on cooling a phenanthrene solution appear to be more complex than hitherto contemplated, for wave-length shifts in different directions occur for band edges in different regions of the spectrum. The far and middle ultra-violet bands from 2000–3000 Å. move on cooling the solution towards the visible end of the spectrum, as do also the longest wave-length bands at 3553 Å., 3713 Å., and 3760 Å. The distinctive band-system from 3000–3500 Å. appears to move 3–5 Å. towards the ultra-violet, a small movement compared to the red-shift of phenanthrene's middle ultra-violet bands (the 2507 Å. band is displaced about 20–30 Å.). In addition to wave-length shifts, multiplication of bands also takes place as the temperature is reduced.

In this very small series of compounds, we have observed many possibilities of change in position and intensity of absorption bands on reducing the temperature. It is evident that even a qualitative explanation of these facts must be complex, and that more than one factor should be taken into account in any theoretical consideration. Changes of various types of energy in the molecule and mutual interaction of solute and solvent molecules must occur, and will be modified by change of temperature.

We wish to express our indebtedness to Professor J. W. Cook who has supplied us with the materials investigated, and to record our gratitude to the International Cancer Research Foundation for a grant to one of us. We wish to thank Dr. Bouwers of Philips (Metalix) for the metal-glass portion of the low-temperature apparatus.

## SUMMARY

The ultra-violet absorption spectra of ethyl alcohol solutions of a number of polycyclic aromatic compounds, some of which are of biological importance, have been investigated. The compounds examined include equilin, oestrone, oestradiol, hexahydrophenanthrene, 9.9.10.10-tetramethyl-9.10-dihydro-1.2.5.6-dibenzanthracene, cholanthrene, 6-isopropyl-1.2-benzanthracene, fluorene, 1.2- and 3.4-benzfluorenes, 1.2.5.6-dibenzfluorene, 1'.2'-naphtha-2'.3-fluorene and 3.4-benz-phenanthrene.

A quantitative technique is described for measurements at low temperatures and results with benzene solutions are recorded. Preliminary qualitative experiments on naphthalene, anthracene, and phenanthrene are reported.

---

Atmospheric Oscillations

By C. L. PEKERIS, D Sc

(Communicated by G. I. Taylor, FRS—Received 10 September, 1936)

## 1—INTRODUCTION

The early researches of Laplace\* on the problem of atmospheric oscillations were aimed at an explanation of the semidiurnal variation of the barometer. It was known to him that the amplitude of the solar component of the semidiurnal barometric oscillation is larger than the corresponding lunar component, although the tidal force of the moon is more than twice as large as that of the sun. His explanation was that the barometric oscillation is not of tidal but of thermal origin. It was pointed out, however, by Sir William Thomson† that if the pressure oscillation were a thermal effect, the diurnal term should be larger than the semidiurnal term—in direct contradiction to the facts. As an alternative explanation, Kelvin made the suggestion that the atmosphere has a period of free oscillation of nearly 12 hours, so that the solar semidiurnal

\* 'Mécanique Céleste'. For a review of the literature up to 1924, see Chapman's article, 'Quart J Roy Met Soc.', vol 50, p 166 (1924).

† 'Proc Roy Soc Edin.', vol 11, p. 396 (1882).

tide is magnified by resonance. The question whether our atmosphere actually has a free oscillation of a period of 12 hours has since been studied extensively, but on account of the various simplifying assumptions common to all these investigations concerning the physical nature of the oscillations and the distribution of temperature in the atmosphere, it still remains open.\* Further collection and analysis of the observational data of the barometric oscillations have tended to support the resonance theory, but evidence has also come from other geophysical phenomena which, apparently, cannot be reconciled with it.

According to Simpson,† the solar semidiurnal barometric oscillation can be represented by

$$p_2 = 0.937 \sin^3 \theta \sin 2t + 154'' \\ + 0.137 (\cos^2 \theta - \frac{1}{2}) \sin (2t - 2\phi + 105^\circ),$$

where  $\theta$  denotes the colatitude,  $t$  local time, and  $\phi$  longitude, and the unit is 1 mm of mercury.

The first term represents a wave travelling from east to west with the sun, while the second term represents a wave which is stationary with respect to the earth and has maximum amplitudes at the poles. A wave of the first type would be expected to be excited either tidally or thermally by the sun, and it was shown by Chapman‡ that the contributions from the two causes are nearly equal. He showed that the magnification is about a hundredfold, and he was also able to explain the phase of this wave. No cause is known for the second wave, but its existence gives strong support to the resonance theory, since it is known that an atmosphere which has a free oscillation of the first type also has a free oscillation of the second type.

The lunar barometric oscillation, for which Laplace looked in vain, is now known at a number of stations, due to the efforts of Chapman§. It is semidiurnal with an amplitude of about 1/16 of the solar wave and a phase of about  $70^\circ$ . It is, however, more variable with locality and seasons than the solar wave. Chapman, Pramanik, and Topping|| have recently discussed the data of the solar and lunar barometric oscillations with a view to testing the resonance theory. They found that on this theory four types of pressure waves should be magnified by resonance,

\* An exception to this statement is the work of Taylor (*infra*)

† 'Quart J Roy Met Soc,' vol 44, p 1 (1918)

‡ 'Quart J Roy Met Soc,' vol 50, p 166 (1924)

§ 'Proc Roy Soc,' A, vol 151, p. 105 (1935)

|| 'Beitr Geophys,' vol. 33, p 246 (1931)

while lunar and solar *diurnal* waves should not occur. All of these six predictions are actually verified by observations

This theory conflicts, however, with the evidence from the propagation of waves of explosion which was brought to bear upon this problem by G I Taylor \* Taylor proved† that the free period of atmospheric oscillations can be computed from the speed of these waves. Now the wave which was caused by the Krakatau eruption in 1883 and which went round the world several times was propagated with a speed, corresponding to a free period of about  $10\frac{1}{2}$  hours. A similar speed was found by Whipple‡ for the wave of the Great Siberian Meteor. Taylor also computed the wave velocity in an atmosphere having a vertical temperature distribution such as is found from balloon observations. The value found was within 2% of the observed speed of the Krakatau wave. A period of  $10\frac{1}{2}$  hours, however, is definitely fatal to the resonance theory, since in order to obtain the observed degree of magnification the free period must be within 6 minutes of 12 hours.

Indirect evidence on this problem can also be obtained from the diurnal variation of the earth's magnetic field. Chapman§ showed that the "dynamo" theory accounts satisfactorily for the principal features of the solar and, especially, the lunar components of the field. He finds, however, that the pressure oscillations in the upper conducting layer, where the dynamo effect is produced, are nearly  $180^\circ$  out of phase with the observed pressure oscillations at the ground. Furthermore, the required conductivity of the layer is larger than the value that can be inferred from radio soundings.

The solution offered here is that the atmosphere has two modes of free oscillations of periods of  $10\frac{1}{2}$  and 12 hours respectively. This is found to be true if we assume a temperature distribution such as is shown by curve T in fig 1 or, with some approximation, by all but F and I of the curves in fig 2. The rise of temperature between about 30 to 60 km, common to all these atmospheres, has been assumed in accordance with results which were obtained by Whipple|| from the abnormal propagation of waves from gun-fire and which are in agreement with the results of similar experiments carried out in Germany. The ratio of the horizontal velocities at any level to the value at the ground is shown for the two modes

\* 'Proc Roy Soc,' A, vol 126, pp 169, 728 (1929), 'Mem Roy Met Soc,' vol 4, No 35 (1932)

† 'Proc Roy Soc,' A, vol 156, p 378 (1936)

‡ 'Quart J Roy Met Soc,' vol 60, p 510 (1934).

§ 'Phil Trans,' A, vol 218, p 1 (1919)

|| 'Quart J Roy Met Soc,' vol 61, p 285 (1935)

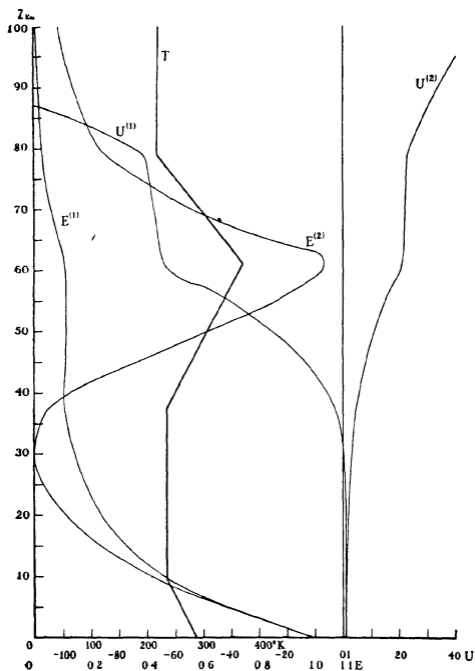


FIG 1

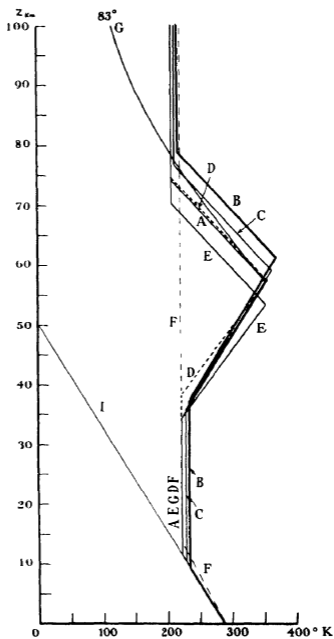


FIG 2

of oscillations by the curves  $U^{(1)}$  and  $U^{(2)}$ . It is seen that the 12-hourly oscillation (2) has a nodal surface at about 30 km, where the horizontal velocities and pressure oscillations vanish. The atmospheres above and below this level move, mainly horizontally, in opposite directions and the pressure changes are of opposite sign in the two regions. Furthermore, the amplitudes of the velocities at the 100 km level which is the probable region of the dynamo effect are, in the 12-hourly oscillation, more than 100 times as large as at the ground. Hence the magnetic data are completely accounted for. The kinetic energy densities, which are proportional to the density of matter and the square of the velocities, vanish ultimately exponentially, as is shown by curves  $E^{(1)}$  and  $E^{(2)}$ . From the run of these curves one might expect that a disturbance like the Krakatau eruption which was concentrated at the ground would excite mode (1) and would therefore be propagated with a corresponding speed. That the Krakatau wave was shallow can be inferred from the fact that the wave-front was considerably modified by the trade winds, as was shown by Taylor.

In the following section we discuss the forced tidal oscillations of a horizontally uniform atmosphere having an arbitrary vertical temperature distribution and for an arbitrary horizontal distribution of the tidal potential. It is shown that for a given period of the tidal disturbance there exists a characteristic set of functions of the horizontal coordinates into which the tidal potential and the motion can conveniently be analysed. With each such function are associated a characteristic value of a certain parameter  $H$  and a definite value of the amplification and vertical distribution of the motion. The first two characteristic functions are given for the solar semidiurnal tide and the first two terms in the expansion of the tidal potential are determined.

In § 3 the boundary condition at infinity for the vertical distribution of the motion is discussed in connexion with the question of the effect of conductivity and viscosity. It is shown that the latter is negligibly small up to 100 km height, but becomes very large at 200 km. A suggestion is made that in certain cases the effect of conductivity and viscosity, though it is small in the lower atmosphere, determines the choice between the two possible solutions for the vertical distribution of the motion. In § 4 details are given of the computations of the free oscillations of some model atmospheres which resemble our atmosphere. It is shown that the existence of a semidiurnal free oscillation restricts in some measure the possible temperature distributions in the upper atmosphere.

## 2—FORCED TIDAL OSCILLATIONS OF A HORIZONTALLY UNIFORM ATMOSPHERE ON A ROTATING GLOBE

The following is a natural sequel to Taylor's\* treatment of the free oscillations of such an atmosphere. We denote the undisturbed values of the variables by the subscript  $_0$  and assume that the disturbed values and the tidal potential  $\Omega$  are proportional to  $e^{i(\sigma t + s\phi)}$ , where  $s$  is a positive or negative integer and  $\phi$  denotes the longitude. We neglect the vertical acceleration, the ellipticity of the earth, and the variation with height of  $\partial\Omega/\partial z$ , of the radius vector, and of  $g$ . The largest error thus introduced is due to the variation of  $g$ , which amounts to about 3% at the 100 km. level. Denoting by  $u, v, w$  the south, east, and vertical components of the velocities, and by  $Q$  the quantity  $\left(\frac{p}{\rho_0} + \Omega\right)$ , we have for the equations of motion and of continuity

$$\frac{\partial u}{\partial t} - 2\omega v \cos \theta = -\frac{1}{a} \frac{\partial Q}{\partial \theta}, \quad (1)$$

$$\frac{\partial v}{\partial t} + 2\omega u \cos \theta = -\frac{1}{a \sin \theta} \frac{\partial Q}{\partial \phi}, \quad (2)$$

$$\frac{\partial p}{\partial z} = -g\rho - \rho_0 \frac{\partial \Omega}{\partial z}, \quad (3)$$

$$\frac{\partial \rho}{\partial t} = -w \frac{\partial \rho_0}{\partial z} - \rho_0 \chi. \quad (4)$$

$z$  is taken positive upwards and

$$\chi = \frac{1}{a \sin \theta} \frac{\partial}{\partial \theta} (u \sin \theta) + \frac{1}{a \sin \theta} \frac{\partial v}{\partial \phi} + \frac{\partial w}{\partial z} \quad (5)$$

If we assume the pressure changes to be adiabatic and denote by  $c$  ( $=\sqrt{\gamma RT_0}$ ) the velocity of sound at any level, then

$$\frac{Dp}{Dt} = c^2 \frac{D\rho}{Dt}, \quad (6)$$

or 
$$\frac{\partial p}{\partial t} = wg\rho_0 - c^2 \rho_0 \chi. \quad (7)$$

On eliminating the pressure from (3) and (7), we get

$$\frac{\partial w}{\partial z} = (1 - \gamma) \chi + \frac{c^2}{g} \frac{\partial \chi}{\partial z} - \frac{i\sigma}{g} \frac{\partial \Omega}{\partial z}. \quad (8)$$

\* \* Proc Roy Soc., A, vol 156, p 378 (1936)

It follows also from (7) that

$$i\sigma Q = gw - c^2\chi + i\sigma\Omega \quad (9)$$

We can now solve for  $u$  and  $v$  from (1) and (2) and substitute in (5) obtaining

$$\begin{aligned} u &= \frac{i\sigma}{4a\omega^2(f^2 - \cos^2\theta)} \left\{ \frac{\partial Q}{\partial\theta} + \frac{s}{f} \cot\theta Q \right\}, \\ v &= \frac{-\sigma}{4a\omega^2(f^2 - \cos^2\theta)} \left\{ \frac{\cos\theta}{f} \frac{\partial Q}{\partial\theta} + \frac{sQ}{\sin\theta} \right\}, \\ \chi - \frac{\partial w}{\partial z} &= i\sigma \left\{ \frac{1}{4a^2\omega^2\sin\theta} \frac{\partial}{\partial\theta} \left[ \frac{\sin\theta}{(f^2 - \cos^2\theta)} \left( \frac{\partial Q}{\partial\theta} + \frac{s}{f} \cot\theta Q \right) \right] \right. \\ &\quad \left. - \frac{1}{4a^2\omega^2(f^2 - \cos^2\theta)} \left[ \frac{s}{f} \cot\theta \frac{\partial Q}{\partial\theta} + \frac{s^2 Q}{\sin^2\theta} \right] \right\} \equiv i\sigma F(Q), \quad (10) \end{aligned}$$

where  $f = \frac{\sigma}{2\omega}$  and  $F$  is defined as the operator of the horizontal coordinates in  $\{ \}$ . On differentiating (8), (9), and (10) with respect to  $z$ , and eliminating  $\partial w/\partial z$  and  $\partial^2 w/\partial z^2$ , we obtain

$$c^2 \frac{\partial^2 \chi}{\partial z^2} + \left( \frac{dc^2}{dz} - \gamma g \right) \frac{\partial \chi}{\partial z} + F \left\{ \chi \left[ g^2(1 - \gamma) - g \frac{dc^2}{dz} \right] \right\} = 0 \quad (11)$$

If we now assume that  $\chi = \chi(z) \psi(\theta)$  and substitute in (11), it easily follows that the operation  $F$  must equal multiplication by a constant which we shall denote by  $-\frac{1}{gH_n}$ . Thus

$$c^2 \frac{d^2 \chi}{dz^2} + \left( \frac{dc^2}{dz} - \gamma g \right) \frac{d\chi}{dz} + \frac{\chi}{H_n} \left[ \frac{dc^2}{dz} + g(\gamma - 1) \right] = 0, \quad (12)$$

and

$$F(Q) = -\frac{1}{gH_n} Q. \quad (13)$$

The differential equation (13) with the condition that  $u$  vanish at the poles and be single-valued everywhere else occurs also in the problem of the free oscillations of an ocean of depth  $H_n$ .<sup>\*</sup> For given values of  $\sigma$  and  $s$  there are an infinite number of possible values of  $H_n$  and corresponding functions  $\psi_n$ . Thus for solar semidiurnal oscillations ( $\sigma = 2\omega$ ) and  $s = 0$ †

$$\psi_n = A_n \cos n\pi\mu + B_n \sin(n + \frac{1}{2})\pi\mu, \quad n = 0, 1, 2, 3, \dots, \mu = \cos\theta,$$

<sup>\*</sup> Lamb, "Hydrodynamics," 6th edit., p. 330 (1932)

† Solberg, "Astrophys. Norveg.," vol. 1, p. 295 (1936)

and

$$H_n = \frac{16a^2 w^2}{g\pi^2 n^2}, \quad (14)$$

where in the last equation  $n$  is an even integer for the symmetrical oscillations and an odd integer for the antisymmetrical oscillations. When  $s = 2$  and  $\sigma = 2w$ , as for the solar semidiurnal tidal potential, the first two symmetrical  $\psi$ 's are:

$$\psi_1 = P_2^2 - 0.0869705 P_4^2 + 4.82147 \times 10^{-3} P_6^2 - 1.65606 \times 10^{-4} P_8^2 \\ + 3.82399 \times 10^{-6} P_{10}^2 - 6.32520 \times 10^{-8} P_{12}^2 + \dots, \quad (15)$$

$$\psi_2 = P_2^2 + 1.29193 P_4^2 - 0.484058 P_6^2 + 0.0811605 P_8^2 \\ - 8.18587 \times 10^{-3} P_{10}^2 + 5.60605 \times 10^{-4} P_{12}^2 \\ - 2.79648 \times 10^{-5} P_{14}^2, \quad (16)$$

$$H_1 = \frac{4a^2 \omega^2}{g} (0.0898557) = 7.87 \text{ km}, \quad (15')$$

$$H_2 = \frac{4a^2 \omega^2}{g} (0.0241938) = 2.12 \text{ km}, \quad (16')$$

if  $a = 6.37 \times 10^8 \text{ cm}$ ,  $g = 980.6$

$\psi_1$  has no nodal lines, while  $\psi_2$  has one nodal circle of latitude, and in general  $\psi_n$  has  $(n-1)$  nodal lines. An important feature of these functions is that they are orthogonal

$$\int_{-1}^1 \psi_n \psi_m d\mu = 0 \quad n \neq m$$

This property can be proved directly from the differential equation (13), and can easily be verified for  $\psi_1$  and  $\psi_2$ . The set of  $\psi$ 's is, moreover, complete, as can be proved from general principles. Hence any function of  $\theta$  can be developed in terms of them. In particular  $P_s^2$ , which represents the horizontal distribution of the semidiurnal tidal potentials of the sun and the moon, has the following development:

$$P_s^2 = 0.940150 \psi_1 + 0.0462273 \psi_2 + \dots \quad (17)$$

The determination of the forced tidal oscillations now proceeds as follows. Assume that

$$\chi = \sum_1^\infty \chi_n(z) \psi_n(\theta), \quad \Omega = \sum_1^\infty \Omega_n(z) \psi_n(\theta), \quad p = \sum_1^\infty p_n(z) \psi_n(\theta), \\ u = \sum_1^\infty u_n(z) \psi_n(\theta), \text{ etc.,}$$

where we have omitted throughout the factor  $e^{i(\sigma t + \phi)}$ . It follows from (10), (13), and (8) that

$$i\sigma \frac{p_n}{\rho_0} = -i\sigma\Omega_n + H_n \left( -\gamma g \chi_n + c^2 \frac{d\chi_n}{dz} - i\sigma \frac{d\Omega_n}{dz} \right) \\ \simeq -i\sigma\Omega_n + H_n \left( -\gamma g \chi_n + c^2 \frac{d\chi_n}{dz} \right), \quad (18)$$

since  $H_n \frac{d\Omega_n}{dz}$  is of the order of  $\frac{H_n}{a} \Omega_n$  and can therefore be neglected in comparison with  $\Omega_n$ . This shows that the tidal action is exerted mainly by the horizontal components of the tidal force, although the vertical component is comparable to them. From (7) we now obtain

$$w'_n = \frac{c^2}{g} \chi_n + H_n \left( -\gamma \chi_n + \frac{c^2}{g} \frac{d\chi_n}{dz} \right) - \frac{i\sigma\Omega_n}{g} \equiv w'_n - \frac{i\sigma\Omega_n}{g} \quad (19)$$

Equation (12), with the appropriate value of  $H_n$  and suitable boundary conditions serves to determine  $\chi_n$ , while equations (18) and (19) serve to determine the vertical distribution of the pressure oscillations and of  $w$  as well as of  $u$  and  $v$ , which are proportional to  $(p/\rho_0)$ . Now the boundary condition at the ground is obviously  $w_n = 0$ , by which the arbitrary constant multiplying  $\chi_n$  (call it  $A$ ) is determined in terms of the value of  $\Omega_n$  at the ground.

For a given temperature distribution in the atmosphere there are certain values  $H_k$  such that when used instead of  $H_n$  in (12) the appropriate solution  $\chi_k$  makes  $w'_k$  vanish at the ground. These are, according to a theorem of Taylor,\* the values of  $H$  which enter in the expression  $c_k = \sqrt{gH_k}$  for the speeds of long waves in the atmosphere. If, then, one of the  $H_k$  is nearly equal to one of the  $H_n$ , the solution  $\chi_n$  of (12) will not differ much from  $\chi_k$ , and  $w'_n$  will nearly vanish at the ground. The resulting value of the factor  $A$  mentioned above will be large. When  $H_k = H_n$ ,  $\chi_k = \chi_n$ ,  $A \rightarrow \infty$  and the atmosphere then possesses a free oscillation of a period appropriate to  $H_n$  and with a distribution of  $\chi$  given by  $e^{i(\sigma t + \phi)} \chi_n(z) \psi_n(\theta)$ †. It is important to notice, however, that besides the proximity of  $H_k$  to  $H_n$  it is also necessary for large amplification that the horizontal distribution of the tidal potential should contain an appreciable term  $\psi_n$ .

In § 4 we shall assume certain temperature distributions and determine some of the  $H_k$ . One of these turns out to be close to  $H_1$  of (15'), and since the distribution of the semidiurnal solar tidal potential has a large

\* 'Proc. Roy. Soc.' A, vol 156, p 378 (1936).

† The other values of  $H_k$  also determine free oscillations but of different periods.

component  $\psi_1$ , we should expect a large semidiurnal tide. In order to compute the actual value of the amplification for a resonating atmosphere, one has to know the value of  $H_1$  to a greater accuracy than 3%. We can, however, compute the maximum percentual difference between  $H_1$  and  $H_2$  which is compatible with the observed amplification. This is found to be less than 4%.

### 3—BOUNDARY CONDITION AT INFINITY AND THE EFFECT OF CONDUCTIVITY AND VISCOSITY

Dropping subscripts we may write (12) as

$$\frac{d^2\chi}{dz^2} + \left(\frac{1}{T} \frac{dT}{dz} - \frac{g}{RT}\right) \frac{d\chi}{dz} + \frac{\chi}{H} \left[\frac{1}{T} \frac{dT}{dz} + \frac{(\gamma-1)g}{\gamma RT}\right] = 0 \quad (20)$$

We shall begin with the simple case of an atmosphere of uniform temperature. Writing  $\frac{RT}{g} = h$  and assuming a solution of the form  $e^{\lambda z}$ , the equation for  $\lambda$  is

$$\lambda^2 - \frac{\lambda}{h} + \frac{(\gamma-1)}{\gamma H h} = 0, \\ \lambda = \frac{1}{2h} \left[ 1 \pm \sqrt{1 - \frac{4(\gamma-1)h}{\gamma H}} \right] = \frac{1}{2h} \left[ 1 \pm \sqrt{1 - \frac{8h}{7H}} \right]. \quad (21)$$

Clearly, we must discard one of the  $\lambda$ 's, but it is seen from (19) and the right-hand side of (18), to which  $u$  and  $v$  are proportional, that for both values of  $\lambda$  the velocities increase exponentially with height. The pressure amplitude has an extra factor  $e^{-s/\lambda}$ , so that its exponent has the two possible values of  $\frac{1}{2h} \left[ -1 \pm \sqrt{1 - \frac{8h}{7H}} \right]$ , both of which are always negative. A suitable criterion for choosing between the two possible solutions is the one suggested by Meissner\* in his treatment of surface waves in an elastic half-space, according to which a physically realizable wave must not have an infinite amount of energy per column of unit cross-section. Now, since the energy density is proportional to  $\rho_0 u^2$ , where  $u$  is the velocity vector, we see from (21) that by the above criterion we must adopt the  $\lambda$  with the negative radical, provided the latter is real. When the radical becomes imaginary, which would happen, for example, in case the higher order  $\psi$ 's occur in the distribution of the tidal potential, the choice between the roots can be made by considering the effect of a small heat-

\* 'Vjschr. naturf. Ges. Zürich,' 66, 181 (1921).

conductivity. Similar considerations would apply to an atmosphere with a different temperature distribution in which the energy density is not integrable.

To illustrate this point, it will suffice to treat the case of an atmosphere of constant temperature and constant thermometric conductivity  $K$ . Equations (2) to (5) are still valid, but instead of equation (6) we now have

$$K \frac{\partial^2 T}{\partial z^2} = \gamma \frac{DT}{Dt} - (\gamma - 1) \frac{T_0}{p_0} \frac{Dp}{Dt} = \gamma \frac{DT}{Dt} - (\gamma - 1) T_0 \left[ \frac{1}{\rho_0} \frac{D\rho}{Dt} + \frac{1}{T_0} \frac{DT}{Dt} \right] \\ = \frac{\partial T}{\partial t} + (\gamma - 1) T_0 \chi, \quad (22)$$

where  $T$  denotes the variation of temperature. It is convenient to express all the variables in terms of  $T$ , which is found to satisfy the following equation:

$$\frac{iK}{\sigma} \left[ \frac{\epsilon^2}{\gamma g} \frac{\partial^4 T}{\partial z^4} - \frac{\partial^2 T}{\partial z^2} \right] + \frac{\epsilon^2}{g} \frac{\partial^2 T}{\partial z^2} - \gamma \frac{\partial T}{\partial z} + \frac{(\gamma - 1)}{H} T = 0 \quad (23)$$

When  $K = 0$ , (23) reduces to the same form as (20), as was to be expected, since by (22)  $T$  then becomes proportional to  $\chi$ . If we assume a solution of (23) of the form  $e^{\lambda z}$ , we have

$$\delta (h\lambda^4 - \lambda^2) + \lambda^2 - \frac{\lambda}{h} + \frac{(\gamma - 1)}{\gamma h H} = 0, \quad \delta \equiv \frac{iK}{\gamma \sigma h}$$

We now assume  $\delta$  to be small and look for roots  $\lambda$  of the form

$$\lambda_0 + \delta \lambda_1 + \delta^2 \lambda_2 +$$

We shall of course use only  $\lambda_0$  for  $\lambda$ , but the sign of the real part of  $\delta \lambda_1$  determines which of the two roots of  $\lambda_0$  we shall choose. Clearly

$$\lambda_0 = \frac{1}{2h} \left[ 1 \pm \sqrt{1 - \frac{8h}{7H}} \right] = \frac{1}{2h} \left[ 1 \pm i\beta \right] = \sqrt{\frac{2}{7hH}} e^{\pm i\phi}, \\ \beta \equiv \sqrt{\frac{8h}{7H} - 1} = \tan^{-1} \phi,$$

$$\lambda_1 = \frac{\lambda_0^3 (1 - h\lambda_0)}{(2\lambda_0 - \frac{1}{h})} = \frac{\left(\frac{2}{7hH}\right)^{3/2} e^{\pm 3i\phi} \left(\sqrt{\frac{2h}{7H}} e^{\mp i\phi}\right)}{(\pm i\frac{\beta}{h})} \quad (24)$$

$$\delta \lambda_1 = \pm \frac{4K e^{\pm 2i\phi}}{49hH^2 \gamma \beta \sigma} = \pm \frac{K}{14hH^2 \gamma \beta \sigma} \left[ 2 - \frac{8h}{7H} \pm i2\beta \right]. \quad (25)$$

The choice between the two possible roots of  $\lambda_0$  depends, then, on the sign of  $\left(2 - \frac{8h}{7H}\right)$ .

We can use equation (23) to estimate the effect of heat conduction on the semidiurnal atmospheric oscillations. It is known *a priori*, as was emphasized by Taylor, that this effect must be negligible in the lower atmosphere, since otherwise the amplification by resonance would be considerably damped. This is true even if we consider the eddy conductivity which can exceed the molecular conductivity by a factor of  $10^5$ . Since, however, the molecular conductivity is inversely proportional to the density, there is a level above which its effect becomes important, so that the results of the following section strictly apply only to the atmosphere below that level. Taking the case of an atmosphere of constant temperature, we have  $\frac{\partial}{\partial z} \sim \frac{1}{h}$ , where  $h = 8 \times 10^5$  cm. The ratio of the conduction terms to the others in (23) is then of the order of magnitude of  $K/\sigma h^2$ , which is of the order of  $10^{-10}$  at the ground. At 100 km height this ratio is still of the order of  $10^{-3}$ , while at 200 km it is over 100. The same relative orders of magnitude will be found for the viscosity terms. Hence damping by conduction and viscosity is certainly negligibly small in the first 100 km but is very large at 200 km.

#### 4—FREE OSCILLATIONS OF THE ATMOSPHERE

In this section we shall obtain a solution of (20) for an assumed temperature distribution which agrees with the mean temperature distribution in the atmosphere in the regions where the latter is known. The temperature in the part of the atmosphere which is accessible to balloon soundings starts with a mean surface value of about  $288^\circ \text{A}$ , decreases in the first 10 km. at the rate of about  $6^\circ \text{C}$  per km, and then remains nearly constant till about 30 km. For the next 20 to 30 km the temperature distribution can be inferred, with less certainty, however, from the abnormal propagation of waves from gun-fire. According to Whipple,\* it can be represented by a temperature rising at the rate of about  $6^\circ \text{C}$  per km. The evidence obtained from these experiments pertains, of course, to the velocity of sound and not directly to the temperature, but it is actually the former which enters in our original equation (12) and we speak of temperature only for convenience. The fact that rays are seldom turned down from levels above 60 km would indicate a decreasing temperature, but besides this vague inference no definite information is available about

\* 'Quart. J. Roy. Met. Soc.', vol. 61, p. 285 (1935)

the temperature distribution above 60 km. We have therefore assumed the simplest type of temperature distribution in these regions which is consistent with the existence in the atmosphere of a free semidiurnal oscillation. This temperature distribution is not unique, but its general feature is an initial fall followed by a constant temperature, as shown in fig. 2. When the "top" of the atmosphere is thus adjusted, the resulting free oscillation is found to possess two characteristics which, according to Chapman, are required by the "dynamo" theory of the diurnal variation of the earth's magnetic field

- (1) The pressure variations in the upper atmosphere are  $180^\circ$  out of phase with the observed pressure variation at the ground
- (2) The amplitudes of the horizontal velocities are larger (by a factor of about 200) than that at the ground

These two results by themselves can be considered as sufficient evidence for the reality of the assumed "top". There is, however, a third characteristic which is verified observationally, namely that

- (3) The atmosphere possesses another mode of free oscillation of a period of about  $10\frac{1}{2}$  hours and a corresponding velocity of the waves of explosion which agrees exactly with the velocity of Krakatau wave

Furthermore, the distribution of energy in the oscillation of the latter mode is such as to lead us to expect that this mode would be excited by a surface disturbance like the Krakatau eruption. The last inference is as yet only of a qualitative nature and its establishment must await the solution of the problem of the propagation of a surface pulse in the assumed atmosphere. Computations were also carried out for slightly different models, as shown in fig. 2, in order to ascertain how the characteristic  $H_k$  depend on the detailed structure of the temperature distribution. Table I gives the values of  $H^{(1)}$  and  $H^{(2)}$ , which are the characteristic  $H_k$ , for the first and second (semidiurnal) modes of oscillation. The results are expressed in the second and third columns in terms of  $H_0$ —the height of the homogeneous atmosphere and which is determined by the surface temperature

$$H_0 = \frac{RT_0}{g}$$

If the surface temperature is  $288^\circ \text{A}$ ,  $H_0 = 8.43 \text{ km}$ , and  $H^{(1)}$  and  $H^{(2)}$  have the values shown in the last two columns.  $H^{(1)}$  has not been determined for all the atmospheres, since it is seen that its variation is

TABLE I

Values of  $H_k$  for the atmospheres shown in fig 2. The speed of the Krakatau wave was 318.8 m./sec, and the corresponding  $H$  is 10.37 km. The mean value of the speed of the Siberian Meteor wave was 318 m/sec.  $H_1$  for solar semidiurnal oscillations is  $7.87 \text{ km} \pm 3\%$ .

	$H^{(1)}/H_0$	$H^{(2)}/H_0$	$H^{(1)}$ km.	$H^{(2)}$ km
A	1.2074	0.9271	10.18	7.815
B	1.2376	0.9718	10.43	8.192
C	—	0.9491	—	8.001
D	—	0.9271	—	7.815
E	—	0.9080	—	7.654
F	1.1954	—	10.08	—
G	1.2102	0.9271	10.20	7.815
I	1.110	0.1684	9.36	1.420

less than that of  $H^{(2)}$ . The extreme values of  $H^{(2)}$  are within 4% of the mean, which can be taken as equal to  $H_1$  since the value of the latter given in (15') is subject to an error of about 3%. Assuming that  $H_1 = 7.889 \text{ km}$ , we find that the pressure variation at the ground in atmosphere B is eight times the statical value, as against the observed magnification of over 50. Since  $H^{(2)}$  of B differs from the assumed  $H_1$  by about 4%, it appears that the variation in the structure of the atmosphere shown in fig 2 is greater than the maximum with which the observed amplification is compatible.

The problem of the free oscillation of our composite atmosphere consists in solving

$$\frac{d^2\chi}{dz^2} + \left( \frac{1}{T} \frac{dT}{dz} - \frac{g}{RT} \right) \frac{d\chi}{dz} + \frac{\chi}{H} \left[ \frac{1}{T} \frac{dT}{dz} + \frac{(\gamma - 1)g}{\gamma RT} \right] = 0, \quad (20)$$

under the conditions that at the ground

$$w = \gamma \left[ \frac{RT}{g} \chi + H \left( -\chi + \frac{RT}{g} \frac{d\chi}{dz} \right) \right] = 0, \quad (26)$$

and that the kinetic energy per column of unit cross-section shall be finite. For an arbitrary  $H$  these conditions are in general not satisfied, so that for a given atmosphere the problem consists in finding those values of  $H$  and the functions  $\chi$  associated with them for which the boundary conditions are satisfied.

Let us denote the boundaries between the sections of the atmosphere by the numbers 0, 1, 2, 3, 4, 0 referring to the ground level. In the

troposphere  $(0-1) T = T_0 - \beta z \equiv \beta y$ , whereby we define a new coordinate  $y$ , which at any level is given by  $T/\beta$ . With  $y$  as an independent variable (26) becomes

$$\frac{d^2\chi}{dy^2} + \frac{(n+2)}{y} \frac{d\chi}{dy} + \frac{m}{y} \chi = 0, \quad (27)$$

where

$$(n+1) = \frac{g}{R\beta} \text{ and } m = \frac{(\gamma-1)n-1}{\gamma H}$$

If  $x$  is defined by  $x^2 = 4my$ , the solution of (27) is

$$\chi = x^{-(n+1)} [AJ_{n+1}(x) + BY_{n+1}(x)], \quad (28)$$

$$\begin{aligned} w &= \frac{\gamma H}{(n+1)} \left[ -(n+1)\chi - y \frac{d\chi}{dy} + \frac{y}{H} \chi \right] \\ &= -\frac{\gamma H}{2(n+1)x^n} \left\{ A \left[ J_n(x) - \frac{\gamma x}{(0.8n-2)} J_{n+1}(x) \right] \right. \\ &\quad \left. + B \left[ Y_n(x) - \frac{\gamma x}{(0.8n-2)} Y_{n+1}(x) \right] \right\}, \quad (29) \end{aligned}$$

$$\begin{aligned} \frac{1}{\rho_0} \frac{\partial p}{\partial t} &= -\gamma g H \left( \chi - \frac{RT}{g} \frac{d\chi}{dz} \right) = -\frac{\gamma g H}{(n+1)} \left[ (n+1)\chi + y \frac{d\chi}{dy} \right] \\ &= -\frac{\gamma g H}{2(n+1)x^n} \{ AJ_n(x) + BY_n(x) \} \quad (30) \end{aligned}$$

At the boundary between two sections of the atmosphere we must have continuity of velocities and of pressure. We shall impose instead the equivalent conditions of the continuity of  $\chi$  and of the quantity  $\left( \frac{w}{\gamma H \chi} \right)$ , which in the troposphere is given by

$$-\frac{w}{\gamma H \chi} = \frac{x \left\{ J_n(x) - \frac{\gamma x}{(0.8n-2)} J_{n+1}(x) \right\} + \frac{B}{A} \left[ Y_n(x) - \frac{\gamma x}{(0.8n-2)} Y_{n+1}(x) \right]}{2(n+1) \left\{ J_{n+1}(x) + \frac{B}{A} Y_{n+1}(x) \right\}}. \quad (31)$$

In the region 1-2 the temperature is constant and it will be convenient to use the same coordinate  $y = \frac{T_0}{\beta} - z$  as for the troposphere. We have

$$\chi = Ce^{\lambda y} + De^{\mu y}, \quad (32)$$

$$\lambda_1 = \frac{1}{2h}[-1 + V], \quad \lambda_2 = \frac{1}{2h}[-1 - V], \quad h_1 = \frac{RT_1}{g}, \quad V = \sqrt{1 - \frac{8h_1}{7H}}.$$

$$w = -\gamma H \left\{ C \left( \frac{1}{2} - \frac{h_1}{H} + \frac{1}{2}V \right) e^{\lambda_1 y} + D \left( \frac{1}{2} - \frac{h_1}{H} - \frac{1}{2}V \right) e^{\lambda_2 y} \right\}, \quad (33)$$

$$\frac{1}{\rho_0} \frac{\partial p}{\partial t} = -\frac{\gamma}{2} g H \{ C(1 + V) e^{\lambda_1 y} + D(1 - V) e^{\lambda_2 y} \}, \quad (34)$$

$$-\frac{w}{\gamma H \chi} = \frac{\left\{ \left( \frac{1}{2} - \frac{h_1}{H} + \frac{1}{2}V \right) e^{(\lambda_1 - \lambda_2)y} + \frac{D}{C} \left( \frac{1}{2} - \frac{h_1}{H} - \frac{1}{2}V \right) \right\}}{\left\{ e^{(\lambda_1 - \lambda_2)y} + \frac{D}{C} \right\}} \quad (35)$$

In the region 2-3 where the temperature is increasing we use the co-ordinate  $z$  defined by  $T = \beta_2 z$ . The origin of this  $z$  is obviously the point of intersection of the temperature line with the zero axis. Equation (20) becomes

$$\frac{d^2 \chi}{dz^2} - \frac{l}{z} \frac{d\chi}{dz} + \frac{s}{z} \chi = 0,$$

where

$$(l+1) = \frac{g}{R\beta_2}, \quad s = \frac{(\gamma-1)l + 2\gamma - 1}{\gamma H} = \frac{0.4l + 1.8}{\gamma H}$$

With  $r$  defined by  $r^2 = 4sz$  we have

$$\chi = r^{(l+1)} \{ E J_{l+1}(r) + F Y_{l+1}(r) \}, \quad (36)$$

$$w = \frac{\gamma H}{(l+1)} \left\{ \frac{z}{H} \chi - (l+1) \chi + z \frac{d\chi}{dz} \right\} = -\frac{\gamma H r^{l+2}}{2(l+1)} \times \left\{ E \left[ J_{l+2}(r) - \frac{\gamma r}{(0.8l+3.6)} J_{l+1}(r) \right] + F \left[ Y_{l+2}(r) - \frac{\gamma r}{(0.8l+3.6)} Y_{l+1}(r) \right] \right\}, \quad (37)$$

$$-\frac{w}{\gamma H \chi} = \frac{r \left\{ J_{l+2}(r) - \frac{\gamma r}{(0.8l+3.6)} J_{l+1}(r) + \frac{F}{E} \left[ Y_{l+2}(r) - \frac{\gamma r}{(0.8l+3.6)} Y_{l+1}(r) \right] \right\}}{(2l+1) \left\{ J_{l+1}(r) + \frac{F}{E} Y_{l+1}(r) \right\}}, \quad (38)$$

$$\frac{1}{\rho_0} \frac{\partial p}{\partial t} = -\frac{\gamma g H}{2(l+1)} r^{l+2} \{ E J_{l+2}(r) + F Y_{l+2}(r) \} \quad (39)$$

The solution for the region 3-4 is formally the same as for 0-1, the only difference being due to the new value of  $n$ . In the region above 4 we have

$$\chi = L e^{\lambda_1 y}, \quad y = \text{constant} - z, \quad \lambda_1 = \frac{1}{2h_4}(-1 + V),$$

$$V = \sqrt{1 - \frac{8h_4}{7H}}, \quad h_4 = \frac{RT_4}{g},$$

$$w = -\gamma HL \left( \frac{1}{2} - \frac{h_4}{H} + \frac{1}{2}V \right) e^{\lambda y}, \quad \frac{1}{\rho_0} \frac{\partial p}{\partial t} = -\frac{\gamma}{2} gHL (1 + V) e^{\lambda y},$$

$$-\frac{w}{\gamma H \chi} = \frac{1}{2} - \frac{h_4}{H} + \frac{1}{2}V.$$

The numerical work proceeds as follows. We assume a certain value for  $H/H_0$  and determine  $x_0$  from the relation

$$\frac{H}{H_0} = \frac{4(n+1)(0.4n-1)}{\gamma x_0^2}$$

$B/A$  is then determined from the condition of the vanishing of  $w$  at the ground

$$\frac{B}{A} = - \frac{J_n(x_0) - \frac{\gamma x_0}{(0.8n-2)} J_{n+1}(x_0)}{Y_n(x_0) - \frac{\gamma x_0}{(0.8n-2)} Y_{n+1}(x_0)}. \quad (40)$$

At the level 1 we have  $x_1 = x_0 (T_1/T_0)^{1/2}$ ,  $\frac{y_1}{h_1} = \frac{T_1}{\beta h_1} = (n+1)$ . On evaluating (31) for  $x = x_1$  and equating it to (35), with  $y = y_1$ , we obtain  $D/C$ . At the level 2 we have  $y_2 = y_1 - \Delta z$ , where  $\Delta z$  is the difference in height between the levels 2 and 1.  $r_2$  is determined from

$$r = x_0 \left[ \frac{(l+1)(0.4l+1.8)T}{(n+1)(0.4n-1)T_0} \right]^{1/2},$$

with  $T_2$  substituted for  $T$ . On equating (35) and (38) we then determine  $F/E$ . We proceed similarly at the levels 3 and 4. If we denote the lapse rate in 3-4 by  $\beta_3$  and define  $q$  by  $(q+1) = \frac{g}{R\beta_2}$  we shall have

$$x_3 = x_0 \left[ \frac{(q+1)(0.4q-1)T_3}{(n+1)(0.4n-1)T_0} \right]^{1/2} \quad (41)$$

We thus evaluate  $\left( -\frac{w}{\gamma H \chi} \right)$  at the level 4, which must equal

$$\left( \frac{1}{2} - \frac{h_4}{H} + \sqrt{1 - \frac{8h_4}{7H}} \right)$$

If this is not true, the computation is repeated with a different value of  $H$  until agreement is finally obtained.

It is to be noted that if we take the temperature distribution up to 60 km and the existence of a semidiurnal free oscillation as given, the value of  $H$  and of the relative distribution of the motion up to that level is

known. In particular, the value of  $\left(-\frac{w}{\gamma H\chi}\right)$  at that level, which is obviously a real quantity, is known. Now in attempting to fit a "top" to the atmosphere it is found that a constant temperature will not do since the radical  $\sqrt{1 - \frac{8h_0}{7H}}$  becomes imaginary. For a given  $H$  the condition of reality of this radical, which ensures an exponentially decreasing kinetic-energy-density, even without the effects of conductivity and viscosity, obviously sets an upper limit to a constant temperature which may exist at the top of the atmosphere. One is thus led first to decrease the temperature linearly from its value at about 60 km and then to superimpose a constant temperature. This linear distribution of temperature is, of course, not unique, as is shown by the fact that the atmosphere G has practically the same  $H_k$  as atmosphere A. In the former the temperature approaches the asymptotic value of  $83^\circ \text{A}$ , its solution being obtained as follows. Let

$$y = - \int_0^z \frac{g dz}{RT}, \quad \frac{d}{dz} = - \frac{g}{RT} \frac{d}{dy}, \quad \frac{d^2}{dz^2} = \frac{g^2}{R^2 T^2} \frac{d^2}{dy^2} + \left( \frac{g}{RT^2} \frac{dT}{dz} \right) \frac{d}{dy}$$

On substituting in (20) we find

$$\frac{d^2 \gamma}{dy^2} + \frac{d\gamma}{dy} + \frac{R\chi}{gH} \left[ - \frac{dT}{dy} + \frac{(\gamma - 1)}{\gamma} T \right] = 0 \quad (42)$$

If we assume

$$T = Ce^{y/3.5} + 3.5B = (T_0 - T_\infty) e^{y/3.5} + T_\infty, \quad (43)$$

then

$$- \frac{dT}{dy} + \frac{(\gamma - 1)}{\gamma} T = B = \frac{T_\infty}{3.5} = \frac{gh_\infty}{3.5R}, \quad h_\infty = \frac{RT_\infty}{g},$$

and

$$\chi = De^{\lambda y}, \quad \lambda = \frac{1}{2} - 1 + \sqrt{1 - \frac{8h_\infty}{7H}},$$

$$- \frac{w}{\gamma H\chi} = \frac{1}{2} - \frac{RT}{gH} + \frac{1}{2} \sqrt{1 - \frac{8h_\infty}{7H}} \quad (44)$$

The last expression is not a constant as in an atmosphere of constant temperature, but varies on account of the variable  $T$ . The height  $z$  above the level 0 at which  $T = T_0$  is given by

$$z = h_0 \left\{ 3.5 \left( 1 - \frac{h_\infty}{h_0} \right) (1 - e^{y/3.5}) - \frac{h_\infty}{h_0} y \right\}. \quad (45)$$

For large values of  $z$ ,  $y \rightarrow -\frac{z}{h_\infty}$  and  $T \rightarrow T_\infty$ . The temperature distribution is found by assuming values of  $y$  and computing the corresponding values of  $z$  and  $T$  from (45) and (43). It may be noted that if  $T_\infty > T_0$ , (43) represents a temperature increasing with height and that for free oscillations

$$H = \frac{h_0}{1 - \frac{T_\infty}{3.5T_0}} \quad (46)$$

This gives for  $H/h_0$  the values  $\gamma$  and 1 for the cases  $T_\infty = T_0$  and  $T = 0$ , which correspond respectively to an atmosphere of uniform temperature and to an atmosphere in convective equilibrium. Equation (46) is, however, valid only for values of  $T_\infty/T_0$  up to 1.75, when  $H = 2h_0$ . This can be shown by considering the energy density which is proportional to

$$\rho_0 \chi^2 \sim \frac{\rho_0}{T_0} e^{2\lambda y} \sim \frac{1}{T} e^{y + y(-1+y)} \rightarrow \frac{1}{T_\infty} e^{y^2}$$

Hence the radical must be positive, and it therefore follows from (44) that  $\frac{RT_0}{gH} = \frac{h_0}{H} \geq \frac{1}{2}$ . When  $T_\infty > 1.75T_0$ , free oscillations are impossible since both boundary conditions cannot be satisfied simultaneously.

TABLE II

	$n$	$y_1/h_1$	$l$	$q$	$T_1/T_0$	$T_2/T_0$	$T_4/T_0$
A	5	2.504	5	3	0.7744	1.2256	0.7229
B	5	1.958	5	3	0.8117	1.2847	0.7578
C	5	2.235	5	3	0.7927	1.2546	0.7400
D	5	1.879	4	3	0.7744	1.2256	0.7229
E	5	2.504	4	3	0.7744	1.2256	0.7229
F	6	—	—	—	0.7744	—	—
G	5	2.504	5	—	0.7744	1.2256	$T_\infty/T_0 = 0.2357$
I	5	—	—	—	—	—	—

Some numerical data for the atmospheres of fig. 2 are given in Table II. It may be noted that in computing the forced oscillation of a given atmosphere one simply uses  $H_1$  for  $H$  and fits the solutions from the level 4 downwards. One thus obtains the value of  $B/A$  by equating the values

of  $\left(-\frac{w}{\gamma H_x}\right)$  at level 1. The amplitude of the pressure variation at the ground is then determined from the relation

$$-\frac{p}{\rho_0 \Omega} = 1 - \frac{J_n(x_0) + \frac{B}{A} Y_n(x_0)}{\left\{ J_n(x_0) - \frac{\gamma x_0}{(0 \ 8n-2)} J_{n+1}(x_0) + \frac{B}{A} \left[ Y_n(x_0) - \frac{\gamma x_0}{(0 \ 8n-2)} Y_{n+1}(x_0) \right] \right\}} \quad (47)$$

The first term on the right-hand side corresponds to the statical pressure. When  $H_x = H_1$ , the second term becomes infinite since  $B/A$  then satisfies equation (40).

I am indebted to Professor S. Chapman for suggesting this problem to me and for his continued interest in the work. My thanks are also due to Professor G. I. Taylor for having put his unpublished manuscript at my disposal and for helpful discussions. For the use of unpublished tables of Bessel's functions I am grateful to Dr. L. J. Comrie.

#### SUMMARY

It is shown that when the increase of temperature between 30 and 60 km., which was inferred by Whipple from the anomalous propagation of sound waves, is assumed it is possible to find a temperature distribution above 60 km. such that the atmosphere has a free oscillation of a period very close to 12 solar hours. In this oscillation there is a horizontal nodal surface at about 30 km. height at which the velocities and pressure variations vanish, the atmospheres below and above this level swinging in opposite directions. The amplitudes of the velocities, which are mainly horizontal, at the 100 km. level are about 200 times larger than at the ground. These two features of the free oscillation remove two difficulties which Chapman encountered in his interpretation of the diurnal variation of the earth's magnetic field by the "dynamo" theory, namely (a) that the pressure oscillation in the conducting layer, where the dynamo effect is produced, is nearly  $180^\circ$  out of phase with the observed pressure oscillation at the ground, and (b) that the required electrical conductivity of the conducting layer is larger than the value that can be inferred from radio soundings.

It is also found that the same atmosphere has another mode of free oscillation, of a period of  $10\frac{1}{2}$  hours and having no nodal surfaces. The existence of this mode of free oscillation is required by the evidence from

the propagation of long waves which was put forward by G. I. Taylor. Taylor has proved that one can determine the period of free oscillation of the atmosphere from the speed of long waves. Now the wave which was caused by the Krakatau eruption in 1883 and which went round the world several times was propagated with a speed which corresponds to a period of free oscillation of about  $10\frac{1}{2}$  hours. A similar speed was found by Whipple for the wave of the Great Siberian Meteor.

A method is given for determining the forced tidal oscillation of a horizontally uniform atmosphere on a rotating globe, and is applied to the atmosphere mentioned above. It is found that the existence of the semi-diurnal free oscillation restricts in some measure the possible temperature distribution in the upper atmosphere.

---

## The Micrography of Metals in Ultra-Violet Light

By J. SMILES, A. R. C. S. (National Institute for Medical Research), and  
H. WRIGHTON, B. Met. (The Research Department, Woolwich)

(Communicated by J. E. Barnard, F. R. S.—Received 11 September, 1936)

[PLATES 28–34]

### INTRODUCTION

The resolution of metallic structures under the microscope has, during many years, been limited to that given by oil immersion apochromatic objectives of N.A. 1.30 or 1.40. With such objectives fine lamellar structure of the order of 140,000 lines per inch can be resolved.

In October, 1933,\* one of the authors published micrographs taken with a new monochromatic objective† for metallurgy designed to work in a narrow band of the visual deep blue at a wave-length of approximately 4395 Å., and having the large numerical aperture of 1.60. With this objective lamellar structure measuring 180,000 lines per inch has been resolved.

\* Wrighton, 'J. R. micro. Soc.', vol. 53, p. 328 (1933).

† This objective was computed by R. J. Bracey, of the British Scientific Instruments Research Association, and made by Messrs. R. & J. Beck, Ltd.

Using direct and dark ground methods of illumination, Barnard has amply demonstrated the superiority of a system using ultra-violet radiation over those used in the visual examination of certain forms of living biological material. He has shown that the greater resolution to be expected on theoretical grounds from the use of shorter wave-lengths is fulfilled, and that the correction of the quartz objectives is of a very high order.

It is only quite recently that any serious attempt has been made to apply dark ground methods of illumination to the metallurgical microscope at the higher powers. Special appliances combining high power objectives, of somewhat restricted aperture, with dark ground illuminating arrangements, are now available, but their use has not as yet become widely adopted. No such equipment is yet available in quartz objective systems.

Ultra-violet radiation has been applied to the metallurgical microscope by a few workers, notably F. Lucas. In June, 1934, however, shortly before the present work was commenced, Lucas\* expressed preference for the results he had obtained using a blue light monochromat of N.A. 1.60 newly introduced by Zeiss. This objective is evidently of similar general character to the one mentioned above.

The apparatus herein described was devised and the photographs with ultra-violet radiation were taken at the National Institute for Medical Research. The investigation there has been undertaken (by one of us, J. S.) with the object of obtaining further knowledge of the fine structure of materials of medical importance and interest, particularly of the teeth. It was necessary, however, in the first instance to test the apparatus and the method on material of which the fine microscopical structure was already known. For this purpose the apparatus has been used with an ultra-violet wave-length on a series of metals and alloys.

This part of the work was therefore designed to explore the possibilities of obtaining higher resolution of the microstructures of metals and alloys by the use of ultra-violet radiation, in comparison with that given by the newly introduced visual light system.

The authors have used the general method of illumination of the metallurgical microscope, that known as "vertical illumination", in which the incident beam of light is passed through the objective to the specimen. The incident beam is, in relation to the reflected image-forming beam, very intense, and reflexion from the air glass surfaces of the objective is liable to set up an amount of glare sufficient to obliterate image detail.

\* Lucas, 'J. Franklin Inst.', vol. 217, p. 661 (1934).

in which contrast is low. This trouble occurs particularly when the outer curvature of the back component of the objective is small. For this reason, objectives for metallurgical work should be computed with bold curvatures, but unfortunately very few objectives are constructed with attention to metallurgical requirements.

In Bracey's computation for the visual light monochromat, glare has been satisfactorily reduced, and the corrections of this objective permit the whole of the numerical aperture to be used without detriment to the image.

The results obtainable with this objective may be accepted as representative of the highest performance as yet attainable with the metallurgical microscope, and these have been used as a standard of comparison in the present work.

The quartz objectives at the authors' disposal were primarily designed for the photography of transparent objects by transmitted light using monochromatic radiation of wave-length 2750 Å. Each consists of a number of simple fused quartz lenses—seven for the highest powers—with the result that the number of air-solid surfaces is greater than for visual objectives of similar aperture.

It was, therefore, not known to what extent the reflexions from these surfaces would impair the quality of the images formed. It was considered that apart from image deterioration arising from this cause, many metal substances should prove almost ideal objects, some, notably aluminium, reflect a high percentage of ultra-violet light, whilst one difficulty of biological work, depth in the object, might not be encountered with suitably prepared specimens.

For this work an illuminating system has been used which is considered to reduce to a minimum the production of glare in any objective, by admitting to the microscope no light other than the strict counterpart of the image-forming beam reflected from the specimen.

In the early days of ultra-violet photomicrography, the success of focussing an object, particularly with a specimen in which the contrast between elements of structure is low, was largely a matter of chance. No microscope adjustment was sufficiently sensitive and free from irregularity to permit of changes in focus of the necessary precision being made, whilst focussing by means of the auxiliary uranium eyepiece was equally insensitive.

Barnard\* has overcome these difficulties by the use of interchangeable objective holding plates designed so as to be replaceable on the microscope.

\* Barnard and Welch, "Practical Photo-Micrography," 3rd edit., 1936, p. 309.

with great precision. The objectives,\* together with their plates, are centred one to another, and, within narrow limits, are parfocal. The objectives may be interchanged without disturbance of the specimen or of the focussing adjustment of the microscope. Barnard has also introduced a fine focussing adjustment capable of moving the objective through definite intervals of one ten-thousandth of a millimetre.

The authors gratefully acknowledge their indebtedness to Mr. Barnard's pioneer work and have taken full advantage of the improvements he has introduced.

#### ILLUMINATION

The visual light illuminating system which has been adopted for this work is shown diagrammatically in fig 1, in which S, a Point-o-lite lamp, is the source



FIG. 1

The lenses  $L_1$ ,  $L_2$ , the slip reflector, and the objective O form a centred optical system, which produces a secondary image of a portion of the source in the plane of the object when the objective is adjusted to form a primary image of the object in the focal plane of the eyepiece. The primary image of the source, formed by the short focus condensing lens  $L_1$ , lies in the plane of the iris  $D_2$  which is mounted concentrically with the axis of the system. The plane of the iris  $D_1$  immediately behind  $L_1$ , and one close to the back surface of the objective are conjugate planes of the lens  $L_2$ . It follows that a sharp image of  $D_2$  will be seen in the image plane of the eyepiece and that the brightness and evenness of illumination of the image will remain unaffected by varying its aperture.

The aperture of  $D_1$  determines the effective working aperture of the objective. The practical features of this system are as follows:

The size of the illuminated field of the specimen may be restricted,

\* These objectives are by Carl Zeiss, Jena.

thereby reducing glare, without in any degree affecting the working aperture of the objective.

The iris  $D_1$  may be adjusted to restrict the light entering the microscope to that just required to fill the aperture of the objective;  $D_1$  may be further restricted to reduce the effective aperture of an objective without any disturbance of the evenness of illumination of the field.

To obtain maximum resolution, objectives should be so free from spherical aberration that the whole of their apertures may be used. In the present work the whole of the aperture of each objective has been used.

The diagram, fig 2, shows the method of introducing the ultra-violet illuminating system. The ultra-violet source  $S'$  is a condensed spark between cadmium electrodes. By means of the lens  $L'_1$  and the dispersing

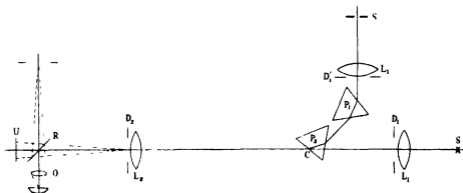


FIG 2

prisms  $P_1$  and  $P_2$ , a primary image in the wave-length 2750 is formed in the plane of the iris  $D_2$ . The quartz objective forms a primary image of the diaphragm and a secondary image of the source in the object plane. The prisms are adjusted for minimum deviation of an axial ray through  $L'_1$ . This ray passes approximately through the centre of each prism face, and on leaving the last of these at the point C is coincident with the axis of the visual system.

A fluorescent screen U is placed behind the slip reflector (which is of fused quartz) at a distance equal to that of the last surface of the objective in front of the slip. In order that the objective may be filled with ultra-violet light, the diameter of the image of  $D'_1$  on the screen U should be the same as that of the last surface of the objective.

The lens  $L_2$ , which is of quartz, is common to both systems, and once adjusted in visual light remains undisturbed. The centralization of the

ultra-violet system is checked by the coincidence of the visual and the ultra-violet images on the screen U. Since the objectives in use are mounted on the Barnard changing plates to be co-axial, they will be axially illuminated by either system.

#### ADJUSTMENT

The illustrations, figs. 3, 4, 5, 6, Plate 28, are general views of the microscope and the illuminating systems and show the method of mounting the optical components of the latter. Fig. 3 shows the microscope with camera attached. The stage is mounted on a separate base, and is provided with suitable adjustments by which the object plane can be set perpendicular to the axis of the objective. The Barnard objective changer is illustrated in fig. 4. Mounted immediately behind, and independent of the objective, is the vertical illuminator. The illuminating systems shown in figs. 5 and 6 are mounted on two optical benches which are fitted with levelling screws. One end of the bench carrying the spark gap and dispersing system is attached to a casting in which are two levelling screws, one of which rests in a conical hole and the other on a horizontal flat, which are carried on a saddle resting on the other bench. The other end of this bench rests on a horizontal flat. The dispersing system can therefore be rotated about a vertical axis. The prism  $P_2$  is mounted on a table so that the axis of rotation lies in the plane of the last face and passes through the point C (fig. 2). The prism table can swing away from the path of the visual system when it is desired to use the latter.

The bench carrying the visual system is also fitted with levelling screws. It is adjusted so that the axis of the illuminating system lies in a horizontal position. The height of the axis is then adjusted by raising the optical components until it passes through the point of intersection of the axis of the objective and the first face of the reflector  $R_1$  (fig. 2). The bench carrying the dispersing system is adjusted so that the axis of  $L'_1$  is horizontal and at the same height as that of the visual system. This can be carried out by adjusting the benches so that the intersections of their bearing faces lie in a horizontal plane. The spark gap and the lens  $L_1$  are placed on the bench carrying the visual system and their heights adjusted to the visual axis. They are then replaced on their own bench.

Final adjustment is carried out by illuminating the object by means of the visual system in conjunction with the quartz objective. The quartz slip of the illuminator, and the lens and iris  $L_2D_2$ , are adjusted to obtain accurate centralization both of the incident light as it enters the objective

and of the illuminated field area. The exact position of the image of the iris  $D_1$  in the plane of the screen  $U$  is then noted. The table carrying the prisms is swung into position, and by rotating the bench carrying the dispersing system, an image of the source  $S'$  in the wave-length 2750 Å. is allowed to fall centrally on the iris  $D_2$ . The position of the image of  $D'_1$  on the screen  $U$  is noted. Should this be horizontally displaced from the position occupied by the image of  $D_1$ , then the two systems will not be co-axial, and this is corrected by adjusting the position of the prism  $P_1$  whilst rotating the bench carrying the dispersing system so as to maintain the image of the spark on the iris  $D_2$ .

The diameter of the iris  $D'_1$  is adjusted so that its image on  $U$  is equal to the diameter of the back lens of the objective.

The first tests were made with a low power quartz objective of a focal length 6 mm. and numerical aperture 0.35. Since all the quartz objectives used were corrected for work with covered objects, a quartz slip was introduced, but in the present work it was found preferable to mount the slip immediately in front of the objective rather than on the specimen in order to minimize the effect of reflexions from its surfaces.

This was followed by the use of a lens of focal length 2.5 mm. and N.A. 0.85 with similar satisfactory results.

Finally the highest power quartz monochromat was used. This has a focal length of 1.7 mm. and N.A. of 1.25. Comparative photographs of almost identical fields in a number of metals and alloys were taken with this lens and with the visual light objective of N.A. 1.60.

The results obtained with this last quartz objective again proved sufficiently glare-free to permit of satisfactory imaging of the finest detail even of surfaces specially delicately etched. The negatives obtained were not quite so contrasty as the corresponding visual light images. This may be due in part to the exceptional freedom from glare of the visual light monochromat, but is in the main due to the low penetration of ultra-violet light in the gelatine of the plate which is a cause of some weakening of contrast in all classes of ultra-violet light microscopy.

With neither of the two lenses is there a large flat field available, and only the centre (approximately one-third diameter) of the field in the  $\times 10$  ocular was photographed. The illuminated field was carefully restricted to cover a plate field of  $2\frac{1}{4}$  inches diameter, thereby further reducing glare, which invariably makes its appearance when a large field is illuminated.

By trial and error methods, and careful examination of many photographs, the optimum tube length for the quartz objective in conjunction with the  $\times 10$  quartz ocular was determined. The fixed extension

camera in use gave with this system a magnification of about 2200 diameters

The visual light photographs were taken at Woolwich with a new photomicrographic outfit recently installed there, the camera being adjusted to give a measured magnification of  $\times 2500$ . The visual light negatives have been printed by contact, whilst the ultra-violet negatives have been printed by projection and enlarged a little to make the illustrations comparable in size.

Under these conditions, when the correct working tube length of the quartz lens had been determined, ultra-violet photographic images were obtained showing sharp definition and high resolution, obviously a little in advance of that given by the visual light monochromat.

The equivalent aperture of the quartz objective is 24% higher than the N.A. of the 1.60 visual light objective. On the other hand, the actual angular aperture of the quartz objective is lower, and this may, under some conditions, tend to reduce its advantage; this point will be referred to below in relation to the preparation of specimens.

#### PREPARATION OF METAL SPECIMENS

In relation to the minuteness of detail seen in the microscope, the methods of preparation of metal specimens seem forceful and crude. In the course of attempts made from time to time to secure the maximum clarity of imaging of fine detail in visual light work, some idea has been formed of the refinements desirable in these processes.

The image formed of a metal specimen is in the main a contour image. It is necessary that the relief or contour produced on the specimen should be substantially uniform in depth from grain to grain in the metal and from point to point on the surface, for high power work the relief should be as delicate as possible, and yet the layer of flowed and distorted material set up in the course of preparation must be completely removed.

It is desirable to carry the final stages of abrasive rubbing as finely as possible with avoidance of undue pressure or heating by friction, so as to require a minimum of surface flowing or polishing treatment.

The harder metal specimens used have been finally polished on a 6-inch diameter disk revolving at about 600 revolutions per minute, covered with selvyt cloth and fed with moistened heavy magnesium oxide. The pieces have been of the order of  $\frac{1}{2}$  inch or  $\frac{3}{4}$  inch square in size, and have required one minute or less of such polishing. Such working results in little surface flow; generally, however, it has been found desirable to

remove the first etch given, by a re-polishing of a few seconds only on the wheel, and then to give a final very light etch

The aluminium alloys, and some other of the softer metals, have been polished by a method described by Taffs,\* using specially prepared alumina on a benzine soaked pad.

A really sharp outline etch of minute structural detail is probably not attainable, the ground material immediately surrounding any attacked element of structure tends to be eaten away and so bevelled, and true image formation is thereby vitiated. The dark spot image of such an attacked particle becomes unduly large and loses shape, and this blurring increases with any reduction of the angular aperture of the optical system. In this respect, the visual light monochromat with its large actual aperture of 1.60 may be at some advantage over the quartz lens

#### DISCUSSION OF RESULTS

The images obtained have shown an increase in resolution and sharpness of detail of an order to be expected from the higher equivalent aperture. There has not been observed any different image formation resulting from selective absorption and reflexion in the ultra-violet when clean etched surfaces reasonably free from deposited etching products have been used. A 4% copper steel examined gave on etching a surface deposit or patina of copper, which, whilst transparent to blue light, was very opaque to the ultra-violet radiation and almost completely masked the structure. This patina was removable by collodion film stripping methods, after which the structure was imaged very clearly in the ultra-violet.

Some non-metallic inclusions have shown selective absorption, whereas brass and bronze, where clearly etched, have photographed quite as might have been expected in a higher aperture visual light system

The increased resolution has, in the steel specimens, resulted in sharper imaging of isolated minute carbide particles, and in a tendency for fine line structures to become resolved into chains of dots. Structural markings in free Ferrite, not shown under an apochromat of N.A. 1.30, are seen faintly appearing under the monochromat of 1.6 N.A. and more clearly imaged in the ultra-violet photographs

In one or two cases the specimens have been photographed in addition with an oil-immersion apochromat of 1.30 N.A., which is the highest power generally available at present. Comparison of these photographs with the ultra-violet images shows very clearly the advance in resolving power which is available

\* 'J. R. micr. Soc.', vol. 56, p. 300 (1936)

In fig. 28, Plate 34, lamellar structure measuring 200,000 lines per inch is resolved.

In conclusion, the authors wish to express their thanks to Mr. J. E. Barnard, F.R.S., for the interest he has taken in the work and for the loan of apparatus, to the Medical Research Council and the Director of the National Institute for Medical Research, and to Dr. R. H. Greaves, Director of Metallurgical Research, Woolwich Arsenal, for the facilities afforded at these different centres.

### EXPLANATION OF PLATES

#### PLATE 29

Pearlitic structure in plain carbon steel.

- FIG 7  $\times$  1000, 2 mm apochromat, N A 1 30  
 FIG 8  $\times$  2500, 2 mm apochromat, N A 1 30.  
 FIG 9  $\times$  2500, 2 mm monochromat, N A 1 60,  $\lambda$  4395  
 FIG 10  $\times$  2500, 1 7 mm. quartz monochromat, N A 1 25,  $\lambda$  2750.

#### PLATE 30

Sorbitic structure in nickel steel

- FIG 11  $\times$  500, 4 mm. apochromat, N A 0 95.  
 FIG 12  $\times$  2500, 2 mm. apochromat, N A 1 30  
 FIG 13  $\times$  2500, 2 mm monochromat, N.A 1 60,  $\lambda$  4395  
 FIG 14  $\times$  2500, 1 7 mm quartz monochromat, N A 1 25,  $\lambda$  2750

#### PLATE 31

Pearlitic structure in 4% copper steel.

- FIG 15  $\times$  2500, 2 mm monochromat, N A 1 60,  $\lambda$  4395  
 FIG 16  $\times$  2500, 1 7 mm quartz monochromat, N A 1 25,  $\lambda$  2750  
 FIG 17  $\times$  2500, 1 7 mm quartz monochromat, N A 1 25,  $\lambda$  2750.

Figs 15 and 16 are photographs of the specimen as prepared by polishing and etching in the usual manner. The film or patina which has formed on the surface is transparent to the visual radiation but almost opaque to the ultra-violet. After removal of this film by collodion stripping, a clear image of the structure is given, as shown in fig 17

#### PLATE 32

Sorbitic structure in nickel chrome steel.

- FIG. 18.  $\times$  2500, 2 mm monochromat, N A 1 60,  $\lambda$  4395  
 FIG. 19  $\times$  2500, 1 7 mm quartz monochromat, N A. 1 25,  $\lambda$  2750.

Venning structure in beryllium-bronze.

- FIG. 20  $\times$  2500, 2 mm monochromat, N A. 1 60,  $\lambda$  4395  
 FIG. 21.  $\times$  2500, 1 7 mm. quartz monochromat, N.A. 1 25,  $\lambda$  2750.



FIG. 3

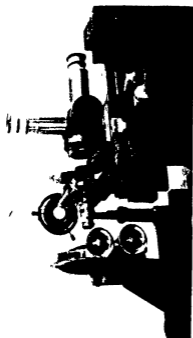


FIG. 4



FIG. 5

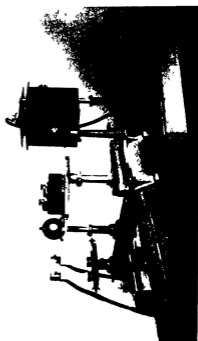


FIG. 6





FIG 7



FIG 8

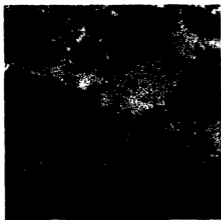


FIG 9



FIG 10





FIG 11



FIG 12



FIG 13



FIG 14





FIG 15



FIG 16



FIG 17





FIG 18



FIG 19



FIG 20



FIG 21





FIG 22



FIG 23



FIG 24





FIG. 25



FIG. 26



FIG. 27



FIG. 28



PLATE 33

Cold worked 70/30 brass

- FIG. 22  $\times 500$ , 4 mm apochromat, N.A. 0.95  
 FIG. 23  $\times 2500$ , 2 mm monochromat, N.A. 1.60,  $\lambda$  4395  
 FIG. 24  $\times 2500$ , 1.7 mm quartz monochromat, N.A. 1.25,  $\lambda$  2750.

PLATE 34

Fine Martensite in nickel chrome steel.

- FIG. 25  $\times 2500$ , 2 mm monochromat, N.A. 1.60,  $\lambda$  4395  
 FIG. 26  $\times 2500$ , 1.7 mm quartz monochromat, N.A. 1.25,  $\lambda$  2750  
 Pearlitic structure in plain carbon steel.  
 FIG. 27  $\times 2500$ , 2 mm monochromat, N.A. 1.60,  $\lambda$  4395.  
 FIG. 28  $\times 2500$ , 1.7 mm quartz monochromat, N.A. 1.25,  $\lambda$  2750.

## The Emission Band Spectrum of Chlorine—I

By A. ELLIOTT, Ph.D., D.Sc., and W. H. B. CAMERON, M.Sc., Physics  
 Department, University of Sheffield

(Communicated by S. R. Milner, F.R.S.—Received 24 September, 1936)

[PLATE 35]

### INTRODUCTION

It has long been known that chlorine, in addition to its atomic line spectrum, can be made to emit both continua and discrete bands, under suitable conditions of excitation. The chief results hitherto obtained are summarized below; other references to work on the band spectrum of chlorine (both in emission and absorption) may be found in Kayser's "Handbuch der Spektroskopie," vols. 7 and 8.

Measurements of the heads of the visible emission bands have been made by Ota and Uchida,\* who have arranged them in three systems. There is, however, serious lack of agreement in the "vibration frequencies" ( $\omega$ 's) where agreement should exist, and this has led us to remeasure the band heads of the whole system. These measurements have been extended considerably in the directions both of higher and of lower frequency, and the use of an improved technique has enabled us

\* "Jap. J. Phys.," vol. 5, p. 53 (1928).

TABLE I

Method of excitation	Spectrum	Observer
Discharge tube (internal electrodes)	Bands, $\lambda\lambda$ 3923–4871 Å	Ota and Uchida *
Tesla discharge . . . . .	Continua maxima at $\lambda\lambda$ 2600 and 3070 Å	Ludlam and West.†
Positive point discharge	Bands, $\lambda\lambda$ 3100–4000 Å., continua $\lambda\lambda$ 2495 and 2960 Å	Campetti ‡
Chlorine in active nitrogen	Continuum, $\lambda\lambda$ 2540–2600 Å	Strutt and Fowler §
Chlorine burning in hydrogen	Bands, $\lambda\lambda$ 5590–6500 Å, identical with absorption bands	Kitagawa
Chlorine at high temperature	Continuum in blue-green region	Kondratjew and Leipunski ¶
Discharge tube (chlorine at a pressure of several cm of mercury)	Continua maxima $\lambda\lambda$ 2570 and 3070 Å, other weaker maxima	v Angerer **

\* 'Jap J Phys,' vol 5, p 53 (1928)

† 'Proc Roy Soc Edin,' vol 44 (2), p 185 (1923–24)

‡ 'Atti Accad Torino,' vol 70, p 618 (1934–35)

§ 'Proc Roy Soc,' A, vol 86, p 105 (1912)

|| 'Rev Phys Chem Jap,' vol 8, p 71 (1934) (abstract and tables in English)

¶ 'Z Phys,' vol 50, p 366 (1928)

\*\* 'Z Phys,' vol 11, p 167 (1922)

to obtain much more accurate measurements of the band heads. These measurements show definitely that the analysis of Ota and Uchida cannot be accepted, as the discrepancies referred to above are greatly in excess of the experimental error. An example is given below, in which are shown the intervals in the  $n'$  progressions ( $n'' = 6$  and 5) of Ota and Uchida's System I.

$$\left. \begin{array}{lllll} n'' = 6 & 301.7 & 306.7 & 319.8 & 306.5 \text{ cm}^{-1} \\ n'' = 5 & & 314.4 & 320.0 & 324.1 \text{ cm}^{-1} \end{array} \right\} \text{Ota and Uchida}$$

The corresponding intervals from our measurements are:

$$\begin{array}{llll} 300.9 & 307.7 & 318.9 & 308.5 \text{ cm}^{-1} \\ & 315.2 & 318.3 & 313.8 \text{ cm}^{-1} \end{array}$$

As the estimated error is of the order of  $1 \text{ cm}^{-1}$ , it is evident that these progressions cannot be genuine.

## EXCITATION AND PHOTOGRAPHY OF THE SPECTRUM

Apart from experiments (described below) conducted for the purpose of examining the influence on the chlorine spectrum of discharge conditions, the high frequency electrical discharge (about  $10^7$  cycles per second) with external electrodes was employed throughout. Chlorine was generated by heating electrically a small quantity of cupric chloride, contained in a horizontal tube, to a temperature in the neighbourhood of  $350^\circ\text{C}$ , and was dried by passage over phosphorus pentoxide. It was then allowed to flow into the discharge tube, and was subsequently absorbed by copper and magnesium turnings. A continuous flow was maintained; the pumps (a Metropolitan-Vickers oil diffusion pump, backed by a Cenco Hyvac) were kept running continuously, and the pressure of chlorine in the tube was regulated by altering the temperature of the cupric chloride. Owing to the chemical activity of chlorine, the measurement of pressure presents great difficulties and was not attempted. The method adopted for the generation and control of chlorine proved to be extremely satisfactory.

The tube was used in the "end-on" position, and the light from it, which was blue in colour and very bright, passed through an aperture to a spectrograph placed in an adjacent constant temperature room. For investigation of the visible and near infra-red regions we used a Littrow spectrograph fitted with a single glass prism and lens of one-metre focal length, and for the ultra-violet region a Hilger E2 quartz spectrograph. In addition, photographs of the fine structure have been obtained with a three-prism Littrow instrument. These will be described in a separate publication. Ilford Special Rapid Panchromatic plates were employed throughout, except for the infra-red, where Ilford Infra-Red plates were used.

## DESCRIPTION OF THE SPECTRUM

Below about  $3400\text{ \AA}$ , the spectrum appears to consist entirely of continua. In addition to two main continua which may be identified with those recorded in the introduction, we have observed several weaker maxima. These have also been observed by Angerer,\* but have not been measured by him. It may be recalled that Curtis and Evans† have discovered a succession of such maxima in the emission spectrum of iodine. A microphotometer record of the chlorine continua is reproduced in Plate 35. Attention should be drawn to the fact that these continua

\* 'Z. Phys.', vol 11, p 167 (1922)

† 'Proc. Roy. Soc., A', vol 141, p. 603 (1933).

extend to the limit of transmission of quartz, and possibly further. The wave-lengths and wave numbers of the maxima are given in Table II.

The discrete bands, degraded to the red, extend from about 3400 Å to at least 5500 Å. A characteristic feature of the spectrum when viewed under low dispersion (*e.g.*, a pocket spectroscope) is a series of strong bands extending from about 5100 Å towards the red. These bands appear to be grouped in pairs at intervals of (very roughly) 300  $\text{cm}^{-1}$ , the members of a pair being about 140  $\text{cm}^{-1}$  apart. They may be seen on the plate, where their presence is indicated by crosses. They show no marked heads, and under higher dispersion become very indefinite, but may readily be seen on a microphotometer record. The region where these bands occur, particularly towards the red, is rich in atomic

TABLE II—WAVE-LENGTHS AND WAVE NUMBERS OF THE MAXIMA IN THE CONTINUOUS SPECTRUM OF CHLORINE

Designation	Wave-length Å	Wave number $\text{cm}^{-1}$
<i>a</i>	3063	32,638
<i>b</i>	2957	33,808
<i>c</i>	2881	34,700
<i>d</i>	2819	35,463
<i>e</i>	2758	36,247
<i>f</i>	2714	36,835
<i>g</i>	2564	38,990
<i>h</i>	2432	39,483

chlorine lines, which makes their investigation difficult. Whilst they have the appearance of diffuse bands, it must be emphasized that the evidence at present available is insufficient to give certainty on this point. Apart from these bands, most of the chlorine bands have fairly well-marked heads.

All attempts to obtain a spectrum free from atomic lines have been unsuccessful. In the infra-red region, an exposure of seven hours failed to reveal any trace of bands, although many chlorine lines were strongly recorded on the plate.

#### INFLUENCE OF CONDITIONS

In attempts to find regularities in the band spectrum, we examined the effect of altering the conditions under which the excitation was made. These alterations were made under several heads, *viz.*, alteration of pressure, of the diameter of the discharge tube; of electrical discharge

conditions; of external temperature, and the alteration produced by admixture of a foreign gas

We found that the intensities of the ultra-violet continua were little affected by a change of pressure, but that the production of the bands and of the lines of chlorine was favoured by lower pressures

A comparison was made between the discharges produced in tubes of 20 mm and 4 mm diameter. When exposure times were arranged to give equal densities of the chlorine bands produced in the two cases, the lines of Cl I were almost equally dense, too. Several of the lines of Cl II appeared strongly in the narrow tube, while the same lines were either much weaker in the wider tube or absent altogether

Four types of electrical excitation were examined, viz., the high frequency discharge with external electrodes, the same applied to a helix surrounding the tube and coaxial with it; a discharge from a small induction coil; and one from a 1200-volt direct current generator. For the two latter, electrodes of copper-nickel wire coated with fused silver chloride were employed. The high frequency discharge, either with external electrodes or helix, was much more effective for the production of the bands than the other two methods. Little difference was to be observed between the discharge with external electrodes and with helix, when high frequency excitation was used

Photographs of the spectra excited by a high frequency discharge (with external electrodes) and by an induction coil were compared when the bands in the two spectra were equally intense. Some of the lines of Cl I, notably the strong lines at 5796.34, 5799.94, 5846.71, 5847.74, and 5856.74 Å., were decidedly stronger in the high frequency discharge, of which they are a prominent feature, than in the induction coil discharge. On the other hand, the lines of Cl II, which were very weak in the high frequency discharge, were much stronger in the induction coil discharge

The influence of helium on the high frequency discharge was then examined. For this purpose, helium from a capillary doser was admitted to the tube and was then made to circulate round a closed system by means of a mercury diffusion pump. Liquid air traps, one of them containing charcoal, served to purify the helium before it was re-introduced into the discharge tube. Chlorine was admitted continuously.

With helium at a pressure of 0.1 mm of mercury, the chlorine bands and continua were greatly reduced in intensity. The lines of Cl I were slightly stronger, and some of the lines of Cl II were strongly developed. As the partial pressure of helium was increased up to 1 mm (the highest pressure used), these effects became more marked, until finally the chlorine bands and continua almost completely vanished.

A similar experiment was tried, using argon instead of helium, but difficulty was experienced on account of the absorption of argon by the charcoal. The results seemed to be similar to those obtained with helium.

In none of the above experiments was any change apparent in the intensity distribution either within a single band or in the band system as a whole

As it appeared that a lower temperature of the chlorine might be expected to give an altered intensity distribution, we tried the effect of cooling the tube with liquid air. This, however, merely quenched the discharge, presumably owing to the pressure of chlorine being too low. As a cooling agent, solid carbon dioxide was next tried, with the expected result that the band heads were rendered relatively more intense. The Cl I lines were weakened, while those of Cl II were less affected. The spectrum was much more suited to measurement of the band heads.

No change of the intensity distribution within the system could be detected with certainty, even though the effect was looked for on microphotometer records made from the spectrum photographs.

From these experiments, certain general conclusions may be drawn. Since pressure has a differential effect upon the intensity of the band system and of the continua, it is clear that these cannot have a common upper level. Strutt and Fowler\* only recorded one continuum in their active nitrogen experiments. If there is any significance in this fact, it would mean that the two main continua have not a common upper level either.

#### MEASUREMENTS

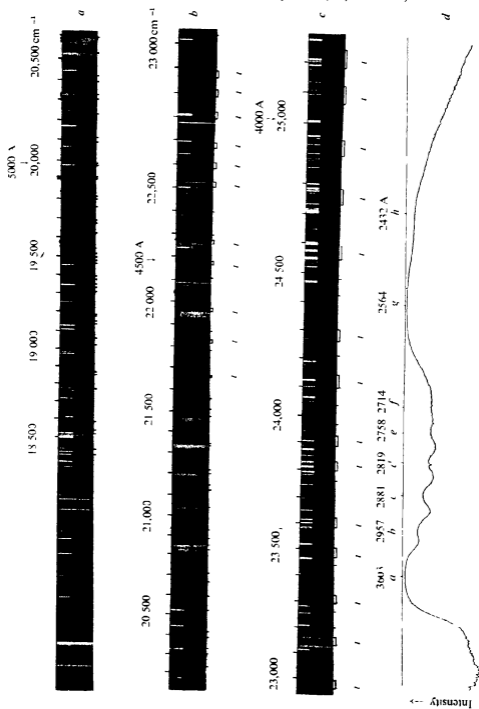
The wave numbers of the maxima of the continua have been measured from microphotometer records and are given in Table II. Little significance can be given to an estimate of their intensities, since it is clear from the reproduction of the microphotometer curve (Plate 35) that the strong maxima at 3063 and 2564 Å extend over the other maxima.

The wave numbers of the discrete band heads have been measured from plates taken with the emission tube cooled in solid carbon dioxide and are given in Table III. Some idea of the relative intensities of these band heads may be obtained by reference to Plate 35.

#### THE VIBRATIONAL ISOTOPE EFFECT

The plate shows a number of bands which have been identified as due to the less abundant molecule Cl<sup>35-37</sup> in addition to the strong bands of

\* 'Proc. Roy. Soc.,' A, vol. 86, p. 105 (1912).





$\text{Cl}^{35-35}$ . It is chiefly at the high frequency end of the spectrum that the identification has been made. None of the very weak bands of  $\text{Cl}^{37-37}$  has been found. The isotope separation is shown plotted against the wave number of the stronger band in fig. 1 for all cases where the identification seems certain. The formulae in common use for the vibrational isotope effect refer to the wave numbers of the band origins, but for the chlorine emission bands, as for the absorption bands, we may be quite certain

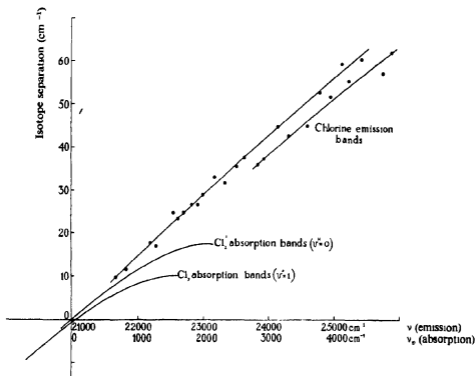


FIG. 1

that the origin and the head lie very near each other, and that no appreciable error will arise if the wave numbers of heads instead of those of the origins are used.

In Jevons's\* notation, the vibrational separation of two isotopic bands is given by

$$v_e' - v_e'' = (\rho - 1) (\omega_e' u' - \omega_e'' u'') - (\rho^2 - 1) (x_e' \omega_e' u'^2 - x_e'' \omega_e'' u''^2) + (\rho^3 - 1) ( \quad ),$$

\* "Report on Band Spectra of Diatomic Molecules," Phys. Soc. Lond. (1932)

or, alternatively, to a very close approximation,

$$\nu_e^i - \nu_e = (\rho - 1) [\nu_e - (x_e' \omega_e' u'^2 - x_e'' \omega_e'' u''^2) + \dots].$$

In these equations  $u = v + \frac{1}{2}$  where  $v$  is the vibrational quantum number (integral).

If the difference in the terms in  $u^2$  be small, then approximately

$$\nu_e^i - \nu_e = (\rho - 1) \nu_e$$

A plot of the observed isotope separations  $\nu^i - \nu$  against  $\nu$  for the main band should be linear, at least for small values of  $\nu^i - \nu$ , and  $\nu^i - \nu$  should extrapolate to zero at a value of  $\nu$  which gives the origin of the system. The slope of the line should be  $\rho - 1$ , which for the molecules  $\text{Cl}^{35-35}$  and  $\text{Cl}^{35-37}$  has the value 0.0137. Fig. 1 shows that, for the emission bands of chlorine, most of the points lie on a line of very slight curvature, but there is a very strong suggestion that a number of points at the high frequency end of the system lie on another line approximately parallel to the first, but displaced along the horizontal axis in the direction of greater frequency by an amount corresponding to  $340 \text{ cm}^{-1}$ . In addition, three points are displaced in the other direction by amounts which are decidedly greater than the estimated error, though as the position of a band head can be falsified by lines belonging to another band too much weight should not be given to this.

The significance of the graph may be realized by comparing it with a similar graph, also shown on fig. 1, constructed from the known vibrational data for the visible absorption bands of chlorine,\* for the progressions with  $v'' = 0$  and 1 respectively. Over the range plotted, the vibrational frequency  $\omega$  is linear in  $v$ . It is obvious from a comparison of the graphs that the terms in  $u^2$  must be much smaller for the emission than for the absorption bands, as the departure of the graph from linearity is much more marked for the absorption bands. It is of interest to consider what is the upper limit to the anharmonicity factor  $x_e$  for the emission bands. If we neglect terms in  $u^2$  and higher powers, then

$$\frac{d(\nu_e^i - \nu_e)}{du'} = (\rho - 1)(\omega_e' - 4x_e' \omega_e' u')$$

for constant  $u''$ , whence it follows that the maximum separation of the isotope bands in a  $v'$  progression occurs when  $u' = \frac{1}{4}x_e'$ . This gives a maximum separation

$$\nu_e^i - \nu_e = \nu^i - \nu = (\rho - 1) \left[ \frac{\omega_e'}{8x_e'} - \omega_e'' u'' + 2x_e'' \omega_e'' u''^2 \right]$$

\* Jevons, *loc. cit.*

The greatest isotope separation observed is  $62.2 \text{ cm}^{-1}$  and the curve has by no means attained its maximum at this point. Hence we may conclude that the quantity in the square brackets above is very much greater than  $62.2/0.0137$  or  $4500 \text{ cm}^{-1}$  at its maximum value, and therefore that  $\frac{\omega'_e}{8x_e} \gg 4500 \text{ cm}^{-1}$  or that  $x'_e \ll \frac{\omega'_e}{36000}$ . This may be compared with the upper level of the absorption bands, for which  $x'_e = \omega'_e/1256 \text{ cm}^{-1}$ .

The existence of two separate curves for the emission bands in fig. 1 seems to point to the fact that we have here at least two distinct electronic systems, whose origins are situated at approximately 21,000 and 21,340  $\text{cm}^{-1}$  respectively.

The development of well-marked heads on the high frequency side of the origin is much greater than on the low frequency side. We have examined our data for isotopic pairs of bands on the less refrangible side, and have found six pairs which might be due to the molecules  $\text{Cl}^{36-35}$  and  $\text{Cl}^{35-37}$ . The observed separations are only in approximate agreement with the expected values. As, however, the bands of frequency lower than about  $20,500 \text{ cm}^{-1}$  are faint and have heads which are not very well marked, this poor agreement may be due to errors of observation. The bands in question (in the range  $19,153\text{--}19,913 \text{ cm}^{-1}$ ) are included in Table III but are not shown on the graph. Where isotopic companions have not been observed, the bands are either faint or close to the system origin.

#### CONCLUDING REMARKS

We have as yet been unable to carry out a vibrational analysis of the chlorine emission bands, and have not, in fact, been able to identify with certainty a single progression. It would appear that many of the bands belong to very incompletely developed progressions. Several identical intervals have been found, of which the chief are 627 and  $632 \text{ cm}^{-1}$ , but it is impossible to say whether either of these represents one of the vibrational frequencies.

An examination of the rotational structure of the bands, now in progress, may assist in the vibrational analysis.

#### SUMMARY

The wave numbers of the band heads of the chlorine emission spectrum, and of the maxima of the continua excited by a high frequency discharge, have been measured.

TABLE III—WAVE NUMBERS OF THE EMISSION BAND HEADS OF CHLORINE

Bands which have been identified as isotopic pairs are bracketted. The weaker member of such a pair is due to  $\text{Cl}^{35-37}$  and is indicated by  $i$ , the other member is due to  $\text{Cl}^{35-36}$ .

Wave Number in $\text{cm}^{-1}$	Wave Number in $\text{cm}^{-1}$	Wave Number in $\text{cm}^{-1}$	Wave Number in $\text{cm}^{-1}$
18,401 4	19,983 6	22,111 5	23,887 8 <i>i</i> }
431 9	20,083 0	168 5 <i>i</i> }	925 2 }
522 0	118 4	186 2 }	964 4 }
541 8	228 2	260 3 <i>i</i> }	24,036 0
546 9	300 1	277 3 }	102 3 <i>i</i> }
589 2	323 8	301	147 3 }
777 3	383 5	402 7	215 2
858 6	416 0	504 5 <i>i</i> }	265 9 <i>i</i> }
873 4	524 1	529 3 }	308 7 }
19,024 3	595 6	585 7 <i>i</i> }	425 4 <i>i</i> }
061 2	668 2	609 3 }	484 8 }
137 9	711 3	671 5 <i>i</i> }	551 7 <i>i</i> }
152 8 }	828 6	696 3 }	596 9 }
182 6 <i>i</i> }	852 3	793 0 <i>i</i> }	735 1 <i>i</i> }
192 6	885 5	819 7 }	788 3 }
311 8	927 2	886 0 <i>i</i> }	896 0 <i>i</i> }
349 4	21,041 7	912 7 }	948 1 }
358 1 }	121 6	961 2 <i>i</i> }	25,062 8 <i>i</i> }
380 0 <i>i</i> }	161 1	990 0 }	122 6 }
396 5	201 5	23,130 3 <i>i</i> }	180 3 <i>i</i> }
463 1	222 0	163 4 }	236 2 }
479 7	339 7	200 9	365 4 <i>i</i> }
500 4 }	349 8	264 9	426 3 }
518 3 <i>i</i> }	476 3	295 5 <i>i</i> }	526 5
624 0	513 5	327 4 }	699 8 <i>i</i> }
676 1 }	559 1	444 7	757 3 }
691 8 <i>i</i> }	659 0 <i>i</i> }	474 0 <i>i</i> }	819 9 <i>i</i> }
758 8	668 7 }	509 9 }	882 4 }
800 3 }	783	586 6 <i>i</i> }	
816 0 <i>i</i> }	819 9 <i>i</i> }	624 2 }	
903 2 }	831 5 }	762 0	
913 3 <i>i</i> }	872 2	797 2 <i>i</i> }	
972 0	959 0 <i>i</i> }	833 3 }	
	976.4 }		

The analysis of the band system proposed by Ota and Uchida is shown to be untenable, but no alternative analysis is put forward

The vibrational isotope effect shows that there is a system whose origin is at  $21,000\text{ cm}^{-1}$ , and probably a second system with origin at  $21,340\text{ cm}^{-1}$

#### DESCRIPTION OF PLATE 35

- a*, *b*, and *c*—Chlorine emission spectrum excited by high frequency discharge at low pressure in tube cooled with solid  $\text{CO}_2$ . Iron arc comparison spectrum. Diffuse bands indicated thus  $\times$ . Isotopic pairs of band heads ( $\text{Cl}^{35-35}$  and  $\text{Cl}^{35-37}$ ) are connected by a bracket and the heads of the bands due to  $\text{Cl}^{35-37}$  indicated by  $\downarrow$ . The exposure times for spectra *a*, *b*, and *c* are different
- d*—Microphotometer record of ultra-violet continua of chlorine excited by high frequency discharge (pressure higher than in *a*, *b*, and *c*, tube at room temperature). The direction of increasing intensity is indicated by the arrow

---

## The *n*-Fatty Acids and Certain of their Derivatives

By F FRANCIS, F J E COLLINS, and S H PIPER,  
University of Bristol

(Communicated by M W Travers, F R S—Received 15 October, 1936)

In an earlier paper\* we have described the properties of all the members of the series of *normal* fatty acids which contain between 14 and 26 carbon atoms, and also of certain of their derivatives

The present communication deals with the redetermination on recently prepared specimens of the melting points and crystal spacings of some of these acids and, in continuation of the investigation, with the properties of all those of even carbon content containing between 28 and 38 carbon atoms, and the single acid with 46 carbon atoms. The properties of the corresponding ethyl esters, alcohols, iodides, and dicarboxylic acids obtained in the course of the syntheses of the fatty acids are also described

The importance of the work lies partly in the fact that there exists no other series of long chain compounds of which so many members can be obtained in a pure and crystalline condition. Also, as some members of these series of compounds occur naturally, their investigation furnishes a set of constants, based on the study of pure synthetic products, which

\* 'Proc. Roy Soc.' A, vol. 128, p. 214 (1930).

will serve as a definite basis for the identification of those occurring naturally.

The paper is divided into two parts: Part I contains an account of the acids and their derivatives, and Part II of some of the properties of palmitic and stearic acids and their mixtures

### I—THE *n*-ALIPHATIC ACIDS AND THEIR DERIVATIVES

#### 1—*Methods of Determining Melting Points, Setting Points, and Crystal Spacings*

The apparatus used for the determination of setting points, and melting points by the capillary tube method, has been described elsewhere \* The values obtained are recorded in Table I

The error in the determination of the setting points of palmitic and stearic acids is  $\pm 0.01^\circ$ , in all the others  $\pm 0.02^\circ$

In the determination of melting points, different observers do not differ by more than  $\pm 0.03^\circ$ . The values are generally lower by  $0.2^\circ$  to  $0.6^\circ$  than those obtained on the same specimen in the apparatus usually employed

Melting points are invariably higher than setting points by amounts that vary from  $0.1^\circ$  to  $0.6^\circ$  in different classes of substances. The divergence is greater, for instance, in the acids than in their ethyl esters.

The temperature, however, at which the specimens in the capillary resolidify—R P in Table I, columns 4 and 8—generally differs for acids or esters by  $\pm 0.1^\circ$ , but never by more than  $\pm 0.2^\circ$ , from the setting point. The accuracy of the observation depends on the presence of a solid nucleus, and on allowing the temperature to fall very slowly. The effect on the resolidification point of the existence of two modifications of the substance under examination will be mentioned later (Part I, §§ 4 and 6).

In fig. 1 the melting points of the acids, iodides, and alcohols are plotted against their carbon content, and those of the ether esters against that of their parent acid. In all cases, smooth curves are obtained. Such graphs as these, and particularly that of the setting point of the ethyl esters, afford checks on the accuracy of the data for melting points, and enabled us to make a critical study of the methods of determining these values (*loc cit*).

With many of the acids, their ethyl esters, and the corresponding alcohols, a marked alteration takes place in the appearance of the solid in the

\* Francis and Collins, 'J. Chem. Soc.', p. 137 (1936).

capillary tube about  $0.3^{\circ}$  to  $0.5^{\circ}$  before the melting point is reached. These derivatives may lose their crystalline appearance and pass into semi-translucent solids or apparently amorphous opaque masses. These

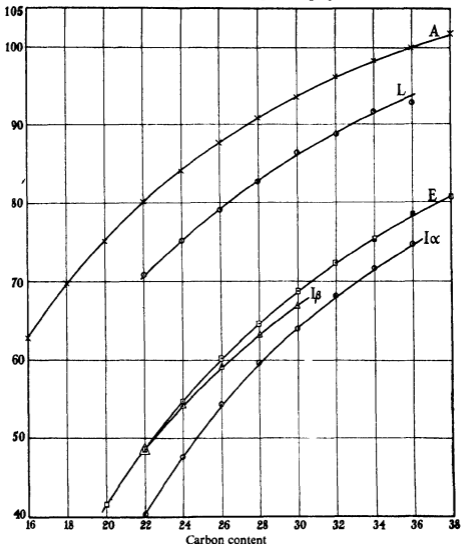


FIG. 1—Melting points. A = acids, L = alcohols, E = ethyl esters, I $\alpha$  and I $\beta$  = iodides

phenomena have not been investigated, and it is possible that they may be correlated with transition temperatures and with the changes observed in the heats of crystallization and in the dipole moments, which occur at temperatures near the melting point.

The method used for the measurement of the crystal spacings by means of X-rays has been described in our previous communication (*loc cit.*) A redetermination of the values for the acids recorded in that paper

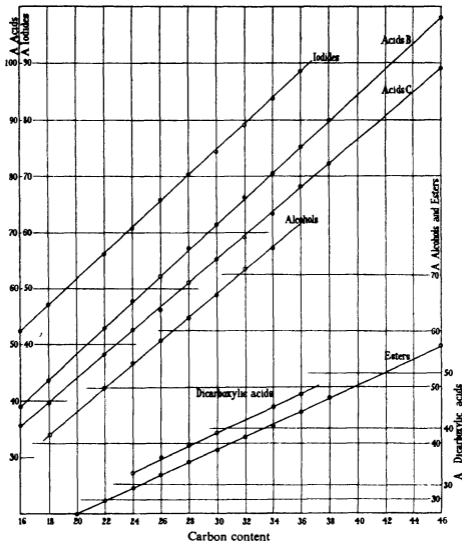


FIG 2—Crystal spacings plotted against carbon content

showed that there was a calibration error in the apparatus which reduced them by about 0.5%. These data, accurate to  $\pm 0.5\%$ , and those for the acids and their derivatives isolated during the course of the present investigation, are given in Table II, and the graphs of the spacings against

carbon content in fig. 2. Further reference will be made to the two spacings of the acids after these substances have been described (§ 3).

*2—The Methods Used in the Synthesis of the Higher n-Fatty Acids, and their Derivatives*

As pointed out in our previous communication, erucic acid is a valuable raw material for the synthesis of the higher members of the *n*-fatty acids. Obtainable in quantity and readily purified, the saturated behenic acid can be prepared from it in a high state of purity. No other acid of higher carbon content is available from any natural source in sufficiently large quantities for such work.

We hoped that it might have been possible to separate in a pure condition, and in suitable quantity, the acid with either 26 or 28 carbon atoms from a mixture of those which constitute the main bulk of the acids obtained from Chinese wax, but this could not be done.\*

The synthesis was commenced with 110 gm. of ethyl behenate. Of an identical preparation, King and Garner† state that it was probably the purest of the many esters of which they had measured the heats of crystallization. This ester and the others were reduced to the corresponding alcohols by a slight modification of the method of Bleyberg and Ulrich.‡ 20 gm. of freshly distilled ester is dissolved in sufficient carefully dried benzene to cover completely the 23 gm. of sodium wire. The flask and condenser used must be perfectly dry, and exits to the atmosphere protected by tubes containing a drying agent. Into the gently boiling benzene solution of the ester there is now run, over a period of 4–5 hours, 120 cc. of dry and freshly distilled butyl alcohol. The flask is continually shaken and the contents refluxed until all the sodium has dissolved. After cooling, ethyl alcohol is added until a clear solution is obtained, and this is again refluxed for 1 hour. When cold, the liquid is repeatedly washed with water until free from alkali, and the solution is distilled on a water bath, the process being completed under reduced pressure. This removes water, benzene, and ethyl and butyl alcohols, and there remains in the flask a dry mixture of the corresponding alcohol with small quantities of the alkali salt of the unreduced acid. From this mixture the alcohol is extracted in a vapour jacketed Soxhlet with dry benzene for the lower members, and with petroleum ether (60°–80°) for the others. The alcohols are purified by distillation under a pressure of  $10^{-5}$  mm., but by

\* Collins, 'J. Soc. Chem. Ind.', vol. 54, p. 33T (1935).

† 'J. Chem. Soc.', p. 1453 (1934).

‡ 'Ber. deutsch. chem. Ges.', p. 2504 (1931).

molecular distillation for those containing more than 28 carbon atoms. This operation is essential, for the alcohol extracted by benzene or petroleum ether is always contaminated with small quantities of the non-volatile sodium salt. The yield of pure alcohol from the reduction of the majority of the esters is in the neighbourhood of 90%.

The alcohols were then converted into the iodides and, by interaction with sodio-malonic ester in benzene, into the malonic ester derivatives. These derivatives were converted into the dicarboxylic acids, which, on heating, gave the monocarboxylic acids with two carbon atoms more than the original material. This process was repeated until an acid with 34 carbon atoms had been prepared. The complete decomposition of the dicarboxylic acid became increasingly difficult to carry out with large quantities of material, and for acids with more than 28 carbon atoms could only be accomplished satisfactorily using 5 to 6 gm of material and completing the process in a vacuum of  $10^{-5}$  mm. The yield of highly purified acid with two carbon atoms more than the one used in the synthesis was 70% with the lower members but less as the series was ascended.

In the course of the investigation a larger quantity of tesserakaitriacontanoic acid was required. It was prepared by the method developed by Mrs G M Robinson\* and used for the preparation of the acid containing 30 carbon atoms†.

For this purpose, behenoyl chloride was condensed with the sodium derivative of ethyl- $\alpha$ -acetyl-brassylate, and the resulting ethyl- $\alpha$ -acetyl- $\alpha$ -behenoyl-brassylate saponified to give the corresponding keto acid,  $C_{31}H_{43}CO(CH_2)_{11}COOH$ . The yield of the keto acid was small, and on reduction it passed readily to tesserakaitriacontanoic acid,  $C_{34}H_{68}O_2$ . (Found, C 80.2%, H 13.5%, calculated, C 80.3%, H 13.4%) This preparation was identical in all respects with that which had been previously synthesized from behenic acid.

From this acid we prepared the two higher members of the series, hexakaitriacontanoic acid,  $C_{36}H_{72}O_2$  (found, C 80.4%, H 13.3%; calculated, C 80.6%, H 13.4%), and octakaitriacontanoic acid,  $C_{38}H_{76}O_2$  (found, C 80.6%, H 13.5%, calculated, C 80.8%, H 13.5%), by the methods previously described.

A small quantity of the acid containing 46 carbon atoms was synthesized in these laboratories by Mr J A. V. Willis. It was prepared by condensing the acid chloride of tesserakaitriacontanoic acid with the

\* 'J. Chem. Soc.', p. 748 (1930).

† 'J. Chem. Soc.', p. 1543 (1934).

sodium derivative of ethyl- $\alpha$ -acetyl-brassylate The resulting derivative on saponification gave the keto acid,  $C_{33}H_{67}CO(CH_2)_{11}COOH$ , which on reduction gave  $C_{46}H_{92}O_2$ , m p  $107.1^\circ$ , resolidification point  $106.5^\circ$  (Found, C 81.6%, H 13.7%, calculated, C 81.7%, H 13.6%.) A full account of this acid, and also those containing 34, 36, and 38 carbon atoms, will be published later

In the course of this work, enneakaeicosanic acid,  $C_{29}H_{58}O_2$ , was prepared from octacosanic iodide and the corresponding nitrile. It melts at  $90.3^\circ$  (resolidification point  $89.8^\circ$ ), and this temperature lies on an extrapolation of the graph connecting melting points and carbon content of the acids containing an odd number of carbon atoms described in a previous communication (*loc cit*) The ethyl ester melts at  $66.6^\circ$  and resolidifies at  $66.3^\circ$ , see p 702 We did not observe, however, the existence of a second crystalline form of this acid, which is so characteristic of those with an odd number of carbon atoms between 9 and 25 The crystal spacing of this acid,  $66.34 \text{ \AA}$ , falls on the extrapolation of the graph connecting these with the carbon content of those acids which had previously only been measured so far as that containing 25.

The purity of the acids depends primarily on that of the alcohols from which they are synthesized Unless the precautions previously mentioned are taken in the purification of these alcohols, and particularly those of higher carbon content, they may be contaminated with the acid from which they were originally prepared If this is so, the final acid containing two carbon atoms more may contain small quantities of that with two less Such a preparation could only be purified with great difficulty, indeed, this would only be possible with the higher members, if considerable quantities were available

All the acids whose constants are described in this communication were obtained from their ethyl esters, which up to that containing 34 carbon atoms were purified by distillation in a vacuum of  $10^{-5}$  mm without any sign of decomposition, but the smaller amounts which were obtained from acids of higher carbon content were subjected to molecular distillation

The acids were prepared from these esters by saponification with an alcoholic solution of potash, the alcohol being removed by distillation before the solution was treated with mineral acids, as experience had shown that the resulting acids might be contaminated with re-formed esters.

The acids were crystallized from either acetone, benzene, or acetic acid, methanol or ethanol was avoided on account of the possibility of ester formation.

### 3—The Properties of the Higher Fatty Acids

The setting points, melting and resolidification temperatures of the acids are given in Table I, columns 2, 3, and 4, and melting points plotted against carbon content in fig. 1

Triaccontanoic acid,  $C_{30}H_{60}O_2$ , synthesized stepwise from behenic acid, was identical with that prepared by Mrs Robinson (*loc cit*), and a similar correspondence was also observed for tesserakaitriacontanoic acid,  $C_{34}H_{68}O_2$ , obtained by these two methods.

The identity of the two specimens of tesserakaitriacontanoic acid, of which we prepared between 30 and 40 gm by the Robinson synthesis, confirmed our opinion that the methods used for the purification of those with smaller carbon content could be relied upon. The impurities that were possible in acids synthesized from behenic acid could not have been present in those prepared by that method. The heat of crystallization of the ethyl ester of this acid has been determined by Miss King and will be published later.

The B crystal spacing of hexakaitesseracontanoic acid containing 46 carbon atoms is 108.2 Å, and the C spacing 99.05 Å. Both points lie on the extrapolated graphs for the lower acids given in fig. 2, and consequently there is no departure from the straight line relationship between carbon content and spacings even for this *n*-fatty acid, which has a greater number of carbon atoms than any yet synthesized.

During the course of this investigation we made the interesting and important observation that the crystals of fatty acids, with an even number of carbon atoms, which separated from glacial acetic acid on recrystallization, show the C crystal spacings, whereas the crystals from either benzene or acetone show the B spacings only. Acids with an odd number of carbon atoms show the B spacings whichever solvent is employed.

In our first communication (*loc cit*) the C spacings had been obtained by measurements on specimens which had been previously melted, but those given in Table II have all been made on crystals of the acids which separated from hot acetic acid on slow cooling.

Experience has shown that when acids are crystallized from a non-polar solvent and show both B and C crystal spacings on the same plate, it is an indication of the presence of impurities which may amount to something between 1% and 3%, or possibly more. The B spacings appear to be less affected by impurity than the C spacings.

When the new values of the B and C spacings are plotted against the corresponding carbon content, fig. 2, the resulting straight lines rise less

TABLE I

Carbon content	Acids				Ethyl esters				Iodides				Alcohols	
	SP	MP		RP	SP	MP		RP	MP	MP		RP	MP	RP
		°C	°C			°C	°C			°C	°C		°C	°C
16	62.53	62.85	62.4	62.4	23.2	(19.4)	24.4	—	—	—	—	—	—	—
18	69.32	69.9	69.45	69.45	31.05	32.0	34.0	30.8	—	—	—	—	—	—
20	—	75.15	74.55	74.55	40.36	40.52	41.65	40.15	—	—	—	—	—	—
22	—	80.2	79.6	79.6	47.8	48.7	48.25	47.7	41.5	48.2	40.6	—	70.8	70.6
24	83.9	84.15	83.8	83.8	54.2	54.77	54.35	54.2	48.1	54.2	47.6	—	75.3	74.8
26	87.4	87.7	87.2	87.2	59.6	60.2	59.95	59.5	54.4	59.1	53.8	—	79.2	78.9
28	—	90.9	90.2	90.2	64.2	64.6	—	64.3	59.6	63.15	59.0	—	82.6	82.25
30	—	93.6	93.0	93.0	68.3	68.45	—	68.35	64.0	67.0	63.8	—	86.5	86.3
32	—	96.2	95.5	95.5	—	72.5	—	72.0	68.2	—	68.0	—	89.2	88.9
34	98.0	98.2	97.8	97.8	75.3	75.4	—	75.2	71.6	—	71.3	—	91.7	—
36	—	99.9	99.4	99.4	78.31	78.6	—	78.3	74.9	—	74.7	—	92.9	92.1
38	—	101.6	100.1	100.1	—	80.55	—	80.3	—	—	—	—	—	—
46	—	107.1	106.5	106.5	90.2	—	90.5	90.3	—	—	—	—	—	—

steeply than when the values given in our previous paper are used. On these straight lines now lie the points relating to all the acids which we have synthesized up to that containing 38 carbon atoms, and also those relating to the acid with 46 carbon atoms, the agreement being very exact. The results of measurements with specimens which we have received from other investigators, including the acid with 30 carbon atoms synthesized by Mrs. Robinson (*loc cit*), are also identical.

A valuable clue to the identity of one of the higher fatty acids, for example, an acid isolated from a natural product, can be obtained by comparing its melting point, and also that of its ethyl ester, with the melting points of the synthetic acid and its ethyl ester. If, however, a comparison is also made of the B or C crystal spacings of the natural and synthetic acids, the identity of the natural product can be established with certainty. Acids with an even number of carbon atoms can be distinguished from those containing an odd number, since the crystals of the former separated from such a solvent as benzene show the B spacings, whereas crystals from acetic acid show the C spacings only. On the other hand, the acids with an odd number of carbon atoms show the B spacings irrespective of the solvent from which they are crystallized.

The presence of impurities consisting of members of the homologous series of acids, and of the order of 1%, does not affect the values for the crystal spacings of the pure acids, but when the quantity of impurity rises to 5%, the differences are measurable. (See Part II, fig 4, p 715.) Melting points, determined by the method we have described, and the behaviour of the specimen in the capillary tube in close proximity to that temperature, enable the presence of 1% of such impurities to be detected.

#### 4—The Properties of the Ethyl Esters

The dimorphism of the esters of the lower *n*-fatty acids has been studied by Smith,\* Phillips and Mumford,† and Malkin,‡ and King and Garner (*loc cit*) have investigated this problem by measuring the heats of crystallization of a series of these compounds. In this communication we give only the setting points of the ethyl esters of the higher fatty acids, together with their melting and resolidification points determined in our apparatus.

If the setting points of the esters (Table I, column 5) are plotted against the carbon content of the corresponding acids from 18 to 38, they fall with striking accuracy on a smooth curve. These setting points are the

\* 'J Chem Soc,' p 802 (1931)

† 'J Chem Soc.,' p 1657 (1934)

‡ 'J Chem Soc,' p 2796 (1931)

TABLE II—CRYSTAL SPACINGS, A

Carbon content	Acids			Ethyl esters		Alcohols		Iodides	Dicarboxylic acids
	B	C		A	B	A	B		
16	39 1	35 6		—	—	—	—	42 6 (M <sub>1</sub> )	—
18	43 75	39 75		—	—	—	—	47 2 (M <sub>1</sub> )	—
22	52 95	48 3		—	29 9	—	—	56 10	—
24	57 75	52 6		—	32 15	—	—	60 7	32 3
26	62 2	56 25		—	34 45	70 7	58 0	65 85	35 0
28	67 15	61 05		—	36 65 (C)	75 95	62 3	70 2	37 1
30	71 4	65 2		—	38 75	—	66 4	74 15	39 4
32	76 3	69 25		—	41 1	—	71 0	79 15	—
34	80 5	73 3		—	43 45	90 8 (C)	74 65 (C)	83 85	44 05
36	85 25	78 1		—	45 65	—	—	88 4	45 65
38	90 0	82 1		53 55	48 05	—	—	—	—
46	108 2	99 05		—	57 45	—	—	—	—

C = Chubnall, 'Bio-chem J', vol 28, p 2175 (1934), M<sub>1</sub> = Malkin, 'J Chem Soc', p 2796 (1931), M<sub>2</sub> = Malkin, 'J Amer Chem Soc', vol 52, p 3739 (1930)

temperatures—accurate to  $\pm 0.02^\circ$ —at which the respective  $\alpha$ -modifications and liquid are in equilibrium. The setting points of the esters of those acids containing an odd number of carbon atoms up to 29, the highest yet examined, also lie on this graph.

On this graph falls the melting point,  $19.4^\circ$ , of the metastable form of ethyl palmitate, whereas the setting point of this compound,  $23.2^\circ$ , corresponds to the temperature at which the  $\beta$ -modification and liquid are in equilibrium. In this respect ethyl palmitate is different from the other esters we have examined, with the possible exception of that of the acid containing 46 carbon atoms, which will be discussed later.

The specimen of ethyl palmitate used in these laboratories by King and Garner (*loc cit*) has a setting point of  $23.20^\circ$  and melts in a capillary tube at  $24.6^\circ$ . Between  $0.5^\circ$  and  $1^\circ$  below this temperature an alteration in the appearance of the solid is noticed and is best seen during liquefaction, when it appears to be a wool-like amorphous mass. If the temperature is allowed to fall slowly before this material has completely melted, it commences to increase at  $24.15^\circ$ , partly but never completely filling the tube at that temperature. As the temperature continues falling, at and below  $23^\circ$ , this amorphous material passes slowly into a crystalline form.

A considerable period is required before the specimen solidifies completely, but if the temperature is raised whilst crystalline solid and liquid are still present, the former melts sharply at  $24.4^\circ$ .

If the substance in the capillary tube is completely melted, then, as the temperature falls, no amorphous solid is formed, and well-defined crystals commence to separate very slowly between  $23^\circ$  and  $21.5^\circ$ . On raising the temperature before complete solidification has taken place these crystals melt at  $24.4^\circ$ .

The phenomena just described may indicate the presence of a second  $\beta$ -modification of ethyl palmitate, noticed by Buckingham\* during density measurements of this substance.

When the melting points of the higher esters are determined by the capillary tube method, those of the  $\beta$ -forms of the esters can be obtained provided the specimens have remained for some time at room temperatures, Table I, column 7. When these data are plotted against carbon content, the graph lies above that of the setting points: the difference is  $2.9^\circ$  for  $C_{18}$ ,  $1.3^\circ$  for  $C_{20}$ ,  $0.9^\circ$  for  $C_{22}$ ,  $0.57^\circ$  for  $C_{24}$ , and  $0.6^\circ$  for  $C_{26}$ .

If the temperature is allowed to fall slowly after the melting point of

\* 'Trans. Faraday Soc.', vol. 30, p. 377 (1934).

the  $\beta$ -modification has been determined, resolidification takes place at temperatures within  $\pm 0.2^\circ$  of their respective setting points. When the temperature is raised immediately, the melting points of the  $\alpha$ -modifications can be obtained, Table I, column 6. Such values are not so accurate as the setting points, but they can be obtained with small quantities of material. Determined by this means the difference between the melting points of the two forms of the esters of  $C_{20}$  is  $1.1^\circ$ ,  $C_{22}$   $0.45^\circ$ ,  $C_{24}$   $0.42^\circ$ , and  $C_{26}$  about  $0.2^\circ$ .

In all these esters the  $\beta$ -modification is that stable at room temperatures; at their melting points King and Garner (*loc cit*) have shown that this also holds for those of the acids  $C_{16}$ ,  $C_{18}$ , and probably  $C_{20}$  and  $C_{22}$ , that of  $C_{24}$  is doubtful, whereas from  $C_{26}$  to  $C_{34}$  it is the  $\alpha$ -modification which is in equilibrium with the melt. Consequently there is an uncertainty in the classification of those of  $C_{20}$ - $C_{24}$  in Table I.

From  $C_{26}$  to  $C_{38}$ , setting points and both melting and resolidification temperatures afford no evidence that the esters exist in two modifications, and in column 6, Table I, they are all grouped under those designated  $\alpha$ . The melting points in fig. 1 determined by the capillary tube method are those of the  $\beta$ -modification up to  $C_{26}$  and beyond of the  $\alpha$ .

The highly purified ethyl ester of hexakostessaracontanoic acid melts at  $90.5^\circ$  and resolidifies at  $90.3^\circ$  (capillary tube method). Now the value for this constant obtained either from the extrapolation of the graph of setting points of the esters against their carbon content or from that of their melting points (fig. 1) is  $88^\circ \pm 0.5^\circ$ , and is  $86.8^\circ$  calculated from the equation for the melting points of the esters of those acids with more than 22 carbon atoms. Consequently we consider that the high melting point of the ester of this  $C_{46}$  acid may be due to its existence in a  $\beta$ -modification in metastable equilibrium with the melt, but this point cannot be settled without X-ray measurements of the long spacing near the melting point.

Measurements of the crystal spacings of the lower ethyl esters were carried out on specimens which had been prepared by crystallization from ethyl alcohol. Such esters are too soluble in benzene for this purpose, although with the higher members of the series this solvent is preferable.

The B crystal spacings of the esters to within  $\pm 0.5\%$  lie on a straight line when plotted against the parent acids of even carbon content for 16 to 38 and extrapolated to 46 (fig. 2). This relationship, shown both by the  $C_{46}$  acid and its ester, is very striking. The ester was purified by molecular distillation followed by crystallization from alcohol and then

benzene, and the resulting specimen gave an exceptionally good X-ray photograph showing nine orders

Only a very small quantity of the ester of the  $C_{38}$  acid was available. Purified in the usual way and recrystallized from alcohol, the crystals gave an A spacing of 53.55 Å, which is almost certainly due to the presence of impurities, small quantities of which always have this effect. On recrystallization from benzene, the B spacing of 48.07 Å. was obtained, showing the value of this solvent for purposes of purification

### 5—*The Properties of the Higher Aliphatic n-Alcohols*

The melting points of the higher alcohols resulting from the reduction of the ethyl esters are given in Table I (*see also* fig. 1). The X-ray data will be found in Table II (*see also* fig. 2). Some of the alcohols show two spacings similar to those observed with the acids, where comparison is possible, the data for both coincide with those obtained with the products isolated by Chibnall from natural sources. The crystal spacings lie on an extrapolation of the graph connecting crystal spacings and carbon content, determined for some of the lower members by Malkin\* using preparations isolated during the course of our previous work.

On determining the melting points of the alcohols with a carbon content greater than 26, in each case an opalescence is observed in the molten material in the capillary, which disappears when the temperature is raised about 0.3°–0.4°. The same phenomenon was also noticed in four of the specimens sent us by Professor Chibnall,† and we are inclined to ascribe it to the formation of liquid crystals and not to the presence of impurities.

### 6—*Properties of the n-Primary Iodides*

The *n*-primary iodides were prepared by the action of iodine and phosphorus on the corresponding alcohols. They crystallize well, are only slightly soluble in alcohol, and readily in cold ether or benzene, although this solubility decreases as the series is ascended.

The iodides with a carbon content of 22 up to 30 occur in two modifications. On standing at room temperatures the  $\alpha$  passes into the  $\beta$ -form, of which the melting points are determined in the usual manner. They are given in Table I, column 10, and fig. 1, I $\beta$ .

\* 'J. Amer. Chem. Soc.', vol. 52, p. 3739 (1930).

† Piper, Chibnall, and Williams, 'Bio-chem. J.', vol. 28, p. 2175 (1934).

With the exception of behenyl iodide, when the temperature is raised  $1^{\circ}$  to  $2^{\circ}$  above the melting points of the  $\beta$ -modifications, and is then allowed to fall, resolidification takes place at temperatures which are lower than the melting points of these forms, by  $6.6^{\circ}$  for that containing 24 carbon atoms, falling to  $3.2^{\circ}$  in that with 30, Table I, columns 10 and 11. On raising the temperature immediately, the melting points of the  $\alpha$ -modifications can be determined, Table I, column 9, and fig. 1, I $\alpha$ . These values differ from the resolidification temperatures by amounts not larger than  $0.6^{\circ}$ .

If the procedure outlined in the preceding paragraph is followed with behenyl iodide, the  $\alpha$ -modification is not formed. When this compound is heated to  $49^{\circ}$  and then cooled, it resolidifies at  $46.4^{\circ}$ , and if the temperature is then raised, it melts at  $48.2^{\circ}$ . If, on the other hand, it is heated to  $60^{\circ}$  and then cooled, it solidifies at  $40.6^{\circ}$ , and if the temperature is not allowed to drop further, but is raised immediately, it melts at  $41.5^{\circ}$ . The former melting point is that of the  $\beta$  and the latter that of the  $\alpha$ -modification.

The liquid  $\alpha$ -iodide passes either to the solid  $\alpha$  or solid  $\beta$  with great ease under conditions which we have not investigated. The stability of  $\alpha$ -behenyl iodide appeared to be analogous to that recorded for the metastable  $\alpha$ -ethyl palmitate.

Dr T. Malkin has investigated the cooling curves of some of the lower iodides and has informed us that he had observed a similar phenomenon. It was only after the temperature had previously been raised  $15^{\circ}$ – $20^{\circ}$  above the melting points of these derivatives that, as the temperature fell, he was able to obtain definite indications of the existence of the  $\alpha$ -forms. This work has not yet been published.

The interesting behaviour of liquid  $\beta$ -behenyl iodide appears to show that at temperatures just above the melting point this modification is oriented in the liquid probably at the surface or in contact with the glass. At higher temperatures this arrangement is destroyed and it passes into the liquid  $\alpha$ -form.

The melting points of the  $\alpha$ -iodides, including  $\alpha$ -behenyl iodide, plotted against their carbon content, fall on a smooth curve on which lie those of carbon content 32 to 36, which only appear to exist in the  $\alpha$ -form, fig. 1, I $\alpha$ .

### 7—The Properties of the Dicarboxylic Acids

The dicarboxylic acids prepared during the course of this investigation can be purified by recrystallization from hot benzene, in which they are moderately soluble. They decompose at the melting point and conse-

quently this temperature cannot be determined as accurately as in all the other cases, but within experimental error they all fuse close to  $126^{\circ}$ , the convergence temperature of this series. The X-ray spacings of these acids are given in Table II. See also fig. 2.

## II—MIXTURES OF PALMITIC AND STEARIC ACIDS

In our previous communication\* we described the C crystal spacings and melting points of various mixtures of equimolar quantities of *n*-fatty acids, these had been measured on specimens prepared by melting together the two acids and allowing them to solidify. These mixtures were eutectic and consequently their melting points were as sharp as those of pure substances.

As we were now able to prepare such mixtures in the crystalline condition by recrystallization from acetic acid or from the diluted acid, we investigated those of palmitic and stearic acids, in which the constituents were present in different proportions. Little is known about the nature of the mixed crystals obtained by such means, and it was hoped that some light might be thrown on this subject by measurements of their X-ray crystal spacings.

### 1—Preparation of Pure Palmitic and Stearic Acids

The purest commercial specimens of these acids that we examined were obtained from Messrs Schering-Kahlbaum. The palmitic acid had a setting point of  $61.37^{\circ}$  and stearic of  $68.0^{\circ}$ , and both preparations gave a dark solution when dissolved in concentrated sulphuric acid at  $70^{\circ}$ . This is a very delicate test for unsaturated substances, which in these cases is most probably oleic acid.

When this specimen of palmitic acid is recrystallized four times from glacial acetic acid, which is by far the best solvent for this purpose, the resulting material is free from oleic acid, and its setting point,  $62.2^{\circ}$ , indicates 0.8% of stearic acid, if that is the impurity which is present.

On the other hand, when the preparation of stearic acid is treated in a similar manner, the resulting material still contains oleic acid, but it can be obtained free from this substance by one crystallization from strong sulphuric acid followed by three from acetic acid. The resulting material has a setting point of  $69.1^{\circ}$ , and, if the impurity is palmitic acid, there is about 1% present. The time spent on the purification of both palmitic

\* Francis, Collins, and Piper (1930).

and stearic acids, and particularly the latter, is much reduced by one or two preliminary crystallizations from strong sulphuric acid.

After the treatment described above, the final purification of both acids was effected by converting them into their ethyl esters, fractionating these *in vacuo*, and reconvertng the constant boiling fraction of each back into the acids, which were then recrystallized from glacial acetic acid until their setting points were constant.

King and Garner (*loc. cit.*) also found it difficult to obtain pure stearic acid for their measurements of the heats of crystallization of the esters of the normal fatty acids. A specimen of carefully purified ethyl stearate gave a heat of crystallization 2% lower than the final recorded value given by the same specimen after it had been recrystallized several times beyond the point at which it had been considered pure. A pure specimen of ethyl palmitate, on the other hand, was obtained without much difficulty.

#### 2—Melting Points of Palmitic and Stearic Acids

The setting point of our preparation of palmitic acid was  $62.53^{\circ} \pm 0.01^{\circ}$ . It was determined in the apparatus described in a previous communication using 2 gm. of material.

De Visser\*, who used 50 gm., gives  $62.618^{\circ}$  for this value, but as he used a thermometer of French *verre dure* the correction to the standard scale gives a value of  $62.528^{\circ}$ , practically identical with that of our preparation.

The preparation of stearic acid had a setting point of  $69.32^{\circ} \pm 0.01^{\circ}$ . De Visser gives  $69.320^{\circ}$ , which after correction is  $69.248^{\circ}$ , that is about  $0.07^{\circ}$  lower than that shown by our material.

These two setting points are the highest recorded in the literature for these acids, though the melting points determined by the capillary tube method are invariably higher. Partington† gives the setting point of palmitic acid as  $62.25^{\circ}$ , but its melting point as  $62.68^{\circ}$ . The melting point of our preparation of this acid in the apparatus we have described was  $61.85^{\circ}$ , and that of stearic acid was  $69.9^{\circ}$ .

In this apparatus the presence of 1% of one acid in the other can be detected. For palmitic acid with 1% of stearic, softening of the material in the capillary tube takes place at  $62.3^{\circ}$ , it melts at  $62.6^{\circ}$ , and resolidifies at  $62.1^{\circ}$ , whereas pure palmitic acid melts at  $62.85^{\circ}$  and resolidifies at  $62.4^{\circ}$ .

\* 'Rec Trav. chim. Pays-Bas,' vol 17, pp 182, 346 (1898).

† 'Phil. Mag.,' vol 48, p 1085 (1924).

A synthetic mixture of stearic acid with 1% of palmitic softens at 69.2°, melts at 69.3°, and resolidifies at 68.7°, whereas the pure acid melts at 69.9° and resolidifies at 69.5°.

### 3—The Setting Points of Mixtures of Palmitic and Stearic Acids

As we proposed to examine by X-rays mixed crystals of palmitic and stearic acids of known composition which were prepared by crystallization from dilute acetic acid, it was necessary to determine the composition of such crystals after this operation, as they would certainly be different from the original mixture whose composition was known. Further, as the composition was to be deduced from setting points, it was necessary to find out whether it was possible to reproduce de Visser's data (*loc cit*) for various mixtures of the acids.

This was done by placing about 2 gm. of the pure substance in the container of the apparatus described in a previous communication (*loc. cit.*, p. 138), its setting point was determined, and then known amounts of the second acid were introduced and a series of observations carried out which are recorded in Table III. The data for the setting point lie accurately on a graph, fig. 3, connecting these temperatures with the stearic acid content of the respective mixtures. This graph can be divided into three sections,  $P_s$ ,  $I_s$ , and  $S_s$ .

On the first section,  $P_s$ , from 0 to 25 mols. % stearic acid, our temperatures and those of de Visser coincide after correction to standard scale. On the second section,  $I_s$ , from 27 to 41 mols. % stearic, our data are lower than his, commencing at 0.3° for the former and falling to 0.2° for the latter mixture, but between 45 and 50 mols. % they again coincide. The form of this section of the graph is slightly different from that of de Visser. From 50 to 100 mols. % stearic acid on section  $S_s$  of the graph there is again good agreement between his determinations of setting points and ours. From 0 to 45 and 50 to 100 mols. % stearic acid the composition of mixtures of the two acids can be determined from the graph with an accuracy of about 1%, but for intermediate mixtures it is between 2 and 3%.

If a supply of one pure acid is available, it is clearly possible to determine the composition of any unknown mixture of these acids by a determination of its setting point, and a second after it has been mixed with a known weight of one of the pure acids.

TABLE III

	Stearic acid mols. %	Setting point  C°	Stearic acid mols %	Melting point capillary tube		
				Commence °C	End °C	Graph °C.
P <sub>e</sub>	0	62 53	0	62 85	—	—
	1	62 02				
	2 01	61 69				
	3 04	61 37				
	5 06	60 64				
	81	60 04				
			7 8	61 3	61 7	61 45
			15	59 5	59 7	59 8
			20 3	57 8	58 4	58 4
	23 09	55 38				
	24 18	55 26				
	25 33	55 04				
	26 89	54 56				
I <sub>e</sub>	27 58	54 70				
	28 29	54 84				
	31 38	55 00 (Graph 55 15)	31 38	55 5	55 8	55 5
			32 7	55 6	55 7	55 65
	39 59	55 89 (Graph 55 95)	40 7	56 15	56 35	56 4
	42 46	56 17				
	45 11	56 35				
			45 7	56 8	56 85	56 8
	47 51	56 43	47 51	56 85	57 2	56 85
	50 49	56 56				
			50 8	57 2	57 6	57 2
S <sub>e</sub>	51 48	56 82				
			53 8	57 9	58 4	58 4
	57 49	58 70	57 49	59 3	60 6	60 5
			67 5	62 1	63 3	63 3
	68 0	61 64*				
			70 0	62 9	63 7	64 05
			83 0	66 5	67 2	67 1
	89 0	66 94*				
			94 0	68 5	69 0	69 0
	84 28	68 11	94 28	68 7	68 9	—
	97 02	68 68				
	98 5	69 00	98 5	69 8	69 9	69 7
	98 97	69 08				
	100	69 32	100	69 9	—	—

\* de Visser (1898)

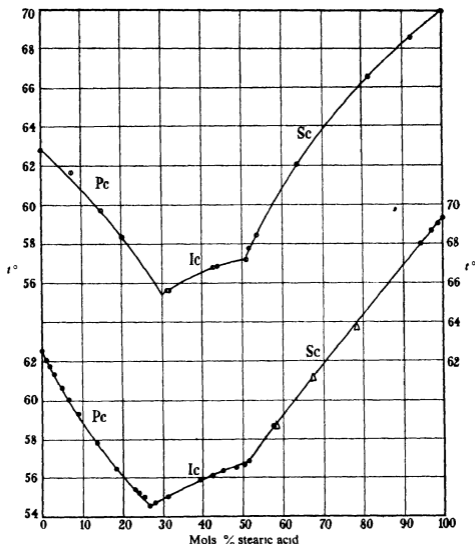


FIG. 3—Melting and setting points of mixtures of palmitic and stearic acids ○ = melting points, ● setting points, △ de Visser

#### 4—Melting Points of Mixtures of Palmitic and Stearic Acids by the Capillary Tube Method

Dr J P Treub, of Gouda, was kind enough to send us a large number of specimens of different mixtures of palmitic and stearic acids. They were sealed in glass tubes containing about 5 gm. each, and on these he had determined the "temperature at which the last crystal disappeared".

These results have not been previously published but with his consent are given in Table IV. His data are close to those determined on a smaller number of mixtures by R. N. Wenzel,\* who used the same criterion for

TABLE IV—"MELTING POINTS" OF MIXTURES OF PALMITIC AND STEARIC ACIDS, BY J. P. TREUB

	Mols. % of stearic	Melting point ° C
P <sub>6</sub>	0	62.2 (W 62.3)
	4.3	61.5 (W)
	9.1	60.7 (W 60.6)
	14.0	59.78 (W)
	16.5	59.0 (A 48.5)
	22.2	57.65
	26.1	56.00 (A 55.6)
I <sub>6</sub>	28.1	55.45 (A 55.5, W 55.5)
	28.6	55.00
	29.5	55.25
	32.1	55.5
	33.6	55.75 (A 55.7)
	35.7	56.00
	37.5	56.3 (W 56.2)
	39.6	56.35
	41.4	56.45
	43.5	56.55 (A 56.6)
	45.4	56.60
	47.6	56.7
	49.5	56.8 (A 56.8)
	50	56.55 (W 56.71)
S <sub>6</sub>	51.0	57.2
	52.4	58.00
	58.1	60.15 (W 60.33)
	65.5	62.6 (A 62.5)
	68.0	63.2 (W)
	73.0	64.3
	84.5	66.4
	100	68.95 (W 69.1)

A, the authors' determinations on same specimen; W, Wenzel, 'Industr. Engng. Chem.', vol. 6 (1934)

the "melting point". \*On repeating some of Dr. Treub's experiments by the capillary tube method, we were able to reproduce his data to within  $\pm 0.2^\circ$ .

\* 'Industr. Engng. Chem., Anal. Edit.', vol. 6, p. 2 (1934).

With mixtures of our pure acids, Table III, column 3, the melting points are given in column 4, and the temperature at which the last trace of solid disappears in column 5.

On the  $P_s$  and  $S_s$  sections of the graph, fig 3 (and Tables III and IV), the melting points cannot be observed with any degree of accuracy. There is a preliminary softening and a fusion range, both characteristic of mixtures of this type. The temperatures in the last column, 6, Table III, have been taken from a graph connecting the temperature at which the last trace of solid disappears with the stearic acid content of the mixtures. On both these sections of the graph our data are invariably higher than those of Dr Treub by about  $0.5^\circ$  at the maximum.

Mixtures of acids, however, lying on the section of the graph  $I_s$  behave in a similar manner to pure substances. Their melting points can be determined to within  $\pm 0.05^\circ$ , the fusion range is either very small or non-existent, and these melting points are about  $0.4^\circ$  higher than the corresponding setting points, which is the difference usually observed with pure substances. In this eutectic region, Dr Treub's data from 30–41 mols. of stearic, and the only two observations of Wenzel at 37.5 and 47.5 mols. %, are within experimental error identical with ours.

All of Dr Treub's specimens contained a trace of unsaturated material, probably oleic acid, and the acids used by Wenzel were not of any high degree of purity. Consequently, it appears that the melting points in the  $I_s$  region are less affected by impurities than are those in the other two.

From such data as those just described, the composition of mixtures of the two acids cannot be deduced as accurately as they can from setting points.

#### *5—Interpretation of Melting Point and Setting Point Data by Dr J. P. Treub*

During the course of this work we got into communication with Dr. J. P. Treub, who allows us to state his views on the interpretation of the melting and setting points of these mixtures. When he refers to melting points, it has been previously stated that they are the temperatures at which the "last trace of solid disappears." The following is an extract from a letter sent to one of us.

"My opinion on de Visser's results is as follows. In the system palmitic acid–stearic acid, we have the two components and a dissociating compound of one mol palmitic + one mol stearic. There is a eutectic point between the compound and palmitic acid. If we call the curve of the liquids on the palmitic side  $P_s$ , and that on the stearic  $S_s$ , and the

intermediate curve  $I_s$ , then there is a eutectic point between  $P_s$  and  $I_s$ , whereas the curve  $S_s$  cuts the curve  $I_s$  so near to the maximum of the latter, that it is not possible to determine whether there is a second eutectic point, or not" (These curves are determined by melting points, plotted against composition, Table III.) "Now de Visser has determined solidifying points, that is, the molten substance is cooled slowly until solidification takes place, and the maximum temperature is determined at which equilibrium exists between solid and liquid

"If the material examined is a pure substance, then the composition of the liquid is not altered in solidification, but if we have a mixture, for example on curve  $P_s$ , then the first crystals separating out contain more palmitic acid than the mixture, so that the composition of the liquid comes nearer to the eutectic point and the maximum temperature determined is *not* the temperature of equilibrium between a liquid having the composition of the mixture examined and solid material

"The more the temperature of equilibrium is influenced by composition, that is, the steeper the curves, the greater will be the difference between the two methods (compare  $P_s$  and  $S_s$ ), whereas the difference will be least in the  $I_s$  part of the graph which is nearly horizontal

"As the solidifying points are determined in such a way that cooling from outside is a minimum, the difference between the two curves seems to be fixed by the under-cooling that takes place"

The evidence of a bimolecular compound, postulated by Dr. Treub, is generally held by those who have investigated the melting and setting points of different mixtures of pairs of aliphatic acids with even numbers of carbon atoms, all of which show eutectic points. Among these investigations the work of Jantzen\* on lauric and myristic acids is of importance, as special precautions were taken to establish equilibrium. Numerical data were not published in his communication, and we have to thank him for a copy of the graph showing the liquidus and solidus phases

#### 6—Crystal Spacings of Mixed Aliphatic Acids, etc.

Recent investigations† have shown that a homogeneous mixture of two solid aliphatic homologous substances does not give a long spacing

\* 'Z angew Chem,' vol 44, p 482 (1931)

† Piper, Malkin, and Austin, 'J Chem Soc,' p 2310 (1926), Francis, Malkin, and Piper, *loc cit*, p 214, Slagle and Ott, 'J Amer Chem. Soc,' pp. 4396, 4404 (1933, a), 'J Phys Chem,' vol. 37, p. 257 (1933, b), Piper and Chubb, 'Biochem. J.,' vol. 25, p 2072 (1931)

intermediate between those of its constituents, although calculations suggest that such a spacing might appear.

A possible exception, however, is found for the A and C spacings of the aliphatic acids with an odd number of carbon atoms \*†

All these measurements were made on specimens prepared by melting the two components together in suitable amounts, remelting a small proportion on a slide, and allowing it to resolidify. Under these conditions equilibrium could not have been attained, and the actual composition of the mixture under investigation was not necessarily identical with that of the whole specimen.

Then Ott and Slagle, for instance, have shown that the spacing of a particular mixture prepared in this way varies with its treatment and history.

On the other hand, Piper and Chibnall, using a uniform technique in preparing *crystalline specimens* of binary mixtures of fatty acids from a solvent, found that the B spacing of any definite mixture was constant. Such spacings in conjunction with mixed melting points and molecular weights, can be used to determine quantitatively the composition of any such mixture.

Our work was limited to mixtures of palmitic and stearic acids, but the setting points of these acids recorded by previous investigations of such mixtures, show that their preparations contained small quantities of impurities.

The aliphatic acids with an even number of carbon atoms crystallize from most solvents in that unstable form showing the B spacings, and these are converted irreversibly into those showing the C spacing at temperatures about 5° below their melting points, but when acetic acid is used as a solvent, the crystals all show this latter spacing.

When mixtures of palmitic and stearic acids are dissolved in this hot solvent containing sufficient water to cause complete separation when it is cold, crystals of different composition will separate continuously as the temperature falls slowly, and these will all show the C spacings.

We desired to ~~compare~~ the spacings of such mixed crystals, in which the crystal modification had not been altered, with those recorded by other investigators who had prepared their specimens by melting the components together.

No measurements of this kind have yet been made and although, as we expected, no interpretation could be offered for the results, many of

\* Chibnall and Piper, 'Bio-chem. J.', vol. 30, p. 180 (1936)

† Piper and Chibnall, 'Bio-chem. J.', vol. 28, p. 2175 (1934).

which were quite unexpected, they are of sufficient interest to outline briefly.

### 7—Preparation and Treatment of Specimens of Palmitic and Stearic Acids

Crystalline specimens were prepared by allowing a mixture of palmitic and stearic acids of known composition to crystallize slowly from dilute acetic acid. The crystals were freed from solvent by washing with an acid of similar concentration and a portion used for the determination of the

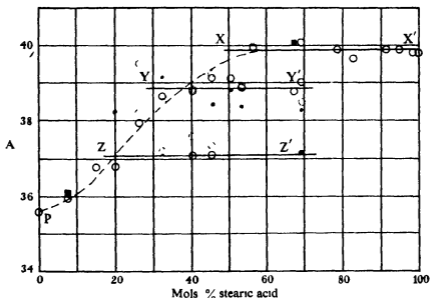


FIG. 4—Spacings of mixed crystals of palmitic and stearic acids ○ crystalline layer, ◐ aged layer, ● melted layer; ■ annealed layer

crystal spacing and another for the setting point, from which its average composition was determined

The specimens were treated as follows. (1) Crystals from acetic acid pressed on a glass plate 1 cm. by 5 mm.; (2) the same crystals after melting and cooling; (3) crystals annealed for some days at temperatures about 1° below their melting points, and then pressed on to the mount, (4) the crystals of No. (3) melted and resolidified; (5) crystals prepared under conditions (1) were rephotographed after an interval of several months.

In fig. 4, spacings are plotted against the average composition of the mixture expressed in mols % stearic acid.

### 8—General Results

Except in mixtures containing small amounts of one component, the reflexions tend to become very diffuse and few orders are registered. This may be caused both by the Debye broadening due to very small crystals, and to variations in the spacing of the different crystals constituting the specimen. There is so much background scattering that photometer curves show very flat maxima and often may not resolve two very diffuse overlapping lines.

These flat maxima make it difficult to measure the spacings of mixtures, containing from 20 to 80 mols % stearic acid, with an accuracy of more than 1%–2%, and the spacing obtained may only be a mean value due to two overlapping lines of unequal intensities.

The spacing of the freshly prepared specimen remains appreciably constant after it has aged for a period of six to eight months, although additional spacings sometimes appear.

### 9—Relationships of Spacings

From the palmitic acid side of the diagram in fig. 4, a dotted curve has been drawn through the maximum spacings measured on freshly prepared crystalline layers. This curve follows the same course as that observed by Piper, Chibnall, and Williams for the B spacings of mixtures of acids with 28 and 30 carbon atoms.

These spacings alone can be used to indicate the composition of crystalline mixtures of the acids up to that containing 55 mols. % stearic acid, but not with higher concentrations.

A melting point or setting point is usually characteristic of two mixtures, and a measurement of the C spacing will establish which of these is under investigation.

The curve rises until 55 mols % stearic acid is reached, the spacing is then close to that of pure stearic acid, and remains unaltered as the concentration of that acid increases.

About 32 mols % stearic acid, a second set of spacings is observed which group themselves along the ZZ' line, and a third set on the YY' line commencing at 40 mols % and appearing most strongly at equimolar proportions. Both these groups of spacings disappear in crystals containing more than 70 mols. % of stearic acid.

These data may be interpreted as giving some support for the existence of a bimolecular compound whose spacing lies at YY', and possibly a second containing a larger proportion of palmitic acid with a spacing

of ZZ'. If this latter compound does exist, however, it would be necessary to postulate that it is only stable at temperatures below the melting point of the eutectic mixture, otherwise its existence would be indicated on the melting or setting point graphs

It is surprising that a mixture of the average composition of 55, and higher, mols. % stearic acid should show spacings very close to that of pure stearic acid. In such mixtures, the crystals of stearic acid certainly do not predominate to the extent that their spacings only are measured. Probably they are due to mixed crystals in which the tilt of the stearic acid molecules is different from what it is in the pure state.

Our thanks are due to the Colston Research Society both for defraying part of the expenses of the work, and for the Mardon Fellowship, which enabled one of us (F. J. E. C.) to take part in the investigation

#### SUMMARY

The properties of all the members of the series of *n*-fatty acids which contain between 14 and 26 carbon atoms have been previously described. The present communication deals with a redetermination of the crystal spacings of some of these acids and, in continuation of the investigation, with the properties of all those of even carbon content between 28 and 38, and the single acid with 46 carbon atoms, together with various derivatives prepared during the course of the syntheses.

The importance of this work lies partly in the fact that there exists no other series of long chain carbon compounds of which so many members can be obtained in the pure and crystalline condition. Also, many of these acids, and the alcohols used in their preparation, occur naturally, and their investigation furnishes a set of constants based on the study of pure synthetic products which will serve as a definite basis for the identification of those occurring naturally.

When the values for the crystal spacings of the acids and their various derivatives are plotted against the corresponding carbon contents, straight lines result in all cases. On those for the acids, for instance, lie accurately the two spacings of all the acids including that containing 46 carbon atoms, which is the largest chain acid yet prepared.

The important observation was made that crystals of the acids with even carbon content obtained by crystallization from acetic acid show the C spacings only, whereas the crystals from non-polar solvents show the B spacings.

The C spacings of a series of crystalline mixtures of palmitic and stearic acids were measured and compared with those previously obtained on specimens prepared by melting the constituents together in different proportions. The manner in which these spacings alter as the amount of stearic acid increases affords data which, in conjunction with either a melting or setting point, enables the composition of such mixtures to be determined.

---

## The Electrical Conductivity of Thin Metallic Films II—Caesium and Potassium on Pyrex Glass Surfaces

By E. T. S. APPLEYARD and A. C. B. LOVELL, H. H. Wills Physical  
Laboratory, University of Bristol

(Communicated by A. M. Tyndall, F.R.S.—Received 25 September, 1936)

### 1—INTRODUCTION

An account of an investigation of the electrical conductivity of thin films of rubidium deposited in high vacua on very clean glass surfaces has been previously published\*. It will be referred to in what follows as Part I. The method has now been used in a similar investigation using caesium and potassium.

The vigorous heat treatment of the surface and vacuum technique described in Part I has again been found necessary in order to attain reproducible results, and the effects on contaminated surfaces are similar. It will be seen that the resistivities of the stable films are consistent with the theory given in Part I; moreover, the greater stability of the caesium films has supplied a test of the theory down to thicknesses of only a few Å. The decay phenomena associated with the unstable films show a marked gradation through these three alkali metals, the stability of a given film increasing in the order potassium—rubidium—caesium.

### 2—EXPERIMENTAL

The experimental tube, vacuum technique, and method of working were identical with those described in Part I. Caesium was prepared by

\* Lovell, 'Nature,' vol. 137, p. 493 (1936); 'Proc. Roy. Soc.,' A, vol. 157, p. 311 (1936).

reduction of the chloride with calcium as for rubidium, and potassium by distilling the cleaned metal *in vacuo*

The intensity of the atomic beam has been found by measuring the positive ion emission from a hot tungsten filament placed in the path of the beam as in § 4, Part I. These measured intensities have fallen within the limits given by the effusion formula (1) (Part I), using the somewhat divergent vapour pressure data available \*

In calculating the film thicknesses from the number of atoms on the surface, the same assumption has been made that these films contain the same number of atoms per  $\text{cm}^2$  as the bulk metal. Then if  $n$  is the number of atoms per  $\text{cm}^2$  on the surface, the film thicknesses at liquid air temperatures are given by

$$t = \frac{n}{9 \cdot 16} \times 10^{-21} \text{ cm for caesium} \quad (1)$$

and

$$t = \frac{n}{1 \cdot 39} \times 10^{-22} \text{ cm for potassium} \quad (2)$$

Then from the definition of a monatomic layer a film of thickness  $t$  Å contains  $t/6 \cdot 05$  atomic layers each containing  $5 \cdot 54 \times 10^{14}$  atoms per  $\text{cm}^2$  for caesium; and  $t/5 \cdot 20$  atomic layers each containing  $7 \cdot 23 \times 10^{14}$  atoms per  $\text{cm}^2$  for potassium.

By following the precautions outlined in § 8, Part I, completely reproducible results have been obtained. The results to be quoted were those obtained on the clean standard surface referred to in Part I.

### 3—MEASUREMENTS WITH CAESIUM

The results obtained with caesium are essentially similar to those previously described for rubidium, but a caesium film of a given thickness deposited at a given temperature shows much greater stability than the corresponding rubidium film. Fig. 1 illustrates measurements on films 24 Å thick deposited at different temperatures, using a constant beam intensity  $2 \cdot 3 \times 10^{12}$  atoms/ $\text{cm}^2/\text{sec}$ .

The relevant data for these films is collected in Table I. In contrast, rubidium films of this thickness showed decay factors of the order of 13 at 90° K. and were still unstable when deposited at 64° K., the resistivities being correspondingly higher.

\* See Scott, 'Phil. Mag.', vol. 47, p. 32 (1924), Killian, 'Phys. Rev.', vol. 27, p. 578 (1926), Kröner, 'Ann. Phys.', vol. 40, p. 438 (1913) for caesium, and Edmonston and Egerton, 'Proc. Roy. Soc., A', vol. 113, p. 520 (1927) for potassium.

The resistance of the end contacts has been found by depositing thick layers as in Part I; in the apparatus from which this data is taken it was 2.0 ohms. As with rubidium, the stable films have given completely reproducible temperature/resistance graphs over the range to 90° K. (see fig. 7).

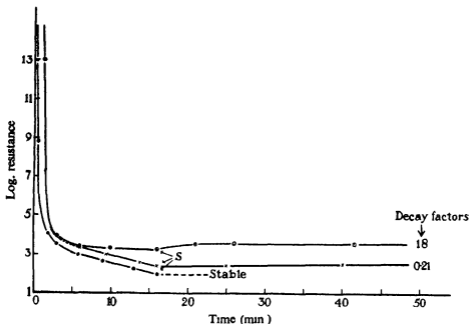


FIG 1—Formation and decay of conductivity for films 24 Å thick deposited at different temperatures of deposition with beam intensity  $2.3 \times 10^{18}$  atoms/cm<sup>2</sup>/sec  
S = shutter closed (cessation of deposition), ○ 90° K, × 77° K; ● 64° K.

TABLE I—DATA FOR CAESIUM FILMS 24 Å THICK

Temperature of deposition ° K.	Beginning of conductivity	Resistivity at instant of closing shutter ohm cm	Decay factor
90	1.7 Å (0.3 layers)	$8.5 \times 10^{-4}$	1.8
77	1.7 Å. (0.3 layers)	$1.1 \times 10^{-4}$	0.21
64	0.35 Å (0.06 layers)	$3.1 \times 10^{-5}$	Stable

#### 4—SUMMARY OF THE EXPERIMENTAL DECAYS AND RESISTIVITIES FOR CAESIUM

Fig. 2 summarizes the measurements of the decay of conductivity for the caesium films, and shows the decay factor ( $\Delta R/R$  in 30 mins. after

cessation of the deposition) as a function of the temperature of deposition for a given number of layers. After a deposition at 64° K., only extremely thin films show any tendency to decay; for example, a film 5.7 Å. thick deposited at this temperature is stable, but decays at the rate 0.43 when the temperature is raised to 90° K.

By comparison with fig. 4 of Part I, the much greater stability of the caesium films over the rubidium films is evident. The caesium films show

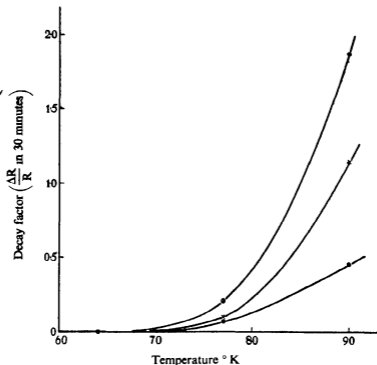


FIG. 2—Decay factors as a function of the temperature of deposition for films of a given thickness deposited with beam intensity  $2.3 \times 10^{13}$  atoms/cm.<sup>2</sup>/sec  
○ 24 Å.; × 50 Å.; ● 57 Å.

some peculiarity in that the decay/thickness at a given temperature passes through a maximum and minimum in the region of 10 Å. and then decreases, as has been found before. This is shown in fig. 2 where the curve for the 5.7 Å. film appears below those for thicker films.

Fig. 3a summarizes the film resistivities against film thickness for various deposition temperatures, and fig. 3b illustrates the influence of the temperature of deposition on the resistivity of films of a given thickness.

The greater stability and consequent lower resistivity of the caesium films is again evident by comparison with fig 5, Part I

As pointed out in § 10, Part I, the experimental points on these figures which are not determinations from stable films are somewhat arbitrary, since the resistance plotted is that measured immediately after completing the deposition with a definite beam intensity.

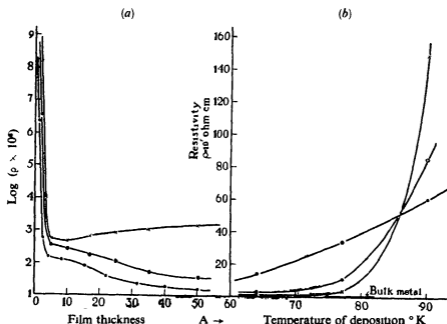


FIG 3—(a) Film resistivities (log scale) as a function of film thicknesses for different deposition temperatures  $\times$  90° K,  $\circ$  77° K,  $\bullet$  64° K (b) Dependence of resistivity (linear scale) on the temperature of deposition for films of a given thickness  $\bullet$  5 Å,  $\circ$  25 Å,  $\times$  50 Å

### 5—MEASUREMENTS WITH POTASSIUM

The thin films of potassium have been the most unstable of the three alkalis investigated. Fig 4 is a comparison diagram showing the behaviour of films 20 Å thick of potassium, rubidium, and caesium deposited at 90° K. with approximately the same beam intensity, and Table II summarizes the data.

As with rubidium and caesium, the potassium films become more stable as the temperature of deposition is lowered, but even at 64° K. a 40 Å film of potassium is on the verge of instability, since although stable at that temperature it decays slightly when the temperature is raised to 90° K.

The interpretation of these measurements will be considered in the discussion.

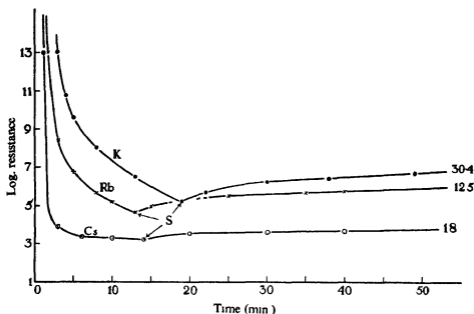


FIG 4—Formation and decay of conductivity for films of K, Rb, Cs deposited at  $90^{\circ}$  K. ● K 20 A with beam intensity  $2.45 \times 10^{12}$  atoms/cm<sup>2</sup>/sec, × Rb 21.8 A with beam intensity  $3.15 \times 10^{12}$  atoms/cm<sup>2</sup>/sec, ○ Cs 21.0 A with beam intensity  $2.30 \times 10^{12}$  atoms/cm<sup>2</sup>/sec. S shutter closed (cessation of deposition)

TABLE II—COMPARISON OF A 20 A FILM OF K, Rb, AND Cs DEPOSITED AT  $90^{\circ}$  K

	Beginning of conductivity A	Resistivity at instant of closing shutter ohm cm	Film resistivity Bulk resistivity*	Decay factor
Potassium	3.2	$5.75 \times 10^{-3}$	34000	30
Rubidium	2.8	$1.2 \times 10^{-3}$	4700	12.5
Caesium	1.7	$7.45 \times 10^{-4}$	140	1.8

\* Resistivity of the bulk metal: Rubidium, Hackspill, 'C.R. Acad. Sci. Paris,' vol. 151, p. 305 (1910); caesium, Hackspill, *loc. cit.*; potassium, Woltjer and Onnes, 1924, 4th Int. Congr. of Refrig. London, also Comm. Phys.-Lab. Leiden, No. 173a.

## 6—DISCUSSION OF RESISTIVITIES OF THE STABLE FILMS

We may briefly summarize the experimental findings concerning thin films of caesium and potassium by saying that the simple theory of Part I

which was found adequate for rubidium satisfactorily accounts for these results too. The stability of extremely thin films of caesium has made a comparison with theory possible down to much smaller thicknesses; with potassium, on the other hand, films thinner than 30 Å. are not stable and so cannot be compared with the calculated values.

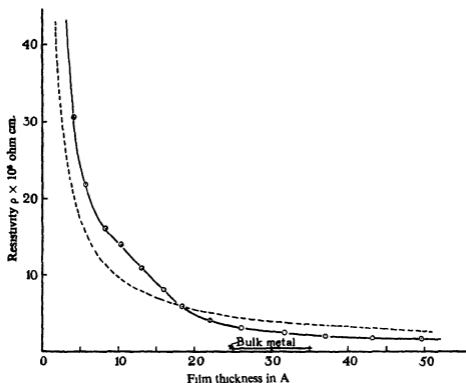


FIG. 5—Theoretical - - -, and experimental ○ Resistivity/thickness curves up to 50 Å. for a caesium film deposited at 64° K.

Figs 5 and 6 exhibit the results for caesium films. The calculated resistivities  $\rho$  (broken curve) in both cases are obtained from the formula of § 11, Part I.

$$\rho = \frac{2mv}{Ne^2} \cdot \frac{1}{t \left[ 1 + \log \frac{\lambda_g}{t} \right]}, \quad (3)$$

where  $e$ ,  $m$ , and  $v$  are respectively the electronic charge, mass, and velocity,  $\lambda_g$  the normal mean free path in the bulk metal at temperature

$0^\circ \text{ K.}$ , and  $N$  is the number of electrons per  $\text{cm.}^3 \simeq 1/\text{atomic volume}$  for the alkalis.\*

This formula takes into account the shortening of the normal mean free path by collisions with the boundaries and should only hold for  $t < \lambda_e$ . Fig. 5 shows the good agreement between experiment and theory down to a few  $\text{\AA.}$  in thickness. Fig. 6, which includes measurements up to 550  $\text{\AA.}$  thickness, shows that the theory begins to break down seriously

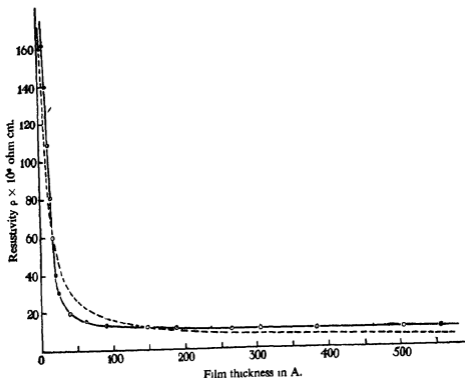


FIG. 6—Theoretical - - -, and experimental  $\bigcirc$  Resistivity/thickness curves up to 550  $\text{\AA.}$  for a caesium film deposited at  $64^\circ \text{ K.}$

at the upper end of the range. Here, however, the thickness becomes comparable with the normal mean free path of the electron in bulk caesium (1450  $\text{\AA.}$  at  $64^\circ \text{ K.}$ ), and the postulates of the simple theory no longer hold. Fig. 7 shows the resistivity/temperature graphs for a 50  $\text{\AA.}$  caesium film deposited at  $64^\circ \text{ K.}$

The resistivities for potassium are hardly worth publication in detail.

\* See R. W. Wood, 'Phys. Rev.', vol. 44, p. 353 (1933), Zener, 'Nature', vol. 132, p. 968 (1933); Mott and Zener, 'Proc. Camb. Phil. Soc.', vol. 30, p. 249 (1934).

The agreement with theory is about as good as that for the rubidium films of Part I, and the deviations in the range of small thicknesses are about what one would expect from the relatively smaller stability of the potassium films

There can therefore be little doubt that if the deposition of rubidium and potassium were carried out at temperatures low enough to obtain completely stable films the agreement with theory would be as satisfactory as it is for caesium.

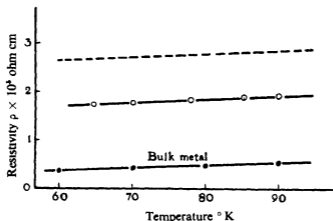


FIG. 7—Theoretical — — —, and experimental  $\bigcirc$  Resistivity/temperature graphs for a film  $49.5 \text{ \AA}$  thick deposited at  $64^{\circ}\text{K}$   $\bullet$  bulk metal

#### 7—DISCUSSION OF THE PHENOMENON OF THE DECAY OF CONDUCTIVITY

In § 12, Part I, to which we refer for details, a qualitative theory was developed to account for the experimental observation that the conductivity of thin films normally decays when the deposition of the metal is stopped. The decay was attributed to the widening of cracks and imperfections in the film under the action of surface tension forces.

The discussion of Part I requires slight correction on one point. It was suggested there that the cracks might extend across the film, and that the current actually passed across the crack. The high and increasing resistance of such cracks was invoked to explain the observed resistivities as the film aged. Our present view is that the cracks are unlikely to extend unbroken from one boundary of the film to the other. They therefore can be regarded as mere insulating barriers, the current being carried by unbroken bridges of metal which, however, become fewer and

smaller as the film disintegrates. This modification of the original hypothesis explains more satisfactorily the tendency for the aged film to settle down to a steady and not inordinately high resistance after a period of hours. It may also be pointed out here that a "crack" is not the only likely form of imperfection. If disintegration starts from a point, then roughly circular holes may develop similar to the "windows" described by Andrade and Martindale.\*

None of the observations of the present paper contradict this hypothesis. On the other hand, one or two new facts about the decay merit a rather fuller discussion.

If we take the crudest form of this hypothesis, we may picture the disintegrating film as a layer of homogeneous metal uniform in thickness except where it is pierced by holes or cracks which are gradually extending under the influence of surface tension forces. Detached "islands" may, of course, also exist. The extension of the cracks is opposed by the rigidity of the metal. Now at ordinary temperatures, at any rate, caesium, rubidium, and potassium increase in mechanical strength in this order. Hence, in order to explain the observed fact that the stability of the films is in the reverse order, we have to suppose that the surface tension forces become progressively stronger as we pass from caesium to potassium. This additional hypothesis is not unreasonable. Fixing attention upon a definite geometrical configuration of the disintegrating film, it is clear that the forces deforming it will be proportional to  $E_1 + E_2$ , where  $E_1$  is the surface energy of a free alkali-metal surface and  $E_2$  the (negative) surface energy of the alkali-glass surface. If  $E_1 + E_2$  were negative, the film would tend to spread (*i.e.*, the alkali metal would "wet" the surface of the glass). If  $E_1 + E_2$  is positive, the film will tend to contract, but the larger the absolute magnitude of  $E_2$  the smaller will be the contracting force. Now  $|E_2|$  is a measure of the energy with which the alkali atoms in contact with the glass surface adhere to it, and we should expect this energy to be greater for caesium than for rubidium or potassium on account of its greater chemical activity. This might then account for the greater relative stability of the caesium films.

Actually there is one significant fact opposed to the above conception of the film as a homogeneous metal phase. Reference to fig. 2 shows that caesium films 5.7 Å. thick actually show a smaller decay than films 24 Å. thick, although on the above picture the surface tension stresses should be much greater at a crack in the thinner films. One is therefore driven to the conclusion that the first atoms of caesium laid down have a much

\* 'Phil. Trans.', A, vol. 235, p. 69 (1935).

smaller mobility than those in the subsequent layers. The observations of Andrade and Martindale (*loc. cit.*) definitely prove that this is so for silver films on glass, and so the result is not unexpected. But the whole foregoing discussion must remain somewhat speculative until further experience has been acquired with other metals on various surfaces.

We wish to acknowledge a grant in aid from the Colston Research Society of the University of Bristol. One of us (A. C. B. L.) is also indebted to the D S I R for a Maintenance Grant during the course of the work.

### 8—SUMMARY

The method recently described for measuring the resistivity of thin films of rubidium on clean substrates in very high vacua has been extended to caesium and potassium.

Conductivity has been observed with caesium films of only 0.3 Å. in thickness. The decay of conductivity normally shown by these films after cessation of the deposition decreases in the order potassium—rubidium—caesium for a film under given conditions. At the lowest temperature used (64° K.), caesium films of only a few Å. in thickness are stable.

The resistivities of the stable films again show excellent agreement with the formula previously derived, for caesium down to a few Å. in thickness.

The work on caesium and potassium has given further support to the hypothesis previously developed to explain the phenomenon of the decay of conductivity.

---

# Ionization, Excitation, and Chemical Reaction in Uniform Electric Fields

## III—The Excitation of the Continuous Spectrum of Hydrogen

By R WINSTANLEY LUNT, C A MEEK, and E C W SMITH (The Sir William Ramsay Laboratories of Inorganic and Physical Chemistry, University College, London, and Messrs. Imperial Chemical Industries, Ltd)

(Communicated by F. G. Donnan, FRS—Received 5 October, 1936)

### I—INTRODUCTION

In a previous communication, Part II,\* Lunt and Meek described the calculation of the energy efficiency,  $\eta$ , for the excitation of the  $^3\Sigma_g^+$  state of the hydrogen molecule, transitions from which to the lowest triplet state,  $^3\Sigma_u^+$ , are accompanied by the emission of the continuous spectrum, these values of  $\eta$  refer to excitation effected by an electron swarm moving in a uniform electric field,  $X$ , through hydrogen molecules in the ground state at the pressure  $p$ . The calculations show that  $\eta$  is a function of  $Xp^{-1}$ , and are based on the assumption of a Maxwellian electron energy distribution, an approximate estimate for the probability cross-section for the excitation of the  $^3\Sigma_g^+$  state by electron impact, and Townsend's data† for the dependence of the electron drift velocity,  $W$ , and the mean electron energy,  $\bar{V}$ , on  $Xp^{-1}$ . Since the only optically allowed transition which molecules in the  $^3\Sigma_g^+$  state can suffer is that giving rise to the continuous spectrum, it follows that the energy efficiency for the emission of this spectrum must be equal to that for the excitation of the  $^3\Sigma_g^+$  state.

These calculations of  $\eta$  are valid for the very low current densities used in the experiments to determine  $W$  and  $\bar{V}$ . Reasons have been discussed in Part II for believing that these calculations may be valid for the much greater current densities in a uniform positive column discharge, a zone in which the conditions approximate closely to those postulated in the theory

\* Lunt and Meek, 'Proc. Roy. Soc., A, vol. 157, p. 146 (1936)

† Townsend, "The Motion of Electrons in Gases," Oxford (1925); cf. also Part I, Emeleus, Lunt, and Meek, 'Proc. Roy. Soc., A, vol. 156, p. 394 (1936)

given in Part II. One line of reasoning is based on the conformity between the data of Chalonge, 1934, for the emission of the hydrogen continuous spectrum in a discharge and the calculated values of the energy efficiency,  $\eta$ , for the intensity of the emission of this spectrum (fig. 1, Part II). In the experiments of Chalonge\* a positive column discharge was maintained by an alternating potential applied to the electrodes apart from the uncertainty as to the values of  $W$  and  $\bar{V}$  under these conditions, the values of  $X$  used in deriving those of  $Xp^{-1}$  are necessarily somewhat uncertain averages, and also involve uncertain allowances for the cathode fall in potential. For these reasons the agreement between experiment and theory, mentioned above, may be due to mutually compensating errors. This paper describes the determination of  $\eta$ , in arbitrary units, as a function of  $Xp^{-1}$  for the emission of the continuous spectrum by a uniform positive column discharge maintained by constant electrode potential, that is, for conditions closely approximating to those postulated in the theory given in Part II, the results reveal a very satisfactory agreement between experiment and theory, and, despite the fact that they are not so extensive as might be desired,† we have therefore felt them to be of sufficient interest to publish.

The determination of the absolute value of  $\eta$  requires the measurement of the total number of  $^3\Sigma_u^+$  molecules suffering the transition to the  $^3\Sigma_g^+$  state per unit volume of discharge zone per second, and per unit of energy required to maintain this unit volume per second, since the radiation emitted by such transitions from the discharge is random in direction, the intensity in a small solid angle subtended by a small zone of the discharge per unit of energy supplied is a quantity proportional to  $\eta$ , and this is the quantity we have measured. Ideally, determinations of the intensity throughout the continuous spectrum are desirable, but since there is no reason to suppose that the intensity distribution changes provided the initial state of the hydrogen molecules is maintained constant, we have contented ourselves with observations in three regions about  $\lambda\lambda$  3100, 2800, and 2600. Further towards the visible the continuous spectrum becomes overlaid by the band spectrum, and further towards the ultra-violet the intensity response of photographic plates is unsatisfactory ‡

\* 'Ann. Phys. Paris,' ser 11, vol 1, p 123 (1934)

† Circumstances unforeseen at the commencement of these experiments have precluded any attempt to demonstrate that the phenomena are independent of the particular discharge tube used

‡ Pearse and Hunter, 'Nature,' vol 138, p 37 (1936)

## II—EXPERIMENTAL

In order that the experimental conditions should approximate closely to those postulated in the theory given in Part II, a number of requirements have to be fulfilled which have necessitated a measure of compromise in the design of the apparatus, and the experimental procedure finally adopted. Ideally, the discharge tube should be so wide that the transverse field due to the walls is negligible, and the main body of the discharge homogeneous, the cross-section of the tube must be such that the positive column remains uniform over a considerable range of pressure, and that by varying the pressure the required range of  $Xp^{-1}$  (about 10–120 volts  $\text{cm}^{-1} \text{mm Hg}^{-1}$ ) can be attained, the length of the discharge tube must be sufficient to enable determinations of the (longitudinal) field,  $X$ , to be made with the desired accuracy, and lastly the cross-section of the tube must be such that, with the available pumping resources, a rapid stream of hydrogen can be passed through the discharge so that, in the region where observations are made, the gas consists mainly of ground state molecules unchanged by the discharge.

The tube finally adopted after a number of trials consisted essentially of a cylindrical quartz tube 38 cm long and of 0.2  $\text{cm}^2$  internal cross-section, and provided with three side tubes arranged symmetrically about the centre and 16 cm apart, through each of which was inserted a probe electrode, the tip of which ended at the axis of the discharge tube, these probes were connected to an electrostatic voltmeter in order to measure the field  $X$ . At each end this discharge tube was fused to larger tubing to which a number of side tubes were attached, in one side tube at each end a water-cooled electrode was inserted, and the others provided connexions to the hydrogen supply, pressure gauge, and the pumping system. Hydrogen was admitted to the system at the cathode end through a large electrically heated palladium tube, the adjustment of the heater current providing a convenient control over the hydrogen flow, this flow was further regulated by taps connecting the "exit" end of the discharge tube to the oil pump. A side tube close to the "inlet" end of the discharge tube was connected to a manometer containing carefully degassed Apiezon oil. By using a pressure range of 1.6 to 0.06 mm. Hg, it was found possible to obtain a uniform (non-striated) positive column in which the corresponding range of  $Xp^{-1}$  was from 25.5 to 248. In this pressure range the rates of flow of gas through the discharge tube used in the experiments, and referred to volumes measured at the actual pressure, were found to be approximately represented by  $730 \times p \text{ cm.}^3 \text{ sec}^{-1}$ .

A number of ground joints sealed with picein wax were used to connect the quartz discharge tube to the various pieces of auxiliary glass apparatus; spectroscopic observations of the discharge showed that these did not contaminate the hydrogen. The discharge was excited by high tension direct current derived from a 4000-volt motor generator unit fed from a large 220-volt battery to ensure steadiness in running; a ballast resistance of  $10^5$  ohms was permanently connected in series with the discharge to secure stability. The current through the discharge was indicated by a sub-standard multi-range milliammeter. The spectrum of the discharge was recorded photographically by using a small (Hilger type No E369) quartz spectroscope aligned transversely to the discharge tube and mid-way between the second and third probe reckoned from the hydrogen "inlet" end; Wellington ortho process quarter plates were used. By using a fairly narrow slit aperture, it was possible to obtain twelve exposures on each plate separated by about 1 mm.

*Experimental Procedure*—The principle on which the procedure was based was to record the spectrum of the discharge at various values of  $Xp^{-1}$  but for an approximately constant value of the energy supplied to the discharge; the intensity of the continuous spectrum is then proportional to the energy efficiency for its excitation,  $\eta$ . Since the current and  $X$  varied considerably with the pressure, this necessitated adjustment of the exposure time for each value of  $Xp^{-1}$ , the standard value of the energy supplied being chosen as a result of preliminary experiments so that the range of photographic blackening of the plate over a range of  $Xp^{-1}$  would be suitable for microphotometer measurements. After the discharge had run for about an hour in streaming hydrogen to remove any residual impurities, the current was adjusted to some suitable value of the order of 5 mA, the pressure then adjusted to give the required value of  $Xp^{-1}$ , the potential across the probes read, and an exposure was then made for such a time that the energy supplied was as near as possible to the standard value; this procedure was then repeated for a series of values of the pressure and  $Xp^{-1}$ . The last four exposures on the plate were made to form an intensity scale for the others by running the discharge under constant conditions and for exposure times in the ratio 1 : 2 : 4 : 8, the absolute values of these exposures being chosen from experience gained in preliminary experiments so that the range of photographic blackening would cover the range concerned in the first eight exposures in which  $Xp^{-1}$  had been varied.

Microphotometer traces of the plate were then taken transversely (*i.e.*, at right angles to the extension of the spectra) at three regions corre-

sponding approximately to  $\lambda\lambda$  3100, 2800, and 2600. The heights of the ordinates of the microphotometer traces were then measured; for each wave-length the heights corresponding to the last four exposures were plotted against an intensity scale 1, 2, 4, 8, and the resulting curve was then used to read off the intensities, in arbitrary units, for the other exposures corresponding to the various values of  $Xp^{-1}$ . Since the actual energy supplied to the discharge deviated slightly from the standard value (the largest deviation amounted to 5%), these intensities were corrected for these deviations by making the plausible assumption that for small changes the blackening was proportional to the energy supplied.

The data now reported were derived in this way from two plates covering overlapping ranges of  $Xp^{-1}$ , the intensities for both plates were expressed in the same (arbitrary) units by adjusting the intensity of the second plate to that of the first at  $Xp^{-1} = 92$  which lies within the common range. Finally, the experimental values for the energy efficiencies of these intensities (in arbitrary units) were multiplied by a numerical factor so that their magnitudes in the neighbourhood of  $Xp^{-1} = 30$  to 40 were comparable with the absolute values of  $\eta$  for the excitation of the  $^3\Sigma_g^+$  state as calculated in Part II. This procedure was carried out for the data at each of the three regions of wave-length at which the microphotometer traces were obtained, the results are given in Table I. It is very satisfactory to find that at all values of  $Xp^{-1}$  below 55 the individual values of the energy efficiencies of the intensity at each wave-length differed from the mean by less than 2%, showing that there was no systematic variation with wave-length.

The mean values of the energy efficiency of the intensity, column 5, Table I, are represented in fig. 1 by points +, together with the values (also in arbitrary units, but similarly adjusted) derived from the data of Chalonge (*cf.* Part II) denoted  $\circ$ , the full curve represents the values of  $\eta$  for the excitation of the  $^3\Sigma_g^+$  state in absolute units as calculated by the procedure described in Part II. Since the experimental data now reported extend to a range of  $Xp^{-1}$  beyond that for which the calculated values of  $\eta$  were given in Part II, the calculations have been extended to  $Xp^{-1} = 250$  by using the same extrapolations for  $W$  and  $\bar{V}$  which were found in Part I (*cf.* Table I) to lead to values of the Townsend coefficient of ionization,  $\alpha p^{-1}$ , in good agreement with experiment. The range of  $Xp^{-1}$  now concerned extends about 100 units beyond that examined in Part I; the validity of the extrapolations in this further range has therefore been checked by calculating  $\alpha_0 p^{-1}$  (*cf.* Part I, Table I). It is found that

TABLE I

The energy efficiency of the intensity of the continuous spectrum of hydrogen (as excited in a positive column) in arbitrary units,  $\eta'$ , as adjusted to be approximately equal to the calculated energy efficiency,  $\eta$ , in the range  $Xp^{-1}$  30-40. The fractional concentration,  $f$ , of hydrogen atoms in the positive column as calculated from the rate of excitation of the  $^3\Sigma_u^+$  state \*

$Xp^{-1}$	$\eta'$			$\eta'_{\text{mean}}$	$f$
	$\lambda$ 3100	$\lambda$ 2800	$\lambda$ 2600		

PLATE I					
25 <sub>s</sub>	4 4	4 3 <sub>s</sub>	4 4	4 4	0 016
29	3 9 <sub>s</sub>	4 0 <sub>s</sub>	3 9 <sub>s</sub>	4 0	0 017
30 <sub>s</sub>	4 4	4 3 <sub>s</sub>	4 3	4 4	0 021
35 <sub>s</sub>	5 3	5 4	5 4	5 4	0 037
42	4 4	5 0	5 1	5 0	0 055
48 <sub>s</sub>	5 4	5 2 <sub>s</sub>	5 5	5 4	0 075
51	4 9 <sub>s</sub>	4 9 <sub>s</sub>	5 0	5 0	0 100
138	1 7 <sub>s</sub>	1 8 <sub>s</sub>	1 7 <sub>s</sub>	1 8	0 033

PLATE II					
92	3 0	3 0	3 0	3 0	—
97	2 5 <sub>s</sub>	2 7	2 5	2 6	—
119	2 1	2·2	2 2	2 2	—
145	1 6	1 6 <sub>s</sub>	1 6	1 6	—
235	1 0 <sub>s</sub>	1 1	1 3 <sub>s</sub>	1 2	—
247	0 7 <sub>s</sub>	0 8 <sub>s</sub>	1 1	0 9	—

\* The significance of  $f$  is discussed on p. 736

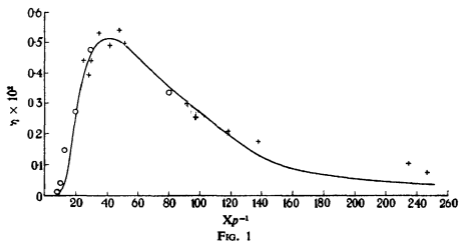


FIG. 1

from  $Xp^{-1} = 150$  to 250 the ratio of the calculated to experimental values,  $\theta_p$ , remained sensibly constant and equal to 0.83.

### III—DISCUSSION OF RESULTS

Although, as shown by fig. 1, the experimental data for  $\eta$  in arbitrary units for the excitation of the continuous spectrum of hydrogen lie close to the theoretically calculated curve of  $\eta$  for the excitation of the  $^3\Sigma_u^+$  state over a wide range of  $Xp^{-1}$ , it is necessary to consider the accuracy of the experimental determinations before discussing the significance of the results.

The positive column was visually uniform, and the field between the central probe electrode and either of the others was constant within 5% for any given conditions, no tests were made for oscillations. A consideration of the accuracy of the individual measurements shows that

- (i) The probable error in determining  $\eta$  in arbitrary units increases to about 5% at the lower end of the range of  $Xp^{-1}$  investigated
- (ii) The probable error in determining  $Xp^{-1}$  was about 5% in the range of  $Xp^{-1}$  below 55, increasing to about 15% at the highest values used

It remains to consider how far the fundamental postulate that the gas consisted mainly of molecules unchanged by the discharge was fulfilled in these experiments. The results given in Part II show that, for this purpose, it is only necessary to consider, in approximate calculations, the excitation and dissociation of the lowest triplet state,  $^3\Sigma_u^+$ , for which the values of  $F_c$  as functions of  $Xp^{-1}$  are given in Part II, Table I. From the definitions given in Part II, the rate of excitation (and therefore of destruction by spontaneous dissociation),  $R_e$ , molecules  $\text{cm}^{-3} \text{sec}^{-1}$ , is given by

$$R_e = X \cdot I_c \cdot F_c / V_c,$$

where  $F_c$  is the fractional energy loss,  $I_c$  the current density in electrons  $\text{cm}^{-2} \text{sec}^{-1}$ , and  $V_c$  the critical energy for the process. Values of  $R_e$  have been calculated in this way as functions of  $Xp^{-1}$  for the values of  $I_c$  in the present experiments. Since the observations of the spectrum were made in the middle of the second half (with respect to the hydrogen flow) of the tube containing the positive column and through which the gas streamed, it is necessary to consider the amount of dissociation produced in the whole positive column having a volume of  $8 \text{ cm}^3$  approximately; the total rate of dissociation was therefore about  $8 \times R_e$ , molecules  $\text{sec}^{-1}$  provided that the gas was mainly unchanged hydrogen. Since the

streaming velocity referred to the actual pressure in the discharge tube was approximately  $730 \times p \text{ cm}^2 \text{ sec}^{-1}$ , it follows that the number of molecules passing through per second was approximately  $730 \times p \times 3.5 \times 10^{14} \times p = 2.6 \times 10^{19} \times p^2$ . Provided that the fraction of molecules dissociated was small, the fraction dissociated,  $f$ , is then given approximately by

$$f = \frac{8 \times R_e}{2.6 \times 10^{19} \times p^2}$$

Values of  $f$  calculated in this way are given in the last column of Table I, from which it is seen that  $f$  never exceeds  $0.10^*$ , the actual value of  $f$  was probably considerably smaller on account of the recombination of atoms at the walls. It is thus clear that the conditions postulated by the theory of Part II, that the gas consists mainly of molecules unchanged by the discharge, was approximately fulfilled in these experiments.

The mean percentage deviation of the  $\eta$  values now reported (points marked + in fig. 1) from the theoretically calculated values is 12% for the range of  $Xp^{-1}$  from 25.5 to 138, this is the range in which the calculations are most reliable, and it is therefore satisfactory to find that the mean deviation lies so close to the estimated probable error in the experimental determinations. For higher values of  $Xp^{-1}$  the experimental values are higher than the theoretical ones, being larger by a factor of about 2.5 at the extreme end of the range investigated. These discrepancies lie beyond the estimated experimental error, on the other hand, the calculations in this region are not very reliable because the energy of (electron) drift motion becomes comparable with that of random motion, and the postulates on which the calculations are based are therefore no longer fulfilled. Furthermore, there is some uncertainty about the range of electron energy in which the cross-section for the excitation of the  $^3\Sigma_g^+$  state is significant (cf. Part II, Appendix, § 4), the approximation adopted almost certainly leads to values of  $\eta$ , which are too small for the higher values of  $Xp^{-1}$ ; calculation shows, however, that the introduction of a correction extending the significant range of cross-section would not account for more than a small fraction of the present discrepancies. Despite these uncertainties in the theoretical calculations for the higher values of  $Xp^{-1}$  (150–250), it is interesting to find that they do still predict the general character of the trend of  $\eta$  with  $Xp^{-1}$ .

Considered in conjunction with the results reported in Part II, the

\* The discontinuous variation of  $f$  with  $Xp^{-1}$  occurs because the values of  $I_e$  used did not vary regularly with  $Xp^{-1}$ .

agreement now reported between the theoretically calculated values of  $\eta$  and those determined experimentally confirm the conclusions reached in Parts I and II, and, moreover, show that, to a close approximation, Townsend's data for the dependence of  $\bar{V}$  on  $Xp^{-1}$ , and the assumption of a Maxwellian electron energy distribution, are still valid in the high current densities of a uniform positive column discharge for the wide range of  $Xp^{-1}$  from 25 to 140. The additional agreement provided by the  $\eta$  values derived from the data of Chalonge (1934) suggests that these conclusions extend down to  $Xp^{-1} \approx 10$ , and that the dependence of  $W$  and  $\bar{V}$  on the mean value of  $Xp^{-1}$  (averaged over a half period) in a positive column maintained by a low frequency (50 cycle) alternating electrode potential is approximately the same as that reported by Townsend for weak currents in a uniform field.

The fact that the assumption of a Maxwellian electron energy distribution, and the extrapolated values of  $W$  and  $\bar{V}$  in the further range of  $Xp^{-1}$  up to 250, give values of  $\alpha p^{-1}$  in satisfactory agreement with experiment (at the same low current densities for which  $W$  and  $\bar{V}$  were determined in the lower range of  $Xp^{-1}$ ), whilst the calculated values of  $\eta$  for the excitation of the continuous spectrum are markedly smaller than the experimental values (for the high current densities of the positive column discharge) indicates that at these high values of  $Xp^{-1}$  the motion of the electrons varies with the current density. Whilst it does not appear possible to infer the nature of the change from the discrepancies in the calculated and experimental values of  $\eta$ , it is interesting to note that if the positive column discharge be regarded as approximately equivalent to a homogeneous beam having energy equal to the extrapolated value of the random energy,  $\bar{V}$ , then for  $Xp^{-1} = 250$ , the value of  $\eta^*$  is then approximately equal to the experimental value (the latter being in arbitrary units, as before, and adjusted to agree with the theoretical values in the neighbourhood of  $Xp^{-1} = 40$ ).

One of the authors (E. C. W. S.) wishes to express his indebtedness to the Department of Scientific and Industrial Research for a grant which has enabled him to participate in this work, and another (R. W. L.) his indebtedness to the Government Grant Committee of the Royal Society for a grant to purchase the motor generator used.

\* For these (assumed) conditions the number of molecules excited per cm. of electron path, which is in the direction of  $X$ , is  $3.15 \times p \times Q_e (\bar{V})$ , the energy efficiency of excitation is therefore (cf. Part II)  $3.15 \times (Xp^{-1})^{-1} \times Q_e (\bar{V})$ .

## SUMMARY

Experiments are described in which the energy efficiency of the excitation of the continuous spectrum of hydrogen ( $^3\Sigma_g^+ - ^3\Sigma_u^+$ ) has been determined in arbitrary units as a function of  $Xp^{-1}$ , the ratio of the field to the pressure, in the uniform positive column discharge through rapidly streaming hydrogen. For values of  $Xp^{-1}$  from 25 to 140 the theoretical values of the energy efficiency derived in Part II are in good agreement with the results of these experiments; the data of Chalonge indicate that the agreement probably extends to  $Xp^{-1} = 10$ . For higher values of  $Xp^{-1}$  the theoretical values of the energy efficiency diminish more rapidly than the experimental ones

---

## INDEX TO VOLUME CLVIII (A)

- Acids, *n*-fatty, and derivatives (Francis, Collins, and Piper), 691
- Alkali metals, a quantum mechanical discussion of (Fröhlich), 97.
- Allsopp (C B) The absorption spectra of triiodides, 167.
- Appleton (E V) and Chapman (F W) On the nature of atmospherics—IV, 1.
- Appleyard (E T S) and Lovell (A C B) The electrical conductivity of thin metallic films II—Caesium and potassium on pyrex glass surfaces, 718.
- Arnott (F L) A new process of negative ion formation—II. III—The energy distribution of the negative ions and accommodation coefficients of the positive ions, 137, 157.
- Atmospherics, nature of (Appleton and Chapman), 1
- Atoms and molecules, interaction of, with solid surfaces VI, VII, VIII (Lennard-Jones and Devonshire, and Devonshire), 242, 253, 269
- Atoms, diffraction of, by a surface (Lennard-Jones and Devonshire), 253
- Baber (W G) The contribution to the electrical resistance of metals from collisions between electrons, 383
- Barriers, potential, permeability of, to light particles (Bell), 128
- Baughan (E C) and Bell (R P) Temperature coefficients in the anion catalysed decomposition of nitramide, 464
- Bayliss (N S) The theory of the continuous absorption spectrum of bromine, 551
- Bell (J) Spectrographic studies of the explosive combustion of methane, 429
- Bell (R P) Exact and approximate expressions for the permeability of potential barriers to light particles, 128
- Bell (R P) *See* Baughan and Bell
- Beta-ray lines of Ra (B + C), Th (B + C), and Ac (B + C), (Li), 571
- Bands of fractional order in aromatic molecules (Penney), 306
- Bromine, continuous absorption spectrum of (Bayliss), 551
- Burton (E F) and Turnbull (L G) Dielectric constants of solids at high frequencies and the influence of water of crystallization on dielectric constant, 182
- Cameron (W. H B) *See* Elliott and Cameron
- Carter (A G) and Travers (Morris W) On the thermal decomposition of methyl nitrite, 495
- Chamberlain (E A C) *See* Townend and Chamberlain
- Chapman (F W) *See* Appleton and Chapman
- Chlorine, emission band spectrum of (Elliott and Cameron), 681
- Collins (F J E) *See* Francis, Collins, and Piper
- Conductivity, electrical, of thin metallic films—II (Appleyard and Lovell), 718
- Cosmic ray showers, studies of (Hu), 581
- Crawford (D P) *See* Henderson, Mushkat, and Crawford
- Crawford (M F), McLay (A B), and Crooker (A M) The spectrum of trebly-ionized lead, Pb IV, 455
- Crooker (A M) *See* Crawford, McLay, and Crooker.
- Deuterium, energy exchange between hydrogen and (Mann and Newell), 397.

Devonshire (A F) The interaction of atoms and molecules with solid surfaces  
VIII—The exchange of energy between a gas and a solid, 269

Devonshire (A. F) *See also* Lennard-Jones and Devonshire

Dielectric constants of solids at high frequencies (Burton and Turnbull), 182.

Eddies, production of small ones from large ones (Taylor and Green), 499

Eggleston (F H) *See* Martin and Eggleston

Elliott (A) and Cameron (W H B) The emission band spectrum of chlorine—I,  
681

Elliptic cylinder, motion of, in fluids (Manohar Ray), 522

Energy exchange between hydrogen and deuterium (Mann and Newell), 397

Energy, exchange of, between gas and solid (Devonshire), 269

Energy, the emission and absorption of, by a solid (Strachan), 591

Essen (L) *See* Wood, Tomlinson, and Essen

Explosion waves and shock waves—IV (Payman and Shepherd), 348

Films, thin metallic, electrical conductivity of (Appleyard and Lovell), 718

Fitzgerald-Lorentz contraction (Wood, Tomlinson, and Essen), 606

Francis (F), Collins (F J. E.), and Piper (S H) The *n*-fatty acids and certain of  
their derivatives, 691

Frohlich (H) A quantum mechanical discussion of the cohesive forces and thermal  
expansion coefficients of the alkali metals, 97

Green (A E) *See* Taylor and Green

Haloes, pleochroic, quantitative study of (Henderson, Mushkat, and Crawford), 199.

Hartree (D R) *See* Myers, Hartree, and Porter

Helium, adsorbed at low temperatures, behaviour of (Lennard-Jones and Devonshire),  
242

Henderson (G H), Mushkat (C M), and Crawford (D P) A quantitative study  
of pleochroic haloes III—Thorium, 199

Hu (C S) Studies of cosmic-ray showers by quintuple coincidences, 581

Hydrocarbons, complex, ultra-violet absorption spectra of (Mayneord and Roe), 634

Hydrogen, excitation of the continuous spectrum of (Lunt, Meek, and Smith), 729

Hyperfine structure and Zeeman effect of the resonance lines of silver (Jackson and  
Kuhn), 372

Ignition, spontaneous, influence of pressure on an ethane-air mixture (Townend and  
Chamberlain), 415

Infeld (L) The Lorentz transformations in the new quantum electrodynamics, 368

Ionization, excitation, and chemical reaction in uniform electric fields—III (Lunt,  
Meek, and Smith), 729

Ion, negative, new process of (Arnot), 137, 157

Ions, positive, accommodation coefficients of (Arnot), 157

Jackson (D A) and Kuhn (H) The hyperfine structure and Zeeman effect of the  
resonance lines of silver, 372

Johnson (M C) and Vick (F A) The modification of apparent thermionic con-  
stants for oxygenated tungsten by the temperature variation of adsorptive  
equilibrium, 55

- Ketones, *n*-long chain, dielectric polarization of (Müller), 403.**
- Kinematics, dynamics, and the scale of time (Milne), 324.**
- Krishnamurty (S. G.) and Rao (K. R.) The spectrum of ionized tellurium, extension of Te III, 562.**
- Kuhn (H.) Pressure broadening of spectral lines and van der Waals forces. I—Influence of argon on the mercury resonance line II—Continuous broadening and discrete bands in pure mercury vapour, 212, 230.**
- Kuhn (H.) See Jackson and Kuhn.**
- Lead, trebly-ionized, spectrum of (Crawford, McLay, and Crooker), 455.**
- Lee (E.) See Tolansky and Lee**
- Lennard-Jones (J. E.) The electronic structure of some polyenes and aromatic molecules I—The nature of the links by the method of molecular orbitals, 280**
- Lennard-Jones (J. E.) and Devonshire (A. F.) The interaction of atoms and molecules with solid surfaces VI—The behaviour of adsorbed helium at low temperatures VII—The diffraction of atoms by a surface, 242, 253**
- Lennard-Jones (J. E.) and Turkevich (J.) The electronic structure of some polyenes and aromatic molecules II—The nature of the links of some aromatic molecules, 297**
- Li (K. T.) On the absolute intensities of the strong beta-ray lines of Ra (B + C), Th (B + C), and Ac (B + C), 571**
- Links, nature of, in aromatic molecules (Lennard-Jones, Lennard-Jones and Turkevich), 280, 297**
- Lorentz transformations in the new quantum electrodynamics (Infeld), 368**
- Lovell (A. C. B.) See Appleyard and Lovell**
- Lunt (R. W.), Meek (C. A.), and Smith (E. C. W.) Ionization, excitation, and chemical reaction in uniform electric fields III—The excitation of the continuous spectrum of hydrogen, 729**
- McLay (A. B.) See Crawford, McLay, and Crooker**
- Mann (W. B.) and Newell (W. C.) The exchanges of energy between a platinum surface and hydrogen and deuterium molecules, 397**
- Martin (L. H.) and Eggleston (F. H.) The Auger effect in xenon and krypton, 46.**
- Martyn (D. F.), Piddington (J. H.), and Munro (G. H.) The polarization of radio echoes, 536**
- Mayneord (W. V.) and Roe (E. M. F.) The ultra-violet absorption spectra of some complex aromatic hydrocarbons, 634**
- Meek (C. A.) See Lunt, Meek, and Smith**
- Mercury vapour, continuous broadening and discrete bands in (Kuhn), 230**
- Metals, electrical resistance in (Baber), 383.**
- Methane and air mixtures, quasi-detonation in (Payman and Shepherd), 348**
- Methane, spectrographic studies of the explosive combustion of (Bell), 429.**
- Methyl nitrite, thermal decomposition of (Carter and Travers), 495.**
- Micrography of metals in ultra-violet light (Smiles and Wrighton), 671.**
- Milne (E. A.) Kinematics, dynamics, and the scale of time, 324.**
- Montserrat, preliminary report on seismic observations (Powell), 479**
- Müller (A.) The dielectric polarization of *n*-long chain ketones near their melting points, 403**

- Munro (G H) *See* Martyn, Piddington, and Munro.
- Mushkat (C. M.) *See* Henderson, Mushkat, and Crawford
- Myers (D M), Hartree (D R), and Porter (A) The effect of space-charge on the secondary current in a triode, 23.
- Neuberger (A) Dissociation constants and structures of zwitterions, 68.
- Newell (W. C.) *See* Mann and Newell
- Nitramide, temperature coefficients in the anion catalysed decomposition of (Baughan and Bell), 464
- Oscillations, atmospheric (Pekeris), 650.
- Payman (W) and Shepherd (W C F) Explosion waves and shock waves IV—Quasi-detonation in mixtures of methane and air, 348.
- Pekeris (C L) Atmospheric oscillations, 650
- Penney (W G) The electronic structure of some polyenes and aromatic molecules III—Bonds of fractional order by the pair method, 306
- Permeability of potential barriers to light particles, expressions for (Bell), 128
- Piddington (J H) *See* Martyn, Piddington, and Munro
- Piper (S. H.) *See* Francis, Collins, and Piper
- Platinum, fine structure and arc spectrum (Tolansky and Lee), 110
- Polyenes and aromatic molecules, structure of (Lennard-Jones, Lennard-Jones and Turkevich, and Penney), 280, 297, 306
- Porter (A) *See* Myers, Hartree, and Porter
- Powell (C F) Royal Society expedition to Montserrat, B W I Preliminary report on seismic observation, 479.
- Pressure broadening of spectral lines (Kuhn), 212, 230
- Radio echoes, polarization of (Martyn, Piddington, and Munro), 536
- Rao (K R) *See* Krishnamurty and Rao
- Ray (Manohar) Motion of an infinite elliptic cylinder in fluids with constant vorticity, 522
- Roe (E M F) *See* Mayneord and Roe
- Shepherd (W C F) *See* Payman and Shepherd
- Silver, hyperfine structure (Jackson and Kuhn), 372.
- Smiles (J) and Wrighton (H) The micrography of metals in ultra-violet light, 671
- Smith (E C W) *See* Lunt, Meek, and Smith
- Space-charge, effects of, on secondary current in a triode (Myers, Hartree, and Porter), 23
- Spectra, absorption, of complex hydrocarbons (Mayneord and Roe), 634
- Spectra, absorption, of triiodides (Allsopp), 167
- Spectral lines, pressure broadening of (Kuhn), 212, 230
- Spectrum, arc of platinum (Tolansky and Lee), 110.
- Spectrum, band, of chlorine (Elliott and Cameron), 681.
- Spectrum, continuous absorption of bromine (Bayliss), 551
- Spectrum of ionized tellurium (Krishnamurty and Rao), 562.
- Spectrum of trebly-ionized lead (Crawford, McLay, and Crooker), 455.
- Spinor-calculus, relations of tensor-calculus to (Whittaker), 38

- Strachan (C.) The interaction of atoms and molecules with solid surfaces. IX—  
The emission and absorption of energy by a solid, 591.
- Taylor (G. I.) and Green (A. E.) Mechanism of the production of small eddies from  
large ones, 499.
- Tellurium, ionized, spectrum of (Krishnamurty and Rao), 562.
- Tensor-calculus, relations of, to spinor-calculus (Whittaker), 38.
- Thorium, pleochroic haloes (Henderson, Mushkat, and Crawford), 199.
- Tolansky (S.) and Lee (E.) Fine structure of the arc spectrum of platinum. (A)  
The nuclear spin of Pt 195, (B) Even isotope displacement, 110.
- Tomlinson (G. A.) See Wood, Tomlinson, and Essen.
- Townend (D. T. A.) and Chamberlain (E. A. C.) The influence of pressure on the  
spontaneous ignition and limits of inflammability of ether-air mixtures, 415.
- Travers (Morris W.) See Carter and Travers.
- Triiodides, absorption spectra of (Allsopp), 167.
- Triode, effect of space charge on secondary current (Myers, Hartree, and Porter), 23.
- Tungsten, thermionic constants for (Johnson and Vick), 55.
- Turkevich (J.) See Lennard-Jones and Turkevich.
- Turnbull (L. G.) See Burton and Turnbull.
- Vick (F. A.) See Johnson and Vick.
- Whittaker (E. T.) On the relations of the tensor-calculus to the spinor-calculus, 38.
- Wood (A. B.), Tomlinson (G. A.), and Essen (L.) The effect of the Fitzgerald-  
Lorentz contraction on the frequency of longitudinal vibration of a rod, 606.
- Wrighton (H.) See Smiles and Wrighton.
- Xenon and krypton, Auger effect in (Martin and Eggleston), 46.
- Zeeman effect of the resonance lines of silver (Jackson and Kuhn), 372.
- Zwitterions, structures of (Neuberger), 68.

END OF THE ONE HUNDRED AND FIFTY-EIGHTH VOLUME (SERIES A)

---



